MODULATING GLIAL CELLS PHENOTYPE: NEW FINDINGS AND THERAPIES

EDITED BY: Alberto Javier Ramos, Yolanda Diz-Chaves and Maria Jose Bellini
PUBLISHED IN: Frontiers in Aging Neuroscience, Frontiers in Molecular Neuroscience and Frontiers in Neuroscience

frontiers Research Topics

ISSN 1664-8714
ISBN 978-2-88966-183-1
DOI 10.3389/978-2-88966-183-1

About Frontiers

Frontiers is more than just an open-access publisher of scholarly articles: it is a pioneering approach to the world of academia, radically improving the way scholarly research is managed. The grand vision of Frontiers is a world where all people have an equal opportunity to seek, share and generate knowledge. Frontiers provides immediate and permanent online open access to all its publications, but this alone is not enough to realize our grand goals.

Frontiers Journal Series

The Frontiers Journal Series is a multi-tier and interdisciplinary set of open-access, online journals, promising a paradigm shift from the current review, selection and dissemination processes in academic publishing. All Frontiers journals are driven by researchers for researchers; therefore, they constitute a service to the scholarly community. At the same time, the Frontiers Journal Series operates on a revolutionary invention, the tiered publishing system, initially addressing specific communities of scholars, and gradually climbing up to broader public understanding, thus serving the interests of the lay society, too.

Dedication to Quality

Each Frontiers article is a landmark of the highest quality, thanks to genuinely collaborative interactions between authors and review editors, who include some of the world's best academicians. Research must be certified by peers before entering a stream of knowledge that may eventually reach the public - and shape society; therefore, Frontiers only applies the most rigorous and unbiased reviews.
Frontiers revolutionizes research publishing by freely delivering the most outstanding research, evaluated with no bias from both the academic and social point of view. By applying the most advanced information technologies, Frontiers is catapulting scholarly publishing into a new generation.

What are Frontiers Research Topics?

Frontiers Research Topics are very popular trademarks of the Frontiers Journals Series: they are collections of at least ten articles, all centered on a particular subject. With their unique mix of varied contributions from Original Research to Review Articles, Frontiers Research Topics unify the most influential researchers, the latest key findings and historical advances in a hot research area! Find out more on how to host your own Frontiers Research Topic or contribute to one as an author by contacting the Frontiers Editorial Office: researchtopics@frontiersin.org

MODULATING GLIAL CELLS PHENOTYPE: NEW FINDINGS AND THERAPIES

Topic Editors:
Alberto Javier Ramos, Consejo Nacional de Investigaciones Científicas y Técnicas (CONICET), Argentina
Yolanda Diz-Chaves, University of Vigo, Spain
Maria Jose Bellini, Consejo Nacional de Investigaciones Científicas y Técnicas (CONICET), Argentina

Citation: Ramos, A. J., Diz-Chaves, Y., Bellini, M. J., eds. (2020). Modulating Glial Cells Phenotype: New Findings and Therapies. Lausanne: Frontiers Media SA. doi: 10.3389/978-2-88966-183-1

Table of Contents

frontiers in Aging Neuroscience

EDITORIAL
published: 23 September 2020
doi: 10.3389/fnagi.2020.594870

Editorial: Modulating Glial Cells Phenotype: New Findings and Therapies

María José Bellini[1]*, *Yolanda Diz-Chaves*[2] and *Alberto Javier Ramos*[1]

[1] Consejo Nacional de Investigaciones Científicas y Técnicas, Buenos Aires, Argentina, [2] Laboratory of Endocrinology, The Biomedical Research Centre (CINBIO), University of Vigo, Vigo, Spain

Keywords: aging, inflammation, microglia, astroglia, therapies

Editorial on the Research Topic

Modulating Glial Cells Phenotype: New Findings and Therapies

Aging and neurodegenerative diseases are closely related, and the common point between both scenarios is neuroinflammation. Neuroinflammation is mainly mediated by glial cells, astrocytes, and microglia; while endothelial cells transfer the pro-inflammatory signals from periphery. The mechanism that underlies glial cells activation and neuroinflammation-related damage is not fully understood, being the study of glial cells during aging as well as neurodegenerative diseases, a key point to identify targets and to develop therapies that modulate adverse outcomes and mitigate neurodegeneration.

This Research Topic has produced a highly informative collection of original research and reviews, that cover multiple aspects for delving neuroinflammation and glial phenotypic changes in neurological diseases and aging. Researchers have presented their work and views to explain cellular and molecular mechanisms acquired by glial cells as well as possible interventions that can modify their functions and phenotypes associated with a broad spectrum of neurological diseases.

Serapide et al. started by focusing on the pivotal role of astrocytes activation in Parkinson's disease (PD), the most common age-dependent movement disorder. These authors tried a new approach to uncover the interaction between the astrocytes and neurons in PD mice brains. They demonstrate that grafting astrocytes alleviate oxidative stress in a parkinsonian brain by using MPTP-induced PD mice. Adding new information, Rabaneda-Lombarte et al. investigated the effect of MPP+ or rotenone to microglial/astroglial functions. Their manuscript provides information on the impact of PD-related toxins on the phenotype of glia, based on the evaluation of the mRNA levels of various gene products.

Deepen on astrocytes functions, the astrocyte-specific enzyme glutamine synthetase plays an essential role in supporting neurotransmission and in limiting ammonium toxicity. Moreover, deficits in Glutamine synthetase activity contribute to epilepsy and neurodegeneration. In this regard, Huyghe et al. extensively investigated the regulation of glutamine synthetase by PKA at T301 using biochemical and cell biological approaches. The authors successfully created two anti-phospho-GS antibodies and demonstrated that phosphorylation of T301 is critical for its activity in astrocytes. This modification results in decreased enzyme activity in a mouse model of epilepsy.

To provide new insights into microglial implication in behavioral changes induced by infections and mediated by pro-inflammatory cytokines, Savage et al. describe for the first time the effects of acute LPS on the ultrastructure of microglia in the mouse hippocampus. The ultrastructural changes found by the authors, provide an excellent starting point to determine pro-inflammatory and phagocytic pathways engaged by in sickness behavior.

Another interesting aspect of glial cells participation on pathological conditions was reviewed by Zang et al.. Their work was focused on the role of epigenetic regulation in the pathogenesis of

OPEN ACCESS

Edited and reviewed by:
Thomas Wisniewski,
New York University, United States

***Correspondence:**
María José Bellini
mariajosebellini@yahoo.com;
mariajosebellini@med.unlp.edu.ar

Received: *14 August 2020*
Accepted: *18 August 2020*
Published: *23 September 2020*

Citation:
Bellini MJ, Diz-Chaves Y and Ramos AJ (2020) Editorial: Modulating Glial Cells Phenotype: New Findings and Therapies. Front. Aging Neurosci. 12:594870. doi: 10.3389/fnagi.2020.594870

glioma and discuss its value as therapeutic target for the treatment of this disease. Authors expand our knowledge on four epigenetic phenomena that occur in glioma: DNA methylation, abnormal microRNA, histone modifications, and chromatin remodeling. They review current epigenetic treatments for glioma, such as inhibitors of DNA methyltransferase and histone deacetylation inhibitors and argument the limitations of their applications due to the complicated pathogenesis of glioma.

Various articles in this collection focus on the role and mechanisms of astrocytes and microglia in the aging brain. Current issues and novel findings in the modulation of glial cells and the pathways able to promote healthy aging will provide a better understanding of cellular and molecular mechanisms toward a neuroprotective or a deleterious glial phenotype. Related with this topic, Matias et al. introduced the concept of astrocyte heterogeneity, which is a hot topic in the field. The review addressed diverse phenotypes of astrocytes with an emphasis on aging and neurodegenerative conditions. The authors discussed historical overview of astrocytes, astrocyte heterogeneity in healthy brain and pathological conditions, concept of "inflammaging," and selective vulnerability. Also, they present the possibility of using glia as target for therapeutic strategies.

Expanding the knowledge of the changes undergone by astrocytes during aging, Zárate et al. investigated the role of Humanin, an astrocyte-release mitochondrial peptide, and the influence of hormonal milieu. They analyzed the role of this protein on synaptic dysfunction in the context of hormonal decline as a model of aging. The study of Humanin regulation by ovarian hormones in the brain is novel and highly interesting, given the plethora of molecular targets that these hormones have and that participate in mediating their neuroprotective and neuro-restorative.

Continuing with the study of glial-cells changes during aging, Falomir-Lockhart et al. investigated the effects of IGF-1 gene therapy on microglia. Importantly, these authors found that IGF1 therapy leads to a region-specific modification of aged microglia population. Microglia cells become dystrophic with aging; which contributes to basal central nervous system neuroinflammation being a risk factor for age-related neurodegenerative diseases. These authors' findings suggest that such a therapy may be useful to alter the function of dystrophic microglia effects.

Another study by Trias et al. explores the emergence of senescent microglia in spinal cord during paralysis progression in amyotrophic lateral sclerosis (ALS) rat model (SOD1G93A). The authors showed nuclear p16INK4a expression in activated microglia during paralysis progression as well as in a subpopulation of spinal motor neurons and astrocytes. They suggest that cellular senescence is closely associated with inflammation and motor neuron loss occurring after paralysis onset in SOD1G93A rats. The emergence of senescent cells could mediate key pathogenic mechanisms in ALS.

With the increment of life expectancy, preventive measures, and treatments for age-related cognitive decline, and dementia are of utmost importance. The work by Ano et al. shows that both chronic and acute administration of Iso-alpha-acids (IAA) prevents the neuroinflammation and cognitive decline associated with aging. The use of natural compounds as IAA, which are hop-derived bitter compounds in beer, represent an interesting therapeutic tool to ameliorate age-related negative outcomes.

Later on, Velasco-Estevez et al. used an aging transgenic rat model of Alzheimer Disease (AD) to study the expression of mechanosensing Piezo1 ion channels in amyloid plaque-reactive astrocytes. Piezo1 is a non-selective mechanosensory mediating cation channel. The authors found that aging and peripheral infection augment amyloid plaque-induced upregulation of mechanoresponsive ion channels, such as Piezo1, in astrocytes. Additional work is required to investigate the role of astrocytic Piezo1 in the Alzheimer's brain and its possible use as a novel drug target for age-related dementia.

Microglia polarization to an anti-inflammatory phenotype has been described to be neuroprotective. In the study by Jin et al., they linked microglial pro-inflammatory polarization to neuroinflammation and autophagy dysfunction, that are closely related to the development of neurodegeneration in Parkinson's disease. They demonstrate that TNF-α inhibits autophagy in microglia through AKT/mTOR signaling pathway, and autophagy enhancement can promote microglia polarization toward anti-inflammatory phenotype and inflammation resolution. This study adds information to establish which specific factors are responsible for disturbing the pro-/anti-inflammatory balance in areas where inflammatory stimuli induce neurodegeneration. Besides the study contributes to understanding the relationship between inflammation and autophagy processes.

Together these articles have brought several interesting understandings of neuroinflammation and glial cells activation in a range of neurological diseases and aging. We expect that this topic would expand our knowledge of the mechanisms whereby reactive glial cells could be detrimental or neuroprotective. Moreover, this comprehension could contribute for the development of therapeutics to limit neuroinflammation or even slow down the process of aging.

AUTHOR CONTRIBUTIONS

MB, YD-C, and AR contributed equally to this editorial, in its conception, writing, and revision. All authors approved the submitted version.

Conflict of Interest: The authors declare that the research was conducted in the absence of any commercial or financial relationships that could be construed as a potential conflict of interest.

frontiers in Aging Neuroscience

ORIGINAL RESEARCH
published: 22 October 2018
doi: 10.3389/fnagi.2018.00332

Infection Augments Expression of Mechanosensing Piezo1 Channels in Amyloid Plaque-Reactive Astrocytes

María Velasco-Estevez[1,2], Myrthe Mampay[1], Hervé Boutin[3], Aisling Chaney[3,4], Peter Warn[5], Andrew Sharp[5], Ellie Burgess[5], Emad Moeendarbary[6,7], Kumlesh K. Dev[2]* and Graham K. Sheridan[1]**

[1] Neuroimmulology & Neurotherapeutics Laboratory, School of Pharmacy and Biomolecular Sciences, University of Brighton, Brighton, United Kingdom, [2] Drug Development, Department of Physiology, School of Medicine, Trinity College Dublin, Dublin, Ireland, [3] Wolfson Molecular Imaging Centre, Faculty of Biology, Medicine and Health and Manchester Academic Health Sciences Centre, The University of Manchester, Manchester, United Kingdom, [4] Department of Radiology, Stanford University, Stanford, CA, United States, [5] Evotec (UK) Ltd., Manchester Science Park, Manchester, United Kingdom, [6] Department of Biological Engineering, Massachusetts Institute of Technology, Cambridge, MA, United States, [7] Department of Mechanical Engineering, University College London, London, United Kingdom

OPEN ACCESS

Edited by:
Alberto Javier Ramos, Consejo Nacional de Investigaciones Científicas y Técnicas (CONICET), Argentina

Reviewed by:
Jingwen Niu, Temple University, United States
Vladimir Parpura, The University of Alabama at Birmingham, United States

***Correspondence:**
Emad Moeendarbary
e.moeendarbary@ucl.ac.uk
Kumlesh K. Dev
devk@tcd.ie
Graham K. Sheridan
G.Sheridan@brighton.ac.uk

Received: 19 June 2018
Accepted: 01 October 2018
Published: 22 October 2018

Citation:
Velasco-Estevez M, Mampay M, Boutin H, Chaney A, Warn P, Sharp A, Burgess E, Moeendarbary E, Dev KK and Sheridan GK (2018) Infection Augments Expression of Mechanosensing Piezo1 Channels in Amyloid Plaque-Reactive Astrocytes. Front. Aging Neurosci. 10:332. doi: 10.3389/fnagi.2018.00332

A defining pathophysiological hallmark of Alzheimer's disease (AD) is the amyloid plaque; an extracellular deposit of aggregated fibrillar $A\beta_{1-42}$ peptides. Amyloid plaques are hard, brittle structures scattered throughout the hippocampus and cerebral cortex and are thought to cause hyperphosphorylation of tau, neurofibrillary tangles, and progressive neurodegeneration. Reactive astrocytes and microglia envelop the exterior of amyloid plaques and infiltrate their inner core. Glia are highly mechanosensitive cells and can almost certainly sense the mismatch between the normally soft mechanical environment of the brain and very stiff amyloid plaques via mechanosensing ion channels. Piezo1, a non-selective cation channel, can translate extracellular mechanical forces to intracellular molecular signaling cascades through a process known as *mechanotransduction*. Here, we utilized an aging transgenic rat model of AD (TgF344-AD) to study expression of mechanosensing Piezo1 ion channels in amyloid plaque-reactive astrocytes. We found that Piezo1 is upregulated with age in the hippocampus and cortex of 18-month old wild-type rats. However, more striking increases in Piezo1 were measured in the hippocampus of TgF344-AD rats compared to age-matched wild-type controls. Interestingly, repeated urinary tract infections with *Escherichia coli* bacteria, a common comorbidity in elderly people with dementia, caused further elevations in Piezo1 channel expression in the hippocampus and cortex of TgF344-AD rats. Taken together, we report that aging and peripheral infection augment amyloid plaque-induced upregulation of mechanoresponsive ion channels, such as Piezo1, in astrocytes. Further research is required to investigate the role of astrocytic Piezo1 in the Alzheimer's brain, whether modulating channel opening will protect or exacerbate the disease state, and most importantly, if Piezo1 could prove to be a novel drug target for age-related dementia.

Keywords: Alzheimer's disease, amyloid plaques, astrocytes, dentate gyrus, mechanosensitive ion channel, Piezo1, TgF344-AD rats, urinary tract infection

INTRODUCTION

The etiology of early-onset Alzheimer's disease (AD) has a strong genetic component and mutations in genes that encode for amyloid precursor protein (APP), presenilin 1 (PSEN1), and presenilin 2 (PSEN2) give rise to a rare but severe form of familial dementia characterized by cortical and hippocampal atrophy and progressive cognitive decline (Saunders, 2001; Nacmias et al., 2014; Lanoiselee et al., 2017). The amyloid cascade hypothesis of AD (Hardy and Allsop, 1991) states that aberrant cleavage of APP by γ-secretase results in the accumulation of cytotoxic oligomeric amyloid-β_{1-42} ($A\beta_{1-42}$) which aggregates and forms β-sheet fibrillar structures that, in turn, clump together and generate extracellular amyloid plaques (Lukiw, 2012; Morris et al., 2014). Amyloid plaques contribute to cortical and hippocampal neurodegeneration and neuroinflammation (Nobakht et al., 2011; Dansokho and Heneka, 2018), although extensive plaque pathology is not necessarily a good indicator of the clinical severity of dementia (Hyman et al., 1993). Structurally, amyloid plaques are very brittle and stiff (with a stiffness of $\sim 3 \times 10^9$ Pa) (Smith et al., 2006), in contrast to brain tissue which we have previously shown to be very soft (with a stiffness of ∼200–500 Pa) (Moeendarbary et al., 2017). Therefore, neurons and glia surrounding the amyloid plaque experience a large perturbation to their mechanical microenvironment. Astrocytes, the most abundant glial cell type in the brain, respond to amyloid plaque accumulation by adopting a 'reactive' phenotype characterized by an increase in intermediate filament expression, e.g., GFAP (Wilhelmsson et al., 2006; Sofroniew, 2009), and synthesis of proinflammatory cytokines (Buffo et al., 2010; Sofroniew, 2014). We hypothesize that, in addition to biochemical signals, astrogliosis in the AD brain is triggered in part by a detectable increase in the stiffness of the mechanical microenvironment experienced by resting glial cells.

Neurons and glia are highly mechanosensitive (Previtera et al., 2010; Blumenthal et al., 2014) and detect changes in the stiffness of underlying cell culture substrates via stretch-activated membrane-spanning ion channels (Cox et al., 2016; Bavi et al., 2017). Microglial cells, for example, display durotaxis, i.e., they migrate toward stiffer areas when cultured on stiffness gradient hydrogels (Bollmann et al., 2015). Astrocytes grown on stiff hydrogels possess longer, thicker processes and appear much more reactive than those cultured on soft hydrogels (Moshayedi et al., 2010). Moreover, astrocytes *in vivo* respond to hard foreign body implants by releasing proinflammatory cytokines, such as Il-1β (Moshayedi et al., 2014). In AD, the build-up of extracellular amyloid plaques causes astrogliosis and, given the stiffness of plaques, we hypothesize that astrocyte reactivity is mediated partly by activation of mechanosensitive ion channels. Therefore, our aim here was to investigate cellular expression of mechanosensitive Piezo1 channels in response to amyloid plaque pathology in an aging rat model of AD.

To carry out this aim, we utilized the TgF344-AD rat model (Cohen et al., 2013) that overexpress human APP with the Swedish mutation (APP_{SWE}) and mutated human PSEN1 (PSEN1ΔE9). In the healthy human brain, Piezo1 mRNA is expressed by neurons but is absent from astrocytes. Post-mortem analysis of AD brains, however, revealed that Piezo1 mRNA is down-regulated in neurons and up-regulated in astrocytes surrounding amyloid plaques (Satoh et al., 2006). Therefore, Piezo1 was previously known as Mib (membrane protein induced by beta-amyloid treatment). Piezo1 is a large protein (>2,500 amino acids) predicted to contain 30–40 putative transmembrane segments (Kamajaya et al., 2014), assembles as a ∼900 kDa homotrimer (Ge et al., 2015) and forms a non-selective calcium (Ca^{2+})-permeable cation channel (Gnanasambandam et al., 2015). Mechanosensitive ion channels translate external physical stimuli, such as shear stress (Ranade et al., 2014), pressure (Gottlieb and Sachs, 2012; Bae et al., 2015) and extracellular matrix (ECM)-associated traction forces (Pathak et al., 2014) to intracellular biochemical signals via mechanotransduction events (Martinac, 2004; Moeendarbary and Harris, 2014). Piezo1 mRNA is highly expressed in tissues subject to regular deformations or shear forces such as lungs, bladder, skin and vasculature endothelium (Coste et al., 2010; Ranade et al., 2014; Li et al., 2015). To date, however, very little is known about the role of Piezo1 in the CNS. We have recently shown that Piezo1 is involved in axon guidance of optic tract retinal ganglion cells (RGCs) in the developing *Xenopus laevis* brain (Koser et al., 2016). Here, we will investigate if glial cells can physically sense and respond to the accumulation of amyloid plaques by quantifying expression of astrocytic Piezo1 channels in the hippocampus and cerebral cortex of the aging TgF344-AD rat model of AD.

Because of their advanced age, elderly people are prone to co-morbidities and peripheral infections that cause low-grade systemic inflammation (Salles and Mégraud, 2007; Doulberis et al., 2018). Interestingly, peripheral infections increase older people's risk of developing AD (Holmes et al., 2009; Tate et al., 2014) and reportedly exacerbate amyloid plaque deposition in the mouse brain (McManus et al., 2014), although the mechanisms underlying this crosstalk between the periphery and CNS is not well-understood. Although most transgenic animal models recapitulate many of the amyloid-related hallmarks of AD, it is important to use clinically-relevant animal models with at least one comorbidity, such as a peripheral infection, to investigate AD pathogenesis. Therefore, we investigated if a peripheral urinary tract infection (UTI) with *E. coli* bacteria, one of the most likely causes of infection in elderly people with dementia (Natalwala et al., 2008; Rowe and Juthani-Mehta, 2013), modifies astrocytic mechano-responsiveness to stiff extracellular amyloid deposits (Leyns and Holtzman, 2017). Our results suggest that restoring homeostatic mechanotransduction pathways and neuron/glial crosstalk around amyloid plaques may lead to the discovery of novel drug targets for neurodegeneration and AD.

Abbreviations: Aβ42, amyloid-β 1–42 peptide; BSA, bovine serum albumin; CMM, conditioned microglial media; CNS, central nervous system; DMEM, Dulbecco's modified Eagle's medium; FBS, fetal bovine serum; GFAP, glial fibrillary acidic protein; HBSS, Hank's buffered salt solution; HRP, horse radish peroxidase; iTG, transgenic with infection; iWT, wild-type with infection; NaCl, sodium chloride; NFH, neurofilament H; PBS, phosphate-buffered saline; PVDF, polyvinylidene difluoride membrane; SDS, sodium dodecylsulfate; TG, transgenic; TNF-α, tumor necrosis factor-alpha; WT, wild-type.

MATERIALS AND METHODS

Ethics Statement

All experiments involving animals and Schedule 1 protocols used to obtain brain tissue were approved by the Animal Welfare and Ethical Review Bodies (AWERB committees) of the University of Brighton and The University of Manchester, as well as the Animal Research Ethics Committee (AREC) in Trinity College Dublin. This study was conducted in accordance with the principles of the Basel Declaration and adhered to the legislation detailed in the United Kingdom Animals (Scientific Procedures) Act 1986 Amendment Regulations (SI 2012/3039). All efforts were taken to maximize animal welfare conditions and to reduce the number of animals used in accordance with the European Communities Council Directive of September 20th, 2010 (2010/63/EU).

Mouse Neuron Cultures

Primary neuron cultures were prepared from the cerebral cortical tissue of male and female postnatal day 0 or 1 (P0 or P1) C57BL/6 mice bred in the BioResources Unit (BRU) of University of Brighton. Briefly, cortices were dissected following decapitation and collected in Ca^{2+}- and Mg^{2+}-free Hank's balanced salt solution (HBSS) (Thermo Fisher Scientific, 14185052). Cells were dissociated using Papain [20 U/mL] (Worthington, 3119) in Ca^{2+}- and Mg-free HBSS supplemented with L-cysteine [1 mM] (Sigma, 168149), EDTA [0.5 mM] (Thermo Fisher Scientific, 15575020) and DNAse I solution [0.125 U/mL] (Thermo Fisher Scientific, 90083). Dissociation was inhibited using Type II-O ovomucoid trypsin inhibitor [0.1%] (Sigma, T9253) in HBSS with bovine serum albumin [0.1%] (Sigma, A9647) and D-APV [D-(-)-2-Amino-5-phosphonopentanoic acid] [50 μM] (Abcam, ab120003). A single-cell suspension was created by gentle manual trituration using fire-polished Pasteur pipettes. Cells were plated on Poly-D-Lysine (Millipore, A-003-E) coated coverslips in 24-well plates [6×10^4 cells/well] with serum-free Neurobasal-A medium (Life Technologies, 10888-022) supplemented with 2% B27 (Thermo Fisher Scientific, 17504044) and L-glutamic acid [25 μM] (Sigma, G1251). Primary neuron cultures were maintained at 37°C and 5% CO_2 in a humidified incubator and after 1 day *in vitro*, half of the plating medium was replaced with maintenance medium (without L-glutamic acid) composed of Neurobasal-A medium supplemented with 2% B27, 2 mM GlutaMAX™ (Gibco, 35050061), and 1% penicillin/streptomycin (Thermo Fisher Scientific, 15140122). This was repeated every 3 days, i.e., 50% of the cell culture medium was replenished with fresh maintenance medium. After 14 days in culture, cells were fixed in ice-cold formalin solution (10%) for immunofluorescent labeling.

Mouse Astrocyte Cultures

Mixed glial cell cultures were prepared from the cerebral cortical tissue of male and female P1 wild-type C57BL/6 mice bred in the BioResources Units of Trinity College Dublin and University of Brighton, following previously described protocols (O'Sullivan et al., 2017, 2018). Briefly, following decapitation the cortices were dissected with sterile forceps and placed in HBSS (Gibco, 14025-050). Cortical tissue was cross-chopped with a sterile scalpel and then placed in pre-warmed Dulbecco's modified Eagle's medium/F12 (DMEM/F12, Hyclone, SH30023) supplemented with 10% FBS (Labtech; FB-1090) and 1% penicillin/streptomycin (Sigma, P4333) and gently triturated until a clear solution was obtained. The resulting solution was passed through a cell strainer (40 μm) and plated into separate T75 flasks. Cells were cultured at 37°C and 5% CO_2 in a humidified incubator and grown in the supplemented DMEM/F12 media previously described. After 12 days in culture, microglial cells were separated from mouse astrocytes by placing them on a rotating shaker for 2 h at 37°C. The supernatant, with detached microglia, was removed and the enriched astrocyte cultures were trypsinised with 0.5% trypsin for 7 minutes (min) and plated accordingly. Mouse astrocyte purity was >97%, as previously described (Healy et al., 2013).

$A\beta_{1-42}$ Conditioned Microglial Media

Microglial cultures were prepared from the cerebral cortical tissue of male and female P1 wild-type C57BL/6 mice bred in the BioResources Unit of Trinity College Dublin, as previously described (Dempsey et al., 2017). Briefly, after 48 h in culture, microglia were treated with 10 μM amyloid-β_{1-42} peptide (Invitrogen, United Kingdom) for 24 h. $A\beta_{1-42}$ conditioned microglial media (CMM) was collected and used to treat the enriched astrocyte cultures described above.

Immunocytochemistry

After each biochemical treatment, mouse astrocytes were fixed in 10% formalin solution (Sigma, F1635) for 5 min on ice. Cells were blocked overnight at 4°C in blocking solution, i.e., 1% BSA + 0.1% Triton X-100. Primary antibodies included chicken anti-neurofilament H (NFH; Millipore, AB5539, RRID: AB_177520) 1:1000 dilution, rabbit anti-GFAP (Abcam, ab7260, RRID: AB_305808) 1:1000 dilution, goat anti-PIEZO1 (N-15; Santa Cruz, sc-164319, RRID: AB_10842990) 1:500 dilution, and rabbit anti-FAM38A (Abcam, ab128245, RRID: AB_11143245) 1:500 dilution in blocking solution, were used and incubated overnight at 4°C. Cells were washed with PBS + 0.1% Triton X-100 for 5 min, three times. Incubations with secondary antibodies were performed in the dark at 22 ± 2°C for an hour. In the case of rabbit anti-FAM38A, it was also incubated with biotinylated goat anti-rabbit antibody (Thermo Fisher, A24535, RRID: AB_2536003) and avidin Alexa 488 conjugate (Life Technologies, A21370) to amplify the fluorescent signal. After washes, cells were coverslipped and mounted on a microscope slide (Clarity, C361) with antifade reagent (Thermo Fisher S36936). Imaging was performed using a Leica SP8 confocal microscope.

Western Blotting

Mouse astrocyte samples were obtained by scraping the cells in radioimmunoprecipitation assay buffer (RIPA) containing 150 mM NaCl (Sigma, A3014), 1% Triton-X (Sigma, T8787), 0.1% SDS (Fisher, S/5200/53) and 50 mM Tris pH 8.0 (Fisher, T/3710/60). Samples were sonicated three times for 10 s at 20% amplitude using a vibracell VCX 130 (Sonics,

United States). Briefly, samples were mixed in 1:1 dilution with Laemmli sample buffer 2× (BioRad, 161-0737) and boiled at 95°C for 5 min. They were run in a 6% polyacrylamide separating gel with 4% stacking gel (Applichem Panreac, A1672) in running buffer at constant voltage 120 V, followed by wet transfer to a PVDF (Millipore, IPVH00010) for 3 h at constant 70 V on ice. Blocking of the membrane was done with 5% BSA (Santa Cruz, sc-2323) in 0.05% PBS/Tween 20 for an hour at 22 ± 2°C. Incubation with primary antibody rabbit anti-FAM38A (Abcam, ab128245, RRID: AB_11143245) or goat anti-PIEZO1 (Santa Cruz, sc-164319, RRID: AB_10842990) was performed at a 1:500 dilution for 48 h at 4°C. The membrane was washed and incubated with secondary antibody HRP-conjugated goat anti-rabbit (GE Healthcare, NA934, RRID: AB_772206) or HRP-conjugated rabbit anti-goat (Sigma, A4174, RRID: AB_258138), respectively, at 1:5000 dilution for 2 h at 22°C. Following further washes, membranes were developed using chemiluminescent HRP substrate (Millipore, WBKLS0500) in a Fujifilm LAS-3000 (Fujifilm, Japan).

Wild-Type Rats

Female Lister hooded rats (Harlan Laboratories, United Kingdom) were socially housed in groups of four and given *ad libitum* access to food and water. The holding room was kept on a 12 h light/dark cycle at 22 ± 2°C. Postnatal day 37 (5-weeks) rats were sacrificed by pentobarbital overdose (intraperitoneal injection) and death was confirmed by decapitation. Immunohistochemical experiments were conducted using post-mortem brain tissue. All experiments on animal tissue were performed in accordance with the United Kingdom Animals (Scientific Procedures) Act 1986 Amendment Regulations (SI 2012/3039).

TgF344-AD Rats

Two male and female WT Fisher and TgF344-AD (TG) rats with the APP_{SWE} and PSEN1ΔE9 mutations were purchased from Prof T. Town laboratory (University of Southern California, United States) and were set-up as breeding pairs in-house at the Biological Services Unit (BSU) in The University of Manchester, United Kingdom. TG rats and WT littermates were randomly split into four groups, i.e., WT and TG non-infected (WT/TG) and infected (iWT/iTG), bearing in mind that the UTI needed to be performed on the entire box of rats. The number of rats per group (n) were as follows; 12m WT ($n = 5$); 18m WT ($n = 5$); 12m TG ($n = 6$); 18m TG ($n = 6$); 12m iWT ($n = 5$); 18m iWT ($n = 5$); 12m iTG ($n = 6$); 18m iTG ($n = 6$). All animals were housed in groups of 2–4 in cages with individual ventilation, environmental enrichment and constant access to food and water. A 12 h light/dark cycle was used, with light from 7 am until 7 pm. All experiments were carried out following internal ethical review and approval by the AWERB committee of The University of Manchester.

Urinary Tract Infection

A UTI was administered to the iWT and iTG groups at 7–8, 10–11, 13–14, and 16–17 months of age using *Escherichia coli* (*E. coli*) UTI89. For infections at 7–8 and 10–11 months of age, a concentration of 1.3×10^9 colony forming units/mL (cfu/mL) was used, and for infections at 13–14 and 16–17 months of age, a concentration of 2.6×10^9 cfu/mL was used. Therefore, before sacrifice, 12-month rats received two rounds of infection and 18-month rats received four rounds. Prior to infection, stocks of *E. coli* were stored as 1.02×10^{11} cfu/mL in 15% glycerol and were rapidly thawed and brought to the correct concentration using sterile PBS. Rats were anesthetized and infected with 0.1 mL of *E. coli* UTI89 by inserting a catheter (polyethylene tubing covering 30-G hypodermic needles) into the urethra and injecting the inoculum into the bladder. Prior to infection, buprenorphine (0.03 mg/kg) was administered and the animals' bladders were emptied by gently pressing on the abdomen to release any bladder content. Infected animals were placed into clean cages and were monitored for 5 days for signs of illness. Urine samples were taken 2 and 5 days post-infection to confirm infection levels. Urine was plated on CLED agar plates and incubated at 37°C for 18–24 h after which colony forming unit counts were performed and scored according to the following classification system: 0 = Zero colonies; 0.5 = Scanty growth (<5 cfu); 2 = Scanty growth (<20 cfu); 3 = moderate growth (>20 cfu); 4 = confluent growth. Non-infected rats tested for infection all scored ≤ 0.5.

Tissue Sectioning

Coronal slices of Lister hooded rat brains (3–4 mm thick) were fixed in 10% formalin solution for 8 h at 4°C and then transferred to 30% sucrose solution overnight (4°C) for cryoprotection. Brain slices were then covered in OCT (Optimal Cutting Temperature compound) and frozen and stored at −80°C. The slices were cryosectioned (14 μm thick) coronally at approximately −3.0 and −10.8 mm with respect to Bregma (Paxinos and Watson, 2014) in order to reveal the dorsal hippocampus and cerebellum regions, respectively. Cryosections were adhered to glass slides coated with poly-L-lysine solution [0.1% (w/v) in H_2O, Sigma]. Sections were permeabilized using a solution of 0.1% Triton™ X-100 (Sigma) in PBS for 25 min.

TgF344-AD and WT rats were sacrificed using an isoflurane overdose, confirmed by cervical dislocation. The brains were collected, snap frozen using isopentane on dry ice and stored at −80°C. Sagittal brain sections (20 μm thick) between 1 and 3.36 mm lateral to Bregma were taken using a cryostat (Leica CM3050s, Leica Biosystems Nussloch GmbH, Germany) and stored at −80°C. Prior to immunofluorescence, frozen sections were allowed to air dry at 22 ± 2°C for 20 min before fixation in 70% ethanol for 30 min. They were permeabilized in 0.2% Triton-X/PBS for 30 min, followed by several PBS washes, and then blocked with 5% BSA/PBS for 1.5 h at 22 ± 2°C.

Immunohistochemistry

Sections from WT Fisher and TgF344-AD rats were incubated overnight at 22 ± 2°C with the following primary antibodies, (1) 1:500 dilution of goat anti-PIEZO1 (N-15; Santa Cruz, sc-164319, RRID: AB_10842990), an affinity-purified goat polyclonal antibody raised against a peptide mapping to the N-terminus of PIEZO1 of human origin; (2) 1:1000 dilution of rabbit anti-amyloid β_{1-42} (mOC98, Abcam, ab201061), a

conformation-specific antibody that recognizes a discontinuous epitope of Aβ that maps to segments AEFRHD and EDVGSNK; (3) 1:1000 dilution of chicken anti-GFAP (Abcam, ab4674, RRID: AB_304558). Slides were then washed in PBS and incubated for 4 h at 22°C with the following secondary antibodies, (1) donkey anti-goat Alexa 488 (Abcam, ab150133), (2) donkey anti-rabbit 555 (Sigma, SAB4600061), (3) donkey anti-chicken IgY (H + L) CF^{TM} 633 (Sigma, SAB4600127). Finally, slides were washed and coverslipped using ProLong® Gold antifade mounting medium with DAPI (Life Technologies, United Kingdom, P36935).

Microscopy and Image Analysis

All images used to quantify Piezo1 expression in sagittal cryosections were captured using an Axio Scan.Z1 slide scanner (Zeiss, Germany) with a 20× magnification objective (Plan-Apochromat). Individual images were montaged together automatically in ZEN software (Zeiss, Germany) to reconstruct a single image of the whole brain section. For quantitative fluorescence intensity analysis, all images were captured in a single uninterrupted run (∼50 h imaging time) and uniform microscope settings were maintained throughout the session. The images were exported as 8-bit tif files for Piezo1 fluorescence intensity quantification. Image analysis was conducted using the software package FIJI[1]. Briefly, Piezo1 expression was quantified by manually selecting 10 regions of interest (ROI) for each brain structure and calculating the average fluorescence intensity within each ROI. Two or three brain sections from 5 or 6 different animals per age group/genotype were analyzed (n = 5–6). More specifically, the number of rats per group were as follows; 12m WT (n = 5); 18m WT (n = 5); 12m TG (n = 6); 18m TG (n = 6); 12m iWT (n = 5); 18m iWT (n = 5); 12m iTG (n = 6); 18m iTG (n = 6). Therefore, 100–180 fluorescence intensity (ROI) measurements were captured depending on the age and genotype of the rat. Piezo1 fluorescence intensities were normalized to the 12m WT value for each region and the percentage (%) change relative to the 12m WT group is represented in each bar graph. To quantify Piezo1 expression in amyloid plaque-reactive astrocytes versus astrocytes located at least 200 μm away from any noticeable amyloid deposits, 25 plaques from the frontal cortex of 18m TG rat brains were randomly selected for analysis. For each image (25 in total) Piezo1 fluorescence intensity was quantified in six astrocytes within the plaque core and in six astrocytes ∼200–500 μm away from the plaque. The average Piezo1 fluorescence intensity values for astrocytes located "outside" the plaque versus "inside" the plaque were calculated for each image, i.e., 150 astrocytes per group were analyzed.

Statistical Analysis

All statistical analysis was performed using GraphPad® Prism 7 (RRID: SCR_015807). Assessment of the normality of data was carried out using column statistics with D'Agostino analysis before any other statistical test was performed. For Western blot assays, repeated measures analysis of variance (ANOVA) tests were performed because data in every experiment was matched. Holm-Sidak multiple comparisons *post hoc* tests were run in conjunction with one-way ANOVAs and all groups were compared with one another. Data are presented as the mean ± standard error of the mean (SEM). To analyze changes in Piezo1 fluorescence intensities *in vivo*, where three independent variables (i.e., age, genotype, and infection) were present, a three-way ANOVA was performed on the raw fluorescence values, followed by a Holm-Sidak multiple comparisons *post hoc* test. Changes in Piezo1 expression *in vivo* were only considered significant when they passed two criteria, i.e., the relative percentage (%) change was $> 20\%$ and the p-value < 0.01. To analyze differences in average astrocytic Piezo1 expression outside versus inside amyloid plaques in the frontal cortex of 18m TG rat brains, a two-tailed paired t-test was performed. Finally, to correlate Piezo1 expression in the DG with that of GFAP and $A\beta_{1-42}$ fluorescence intensities, Pearson r-values were calculated using the raw fluorescence intensity values. A correlation was only deemed significant if $r > 0.5$ and $p < 0.0001$.

RESULTS

Mechanosensitive Piezo1 Channel Expression in the Juvenile and Adult Rat Brain

To characterize Piezo1 channel expression in distinct regions of the young rat brain, coronal sections were cut at −3.0 and −10.8 mm with respect to Bregma revealing hippocampal (**Figure 1A**) and cerebellar (**Figure 1B**) structures. In agreement with our previous findings in the brain of embryonic *Xenopus laevis* (Koser et al., 2016), the juvenile rat optic tract expresses relatively high levels of Piezo1 channels (**Figure 1A**, red arrow). Moreover, axonal tracts of the corpus callosum, hippocampal fimbriae, and arbor vitae of the cerebellum (**Figure 1B**, white arrow) express high levels of Piezo1 channels. In contrast, the molecular and granule layers of the cerebellum, and non-neuronal areas of the hippocampus, express much fewer Piezo1 channels (**Figures 1A,B**). These regional differences were confirmed by Western blot (WB) using two distinct antibodies, i.e., one which binds the N-terminus of Piezo1 (Santa Cruz; **Figures 1C,D**) and one that binds the C-terminus (Abcam; **Figures 1E,F**). For WB, the brains of juvenile rats were dissected into four areas, i.e., cerebellum (Crb), hippocampus (Hip), cerebral cortex (Ctx), and brain stem/thalamus (BS/T) combined. There were no statistically significant differences in Piezo1 expression between brain structures (repeated measures one-way ANOVA, $p > 0.05$). However, the hippocampus consistently displayed lower levels of Piezo1, both with immunofluorescence and WB techniques.

Next, sagittal sections from adult (12 months) rat brains were imaged to characterize Piezo1 localisation in several other structures along the anterior–posterior axis (**Figures 2A–D**). Similar to juvenile rats, Piezo1 was highly expressed along axonal tracts of the corpus callosum and cerebellar arbor vitae as well as on Purkinje cell bodies (**Figure 2J**), medulla, pons, thalamus (**Figure 2M**) as well as on Purkinje cell bodies (**Figure 2J**), medulla, pons, thalamus (**Figure 2M**), striatum (**Figure 2N**) and

[1]http://fiji.sc/Fiji

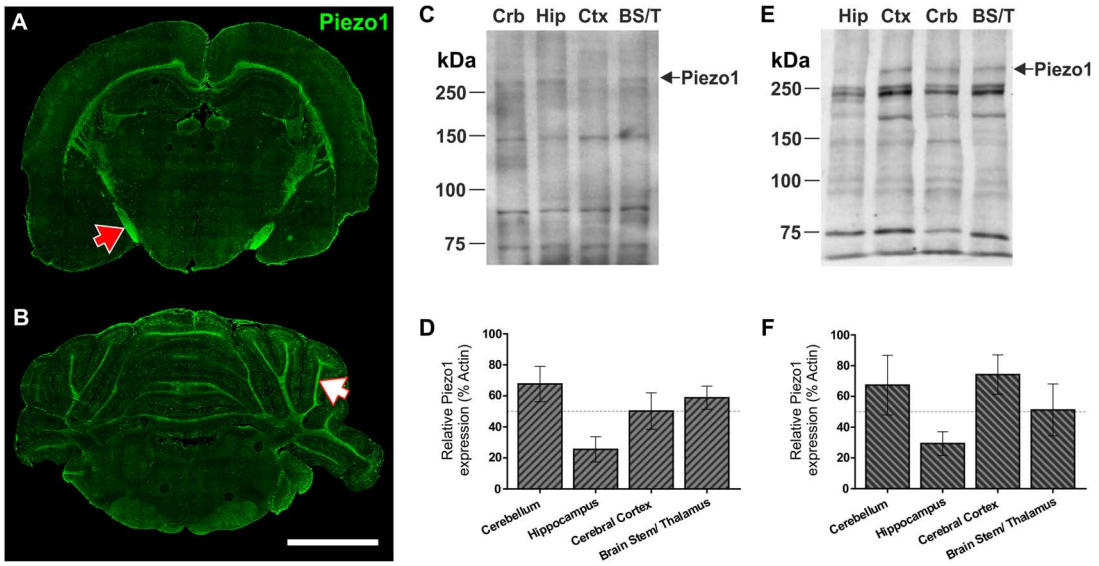

FIGURE 1 | Piezo1 channels are highly expressed by neurons in the optic tract, corpus callosum, and arbor vitae of the cerebellum. Coronal sections of the 5-week old rat brain were cut at –3.3 mm **(A)** and –10.8 mm **(B)** with respect to Bregma and immunofluorescently stained for Piezo1 (N-terminal antibody) (n = 4), scale bar = 4,000 μm. The red arrow points to the optic tract in the right hemisphere and the white arrow points to the arbor vitae of the Ansiform lobule Crus 1 of the cerebellum. 5-week old rat brains were also dissected into four parts for Western blotting (WB), i.e., cerebellum (Crb), hippocampus (Hip), cerebral cortex (Ctx) and brainstem/thalamus (BS/T). WB were run for Piezo1 using an N-terminal binding antibody **(C,D)** from Santa Cruz (n = 3) and a C-terminal binding antibody **(E,F)** from Abcam (n = 3). The hippocampus consistently showed the lowest levels of Piezo1 protein expression.

the rostral migratory stream which links the subventricular zone to the olfactory bulb (**Figure 2B**, blue arrow). Areas of low Piezo1 expression included the dorsal midbrain (**Figure 2K**) and non-neuronal regions of the hippocampus. Pyramidal and granule neurons of the CA1 (**Figure 2E**), CA3 (**Figure 2F**), and dentate gyrus (**Figure 2G**), however, expressed higher levels of Piezo1. Interestingly, layer V cortical cells (**Figure 2H**) expressed more Piezo1 channels than prefrontal cortical cells (**Figure 2I**). It was also noted that epithelial cells of the choroid plexus within the lateral ventricle (**Figure 2L**) express relatively high levels of Piezo1 protein.

Reactive Astrocytes Surrounding Amyloid Plaques Upregulate Piezo1

The pattern of expression in the rat brain suggested that Piezo1 is predominantly localized to neurons, in agreement with human studies of mRNA (Satoh et al., 2006). To examine if Piezo1 protein expression in mouse brain *in situ* matched that of the rat brain at the same age, we sectioned and immunofluorescently-labeled juvenile (5 weeks) mouse brains for Piezo1 and observed a strikingly similar expression pattern to the young rat brain; a result that matches the highly conserved amino acid sequence between mouse and rat Piezo1[2]. It was noted that Piezo1 expression in mouse brain also appeared predominantly neuronal (*data not shown*). To confirm cellular localisation, primary neuron cultures and enriched astrocyte cultures (∼97% pure) were prepared from newborn C57BL/6 mice and double-stained for either Piezo1 and GFAP (**Figures 3A–D**) or Piezo1 and neurofilament H (NFH; **Figures 3E–H**). Piezo1 co-localized with neurofilament H in mouse cortical neurons but was almost completely absent from primary astrocyte cultures under basal conditions.

To investigate if neuroinflammatory cell stressors are capable of upregulating Piezo1 channels in astrocytes, we exposed astrocytes to 5 μM hydrogen peroxide (H_2O_2) or to a cytokine cocktail consisting of TNF-α (10 ng/mL) and IL17A (250 ng/mL) for 24 h. Neither stressor induced Piezo1 expression in astrocytes (**Figures 3M,N**). Satoh et al. (2006), however, have reported previously that Piezo1 mRNA (then known as membrane protein induced by beta amyloid, Mib), is upregulated in astrocytes surrounding amyloid plaques in human post-mortem brain tissue. To examine if mouse astrocytes in culture can also be forced to express Piezo1 under similar pathophysiological conditions, we first treated mouse microglial cells with 10 μM amyloid beta-42 ($A\beta_{1-42}$; Invitrogen, United Kingdom) for 24 h and collected the inflammatory cell culture media. Mouse astrocytes were then incubated with $A\beta_{1-42}$ CMM for 48 h and stained for Piezo1 channels (**Figures 3I–L**). $A\beta_{1-42}$ CMM induced Piezo1 expression in 30–40% of cortical astrocytes (**Figures 3I,M,N**).

Next, we investigated if upregulation of Piezo1 channels is also evident *in vivo* in an aging rat model of Alzheimer's disease pathology (TgF344-AD). To achieve this, the brains of 18-month old TgF344-AD (18m TG) rats were sectioned in the sagittal plane and triple-immunolabeled for Piezo1, conformation-specific $A\beta_{1-42}$ [mOC98], and GFAP. High magnification (100×) z-stack projections clearly demonstrate an upregulation of Piezo1 in reactive astrocytes surrounding prefrontal cortical

[2]http://www.uniprot.org/

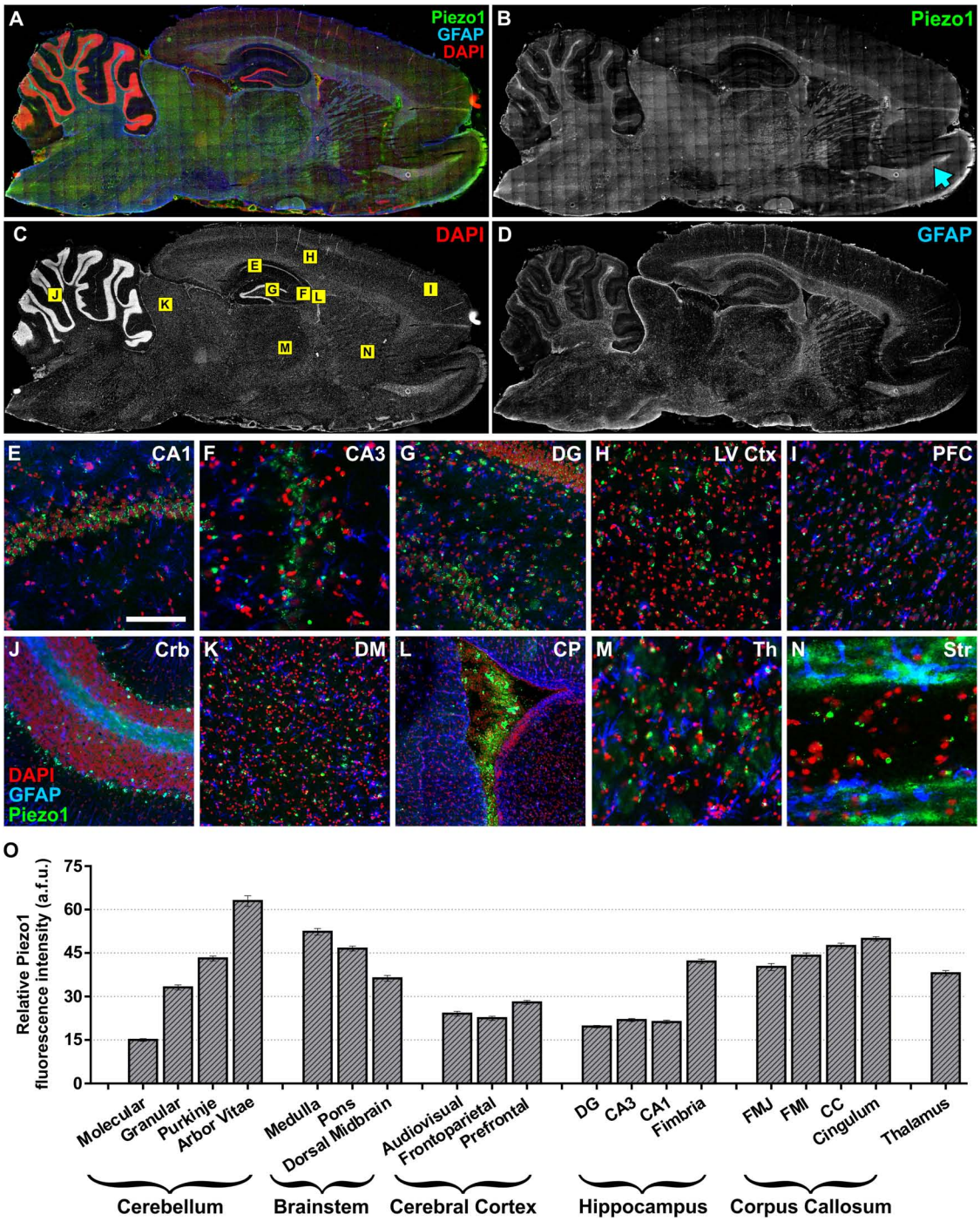

FIGURE 2 | Piezo1 channel expression in the adult rat brain. **(A)** The brains of adult (12 month) Fisher rats were sectioned in the sagittal plane (lateral –1.9 mm) and stained for **(B)** Piezo1 (N-terminal antibody), **(C)** DAPI, and **(D)** GFAP (n = 5). Images were captured using a 20× magnification objective on an Axio Scan.Z1 slide scanner (Zeiss, Germany) and montaged in ZEN software. 20× magnification images of the hippocampal **(E)** CA1 (scale bar = 150 μm), **(F)** CA3 and **(G)** dentate gyrus (DG) show that Piezo1 expression is greater in pyramidal and granule neurons compared to GFAP-positive astrocytes. In the cerebral cortex, **(H)** layer V pyramidal neurons (LV Ctx) appear to express more Piezo1 channels than **(I)** prefrontal cortical (PFC) neurons. In the cerebellum **(J)**, Purkinje neuron cell bodies and axons (arbor vitae) express higher levels of Piezo1 compared to neurons in the granule and molecular cell layers. **(K)** The dorsal midbrain (DM) expresses moderate levels of Piezo1, whereas **(L)** epithelial cells of the choroid plexus (CP) express greater amounts of Piezo1 protein. It was also noted that white matter tracts in **(M)** the thalamus (Th) and **(N)** striatum (Str) express more Piezo1 than gray matter areas of these brain regions. The areas depicted in images **(E–N)** are shown as yellow boxes in **(C)**. Relative fluorescence intensity (arbitrary fluorescence units, a.f.u.) of Piezo1 staining in each brain region was quantified **(O)**. Axonal tracts including the cerebellar arbor vitae, hippocampal fimbriae, cingulum and corpus callosum, as well as the medulla and pons of the brainstem, had the highest expression of Piezo1 protein.

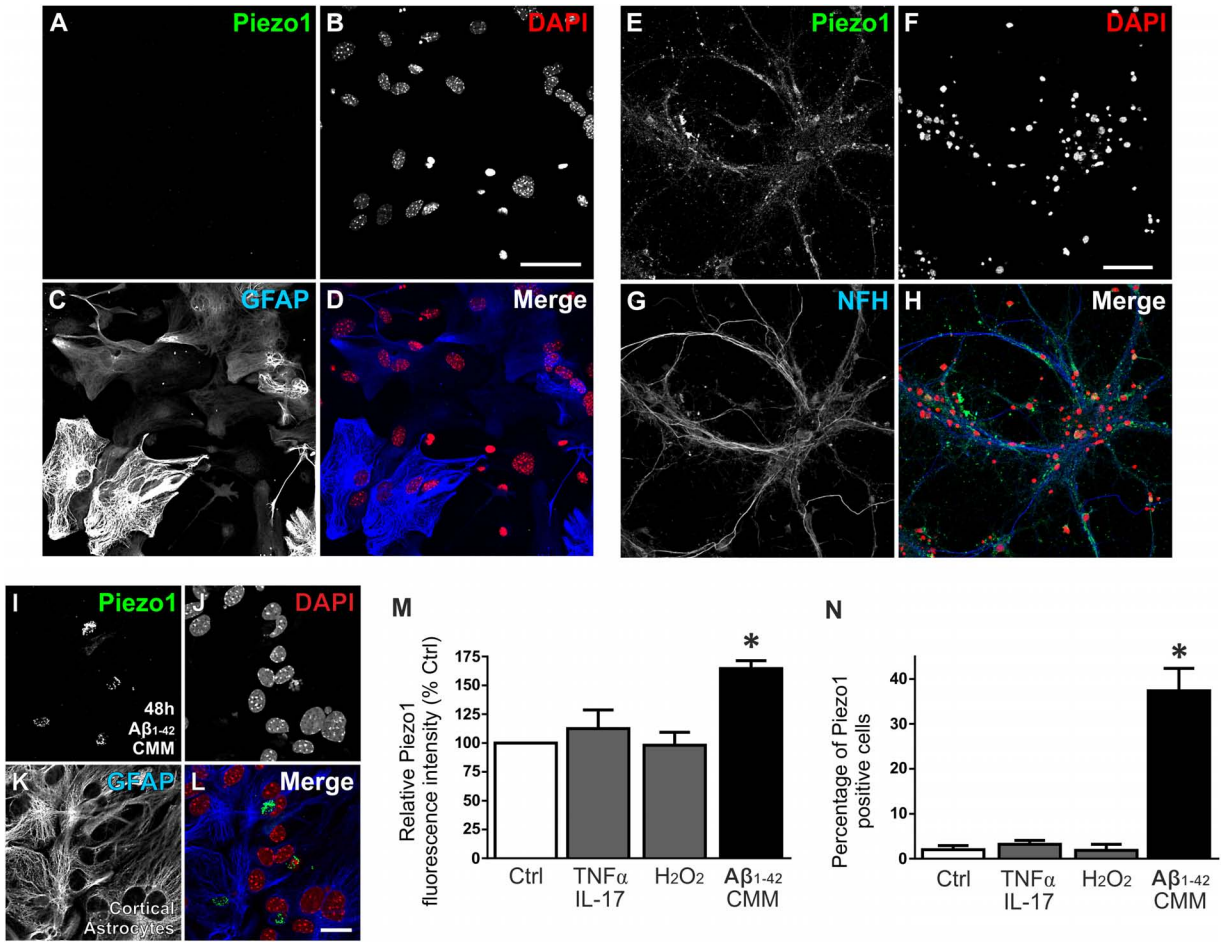

FIGURE 3 | $A\beta_{1-42}$ CMM upregulates Piezo1 expression in cortical astrocyte cultures. To check cellular localisation of Piezo1 in the brain, enriched astrocyte cultures **(A–D)** and cortical neuronal cultures **(E–H)** from newborn mice were stained for **(A,E)** Piezo1 (N-terminal antibody) and **(C)** GFAP or **(G)** neurofilament H (NFH), respectively (n = 3). Piezo1 co-localized with NFH staining in neurons **(H)** but was almost completely absent from astrocytes under basal conditions **(D)**. To investigate if neuroinflammatory stimuli can induce Piezo1 expression in astrocytes, mouse microglia were exposed to human $A\beta_{1-42}$ (Invitrogen, United Kingdom) for 24 h and the inflammatory media was collected. Enriched mouse astrocyte cultures were then exposed to this $A\beta_{1-42}$ CMM for 48 h. Astrocytes were immunofluorescently stained for **(I)** Piezo1 (C-terminus antibody), **(J)** DAPI, **(K)** GFAP, and **(L)** is the merge of each channel. Scale bar = 20 μm. Exposure to $A\beta_{1-42}$ CMM upregulated Piezo1 protein expression in approximately 30–40% of astrocytes **(M,N)**. Astrocytes were also treated for 24 h with either 5 μM hydrogen peroxide (H_2O_2) or a cytokine cocktail consisting of TNF-α (10 ng/mL) and IL17A (250 ng/mL). Neither H_2O_2 nor TNF-α/IL17A increased Piezo1 expression indicating that Piezo1 upregulation is not a common response to all cell stressors but specific to certain inflammatory stimuli including $A\beta_{1-42}$ and factors released by reactive amyloid-stimulated microglia. Data are represented as mean ± SEM (n = 8). A repeated measures one-way ANOVA with Holm-Sidak *post hoc* test was performed. *Represents a statistically significant difference ($p < 0.05$) from control (Ctrl), TNF-α/IL17A, and H_2O_2 treatment groups.

amyloid plaques (**Figures 4A–E**). On average, there was a threefold upregulation in Piezo1 expression in amyloid plaque-reactive astrocytes compared to astrocytes located at least 200 μm away from any plaque in the prefrontal cortex (**Figures 4F,G**). One must remember, however, that GFAP staining only covers ∼15% of the total volume of astrocytes (Sun and Jakobs, 2012) and therefore, the reported percentage of cells expressing Piezo1 might be somewhat of an underestimation. Interestingly, *in vivo* Piezo1 expression closely matches our *in vitro* results following incubation of enriched astrocyte cultures with $A\beta_{1-42}$ CMM, i.e., only a proportion of astrocytes (∼30%) express Piezo1 channels and the expression appears perinuclear in reactive astrocytes *in vivo*.

Aging and Amyloid Plaque Pathology Increase Piezo1 Expression in Anterior Cortical Regions

We next characterized spatiotemporal changes in Piezo1 expression in different areas of the cerebral cortex in 12- and 18-month old wild-type (WT) and TgF344-AD (TG) rats. Low magnification (20× montage) images of the prefrontal cortex reveal an upregulation of Piezo1 and GFAP around amyloid plaques (**Figures 5A–J**). Piezo1 expression in the prefrontal cortex increased 32 ± 3% from 12 to 18 months of age in WT rats (**Figure 5K**; $p < 0.0001$). However, frontoparietal (**Figure 5L**) and audiovisual (**Figure 5M**)

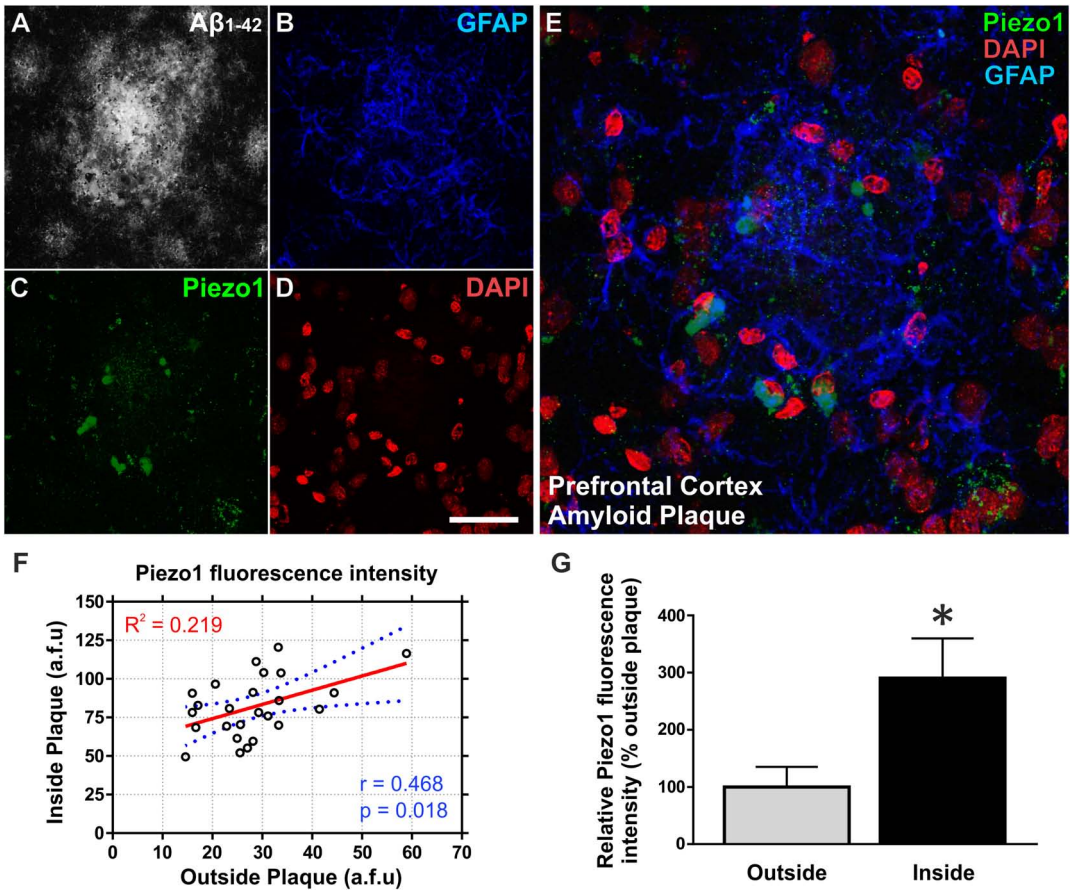

FIGURE 4 | $A\beta_{1-42}$ pathology *in vivo* upregulates Piezo1 expression in astrocytes surrounding amyloid plaques. 18-Month old TgF344-AD rat brains were immunofluorescently stained for **(A)** conformation-specific $A\beta_{1-42}$, **(B)** GFAP, **(C)** Piezo1 (N-terminal antibody), and **(D)** DAPI. Scale bar = 40 μm. **(E)** High magnification (100× objective) z-stack projections of prefrontal cortex amyloid plaques reveal an upregulation of GFAP in reactive astrocytes surrounding the amyloid plaque. Piezo1 protein is also upregulated in a proportion of astrocytes in and around the core of the plaque. Piezo1 appears localized predominantly to the perinuclear compartment of $A\beta_{1-42}$ reactive astrocytes. **(F)** Astrocytic Piezo1 fluorescence intensity was calculated for astrocytes inside the amyloid plaque versus astrocytes located 200–500 μm away from any noticeable plaque deposits. Piezo1 fluorescence intensity was averaged for six astrocytes "inside" and six astrocytes "outside" the plaque and 25 images from the frontal cortex of 18 m TG rats (n = 6) were analyzed. There was no correlation (Pearson r = 0.468) between Piezo1 expression inside versus outside amyloid plaques. **(G)** However, on average there was a 190% increase in Piezo1 expression in astrocytes within the plaque core (Inside) versus astrocytes at least 200 μm away from the edge of any amyloid plaque (Outside). A two-tailed paired t-test was performed. *Represents a statistically significant difference ($p < 0.001$) inside versus outside of the plaque.

cortical regions did not display any significant changes in Piezo1 expression in WT rats from 12 to 18 months. Piezo1 channel expression also increased in the prefrontal (34 ± 2%) and frontoparietal (31 ± 2%) cortices of TG rats from 12- to 18-months of age but not in the audiovisual area (17 ± 2%). Taken together, both aging and amyloid plaque pathology trigger increases in Piezo1 channel expression, particularly in the prefrontal cortex, of TgF344-AD rats (**Figures 5K–N**).

Peripheral Bacterial Infection Enhances Piezo1 Expression in the Cerebral Cortex of TgF344-AD Rats

Twelve month old TgF344-AD rats had previously been exposed to a UTI (*E. coli*) at 8 and 11 months of age (iTG). This bacterial infection caused a significant upregulation of Piezo1 channels in the prefrontal (21 ± 3%; **Figure 5K**) and frontoparietal (23 ± 3%; **Figure 5L**) cortices of 12-month old iTG rats, but not the audiovisual cortex (16 ± 2%; **Figure 5M**). In contrast, in older 18-month iTG rats that had been infected with *E. coli* at 8, 11, 14, and 17 months of age, no changes in Piezo1 channel expression were measured in prefrontal (12 ± 2%; **Figure 5K**) or frontoparietal (12 ± 3%; **Figure 5L**) cortices compared to non-infected TgF344-AD counterparts. However, Piezo1 expression in the audiovisual cortex did display significant upregulations (21 ± 3%; **Figure 5M**) in 18-month iTG rats in response to repeated peripheral infections. Interestingly, peripheral *E. coli* infections did not increase Piezo1 expression in the prefrontal cortex of WT rats at 12 months (15 ± 3%) nor at 18 months (12 ± 3%) of age compared to WT controls. Taken together, our results indicate that repeated UTI enhances Piezo1 expression in

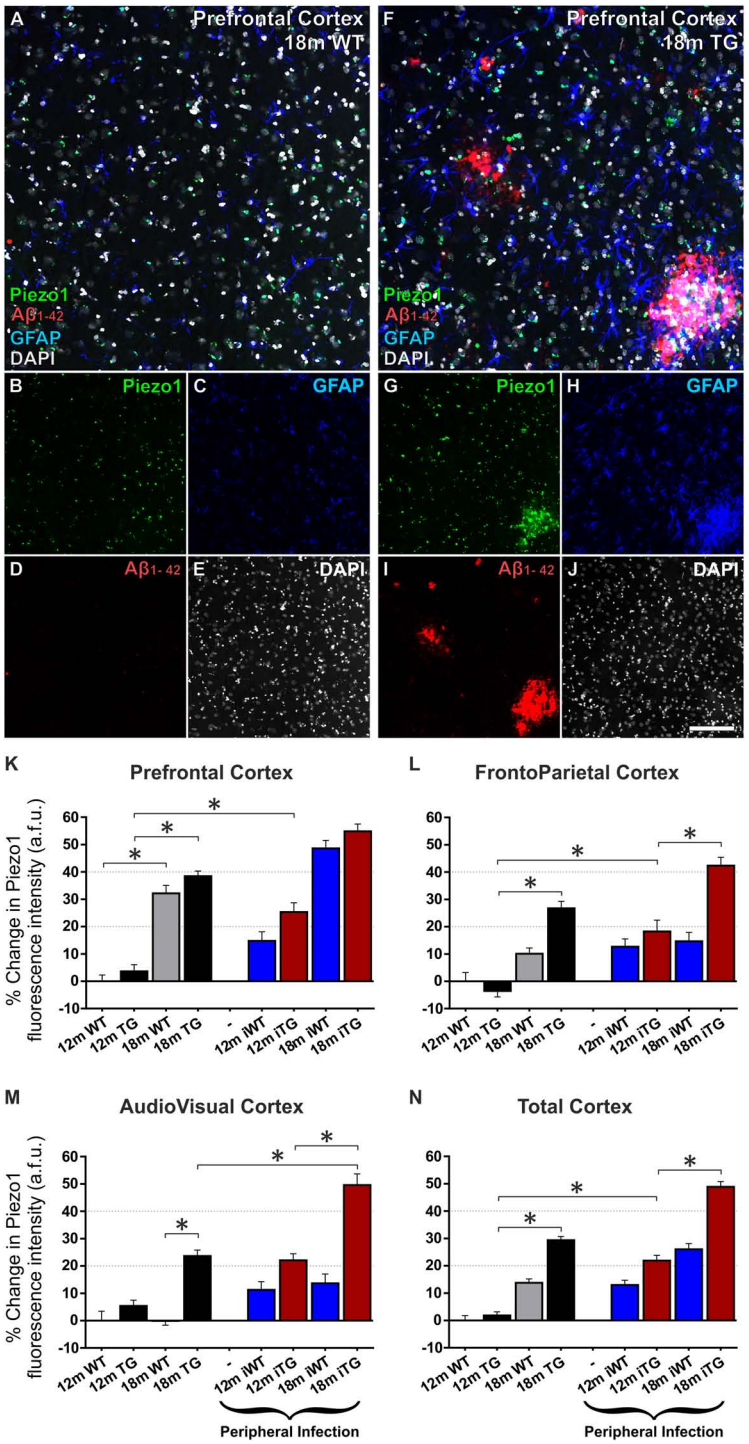

FIGURE 5 | Mechanosensing Piezo1 channel expression increases in the cerebral cortex of TgF344-AD rats with a urinary tract infection (UTI). Sagittal sections (lateral –1.9 mm) of wild-type (WT) Fisher and TgF344-AD rat brains were immunofluorescently stained for Piezo1 (N-terminal antibody), conformation-specific $A\beta_{1-42}$, GFAP, and DAPI. Shown are representative images of the prefrontal cortex of an 18-month WT rat **(A–E)** and an 18-month TgF344-AD (18 m TG) **(F–J)**. Scale bar = 150 μm. Elevations in Piezo1 channel expression with age, Alzheimer's disease (AD) pathology and peripheral infection were measured in three distinct areas of the cerebral cortex, i.e., the prefrontal cortex **(K)**, the frontoparietal cortex **(L)**, and the audiovisual cortex **(M)**. In addition, Piezo1 expression was averaged over all three regions to illustrate changes in channel expression in the total cerebral cortex **(N)**. Data were normalized to 12 month wild-type (12m WT) values for each cortical region and are represented as the mean ± SEM of the percentage change from the 12m WT groups. Three-way ANOVAs with Holm-Sidak *post hoc* tests were performed to test for interactions between age, genotype, and peripheral infection. *Represents a change > 20% and a p-value < 0.01. There were 5–6 rats per group and 2–3 brain sections per animal. Ten regions of interest (ROI) were analyzed per cortical region per section, i.e., 100–180 ROIs analyzed per group.

the cerebral cortex of TgF344-AD rats over and above that seen in response to amyloid plaques alone (**Figure 5N**).

Piezo1 Upregulation in the Hippocampus of TgF344-AD Rats Precedes Changes in the Cerebral Cortex

Just as normal aging increased expression of Piezo1 channels in the prefrontal cortex, increases in Piezo1 were also evident in the CA1 (34 ± 4%) and DG (24 ± 3%) of the hippocampus, but not in the CA3 region, from 12 to 18 months in WT rats (**Figures 6A–W**). Notably, there were also large relative increases in Piezo1 expression in the DG (99 ± 7%; **Figure 6U**), CA3 (58 ± 6%; **Figure 6V**) and CA1 (78 ± 6%; **Figure 6W**) of 12-month TG rats compared to their 12-month WT conspecifics. Interestingly, however, there were no further significant increases in hippocampal Piezo1 expression in TG rats from 12 to 18 months of age, suggesting that amyloid deposition and plaque load begin in the hippocampus before spreading further to cortical regions.

Peripheral Infection Upregulates Hippocampal Piezo1 Expression in Wild-Type and TgF344-AD Rats

Unlike the cerebral cortex, upregulations in Piezo1 expression were measured in the hippocampal CA1 region (28 ± 5%) in response to peripheral *E. coli* infection at 12 months of age in iWT rats (**Figure 6W**). However, no further increases in Piezo1 expression were evident in the CA1 of infected 18-month iWT rats. Peripheral infection at 8 and 11 months did, however, cause an upregulation of Piezo1 channels in the CA3 region of iTG rats at 12 months of age (20 ± 7%; **Figure 6V**). Moreover, repeated peripheral infection at 8, 11, 14, and 17 months of age caused a large increase in Piezo1 channels in the dentate gyrus of 18-month iTG rats (25 ± 8%) compared to their non-infected and age-matched TG counterparts (**Figure 6U**).

Piezo1 Expression Strongly Correlates With Amyloid Plaque Deposition in the Hippocampal Dentate Gyrus

It is clear from our immunofluorescence data that both GFAP reactivity and Piezo1 expression are greater around amyloid plaques, especially in the hippocampus. Apart from the molecular layer of the cerebellum, the dentate gyrus displayed the lowest levels of Piezo1 expression in 12-month old WT rats (**Figure 2O**). Because basal levels of Piezo1 in the DG are low, the relative (%) increases in Piezo1 protein expression in 12-month old, 18-month old, and 18-month infected Tg-344AD rats were large (**Figure 6U**). To assess the relationship between Piezo1 expression and amyloid plaque pathology in adult and aged rats with and without repeated peripheral infections, we correlated Piezo1 fluorescence intensity with both GFAP and $A\beta_{1-42}$ expression in the dentate gyrus of all groups (**Figure 7**). In agreement with our *in vitro* studies, Piezo1 expression did not correlate with GFAP expression in 12-month WT, 18-month WT, or 12-month iWT (**Figures 7A–C**). However, DG Piezo1 expression showed a moderate correlation with GFAP intensity in 18-month iWT rats exposed to repeated peripheral infections (**Figure 7D**; Pearson $r = 0.523$, $p < 0.0001$). Similarly, there was no correlation between GFAP fluorescence intensity and Piezo1 expression in the DG of 12-month TG, 18-month TG, or 12-month iTG (**Figures 7E–G**). In 18-month iTG, however, increases in GFAP reactivity in the DG did correlate with increased Piezo1 expression (**Figure 7H**; Pearson $r = 0.519$, $p < 0.0001$). Peripheral infection of older rats led to an upregulation of GFAP in the hippocampal DG and these reactive astrocytes were more likely to express Piezo1 channels. GFAP expression in the DG of older iTG rats that had repeated peripheral infections also correlated with high amyloid plaque pathology (**Figure 7L**; Pearson $r = 0.586$, $p < 0.0001$), when compared to 18-month TG rats without infection (**Figure 7K**). Finally, Piezo1 expression in the DG displayed very strong correlations with $A\beta_{1-42}$ fluorescence intensity in 12- and 18-month TgF344-AD rats either with or without peripheral infection (**Figures 7M–P**). This suggests that whilst peripheral *E. coli* infection alone can upregulate astrocytic Piezo1; $A\beta_{1-42}$ CMM and *in vivo* amyloid plaque pathology are stronger triggers of mechanosensing Piezo1 channel expression in reactive astrocytes.

DISCUSSION

TgF344-AD transgenic rats overexpress mutated human PSEN1 (PSEN1ΔE9) and human APP with the Swedish mutation (APP_{SWE}) and were developed with the intention of creating an improved animal model of AD that recapitulates a broader spectrum of neuropathological features seen in the human AD brain (Cohen et al., 2013). As such, TgF344-AD rats display neuronal tau deposition in contrast to what is generally observed in transgenic mice with these particular gene mutations (Duyckaerts et al., 2008; Stancu et al., 2014). Unless tau-associated genes are also mutated, transgenic mice tend not to spontaneously form neurofibrillary tau tangles (Holcomb et al., 1998; Jankowsky et al., 2001). By combining this improved transgenic rat model with a UTI, a common comorbidity of elderly people who develop AD, the model we present here more closely mimics the systemic inflammation and the spatiotemporal deposition of amyloid plaques observed in the hippocampus and cortex of aging human AD subjects.

Utilizing the TgF344-AD rat model (Cohen et al., 2013), we show here that Piezo1 protein expression increases in several key brain structures in response to aging, peripheral infection and amyloid plaque pathology. Piezo1 channels increase in the prefrontal cortex and the hippocampal CA1 and dentate gyrus with normal aging. These brain regions are particularly important for processing salient sensory information (Barbas and Zikopoulos, 2007; Lester et al., 2017), for learning and memory (Kane and Engle, 2002; Guo et al., 2018) and for higher executive functions (Arnsten and Li, 2005; Suwabe et al., 2017), all of which deteriorate in the elderly (Zimprich and Kurtz, 2013; Thomé et al., 2016; Wiegand et al., 2016). Since an increase in stretch-activated Ca^{2+} channel expression could, in theory, predispose

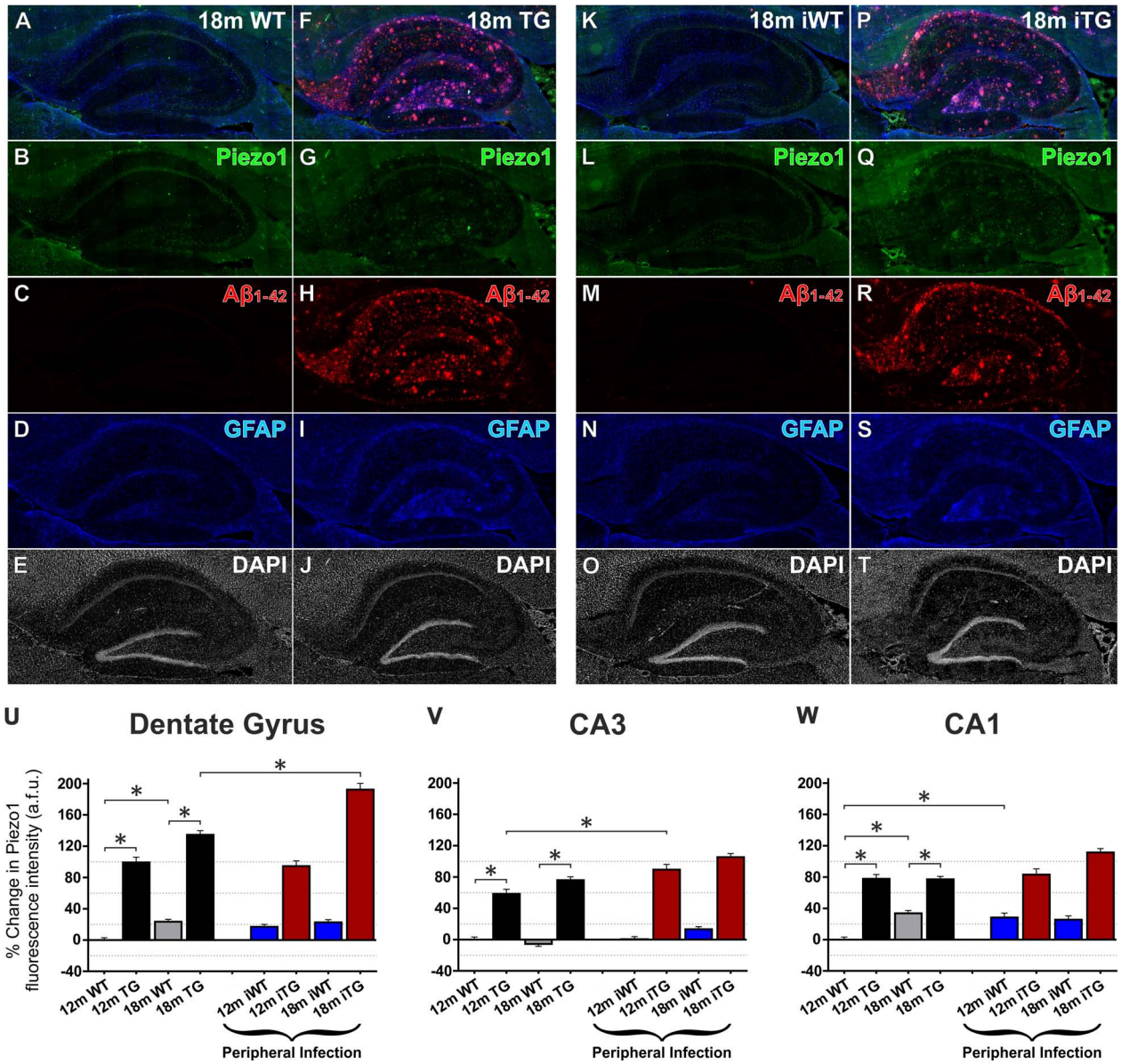

FIGURE 6 | Aging, $A\beta_{1-42}$ pathology and peripheral infection upregulate Piezo1 expression in the hippocampus of TgF344-AD rats. Sagittal sections (lateral −1.9 mm) of WT Fisher and TgF344-AD rat brains were immunofluorescently stained for Piezo1 (N-terminal antibody), conformation-specific $A\beta_{1-42}$, GFAP, and DAPI. Shown are representative images of the hippocampus of an 18-month wild-type (18m WT) rat **(A–E)**, an 18-month TgF344-AD 18m TG **(F–J)**, an 18-month WT with infection (18m iWT) **(K–O)**, and an 18-month TgF344-AD with infection (18m iTG) **(P–T)**. TgF344-AD rats with and without an infection show clear upregulations of GFAP **(I,S)** in hippocampal areas with dense amyloid deposition **(H,R)**, particularly the hilus, the outer molecular layer of the dentate gyrus, and the stratum oriens of the CA1. Moreover, amyloid plaques surrounded by a dense meshwork of GFAP-positive astrocytes generally showed concomitant upregulations of Piezo1 expression, particularly in 18m TG rats with or without an infection **(G,Q)**. Next, changes in Piezo1 expression with age, infection and genotype were quantified in the neuronal cell body layers of the dentate gyrus **(U)**, CA3 **(V)**, and CA1 **(W)**. Piezo1 expression increased from 12- to 18-months in WT rats in the DG and CA1, but not CA3 neurons. A much more potent trigger of Piezo1 expression in the hippocampus, however, was genotype with TgF344-AD rats expressing much larger levels of Piezo1 in the DG **(U)**, CA3 **(V)**, and CA1 **(W)** at 12-months of age. There were no further increases in Piezo1 expression in 18-month old TgF344-AD rats. However, peripheral infection caused a significant increase in Piezo1 expression in the dentate gyrus **(U)** of TgF344-AD rats (18m iTG). Data were normalized to 12m WT values for each hippocampal region and are represented as the mean ± SEM of the percentage change from the 12m WT groups. Three-way ANOVAs with Holm-Sidak *post hoc* tests were performed to test for interactions between age, genotype, and peripheral infection. *Represents a change of $> 20\%$ and a p-value < 0.01. There were 5–6 rats per group and 2–3 brain sections per animal. Ten ROI were analyzed per hippocampal region per section, i.e., 100–180 ROIs analyzed per group.

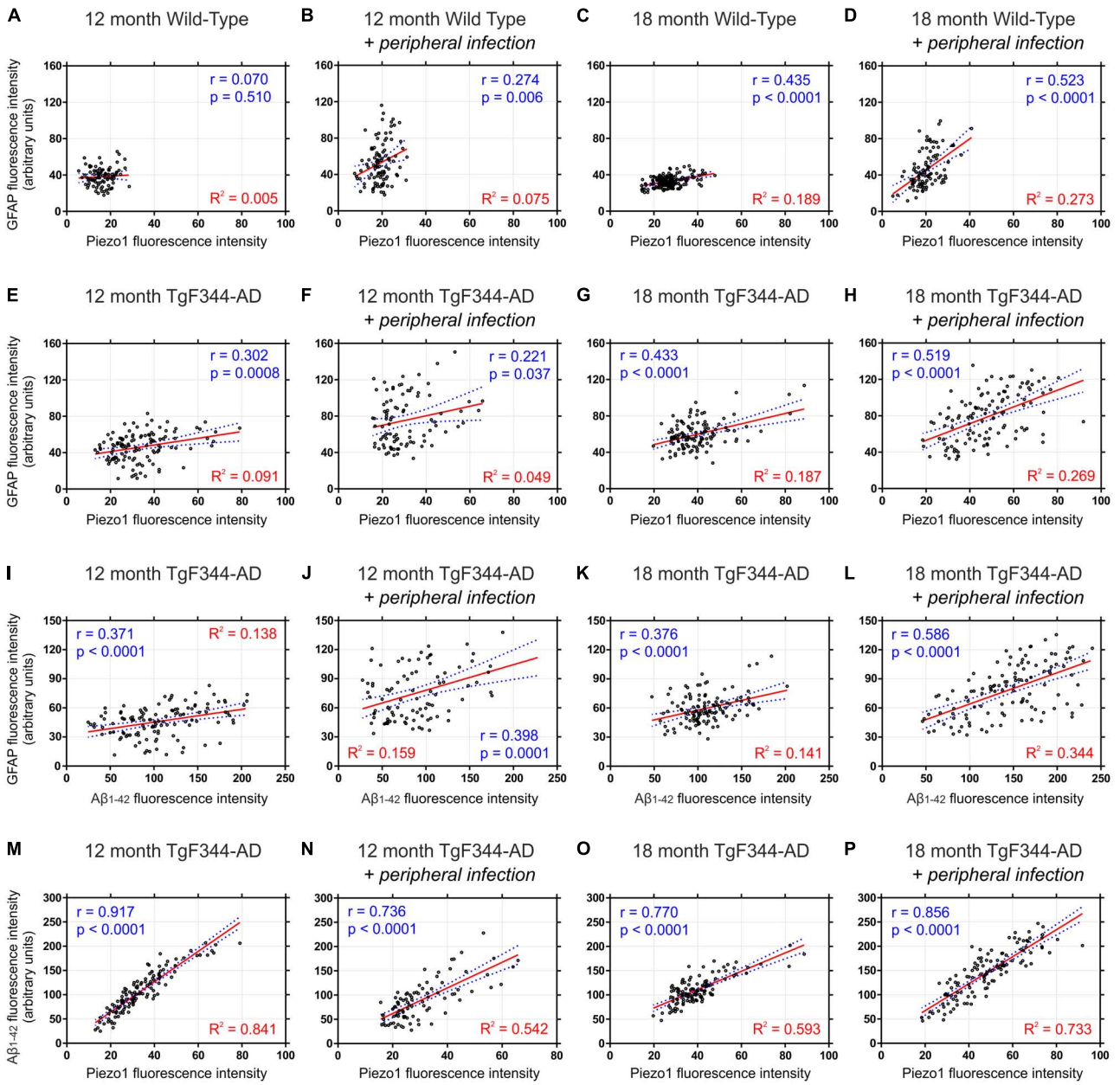

FIGURE 7 | Piezo1 expression in the hippocampal dentate gyrus correlates with GFAP in aged rats with peripheral infection and strongly correlates with amyloid plaques in TgF344-AD rats. Sagittal brain sections were triple-stained for Piezo1, GFAP and conformation-specific $A\beta_{1-42}$ and Pearson correlations (*r* values) were performed to measure changes in Piezo1 channel expression in astrocytes (GFAP vs. Piezo1) with age and peripheral infection in WT **(A–D)** and TgF344-AD **(E–H)** rats. There was a moderate Pearson correlation between GFAP and Piezo1 in the infected 18-month WT ($r = 0.523$) and infected 18-month TgF344-AD rats ($r = 0.519$). However, the linear regression (R^2) values were relatively weak for both groups suggesting that the GFAP fluorescence intensity is not a good predictor of Piezo1 channel expression. Next, Pearson correlations were performed to measure changes in GFAP expression around amyloid plaques (GFAP vs. $A\beta_{1-42}$) in the dentate gyrus with age and peripheral infection in TgF344-AD rats **(I–L)**. There was a moderate Pearson correlation between GFAP and $A\beta_{1-42}$ in the infected 18-month old TgF344-AD rats ($r = 0.586$) but a relatively weak linear regression (R^2) value suggesting that $A\beta_{1-42}$ fluorescence intensity is not a good predictor of GFAP expression. Finally, Pearson correlations were performed to measure changes in Piezo1 channel expression in and around amyloid plaques ($A\beta_{1-42}$ vs. Piezo1) in the dentate gyrus with age and peripheral infection in TgF344-AD rats **(M–P)**. There were strong Pearson correlations between $A\beta_{1-42}$ and Piezo1 in 12-month old TgF344-AD rats ($r = 0.917$), 12-month old TgF344-AD rats with peripheral infection ($r = 0.736$), 18-month old TgF344-AD rats ($r = 0.770$), and 18-month old TgF344-AD rats with peripheral infection ($r = 0.856$). In addition, the high linear regression (R^2) values for each group **(M–P)** suggests that $A\beta_{1-42}$ fluorescence intensity is a good predictor of Piezo1 channel expression in the dentate gyrus of TgF344-AD rats.

aging neurons to Ca^{2+} dysregulations (Nagarajan et al., 2014), it would be interesting to further investigate if Piezo1 channel expression modulates neuronal Ca^{2+} homeostasis. Intrinsic neuronal properties and synaptic plasticity are intimately linked with tight control of cellular Ca^{2+} concentrations (Catterall et al., 2013; Maggio and Vlachos, 2014) and, therefore, mechanosensitive channels that regulate calcium levels may play an important role in cognition in the aging hippocampus or prefrontal cortex. In this regard, various members of the transient receptor potential (TRP) channel family have been implicated in both mechanosensation (Kwan et al., 2006) and Ca^{2+} dysregulations in neurons and astrocytes in AD (Yamamoto et al., 2007). In the present study, the age-dependent increases in Piezo1 channel expression measured in the prefrontal cortex, CA1 and DG of wild-type rats appeared predominantly neuronal whereas in the TgF344-AD rat model, peripheral infection and amyloid plaque pathology caused an upregulation of Piezo1 predominantly in reactive astrocytes, although concomitant increases in neurons and reactive microglia are also likely to occur. This is interesting because the role of Piezo1 in CNS neurons could be different to its function in astrocytes since neurons constitutively express mechanosensing Piezo1 channels on axonal growth cones and the outer cell membrane, whereas astrocytes exposed to neuroinflammatory stimuli, such as $A\beta_{1-42}$ CMM, upregulate and accumulate Piezo1 channels within the perinuclear compartment. Indeed, in epithelial cell types Piezo1 reportedly co-localizes with the endoplasmic reticulum where it regulates intracellular Ca^{2+} release from stores (McHugh et al., 2010). Moreover, separating the physiological role of Piezo1-mediated extracellular calcium influx from Piezo1-regulated Ca^{2+} release from intracellular stores will reveal subsets of novel mechanotransduction cascades that originate from either outer membrane-spanning Piezo1 channels or from intracellular Ca^{2+} stores (Clapham, 2007). Our results suggest that Piezo1 channels regulate glial mechanosensation and may trigger astrogliosis in the AD brain. Moreover, amyloid plaque-associated microglia and the biochemical factors they release when activated likely play a key role in controlling Piezo1 expression in reactive astrocytes. As such, TgF344-AD rats infected with *E. coli* show enhanced Piezo1 expression in the cortex and hippocampus compared to non-infected transgenic animals. Moreover, microglia have been shown to regulate the pathogenic activities of astrocytes in a mouse model of multiple sclerosis (Rothhammer et al., 2018). Therefore, determining whether Piezo1 regulates neurodegenerative or neuroprotective mechanotransduction signaling in reactive astrocytes surrounding amyloid plaques is an important topic for future research.

Astrocytic Piezo1 in Alzheimer's Disease

Satoh et al. (2006) discovered that astrocytes surrounding amyloid plaques in the cerebral cortex of AD patients express hMib mRNA. Coste et al. (2010) renamed Mib (also known as FAM38A), Piezo1, and described how it forms a stretch-activated calcium-permeable channel in the neuroblastoma cell line, Neuro2A. Elegant new research has revealed the tertiary structure of Piezo1 at near atomic level (Ge et al., 2015) and describes how non-selective cationic channels are formed from homotrimers which exhibit large mechanosensitive 'propeller-like' structures on the outer surface of membranes (Coste et al., 2012; Li et al., 2014). Astrocytes are very sensitive to changes in their local mechanical environment (Leipzig and Shoichet, 2009; Blumenthal et al., 2014) and our data suggests that perturbations caused by stiff amyloid plaques trigger the transcriptional upregulation of mechanosensing Piezo1 channels in astrocytes which are normally devoid of Piezo1 protein (**Figure 3E**). But why might a sub-population of reactive astrocytes upregulate mechanosensing Piezo1 channels? Interestingly, Liddelow et al. (2017) showed that ∼60% of GFAP-positive astrocytes in the prefrontal cortex of human AD patients were of the A1 phenotype, i.e., a neurotoxic subtype of reactive astrocyte that drives neuroinflammation and causes neurotoxicity. It would be interesting to determine if the 30–40% of Piezo1-expressing astrocytes around amyloid plaques in the TgF344-AD rat model stain positive for A1 astrocyte markers (e.g., Serping1), or for astrocytes of the A2 phenotype (e.g., S100A10) which reportedly release neurotrophic factors and are mainly neuroprotective (Liddelow et al., 2017). More research is needed to determine what makes Piezo1-expressing astrocytes around amyloid plaques different to their Piezo1-negative neighbors and to characterize both subpopulations based on their 'neuroinflammatory phenotype.'

Piezo1 as a Regulator of Neuron/Glial Communication

Blumenthal et al. (2014) suggest that neuronal Piezo1 is important for sensing the topography of cells at the nanometre scale. Hippocampal neurons cultured *in vitro* form many neuron/glial interactions when grown on relatively smooth glass substrates but blocking mechanosensitive channels with GsMTx4, a peptide component of the *Grammostola rosea* tarantula venom, promotes decoupling of neurons from astrocytes and leads to fewer cell contacts. This suggests that Piezo1 can regulate the physical communication between neurons and astrocytes. Moreover, they also showed that the surface topography of brain tissue becomes rougher in response to amyloid plaque pathology which can increase the nanoroughness of astrocytes, thus contributing to neurodegeneration (Blumenthal et al., 2014). If Piezo1 does indeed regulate neuron/glial communication *in vivo*, this supports our previous work which revealed that Piezo1 channels are involved in neuronal mechanosensation and axon guidance during brain development (Koser et al., 2016), enabling migrating growth cones to detect changes in the stiffness of their local environment. Here, we confirm that the rat optic tract also expresses relatively high levels of Piezo1 channels (**Figure 1A**), as well as the corpus callosum and cerebellar arbor vitae, suggesting that Piezo1 may play a more general role in axonal pathfinding during brain development. Indeed, migrating axons and growth cones are highly mechano-responsive and likely receive constant feedback about the stiffness of the local ECM or the apparent density of glial cell networks as they grow through different brain regions toward their final targets. Moreover, glial cells are softer than neurons (Lu et al., 2006)

and recent studies have shown that SH-SY5Y cells (a human neuroblastoma cell line) that overexpress mutated APP_{SWE} are stiffer than normal SH-SY5Y cells (Lu et al., 2017). Therefore, astrocytes capable of engulfing and phagocytosing neurotoxic $A\beta_{1-42}$ peptides may change their mechanical properties or surface topography in the AD brain. Neurons in contact with reactive astrocytes that engulf neurotoxic amyloid peptides may be able to sense a change in their cellular stiffness or membrane nanoroughness and detach from them. Therefore, widespread loss of cell contacts in the hippocampus and cortex, or a disruption to neuron/glial communication caused by changes in the mechano-responsiveness of cells, may accelerate neurodegeneration (Blumenthal et al., 2014) and cognitive decline in the AD brain.

Recent evidence also suggests that dysregulated mechanosensitive signaling can contribute to astrogliopathy in Alexander disease, leading to an increase in brain stiffness (Wang et al., 2018). Alexander disease is a rare neonatal neurodegenerative disorder caused by accumulation of pathogenic Rosenthal fibers due to mutations in astrocytic GFAP. In contrast, we have recently shown that glial scars rich in GFAP- and Vimentin-expressing glial cells, which form following cortical stab injury or contusive spinal cord injury, are much softer than surrounding healthy CNS tissue (Moeendarbary et al., 2017). Therefore, astrogliosis can apparently lead to either increases or decreases in brain tissue stiffness depending on the underlying causes of tissue injury or disease. As such, reactive astrogliosis can be classified as isomorphic (conserved morphology) or anisomorphic (astrocyte hypertrophy and proliferation) (Verkhratsky et al., 2013). These reactive states differ, not only in morphology, but also in their (patho)physiological functions. For instance, isomorphic gliosis is thought to aid regeneration of neuronal networks by providing a permissive biochemical microenvironment for growth cones to migrate through on their journey to relocate their correct synaptic targets. On the other hand, anisomorphic astrogliosis contributes to glial scar formation which is initially beneficial because it prevents extensive neurodegeneration, but as the primary trauma heals, the glial scar can also inhibit axonal re-growth across the lesion site due to secretion of factors such as chondroitin sulfate proteoglycans (Bradbury et al., 2002; Fawcett, 2006). Interestingly, we have shown that addition of chondroitin sulfate to the *Xenopus* brain *in vivo* causes widespread softening of brain tissue (Koser et al., 2016). Therefore, differences in the secretome of phenotypically and functionally distinct types of reactive astrocyte could, in theory, explain the dichotomy in brain tissue stiffness observed in Alexander disease (Wang et al., 2018) versus cortical glial scars caused by a traumatic stab injury (Moeendarbary et al., 2017). In both cases, however, astrogliosis will likely disrupt neuronal mechanobiological signaling and may trigger either neurodegenerative or neuroprotective/pro-regenerative mechanisms. An important area for future research will involve characterizing the role of Piezo1 in neurons and glial cells in the injured or degenerating brain. With this aim in mind, Piezo1 channel opening reportedly regulates the Hippo signaling pathway (Pathak et al., 2014), which controls cell proliferation and apoptosis. Piezo1 knockdown also decreases levels of the mechanoresponsive transcriptional coactivator, Yes-associated protein (YAP), in neural stem cells (Pathak et al., 2014) suggesting that Piezo1 activation triggers YAP transcriptional activity. Notably, YAP is highly expressed by astrocytes and deletion of the YAP gene induces astrogliosis (Huang et al., 2016). In Alexander disease, astrocytes overexpress nuclear YAP, potentially as a result of increased brain tissue stiffness (Wang et al., 2018). Whether upregulation of YAP is detrimental to astrocytes or induces a protective phenotype is not yet known. YAP has some protective functions and can activate suppressor of cytokine signaling (SOCS) gene expression and, therefore, can prevent astrocyte reactivity by downregulating the JAK–STAT inflammatory pathway (Huang et al., 2016). Taken together, the upregulation of astrocytic Piezo1 that we see around amyloid plaques in the hippocampus and cortex of TgF344-AD rats could, on the one hand, contribute to AD-associated astrogliopathy and neurodegeneration but, on the contrary, astrocytic Piezo1 may instead drive anti-inflammatory signaling cascades through YAP-mediated suppression of cytokine signaling that work in concert to reduce reactive astrogliosis and neuroinflammation in the aging AD brain.

CONCLUSION

The data presented here suggests that mechanoresponsive astrocytes surrounding stiff amyloid plaques in the AD brain upregulate Piezo1 channels for, as yet, unknown reasons. Moreover, peripheral infection, a common comorbidity in elderly people with AD, augments Piezo1 channel expression in astrocytes. This suggests a potential role for pro-inflammatory microglia in regulating astrocytic Piezo1 levels. Future studies will focus on the signaling cascades triggered by Piezo1-mediated currents in reactive astrocytes and Piezo1 as a potential therapeutic target for amyloid plaque-induced neurodegeneration in AD.

AUTHOR CONTRIBUTIONS

GS and KD conceived the project and designed the research. MV-E, MM, HB, AC, EM, and GS performed the experiments. MV-E, KD, and GS analyzed the data. PW, AS, and EB performed the infections in WT and TG rats. MV-E and GS wrote the manuscript with contributions from all authors. All authors discussed the data and results.

FUNDING

This work was supported by an Irish Research Council Ph.D. scholarship for MV-E, a University of Brighton Ph.D. scholarship for MM, and a Ph.D. studentship from the BioImaging Institute, The University of Manchester for AC. Purchase of TgF344-AD rats was jointly supported by the European Union's Seventh Framework Programme

(FP7/2007-2013) under Grant Agreement No. HEALTH-F2-2011-278850 (INMiND) and Alzheimer Research United Kingdom network funds. Breeding and maintenance costs for the TgF344-AD rat colony was supported by the European Union's Seventh Framework Programme (FP7/2007-2013) under Grant Agreement No. HEALTH-F2-2011-278850 (INMiND). EM was grateful for funding from Cancer Research United Kingdom [C57744/A22057]. GS was grateful for a *Rising Stars* award and for support from the Chemistry-Biology Collaborative Research Fund, University of Brighton.

ACKNOWLEDGMENTS

We thank Karen Bryson (Trinity College Dublin) for providing the $A\beta_{1-42}$ CMM for cell culture experiments and Sinead O'Sullivan (University of Chicago) for experimental support during the early parts of this study. We would like to thank Christopher Thrasivoulou and Tim Robson (University College London) for technical support with fluorescence imaging. We also thank the Centre for Stress and Age-Related Disease (University of Brighton) for supporting this research project.

REFERENCES

Arnsten, A. F., and Li, B. M. (2005). Neurobiology of executive functions: catecholamine influences on prefrontal cortical functions. *Biol. Psychiatry* 57, 1377–1384. doi: 10.1016/j.biopsych.2004.08.019

Bae, C., Sachs, F., and Gottlieb, P. A. (2015). Protonation of the human PIEZO1 ion channel stabilizes inactivation. *J. Biol. Chem.* 290, 5167–5173. doi: 10.1074/jbc.M114.604033

Barbas, H., and Zikopoulos, B. (2007). The prefrontal cortex and flexible behavior. *Neuroscientist* 13, 532–545. doi: 10.1177/1073858407301369

Bavi, N., Nikolaev, Y. A., Bavi, O., Ridone, P., Martinac, A. D., Nakayama, Y., et al. (2017). "Principles of mechanosensing at membrane interface," in *The Biophysics of Cell Membranes*, 19 Edn, eds R. M. Epand and J.-M. Ruysschaert (Berlin: Springer Series in Biophysics Springer), 85–119. doi: 10.1007/978-981-10-6244-5_4

Blumenthal, N. R., Hermanson, O., Heimrich, B., and Shastri, V. P. (2014). Stochastic nanoroughness modulates neuron-astrocyte interactions and function via mechanosensing cation channels. *Proc. Natl. Acad. Sci. U.S.A.* 111, 16124–16129. doi: 10.1073/pnas.1412740111

Bollmann, L., Koser, D. E., Shahapure, R., Gautier, H. O., Holzapfel, G. A., Scarcelli, G., et al. (2015). Microglia mechanics: immune activation alters traction forces and durotaxis. *Front. Cell. Neurosci.* 9:363. doi: 10.3389/fncel.2015.00363

Bradbury, E. J., Moon, L. D., Popat, R. J., King, V. R., Bennett, G. S., Patel, P. N., et al. (2002). Chondroitinase ABC promotes functional recovery after spinal cord injury. *Nature* 416, 636–640. doi: 10.1038/416636a

Buffo, A., Rolando, C., and Ceruti, S. (2010). Astrocytes in the damaged brain: molecular and cellular insights into their reactive response and healing potential. *Biochem. Pharmacol.* 79, 77–89. doi: 10.1016/j.bcp.2009.09.014

Catterall, W. A., Leal, K., and Nanou, E. (2013). Calcium channels and short-term synaptic plasticity. *J. Biol. Chem.* 288, 10742–10749. doi: 10.1074/jbc.R112.411645

Clapham, D. E. (2007). Calcium signaling. *Cell* 131, 1047–1058. doi: 10.1016/j.cell.2007.11.028

Cohen, R. M., Rezai-Zadeh, K., Weitz, T. M., Rentsendorj, A., Gate, D., Spivak, I., et al. (2013). A transgenic Alzheimer rat with plaques, tau pathology, behavioral impairment, oligomeric abeta, and frank neuronal loss. *J. Neurosci.* 33, 6245–6256. doi: 10.1523/JNEUROSCI.3672-12.2013

Coste, B., Mathur, J., Schmidt, M., Earley, T. J., Ranade, S., Petrus, M. J., et al. (2010). Piezo1 and Piezo2 are essential components of distinct mechanically activated cation channels. *Science* 330, 55–60. doi: 10.1126/science.1193270

Coste, B., Xiao, B., Santos, J. S., Syeda, R., Grandl, J., Spencer, K. S., et al. (2012). Piezo proteins are pore-forming subunits of mechanically activated channels. *Nature* 483, 176–181. doi: 10.1038/nature10812

Cox, C. D., Bae, C., Ziegler, L., Hartley, S., Nikolova-Krstevski, V., Rohde, P. R., et al. (2016). Removal of the mechanoprotective influence of the cytoskeleton reveals PIEZO1 is gated by bilayer tension. *Nat. Commun.* 7:10366. doi: 10.1038/ncomms10366

Dansokho, C., and Heneka, M. T. (2018). Neuroinflammatory responses in Alzheimer's disease. *J. Neural Transm.* 125, 771–779. doi: 10.1007/s00702-017-1831-7

Dempsey, C., Rubio Araiz, A., Bryson, K. J., Finucane, O., Larkin, C., Mills, E. L., et al. (2017). Inhibiting the NLRP3 inflammasome with MCC950 promotes non-phlogistic clearance of amyloid-beta and cognitive function in APP/PS1 mice. *Brain Behav. Immun.* 61, 306–316. doi: 10.1016/j.bbi.2016.12.014

Doulberis, M., Kotronis, G., Thomann, R., Polyzos, S. A., Boziki, M., Gialamprinou, D., et al. (2018). Review: impact of *Helicobacter pylori* on Alzheimer's disease: what do we know so far? *Helicobacter* 23:e12454. doi: 10.1111/hel.12454

Duyckaerts, C., Potier, M. C., and Delatour, B. (2008). Alzheimer disease models and human neuropathology: similarities and differences. *Acta Neuropathol.* 115, 5–38. doi: 10.1007/s00401-007-0312-8

Fawcett, J. W. (2006). Overcoming inhibition in the damaged spinal cord. *J. Neurotrauma* 23, 371–383. doi: 10.1089/neu.2006.23.371

Ge, J., Li, W., Zhao, Q., Li, N., Chen, M., Zhi, P., et al. (2015). Architecture of the mammalian mechanosensitive Piezo1 channel. *Nature* 527, 64–69. doi: 10.1038/nature15247

Gnanasambandam, R., Bae, C., Gottlieb, P. A., and Sachs, F. (2015). Ionic selectivity and permeation properties of human PIEZO1 channels. *PLoS One* 10:e0125503. doi: 10.1371/journal.pone.0125503

Gottlieb, P. A., and Sachs, F. (2012). Piezo1: properties of a cation selective mechanical channel. *Channels* 6, 214–219. doi: 10.4161/chan.21050

Guo, N., Soden, M. E., Herber, C., Kim, M. T., Besnard, A., Lin, P., et al. (2018). Dentate granule cell recruitment of feedforward inhibition governs engram maintenance and remote memory generalization. *Nat. Med.* 24, 438–449. doi: 10.1038/nm.4491

Hardy, J., and Allsop, D. (1991). Amyloid deposition as the central event in the aetiology of Alzheimer's disease. *Trends Pharmacol. Sci.* 12, 383–388. doi: 10.1016/0165-6147(91)90609-V

Healy, L. M., Sheridan, G. K., Pritchard, A. J., Rutkowska, A., Mullershausen, F., and Dev, K. K. (2013). Pathway specific modulation of S1P1 receptor signalling in rat and human astrocytes. *Br. J. Pharmacol.* 169, 1114–1129. doi: 10.1111/bph.12207

Holcomb, L., Gordon, M. N., McGowan, E., Yu, X., Benkovic, S., Jantzen, P., et al. (1998). Accelerated Alzheimer-type phenotype in transgenic mice carrying both mutant amyloid precursor protein and presenilin 1 transgenes. *Nat. Med.* 4, 97–100. doi: 10.1038/nm0198-097

Holmes, C., Cunningham, C., Zotova, E., Woolford, J., Dean, C., Kerr, S., et al. (2009). Systemic inflammation and disease progression in Alzheimer disease. *Neurology* 73, 768–774. doi: 10.1212/WNL.0b013e3181b6bb95

Huang, Z., Wang, Y., Hu, G., Zhou, J., Mei, L., and Xiong, W. C. (2016). YAP is a critical inducer of SOCS3, preventing reactive astrogliosis. *Cereb. Cortex* 26, 2299–2310. doi: 10.1093/cercor/bhv292

Hyman, B. T., Marzloff, K., and Arriagada, P. V. (1993). The lack of accumulation of senile plaques or amyloid burden in Alzheimer's disease suggests a dynamic balance between amyloid deposition and resolution. *J. Neuropathol. Exp. Neurol.* 52, 594–600. doi: 10.1097/00005072-199311000-00006

Jankowsky, J. L., Slunt, H. H., Ratovitski, T., Jenkins, N. A., Copeland, N. G., and Borchelt, D. R. (2001). Co-expression of multiple transgenes in mouse CNS: a comparison of strategies. *Biomol. Eng.* 17, 157–165. doi: 10.1016/S1389-0344(01)00067-3

Kamajaya, A., Kaiser, J. T., Lee, J., Reid, M., and Rees, D. C. (2014). The structure of a conserved piezo channel domain reveals a topologically distinct beta sandwich fold. *Structure* 22, 1520–1527. doi: 10.1016/j.str.2014.08.009

Kane, M. J., and Engle, R. W. (2002). The role of prefrontal cortex in working-memory capacity, executive attention, and general fluid intelligence: an

individual-differences perspective. *Psychon. Bull. Rev.* 9, 637–671. doi: 10.3758/BF03196323

Koser, D. E., Thompson, A. J., Foster, S. K., Dwivedy, A., Pillai, E. K., Sheridan, G. K., et al. (2016). Mechanosensing is critical for axon growth in the developing brain. *Nat. Neurosci.* 19, 1592–1598. doi: 10.1038/nn.4394

Kwan, K. Y., Allchorne, A. J., Vollrath, M. A., Christensen, A. P., Zhang, D. S., Woolf, C. J., et al. (2006). TRPA1 contributes to cold, mechanical, and chemical nociception but is not essential for hair-cell transduction. *Neuron* 50, 277–289. doi: 10.1016/j.neuron.2006.03.042

Lanoiselee, H. M., Nicolas, G., Wallon, D., Rovelet-Lecrux, A., Lacour, M., Rousseau, S., et al. (2017). APP, PSEN1, and PSEN2 mutations in early-onset Alzheimer disease: a genetic screening study of familial and sporadic cases. *PLoS Med.* 14:e1002270. doi: 10.1371/journal.pmed.1002270

Leipzig, N. D., and Shoichet, M. S. (2009). The effect of substrate stiffness on adult neural stem cell behavior. *Biomaterials* 30, 6867–6878. doi: 10.1016/j.biomaterials.2009.09.002

Lester, A. W., Moffat, S. D., Wiener, J. M., Barnes, C. A., and Wolbers, T. (2017). The aging navigational system. *Neuron* 95, 1019–1035. doi: 10.1016/j.neuron.2017.06.037

Leyns, C. E. G., and Holtzman, D. M. (2017). Glial contributions to neurodegeneration in tauopathies. *Mol. Neurodegener.* 12:50. doi: 10.1186/s13024-017-0192-x

Li, C., Rezania, S., Kammerer, S., Sokolowski, A., Devaney, T., Gorischek, A., et al. (2015). Piezo1 forms mechanosensitive ion channels in the human MCF-7 breast cancer cell line. *Sci. Rep.* 5:8364. doi: 10.1038/srep08364

Li, J., Hou, B., Tumova, S., Muraki, K., Bruns, A., Ludlow, M. J., et al. (2014). Piezo1 integration of vascular architecture with physiological force. *Nature* 515, 279–282. doi: 10.1038/nature13701

Liddelow, S. A., Guttenplan, K. A., Clarke, L. E., Bennett, F. C., Bohlen, C. J., Schirmer, L., et al. (2017). Neurotoxic reactive astrocytes are induced by activated microglia. *Nature* 541, 481–487. doi: 10.1038/nature21029

Lu, Y. B., Franze, K., Seifert, G., Steinhauser, C., Kirchhoff, F., Wolburg, H., et al. (2006). Viscoelastic properties of individual glial cells and neurons in the CNS. *Proc. Natl. Acad. Sci. U.S.A.* 103, 17759–17764. doi: 10.1073/pnas.0606150103

Lu, Z., Li, H., Hou, C., Peng, Y., Long, J., and Liu, J. (2017). Endogenously generated amyloid-beta increases stiffness in human neuroblastoma cells. *Eur. Biophys. J.* 46, 415–424. doi: 10.1007/s00249-016-1185-3

Lukiw, W. J. (2012). Amyloid beta (Abeta) peptide modulators and other current treatment strategies for Alzheimer's disease (AD). *Expert Opin. Emerg. Drugs* 17, 43–60. doi: 10.1517/14728214.2012.672559

Maggio, N., and Vlachos, A. (2014). Synaptic plasticity at the interface of health and disease: new insights on the role of endoplasmic reticulum intracellular calcium stores. *Neuroscience* 281, 135–146. doi: 10.1016/j.neuroscience.2014.09.041

Martinac, B. (2004). Mechanosensitive ion channels: molecules of mechanotransduction. *J. Cell Sci.* 117, 2449–2460. doi: 10.1242/jcs.01232

McHugh, B. J., Buttery, R., Lad, Y., Banks, S., Haslett, C., and Sethi, T. (2010). Integrin activation by Fam38A uses a novel mechanism of R-Ras targeting to the endoplasmic reticulum. *J. Cell Sci.* 123(Pt 1), 51–61. doi: 10.1242/jcs.056424

McManus, R. M., Higgins, S. C., Mills, K. H., and Lynch, M. A. (2014). Respiratory infection promotes T cell infiltration and amyloid-beta deposition in APP/PS1 mice. *Neurobiol. Aging* 35, 109–121. doi: 10.1016/j.neurobiolaging.2013.07.025

Moeendarbary, E., and Harris, A. R. (2014). Cell mechanics: principles, practices, and prospects. *Wiley Interdiscip. Rev. Syst. Biol. Med.* 6, 371–388. doi: 10.1002/wsbm.1275

Moeendarbary, E., Weber, I. P., Sheridan, G. K., Koser, D. E., Soleman, S., Haenzi, B., et al. (2017). The soft mechanical signature of glial scars in the central nervous system. *Nat. Commun.* 8:14787. doi: 10.1038/ncomms14787

Morris, G. P., Clark, I. A., and Vissel, B. (2014). Inconsistencies and controversies surrounding the amyloid hypothesis of Alzheimer's disease. *Acta Neuropathol. Commun.* 2:135. doi: 10.1186/s40478-014-0135-5

Moshayedi, P., Costa Lda, F., Christ, A., Lacour, S. P., Fawcett, J., Guck, J., et al. (2010). Mechanosensitivity of astrocytes on optimized polyacrylamide gels analyzed by quantitative morphometry. *J. Phys. Condens. Matter* 22, 194114. doi: 10.1088/0953-8984/22/19/194114

Moshayedi, P., Ng, G., Kwok, J. C., Yeo, G. S., Bryant, C. E., Fawcett, J. W., et al. (2014). The relationship between glial cell mechanosensitivity and foreign body reactions in the central nervous system. *Biomaterials* 35, 3919–3925. doi: 10.1016/j.biomaterials.2014.01.038

Nacmias, B., Piaceri, I., Bagnoli, S., Tedde, A., Piacentini, S., and Sorbi, S. (2014). Genetics of Alzheimer's disease and frontotemporal dementia. *Curr. Mol. Med.* 14, 993–1000. doi: 10.2174/1566524014666141010152143

Nagarajan, A., Ning, Y., Reisner, K., Buraei, Z., Larsen, J. P., Hobert, O., et al. (2014). Progressive degeneration of dopaminergic neurons through TRP channel-induced cell death. *J. Neurosci.* 34, 5738–5746. doi: 10.1523/JNEUROSCI.4540-13.2014

Natalwala, A., Potluri, R., Uppal, H., and Heun, R. (2008). Reasons for hospital admissions in dementia patients in Birmingham, UK, during 2002-2007. *Dement. Geriatr. Cogn. Disord.* 26, 499–505. doi: 10.1159/000171044

Nobakht, M., Hoseini, S. M., Mortazavi, P., Sohrabi, I., Esmailzade, B., Rahbar Rooshandel, N., et al. (2011). Neuropathological changes in brain cortex and hippocampus in a rat model of Alzheimer's disease. *Iran Biomed. J.* 15, 51–58.

O'Sullivan, S. A., O'Sullivan, C., Healy, L. M., Dev, K. K., and Sheridan, G. K. (2018). Sphingosine 1-phosphate receptors regulate TLR4-induced CXCL5 release from astrocytes and microglia. *J. Neurochem.* 144, 736–747. doi: 10.1111/jnc.14313

O'Sullivan, S. A., Velasco-Estevez, M., and Dev, K. K. (2017). Demyelination induced by oxidative stress is regulated by sphingosine 1-phosphate receptors. *Glia* 65, 1119–1136. doi: 10.1002/glia.23148

Pathak, M. M., Nourse, J. L., Tran, T., Hwe, J., Arulmoli, J., Le, D. T., et al. (2014). Stretch-activated ion channel Piezo1 directs lineage choice in human neural stem cells. *Proc. Natl. Acad. Sci. U.S.A.* 111, 16148–16153. doi: 10.1073/pnas.1409802111

Paxinos, G., and Watson, C. (2014). *The Rat Brain in Stereotaxic Coordinates*, 7 Edn. San Diego: Academic Press.

Previtera, M. L., Langhammer, C. G., Langrana, N. A., and Firestein, B. L. (2010). Regulation of dendrite arborization by substrate stiffness is mediated by glutamate receptors. *Ann. Biomed. Eng.* 38, 3733–3743. doi: 10.1007/s10439-010-0112-5

Ranade, S. S., Qiu, Z., Woo, S. H., Hur, S. S., Murthy, S. E., Cahalan, S. M., et al. (2014). Piezo1, a mechanically activated ion channel, is required for vascular development in mice. *Proc. Natl. Acad. Sci. U.S.A.* 111, 10347–10352. doi: 10.1073/pnas.1409233111

Rothhammer, V., Borucki, D. M., Tjon, E. C., Takenaka, M. C., Chao, C. C., Ardura-Fabregat, A., et al. (2018). Microglial control of astrocytes in response to microbial metabolites. *Nature* 557, 724–728. doi: 10.1038/s41586-018-0119-x

Rowe, T. A., and Juthani-Mehta, M. (2013). Urinary tract infection in older adults. *Aging Health* 9, 519–528. doi: 10.2217/ahe.13.38

Salles, N., and Mégraud, F. (2007). Current management of *Helicobacter pylori* infections in the elderly. *Expert Rev. Anti Infect. Ther.* 5, 845–856. doi: 10.1586/14787210.5.5.845

Satoh, K., Hata, M., Takahara, S., Tsuzaki, H., Yokota, H., Akatsu, H., et al. (2006). A novel membrane protein, encoded by the gene covering KIAA0233, is transcriptionally induced in senile plaque-associated astrocytes. *Brain Res.* 1108, 19–27. doi: 10.1016/j.brainres.2006.06.050

Saunders, A. M. (2001). Gene identification in Alzheimer's disease. *Pharmacogenomics* 2, 239–249. doi: 10.1517/14622416.2.3.239

Smith, J. F., Knowles, T. P., Dobson, C. M., Macphee, C. E., and Welland, M. E. (2006). Characterization of the nanoscale properties of individual amyloid fibrils. *Proc. Natl. Acad. Sci. U.S.A.* 103, 15806–15811. doi: 10.1073/pnas.0604035103

Sofroniew, M. V. (2009). Molecular dissection of reactive astrogliosis and glial scar formation. *Trends Neurosci.* 32, 638–647. doi: 10.1016/j.tins.2009.08.002

Sofroniew, M. V. (2014). Multiple roles for astrocytes as effectors of cytokines and inflammatory mediators. *Neuroscientist* 20, 160–172. doi: 10.1177/1073858413504466

Stancu, I. C., Vasconcelos, B., Terwel, D., and Dewachter, I. (2014). Models of beta-amyloid induced Tau-pathology: the long and "folded" road to understand the mechanism. *Mol. Neurodegener.* 9:51. doi: 10.1186/1750-1326-9-51

Sun, D., and Jakobs, T. C. (2012). Structural remodeling of astrocytes in the injured CNS. *Neuroscientist* 18, 567–588. doi: 10.1177/1073858411423441

Suwabe, K., Hyodo, K., Byun, K., Ochi, G., Yassa, M. A., and Soya, H. (2017). Acute moderate exercise improves mnemonic discrimination in young adults. *Hippocampus* 27, 229–234. doi: 10.1002/hipo.22695

Tate, J. A., Snitz, B. E., Alvarez, K. A., Nahin, R. L., Weissfeld, L. A., Lopez, O., et al. (2014). Infection hospitalization increases risk of dementia in the elderly. *Crit. Care Med.* 42, 1037–1046. doi: 10.1097/CCM.0000000000000123

Thomé, A., Gray, D. T., Erickson, C. A., Lipa, P., and Barnes, C. A. (2016). Memory impairment in aged primates is associated with region-specific network dysfunction. *Mol. Psychiatry* 21, 1257–1262. doi: 10.1038/mp.2015.160

Verkhratsky, A., Rodríguez, J. J., and Parpura, V. (2013). Astroglia in neurological diseases. *Future Neurol.* 8, 149–158. doi: 10.2217/fnl.12.90

Wang, L., Xia, J., Li, J., Hagemann, T. L., Jones, J. R., Fraenkel, E., et al. (2018). Tissue and cellular rigidity and mechanosensitive signaling activation in Alexander disease. *Nat. Commun.* 9:1899. doi: 10.1038/s41467-018-04269-7

Wiegand, J. P., Gray, D. T., Schimanski, L. A., Lipa, P., Barnes, C. A., and Cowen, S. L. (2016). Age is associated with reduced sharp-wave ripple frequency and altered patterns of neuronal variability. *J. Neurosci.* 36, 5650–5660. doi: 10.1523/JNEUROSCI.3069-15.2016

Wilhelmsson, U., Bushong, E. A., Price, D. L., Smarr, B. L., Phung, V., Terada, M., et al. (2006). Redefining the concept of reactive astrocytes as cells that remain within their unique domains upon reaction to injury. *Proc. Natl. Acad. Sci. U.S.A.* 103, 17513–17518. doi: 10.1073/pnas.0602841103

Yamamoto, S., Wajima, T., Hara, Y., Nishida, M., and Mori, Y. (2007). Transient receptor potential channels in Alzheimer's disease. *Biochim. Biophys. Acta* 1772, 958–967. doi: 10.1016/j.bbadis.2007.03.006

Zimprich, D., and Kurtz, T. (2013). Individual differences and predictors of forgetting in old age: the role of processing speed and working memory. *Neuropsychol. Dev. Cogn. B Aging Neuropsychol. Cogn.* 20, 195–219. doi: 10.1080/13825585.2012.690364

Conflict of Interest Statement: Evotec (UK) Ltd. was involved in the design of the urinary tract infection study performed on wild-type and TgF344-AD rats and analyzed the urine samples for bacterial load. Evotec (UK) Ltd. was not involved in the design or analysis of any other experiments.

The authors declare that the research was conducted in the absence of any commercial or financial relationships that could be construed as a potential conflict of interest.

frontiers in Molecular Neuroscience

REVIEW
published: 15 November 2018
doi: 10.3389/fnmol.2018.00408

Potential Epigenetic-Based Therapeutic Targets for Glioma

Lanlan Zang[1,2], Shukkoor Muhammed Kondengaden[3], Fengyuan Che[1,4], Lijuan Wang[1] and Xueyuan Heng[4]**

[1]Central Laboratory and Key Laboratory of Neurophysiology, Linyi People's Hospital, Shandong University, Linyi, China, [2]Department of Medicinal Chemistry, Key Laboratory of Chemical Biology (Ministry of Education), School of Pharmaceutical Sciences, Shandong University, Jinan, China, [3]Chemistry Department and Center for Diagnostics and Therapeutics, Georgia State University, Atlanta, GA, United States, [4]Department of Neurology, Linyi People's Hospital, Shandong University, Linyi, China

Glioma is characterized by a high recurrence rate, short survival times, high rates of mortality and treatment difficulties. Surgery, chemotherapy and radiation (RT) are the standard treatments, but outcomes rarely improve even after treatment. With the advancement of molecular pathology, recent studies have found that the development of glioma is closely related to various epigenetic phenomena, including DNA methylation, abnormal microRNA (miRNA), chromatin remodeling and histone modifications. Owing to the reversibility of epigenetic modifications, the proteins and genes that regulate these changes have become new targets in the treatment of glioma. In this review, we present a summary of the potential therapeutic targets of glioma and related effective treating drugs from the four aspects mentioned above. We further illustrate how epigenetic mechanisms dynamically regulate the pathogenesis and discuss the challenges of glioma treatment. Currently, among the epigenetic treatments, DNA methyltransferase (DNMT) inhibitors and histone deacetylase inhibitors (HDACIs) can be used for the treatment of tumors, either individually or in combination. In the treatment of glioma, only HDACIs remain a good option and they provide new directions for the treatment. Due to the complicated pathogenesis of glioma, epigenetic applications to glioma clinical treatment are still limited.

Keywords: glioma, epigenetics, DNA methylation, miRNA, chromatin remodeling, histone modifications

OPEN ACCESS

Edited by:
Alberto Javier Ramos, Consejo Nacional de Investigaciones Científicas y Técnicas (CONICET), Argentina

Reviewed by:
Marianela Candolfi, Consejo Nacional de Investigaciones Científicas y Técnicas (CONICET), Argentina
Timothy J. Jarome, Virginia Tech, United States

****Correspondence:***
Lijuan Wang
wanglj730@163.com
Xueyuan Heng
hengxueyuan12@163.com

Received: *12 July 2018*
Accepted: *16 October 2018*
Published: *15 November 2018*

Citation:
Zang L, Kondengaden SM, Che F, Wang L and Heng X (2018) Potential Epigenetic-Based Therapeutic Targets for Glioma. Front. Mol. Neurosci. 11:408. doi: 10.3389/fnmol.2018.00408

INTRODUCTION

Glioma is the most common form of primary malignant brain tumors, accounting for nearly 30% of all brain tumors, and also one of the most lethal (Chien et al., 2016). Some symptoms of glioma may be subtle and gradually worsen, while others may be present as an acute illness. The exact mechanism of occurrence of glioma remains unclear.

Recently, the World Health Organization (WHO) Classification of Tumors of the Central Nervous System (CNS; Wen and Huse, 2017) categorized glioma into four grades. Grades I and II are considered low-grade glioma, whereas grades III and IV are high-grades, with the degree of malignancy increasing in the higher grades. The types of glioma include low-grade glioma (WHO II: mainly refers to diffuse astrocytoma, oligodendroglioma, and oligodendrocyte astrocytoma), anaplastic glioma (WHO III), glioblastoma (GBM, WHO IV), brain gliomatosis (pathologically astrocytoma-based, can be divided into WHO II, III, IV) and ependymomas (WHO II, III). Each grade has a relatively specific prognosis to guide the clinical treatment, but most of the glioma

are WHO III grade anaplastic glioma and WHO grade IV GBM, which is devoid of cure with the current therapeutic options.

Unfortunately, most high-grade gliomas do not have a definitive cure. The current treatment for these high-grade tumors mainly focuses on surgical resection, followed by chemotherapy and radiotherapy. Temozolomide (TMZ) can traverse the blood-brain barrier and it is often used to treat these tumors. However, various side effects and adverse prognosis exist, such as the hematological toxicity (Stupp et al., 2005), and glioma have proven to be particularly resistant to radiotherapy and chemotherapy. The main mechanism of drug resistance is correlated with the O6-methyl guanine-DNA methyltransferase (MGMT; Hegi et al., 2005), which can bind to an alkyl compound on the O6 of DNA guanine and reduce it so that protein complexes cannot recognize the mismatched base pair, resulting in cell tolerance to O6 guanine methylation. As a result, the efficacy of these treatments is not promising and the prognosis of patients remains poor.

Therapies aimed to overcome these limitations have been presented in recent preclinical and clinical studies, including targeted molecular therapy, immunotherapy, gene therapy and stem cell therapy. The success of targeted molecular therapy for some tumor types, such as non-small cell lung cancer (Antonelli et al., 2016), malignant melanoma (Sullivan and Atkins, 2009) and chronic myeloid leukemia (Smirnikhina et al., 2016), has important guiding significance for targeted malignant glioma therapy.

With the advancement of the molecular pathology of malignant glioma, it is now evident that epigenetic abnormalities, including aberrant DNA methylation, abnormal microRNA (miRNA), chromatin remodeling and histone modifications, are closely related to the occurrence of glioma (Kondo et al., 2014; Hashizume, 2017; **Figure 1**). Multiple enzymes and genes that regulate the epigenetic modifications have become new targets not only for glioma treatments but for the treatment of other cancers as well.

This review summarizes the potential epigenetic-based therapeutic targets and related drugs for glioma. We illustrate how the epigenetic mechanisms dynamically regulate the pathogenesis of the disease. To provide information that will assist clinicians, we discuss preclinical and clinical trials of epigenetic-based treatments of glioma and include the results from these studies. This review also highlights the limitations of the current treatment and suggests future potential areas for research and advancements in the prognosis of the disease.

DNA METHYLATION

DNA methylation is one of the earliest discovered epigenetic modifications pathways. There are four possible sites for DNA methylation (Jones, 2012; Lovkvist et al., 2016)—the N-6 position of adenine, the N-4 position of cytosine, the N-7 position of guanine and the C-5 position of cytosine. In mammalian cells, DNA methylation occurs predominantly in cytosine of 5'-CpG-3' to produce 5-methylcytosine (5mC). The methylation reaction is site-specific and it is performed by the enzyme DNMT with the help of methyl donor s-adenosylmethionine (SAM) as a co-factor (Bird, 2002). Currently, according to the differences in their structure and function, these DNMTs are divided into three categories, DNMT1, DNMT2, DNMT3 (DNMT3a and DNMT3b), with DNMT1 and DNMT3 as the representatives. DNMT1 is involved in the maintenance and extension of methylation, a necessity for non-CpG site methylation. DNMT3a and DNMT3b are *de novo* methyltransferases that methylate CpG. *De novo* methyltransferases may be involved in the regulation of cell growth and differentiation, in which DNMT3b plays an important role in tumor gene methylation (Chédin, 2011). DNMT2 binds to a specific site on DNA and its main target is tRNA (Kaiser et al., 2017). A number of studies (Hashimshony et al., 2003; Krausz et al., 2012; Shimooka et al., 2013) show that DNA methylation can contribute to changes in chromatin structure, DNA conformation, DNA stability, interactions between DNA and proteins, and can also control gene expression. DNA methylation has additionally become an important study of epigenetics and epigenetic genomics due to the close relationship between DNA methylation, human development and tumor diseases, particularly the transcriptional inactivation of tumor suppressor genes caused by methylation of CpG islands content.

Aberrant DNA Methylation in Glioma

Many studies (de Souza et al., 2018; Liao et al., 2018) have shown that the patterns of DNA methylation in glioma cells are different from those in normal cells. Most notably, the coexistence of extensive hypomethylation and CpG island hypermethylation are characteristic of tumor cells. The DNA methylation status of some relevant genes in glioma is therefore a good biomarker for clinical glioma diagnosis (**Figure 1**; Qu et al., 2013; Choudhury et al., 2015). Hypermethylation of the gene promoter region is the clearest epigenetic change that occurs in the tumor. The methylation status of the promoter region in the human genome regulates gene expression. Almost all housekeeping genes and roughly half of the tissue-specific genes are under the control of the promoter region. Under normal physiological conditions, most CpG islands are in a hypomethylated state; however, some housekeeping genes, such as DNA repair genes and tumor suppressor genes, are often hypermethylated in tumor tissues (Jin et al., 2017). This aberrant methylation can lead to gene transcription suppression and the loss of their biological function. DNA-5-hydroxymethylcytosine (5hmC), an epigenetic mark resulting from 5mC oxidation, correlates with the progression of glioma (Fernandez et al., 2018). Recent evidence (Kraus et al., 2012) has shown that DNA 5hmC negatively correlates with tumor grade. The CpG island methylator phenotype (G-CIMP) is also used as an indicator of glioma prognosis in infancy, pediatric and adults (Mack et al., 2014; Malta et al., 2018). Importantly, another study (Jha et al., 2014) found that pediatric GBM have a distinct methylome compared with that of adults, suggesting that the G-CIMP indicator of glioma prognosis in adult GBM cannot simply be extrapolated to pediatric GBM and there is a strong need for identification of separate prognostic markers.

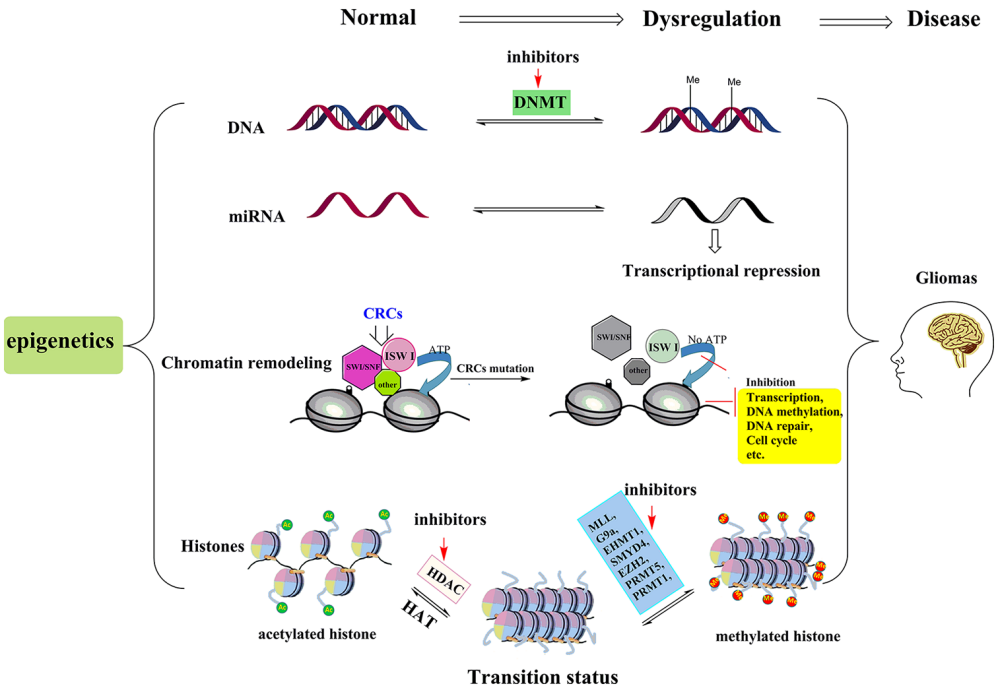

FIGURE 1 | Pathogenesis and treatment options for glioma. The pathogenesis of glioma involves multiple processes. Here we show four epigenetic abnormalities (from top to bottom) linked to the occurrence of glioma: aberrant DNA methylation, abnormal microRNA (miRNA), chromatin remodeling and histone modifications. Among them, chromatin remodeling complexes (CRCs, such as SWI/SNF, ISW I, and other types of complexes) rely on the hydrolysis of ATP to provide energy to complete the chromatin structure changes. When the key proteins of the CSCs are mutated, this leads to abnormalities in the expression of tumor suppressor genes or those genes involved in cell cycle regulation, leading to the occurrence of glioma. In histone modification section, by inhibiting the activities of histone methyltransferases and histone deacetylase (HDAC), more sites in histone tails are free to be acetylated and this process can reverse the aberrant histone modifications, and then further suppress tumor cell proliferation and induce apoptosis. The red arrows represent potential epigenetic-based therapeutic approaches against glioma. For example, in DNA methylation section, DNMT inhibitor, 5-aza-20-deoxycytidine is the representative drug. In histone modifications, the HDACIs (vorinostat, panobinostat, valproic acid, etc.) and relevant histone methyltransferases inhibitors are potential treatment drugs in clinic.

Abnormal DNA methylation is an important indicator of the inactivation of tumor suppressor genes. Many tumor suppressor genes in glioma have also been identified, including $p16^{INK4a}$ (Lee et al., 2000), p14ARF (Watanabe et al., 2007), MLH1 (Gömöri et al., 2007) and NDRG2 (Kolodziej et al., 2016; see **Table 1**). The $p16^{INK4a}$ gene maintains the dephosphorylated activating state of the retinoblastoma tumor suppressor protein (pRb) in the normal cyclinD-Rb pathway to control cell cycle progression. A high frequency (more than 50%) of homozygous $p16^{INK4a}$ gene deletion has been demonstrated in GBM tissues, and $p16^{INK4a}$ is altered in 80% of glioma cell lines. Therefore, restoration of $p16^{INK4a}$ would suppress cell proliferation and induce cell growth arrest (Lee et al., 2000). MGMT is a crucial DNA damage repair gene that can repair alkyl damage caused by BCNU. Esteller et al. (2000) found that MGMT promoter hypermethylation existed in approximately 40% of glioma tissues. The methylation level is related to the occurrence and prognosis of the tumor, which is more important than the prognosis of age and tumor grade (Mur et al., 2015). Besides, the methylation level of MGMT promoter is the most important indicator to assess TMZ sensitivity in glioma treatment, and down-regulated MGMT can substantially restore TMZ chemosensitivity *in vitro* and *in vivo* (Xipell et al., 2016; Yu et al., 2018). Except for the genes mentioned above, the CpG island methylation in gene promoter regions of p73 (Watanabe et al., 2002), LATS1, LATS2 (Jiang et al., 2006), and the genes that are listed in **Table 1** are also closely related with the occurrence and development of glioma.

Isocitrate dehydrogenases 1 (IDH1) is not only a major source of NADPH in the human brain (Bleeker et al., 2010) but also in other body tissues (Kim et al., 2009). The mutations of methylation regulatory proteins IDH1/2 can be detected in most low-grade diffuse astrocytoma (75% mutation rate) and anaplastic astrocytoma (66% mutation rate) as well as oligodendroglioma, mixed promyelocytoma and secondary sex polymorphic neuroblastoma (GBM, 76% mutation rate). Noushmehr et al. (2010) found that the IDH1 mutation is highly correlated with the G-CIMP, and its mutation was associated with the prognosis of secondary GBM and positively correlated with the survival rate of patients (Rossetto et al., 2011). Studies have shown that the hypermethylated phenotype of IDH mutations causes insulator proteins to separate from IDH mutant binding sites (Flavahan et al., 2016). These free insulator proteins are then linked to the normally resting platelet-derived growth factor receptor (PDGFRA) oncogene promoter to form a complex that can further stimulate tumor

TABLE 1 | DNA Methylation in glioma.

Genes/proteins DNA methylation	Location	Pathway	References
$p16^{INK4a}$	9p21	Cell cycle	Lee et al. (2000)
p14ARF	9p21	Cell cycle	Watanabe et al. (2007)
PTPRD	9p23-p24.3	Cell proliferation	Veeriah et al. (2009)
EMP3	19q13.3	Cell proliferation	Alaminos et al. (2005), Kunitz et al. (2007)
KLF4	9q31	Cell proliferation	Nakahara et al. (2010)
P73	1p36.3	Cell cycle and apoptosis	Watanabe et al. (2002)
NDRG2	14q11.2	Cell cycle and proliferation	Kolodziej et al. (2016)
MKP-2	8p12-p11	Cell proliferation	Waha et al. (2010)
NSD1	5q35	Cell proliferation	Berdasco et al. (2009)
miR129-2	11p11.2	Cell proliferation, apoptosis, invasion, and migration	Yadavilli et al. (2015)
HTATIP2	11p15.1	Cell proliferation	Dong et al. (2015)
SLC22A18	11p15.5	Cell proliferation, apoptosis	Chu et al. (2011)
hMLH1	3p21.3	DNA repair	Gömöri et al. (2007)
MGMT	10q26	DNA repair	Weller (2013), Kanemoto et al. (2014), Berghoff et al. (2015)
RANK (TNFRSF11A)	18q22.1	Cell apoptosis	von dem Knesebeck et al. (2012)
Neogenin	15q22.3-q23	Cell apoptosis	Wu et al. (2012)
NAG-1	19p13.11	Cell apoptosis	Kadowaki et al. (2012)
GLIPR1	12q21.2	Cell apoptosis	Li L. et al. (2013)
TES	7q31.2	Cell apoptosis	Bai et al. (2014)
BEX1	Xq22.1	Cell apoptosis	Foltz et al. (2006)
BEX2	Xq22	Cell apoptosis	Foltz et al. (2006)
WNK2	9q22.3	Invasion and migration	Moniz et al. (2013)
AJAP1	1p36.32	Migration	Lin et al. (2012)
CST6	11q13	Invasion	Qiu et al. (2008)
SLIT2	4p15.2	Invasion and migration	Xu et al. (2010)
MiR-124a	8p23.1	Invasion and migration	Fowler et al. (2011)
TFPI-2	7q22	Invasion and migration	Gessler et al. (2011), Vaitkiene et al. (2012)
PCDH10	4q28.3	Cell proliferation, cell cycle progression, and cell migration	Echizen et al. (2014)
RUNX3	1p36	Invasion and migration	Mei et al. (2011)
SOCS3	17q25.3	STAT signal pathway	Martini et al. (2008)
RASSF1A	3p21.3	Ras/STAT signal pathway	Horiguchi et al. (2003), Gao et al. (2004)
RASSF10	11p15.2	Ras signal pathway	Hill et al. (2011)
SFRP1	8p11.21	Wnt signal pathway	Majchrzak-Celinska et al. (2016)
SFRP5	10q24.1	Wnt signal pathway	Götze et al. (2010)
DKK1	10q11.2	Wnt signal pathway	Mueller et al. (2005)
DKK3	11p15.2	Wnt signal pathway	Hara et al. (2015)
NKD1	16q12.1	Wnt signal pathway	Götze et al. (2010)
NKD2	5p15.3	Wnt signal pathway	Götze et al. (2010)
SOX2	3q26.3-27	Migration	Luo et al. (2017)

cell growth. By using demethylated drugs to restore normal function in these insulator proteins, PDGFRA can inhibit the growth of IDH mutant astrocytoma cells (Flavahan et al., 2016). In another study, they associated known subtypes with specific alterations in NF1 and PDGFRA/IDH1 in order to provide a framework for the investigation of targeted therapies (Verhaak et al., 2010). As a critical gene of glioma, IDH has vast potential for the diagnosis, treatment and prognosis of glioma.

MicroRNA

MiRNAs are short non-coding endogenous RNAs that involve in post-transcriptional gene expression regulation in animals and plants (Bartel, 2004). miRNAs can target complementary regions of the 3'-UTR of the mRNA, inhibiting post-transcriptional processes or degrading mRNA and ultimately reducing protein levels (Pileggi et al., 2013). There are many miRNAs in the human genome, targeting tens of thousands of mRNAs.

MicroRNAs and Glioma

In recent years, some studies have shown that miRNAs play key roles in the transcriptional regulation and growth and proliferation of various tumor genes (Yan et al., 2017). Therefore, miRNA-based individual therapy and gene editing methods may play important roles in the diagnosis and treatment of glioma. It is currently estimated that about half of the miRNA genes are located in glioma cancer genes or their fragile sites (**Table 2**), and these miRNA genes can regulate 3% of the entire glioma tumor genes and 30% of the coding genes. Also, a single miRNA can simultaneously affect a hundred mRNAs of GBM (Berindan-Neagoe et al., 2014), whereas a single mRNA of glioma can be modulated by one or more miRNAs (Lakomy et al., 2011).

miRNAs play many critical roles in the progression of glioma diseases. In particular, miRNAs regulate the expression of cancer-related genes, participate in the regulation of tumorigenesis and regulatory pathways, regulate the differentiation of glioma stem cells, and are encoded by oncolytic

TABLE 2 | Role of microRNA in glioma biology.

MicroRNA					
mi-RNA	**Target gene**	**References**	**mi-RNA**	**Target gene**	**References**
Down-regulation					
miR-873	GLI1, Bcl-2,	Chen et al. (2015), Zhang J. S. et al. (2017)	miR-152	Runx2	Zhang P. et al. (2017)
miR-34a	PD-L1	Wang and Wang (2017)	miR-152-3p	NF2	Sun J. et al. (2017)
miR-373	CD44, TGFBR2	Wei F. et al. (2016), Jing et al. (2017)	miR-153	Irs-2	Xu et al. (2011), Ghasemi et al. (2016)
miR-146a	Notch	Hu et al. (2016)	miR-181	VCAM-1, Bcl-2	Chen et al. (2010), Liu et al. (2017)
miR-7	EGFR, PI3K/ATK, Raf/MEK/ERK	Liu X. et al. (2013), Liu et al. (2014)	miR-184	FIH1, SND1	Yuan et al. (2014), Emdad et al. (2015)
miR-128	RhoE	Shang et al. (2016b)	miR-204	IGFBP2	Chen et al. (2016)
miR-195	E2F3, Cyclosporin	Zhang Q. Q. et al. (2012), Yilaz Susluer et al. (2015)	miR-218	Robo1, E2F2, NF-kappaB	Xia et al. (2013), Zhang et al. (2015), Gu et al. (2016)
miR-124	SCP1, Capn4	Cai et al. (2016), Sun A. G. et al. (2017)	miR-326	SMO	Du et al. (2015)
miR-137	PTP4A3, CSE1L	Li K. K. et al. (2013), Wang et al. (2016)	miR-410	MET	Chen et al. (2012)
miR-15b	Cyclin D1, NRP-2 and MMP-3	Zheng et al. (2013), Sun et al. (2014)	miR-483-5p	ERK1	Wang et al. (2012)
miR-16-1	Zyxin	Li X. et al. (2013)	miR-125b	Connexin43	Jin et al. (2013)
miR-31	radixin	Hua et al. (2012)	miR-138	Immune,	Wei J. et al. (2016)
miR-101	COX-2,	Ma et al. (2016)	miR-145	ABCG2, SOX9, adducin 3	Rani et al. (2013), Shi et al. (2014)
miR-491-5p	EGFR, CDK6 and Bcl-xL	Li et al. (2015)	miR-149	Akt/mTOR, signaling,	Xue et al. (2015)
miR-491-3p	IGFBP2 and CDK6	Li et al. (2015)			
Up-regulation					
miR-21	Spry2	Kwak et al. (2011)	miR-18a	Neogenin, zonula occluden-1, claudin-5, and occludin	Song et al. (2014), Zhao et al. (2015)
miR-26a	PTEN, TUG1	Huse et al. (2009), Li et al. (2016)	miR-20a	TIMP-2, LRIG1	Wang et al. (2015), Wei et al. (2015)
miR-10b	RHOC	Dong et al. (2012)	miR-23b	TUSC7, TFAM	Jiang et al. (2013), Shang et al. (2016a)
miR-30e	CBL-B	Kwak et al. (2015)	miR-93	integrin-beta8, IL-8,	Fang et al. (2011), Fabbri et al. (2015)
miR-221/222	TIMP2, PTPμ, Cx43, P27Kip1,	Zhang C. et al. (2009), Hao et al. (2012), Quintavalle et al. (2012), Yang et al. (2015)	miR-125b-2	mitochondrial pathway of apoptosis,	Shi et al. (2012)
miR-17-92	CTGF	Ernst et al. (2010)	miR-296-3p	EAG1	Bai et al. (2013)
miR-9/9*	CAMTA1	Schraivogel et al. (2011)	miR-451	SMAD	Gal et al. (2008)

miR-9 is the complementary sequence of miR-9.*

viruses and involved in tumor processes. Zhang C. et al. (2012), for instance, found miR-221/222 positively correlated with the degree of glioma infiltration and cell invasion, whereas knockdown of miR-221/222 decreased cell invasion via modulating the levels of the TIMP3 target. Knockdown of miR-221/222 additionally increased TIMP3 expression and considerably inhibited tumor growth in a xenograft model. Another study indicated that the over-expression of miR-221/222 reduced p27kipl levels (Zhang C. et al., 2009). P27kipl prevented cell cycle from G1 to S phase by binding to CDK2 and cyclin E complexes. Therefore, down-regulated miR-221/222 can up-regulate p27kipl to inhibit tumor proliferation.

CHROMATIN REMODELING

Chromatin remodeling complexes (CRCs) have ATPase activity and they rely on the hydrolysis of ATP to provide energy to complete the chromatin structure changes (Stanton et al., 2017). Depending on the different subunits that can hydrolyze ATP, the complexes can be divided into SWI/SNF, ISW I and other types of complexes (**Figure 1**). The SWI/SNF complex and the ISW I complex family were the first to be found in yeast and *Drosophila* (Biegel et al., 2014). The human SWI/SNF complex is a polymer with many molecules, including BRG1, hBMR and tumor suppressor protein Hsnf5, which mainly activates gene transcription and is also involved in the recombination of immunoglobulin and TCR genes (Pulice and Kadoch, 2016). The ISW I complex family include three complexes—RSF, HuCHRAC and CAF1 (Loyola et al., 2003). RSF is a heterodimer that mainly consists of Hsnf-h, which is involved in transcription initiation (Sheu et al., 2010); HucHRAC contains Hsnf-2 h and chromatin assembly factor Hacf1, which is related to the maintenance of the heterochromatin replication status (Hanai et al., 2008); CAF1 is involved in chromatin assembly, altering the state of chromatin to correlate with DNA function (Endo et al., 2017). These complexes and related proteins are associated with activation and inhibition of transcription, DNA methylation, DNA repair and cell cycle.

Chromatin Remodeling and Glioma

Human diseases caused by abnormal chromatin remodeling are often due to mutations in the key proteins of the remodeling complex. This can lead to the failure of chromatin remodeling in which nucleosomes cannot be correctly positioned, preventing basic transcriptional machinery and the complexes that can repair DNA damage from accessing DNA, which can lead to aberrant gene expression. If these mutations lead to abnormalities of tumor suppressor genes or proteins that regulate cell cycle, they can finally lead to the occurrence of cancer (Marfella et al., 2008; Choi et al., 2015).

Liau et al. (2017) recently indicated that chromatin remodeling regulated GBM drug resistance. GBM stem cells (GSC) can reversibly change to a slow-cycling, long-lasting state when targeted by kinase inhibitors. Under this state, the notch signaling pathway is activated and histone demethylase KDM6A/B is significantly up-regulated. This leads to the removing of trimethylation of H3K27 in genome cis-regulatory region and further leads to the increased levels of H3K27Ac. Chromatin remodeling played a key role in this cellular shift, and this research provided a novel target for the development of effective treatments in the future. By targeting epigenetic and developmental pathways, it is possible to eradicate drug-resistant tumor cells and prevent disease recurrence. Another study (Xiao et al., 2017) revealed evidence demonstrating up-regulated chromatin remodeling factor lymphoid-specific helicase (LSH) promoted the development of glioma. Research (Xiao et al., 2017) indicates that the up-regulated transcription factor E2F1 and glycogen synthase kinase-3β (GSK-3β, an intact complex of E2F1) in astrocytomas and GBM were associated with the progression of glioma and correlated with LSH expression. The depletion of E2F1 decreased LSH expression and cell growth, while inhibition of GSK3β increased the enrichment of E2F1 to the LSH promoter, and increased LSH expression. Lipoprotein receptor-related protein 6 (LRP6), an upstream regulator of GSK3β signaling pathway, was also over expressed in glioma tissue. Knockdown of LRP6 reduced LSH expression level through decreased recruitment of E2F1 to the LSH promoter, finally leading to inhibition of cell growth. Taken together, a mechanistic link between LSH expression and activation of the LPR6/GSK3β/E2F1 axis in glioma illustrates a novel role of LSH in malignant astrocytomas and GBM. Understanding the roles of LSH in glioma progression will not only enrich our knowledge of glioma but also frame LSH as a potential therapeutic target for the treatment of these deadly brain cancers.

HISTONE MODIFICATIONS

In the mammalian epigenome, histone modifications can occur in many ways. The basic unit of histone, called nucleosome, is an octamer that consists of two H2A, two H2B, two H3, two H4 and 147 base pairs wound outside of the composition (de Ruijter et al., 2003; **Figure 1**). The core histone has C-terminal and N-terminal binding regions. Of these, the N-terminal is particularly relevant, since lysine residue of the N-terminal extends out of the nucleosome and is accessible for modifications, including acetylation, methylation, phosphorylation, ubiquitination and ADP ribosylation. These modifications subsequently alter the expression of the gene without altering the base pair (Wang et al., 2014; Mathias et al., 2015). The total process, known as epigenetic regulation, involves a variety of enzymes. Scientists have classified these enzymes according to their functions (Liu et al., 2011): "writers" (enzymes that add groups such as methyl, acetyl and glycans), "erasers" (enzymes that remove post-translational modifications) and "readers" (enzymes that recognize these epigenetic markers and regulate epigenetic effects). The protein complexes that promote the movement of nucleosomes on chromatin are called "movers." From this enormous pool, many therapeutic targets are derived as a single target or as combinations, apart from the most prominent DNMTs and histone deacetylases (HDACs).

Dysregulation of Histone Modifications in Glioma

Aberrant histone modifications can lead to transcriptional abnormalities in gene expression that eventually lead to the development and progression of glioma. Among the various histone modification proteins, two have attracted more attention than the others—HDACs, which cause histone deacetylation, and histone methyltransferases, which cause methylation at various sites of histone (Zang et al., 2014). Among the different classes of HDAC enzymes, HDAC1 (Wang et al., 2017), HDAC2, HDAC3 (Leng et al., 2016), HDAC5 and HDAC9 (Milde et al., 2010) have undergone significant changes in glioma cells. H3 acetylation levels are elevated in high-grade astrocytoma compared to low-grade medulloblastoma and normal brain tissues, as are the expression of HDAC5 and HDAC9 (Milde et al., 2010) in high-grade medulloblastoma. One survey demonstrated that mRNA levels of class II and IV HDACs were down-regulated in GBM compared to low-grade astrocytomas and normal brain tissues (Lucio-Eterovic et al., 2008). The use of HDAC inhibitors (HDACIs) for the treatment of cancer is an area of active investigation. In glioma treatment, HDACIs have been used for the treatment of GBM in combination with RT therapy and chemotherapy (Shi et al., 2016; Ghiaseddin et al., 2018). The anti-tumor mechanism of HDACIs includes blocking cell cycle and promoting cell differentiation, and inducing apoptosis and inhibiting angiogenesis, which can inhibit proliferation and apoptosis of various tumor cells (Marks and Breslow, 2007).

In glioma cells, histone methyltransferases G9a, EZH2, MLL1 and MLL2 (Chang et al., 2009; Cheung et al., 2012; Liu F. et al., 2013; Kondengaden et al., 2016; Wiese et al., 2016; Banasavadi-Siddegowda et al., 2018) regulated the methylation level of lysine located in histone (**Table 3**); these modifications were closely related to gene transcription regulation and genome integration (Heddleston et al., 2012; Zhou et al., 2016). Protein arginine methyltransferase 5 (PRMT5) is another candidate gene for the diagnosis and treatment of glioma, its nuclear expression correlates with poor survival in glioma patients. Banasavadi-Siddegowda et al. (2018) revealed that GBM cells treated with PRMT5 inhibitor mirrored the effects of PRMT5 knockdown, wherein it led to apoptosis of differentiated GBM cells and drove undifferentiated primary patient-derived GBM cells into a non-replicative senescent state.

Inhibiting the activities of histone methyltransferases or HDACs can suppress glioma cell proliferation and induce apoptosis (Sharma et al., 2010; Vargas et al., 2014), suggesting that the inhibitors of these proteins could be candidate drugs for the treatment of glioma. Recently, Ghildiyal and Sen (2017) reported that histone methyltransferase G9a that regulated H3K9 dimethylation has also correlated with the development and progression of glioma, and its inhibitors have also been reported as potential agents for the treatment of glioma (Guo et al., 2016).

It is worth noting that no post-translational modifications processes exist in isolation but rather act with mutual influence and coordination, usually referred to as histone crosstalk. In our earlier research (Zang et al., 2017), we found that simultaneously inhibiting the activity of HDAC and G9a would yield better effects than inhibiting single targets. In our anti-proliferation experiment, multiple cancer phenotypes including leukemia, prostatic carcinoma, hepatocellular carcinoma and pulmonary carcinoma and breast carcinoma were used in this study. Compared to the single target suppression effect, simultaneous inhibition of the activities for two protein targets showed a better anti-proliferation effect in parts of the tumor cell lines, such as breast carcinoma. As illustrated in **Figure 1**, under the cooperation of G9a inhibitor and HDACIs, more sites in histone tails are free to be acetylated. This acetylation status can activate cancer suppression gene transcription and alleviate the disease. Thus, developing high activity HDAC and G9a hybrid inhibitors is another effective route in targeted epigenetic therapy.

The Polycomb group (PcG) protein family is a group of gene regulatory factors that play a role in embryonic development (Zhao et al., 2017). They are divided into two protein complexes based on function, namely PRC1 and PRC2 (Collinson et al., 2016). PRC2 is a multi-protein complex responsible for the methylation of H3 at lysine 27 (H3K27Me). Zeste Gene Enhancer Homolog 2 (EZH2) is a catalytic subunit that constitutes the PRC2 protein complex (Collinson et al., 2016). Current studies (Orzan et al., 2011; Chen et al., 2017) indicated that EZH2 is over expressed in many tumor tissues, including glioma, and is closely related to the malignant progression, invasion and metastasis of the tumors. In the cellular level of research, EZH2 gene silencing technology or using EZH2 inhibitors prevented glioma cell proliferation (Kurmasheva et al., 2017). Therefore, focusing on EZH2 as a new target may pave a new way for the treatment of clinical glioma (Zhang Y. et al., 2017). In pediatric GBM, H3F3A involves two critical single-point mutations in the histone tail at lysine (K) 27 (K27M) and glycine (G) 34 (G34R/V) that are both involved with key regulatory post-transcriptional modifications (Schwartzentruber et al., 2012). The discovery of these molecular markers provides a basis for the diagnosis of this type of glioma and

TABLE 3 | Enzymes and inhibitors related to the pathogenesis of glioma.

Class	Proteins	Inhibitors	References
Histone deacetylases	HDAC2, HDAC9, HDAC1, HDAC3,	Vorinostat, Panobinostat, Romidepsin, Valproic acid,	Lucio-Eterovic et al. (2008)
Histone methyltransferases	MLL, G9a, EHMT1, SMYD4, EZH2, PRMT5, PRMT1	BIX01294, UNC0642, DCG066, EPZ-6438	Chang et al. (2009), Cheung et al. (2012), Liu F. et al. (2013), Kondengaden et al. (2016), Wiese et al. (2016), Banasavadi-Siddegowda et al. (2018)

will lay the foundation for further diagnosis and treatment research.

PRESENT CLINICAL WORKFLOW

DNA methylation by DNMT leads to the gene silencing of tumor suppressor genes (Dammann et al., 2017). The inhibition of DNMTs can achieve reactivation of transcription of these critical genes (Castillo-Aguilera et al., 2017). Thus, the study of DNMT inhibitors has become a new bright spot in the treatment of glioma. Among the DNMT inhibitors that have now entered the clinical trials, 5-aza-2′-deoxycytidine (Chu et al., 2013) is the most representative. In tumor cells, 5-aza-2′-deoxycytidine is blended with DNA in the form of phosphate, and then inhibit DNMT activity, eventually leading to the desired low methylation status to exert antitumor effects (Sun et al., 2011). Currently the clinical research of 5-aza-2′-deoxycytidine is limited in leukemia (Roboz et al., 2018) and part of solid tumors (Garrido-Laguna et al., 2013; Fan et al., 2014; lung cancer, etc., not including glioma). For glioma treatment, most of the studies with 5-aza-2′-deoxycytidine are still in pre-clinical research stage (Oi et al., 2009; Zhang et al., 2014).

HDACIs can inhibit glioma oncogene transcription and have a variety of effects on cell life cycle. HDACIs can arrest cell division in G1 and G2 phases, induce cell differentiation and apoptosis (Hazane-Puch et al., 2016), destroy the combination of heat shock protein and substrate protein, promote degradation of oncoprotein, and also inhibit the growth and proliferation of glioma by inhibiting tumor angiogenesis (Pei et al., 2016). DNMT inhibitors and HDACIs can be used for the treatment of various tumors, either individually or as a synergistic combination (Xu et al., 2014; Pathania et al., 2016). In glioma, as a new therapeutic drug, HDACIs provide new directions for the treatment of glioma. Already many HDACIs have entered the phase I/II clinical trials (**Table 4**) alone or in combination with other chemotherapeutic agents such as TMZ and radiotherapy for the treatment of various types of glioma, including diffuse intrinsic pontine glioma (DIPG), progressive, or recurrent GBM (Lee et al., 2012; Krauze et al., 2015; Kim et al., 2017).

One phase I study conducted by the Children's Oncology Group (COG) investigated vorinostat with TMZ in relapsed or refractory primary CNS tumors (Hummel et al., 2013). Five-day cycles of vorinostat in combination with TMZ were well tolerated in children with recurrent CNS malignancies, with myelosuppression as the dose-limiting toxicities (DLT). Accumulation of acetylated H3 in peripheral blood mononuclear cells (PBMC) was observed after administration of vorinostat. One phase II trial of vorinostat on recurrent GBM was reported by the North Central Cancer Treatment Group (Galanis et al., 2009). In this study, vorinostat monotherapy was well tolerated in patients with recurrent GBM, and there were obvious increases in acetylation levels of H2B, H3 and H4 after treatment. Microarray RNA analysis showed changes in genes regulated by vorinostat, such as up-regulation of E-cadherin.

TABLE 4 | Summary of epigenetic drugs for glioma that entered in phase I/II clinical trials.

	Clinical trial	Population	Phase	References
Vorinostat	Vorinostat;	Adult: recurrent GBM; Pediatric: refractory solid tumors	II	Galanis et al. (2009), Fouladi et al. (2010)
	Vorinostat and temozolomide;	Pediatric: relapsed or refractory primacy CNS tumors; Adult: high-grade glioma	I	Lee et al. (2012), Hummel et al. (2013)
	Vorinostat and bortezomib;	Pediatric: refractory or recurrent solid tumors; Adult: advanced malignancies	I/II	Muscal et al. (2013), Schelman et al. (2013)
	Vorinostat, erlotinib and radiation;	Adult: GBM (ineffective)	I	Peereboom et al. (2010)
	Vorinostat, temozolomide and radiotherapy;	Adult: GBM	I/II	Galanis et al. (2018)
	Vorinostat and bevacizumab;	Adult: recurrent World Health Organization Grade 4 malignant glioma	II	Ghiaseddin et al. (2018)
	Vorinostat, bevacizumab and temozolomide;	Adult: GBM	I/II	Krauze et al. (2015)
Panobinostat	Panobinostat and bevacizumab;	Adult: recurrent glioblastoma and anaplastic glioma; (no continued accrual)	II	Lee et al. (2015)
	Panobinostat with fractionated stereotactic re-irradiation;	Adult: recurrent HGG	I	Shi et al. (2016)
Romidepsin	Romidepsin;	Adult: recurrent GBM; (ineffective)	I	Iwamoto et al. (2011)
valproic acid	valproic acid;	Pediatric: refractory solid or CNS tumors	I	Su et al. (2011)
	valproic acid, temozolomide and radiotherapy;	Adult: GBM	II	Krauze et al. (2015)

With regards to panobinostat, one phase II study of panobinostat in combination with bevacizumab (BEV) was attempted in individuals with recurrent GBM and anaplastic glioma, but part of this study did not meet the criteria for continued accrual and was closed (Lee et al., 2015). Prior to closure, the treatment was reasonably well tolerated in both cohorts, but the addition of panobinostat to BEV did not significantly improve 6-month progression-free survival (PFS6) compared to historical controls of BEV monotherapy in either cohort. More preclinical evidences have shown that panobinostat may act as a radiosensitizer. A phase I trial combining panobinostat with stereotactic re-irradiation in patients with recurrent HGG has been reported (Shi et al., 2016). The results were more promising than panobinostat with BEV, with a PFS6 of 83% in the panobinostat and stereotactic re-irradiation therapy group, compared to 30.4% in the panobinostat with BEV group.

Another phase I study of valproic acid (VPA) in pediatric patients with refractory solid or CNS tumors was conducted by COG (Su et al., 2011). Histone hyperacetylation was observed in half of the patients at steady state. Krauze et al. (2015) recently conducted a phase II study of concurrent radiation therapy, TMZ, and VPA for patients with GBM. The results of this study demonstrated that the addition of VPA to concurrent RT/TMZ in patients with newly diagnosed GBM was well tolerated. VPA may result in improved outcomes compared to historical data and merits further study.

Overall, HDACIs as monotherapy or a combination therapy seem promising in improving prognosis in this difficulty to treat malignancy glioma (**Table 4**). For the possible toxicity that epigenetic drugs may present during treatment, improving the dosage regimen (Issa et al., 2004) or developing new epigenetic therapies or gaining knowledge of how to synchronize them with other treatment modalities are good choices to alleviate this toxic effect. So far, HDAC inhibitors, vorinostat and valproic acid can both combine with TMZ and/or RT to exert good effects in clinical trials to treat children with refractory or recurrent CNS malignancies or adult GBM (Lee et al., 2012; Hummel et al., 2013; Krauze et al., 2015). This is a good trend for our future clinical research. Vorinostat combined with erlotinib or panobinostat with BEV did not show obvious effects (Peereboom et al., 2010; Lee et al., 2015). Though the results are not optimistic, they provide valuable information for future research. In recent years, immunotherapy combined with other drugs has been a hot topic in cancer treatment, but few clinical trials were reported on combining the HDACIs with Gene-Mediated Cytotoxic Immunotherapy (G-MCI). Most G-MCI were preferred to combine with TMZ and standard of care (SOC) radiation after surgery, and survival outcomes were most notably improved in patients with minimal residual disease after gross total resection (Chiocca et al., 2011; Wheeler et al., 2016).

Although there are few clinical trials on the combination of glioma immunotherapy and epigenetics, many basic studies on immunotherapy and epigenetics of glioma were reported recently (Gallagher et al., 2017; Bhat et al., 2018). Studies have shown that tumor cells can use epigenetic mechanisms to alter their autoimmune origin and disrupt the process of recognition between tumor cells and the immune system. By DNA methylation or histone modifications, tumor cells can directly or indirectly down-regulate the expression levels of key molecules in the tumor immunoreaction process, thereby destroying the immune recognition and killing tumor cells (Maio et al., 2015). At present, the immunotherapeutic drugs that can combine with epigenetic drugs mainly include cytokines immunosuppressive agents, polypeptide vaccines, immunological adjuvants and tumor cell vaccine agents. Epigenetic drugs combined with tumor immunotherapy drugs will become an important research direction for the future treatment of tumors, and also provide new ideas for the treatment of glioma. With the development of improved medical standards, we believe more high-quality phase trials in newly diagnosed and recurrent GBM are imperative.

CONCLUSIONS AND PERSPECTIVES

Glioma is a common primary malignant brain tumor with high recurrence rates, short survival times, high rates of mortality and treatment difficulties. For all grades of glioma patients, the largest range of safe resection remains the central step in current comprehensive treatment strategies (Kreth et al., 2013). Prior treatments of these tumors had taught us that conventional surgeries and chemo-radiotherapy protocols can only minimally improve the quality of life and slightly prolong the survival of some patients. The postoperative treatments, including radiation, chemotherapy, the dose and the cycle, should be implemented after comprehensive evaluation based on factors such as patient's age, operation circumstances, histopathological classification and molecular characteristics (Jiang et al., 2016). Further investigations and reviews of the treatment strategies for malignant glioma are needed.

The genetic instability and heterogeneity of glioma are prominent. The mutual regulation mechanisms of related signal transduction pathways, which are not yet fully understood, are essential for the determination of therapeutic targets and drug development process. In the study of epigenetic therapy, multi-target combined inhibition is a critical concept in targeted drug development. In addition to single drug with multi-target inhibition, the combined use of multiple targeted drugs is also important, including those mentioned in this study (e.g., HDAC and G9a). However, even if the targeted drugs are tested in combination, the number of trials is quite large and pre-clinical pre-screening of drugs is therefore necessary. Whether the targeted drug can act on the expected target site and whether it can effectively inhibit the downstream signaling pathways, the potential toxic and side effects, are related to the safety and efficacy of targeted therapy. These issues need to be studied in depth.

Overall, epigenetic modifications are closely related to glioma proliferation, metastasis, invasion and prognosis. Various epigenetic modifications closely interact to participate in the occurrence and progression of glioma. Breakthroughs in the treatment of glioma require advances in scientific research,

improvements in therapeutic technologies and protocols, and the development of diagnosis and treatment around individualized protocols. The epigenetic phenomena of glioma, including DNA methylation, abnormal microRNA, chromatin remodeling and histone modifications, have excellent potential significance and application to the diagnosis, treatment, and prognosis of glioma. Among the four fields, the methylation level of the gene promoter region can be taken as a guide for glioma diagnosis, and also related to the prognosis of the glioma (Mur et al., 2015), miRNAs play many critical roles in the progression of glioma (Zhang C. et al., 2012), the protein levels of enzymes that regulate histone modifications are candidates for the diagnosis of the glioma, and its inhibitors are good candidate drugs for the treatment of glioma (Sharma et al., 2010; Vargas et al., 2014). These phenomena might also help monitor high-risk groups, and assist in tumor risk assessment, judgment of tumor recurrence, prediction of tumor treatment efficacy and prognosis and development of specific new target drugs. It is believed that with the improvement of detection methods and experimental methods, promising results will be achieved in the fields of glioma prevention, diagnosis and treatment. Biotherapy, including gene therapy, immunotherapy and targeted molecular therapy, provides a new hope for the treatment of glioma. Some of these therapies have been shown to be effective in preclinical studies and safe in phase I clinical trials (Maio et al., 2015). Yet, clinical trials in phase II and III have been conducted. Based on our review, except HDACIs, a new therapeutic and epigenetic drug that can be taken alone or combined with other drugs or other treatments, the combination of epigenetic drugs with biotherapy is also a particularly interesting and novel direction for the future treatment of tumors. Due to the complicated pathogenesis of glioma, epigenetic applications to glioma clinical treatment are still limited. Discovering more effective therapeutic targets, developing novel targeted drugs, improving the efficacy of existing drugs in clinical research, and reducing the side effects of existing drugs are the problems that we need to face and solve in clinical treatment. With continued research, epigenetics understanding is certain to improve and, so is the epigenetic-based treatment of glioma.

AUTHOR CONTRIBUTIONS

XH and LZ conceived and designed the project. Each author has contributed significantly to the submitted work. LZ drafted the manuscript. SK, FC and LW revised the manuscript. All authors read and approved the final manuscript.

FUNDING

This work was supported by the China Postdoctoral Science Foundation (number 2018M632679); Medical and Health Science and Technology Development Project of Shandong Province (number 2017WS639); Linyi Science and Technology Development Project (number 201717024); Linyi People's Hospital Doctoral Research Foundation (number 2016LYBS02); Key Research Project program of Shandong Province (number 2016GSF201056); and the Natural Science Foundation of Shandong Province (number ZR2014HM077).

REFERENCES

Alaminos, M., Dávalos, V., Ropero, S., Setién, F., Paz, M. F., Herranz, M., et al. (2005). *EMP3*, a myelin-related gene located in the critical 19q13.3 region, is epigenetically silenced and exhibits features of a candidate tumor suppressor in glioma and neuroblastoma. *Cancer Res.* 65, 2565–2571. doi: 10.1158/0008-5472.can-04-4283

Antonelli, G., Libra, M., Panebianco, V., Russo, A. E., Vitale, F. V., Colina, P., et al. (2016). Molecular-targeted therapy for elderly patients with advanced non-small cell lung cancer. *Oncol. Lett.* 11, 3–8. doi: 10.3892/ol.2015.3901

Bai, Y., Liao, H., Liu, T., Zeng, X., Xiao, F., Luo, L., et al. (2013). MiR-296–3p regulates cell growth and multi-drug resistance of human glioblastoma by targeting ether-à-go-go (EAG1). *Eur. J. Cancer* 49, 710–724. doi: 10.1016/j.ejca.2012.08.020

Bai, Y., Zhang, Q.-G., and Wang, X.-H. (2014). Downregulation of TES by hypermethylation in glioblastoma reduces cell apoptosis and predicts poor clinical outcome. *Eur. J. Med. Res.* 19:66. doi: 10.1186/s40001-014-0066-4

Banasavadi-Siddegowda, Y. K., Welker, A. M., An, M., Yang, X., Zhou, W., Shi, G., et al. (2018). PRMT5 as a druggable target for glioblastoma therapy. *Neuro Oncol.* 20, 753–763. doi: 10.1093/neuonc/nox206

Bartel, D. P. (2004). MicroRNAs: genomics, biogenesis, mechanism, and function. *Cell* 116, 281–297. doi: 10.1016/S0092-8674(04)00045-5

Berdasco, M., Ropero, S., Setien, F., Fraga, M. F., Lapunzina, P., Losson, R., et al. (2009). Epigenetic inactivation of the Sotos overgrowth syndrome gene histone methyltransferase NSD1 in human neuroblastoma and glioma. *Proc. Natl. Acad. Sci. U S A* 106, 21830–21835. doi: 10.1073/pnas.0906831106

Berghoff, A. S., Hainfellner, J. A., Marosi, C., and Preusser, M. (2015). Assessing MGMT methylation status and its current impact on treatment in glioblastoma. *CNS Oncol.* 4, 47–52. doi: 10.2217/cns.14.50

Berindan-Neagoe, I., Monroig Pdel, C., Pasculli, B., and Calin, G. A. (2014). MicroRNAome genome: a treasure for cancer diagnosis and therapy. *CA Cancer J. Clin.* 64, 311–336. doi: 10.3322/caac.21244

Bhat, J., Kouakanou, L., Peters, C., Yin, Z., and Kabelitz, D. (2018). Immunotherapy with human gamma delta T cells—synergistic potential of epigenetic drugs? *Front. Immunol.* 9:512. doi: 10.3389/fimmu.2018.00512

Biegel, J. A., Busse, T. M., and Weissman, B. E. (2014). SWI/SNF chromatin remodeling complexes and cancer. *Am. J. Med. Genet. C Semin. Med. Genet.* 166C, 350–366. doi: 10.1002/ajmg.c.31410

Bird, A. (2002). DNA methylation patterns and epigenetic memory. *Genes Dev.* 16, 6–21. doi: 10.1101/gad.947102

Bleeker, F. E., Atai, N. A., Lamba, S., Jonker, A., Rijkeboer, D., Bosch, K. S., et al. (2010). The prognostic $IDH1^{R132}$ mutation is associated with reduced $NADP^{+}$-dependent IDH activity in glioblastoma. *Acta Neuropathol.* 119, 487–494. doi: 10.1007/s00401-010-0645-6

Cai, J. J., Qi, Z. X., Chen, L. C., Yao, Y., Gong, Y., and Mao, Y. (2016). miR-124 suppresses the migration and invasion of glioma cells *in vitro* via Capn4. *Oncol. Rep.* 35, 284–290. doi: 10.3892/or.2015.4355

Castillo-Aguilera, O., Depreux, P., Halby, L., Arimondo, P. B., and Goossens, L. (2017). DNA methylation targeting: the DNMT/HMT crosstalk challenge. *Biomolecules* 7:E3. doi: 10.3390/biom7010003

Chang, Y., Zhang, X., Horton, J. R., Upadhyay, A. K., Spannhoff, A., Liu, J., et al. (2009). Structural basis for G9a-like protein lysine methyltransferase inhibition by BIX-01294. *Nat. Struct. Mol. Biol.* 16, 312–317. doi: 10.1038/nsmb.1560

Chédin, F. (2011). The DNMT3 family of mammalian *de novo* DNA methyltransferases. *Prog. Mol. Biol. Transl. Sci.* 101, 255–285. doi: 10.1016/b978-0-12-387685-0.00007-x

Chen, P. H., Chang, C. K., Shih, C. M., Cheng, C. H., Lin, C. W., Lee, C. C., et al. (2016). The miR-204–3p-targeted IGFBP2 pathway is involved in xanthohumol-induced glioma cell apoptotic death. *Neuropharmacology* 110, 362–375. doi: 10.1016/j.neuropharm.2016.07.038

Chen, X., Ma, H., Wang, Z., Zhang, S., Yang, H., and Fang, Z. (2017). EZH2 palmitoylation mediated by ZDHHC5 in p53-mutant glioma drives malignant development and progression. *Cancer Res.* 77, 4998–5010. doi: 10.1158/0008-5472.can-17-1139

Chen, L., Zhang, J., Feng, Y., Li, R., Sun, X., Du, W., et al. (2012). MiR-410 regulates MET to influence the proliferation and invasion of glioma. *Int. J. Biochem. Cell Biol.* 44, 1711–1717. doi: 10.1016/j.biocel.2012.06.027

Chen, X., Zhang, Y., Shi, Y., Lian, H., Tu, H., Han, S., et al. (2015). MiR-873 acts as a novel sensitizer of glioma cells to cisplatin by targeting Bcl-2. *Int. J. Oncol.* 47, 1603–1611. doi: 10.3892/ijo.2015.3143

Chen, G., Zhu, W., Shi, D., Lv, L., Zhang, C., Liu, P., et al. (2010). MicroRNA-181a sensitizes human malignant glioma U87MG cells to radiation by targeting Bcl-2. *Oncol. Rep.* 23, 997–1003. doi: 10.3892/or_00000725

Cheung, H. C., Yatsenko, S. A., Kadapakkam, M., Legay, H., Su, J., Lupski, J. R., et al. (2012). Constitutional tandem duplication of 9q34 that truncates *EHMT1* in a child with ganglioglioma. *Pediatr. Blood Cancer* 58, 801–805. doi: 10.1002/pbc.23219

Chien, L.-N., Gittleman, H., Ostrom, Q.-T., Hung, K.-S., Sloan, A.-E., Hsieh, Y.-C., et al. (2016). Comparative brain and central nervous system tumor incidence and survival between the united states and taiwan based on population-based registry. *Front. Public Health* 4:151. doi: 10.3389/fpubh.2016.00151

Chiocca, E. A., Aguilar, L. K., Bell, S. D., Kaur, B., Hardcastle, J., Cavaliere, R., et al. (2011). Phase IB study of gene-mediated cytotoxic immunotherapy adjuvant to up-front surgery and intensive timing radiation for malignant glioma. *J. Clin. Oncol.* 29, 3611–3619. doi: 10.1200/JCO.2011.35.5222

Choi, Y. J., Yoo, N. J., and Lee, S. H. (2015). Mutation of HELLS, a chromatin remodeling gene, gastric and colorectal cancers. *Pathol. Oncol. Res.* 21, 851–852. doi: 10.1007/s12253-014-9862-y

Choudhury, S. R., Cui, Y., Milton, J. R., Li, J., and Irudayaraj, J. (2015). Selective increase in subtelomeric DNA methylation: an epigenetic biomarker for malignant glioma. *Clin. Epigenetics* 7:107. doi: 10.1186/s13148-015-0140-y

Chu, S. H., Feng, D. F., Ma, Y. B., Zhang, H., Zhu, Z. A., Li, Z. Q., et al. (2011). Promoter methylation and downregulation of SLC22A18 are associated with the development and progression of human glioma. *J. Transl. Med.* 9:156. doi: 10.1186/1479-5876-9-156

Chu, B. F., Karpenko, M. J., Liu, Z., Aimiuwu, J., Villalona-Calero, M. A., Chan, K. K., et al. (2013). Phase I study of 5-aza-2'-deoxycytidine in combination with valproic acid in non-small-cell lung cancer. *Cancer Chemother. Pharmacol.* 71, 115–121. doi: 10.1007/s00280-012-1986-8

Collinson, A., Collier, A. J., Morgan, N. P., Sienerth, A. R., Chandra, T., Andrews, S., et al. (2016). Deletion of the polycomb-group protein EZH2 leads to compromised self-renewal and differentiation defects in human embryonic stem cells. *Cell Rep.* 17, 2700–2714. doi: 10.1016/j.celrep.2016.11.032

Dammann, R. H., Richter, A. M., Jiménez, A. P., Woods, M., Kuster, M., and Witharana, C. (2017). Impact of natural compounds on DNA methylation levels of the tumor suppressor gene *RASSF1A* in cancer. *Int. J. Mol. Sci.* 18:E2160. doi: 10.3390/ijms18102160

de Ruijter, A. J., van Gennip, A. H., Caron, H. N., Kemp, S., and van Kuilenburg, A. B. (2003). Histone deacetylases (HDACs): characterization of the classical HDAC family. *Biochem. J.* 370, 737–749. doi: 10.1042/bj20021321

de Souza, C. F., Sabedot, T. S., Malta, T. M., Stetson, L., Morozova, O., Sokolov, A., et al. (2018). A distinct DNA methylation shift in a subset of glioma CpG island methylator phenotypes during tumor recurrence. *Cell Rep.* 23, 637–651. doi: 10.1016/j.celrep.2018.03.107

Dong, X., Deng, Q., Nie, X., Zhang, M., Jia, W., Chen, C., et al. (2015). Downregulation of HTATIP2 expression is associated with promoter methylation and poor prognosis in glioma. *Exp. Mol. Pathol.* 98, 192–199. doi: 10.1016/j.yexmp.2015.01.013

Dong, C. G., Wu, W. K., Feng, S. Y., Wang, X. J., Shao, J. F., and Qiao, J. (2012). Co-inhibition of microRNA-10b and microRNA-21 exerts synergistic inhibition on the proliferation and invasion of human glioma cells. *Int. J. Oncol.* 41, 1005–1012. doi: 10.3892/ijo.2012.1542

Du, W., Liu, X., Chen, L., Dou, Z., Lei, X., Chang, L., et al. (2015). Targeting the SMO oncogene by miR-326 inhibits glioma biological behaviors and stemness. *Neuro Oncol.* 17, 243–253. doi: 10.1093/neuonc/nou217

Echizen, K., Nakada, M., Hayashi, T., Sabit, H., Furuta, T., Nakai, M., et al. (2014). PCDH10 is required for the tumorigenicity of glioblastoma cells. *Biochem. Biophys. Res. Commun.* 444, 13–18. doi: 10.1016/j.bbrc.2013.12.138

Emdad, L., Janjic, A., Alzubi, M. A., Hu, B., Santhekadur, P. K., Menezes, M. E., et al. (2015). Suppression of miR-184 in malignant gliomas upregulates SND1 and promotes tumor aggressiveness. *Neuro Oncol.* 17, 419–429. doi: 10.1093/neuonc/nou220

Endo, A., Ly, T., Pippa, R., Bensaddek, D., Nicolas, A., and Lamond, A. I. (2017). The chromatin assembly factor complex 1 (CAF1) and 5-azacytidine (5-AzaC) affect cell motility in src-transformed human epithelial cells. *J. Biol. Chem.* 292, 172–184. doi: 10.1074/jbc.m116.751024

Ernst, A., Campos, B., Meier, J., Devens, F., Liesenberg, F., Wolter, M., et al. (2010). De-repression of CTGF via the miR-17–92 cluster upon differentiation of human glioblastoma spheroid cultures. *Oncogene* 29, 3411–3422. doi: 10.1038/onc.2010.83

Esteller, M., Garcia-Foncillas, J., Andion, E., Goodman, S. N., Hidalgo, O. F., Vanaclocha, V., et al. (2000). Inactivation of the DNA-repair gene MGMT and the clinical response of gliomas to alkylating agents. *N. Engl. J. Med.* 343, 1350–1354. doi: 10.1056/NEJM200011093431901

Fabbri, E., Brognara, E., Montagner, G., Ghimenton, C., Eccher, A., Cantu, C., et al. (2015). Regulation of IL-8 gene expression in gliomas by microRNA miR-93. *BMC Cancer* 15:661. doi: 10.1186/s12885-015-1659-1

Fan, H., Lu, X., Wang, X., Liu, Y., Guo, B., Zhang, Y., et al. (2014). Low-dose decitabine-based chemoimmunotherapy for patients with refractory advanced solid tumors: a phase I/II report. *J. Immunol. Res.* 2014:371087. doi: 10.1155/2014/371087

Fang, L., Deng, Z., Shatseva, T., Yang, J., Peng, C., Du, W. W., et al. (2011). MicroRNA miR-93 promotes tumor growth and angiogenesis by targeting integrin-β8. *Oncogene* 30, 806–821. doi: 10.1038/onc.2010.465

Fernandez, A. F., Bayón, G. F., Sierra, M. I., Urdinguio, R. G., Toraño, E. G., García, M., et al. (2018). Loss of 5hmC identifies a new type of aberrant DNA hypermethylation in glioma. *Hum. Mol. Genet.* 27, 3046–3059. doi: 10.1093/hmg/ddy214

Flavahan, W. A., Drier, Y., Liau, B. B., Gillespie, S. M., Venteicher, A. S., Stemmer-Rachamimov, A. O., et al. (2016). Insulator dysfunction and oncogene activation in IDH mutant gliomas. *Nature* 529, 110–114. doi: 10.1038/nature16490

Foltz, G., Ryu, G. Y., Yoon, J. G., Nelson, T., Fahey, J., Frakes, A., et al. (2006). Genome-wide analysis of epigenetic silencing identifies BEX1 and BEX2 as candidate tumor suppressor genes in malignant glioma. *Cancer Res.* 66, 6665–6674. doi: 10.1158/0008-5472.can-05-4453

Fouladi, M., Park, J. R., Stewart, C. F., Gilbertson, R. J., Schaiquevich, P., Sun, J., et al. (2010). Pediatric phase I trial and pharmacokinetic study of vorinostat: a Children's Oncology Group phase I consortium report. *J. Clin. Oncol.* 28, 3623–3629. doi: 10.1200/JCO.2009.25.9119

Fowler, A., Thomson, D., Giles, K., Maleki, S., Mreich, E., Wheeler, H., et al. (2011). miR-124a is frequently down-regulated in glioblastoma and is involved in migration and invasion. *Eur. J. Cancer* 47, 953–963. doi: 10.1016/j.ejca.2010.11.026

Gal, H., Pandi, G., Kanner, A. A., Ram, Z., Lithwick-Yanai, G., Amariglio, N., et al. (2008). MIR-451 and Imatinib mesylate inhibit tumor growth of Glioblastoma stem cells. *Biochem. Biophys. Res. Commun.* 376, 86–90. doi: 10.1016/j.bbrc.2008.08.107

Galanis, E., Anderson, S. K., Miller, C. R., Sarkaria, J. N., Jaeckle, K., Buckner, J. C., et al. (2018). Phase I/II trial of vorinostat combined with temozolomide and radiation therapy for newly diagnosed glioblastoma: results of Alliance N0874/ABTC 02. *Neuro Oncol.* 20, 546–556. doi: 10.1093/neuonc/nox161

Galanis, E., Jaeckle, K. A., Maurer, M. J., Reid, J. M., Ames, M. M., Hardwick, J. S., et al. (2009). Phase II trial of vorinostat in recurrent glioblastoma multiforme: a north central cancer treatment group study. *J. Clin. Oncol.* 27, 2052–2058. doi: 10.1200/JCO.2008.19.0694

Gallagher, S. J., Shklovskaya, E., and Hersey, P. (2017). Epigenetic modulation in cancer immunotherapy. *Curr. Opin. Pharmacol.* 35, 48–56. doi: 10.1016/j.coph.2017.05.006

Gao, Y., Guan, M., Su, B., Liu, W., Xu, M., and Lu, Y. (2004). Hypermethylation of the RASSF1A gene in gliomas. *Clin. Chim. Acta* 349, 173–179. doi: 10.1016/j.cccn.2004.07.006

Garrido-Laguna, I., McGregor, K. A., Wade, M., Weis, J., Gilcrease, W., Burr, L., et al. (2013). A phase I/II study of decitabine in combination with panitumumab in patients with wild-type (wt) KRAS metastatic colorectal cancer. *Invest. New Drugs* 31, 1257–1264. doi: 10.1007/s10637-013-9947-6

Gessler, F., Voss, V., Seifert, V., Gerlach, R., and Kögel, D. (2011). Knockdown of TFPI-2 promotes migration and invasion of glioma cells. *Neurosci. Lett.* 497, 49–54. doi: 10.1016/j.neulet.2011.04.027

Ghasemi, A., Fallah, S., and Ansari, M. (2016). MiR-153 as a tumor suppressor in glioblastoma multiforme is downregulated by DNA methylation. *Clin. Lab.* 62, 573–580. doi: 10.7754/clin.lab.2015.150738

Ghiaseddin, A., Reardon, D., Massey, W., Mannerino, A., Lipp, E. S., Herndon, J. E., et al. (2018). Phase II study of bevacizumab and vorinostat for patients with recurrent world health organization grade 4 malignant glioma. *Oncologist* 23:157-e21. doi: 10.1634/theoncologist.2017-0501

Ghildiyal, R., and Sen, E. (2017). Concerted action of histone methyltransferases G9a and PRMT-1 regulates PGC-1α-RIG-I axis in IFNγ treated glioma cells. *Cytokine* 89, 185–193. doi: 10.1016/j.cyto.2015.12.008

Gömöri, E., Pál, J., Mészáros, I., Dóczi, T., and Matolcsy, A. (2007). Epigenetic inactivation of the hMLH1 gene in progression of gliomas. *Diagn. Mol. Pathol.* 16, 104–107. doi: 10.1097/pdm.0b013e318033f140

Götze, S., Wolter, M., Reifenberger, G., Müller, O., and Sievers, S. (2010). Frequent promoter hypermethylation of Wnt pathway inhibitor genes in malignant astrocytic gliomas. *Int. J. Cancer* 126, 2584–2593. doi: 10.1002/ijc.24981

Gu, J. J., Gao, G. Z., and Zhang, S. M. (2016). MiR-218 inhibits the tumorgenesis and proliferation of glioma cells by targeting Robo1. *Cancer Biomark.* 16, 309–317. doi: 10.3233/cbm-160568

Guo, A. S., Huang, Y. Q., Ma, X. D., and Lin, R. S. (2016). Mechanism of G9a inhibitor BIX01294 acting on U251 glioma cells. *Mol. Med. Rep.* 14, 4613–4621. doi: 10.3892/mmr.2016.5815

Hanai, K., Furuhashi, H., Yamamoto, T., Akasaka, K., and Hirose, S. (2008). RSF governs silent chromatin formation via histone H2Av replacement. *PLoS Genet.* 4:e1000011. doi: 10.1371/journal.pgen.1000011

Hao, J., Zhang, C., Zhang, A., Wang, K., Jia, Z., Wang, G., et al. (2012). miR-221/222 is the regulator of Cx43 expression in human glioblastoma cells. *Oncol. Rep.* 27, 1504–1510. doi: 10.3892/or.2012.1652

Hara, K., Kageji, T., Mizobuchi, Y., Kitazato, K. T., Okazaki, T., Fujihara, T., et al. (2015). Blocking of the interaction between Wnt proteins and their co-receptors contributes to the anti-tumor effects of adenovirus-mediated DKK3 in glioblastoma. *Cancer Lett.* 356, 496–505. doi: 10.1016/j.canlet.2014.09.045

Hashimshony, T., Zhang, J., Keshet, I., Bustin, M., and Cedar, H. (2003). The role of DNA methylation in setting up chromatin structure during development. *Nat. Genet.* 34, 187–192. doi: 10.1038/ng1158

Hashizume, R. (2017). Epigenetic targeted therapy for diffuse intrinsic pontine glioma. *Neurol. Med. Chir.* 57, 331–342. doi: 10.2176/nmc.ra.2017-0018

Hazane-Puch, F., Arnaud, J., Trocmé, C., Faure, P., Laporte, F., and Champelovier, P. (2016). Sodium selenite decreased HDAC activity, cell proliferation and induced apoptosis in three human glioblastoma cells. *Anticancer Agents Med. Chem.* 16, 490–500. doi: 10.2174/1871520615666150819095426

Heddleston, J. M., Wu, Q., Rivera, M., Minhas, S., Lathia, J. D., Sloan, A. E., et al. (2012). Hypoxia-induced mixed-lineage leukemia 1 regulates glioma stem cell tumorigenic potential. *Cell Death Differ.* 19, 428–439. doi: 10.1038/cdd.2011.109

Hegi, M. E., Diserens, A. C., Gorlia, T., Hamou, M. F., de Tribolet, N., Weller, M., et al. (2005). MGMT gene silencing and benefit from temozolomide in glioblastoma. *N. Engl. J. Med.* 352, 997–1003. doi: 10.1016/s0513-5117(08)70328-4

Hill, V. K., Underhill-Day, N., Krex, D., Robel, K., Sangan, C. B., Summersgill, H. R., et al. (2011). Epigenetic inactivation of the RASSF10 candidate tumor suppressor gene is a frequent and an early event in gliomagenesis. *Oncogene* 30, 978–989. doi: 10.1038/onc.2010.471

Horiguchi, K., Tomizawa, Y., Tosaka, M., Ishiuchi, S., Kurihara, H., Mori, M., et al. (2003). Epigenetic inactivation of RASSF1A candidate tumor suppressor gene at 3p21.3 in brain tumors. *Oncogene* 22, 7862–7865. doi: 10.1038/sj.onc.1207082

Hua, D., Ding, D., Han, X., Zhang, W., Zhao, N., Foltz, G., et al. (2012). Human miR-31 targets radixin and inhibits migration and invasion of glioma cells. *Oncol. Rep.* 27, 700–706. doi: 10.3892/or.2011.1555

Hu, H.-Q., Sun, L.-G., and Guo, W.-J. (2016). Decreased miRNA-146a in glioblastoma multiforme and regulation of cell proliferation and apoptosis by target Notch1. *Int. J. Biol. Markers* 31, e270–e275. doi: 10.5301/jbm.5000194

Hummel, T. R., Wagner, L., Ahern, C., Fouladi, M., Reid, J. M., McGovern, R. M., et al. (2013). A pediatric phase 1 trial of vorinostat and temozolomide in relapsed or refractory primary brain or spinal cord tumors: a Children's Oncology Group phase 1 consortium study. *Pediatr. Blood Cancer* 60, 1452–1457. doi: 10.1002/pbc.24541

Huse, J. T., Brennan, C., Hambardzumyan, D., Wee, B., Pena, J., Rouhanifard, S. H., et al. (2009). The PTEN-regulating microRNA miR-26a is amplified in high-grade glioma and facilitates gliomagenesis *in vivo*. *Genes Dev.* 23, 1327–1337. doi: 10.1101/gad.1777409

Issa, J. P., Garcia-Manero, G., Giles, F. J., Mannari, R., Thomas, D., Faderl, S., et al. (2004). Phase 1 study of low-dose prolonged exposure schedules of the hypomethylating agent 5-aza-2'-deoxycytidine (decitabine) in hematopoietic malignancies. *Blood* 103, 1635–1640. doi: 10.1182/blood-2003-03-0687

Iwamoto, F. M., Lamborn, K. R., Kuhn, J. G., Wen, P. Y., Yung, W. K., Gilbert, M. R., et al. (2011). A phase I/II trial of the histone deacetylase inhibitor romidepsin for adults with recurrent malignant glioma: north american brain tumor consortium study 03–03. *Neuro Oncol.* 13, 509–516. doi: 10.1093/neuonc/nor017

Jha, P., Pia Patric, I. R., Shukla, S., Pathak, P., Pal, J., Sharma, V., et al. (2014). Genome-wide methylation profiling identifies an essential role of reactive oxygen species in pediatric glioblastoma multiforme and validates a methylome specific for H3 histone family 3A with absence of G-CIMP/isocitrate dehydrogenase 1 mutation. *Neuro Oncol.* 16, 1607–1617. doi: 10.1093/neuonc/nou113

Jiang, Z., Li, X., Hu, J., Zhou, W., Jiang, Y., Li, G., et al. (2006). Promoter hypermethylation-mediated down-regulation of LATS1 and LATS2 in human astrocytoma. *Neurosci. Res.* 56, 450–458. doi: 10.1016/j.neures.2006.09.006

Jiang, T., Mao, Y., Ma, W., Mao, Q., You, Y., Yang, X., et al. (2016). CGCG clinical practice guidelines for the management of adult diffuse gliomas. *Cancer Lett.* 375, 263–273. doi: 10.1016/j.canlet.2016.01.024

Jiang, J., Yang, J., Wang, Z., Wu, G., and Liu, F. (2013). TFAM is directly regulated by miR-23b in glioma. *Oncol. Rep.* 30, 2105–2110. doi: 10.3892/or.2013.2712

Jin, C., Li, M., Ouyang, Y., Tan, Z., and Jiang, Y. (2017). MiR-424 functions as a tumor suppressor in glioma cells and is down-regulated by DNA methylation. *J. Neurooncol.* 133, 247–255. doi: 10.1007/s11060-017-2438-4

Jin, Z., Xu, S., Yu, H., Yang, B., Zhao, H., and Zhao, G. (2013). miR-125b inhibits Connexin43 and promotes glioma growth. *Cell. Mol. Neurobiol.* 33, 1143–1148. doi: 10.1007/s10571-013-9980-1

Jing, S.-Y., Jing, S.-Q., Liu, L.-L., Xu, L.-F., Zhang, F., and Gao, J.-L. (2017). Down-expression of miR-373 predicts poor prognosis of glioma and could be a potential therapeutic target. *Eur. Rev. Med. Pharmacol. Sci.* 21, 2421–2425.

Jones, P. A. (2012). Functions of DNA methylation: islands, start sites, gene bodies and beyond. *Nat. Rev. Genet.* 13, 484–492. doi: 10.1038/nrg3230

Kadowaki, M., Yoshioka, H., Kamitani, H., Watanabe, T., Wade, P. A., and Eling, T. E. (2012). DNA methylation-mediated silencing of nonsteroidal anti-inflammatory drug-activated gene (NAG-1/GDF15) in glioma cell lines. *Int. J. Cancer* 130, 267–277. doi: 10.1002/ijc.26082

Kaiser, S., Jurkowski, T. P., Kellner, S., Schneider, D., Jeltsch, A., and Helm, M. (2017). The RNA methyltransferase Dnmt2 methylates DNA in the structural context of a tRNA. *RNA Biol.* 14, 1241–1251. doi: 10.1080/15476286.2016.1236170

Kanemoto, M., Shirahata, M., Nakauma, A., Nakanishi, K., Taniguchi, K., Kukita, Y., et al. (2014). Prognostic prediction of glioblastoma by quantitative assessment of the methylation status of the entire MGMT promoter region. *BMC Cancer* 14:641. doi: 10.1186/1471-2407-14-641

Kim, J., Kim, K. Y., Jang, H.-S., Yoshida, T., Tsuchiya, K., Nitta, K., et al. (2009). Role of cytosolic $NADP^+$-dependent isocitrate dehydrogenase in ischemia-reperfusion injury in mouse kidney. *Am. J. Physiol. Renal Physiol.* 296, F622–F633. doi: 10.1152/ajprenal.90566.2008

Kim, W. J., Newman, W. C., and Amankulor, N. M. (2017). Phase I/II trial of combination of temozolomide chemotherapy and immunotherapy

with fusions of dendritic and glioma cells in patients with glioblastoma. *Neurosurgery* 81:N11. doi: 10.1093/neuros/nyx263

Kolodziej, M. A., Weischer, C., Reinges, M. H. T., Uhl, E., Weigand, M. A., Schwarm, F. P., et al. (2016). NDRG2 and NDRG4 expression is altered in glioblastoma and influences survival in patients with *MGMT*-methylated tumors. *Anticancer Res.* 36, 887–897.

Kondengaden, S. M., Luo, L. F., Huang, K., Zhu, M., Zang, L., Bataba, E., et al. (2016). Discovery of novel small molecule inhibitors of lysine methyltransferase G9a and their mechanism in leukemia cell lines. *Eur. J. Med. Chem.* 122, 382–393. doi: 10.1016/j.ejmech.2016.06.028

Kondo, Y., Katsushima, K., Ohka, F., Natsume, A., and Shinjo, K. (2014). Epigenetic dysregulation in glioma. *Cancer Sci.* 105, 363–369. doi: 10.1111/cas.12379

Kraus, T. F., Globisch, D., Wagner, M., Eigenbrod, S., Widmann, D., Münzel, M., et al. (2012). Low values of 5-hydroxymethylcytosine (5hmC), the "sixth base," are associated with anaplasia in human brain tumors. *Int. J. Cancer* 131, 1577–1590. doi: 10.1002/ijc.27429

Krausz, C., Sandoval, J., Sayols, S., Chianese, C., Giachini, C., Heyn, H., et al. (2012). Novel insights into DNA methylation features in spermatozoa: stability and peculiarities. *PLoS One* 7:e44479. doi: 10.1371/journal.pone.0044479

Krauze, A. V., Myrehaug, S. D., Chang, M. G., Holdford, D. J., Smith, S., Shih, J., et al. (2015). A phase 2 study of concurrent radiation therapy, temozolomide and the histone deacetylase inhibitor valproic acid for patients with glioblastoma. *Int. J. Radiat. Oncol. Biol. Phys.* 92, 986–992. doi: 10.1016/j.ijrobp.2015.04.038

Kreth, F. W., Thon, N., Simon, M., Westphal, M., Schackert, G., Nikkhah, G., et al. (2013). Gross total but not incomplete resection of glioblastoma prolongs survival in the era of radiochemotherapy. *Ann. Oncol.* 24, 3117–3123. doi: 10.1093/annonc/mdt388

Kunitz, A., Wolter, M., van den Boom, J., Felsberg, J., Tews, B., Hahn, M., et al. (2007). DNA hypermethylation and aberrant expression of the EMP3 gene at 19q13.3 in Human Gliomas. *Brain Pathol.* 17, 363–370. doi: 10.1111/j.1750-3639.2007.00083.x

Kurmasheva, R. T., Sammons, M., Favours, E., Wu, J., Kurmashev, D., Cosmopoulos, K., et al. (2017). Initial testing (stage 1) of tazemetostat (EPZ-6438), a novel EZH2 inhibitor, by the pediatric preclinical testing program. *Pediatr. Blood Cancer* 64:e26218. doi: 10.1002/pbc.26218

Kwak, S. Y., Kim, B. Y., Ahn, H. J., Yoo, J. O., Kim, J., Bae, I. H., et al. (2015). Ionizing radiation-inducible miR-30e promotes glioma cell invasion through EGFR stabilization by directly targeting CBL-B. *FEBS J.* 282, 1512–1525. doi: 10.1111/febs.13238

Kwak, H. J., Kim, Y. J., Chun, K. R., Woo, Y. M., Park, S. J., Jeong, J. A., et al. (2011). Downregulation of Spry2 by miR-21 triggers malignancy in human gliomas. *Oncogene* 30, 2433–2442. doi: 10.1038/onc.2010.620

Lakomy, R., Sana, J., Hankeova, S., Fadrus, P., Kren, L., Lzicarova, E., et al. (2011). MiR-195, miR-196b, miR-181c, miR-21 expression levels and O-6-methylguanine-DNA methyltransferase methylation status are associated with clinical outcome in glioblastoma patients. *Cancer Sci.* 102, 2186–2190. doi: 10.1111/j.1349-7006.2011.02092.x

Lee, S. H., Kim, M. S., Kwon, H. C., Park, I. C., Park, M. J., Lee, C. T., et al. (2000). Growth inhibitory effect on glioma cells of adenovirus-mediated p16/INK4a gene transfer *in vitro* and *in vivo*. *Int. J. Mol. Med.* 6, 559–563. doi: 10.3892/ijmm.6.5.559

Lee, E. Q., Puduvalli, V. K., Reid, J. M., Kuhn, J. G., Lamborn, K. R., Cloughesy, T. F., et al. (2012). Phase I study of vorinostat in combination with temozolomide in patients with high-grade gliomas: north american brain tumor consortium study 04–03. *Clin. Cancer Res.* 18, 6032–6039. doi: 10.1158/1078-0432.ccr-12-1841

Lee, E. Q., Reardon, D. A., Schiff, D., Drappatz, J., Muzikansky, A., Grimm, S. A., et al. (2015). Phase II study of panobinostat in combination with bevacizumab for recurrent glioblastoma and anaplastic glioma. *Neuro Oncol.* 17, 862–867. doi: 10.1093/neuonc/nou350

Leng, Y., Wang, J., Wang, Z., Liao, H.-M., Wei, M., Leeds, P., et al. (2016). Valproic acid and other HDAC inhibitors upregulate FGF21 gene expression and promote process elongation in glia by inhibiting HDAC2 and 3. *Int. J. Neuropsychopharmacol.* 19:pyw035. doi: 10.1093/ijnp/pyw035

Li, J., An, G., Zhang, M., and Ma, Q. (2016). Long non-coding RNA TUG1 acts as a miR-26a sponge in human glioma cells. *Biochem. Biophys. Res. Commun.* 477, 743–748. doi: 10.1016/j.bbrc.2016.06.129

Li, X., Ling, N., Bai, Y., Dong, W., Hui, G. Z., Liu, D., et al. (2013). MiR-16–1 plays a role in reducing migration and invasion of glioma cells. *Anat. Rec.* 296, 427–432. doi: 10.1002/ar.22626

Li, X., Liu, Y., Granberg, K. J., Wang, Q., Moore, L. M., Ji, P., et al. (2015). Two mature products of MIR-491 coordinate to suppress key cancer hallmarks in glioblastoma. *Oncogene* 34, 1619–1628. doi: 10.1038/onc.2014.98

Li, K. K., Yang, L., Pang, J. C., Chan, A. K., Zhou, L., Mao, Y., et al. (2013). MIR-137 suppresses growth and invasion, is downregulated in oligodendroglial tumors and targets CSE1L. *Brain Pathol.* 23, 426–439. doi: 10.1111/bpa.12015

Li, L., Yang, G., Ren, C., Tanimoto, R., Hirayama, T., Wang, J., et al. (2013). Glioma pathogenesis-related protein 1 induces prostate cancer cell death through Hsc70-mediated suppression of AURKA and TPX2. *Mol. Oncol.* 7, 484–496. doi: 10.1016/j.molonc.2012.12.005

Liao, P., Ostrom, Q. T., Stetson, L., and Barnholtz-Sloan, J. S. (2018). Models of epigenetic age capture patterns of DNA methylation in glioma associated with molecular subtype, survival and recurrence. *Neuro Oncol.* 20, 942–953. doi: 10.1093/neuonc/noy003

Liau, B. B., Sievers, C., Donohue, L. K., Gillespie, S. M., Flavahan, W. A., Miller, T. E., et al. (2017). Adaptive chromatin remodeling drives glioblastoma stem cell plasticity and drug tolerance. *Cell Stem Cell* 20, 233.e7–246.e7. doi: 10.1016/j.stem.2016.11.003

Lin, N., Di, C., Bortoff, K., Fu, J., Truszkowski, P., Killela, P., et al. (2012). Deletion or epigenetic silencing of AJAP1 on 1p36 in glioblastoma. *Mol. Cancer Res.* 10, 208–217. doi: 10.1158/1541-7786.mcr-10-0109

Liu, F., Barsyte-Lovejoy, D., Allali-Hassani, A., He, Y., Herold, J. M., Chen, X., et al. (2011). Optimization of cellular activity of G9a inhibitors 7-aminoalkoxy-quinazolines. *J. Med. Chem.* 54, 6139–6150. doi: 10.1021/jm200903z

Liu, F., Barsyte-Lovejoy, D., Li, F., Xiong, Y., Korboukh, V., Huang, X. P., et al. (2013). Discovery of an *in vivo* chemical probe of the lysine methyltransferases G9a and GLP. *J. Med. Chem.* 56, 8931–8942. doi: 10.1021/jm401480r

Liu, X., Li, G., Su, Z., Jiang, Z., Chen, L., Wang, J., et al. (2013). Poly(amido amine) is an ideal carrier of miR-7 for enhancing gene silencing effects on the EGFR pathway in U251 glioma cells. *Oncol. Rep.* 29, 1387–1394. doi: 10.3892/or.2013.2283

Liu, Y. S., Lin, H. Y., Lai, S. W., Huang, C. Y., Huang, B. R., Chen, P. Y., et al. (2017). MiR-181b modulates EGFR-dependent VCAM-1 expression and monocyte adhesion in glioblastoma. *Oncogene* 36, 5006–5022. doi: 10.1038/onc.2017.129

Liu, Z., Jiang, Z., Huang, J., Huang, S., Li, Y., Yu, S., et al. (2014). miR-7 inhibits glioblastoma growth by simultaneously interfering with the PI3K/ATK and Raf/MEK/ERK pathways. *Int. J. Oncol.* 44, 1571–1580. doi: 10.3892/ijo.2014.2322

Lovkvist, C., Dodd, I. B., Sneppen, K., and Haerter, J. O. (2016). DNA methylation in human epigenomes depends on local topology of CpG sites. *Nucleic Acids Res.* 44, 5123–5132. doi: 10.1093/nar/gkw124

Loyola, A., Huang, J. Y., LeRoy, G., Hu, S., Wang, Y. H., Donnelly, R. J., et al. (2003). Functional analysis of the subunits of the chromatin assembly factor RSF. *Mol. Cell. Biol.* 23, 6759–6768. doi: 10.1128/mcb.23.19.6759-6768.2003

Lucio-Eterovic, A. K., Cortez, M. A., Valera, E. T., Motta, F. J., Queiroz, R. G., Machado, H. R., et al. (2008). Differential expression of 12 histone deacetylase (HDAC) genes in astrocytomas and normal brain tissue: class II and IV are hypoexpressed in glioblastomas. *BMC Cancer* 8:243. doi: 10.1186/1471-2407-8-243

Luo, G., Luo, W., Sun, X., Lin, J., Wang, M., Zhang, Y., et al. (2017). MicroRNA21 promotes migration and invasion of glioma cells via activation of Sox2 and βcatenin signaling. *Mol. Med. Rep.* 15, 187–193. doi: 10.3892/mmr.2016.5971

Ma, C., Zheng, C., Bai, E., and Yang, K. (2016). miR-101 inhibits glioma cell invasion via the downregulation of COX-2. *Oncol. Lett.* 12, 2538–2544. doi: 10.3892/ol.2016.4939

Mack, S. C., Witt, H., Piro, R. M., Gu, L., Zuyderduyn, S., Stutz, A. M., et al. (2014). Epigenomic alterations define lethal CIMP-positive ependymomas of infancy. *Nature* 506, 445–450. doi: 10.1038/nature13108

Maio, M., Covre, A., Fratta, E., Di Giacomo, A. M., Taverna, P., Natali, P. G., et al. (2015). Molecular pathways: at the crossroads of cancer epigenetics and

immunotherapy. *Clin. Cancer Res.* 21, 4040–4047. doi: 10.1158/1078-0432.ccr-14-2914

Majchrzak-Celinska, A., Slocinska, M., Barciszewska, A. M., Nowak, S., and Baer-Dubowska, W. (2016). Wnt pathway antagonists, SFRP1, SFRP2, SOX17, and PPP2R2B, are methylated in gliomas and SFRP1 methylation predicts shorter survival. *J. Appl. Genet.* 57, 189–197. doi: 10.1007/s13353-015-0312-7

Malta, T. M., de Souza, C. F., Sabedot, T. S., Silva, T. C., Mosella, M. Q. S., Kalkanis, S. N., et al. (2018). Glioma CpG island methylator phenotype (G-CIMP): biological and clinical implications. *Neuro Oncol.* 20, 608–620. doi: 10.1093/neuonc/nox183

Marfella, C. G., Henninger, N., LeBlanc, S. E., Krishnan, N., Garlick, D. S., Holzman, L. B., et al. (2008). A mutation in the mouse Chd2 chromatin remodeling enzyme results in a complex renal phenotype. *Kidney Blood Press. Res.* 31, 421–432. doi: 10.1159/000190788

Marks, P. A., and Breslow, R. (2007). Dimethyl sulfoxide to vorinostat: development of this histone deacetylase inhibitor as an anticancer drug. *Nat. Biotechnol.* 25, 84–90. doi: 10.1038/nbt1272

Martini, M., Pallini, R., Luongo, G., Cenci, T., Lucantoni, C., and Larocca, L. M. (2008). Prognostic relevance of SOCS3 hypermethylation in patients with glioblastoma multiforme. *Int. J. Cancer* 123, 2955–2960. doi: 10.1002/ijc.23805

Mathias, R. A., Guise, A. J., and Cristea, I. M. (2015). Post-translational modifications regulate class IIa histone deacetylase (HDAC) function in health and disease. *Mol. Cell. Proteomics* 14, 456–470. doi: 10.1074/mcp.o114.046565

Mei, P. J., Bai, J., Liu, H., Li, C., Wu, Y. P., Yu, Z. Q., et al. (2011). RUNX3 expression is lost in glioma and its restoration causes drastic suppression of tumor invasion and migration. *J. Cancer Res. Clin. Oncol.* 137, 1823–1830. doi: 10.1007/s00432-011-1063-4

Milde, T., Oehme, I., Korshunov, A., Kopp-Schneider, A., Remke, M., Northcott, P., et al. (2010). HDAC5 and HDAC9 in medulloblastoma: novel markers for risk stratification and role in tumor cell growth. *Clin. Cancer Res.* 16, 3240–3252. doi: 10.1158/1078-0432.ccr-10-0395

Moniz, S., Martinho, O., Pinto, F., Sousa, B., Loureiro, C., Oliveira, M. J., et al. (2013). Loss of WNK2 expression by promoter gene methylation occurs in adult gliomas and triggers Rac1-mediated tumour cell invasiveness. *Hum. Mol. Genet.* 22, 84–95. doi: 10.1093/hmg/dds405

Mueller, W., Lass, U., Wellmann, S., Kunitz, F., and von Deimling, A. (2005). Mutation analysis of DKK1 and *in vivo* evidence of predominant p53-independent DKK1 function in gliomas. *Acta Neuropathol.* 109, 314–320. doi: 10.1007/s00401-004-0969-1

Mur, P., Rodríguez de Lope, Á., Díaz-Crespo, F. J., Hernández-Iglesias, T., Ribalta, T., Fiaño, C., et al. (2015). Impact on prognosis of the regional distribution of MGMT methylation with respect to the CpG island methylator phenotype and age in glioma patients. *J. Neurooncol.* 122, 441–450. doi: 10.1007/s11060-015-1738-9

Muscal, J. A., Thompson, P. A., Horton, T. M., Ingle, A. M., Ahern, C. H., McGovern, R. M., et al. (2013). A phase I trial of vorinostat and bortezomib in children with refractory or recurrent solid tumors: a Children's Oncology Group phase I consortium study (ADVL0916). *Pediatr. Blood Cancer* 60, 390–395. doi: 10.1002/pbc.24271

Nakahara, Y., Northcott, P. A., Li, M., Kongkham, P. N., Smith, C., Yan, H., et al. (2010). Genetic and epigenetic inactivation of Kruppel-like factor 4 in medulloblastoma. *Neoplasia* 12, 20–27. doi: 10.1593/neo.91122

Noushmehr, H., Weisenberger, D. J., Diefes, K., Phillips, H. S., Pujara, K., Berman, B. P., et al. (2010). Identification of a CpG island methylator phenotype that defines a distinct subgroup of glioma. *Cancer Cell* 17, 510–522. doi: 10.1016/j.ccr.2010.03.017

Oi, S., Natsume, A., Ito, M., Kondo, Y., Shimato, S., Maeda, Y., et al. (2009). Synergistic induction of NY-ESO-1 antigen expression by a novel histone deacetylase inhibitor, valproic acid, with 5-aza-2'-deoxycytidine in glioma cells. *J. Neurooncol.* 92, 15–22. doi: 10.1007/s11060-008-9732-0

Orzan, F., Pellegatta, S., Poliani, P. L., Pisati, F., Caldera, V., Menghi, F., et al. (2011). Enhancer of Zeste 2 (EZH2) is up-regulated in malignant gliomas and in glioma stem-like cells. *Neuropathol. Appl. Neurobiol.* 37, 381–394. doi: 10.1111/j.1365-2990.2010.01132.x

Pathania, R., Ramachandran, S., Mariappan, G., Thakur, P., Shi, H., Choi, J. H., et al. (2016). Combined inhibition of DNMT and HDAC blocks the tumorigenicity of cancer stem-like cells and attenuates mammary tumor growth. *Cancer Res.* 76, 3224–3235. doi: 10.1158/0008-5472.can-15-2249

Peereboom, D. M., Shepard, D. R., Ahluwalia, M. S., Brewer, C. J., Agarwal, N., Stevens, G. H., et al. (2010). Phase II trial of erlotinib with temozolomide and radiation in patients with newly diagnosed glioblastoma multiforme. *J. Neurooncol.* 98, 93–99. doi: 10.1007/s11060-009-0067-2

Pei, Y., Liu, K. W., Wang, J., Garancher, A., Tao, R., Esparza, L. A., et al. (2016). HDAC and PI3K antagonists cooperate to inhibit growth of MYC-driven medulloblastoma. *Cancer Cell* 29, 311–323. doi: 10.1016/j.ccell.2016.02.011

Pileggi, A., Klein, D., Fotino, C., Bravo-Egaña, V., Rosero, S., Doni, M., et al. (2013). MicroRNAs in islet immunobiology and transplantation. *Immunol. Res.* 57, 185–196. doi: 10.1007/s12026-013-8436-5

Pulice, J. L., and Kadoch, C. (2016). Composition and function of mammalian SWI/SNF chromatin remodeling complexes in human disease. *Cold Spring Harb. Symp. Quant. Biol.* 81, 53–60. doi: 10.1101/sqb.2016.81.031021

Qiu, J., Ai, L., Ramachandran, C., Yao, B., Gopalakrishnan, S., Fields, C. R., et al. (2008). Invasion suppressor cystatin E/M (CST6): high-level cell type-specific expression in normal brain and epigenetic silencing in gliomas. *Lab. Invest.* 88, 910–925. doi: 10.1038/labinvest.2008.66

Qu, Y., Dang, S., and Hou, P. (2013). Gene methylation in gastric cancer. *Clin. Chim. Acta* 424, 53–65. doi: 10.1016/j.cca.2013.05.002

Quintavalle, C., Garofalo, M., Zanca, C., Romano, G., Iaboni, M., del Basso De Caro, M., et al. (2012). miR-221/222 overexpression in human glioblastoma increases invasiveness by targeting the protein phosphate PTPmu. *Oncogene* 31, 858–868. doi: 10.1038/onc.2011.280

Rani, S. B., Rathod, S. S., Karthik, S., Kaur, N., Muzumdar, D., and Shiras, A. S. (2013). MiR-145 functions as a tumor-suppressive RNA by targeting Sox9 and adducin 3 in human glioma cells. *Neuro Oncol.* 15, 1302–1316. doi: 10.1093/neuonc/not090

Roboz, G. J., Ritchie, E. K., Dault, Y., Lam, L., Marshall, D. C., Cruz, N. M., et al. (2018). Phase I trial of plerixafor combined with decitabine in newly diagnosed older patients with acute myeloid leukemia. *Haematologica* 103, 1308–1316. doi: 10.3324/haematol.2017.183418

Rossetto, M., Ciccarino, P., Boisselier, B., Labussiere, M., and Sanson, M. (2011). Metabolism of glioma and IDH1/IDH2 mutations. *Rev. Neurol. Paris.* 167, 699–703. doi: 10.1016/j.neurol.2011.08.002

Schelman, W. R., Traynor, A. M., Holen, K. D., Kolesar, J. M., Attia, S., Hoang, T., et al. (2013). A phase I study of vorinostat in combination with bortezomib in patients with advanced malignancies. *Invest. New Drugs* 31, 1539–1546. doi: 10.1007/s10637-013-0029-6

Schraivogel, D., Weinmann, L., Beier, D., Tabatabai, G., Eichner, A., Zhu, J. Y., et al. (2011). CAMTA1 is a novel tumour suppressor regulated by miR-9/9* in glioblastoma stem cells. *EMBO J.* 30, 4309–4322. doi: 10.1038/emboj.2011.301

Schwartzentruber, J., Korshunov, A., Liu, X. Y., Jones, D. T., Pfaff, E., Jacob, K., et al. (2012). Driver mutations in histone H3.3 and chromatin remodelling genes in paediatric glioblastoma. *Nature* 482, 226–231. doi: 10.1038/nature10833

Shang, C., Guo, Y., Hong, Y., and Xue, Y. X. (2016a). Long non-coding RNA TUSC7, a target of miR-23b, plays tumor-suppressing roles in human gliomas. *Front. Cell. Neurosci.* 10:235. doi: 10.3389/fncel.2016.00235

Shang, C., Hong, Y., Guo, Y., Liu, Y. H., and Xue, Y. X. (2016b). miR-128 regulates the apoptosis and proliferation of glioma cells by targeting RhoE. *Oncol. Lett.* 11, 904–908. doi: 10.3892/ol.2015.3927

Sharma, V., Koul, N., Joseph, C., Dixit, D., Ghosh, S., and Sen, E. (2010). HDAC inhibitor, scriptaid, induces glioma cell apoptosis through JNK activation and inhibits telomerase activity. *J. Cell. Mol. Med.* 14, 2151–2161. doi: 10.1111/j.1582-4934.2009.00844.x

Sheu, J. J., Guan, B., Choi, J. H., Lin, A., Lee, C. H., Hsiao, Y. T., et al. (2010). Rsf-1, a chromatin remodeling protein, induces DNA damage and promotes genomic instability. *J. Biol. Chem.* 285, 38260–38269. doi: 10.1074/jbc.m110.138735

Shi, W., Palmer, J. D., Werner-Wasik, M., Andrews, D. W., Evans, J. J., Glass, J., et al. (2016). Phase I trial of panobinostat and fractionated stereotactic re-irradiation therapy for recurrent high grade gliomas. *J. Neurooncol.* 127, 535–539. doi: 10.1007/s11060-016-2059-3

Shi, L., Wang, Z., Sun, G., Wan, Y., Guo, J., and Fu, X. (2014). miR-145 inhibits migration and invasion of glioma stem cells by targeting ABCG2. *Neuromolecular Med.* 16, 517–528. doi: 10.1007/s12017-014-8305-y

Shi, L., Zhang, S., Feng, K., Wu, F., Wan, Y., Wang, Z., et al. (2012). MicroRNA-125b-2 confers human glioblastoma stem cells resistance to temozolomide

through the mitochondrial pathway of apoptosis. *Int. J. Oncol.* 40, 119–129. doi: 10.3892/ijo.2011.1179

Shimooka, Y., Nishikawa, J., and Ohyama, T. (2013). Most methylation-susceptible DNA sequences in human embryonic stem cells undergo a change in conformation or flexibility upon methylation. *Biochemistry* 52, 1344–1353. doi: 10.1021/bi301319y

Smirnikhina, S. A., Lavrov, A. V., Chelysheva, E. Y., Adilgereeva, E. P., Shukhov, O. A., Turkina, A., et al. (2016). Whole-exome sequencing reveals potential molecular predictors of relapse after discontinuation of the targeted therapy in chronic myeloid leukemia patients. *Leuk. Lymphoma* 57, 1669–1676. doi: 10.3109/10428194.2015.1132420

Song, Y., Wang, P., Zhao, W., Yao, Y., Liu, X., Ma, J., et al. (2014). MiR-18a regulates the proliferation, migration and invasion of human glioblastoma cell by targeting neogenin. *Exp. Cell Res.* 324, 54–64. doi: 10.1016/j.yexcr.2014.03.009

Stanton, B. Z., Hodges, C., Crabtree, G. R., and Zhao, K. (2017). A general non-radioactive ATPase assay for chromatin remodeling complexes. *Curr. Protoc. Chem. Biol.* 9, 1–10. doi: 10.1002/cpch.16

Stupp, R., Mason, W. P., van den Bent, M. J., Weller, M., Fisher, B., Taphoorn, M. J., et al. (2005). Radiotherapy plus concomitant and adjuvant temozolomide for glioblastoma. *N. Engl. J. Med.* 352, 987–996. doi: 10.1016/j.canrad.2005.05.001

Su, J. M., Li, X.-N., Thompson, P., Ou, C. N., Ingle, A. M., Russell, H., et al. (2011). Phase 1 study of valproic acid in pediatric patients with refractory solid or CNS tumors: a children's oncology group report. *J. Clin. Oncol.* 17, 589–597. doi: 10.1158/1078-0432.ccr-10-0738

Sullivan, R. J., and Atkins, M. B. (2009). Molecular-targeted therapy in malignant melanoma. *Expert Rev. Anticancer Ther.* 9, 567–581. doi: 10.1586/era.09.20

Sun, G., Shi, L., Yan, S., Wan, Z., Jiang, N., Fu, L., et al. (2014). MiR-15b targets cyclin D1 to regulate proliferation and apoptosis in glioma cells. *Biomed. Res. Int.* 2014:687826. doi: 10.1155/2014/687826

Sun, J., Tian, X., Zhang, J., Huang, Y., Lin, X., Chen, L., et al. (2017). Regulation of human glioma cell apoptosis and invasion by miR-152–3p through targeting DNMT1 and regulating NF2: MiR-152-3p regulate glioma cell apoptosis and invasion. *J. Exp. Clin. Cancer Res.* 36:100. doi: 10.1186/s13046-017-0567-4

Sun, A. G., Wang, M. G., Li, B., and Meng, F. G. (2017). Down-regulation of miR-124 target protein SCP-1 inhibits neuroglioma cell migration. *Eur. Rev. Med. Pharmacol. Sci.* 21, 723–729. doi: 10.1007/s13577-017-0180-z

Sun, J.-Z., Yang, X.-X., Li, X.-H., Xu, W.-W., Wang, Y., Zhu, W., et al. (2011). Aberrant CpG island hypermethylation and down-regulation of *Oct-6* mRNA expression in human hepatocellular carcinoma. *Dig. Dis. Sci.* 56, 3072–3077. doi: 10.1007/s10620-011-1686-y

Vaitkiene, P., Skiriute, D., Skauminas, K., and Tamasauskas, A. (2012). Associations between TFPI-2 methylation and poor prognosis in glioblastomas. *Medicina* 48, 345–349. doi: 10.3390/medicina48070051

Vargas, J. E., Filippi-Chiela, E. C., Suhre, T., Kipper, F. C., Bonatto, D., and Lenz, G. (2014). Inhibition of HDAC increases the senescence induced by natural polyphenols in glioma cells. *Biochem. Cell Biol.* 92, 297–304. doi: 10.1139/bcb-2014-0022

Veeriah, S., Brennan, C., Meng, S., Singh, B., Fagin, J. A., Solit, D. B., et al. (2009). The tyrosine phosphatase PTPRD is a tumor suppressor that is frequently inactivated and mutated in glioblastoma and other human cancers. *Proc. Natl. Acad. Sci. U S A* 106, 9435–9440. doi: 10.1073/pnas.0900571106

Verhaak, R. G., Hoadley, K. A., Purdom, E., Wang, V., Qi, Y., Wilkerson, M. D., et al. (2010). Integrated genomic analysis identifies clinically relevant subtypes of glioblastoma characterized by abnormalities in PDGFRA, IDH1, EGFR, and NF1. *Cancer Cell* 17, 98–110. doi: 10.1016/j.ccr.2009.12.020

von dem Knesebeck, A., Felsberg, J., Waha, A., Hartmann, W., Scheffler, B., Glas, M., et al. (2012). RANK (*TNFRSF11A*) is epigenetically inactivated and induces apoptosis in gliomas. *Neoplasia* 14, 526–534. doi: 10.1596/neo.12360

Waha, A., Felsberg, J., Hartmann, W., von dem Knesebeck, A., Mikeska, T., Joos, S., et al. (2010). Epigenetic downregulation of mitogen-activated protein kinase phosphatase MKP-2 relieves its growth suppressive activity in glioma cells. *Cancer Res.* 70, 1689–1699. doi: 10.1158/0008-5472.can-09-3218

Wang, X.-Q., Bai, H.-M., Li, S.-T., Sun, H., Min, L.-Z., Tao, B.-B., et al. (2017). Knockdown of HDAC1 expression suppresses invasion and induces apoptosis in glioma cells. *Oncotarget* 8, 48027–48040. doi: 10.18632/oncotarget.18227

Wang, L., Liu, J., Zhong, Z., Gong, X., Liu, W., Shi, L., et al. (2016). PTP4A3 is a target for inhibition of cell proliferatin, migration and invasion through Akt/mTOR signaling pathway in glioblastoma under the regulation of miR-137. *Brain Res.* 1646, 441–450. doi: 10.1016/j.brainres.2016.06.026

Wang, C., Schroeder, F. A., and Hooker, J. M. (2014). Visualizing epigenetics: current advances and advantages in HDAC PET imaging techniques. *Neuroscience* 264, 186–197. doi: 10.1016/j.neuroscience.2013.09.018

Wang, L., Shi, M., Hou, S., Ding, B., Liu, L., Ji, X., et al. (2012). MiR-483–5p suppresses the proliferation of glioma cells via directly targeting ERK1. *FEBS Lett.* 586, 1312–1317. doi: 10.1016/j.febslet.2012.03.035

Wang, Y., and Wang, L. (2017). miR-34a attenuates glioma cells progression and chemoresistance via targeting PD-L1. *Biotechnol. Lett.* 39, 1485–1492. doi: 10.1007/s10529-017-2397-z

Wang, Z., Wang, B., Shi, Y., Xu, C., Xiao, H. L., Ma, L. N., et al. (2015). Oncogenic miR-20a and miR-106a enhance the invasiveness of human glioma stem cells by directly targeting TIMP-2. *Oncogene* 34, 1407–1419. doi: 10.1038/onc.2014.75

Watanabe, T., Huang, H., Nakamura, M., Wischhusen, J., Weller, M., Kleihues, P., et al. (2002). Methylation of the p73 gene in gliomas. *Acta Neuropathol.* 104, 357–362. doi: 10.1007/s00401-002-0549-1

Watanabe, T., Katayama, Y., Yoshino, A., Yachi, K., Ohta, T., Ogino, A., et al. (2007). Aberrant hypermethylation of p14ARF and O6-methylguanine-DNA methyltransferase genes in astrocytoma progression. *Brain Pathol.* 17, 5–10. doi: 10.1111/j.1750-3639.2006.00030.x

Wei, J., Nduom, E. K., Kong, L. Y., Hashimoto, Y., Xu, S., Gabrusiewicz, K., et al. (2016). MiR-138 exerts anti-glioma efficacy by targeting immune checkpoints. *Neuro Oncol.* 18, 639–648. doi: 10.1093/neuonc/nov292

Wei, J., Qi, X., Zhan, Q., Zhou, D., Yan, Q., Wang, Y., et al. (2015). miR-20a mediates temozolomide-resistance in glioblastoma cells via negatively regulating LRIG1 expression. *Biomed. Pharmacother.* 71, 112–118. doi: 10.1016/j.biopha.2015.01.026

Wei, F., Wang, Q., Su, Q., Huang, H., Luan, J., Xu, X., et al. (2016). miR-373 inhibits glioma cell u251 migration and invasion by down-regulating CD44 and TGFBR2. *Cell. Mol. Neurobiol.* 36, 1389–1397. doi: 10.1007/s10571-016-0338-3

Weller, M. (2013). Assessing the MGMT status in glioblastoma: one step forward, two steps back? *Neuro Oncol.* 15, 253–254. doi: 10.1093/neuonc/not014

Wen, P. Y., and Huse, J. T. (2017). 2016 world health organization classification of central nervous system tumors. *Continuum* 23, 1531–1547. doi: 10.1212/CON.0000000000000536

Wheeler, L. A., Manzanera, A. G., Bell, S. D., Cavaliere, R., McGregor, J. M., Grecula, J. C., et al. (2016). Phase II multicenter study of gene-mediated cytotoxic immunotherapy as adjuvant to surgical resection for newly diagnosed malignant glioma. *Neuro Oncol.* 18, 1137–1145. doi: 10.1093/neuonc/now002

Wiese, M., Schill, F., Sturm, D., Pfister, S., Hulleman, E., Johnsen, S. A., et al. (2016). No significant cytotoxic effect of the EZH2 inhibitor tazemetostat (EPZ-6438) on pediatric glioma cells with wildtype histone 3 or mutated histone 3.3. *Hum. Pathol.* 228, 113–117. doi: 10.1055/s-0042-105292

Wu, X., Li, Y., Wan, X., Kayira, T. M., Cao, R., Ju, X., et al. (2012). Down-regulation of neogenin accelerated glioma progression through promoter Methylation and its overexpression in SHG-44 induced apoptosis. *PLoS One* 7:e38074. doi: 10.1371/journal.pone.0038074

Xia, H., Yan, Y., Hu, M., Wang, Y., Wang, Y., Dai, Y., et al. (2013). MiR-218 sensitizes glioma cells to apoptosis and inhibits tumorigenicity by regulating ECOP-mediated suppression of NF-κB activity. *Neuro Oncol.* 15, 413–422. doi: 10.1093/neuonc/nos296

Xiao, D., Huang, J., Pan, Y., Li, H., Fu, C., Mao, C., et al. (2017). Chromatin remodeling factor LSH is upregulated by the LRP6-GSK3β-E2F1 axis linking reversely with survival in gliomas. *Theranostics* 7, 132–143. doi: 10.7150/thno.17032

Xipell, E., Aragón, T., Martínez-Velez, N., Vera, B., Idoate, M. A., Martínez-Irujo, J. J., et al. (2016). Endoplasmic reticulum stress-inducing drugs sensitize glioma cells to temozolomide through downregulation of MGMT, MPG, and Rad51. *Neuro Oncol.* 18, 1109–1119. doi: 10.1093/neuonc/now022

Xu, J., Liao, X., Lu, N., Liu, W., and Wong, C. W. (2011). Chromatin-modifying drugs induce miRNA-153 expression to suppress Irs-2 in glioblastoma cell lines. *Int. J. Cancer* 129, 2527–2531. doi: 10.1002/ijc.25917

Xu, Y., Li, W. L., Fu, L., Gu, F., and Ma, Y. J. (2010). Slit2/Robo1 signaling in glioma migration and invasion. *Neurosci. Bull.* 26, 474–478. doi: 10.1007/s12264-010-0730-9

Xu, S., Ren, J., Chen, H. B., Wang, Y., Liu, Q., Zhang, R., et al. (2014). Cytostatic and apoptotic effects of DNMT and HDAC inhibitors in endometrial cancer cells. *Curr. Pharm. Des.* 20, 1881–1887. doi: 10.2174/13816128113199990527

Xue, L., Wang, Y., Yue, S., and Zhang, J. (2015). Low MiR-149 expression is associated with unfavorable prognosis and enhanced Akt/mTOR signaling in glioma. *Int. J. Clin. Exp. Pathol.* 8, 11178–11184.

Yadavilli, S., Scafidi, J., Becher, O. J., Saratsis, A. M., Hiner, R. L., Kambhampati, M., et al. (2015). The emerging role of NG2 in pediatric diffuse intrinsic pontine glioma. *Oncotarget* 6, 12141–12155. doi: 10.18632/oncotarget.3716

Yan, Y., Xu, Z., Li, Z., Sun, L., and Gong, Z. (2017). An insight into the increasing role of LncRNAs in the pathogenesis of gliomas. *Front. Mol. Neurosci.* 10:53. doi: 10.3389/fnmol.2017.00053

Yang, F., Wang, W., Zhou, C., Xi, W., Yuan, L., Chen, X., et al. (2015). MiR-221/222 promote human glioma cell invasion and angiogenesis by targeting TIMP2. *Tumour Biol.* 36, 3763–3773. doi: 10.1007/s13277-014-3017-3

Yilaz Susluer, S., Biray Avci, C., Dodurga, Y., Ozlem Dogan Sigva, Z., Oktar, N., and Gunduz, C. (2015). Downregulation of miR-195 via cyclosporin A in human glioblastoma cells. *J. BUON.* 20, 1337–1340.

Yu, Z., Chen, Y., Wang, S., Li, P., Zhou, G., and Yuan, Y. (2018). Inhibition of NF-kappaB results in anti-glioma activity and reduces temozolomide-induced chemoresistance by down-regulating MGMT gene expression. *Cancer Lett.* 428, 77–89. doi: 10.1016/j.canlet.2018.04.033

Yuan, Q., Gao, W., Liu, B., and Ye, W. (2014). Upregulation of miR-184 enhances the malignant biological behavior of human glioma cell line A172 by targeting FIH-1. *Cell. Physiol. Biochem.* 34, 1125–1136. doi: 10.1159/000366326

Zang, L., Kondengaden, S. M., Zhang, Q., Li, X., Sigalapalli, D. K., Kondengadan, S. M., et al. (2017). Structure based design, synthesis and activity studies of small hybrid molecules as HDAC and G9a dual inhibitors. *Oncotarget* 8, 63187–63207. doi: 10.18632/oncotarget.18730

Zang, L.-L., Wang, X.-J., Li, X.-B., Wang, S.-Q., Xu, W.-R., Xie, X.-B., et al. (2014). SAHA-based novel HDAC inhibitor design by core hopping method. *J. Mol. Graph. Model.* 54, 10–18. doi: 10.1016/j.jmgm.2014.08.005

Zhang, Y., Dong, W., Zhu, J., Wang, L., Wu, X., and Shan, H. (2017). Combination of EZH2 inhibitor and BET inhibitor for treatment of diffuse intrinsic pontine glioma. *Cell Biosci.* 7:56. doi: 10.1186/s13578-017-0184-0

Zhang, Y., Han, D., Wei, W., Cao, W., Zhang, R., Dong, Q., et al. (2015). MiR-218 inhibited growth and metabolism of human glioblastoma cells by directly targeting E2F2. *Cell. Mol. Neurobiol.* 35, 1165–1173. doi: 10.1007/s10571-015-0210-x

Zhang, C., Kang, C., You, Y., Pu, P., Yang, W., Zhao, P., et al. (2009). Co-suppression of miR-221/222 cluster suppresses human glioma cell growth by targeting p27kip1 *in vitro* and *in vivo*. *Int. J. Oncol.* 34, 1653–1660. doi: 10.3892/ijo_00000296

Zhang, Q.-M., Shen, N., Xie, S., Bi, S.-Q., Luo, B., Lin, Y.-D., et al. (2014). MAGED4 expression in glioma and upregulation in glioma cell lines with 5-aza-2′-deoxycytidine treatment. *Asian Pac. J. Cancer Prev.* 15, 3495–3501. doi: 10.7314/apjcp.2014.15.8.3495

Zhang, P., Sun, H., Yang, B., Luo, W., Liu, Z., Wang, J., et al. (2017). miR-152 regulated glioma cell proliferation and apoptosis via Runx2 mediated by DNMT1. *Biomed. Pharmacother.* 92, 690–695. doi: 10.1016/j.biopha.2017.05.096

Zhang, Q.-Q., Xu, H., Huang, M.-B., Ma, L.-M., Huang, Q.-J., Yao, Q., et al. (2012). MicroRNA-195 plays a tumor-suppressor role in human glioblastoma cells by targeting signaling pathways involved in cellular proliferation and invasion. *Neuro Oncol.* 14, 278–287. doi: 10.1093/neuonc/nor216

Zhang, C., Zhang, J., Hao, J., Shi, Z., Wang, Y., Han, L., et al. (2012). High level of miR-221/222 confers increased cell invasion and poor prognosis in glioma. *J. Transl. Med.* 10:119. doi: 10.1186/1479-5876-10-119

Zhang, J.-S., Zhao, Y., Lv, Y., Liu, P.-Y., Ruan, J.-X., Sun, Y.-L., et al. (2017). miR-873 suppresses H9C2 cardiomyocyte proliferation by targeting *GLI1*. *Gene* 626, 426–432. doi: 10.1016/j.gene.2017.05.062

Zhao, W., Tong, H., Huang, Y., Yan, Y., Teng, H., Xia, Y., et al. (2017). Essential role for polycomb group protein Pcgf6 in embryonic stem cell maintenance and a noncanonical polycomb repressive complex 1 (PRC1) integrity. *J. Biol. Chem.* 292, 2773–2784. doi: 10.1074/jbc.m116.763961

Zhao, Y.-Y., Zhao, L.-N., Wang, P., Miao, Y.-S., Liu, Y.-H., Wang, Z.-H., et al. (2015). Overexpression of miR-18a negatively regulates myocyte enhancer factor 2D to increase the permeability of the blood-tumor barrier via Krüppel-like factor 4-mediated downregulation of zonula occluden-1, claudin-5, and occludin. *J. Neurosci. Res.* 93, 1891–1902. doi: 10.1002/jnr.23628

Zheng, X., Chopp, M., Lu, Y., Buller, B., and Jiang, F. (2013). MiR-15b and miR-152 reduce glioma cell invasion and angiogenesis via NRP-2 and MMP-3. *Cancer Lett.* 329, 146–154. doi: 10.1016/j.canlet.2012.10.026

Zhou, C., Zhang, Y., Dai, J., Zhou, M., Liu, M., Wang, Y., et al. (2016). Pygo2 functions as a prognostic factor for glioma due to its up-regulation of H3K4me3 and promotion of MLL1/MLL2 complex recruitment. *Sci. Rep.* 6:22066. doi: 10.1038/srep22066

Conflict of Interest Statement: The authors declare that the research was conducted in the absence of any commercial or financial relationships that could be construed as a potential conflict of interest.

The reviewer MC and handling editor declared their shared affiliation at the time of the review.

frontiers in Aging Neuroscience

ORIGINAL RESEARCH
published: 20 November 2018
doi: 10.3389/fnagi.2018.00378

A Critical Role of Autophagy in Regulating Microglia Polarization in Neurodegeneration

Meng-meng Jin[1,2,3†], Fen Wang[4†], Di Qi[4], Wen-wen Liu[4], Chao Gu[2,4], Cheng-Jie Mao[2], Ya-Ping Yang[2], Zhong Zhao[1], Li-Fang Hu[4,5] and Chun-Feng Liu[1,2,4*]*

[1] Department of Neurology, Suzhou Clinical Research Center of Neurological Disease, Suzhou Municipal Hospital of Nanjing Medical University, Suzhou, China, [2] Department of Neurology, The Second Affiliated Hospital of Soochow University, Suzhou, China, [3] Department of Neurology, University Hospital Carl Gustav Carus, Technical University of Dresden, Dresden, Germany, [4] Jiangsu Key Laboratory of Neuropsychiatric Diseases, Institute of Neuroscience, Soochow University, Suzhou, China, [5] Department of Pharmacology, College of Pharmaceutical Sciences, Soochow University, Suzhou, China

Neuroinflammation and autophagy dysfunction are closely related to the development of neurodegeneration such as Parkinson's disease (PD). However, the role of autophagy in microglia polarization and neuroinflammation is poorly understood. TNF-α, which is highly toxic to dopaminergic neurons, is implicated as a major mediator of neuroinflammation in PD. In this study, we found that TNF-α resulted in an impairment of autophagic flux in microglia. Concomitantly, an increase of M1 marker (iNOS/NO, IL-1β, and IL-6) expression and reduction of M2 marker (Arginase1, Ym1/2, and IL-10) were observed in TNF-α challenged microglia. Upregulation of autophagy via serum deprivation or pharmacologic activators (rapamycin and resveratrol) promoted microglia polarization toward M2 phenotype, as evidenced by suppressed M1 and elevated M2 gene expression, while inhibition of autophagy with 3-MA or Atg5 siRNA consistently aggravated the M1 polarization induced by TNF-α. Moreover, Atg5 knockdown alone was sufficient to trigger microglia activation toward M1 status. More important, TNF-α stimulated microglia conditioned medium caused neurotoxicity when added to neuronal cells. The neurotoxicity was further aggravated when Atg5 knockdown in BV2 cells but alleviated when microglia pretreatment with rapamycin. Activation of AKT/mTOR signaling may contribute to the changes of autophagy and inflammation as the AKT specific inhibitor perifosine prevented the increase of LC3II (an autophagic marker) in TNF-α stimulated microglia. Taking together, our results demonstrate that TNF-α inhibits autophagy in microglia through AKT/mTOR signaling pathway, and autophagy enhancement can promote microglia polarization toward M2 phenotype and inflammation resolution.

Keywords: microglia polarization, TNF-α, autophagy, inflammation, neurodegeneration

OPEN ACCESS

Edited by:
Alberto Javier Ramos, Consejo Nacional de Investigaciones Científicas y Técnicas (CONICET), Argentina

Reviewed by:
Carsten Culmsee, Philipps-Universität Marburg, Germany
Cristina Pintado, Universidad de Castilla-La Mancha, Spain

***Correspondence:**
Li-Fang Hu
hulifang@suda.edu.cn
Chun-Feng Liu
liuchunfeng@suda.edu.cn

† These authors have contributed equally to this work

Received: *06 June 2018*
Accepted: *31 October 2018*
Published: *20 November 2018*

Citation:
Jin M-m, Wang F, Qi D, Liu W-w, Gu C, Mao C-J, Yang Y-P, Zhao Z, Hu L-F and Liu C-F (2018) A Critical Role of Autophagy in Regulating Microglia Polarization in Neurodegeneration. Front. Aging Neurosci. 10:378. doi: 10.3389/fnagi.2018.00378

INTRODUCTION

Parkinson's disease (PD) is a leading neurodegenerative movement disorder, caused by the demise of dopaminergic neurons in the substantia nigra (SN). Although the molecular mechanisms that underlie dopaminergic neuron losses are still unclear, it is increasingly recognized that microglia-mediated neuroinflammation serves as a pathogenic factor in PD (Glass et al., 2010). Accumulation

of proinflammatory cytokines, such as tumor necrosis factor-α (TNF-α), interleukin-1β (IL-1β), and interleukin-6 (IL-6) was reported in the brain, cerebrospinal fluid and serum of patients with PD, and animal models as well (Hunot and Hirsch, 2003). The polymorphism of human TNF-α encoding gene increases the risk of developing PD. The plasma TNF-α level correlates with some of the non-motor symptoms in PD including cognition decline, sleep disruption, and depression (Menza et al., 2010). At the molecular level, our previous study identified the autophagy deficits in TNF-α treated dopaminergic cells (Wang et al., 2015). All these suggest that TNF-α is a critical mediator in PD pathogenesis (Mccoy et al., 2011).

The microglia density is remarkably higher in the SN compared to other regions (Kim et al., 2000). Microglia exerts neurotoxic and neuroprotective effects, depending on their diverse functional phenotypes in response to specific stimuli (Orihuela et al., 2016). "Classic M1 polarization" of microglia is characterized by the production of pro-inflammatory mediators. In contrast, alternatively polarized M2 microglia limit inflammation and are typically characterized by the yield of anti-inflammatory factors (Kigerl et al., 2009; Hu et al., 2012). The enhanced microglial M1 activation contributes to neurodegeneration, such as PD and Alzheimer's disease (Wyss-Coray and Rogers, 2012; Vivekanantham et al., 2015). However, the molecular pathway that drives the microglia phenotypic changes during neurodegeneration remains unclear.

Autophagy is a catabolic mechanism which removes unnecessary or dysfunctional proteins and damaged organelles via the lysosome machinery (Mizushima, 2007). Autophagy dysregulation, along with neuroinflammation, is implicated in PD pathogenesis (Plaza-Zabala et al., 2017). The interaction between autophagy and inflammation is very complicated and controversial. For instance, in lipopolysaccharide (LPS)-challenged macrophages, Atg16L1 (an autophagy-related protein) deficiency enhanced IL-1β production (Saitoh et al., 2008). Nevertheless, there was also study reported that rapamycin, an autophagy activator, can inhibit M2 macrophage polarization (Wang et al., 2017). However, it remains unclear how autophagy regulates the shifting between M1 and M2 phenotypes in microglia, the macrophage counterpart in the brain. Therefore, our present study was to explore if autophagy has any impact on the microglial polarization upon TNF-α exposure, and the molecular mechanisms involved.

MATERIALS AND METHODS

Reagents and Antibodies

The chemicals such as 3-methyladenine (3-MA), bafilomycin A1 (BafA1), resveratrol, rapamycin were purchased from Sigma-Aldrich (St. Louis, MO, United States). TNF-α was purchased from PEPROTECH (Rocky Hill, NJ, United States). The Perifosine was purchased from Selleck Chemicals (Houston, TX, United States). The sources for primary antibodies were listed as follows: anti-β-actin, anti-p62, anti-lysosome-associated membrane protein 1 (LAMP1) and anti-β-tubulin from Sigma-Aldrich (St. Louis, MO, United States); anti-LC3, anti-histone 2B and anti-LAMP2 (Abcam, Cambridge, United Kingdom), anti-p-mammalian target of rapamycin (mTOR) [Cell Signaling Technology (CST), 5536s], anti-mTOR (CST, 2983s), anti-p-AKT (CST, 4060), anti-AKT (CST, 4691) and anti-cleaved caspase-3 (CST, 9664); anti-transcription factor EB (TFEB) (Proteintech, Chicago, IL, United States), and anti-GAPDH (Millipore, Billerica, MA, United States). All the reagents for cell culture were bought from Gibco (Grand Island, United States).

Cell Culture and Treatment

Murine BV2 microglial cells were cultured in Dulbecco modified Eagle's medium (DMEM) supplemented with 10% fetal bovine serum (FBS) and 1% penicillin/streptomycin in an incubator with 95% air atmosphere/5% CO_2 at 37°C. MES23.5 cells were cultured in DMEM/F12 with Sato's components containing 5% heat-inactivated FBS with 1% penicillin/streptomycin in the incubator. Cells were regularly subcultured three times a week and seeded into 35 mm dishes or 24-well plates prior to experimentation.

Primary microglia culture was prepared from 1 to 2-day-old neonatal C57BL/6J mice. Briefly, the cortex was dissected, minced and dissociated in 0.125% Trypsin for 4 min at 37°C. Trypsin was then neutralized with complete media (DMEM/F12 supplemented with 15% heat-inactivated FBS) and strained through a 200 μm mesh filter. After brief centrifugation, cells were harvested and plated in T75 cell culture flasks. The culture medium was replaced every 3 days. Once the lower layer reached confluence (about 10 days after culture), microglia cells were harvested by mechanical agitation at 180 rpm for 60–90 min and subsequently plated in DMEM/F12 supplemented with 10% FBS at a desired density for further experimentation.

Quantitative PCR

Total RNA was extracted using Trizol reagent and reverse transcribed using cDNA synthesis kit (Fermentas, Vilnius, Lithuania). Quantitative PCR (qPCR) was performed as we previously elaborated (Zhou et al., 2014). The primers used were listed in **Table 1**. 18s RNA was used as an internal control. The results were normalized and expressed as ratios of the target gene over 18s mRNA level.

Nitrite Quantification

The nitric oxide (NO) production in the culture supernatant was detected using a kit from Beyotime Biotechnology (Shanghai, China). Briefly, 50 μl culture supernatant was collected after treatment and transferred into a 96-well plate. Then, 50 μl Griess reagent was added and incubated at room temperature for 10 min. The absorbance was measured by a Microplate Reader (Tecan M200, Grodig) with a wavelength at 540 nm. The NO level was calculated with a standard curve plotted by sodium nitrite.

Cytokine Assay

The content of the cytokines IL-6 and IL-10 in the culture supernatant was detected using the ELISA kits from BOSTER (Wuhan, China), according to the manufacturer's instructions.

TABLE 1 | The Primers Used for Quantitative PCR.

Primer	Forward (5′ to 3′)	Reverse (5′ to 3′)
p62	CAGGCGCACTACCGCGATGA	TCGCACACGCTGCACAGGTC
iNOS	CAGGAGGAGAGAGATCCGATTTA	GCATTAGCATGGAAGCAAAGA
IL-1β	TGGAAAAGCGGTTTGTCTTC	TACCAGTTGGGGAACTCTGC
Arginase1	GAACACGGCAGTGGCTTTAAC	TGCTTAGCTCTGTCTGCTTTGC
Ym1/2	CAGGGTAATGAGTGGGTTGG	CACGGCACCTCCTAAATTGT
18 s	TCAACACGGGAAACCTCAC	CGCTCCACCAACTAAGAAC

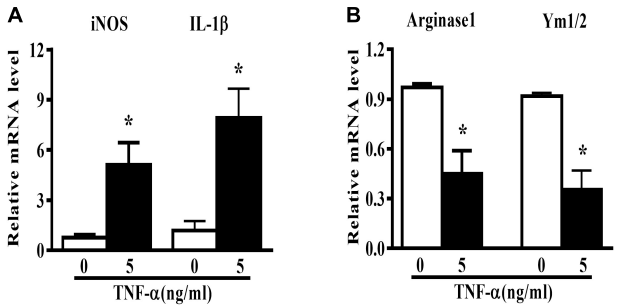

FIGURE 1 | TNF-α enhances M1 but reduces M2 markers in mouse primary microglia. Quantitative PCR (qPCR)analysis of M1 genes (iNOS, IL-1β, **A**) and M2 genes (Arginase1 and Ym1/2, **B**) mRNA levels in mouse primary microglia at 6 h after 5 ng/ml TNF-α stimulation, $n = 4$. Graphs show relative mRNA levels after normalization with those of housekeeping gene 18 s correspondingly. Results are expressed as mean ± SEM of four independent experiments. Student *t*-test. $^*P < 0.05$ vs. untreated controls.

Western Blot Analysis

Whole cell lysates were washed prepared by washing cells with phosphate-buffered saline (PBS) and lysed in ice-cold lysis buffer (150 mM NaCl, 25 mM Tris, 5 mM EDTA, 1% Nonidet P-40, pH 7.5) as previously described (Du et al., 2014). Lysates were separated by 10% sodium dodecyl sulfate-polyacrylamide gels and transferred onto nitrocellulose membranes. Next, membranes were blocked in 5% (w/v) non-fat dry milk powder in 0.1% Tris-buffered saline/Tween 20 (TBST) for 1 h and then incubated with the primary antibodies at optimized dilutions at 4°C overnight. After that, membranes were washed with TBST and incubated with HRP-conjugated secondary antibodies for another 1 h. Blots were finally visualized with chemiluminescence (Thermo Company, West Chester, PA, United States) and band densities were analyzed with ImageJ software (National Institute of Health, United States).

RFP-GFP-Tandem Fluorescent-Tagged LC3 (tf-LC3) and Atg5 siRNA Transfection

For transfection, 0.8 μg RFP-GFP-LC3 cDNA (Addgene, United States) were transfected into BV2 cells using 2 μl Lipofectamine 2000 (Invitrogen, Eugene, OR, United States). To monitor autophagic flux, cells were exposed to TNF-α or vehicle with or without the lysosome inhibitor BafA1 at 24 h post-transfection with tf-LC3 plasmids. The yellow and red LC3 puncta were manually counted, and at least 30 cells per group were randomly selected for counting. The small-interfering RNAs (siRNA) targeting mouse Atg5 (5′GACGUUGGUAACUGACAAATT3′ and 5′UUUGUCAGUUACCAACGUCTT3′) and scrambled siRNA duplexes were synthesized by GenePharma (Shanghai, China), and were transfected using Lipofectamine RNAiMAX (Thermo Company). The knockdown efficiency was determined by western blotting at 24 h post-transfection.

Subcellular Fractionation

Cells were lysed in the fractionation buffer including 3 mM $CaCl_2$, 2 mM MgAc, 320 mM sucrose, 0.1 mM EDTA, 1 mM DTT, 0.5 mM phenylmethylsulfonyl fluoride (PMSF), and 0.5% NP-40, kept on ice for 20 min and then centrifuged at 600 *g* 4°C for 15 min. The supernatants were collected as the cytosolic fraction. The pellets were washed with fractionation buffer without NP-40 twice, lysed with the nuclear lysis buffer comprising 280 mM KCl, 0.2 mM EDTA, 1 mM DTT, 0.5 mM PMSF, 20 mM Hepes (pH 7.9), 25% glycerol, 1.5 mM $MgCl_2$, and 0.3% NP-40 and then centrifuged. The resulting supernatant was then used for the nuclear fraction.

Conditioned Medium-Induced Neuronal Cell Death Assay

BV2 cells were transfected with Atg5 siRNA or control siRNA for 48 h as mentioned above. For rapamycin group, cells were pretreated with 0.2 μg/ml rapamycin for 0.5 h. Cells were then treated with TNF-α for 24 h, and replaced by culture in fresh medium for another 24 h to produce the microglia conditioned medium (CM). After that, the microglia CM was transferred into MES23.5 cells and cultured for 24 h. Thereafter, cells were incubated with Hochest 33342 (Sigma) and propidium iodide (PI, Beyotime, Shanghai, China) for 5 min, and then washed with PBS. Images were taken using an inverted IX71 microscope system (Olympus, Tokyo, Japan). The hochest and PI stained cells were counted manually, and at least 500 cells per group were counted.

Statistical Analysis

All results are presented as mean ± SEM, obtained from a minimum of 3 independent experiments unless otherwise stated. Statistical significance was analyzed using Student *t*-test for two-group comparison or one-way analysis of variance (ANOVA) followed by Tukey *post hoc* analysis using the GraphPad Prism. The significance level was set at $P < 0.05$.

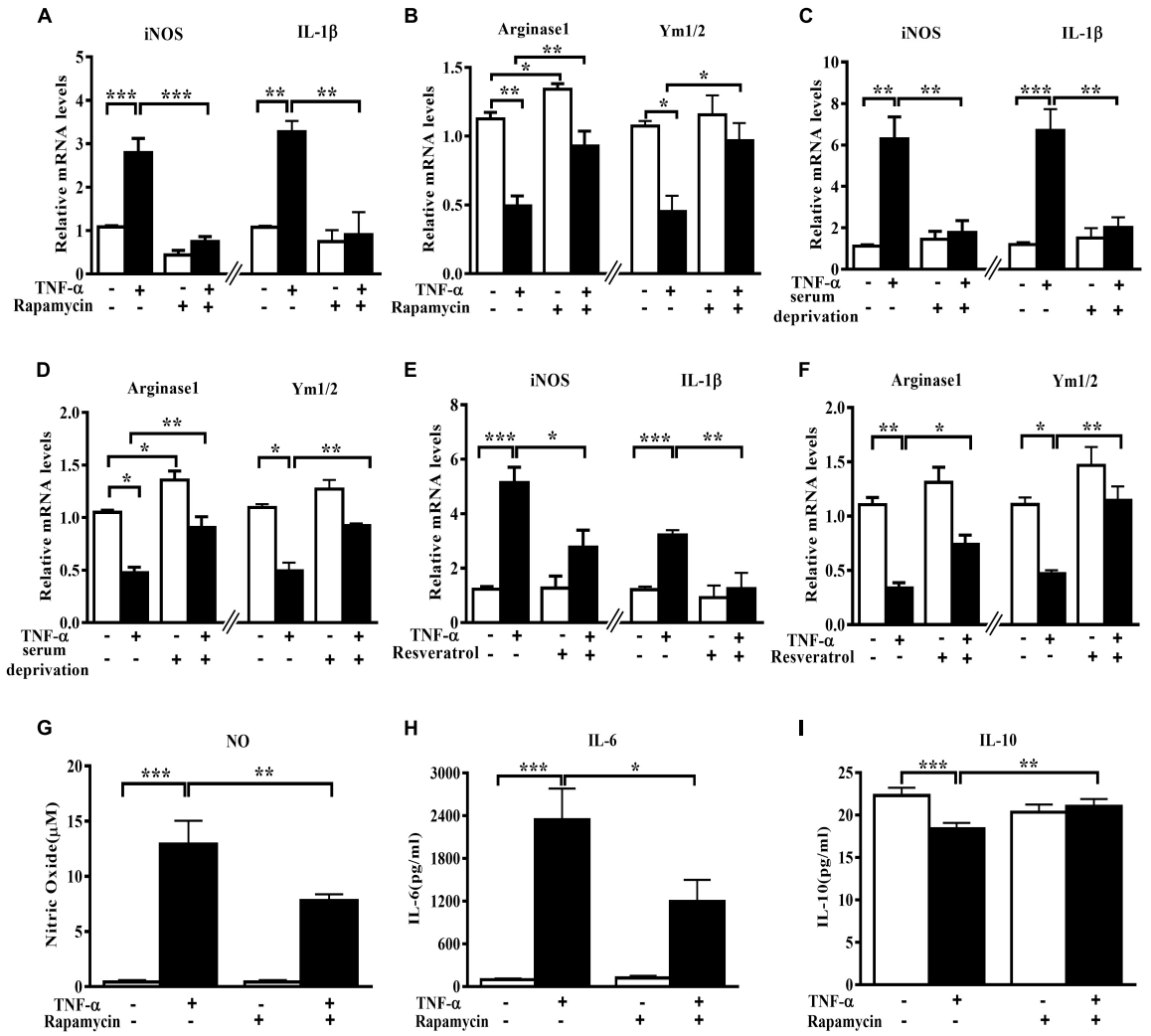

FIGURE 2 | Autophagy stimulation enhances M2 but reduces M1 markers in primary microglia. **(A–F)** qPCR analysis of M1 and M2 genes mRNA levels in TNF-α-treated primary microglia with or without autophagy stimulation by different methods. **(A,B)** 0.2 μg/ml rapamycin pretreatment. **(C,D)** serum deprivation. **(E,F)** autophagy stimulation by 50 μM resveratrol pretreatment. Graphs show relative mRNA levels after normalization with those of corresponding housekeeping gene 18 s, $n = 4$. **(G–I)** Cytokines including NO **(G)**, IL-6 **(H)** and IL-10 levels **(I)**, measured by Griess reagent and ELISA, in cell-free culture supernatant from TNF-α-challenged primary microglia with or without rapamycin pretreatment. $N = 4$. All of the results are expressed as mean ± SEM, one-way ANOVA followed by Tukey analysis. $^*P < 0.05$, $^{**}P < 0.01$, and $^{***}P < 0.001$ vs. controls. NS, not significant.

RESULTS

TNF-α Enhances M1 but Reduces M2 Markers in Microglia

Microglia polarization is commonly characterized by the expression of signature genes that are associated with M1 or M2 phenotype (Mantovani et al., 2013). Neuroinflammation is featured by an alteration of microglia polarization toward M1 status. In this study, we observed that 5 ng/ml TNF-α stimulation not only induced an elevation in M1 genes (iNOS and IL-1β) expression (**Figure 1A**), but also caused a reduction in the M2 signature genes level (Arginase1 and Ym1/2, **Figure 1B**) in mouse primary microglia, indicating a shift toward M1 phenotype following TNF-α stimulation.

Autophagy Activation Enhances M2 but Reduces M1 Markers in Microglia

In order to assess the role of autophagy in microglia polarization, we induced autophagy activation in primary microglia using serum deprivation or two structure-unrelated autophagy inducers (rapamycin and resveratrol). Although none of the three tested autophagy inducers produced any obvious effect on the basal level of M1 genes, they increased the Arginase1 mRNA levels under normal conditions. A mild but not significant elevation of Ym1/2 mRNA was also observed. Importantly, both serum deprivation and pharmacologic autophagy inducers (rapamycin and resveratrol) potently suppressed the increase of M1 (iNOS and IL-1β) mRNA level and alleviated the decline of M2 gene expression (Arginase1 and Ym1/2) in TNF-α-stimulated

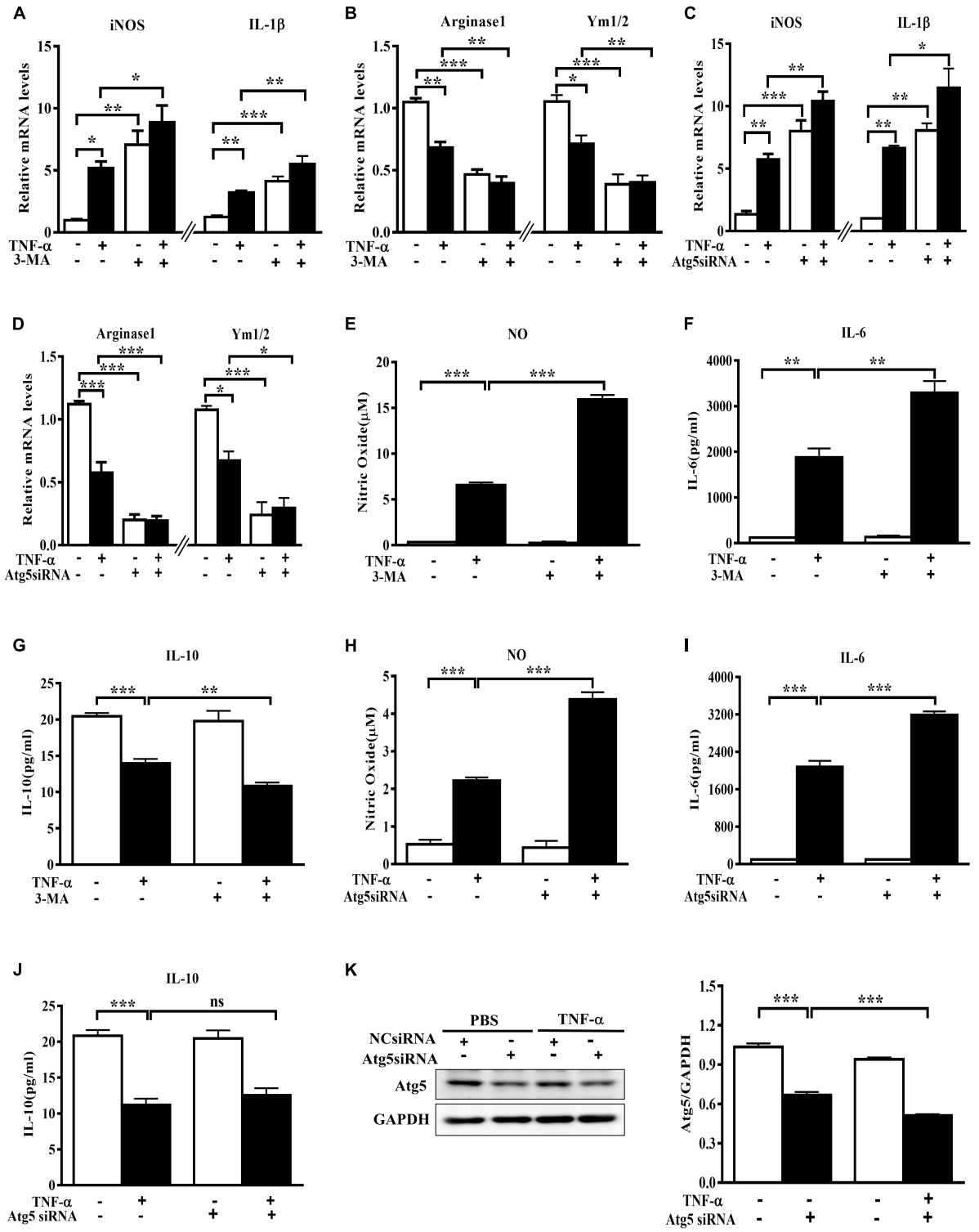

FIGURE 3 | Autophagy inhibition enhances M1 but reduces M2 markers in microglia. **(A–D)** qPCR measurement of M1 and M2 genes mRNA levels in TNF-α-treated cells with or without autophagy inhibition by 10 mM 3-MA (**A,B**, primary microglia) or Atg5 knockdown (**C,D**, BV2 microglial cell line). Atg5 siRNA or scrambled siRNA were transfected into BV2 cells by Lipofectamine RNAiMAX, followed by 5 ng/ml TNF-α treatment at 24 h later. mRNA levels were analyzed at 6 h after TNF-α addition. Graphs show relative mRNA levels after normalization with those of corresponding housekeeping gene 18 s. $N = 3$–6. **(E–J)** NO, IL-6 and IL-10 levels in the culture supernatants from TNF-α-treated microglia with 3-MA or Atg5 siRNA as described above, $n = 4$. **(K)** Western blot study of Atg5 expression in Atg5 siRNA-transfected BV2 cells following TNF-α treatment, $n = 3$. Housekeeping protein GAPDH was used as loading control for semi-quantitative densitometry. $^*P < 0.05$, $^{**}P < 0.01$, and $^{***}P < 0.001$ vs. controls, one-way ANOVA followed by Tukey analysis.

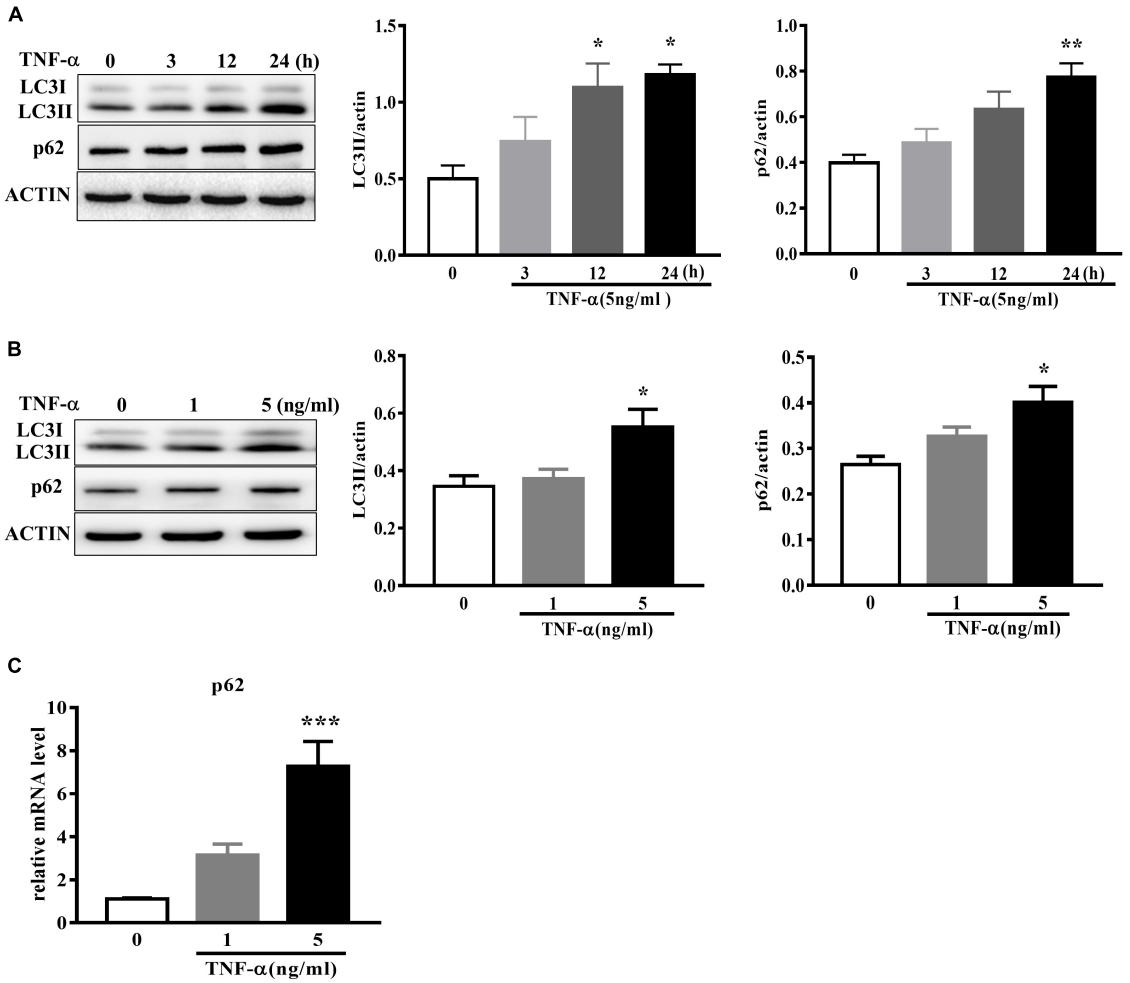

FIGURE 4 | TNF-α disrupts autophagy in microglia. **(A,B)** Western blot analysis of the time- and dose-dependent effects of TNF-α on the autophagy markers LC3II and p62 protein levels in primary microglia. Actin served ad as loading controls, $n = 4$. **(C)** qPCR measurement of p62 mRNA expression in microglia following TNF-α treatment for 6 h. Relative p62 mRNA level was obtained by normalizing to that of housekeeping 18 s, $n = 4$. $^{*}P < 0.05$, $^{**}P < 0.01$, and $^{***}P < 0.001$ vs. controls, one-way ANOVA followed by Tukey analysis.

primary microglia (**Figures 2A–F**). Measurement of the cytokines level in the culture supernatant displayed that the autophagy activator rapamycin reduced the NO (**Figure 2G**) and IL-6 (**Figure 2H**) production but enhanced IL-10 yield (**Figure 2I**) in TNF-α-stimulated primary microglia. These data imply that autophagy activation is able to promote microglia polarization toward M2 phenotype under both basal and inflamed status.

Autophagy Inhibition Enhances M1 but Reduces M2 Markers in Microglia

To evaluate the role of autophagy inhibition in microglia phenotype transition, we used both the autophagy inhibitor 3-MA and the siRNA against autophagy-related protein Atg5 and observed the changes of polarization markers in TNF-α-challenged microglia cells. The autophagy inhibitor 3-MA enhanced the basal and TNF-α-induced iNOS and IL-1β transcription (**Figure 3A**). Meanwhile, it downregulated the basal level of Arginase1 and Ym1/2 and caused a further decline of these two M2 markers in TNF-α-exposed primary microglia (**Figure 3B**). In line with this, Atg5 knockdown in BV2 cells was also found to increase the basal level of M1 gene expression (iNOS, IL-1β) and reduce the M2 gene expression (Arginase1, Ym1/2) (**Figures 3C–D**), and reinforced the alterations of the polarization markers in TNF-α-stimulated cells. These observations were confirmed by cytokines assay. As shown in **Figures 3E–J**, autophagy inhibition with 3-MA or Atg5 siRNA consistently caused a further increase of NO and IL-6 generation and a moderate decrease of IL-10 in the supernatant of TNF-α-treated microglia. Western blot study revealed the successful knockdown of Atg5 by small RNA interference in TNF-α-treated BV2 cells (**Figure 3K**). These data indicate that autophagy not only negatively regulates microglia activation under basal conditions but also affects microglia polarization in response to inflammatory stimulation.

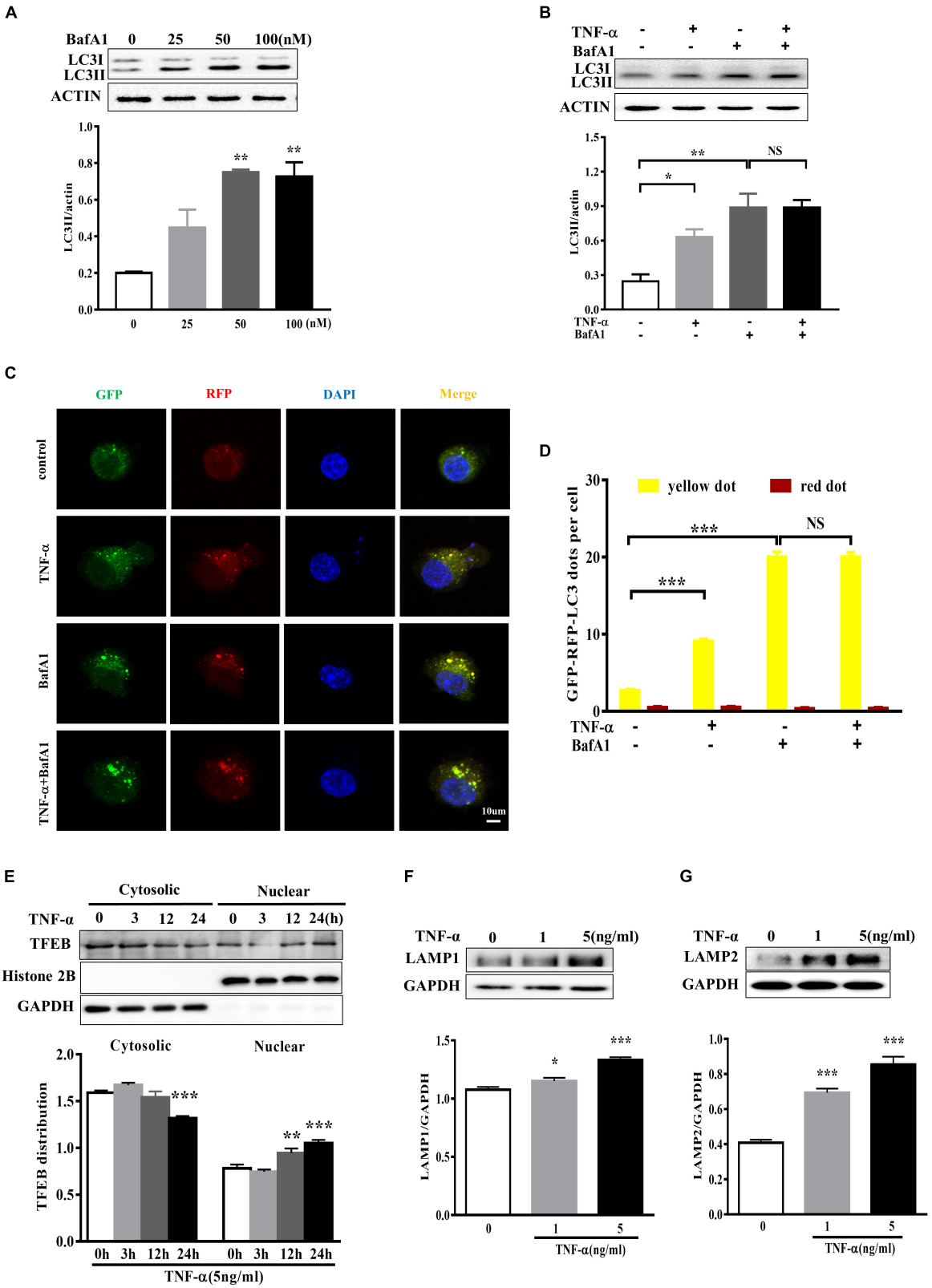

FIGURE 5 | TNF-α disrupted the autophagic flux in microglia. **(A)** Dose-dependent effect of the lysosome inhibitor BafA1 treatment for 2 h on LC3II accumulation in BV2 cells, as evaluated by western blotting. *N* = 3. **(B)** Effect of TNF-α on LC3II levels during lysosome inhibition. BV2 cells were treated with 5 ng/ml TNF-α for 24 h, *(Continued)*

FIGURE 5 | Continued
and then added with BafA1(50 nM) for 2 h before subjected to western blotting. Actin served as loading controls in panels **A,B**. $N = 4$. **(C,D)** Autophagic assay in microglia treated with TNF-α, BafA1, or in combination. BV2 cells were transfected with RFP-GFP-tandem fluorescent LC3 cDNA for 24 h before treatment. Confocal microscope pictures showing yellow (GFP and RFP overlap) and red LC3 puncta formation in different groups. Scale bar, 10 μm. LC3 dots were visualized and quantified from at least 30 cells per group. **(E)** Effect of TNF-α on lysosomal biogenesis. BV2 cells were treated with 5 ng/ml TNF-α for 3, 12, or 24 h. The cytosolic and nuclear fractions were subjected to western blotting analysis of TFEB, with GAPDH and Histone 2B as the cytosolic and nuclear loading controls, respectively. **(F,G)** Effect of TNF-α on lysosomal protein LAMP1 **(F)** and LAMP2 **(G)** levels in BV2 cells. $N = 3$. $^{*}P < 0.05$, $^{**}P < 0.01$, and $^{***}P < 0.001$ vs. controls. NS, not significant. One way ANOVA followed by Tukey analysis.

TNF-α Disrupts Microglia Autophagic Flux

To examine the effect of TNF-α on microglia autophagy, we study several autophagy-related markers including LC3 and p62 (also named sequestosome1, SQSTM1) protein expressions. Western blotting analysis showed that TNF-α treatment resulted in an increase of microglia LC3II and p62 in a time- and dose-dependent manner (**Figures 4A–B**). As several studies previously reported the p62 transcription by inflammatory stimuli (Fujita et al., 2011), here we also examined p62 mRNA level. qPCR analysis showed a substantial increase of p62 transcription in response to TNF-α stimulation (**Figure 4C**).

To determine whether the LC3II increase resulted from autophagy induction or lysosomal degradation impairment, we studied the effect of TNF-α on LC3II in the presence of BafA1, a vacuolar H^+-ATPase inhibitor that blocks autolysosome degradation. As shown in **Figure 5A**, showed that 50 nM BafA1 was sufficient to fully block of lysosomal degradation as 100 nM BafA1 did not result in a further increase of LC3II level in BV2 cells. Therefore, 50 nM BafA1 was used in the following study for lysosomal inhibition. TNF-α failed to further enhance the LC3II protein level in the presence of BafA1 (**Figure 5B**), indicating that the TNF-α-induced LC3II increase may result from lysosome degradation impairment. This is consistent with the tf-LC3 assay which allows us to monitor the autophagic flux (Mizushima et al., 2010). As shown in **Figure 5C**, tf-LC3 transfected BV2 microglia had some basal level of autophagy, as exhibited by a few green/red dots staining in control. Similar to the impact of BafA1, TNF-α caused an obvious elevation in the number of yellow dots, with almost no detectable red dots in cells. TNF-α plus BafA1 co-treatment did not show any further impact on the yellow/red dots when compared to BafA1 treatment alone (**Figures 5C,D**). These data suggest the disruption of autophagic flux in TNF-α challenged microglia.

Anti-transcription factor EB served as a master regulator of the autophagy-lysosome system which coordinates autophagy and lysosomal biogenesis (Sardiello et al., 2009). To clarify the role of TFEB in TNF-α treated microglia, we studied and found that a time-dependent TFEB translocation from cytosol to nuclear fraction in response to TNF-α compared with untreated BV2 cells (**Figure 5E**). Moreover, the lysosome proteins LAMP1 and LAMP2 expression also increased after TNF-α treatment (**Figures 5F,G**).

AKT Signaling Is Involved in TNF-α Induced Autophagy Flux Disruption in Microglia

The signaling mechanism that underlies TNF-α induced autophagy flux disruption was also examined. We observed a rapid activation of AKT in BV2 cells following 5 ng/ml TNF-α treatment, as AKT phosphorylation (Ser473) increased and reached its peak at 6 h after treatment (**Figure 6A**). This was accompanied by a consistent elevation in the phosphorylation of mTOR, the master regulator of autophagy and downstream target of AKT (**Figure 6B**). As expected, treatment with the AKT-specific inhibitor perifosine (100 nM) caused a LC3II increase, correlated with a reduction in Akt phosphorylation in BV2 cells. Of note, TNF-α did not further enhance the LC3II protein level in the presence of perifosine compared with perifosine treatment group (**Figures 6C,D**). This implies that the AKT/mTOR signaling pathway was involved in the autophagy regulation in TNF-α-stimulated microglia.

TNF-α-Challenged Microglia Conditioned Medium Produced Toxicity to Co-cultured Neuronal Cells

In order to evaluate the effect of microglia polarization on neurons around, we established a system in which the cell-free culture supernatant from TNF-α or vehicle challenged BV2 cells (defined as a microglia conditioned medium) was harvested and then transferred into MES23.5 cells, a dopaminergic cell line. To assess the CM-associated impact and avoid the carryover from microglia treatment, BV2 cells were challenged with TNF-α for 24 h, washed, and cultured with fresh medium for another 24 h. After that, the microglia culture supernatant was collected as CM and applied in subsequent experimentation. To determine the influence of microglia autophagy regulation on neurons survival, BV2 cells were transfected with Atg5 siRNA or pretreated with rapamycin before exposure to TNF-α. The hochest and PI staining showed that treatment with TNF-α challenged CM for 24 h resulted in a 13.1 ± 1.2% cell death in MES23.5 cells compared to control CM group (2.2 ± 0.8%), implying TNF-α challenged CM produced toxicity to neuronal cells. This neurotoxicity was enhanced by Atg5 knockdown but attenuated when BV2 cells pretreatment with rapamycin (**Figures 7A,B**). The results were confirmed with the caspase-3 assay. Western blotting showed that treatment with TNF-α challenged CM caused an increase of cleaved caspase-3 level in MES23.5 cells. Transfection with Atg5 siRNA in BV2 microglia led to a further increase in cleaved caspase-3 compared to control siRNA. In

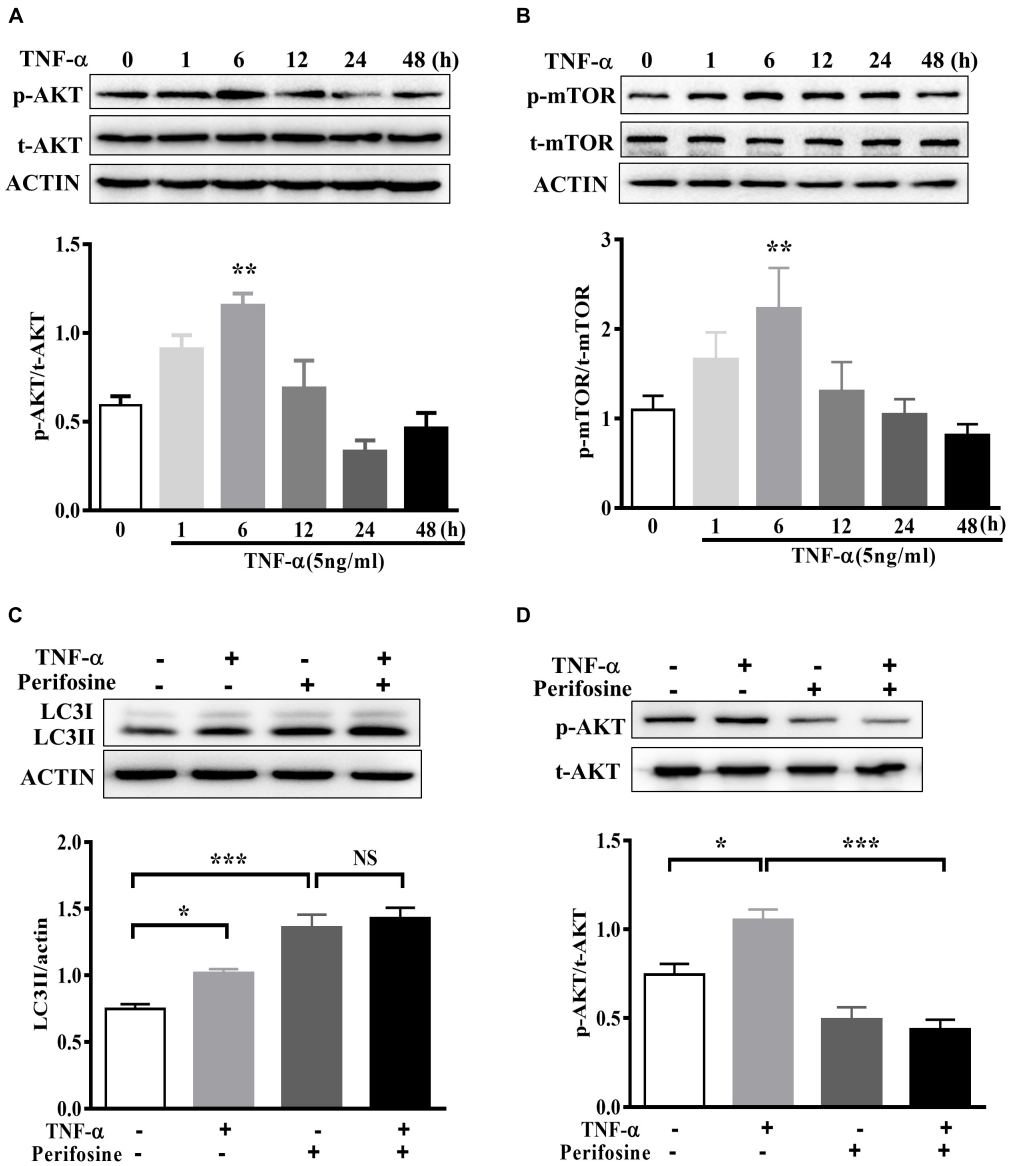

FIGURE 6 | AKT signaling mediates TNF-α-induced autophagy inhibition. **(A,B)** Time-dependent effect of TNF-α on AKT and mTOR signaling. BV2 cells were treated with 5 ng/ml TNF-α for the indicating time. The changes of p-AKT, AKT, p-mTOR, and mTOR proteins level were analyzed by western blotting, $n = 4$. **(C,D)** Effect of TNF-α on LC3II protein level in the presence of AKT inhibitor perifosine (100 nM). $N = 5$. Actin served as loading controls. $^{*}P < 0.05$, $^{**}P < 0.01$, and $^{***}P < 0.001$ vs. controls. One way ANOVA followed by Tukey analysis. NS, not significant.

contrast, microglia pretreatment with rapamycin attenuated the cleaved caspase-3 increase (**Figure 7C**). These results indicate that modulation of microglia autophagy could have an impact on the neuronal survival probably by affecting microglia polarization and associated neuroinflammation.

DISCUSSION

In this study we provide the evidence that pro-inflammatory cytokine TNF-α inhibits autophagy flux and drives microglia shift toward M1 phenotype via activating AKT/mTOR signaling. Our findings demonstrate that autophagy enhancement could guide microglia activation toward M2 status and attenuate the neurotoxicity of TNF-α challenged microglia CM, while microglia autophagy inhibition produces the opposite effects (as summarized in **Figure 8**).

Neuroinflammation and autophagy dysregulation closely linked with neurodegeneration. Recent studies identify a complex interaction between these two processes. Here we clearly show that TNF-α inhibits microglia autophagy flux, and reveal a role of autophagy flux inhibition in M1 microglia polarization and thereby the neurotoxicity. This is consistent with recent reports that autophagy may regulate LPS-stimulated inflammation in

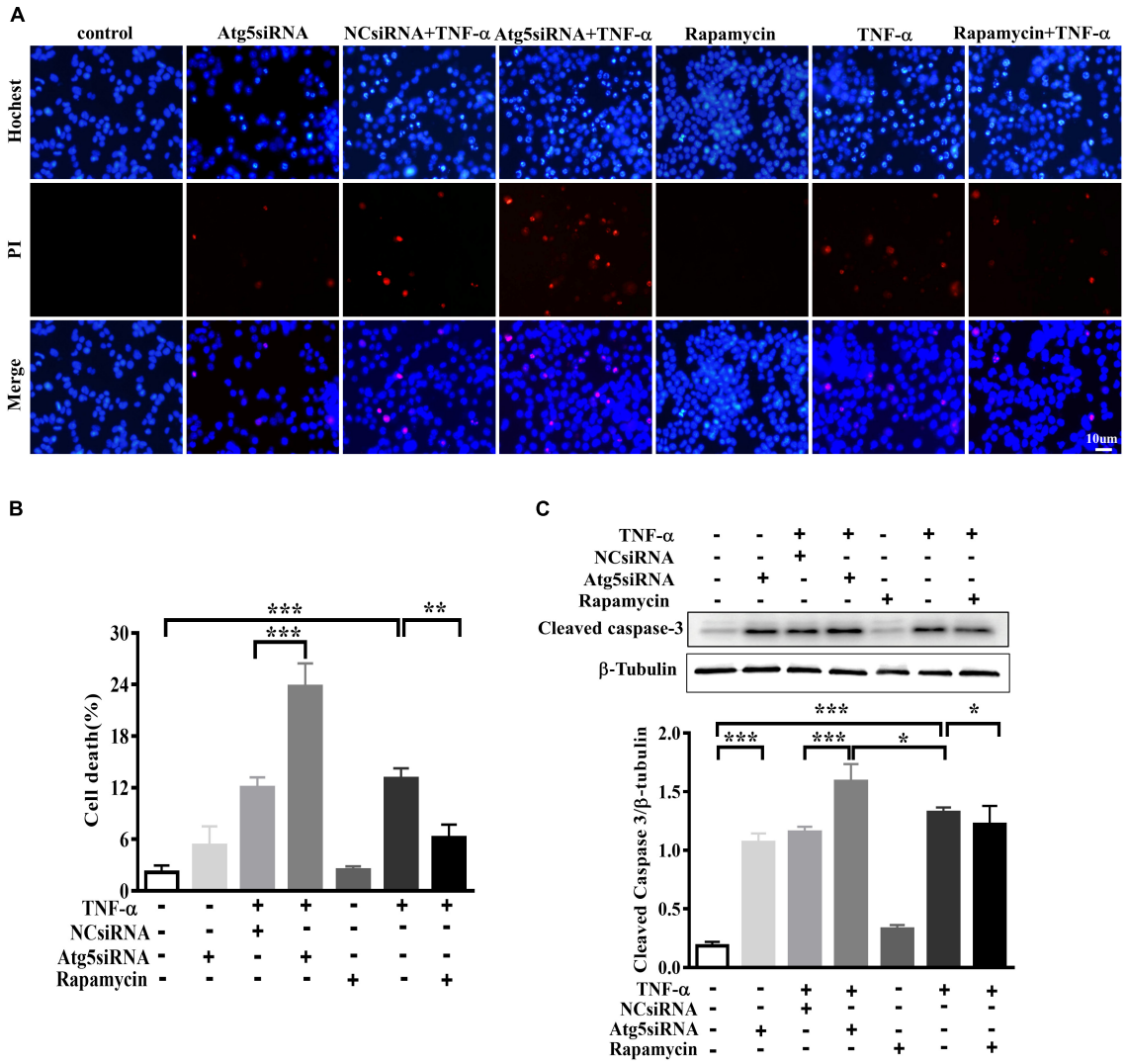

FIGURE 7 | Effect of TNF-α-challenged microglia conditioned medium on dopaminergic cell damage. **(A–C)** MES23.5 cells were cultured for 24 h with different microglia CM as described in materials and methods. After that, MES23.5 cells were subjected to Hoechst/PI staining or western blot analysis of cleaved caspase-3 protein levels. The results were independently repeated three times. Scale bar, 10 μm.*$P < 0.05$, **$P < 0.01$, and ***$P < 0.001$ vs. controls. One way ANOVA followed by Tukey analysis.

microglia and its associated neurotoxicity (Bussi et al., 2017; He et al., 2018). These lines of evidence highlight a possibility that autophagy serves as the common machinery in regulating microglia-mediated inflammation in response to a multitude of inflammatory stimuli. Yet, another study demonstrated that LPS injection induced autophagy activation in rat hippocampus (Pintado et al., 2017). Autophagy is a catabolic process that can be activated during starvation, stress and nutrient deprivation by different signaling pathways. It is conceivable that microglia autophagy could be altered by diverse conditions. Also, the isolation and culture conditions could yield an impact on microglia *in vitro*. Thus, the *in vivo* study, in combination with microglia-specific genetic manipulation, may further our understanding of the relationship between inflammation and autophagy.

We previously reported that TNF-α can disrupt the autophagic flux and result in α-synuclein accumulation in PC12 cells and midbrain neurons (Wang et al., 2015). This and the present study consistently show TNF-α causes autophagy dysfunction in both neuron and microglia, which may produce a positive loop between microglia and neurons and thus lead to neurodegeneration. However, we did not observe any change in TFEB or LAMP1 expression in TNF-α-treated neurons (Wang et al., 2015). By contrast, in this study we detected TFEB nuclear translocation induced by TNF-α in microglia, correlating with the increases of LAMP1 and LAMP2 expression. This may act as a compensatory mechanism to autophagy flux disruption during TNF-α stimulation. This discrepancy may be attributed to the higher activity of lysosomal biogenesis in microglia. The TNF-α induced autophagy flux inhibition seemed to be dependent, at

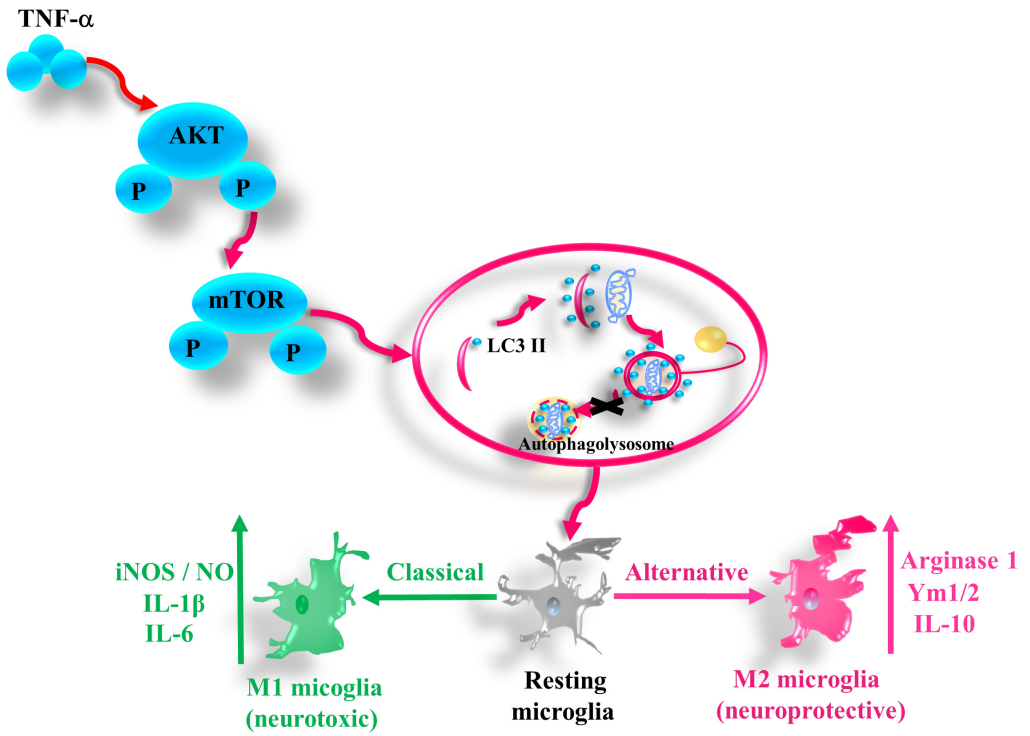

FIGURE 8 | A simplified summary of TNF-α induced autophagy flux inhibition and subsequent inflammation through AKT/mTOR signaling in microglia. TNF-α triggers the phosphorylation of AKT and mTOR, which plays a role in the autophagy flux disruption and causes a shift toward M1 phenotype in microglia. As a result, the microglia expression of the M1 markers such as iNOS/NO, IL-6, and IL-1β increases, while that of M2 genes including arginase, Ym1/2, and IL-10 decreases.

least in part, on AKT activation. An early activation of AKT, accompanied by mTOR activation, was observed in microglia after TNF-α stimulation. In the presence of the AKT inhibitor, TNF-α failed to alter the autophagic marker LC3II. Therefore, activation of AKT/mTOR signaling may contribute to TNF-α-induced autophagy inhibition in microglia. A recent study also identifies the role of AKT activation in regulating autophagy during the late stage (Matsuda-Lennikov et al., 2014). Phafin2 (EAPF or PLEKHF2), a lysosomal protein interacts with and recruits cytosolic Akt to the lysosome, and thus affects the autophagy-lysosome pathway.

The identification of different phenotypes is a breakthrough in microglia biology. M1 or M2 polarization reflects different microglia functions. Generally, M1 is pro-inflammatory and neurotoxic while M2 is anti-inflammatory and neuroprotective (Moehle and West, 2015). This opens up a novel avenue for the treatment of neuroinflammation related disorders. Notably, M1 or M2 markers are not exclusively expressed in microglia. Their phenotypic changes during neurodegeneration may be driven by extracellular and intracellular factors. The extracellular triggers were extensively reported, such as beta-amyloid and LPS (Qin et al., 2007; Hickman et al., 2008). Only a few molecules including AMPK, hydrogen sulfide, and A1 adenosine receptor, have been reported to modulate microglia polarization (Tsutsui et al., 2004; Zhou et al., 2014; Xu et al., 2015). Hence, the intracellular machinery warrants intensive study. Our study reveals autophagy as an endogenous "brake" on microglia phenotype shift toward M1 polarization. Atg5 (an autophagy-related protein) knockdown was sufficient to trigger M1 microglia activation in the absence of inflammatory stimulation. In TNF-α-challenged microglia, autophagic flux was impaired, associated with the increase of M1 marker (iNOS/NO, IL-1β, and IL-6) and the decrease in M2 marker (Arginase1, Ym1/2, and IL-10) expression. Upregulation of autophagy with serum deprivation or with pharmacologic activators (rapamycin and resveratrol) promoted microglia polarization toward M2 phenotype while inhibition of autophagy with 3-MA or Atg5 siRNA consistently aggravated the M1 polarization induced by TNF-α. These findings suggest that autophagy acts as an endogenous "brake" on microglia shift toward M1 in normal situation. In disease conditions, microglia autophagy deficiency may sensitize the cells to simulation and boost neuroinflammation.

Persistent microglia activation toward M1 phenotype could have physiologic relevance in brain regions with high microglia density such as SN (Pintado et al., 2011; Leal et al., 2013). This may contribute to dopaminergic neurodegeneration in PD. In support of this, here we found TNF-α-challenged microglia CM produced toxicity to the cocultured MES23.5 cells. The neurotoxicity was boosted if inhibiting microglia autophagy, but alleviated when microglia autophagy was activated. This CM-derived toxicity may derive from an accumulation of neurotoxic and pro-inflammatory molecules in the challenged CM. Consistently, the cytokines assay (**Figures 2**, **3**)

demonstrated a role of autophagy in modulating cytokines generation in microglia. Sure, other untested factors may also contribute to the toxicity.

In sum, our study demonstrates that TNF-α inhibits autophagy flux in microglia through activating AKT/mTOR signaling pathway, and identifies that autophagy serves as a negative regulator of microglia polarization in both normal and inflamed conditions. This study also highlights the potential of autophagy inducers in the treatment of neuroinflammation-associated degeneration.

AUTHOR CONTRIBUTIONS

C-FL and L-FH designed this study. M-mJ, FW, and W-wL carried out all the experiments. CG, DQ, ZZ, C-JM, and Y-PY revised the manuscript. L-FH and M-mJ contributed to writing the manuscript. All authors read and approved the final version of the manuscript.

FUNDING

This work was supported by grants from the National Natural Science Foundation of China (81571233 and 81671250), Jiangsu Provincial Medical Key Discipline Project (ZDXKB2016022), Jiangsu Key Laboratory of Neuropsychiatric Diseases (BM2013003), Suzhou Clinical Research Center of Neurological Disease (Szzx201503), Jiangsu Province's Young Medical Talents Program (QNRC2016872), and also partly supported by Priority Academic Program Development of Jiangsu Higher Education Institutions (PAPD).

REFERENCES

Bussi, C., Peralta Ramos, J. M., Arroyo, D. S., Gaviglio, E. A., Gallea, J. I., Wang, J. M., et al. (2017). Autophagy down regulates pro-inflammatory mediators in BV2 microglial cells and rescues both LPS and alpha-synuclein induced neuronal cell death. *Sci. Rep.* 7:43153. doi: 10.1038/srep43153

Du, C., Jin, M., Hong, Y., Li, Q., Wang, X. H., Xu, J. M., et al. (2014). Downregulation of cystathionine beta-synthase/hydrogen sulfide contributes to rotenone-induced microglia polarization toward M1 type. *Biochem. Biophys. Res. Commun.* 451, 239–245. doi: 10.1016/j.bbrc.2014.07.107

Fujita, K., Maeda, D., Xiao, Q., and Srinivasula, S. M. (2011). Nrf2-mediated induction of p62 controls Toll-like receptor-4-driven aggresome-like induced structure formation and autophagic degradation. *Proc. Natl. Acad. Sci. U.S.A.* 108, 1427–1432. doi: 10.1073/pnas.1014156108

Glass, C. K., Saijo, K., Winner, B., Marchetto, M. C., and Gage, F. H. (2010). Mechanisms underlying inflammation in neurodegeneration. *Cell* 140, 918–934. doi: 10.1016/j.cell.2010.02.016

He, Y., She, H., Zhang, T., Xu, H., Cheng, L., Yepes, M., et al. (2018). p38 MAPK inhibits autophagy and promotes microglial inflammatory responses by phosphorylating ULK1. *J. Cell Biol.* 217, 315–328. doi: 10.1083/jcb.201701049

Hickman, S. E., Allison, E. K., and El Khoury, J. (2008). Microglial dysfunction and defective beta-amyloid clearance pathways in aging Alzheimer's disease mice. *J. Neurosci.* 28, 8354–8360. doi: 10.1523/JNEUROSCI.0616-08.2008

Hu, X., Li, P., Guo, Y., Wang, H., Leak, R. K., Chen, S., et al. (2012). Microglia/macrophage polarization dynamics reveal novel mechanism of injury expansion after focal cerebral ischemia. *Stroke* 43, 3063–3070. doi: 10.1161/STROKEAHA.112.659656

Hunot, S., and Hirsch, E. C. (2003). Neuroinflammatory processes in Parkinson's disease. *Ann. Neurol.* 53(Suppl. 3), S49–S58. doi: 10.1002/ana.10481

Kigerl, K. A., Gensel, J. C., Ankeny, D. P., Alexander, J. K., Donnelly, D. J., and Popovich, P. G. (2009). Identification of two distinct macrophage subsets with divergent effects causing either neurotoxicity or regeneration in the injured mouse spinal cord. *J. Neurosci.* 29, 13435–13444. doi: 10.1523/JNEUROSCI.3257-09.2009

Kim, W. G., Mohney, R. P., Wilson, B., Jeohn, G. H., Liu, B., and Hong, J. S. (2000). Regional difference in susceptibility to lipopolysaccharide-induced neurotoxicity in the rat brain: role of microglia. *J. Neurosci.* 20, 6309–6316. doi: 10.1523/JNEUROSCI.20-16-06309.2000

Leal, M. C., Casabona, J. C., Puntel, M., and Pitossi, F. J. (2013). Interleukin-1beta and tumor necrosis factor-alpha: reliable targets for protective therapies in Parkinson's disease? *Front. Cell Neurosci.* 7:53. doi: 10.3389/fncel.2013.00053

Mantovani, A., Biswas, S. K., Galdiero, M. R., Sica, A., and Locati, M. (2013). Macrophage plasticity and polarization in tissue repair and remodelling. *J. Pathol.* 229, 176–185. doi: 10.1002/path.4133

Matsuda-Lennikov, M., Suizu, F., Hirata, N., Hashimoto, M., Kimura, K., Nagamine, T., et al. (2014). Lysosomal interaction of Akt with Phafin2: a critical step in the induction of autophagy. *PLoS One* 9:e79795. doi: 10.1371/journal.pone.0079795

Mccoy, M. K., Ruhn, K. A., Blesch, A., and Tansey, M. G. (2011). TNF: a key neuroinflammatory mediator of neurotoxicity and neurodegeneration in models of Parkinson's disease. *Adv. Exp. Med. Biol.* 691, 539–540. doi: 10.1007/978-1-4419-6612-4_56

Menza, M., Dobkin, R. D., Marin, H., Mark, M. H., Gara, M., Bienfait, K., et al. (2010). The role of inflammatory cytokines in cognition and other non-motor symptoms of Parkinson's disease. *Psychosomatics* 51, 474–479. doi: 10.1176/appi.psy.51.6.474

Mizushima, N. (2007). Autophagy: process and function. *Genes Dev.* 21, 2861–2873. doi: 10.1101/gad.1599207

Mizushima, N., Yoshimori, T., and Levine, B. (2010). Methods in mammalian autophagy research. *Cell* 140, 313–326. doi: 10.1016/j.cell.2010.01.028

Moehle, M. S., and West, A. B. (2015). M1 and M2 immune activation in Parkinson's disease: foe and ally? *Neuroscience* 302, 59–73. doi: 10.1016/j.neuroscience.2014.11.018

Orihuela, R., Mcpherson, C. A., and Harry, G. J. (2016). Microglial M1/M2 polarization and metabolic states. *Br. J. Pharmacol.* 173, 649–665. doi: 10.1111/bph.13139

Pintado, C., Macias, S., Dominguez-Martin, H., Castano, A., and Ruano, D. (2017). Neuroinflammation alters cellular proteostasis by producing endoplasmic reticulum stress, autophagy activation and disrupting ERAD activation. *Sci. Rep.* 7:8100. doi: 10.1038/s41598-017-08722-3

Pintado, C., Revilla, E., Vizuete, M. L., Jimenez, S., Garcia-Cuervo, L., Vitorica, J., et al. (2011). Regional difference in inflammatory response to LPS-injection in the brain: role of microglia cell density. *J. Neuroimmunol.* 238, 44–51. doi: 10.1016/j.jneuroim.2011.06.017

Plaza-Zabala, A., Sierra-Torre, V., and Sierra, A. (2017). Autophagy and microglia: novel partners in neurodegeneration and aging. *Int. J. Mol. Sci.* 18:E598. doi: 10.3390/ijms18030598

Qin, L., Wu, X., Block, M. L., Liu, Y., Breese, G. R., Hong, J. S., et al. (2007). Systemic LPS causes chronic neuroinflammation and progressive neurodegeneration. *Glia* 55, 453–462. doi: 10.1002/glia.20467

Saitoh, T., Fujita, N., Jang, M. H., Uematsu, S., Yang, B. G., Satoh, T., et al. (2008). Loss of the autophagy protein Atg16L1 enhances endotoxin-induced IL-1beta production. *Nature* 456, 264–268. doi: 10.1038/nature07383

Sardiello, M., Palmieri, M., Di Ronza, A., Medina, D. L., Valenza, M., Gennarino, V. A., et al. (2009). A gene network regulating lysosomal biogenesis and function. *Science* 325, 473–477. doi: 10.1126/science.1174447

Tsutsui, S., Schnermann, J., Noorbakhsh, F., Henry, S., Yong, V. W., Winston, B. W., et al. (2004). A1 adenosine receptor upregulation and activation attenuates neuroinflammation and demyelination in a model of multiple sclerosis. *J. Neurosci.* 24, 1521–1529. doi: 10.1523/JNEUROSCI.4271-03.2004

Vivekanantham, S., Shah, S., Dewji, R., Dewji, A., Khatri, C., and Ologunde, R. (2015). Neuroinflammation in Parkinson's disease: role in neurodegeneration

and tissue repair. *Int. J. Neurosci.* 125, 717–725. doi: 10.3109/00207454.2014.982795

Wang, M. X., Cheng, X. Y., Jin, M., Cao, Y. L., Yang, Y. P., Wang, J. D., et al. (2015). TNF compromises lysosome acidification and reduces alpha-synuclein degradation via autophagy in dopaminergic cells. *Exp. Neurol.* 271, 112–121. doi: 10.1016/j.expneurol.2015.05.008

Wang, Y., Li, Y., Li, H., Song, H., Zhai, N., Lou, L., et al. (2017). Brucella Dysregulates Monocytes and Inhibits Macrophage Polarization through LC3-Dependent Autophagy. *Front. Immunol.* 8:691. doi: 10.3389/fimmu.2017.00691

Wyss-Coray, T., and Rogers, J. (2012). Inflammation in Alzheimer disease-a brief review of the basic science and clinical literature. *Cold Spring Harb. Perspect. Med.* 2:a006346. doi: 10.1101/cshperspect.a006346

Xu, Y., Xu, Y., Wang, Y., Wang, Y., He, L., Jiang, Z., et al. (2015). Telmisartan prevention of LPS-induced microglia activation involves M2 microglia polarization via CaMKKbeta-dependent AMPK activation. *Brain Behav. Immun.* 50, 298–313. doi: 10.1016/j.bbi.2015.07.015

Zhou, X., Cao, Y., Ao, G., Hu, L., Liu, H., Wu, J., et al. (2014). CaMKKbeta-dependent activation of AMP-activated protein kinase is critical to suppressive effects of hydrogen sulfide on neuroinflammation. *Antioxid. Redox. Signal.* 21, 1741–1758. doi: 10.1089/ars.2013.5587

Conflict of Interest Statement: The authors declare that the research was conducted in the absence of any commercial or financial relationships that could be construed as a potential conflict of interest.

frontiers in Molecular Neuroscience

ORIGINAL RESEARCH
published: 10 January 2019
doi: 10.3389/fnmol.2018.00479

Parkinsonian Neurotoxins Impair the Pro-inflammatory Response of Glial Cells

*Neus Rabaneda-Lombarte[1,2], Efren Xicoy-Espaulella[1], Joan Serratosa[1], Josep Saura[2] and Carme Solà[1]**

[1]*Department of Brain Ischemia and Neurodegeneration, Institut d'Investigacions Biomèdiques de Barcelona (IIBB)—Consejo Superior de Investigaciones Científicas (CSIC), Institut d'Investigacions Biomèdiques August-Pi i Sunyer (IDIBAPS), Barcelona, Spain,* [2]*Biochemistry and Molecular Biology Unit, School of Medicine, Institut d'Investigacions Biomèdiques August-Pi i Sunyer (IDIBAPS), University of Barcelona, Barcelona, Spain*

In the case of Parkinson's disease (PD), epidemiological studies have reported that pesticide exposure is a risk factor for its pathology. It has been suggested that some chemical agents, such as rotenone and paraquat, that inhibit the mitochondrial respiratory chain (in the same way as the PD mimetic toxin 1-methyl-4-phenylpyridinium, MPP+) are involved in the development of PD. However, although the neurotoxic effect of such compounds has been widely reported using *in vivo* and *in vitro* experimental approaches, their direct effect on the glial cells remains poorly characterized. In addition, the extent to which these toxins interfere with the immune response of the glial cells, is also underexplored. We used mouse primary mixed glial and microglial cultures to study the effect of MPP+ and rotenone on glial activation, in the absence and the presence of a pro-inflammatory stimulus (lipopolysaccharide plus interferon-γ, LPS+IFN-γ). We determined the mRNA expression of the effector molecules that participate in the inflammatory response (pro-inflammatory cytokines and enzymes), as well as the nitric oxide (NO) and cytokine production. We also studied the phagocytic activity of the microglial cells. In addition, we evaluated the metabolic changes associated with the observed effects, through the measurement of adenosine triphosphate (ATP) production and the expression of genes involved in the control of metabolic pathways. We observed that exposure of the glial cultures to the neurotoxins, especially rotenone, impaired the pro-inflammatory response induced by LPS/IFN-γ. MPP+ and rotenone also impaired the phagocytic activity of the microglial cells, and this effect was potentiated in the presence of LPS/IFN-γ. The deficit in ATP production that was detected, mainly in MPP+ and rotenone-treated mixed glial cultures, may be responsible for the effects observed. These results show that the response of glial cells to a pro-inflammatory challenge is altered in the presence of toxins inhibiting mitochondrial respiratory chain

OPEN ACCESS

Edited by:
Yolanda Diz-Chaves, University of Vigo, Spain

Reviewed by:
Tarja Maarit Malm, University of Eastern Finland, Finland
Hong Qing, Beijing Institute of Technology, China

****Correspondence:***
Carme Solà
carme.sola@iibb.csic.es

Received: *02 October 2018*
Accepted: *07 December 2018*
Published: *10 January 2019*

Citation:
Rabaneda-Lombarte N, Xicoy-Espaulella E, Serratosa J, Saura J and Solà C (2019) Parkinsonian Neurotoxins Impair the Pro-inflammatory Response of Glial Cells. Front. Mol. Neurosci. 11:479. doi: 10.3389/fnmol.2018.00479

Abbreviations: ATP, adenosine triphosphate; BSA, bovine serum albumin; (COX-2), cyclooxygenase-2; Carkl, carbohydrate kinase-like protein; CNS, central nervous system; Glut, glucose transporter; gp91phox, NADPH oxidase, catalytic subunit; Hif, hypoxia-inducible factor; Hk, hexokinase; IL, interleukin; IFN-γ, interferon-γ; iNOS, inducible nitric oxide synthase; LPS, lipopolysaccharide; MPP+, 1-methyl-4-phenylpyridinium; MPTP, 1-methyl-4-phenyl-1,2,3,6-tetrahydropyridine; MTT, 3-(4,5-dimethylthiazol-2-yl)-2,5-diphenyltetrazolium bromide; NO, nitric oxide; PBS, Phosphate-buffered saline; PCR, polymerase chain reaction; PFK-P, phosphofructokinase; PI, propidium iodide; PD, Parkinson's disease; qRT-PCR, quantitative real time PCR; Rot, rotenone; TNF, tumor necrosis factor.

activity, suggesting that the glial immune response is impaired by such agents. This may have relevant consequences for brain function and the central nervous system's (CNS's) response to insults.

Keywords: glial activation, mixed glia, microglia, immune response, MPP+, rotenone, glial metabolism, Parkinson's disease

INTRODUCTION

Microglia are the main endogenous immune cells of the central nervous system (CNS). Under physiological conditions, they constantly patrol the CNS parenchyma, ready to detect alterations that could interfere with normal brain function. In response to noxious stimuli, microglial cells develop a wide range of reactive phenotypes aimed at re-establishing cerebral homeostasis and minimizing neuronal damage. In this way, they can respond to alterations in the CNS homeostasis due to the presence of exogenous pathogens or anomalous protein aggregates resulting from pathological processes. In addition, they are also able to respond to neuronal damage resulting from brain lesions, brain ischemia, neurodegenerative diseases or exposure to neurotoxic agents (Salter and Stevens, 2017).

In fact, exposure to neurotoxic agents, such as pesticides, may contribute to the development of some neurodegenerative diseases (Mostafalou and Abdollahi, 2013). In 1982, the accidental exposure to 1-methyl-4-phenyl-1,2,3,6-tetrahydropyridine (MPTP) in drug abusers caused parkinsonism (Langston et al., 1983). Epidemiological studies show that exposure to the pesticides rotenone and paraquat, which are functional and structural analogs of MPTP respectively, as well as to other pesticides, is a risk factor for Parkinson's disease (PD; Tanner et al., 2011; Goldman, 2013; Kamel, 2013). MPTP and its analogs are inhibitors of the mitochondrial respiratory chain and it has been suggested that mitochondrial dysfunction is involved in the induction of oxidative damage in dopaminergic neurons in parkinsonism (Dauer and Przedborski, 2003; Goldman, 2013). Due to the particular sensitivity of dopaminergic neurons to the effect of these neurotoxins, experimental models of PD have been developed by exposing neuronal cell cultures or laboratory animals to these agents (Bové and Perier, 2012). These experimental models are useful for studying mechanisms of dopaminergic neuronal cell degeneration and testing potential therapeutic approaches. However, although the toxic effect of MPTP [or its active metabolite 1-methyl-4-phenylpyridinium (MPP+)] and rotenone on dopaminergic neurons has been widely described using both *in vivo* and *in vitro* approaches, reports of their direct effect on glial cells are scarce. In addition, there is some controversy regarding the results already obtained. Either no direct effect of MPP+ on microglial cell function (Gao et al., 2003; Jin et al., 2012), or an increase in the expression of pro-inflammatory markers in microglial cells after MPP+ exposure (Bournival et al., 2012; Chen et al., 2015) has been reported. Similarly, either an increase in the expression of pro-inflammatory factors (Gao et al., 2013; Yuan et al., 2013; Du et al., 2014) or no direct effect on the production of inflammatory factors (Klintworth et al., 2009) has been observed in rotenone-treated microglial cell cultures.

Since reciprocal communication exists in the CNS between neuronal and glial cells, alterations in neuronal function may affect glial function and vice versa. In fact, a possible role of glial activation in the development of neuronal damage in neurodegenerative diseases has been repeatedly proposed (Perry et al., 2010; Colonna and Butovsky, 2017). In addition, communication also exists between glial cells, and alterations in a given cell type may affect the function of other glial cell types. Consequently, alterations in glial function due to exposure to neurotoxic compounds merit study, especially in the context of neurodegenerative diseases in which such exposure is considered a risk factor. The aim of this study was therefore to characterize the effects of MPP+ and rotenone on glial activation using primary mixed glial cultures, (mainly composed of astrocytes and microglia) and microglial cultures. We determined the direct effect of these neurotoxins on glial cell function, and also whether they could interfere with glial activation induced by a classical pro-inflammatory stimulus such as lipopolysaccharide (LPS)/interferon-γ (IFN-γ). We observed that MPP+ and rotenone did not induce the expression of pro-inflammatory markers by glial cells *per se*. However, the LPS/IFN-γ-induced pro-inflammatory response was modified in glial cultures in the presence of MPP+ and rotenone. These neurotoxins induced modifications in the mRNA expression of pro-inflammatory genes and phagocytic activity. Alterations in adenosine triphosphate (ATP) production could account for the effects observed. These results show that insults affecting the metabolic activity of glial cells, result in an altered immune response, which may have relevant consequences for normal brain function and the CNS response to insults.

MATERIALS AND METHODS

Experiments were carried out in accordance with European Union directives (86/609/EU) and Spanish regulations (BOE 67/8509-12, 1988) on the use of laboratory animals, and were approved by the Ethics and Scientific Committees of the University of Barcelona and CSIC.

Cell Cultures

Primary mixed glial cultures were prepared from the cerebral cortex of 1–3-day old C57Bl/6 mice as previously described (Gresa-Arribas et al., 2010). The culture medium used was the Dulbecco's modified Eagle medium-F12 nutrient mixture (GIBCO) supplemented with 10% heat-inactivated fetal bovine serum (FBS, Invitrogen, Molecular Probes, Eugene, OR, USA),

20 U/mL penicillin-20 μg/mL streptomycin (Invitrogen), and 0.5 μg/mL amphotericin B (Fungizone®, Invitrogen). The cells were seeded at a density of 3.5×10^5 cells/mL (100 μL, 300 μL and 2.5 mL per well into 96-, 48- and 6-well culture plates) and cultured at 37°C in a humidified 5% CO_2 atmosphere. The medium was replaced once a week. The cultures were used at 21 DIV.

Primary microglia enriched cultures were obtained from 21 DIV mixed glial cultures using the mild trypsinization method as previously described (Saura et al., 2003). Microglia enriched cultures were used 24 h after isolation by this procedure.

Cell Culture Treatments

LPS and IFN-γ treatment: Cells were treated with 100 ng/ml LPS (*E. coli* 026:B6, Sigma-Aldrich, St. Louis, MO, USA) and 0.1 ng/ml IFN-γ (Sigma-Aldrich) for 6 h or 24 h. Stock solutions of 1 mg/mL LPS in a serum-free culture medium and 10 μg/mL IFN-γ in a serum-containing culture medium, were prepared and stored at −20°C.

MPP+ and rotenone treatment: Cells were treated with 10, 25, 50 and 100 μM MPP+ or 20, 40, 100 and 150 nM rotenone (both from Sigma-Aldrich) for 6 h or 24 h, in the absence or presence of LPS/IFN-γ. Stock solutions of 50 mM MPP+ in milliQ H_2O and 10 mM rotenone in DMSO were freshly prepared on the day of treatment. DMSO in the cell cultures was always below 1/1,000.

Treatments were added directly to the culture medium.

Nitric Oxide Production

Nitric oxide (NO) production was estimated from the nitrite accumulation in the culture supernatant using the colorimetric Griess reaction. Briefly, the culture supernatant from the glial cells seeded into 96-well culture plates, was collected 24 and 48 h after treatments and stored at −20°C until used. Fifty microliter aliquots of the culture supernatant were incubated with equal volumes of the Griess reagent for 10 min at 20–25°C. Optical density at 540 nm was measured using a microplate reader (Multiskan Spectrum, Thermo Fisher Scientific, Vantaa, Finland). Nitrite concentration was determined from a sodium nitrate standard curve.

Cell Viability Measurements

Glial cells seeded into 96-well culture plates were used to estimate cell viability from the metabolic activity by a 3-(4,5-dimethylthiazol-2-yl)-2,5-diphenyl tetrazolium bromide (MTT) colorimetric assay, 24 h after treatments. Briefly, MTT (Sigma-Aldrich) was added to the cell cultures to reach a final concentration of 1 mg/mL. After incubation for 30 min (mixed glial cultures) or 90 min (microglial cultures) at 37°C, the medium was removed and 200 μL of DMSO was added to each well. The optical density of the resulting blue formazan was measured at 570 nm using a microplate reader (Multiskan Spectrum, Thermo Fisher Scientific). Readings were taken at 650 nm to obtain background levels. Results were expressed as percentages of the control.

Propidium iodide (PI) and Hoechst labeling were performed to corroborate data obtained in the MTT assay. Briefly, cells were incubated with PI (7.5 μg/ml, Molecular Probes, Eugene, OR, USA) and Hoechst 33342 (3 μg/ml, Molecular Probes) for 10 min. Microscopy images were obtained using an Olympus IX70 microscope (Olympus, Okoya, Japan) and a digital camera (CC-12, Olympus Soft Imaging Solutions GmbH, Hamburg, Germany). The extent of cell death was calculated from the ratio between PI positive nuclei, corresponding to dead cells, vs. Hoechst positive total nuclei.

RNA Extraction and Quantitative Real Time PCR

Glial cells seeded into six-well culture plates were used (one or two wells per experimental condition for mixed glia and microglia, respectively) to assess the mRNA expression of pro-inflammatory markers by quantitative real time polymerase chain reaction (PCR) 6 h after treatments. A High Pure RNA Isolation Kit (Roche Diagnostics Scheiwz AG, Rotkreuz, Switzerland) was used to isolate the total RNA from the mixed glial cultures. A PureLink RNA micro kit (Invitrogen) was used to isolate the total RNA from the primary microglial cultures. The RNA (0.5–1 μg) was reverse transcribed with random primers using the Transcriptor Reverse Transcriptase Kit (Roche Diagnostics). Three nanograms of cDNA were used to perform quantitative real time PCR (qRT-PCR) with the IQ SYBRGREEN SuperMix (Bio-Rad Laboratories, Hercules, CA, USA) using an iCycler MyIQ apparatus (Bio-Rad Laboratories) as previously described (Dentesano et al., 2014). The primers used (Integrated DNA Technology, IDT, Skokie, IL, USA) are shown in **Table 1**. Samples were run for 40 cycles (95°C for 15 s, 60°C for 30 s, and 72°C for 15 s). The amplification specificity was confirmed by the analysis of melting curves. Relative gene expression values were calculated using the ΔΔCt method (Livak and Schmittgen, 2001). β-Actin and 18S ribosomal RNA (Rn18s) were used as the reference genes.

ELISAs

The interleukin (IL) 1β, IL6 and tumor necrosis factor α (TNFα) release in the culture supernatant was determined using ELISA kits specific for each cytokine (mouse IL1-β ELISA Ready-SET-GO!, mouse IL6 ELISA Ready-SET-GO! and mouse TNFα ELISA Ready-SET-GO!, eBioscience-Affimetrix, Inc., San Diego, CA, USA), following the manufacturer's instructions. The culture supernatant from 48-well culture plates was collected 24 h after treatments and stored at −80°C until use. IL1β, IL6 and TNFα concentrations were determined from the standard curves.

Phagocytosis Assay

The phagocytic activity of the microglial cells was assessed 24 h after treatments. Briefly, the microglial cell cultures in 48-well plates were incubated for 1 h at 37°C with fluorescent latex beads (FluoSpheres, carboxylate-modified microspheres, 2.0 μm, red fluorescent (580/605), 2% solids; Thermofisher Scientific; 1/1,000) 23 h after treatments. Then, the cells were washed three times with a phosphate-buffered saline (PBS) and fixed with 4% paraformaldehyde for 15 min.

Immunocytochemistry was performed using a rabbit polyclonal anti-Iba1 primary antibody (1/500, WAKO; Japan), a specific marker for microglial cells. Cells were first incubated with 0.3% Triton-X-100 in PBS containing 1% bovine serum

TABLE 1 | Primers used for quantitative real time polymerase chain reaction (qRT-PCR).

Target mRNA	Accession number	Forward primer (5′→3′)	Reverse primer (5′→3′)
Carkl	NM_029031.3	CAGGCCAAGGCTGTGAAT	GCCAGCTGCATCATAGGACT
COX2	NM_011198.4	TGCAGAATTGAAAGCCCTCT	CCCCAAAGATAGCATCTGGA
Glut1	NM_011400.3	CATCCTTATTGCCCAGGTGTTT	GAAGATGACACTGAGCAGCAGA
gp91phox	NM_007807.5	ACTCCTTGGGTCAGCACTGGCT	GCAACACGCACTGGAACCCCT
Hifα	NM_010431.2	ACAAGTCACCACAGGACAG	AGGGAGAAAATCAAGTCG
Hk1	NM_010438.3	GATGGAGGTGAAGAAGAAGC	GGAAACGAGAAGGTGAAGC
Hk2	NM_013820.3	CGGTACACTCAATGACATCC	GTAGACAGAGCCATCCACG
IL1β	NM_008361.4	TGGTGTGTGACGTTCCCATTA	CAGCACGAGGCTTTTTTGTTG
IL6	NM_031168.2	CCAGTTTGGTAGCATCCATC	CCGGAGAGGAGACTTCACAG
iNOS	NM_010927.3	GGCAGCCTGTGAGACCTTTG	GCATTGGAAGTGAAGCGTTTC
Pfkp	NM_019703.4	AAGCTATCGGTGTCCTGACC	TCCCACCCACTTGCAGAAT
TNFα	NM_013693.3	TGATCCGCGACGTGGAA	ACCGCCTGGAGTTCTGGAA
Reference genes:			
β-Actin	NM_007393.5	CAACGAGCGGTTCCGATG	GCCACAGGATTCCATACCCA
Rn18s	NR_003278.3_	GTAACCCGTTGAACCCCATT	CCATCCAATCGGTAGTAGCG

β-Actin, Actin, beta; Carkl, sedoheptulokinase; COX2, cyclooxygenase-2; Glut1, Glucose transporter 1; gp91phox, catalytic subunit of NAPH oxidase; Hifα, hypoxia inducible factor 1, alpha subunit; Hk1, hexokinase 1, Hk2, hexokinase 2; IL1β, interleukin 1, beta; IL6, interleukin 6; iNOS, inducible nitric oxide synthase; Pfkp, phosphofructokinase, platelet; TNFα, tumor necrosis factor alpha; Rn18s, 18S ribosomal RNA.

albumin (BSA) and 10% normal donkey serum for 20 min at room temperature, and then overnight at 4°C with the primary antibody. Once they had been rinsed in PBS, cells were incubated for 1 h at room temperature with an ALEXA 488 donkey anti-rabbit secondary antibody (1/1,000; Invitrogen). Antibodies were diluted in 0.3% Triton X-100 in PBS containing 1% BSA and 10% normal donkey serum.

Images of three microscopic fields using a 20× objective were obtained with an Olympus IX70 fluorescence microscope and a digital camera (CC-12, Olympus Soft Imaging Solutions GmbH). Two to three wells per experimental condition were processed and each experimental condition was repeated at least four times. Visual counting of the FluoSpheres was performed. The percentage of phagocytic cells and the average number of fluorescent microspheres per microglial cell were calculated. To further characterize the phagocytic activity, we also calculated the percentage of cells showing lower phagocytic activity (microspheres/cell) than the controls and the percentage of cells showing higher phagocytic activity than the controls.

ATP Production

The intracellular production of ATP was determined using a luminescence assay kit (ATPlite Luminescence ATP Detection Assay System, PerkinElmer, Waltham, MA, USA) following the manufacturer's instructions. Briefly, cells in 96-well plates (mixed glia) or 6-well-plates (microglia) were lysed 24 h after treatments and the ATP concentration was measured based on the production of light, caused by the reaction of the ATP with added luciferase and D-luciferin. The emitted light was quantified using a luminometer (Orion Microplate Luminometer, Berthold Detection System, Germany). The ATP concentration in the samples was calculated from an ATP standard curve.

Data Presentation and Statistical Analysis

The results are presented as the mean + SEM. At least three independent experiments were performed for analysis. Data were statistically analyzed with the GraphPad Prism software. Statistical analyses were performed using the one-way analysis of variance (ANOVA) followed by the Newman-Keuls post-test, and a two-way ANOVA followed by the Bonferroni post-test. Values of $p < 0.05$ were considered statistically significant.

RESULTS

Effects of MPP+ and Rotenone on Glial Cell Viability

In a preliminary study, we performed dose-response experiments in order to select working concentrations of MPP+ and rotenone that did not result in significant alterations in cell viability after 24 h exposure. We evaluated glial cell viability after treating the mixed glial or the microglial cultures with increasing concentrations of MPP+ (10, 25, 50 and 100 μM) or rotenone (20, 40, 100 and 150 nM), both in the absence and in the presence of LPS/IFN-γ, considering the MTT assay and PI staining. In mixed glial cell cultures, MPP+ induced a concentration-dependent decrease in MTT reduction that was accentuated in the presence of LPS/IFN-γ (**Figure 1A**). On the contrary, no alterations in MTT reduction were observed in microglial cell cultures treated with MPP+, both in the absence and presence of LPS/IFN-γ (**Figure 1B**). Rotenone-treated mixed glial cell cultures showed a significant decrease in MTT reduction from 100 nM rotenone. In the presence of LPS/IFN-γ, there was a significant decrease in MTT reduction even at 20 nM rotenone (**Figure 1C**). As in the case of MPP+ treatments, no alterations in MTT reduction were observed in microglial cell cultures treated with rotenone or rotenone and LPS/IFN-γ (**Figure 1D**). To determine whether the decrease in MTT reduction in MPP+ and rotenone-treated mixed glial cell cultures was due to a decrease in metabolic activity or due to cell death, PI staining was performed. Mixed glial cultures treated with 50 and 100 μM MPP+ showed a significant increase in the percentage of PI positive nuclei. This effect was accentuated in the presence

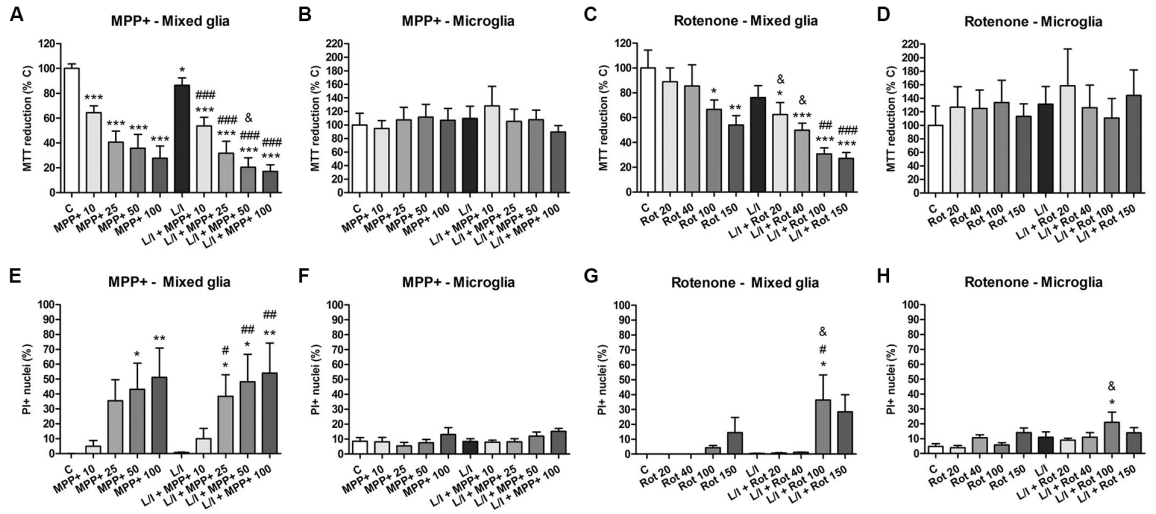

FIGURE 1 | Effect of 1-methyl-4-phenylpyridinium (MPP+) and rotenone on glial cell viability. **(A–D)** MPP+ and rotenone induced alterations in 3-(4,5-dimethylthiazol-2-yl)-2,5-diphenyltetrazolium bromide (MTT) reduction in the primary glial cultures. Effect of 10, 25, 50 and 100 μM MPP+ treatment for 24 h on the mixed glial cultures **(A)** and microglial cultures **(B)**, both in the absence and the presence of lipopolysaccharide (LPS)/interferon-γ (IFN-γ; L/I). Effect of 20, 40, 100 and 150 nM rotenone (Rot) treatment for 24 h on the mixed glial cultures **(C)** and microglial cultures **(D)**, both in the absence and the presence of L/I. **(E–H)** Percentage of propidium iodide (PI) positive nuclei in the mixed glial cultures **(E)** and microglial cultures **(F)** treated for 24 h with 10, 25, 50 and 100 μM MPP+, both in the absence and the presence of LPS/IFN-γ (L/I). Percentage of PI positive nuclei in the mixed glial cultures **(G)** and microglial cultures **(H)** treated for 24 h with 20, 40, 100 and 150 nM rotenone (Rot), both in the absence and the presence of L/I. Bars are means ± SEM of four independent experiments. $^{*}p < 0.05$, $^{**}p < 0.01$ and $^{***}p < 0.001$ vs. control (C); $^{\#}p < 0.05$, $^{\#\#}p < 0.01$ and $^{\#\#\#}p < 0.001$ vs. L/I; $^{\&}p < 0.05$ vs. MPP+ or Rot alone; one-way analysis of variance (ANOVA; repeated measures) and Newman-Keuls post-test.

of LPS/IFN-γ, and a significant increase was also detected at 25 μM MPP+ (**Figure 1E**). No alterations in the percentage of PI-positive nuclei were observed in microglial cultures treated with MPP+ (**Figure 1F**). In addition, no significant increases in the percentage of PI-positive nuclei were observed in rotenone-treated mixed glial cell cultures or microglial cultures (**Figures 1G,H**), with the exception of cells treated with 100 μM rotenone and LPS/IFN-γ.

The concentrations of 10 and 25 μM MPP+ and 40 and 100 nM rotenone were used in subsequent studies. Representative images of the cultures in these experimental conditions are shown in **Figure 2**, which corroborate the lack of a toxic effect of the concentrations of MPP+ (**Figure 2A**) and rotenone (**Figure 2B**) selected for further experiments.

MPP+ and Rotenone Induce Alterations in the Expression of Pro-inflammatory Genes in LPS/IFN-γ-Treated Primary Glial Cultures

We next determined whether MPP+ and rotenone induced a pro-inflammatory phenotype in primary glial cell cultures, as well as whether they had some effect on the development of the pro-inflammatory response induced by LPS/IFN-γ. We determined the mRNA expression of the cytokines IL1β, IL6 and TNFα and the enzymes inducible NO synthase (iNOS), cyclooxygenase 2 (COX2) and gp91phox (the catalytic subunit of NADPH oxidase), as markers of a pro-inflammatory response. In general, MPP+ (**Figure 3**) and rotenone (**Figure 4**) treatment did not significantly induce the mRNA expression of these pro-inflammatory markers in the primary glial cell cultures, although a trend towards increased expression was observed for some mRNAs, especially in rotenone-treated mixed glial cultures. On the contrary, 6 h after LPS/IFN-γ treatment, the mRNA expression of all the pro-inflammatory markers tested was clearly induced (**Figures 3**, **4**). However, MPP+ and especially rotenone induced alterations in the pattern of expression of these markers in LPS/IFN-γ treated cultures. When glial cell cultures were treated with LPS/IFN-γ in the presence of MPP+, the induction of IL1β mRNA expression was significantly inhibited in the mixed glial and microglial cultures (**Figures 3A,B**), while COX2 mRNA expression was further increased in the mixed glial cultures (**Figure 3A**) and gp91phox mRNA was induced in the microglial cultures (**Figure 3B**). More importantly, rotenone exposure significantly abrogated LPS/IFN-γ induction of the mRNA expression of all pro-inflammatory markers in the mixed glial cultures (**Figure 4A**), as well as IL1β, IL6 and COX2 mRNA expression in microglial cultures (**Figure 4B**).

MPP+ and Rotenone Inhibit LPS/IFN-γ-Induced NO and Pro-inflammatory Cytokine Production in Primary Glial Cultures

We also analyzed the effect of MPP+ and rotenone on NO, IL1β, IL6 and TNFα release into the culture medium. MPP+ alone induced a decrease in NO production and an increase

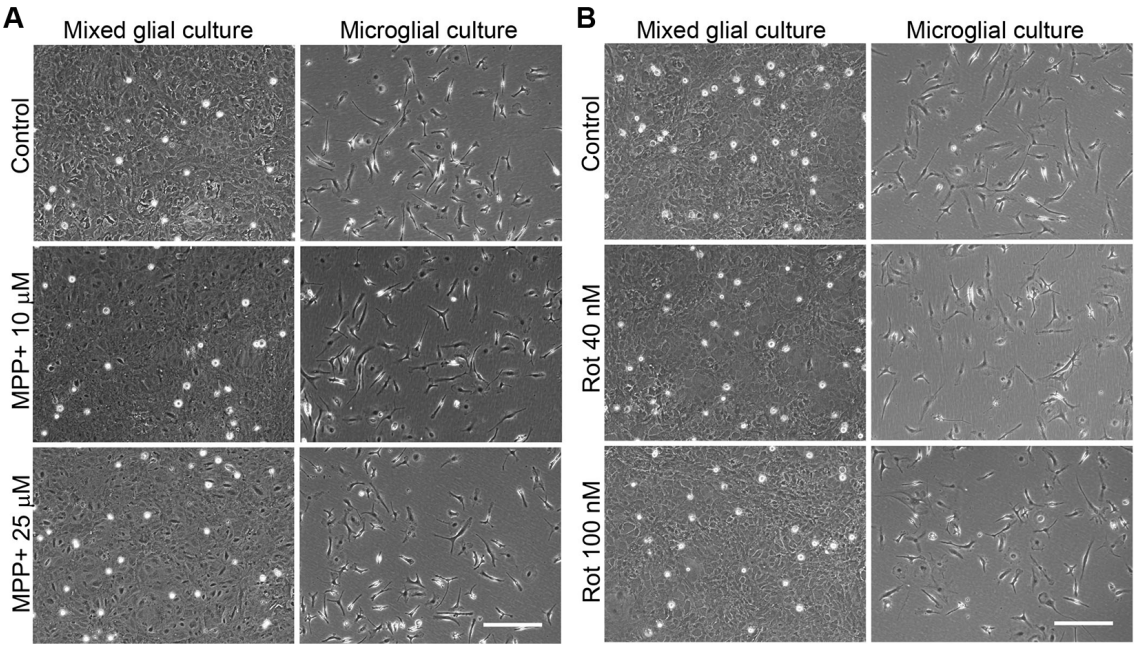

FIGURE 2 | Phase contrast images of the MPP+- and rotenone-treated primary glial cultures. Images show the appearance of the mixed glial cultures and microglial cultures treated for 24 h with 10 and 25 μM MPP+ **(A)** or 40 and 100 nM rotenone (Rot; **B**), the working concentrations used in further studies. Bar = 200 μm.

in IL6 release into the culture medium in mixed glial cell cultures 24 h after treatment (**Figure 5A**). The latter effect was also observed in the MPP+-treated microglial cultures (**Figure 5B**), as well as in the rotenone-treated mixed glial (**Figure 5C**) and microglial cultures (**Figure 5D**). LPS/IFN-γ-treatment clearly increased NO production in the mixed glial cultures, and MPP+ (25 μM) and rotenone (40 and 100 nM) significantly inhibited this effect (**Figures 5A,C**). Significant NO production was not detected in the microglial cultures treated with LPS/IFN-γ for 24 h (**Figures 5B,D**). However, an increase in NO production was observed when the microglial cultures were treated with LPS/IFN-γ for 48 h, but MPP+ and rotenone did not modify this effect (data not shown). With regards to cytokine release, LPS/IFN-γ-treatment resulted in drastic increases in IL1β, IL6 and TNFα levels in the mixed glial (**Figures 5A,C**) and microglial (**Figures 5B,D**) cultures. MPP+ exposure (25 μM) significantly inhibited LPS/IFN-γ-induced release of IL1β and IL6, but not TNFα, in the mixed glia (**Figure 5A**), while it had no significant effect on the production of these cytokines in the microglial cell cultures (**Figure 5B**). Interestingly, rotenone (40 and 100 nM) significantly inhibited IL1β, IL6 and TNFα release induced by LPS/IFN-γ in both the mixed glial (**Figure 5C**) and microglial cultures (**Figure 5D**).

MPP+ and Rotenone Treatment Inhibit the Phagocytic Activity of Microglial Cells

We then evaluated whether MPP+ and rotenone modified the phagocytic activity of the microglial cells, another important parameter used to characterize the microglial activation phenotype. Both MPP+ and rotenone treatment showed a tendency to decrease the percentage of phagocytic microglial cells that were statistically significant when the cells were also treated with LPS/IFN-γ (**Figure 6A**). In addition, MPP+ and rotenone treatment resulted in a significant increase in the percentage of microglial cells showing low phagocytic activity (number of microspheres per cell lower than control) and a subsequent significant decrease in the percentage of cells showing high phagocytic activity (number of microspheres per cell higher than control; **Figure 6B**). These effects were accentuated in the presence of LPS/IFN-γ.

ATP Production Is Compromised in MPP+- and Rotenone-Treated Glial Cell Cultures

In an attempt to better characterize the metabolic status of the cells, we determined the intracellular ATP production in response to MPP+, rotenone and LPS/IFN-γ treatments. In general, ATP production was modified in the mixed glial cultures in our MPP+ and rotenone experimental models ($p < 0.001$, one-way ANOVA; **Figure 7**). In particular, ATP production was significantly decreased after 25 μM MPP+ treatment (**Figure 7A**). On the contrary, a significant increase in ATP production was detected in the LPS/IFN-γ-treated mixed glial cultures, which was abrogated in the presence of MPP+ and rotenone (**Figures 7A,B**). ATP production was also modified in the microglial cultures in the MPP+ and rotenone experimental models ($p < 0.05$, one-way ANOVA), but to a lesser extent than in the mixed glial cultures (**Figures 7C,D**).

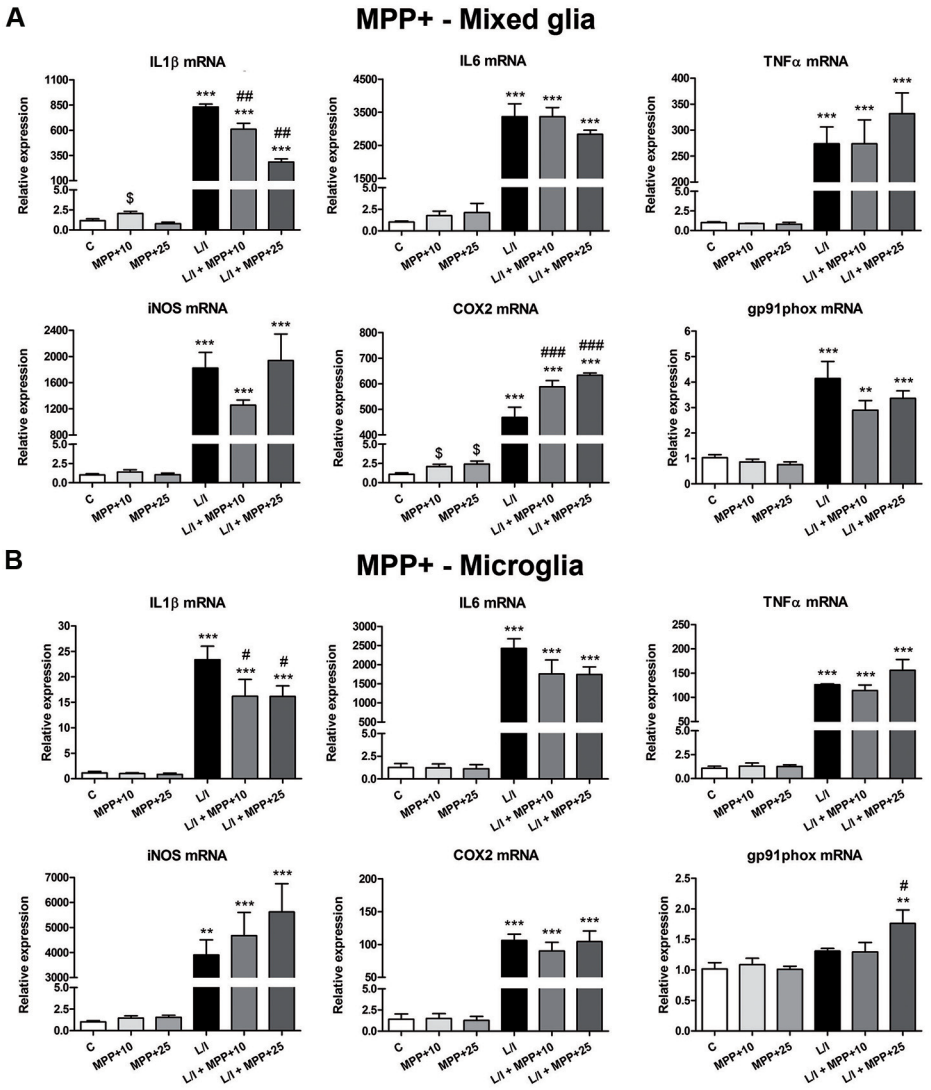

FIGURE 3 | Effect of MPP+ treatment on the mRNA expression of pro-inflammatory markers. mRNA expression of pro-inflammatory cytokines [interleukin-1β (IL-1β), IL-6 and tumor necrosis factor-α (TNF-α)] and enzymes [inducible nitric oxide synthase (iNOS), cyclooxygenase-2 (COX-2), gp91phox] in the primary mixed glial cultures **(A)** and microglial cultures **(B)** treated for 6 h with 10 and 25 μM MPP+, both in the absence and the presence of LPS/IFN-γ (L/I). 18S ribosomal RNA (Rn18s) and β-actin were used as housekeeping genes. Bars are means ± SEM of four independent experiments. $^{**}p < 0.01$ and $^{***}p < 0.001$ vs. C; $^{\#}p < 0.05$, $^{\#\#}p < 0.01$ and $^{\#\#\#}p < 0.001$ vs. L/I; one-way ANOVA and Newman-Keuls post-test. $^{\$}p < 0.05$ MPP+ alone vs. C, one-way ANOVA and Newman-Keuls post-test only considering the L/I-free groups. This latter analysis was performed to detect whether the high values observed in the L/I group may hinder the detection of statistical significance of the effects of MPP+ alone.

Metabolic Changes in LPS/IFN-γ-Treated Glial Cultures: Effect of MPP+ and Rotenone

In immune cells, the development of specific immune responses is associated with specific metabolic changes. Increased glycolysis and potentiation of the pentose phosphate pathway, together with the inhibition of oxidative phosphorylation has been reported for immune cells showing a pro-inflammatory phenotype. We checked whether this was the case in our glial cultures treated with LPS/IFN-γ and whether MPP+ and rotenone were able to modify it. We determined the mRNA expression of genes encoding critical proteins for the switch to glycolysis: glucose transporter 1 (Glut1; glucose entrance into the cell), key glycolytic enzymes such as hexokinase 1 (Hk1) (glycolysis initial rate limiting step) and phosphofructokinase 1 (PFK1) (master regulator of glycolysis), the glycolysis activator hypoxia-inducible factor 1α (Hif1α) and carbohydrate kinase-like protein (Carkl), involved in the control of the pentose phosphate pathway. In the microglial cell cultures, MPP+ and rotenone alone did not modify the expression of these genes *per se* (**Figure 8**). On the contrary, as expected, LPS/IFN-γ treatment induced an increase in their

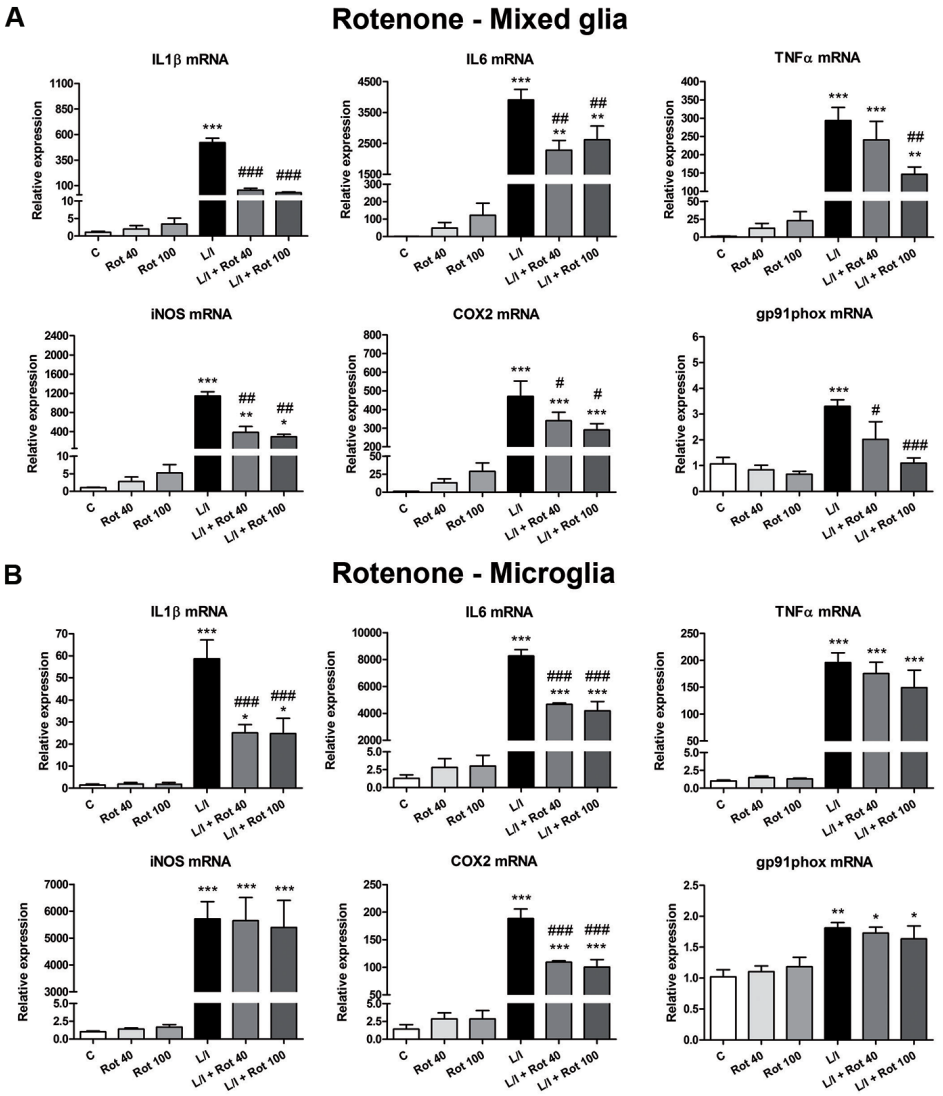

FIGURE 4 | Effect of rotenone treatment on the mRNA expression of pro-inflammatory markers. mRNA expression of pro-inflammatory cytokines (IL-1β, IL-6 and TNF-α) and enzymes (iNOS, COX-2, gp91phox) in the primary mixed glial cultures **(A)** and microglial cultures **(B)** treated for 6 h with 40 and 100 nM rotenone (Rot), both in the absence and the presence of LPS/IFN-γ (L/I). Rn18s and β-actin were used as housekeeping genes. Bars are means ± SEM of four independent experiments. $^{*}p < 0.5$, $^{**}p < 0.01$ and $^{***}p < 0.001$ vs. control (C); $^{\#}p < 0.05$, $^{\#\#}p < 0.01$ and $^{\#\#\#}p < 0.001$ vs. L/I; one-way ANOVA and Newman-Keuls post-test.

expression (**Figure 8**), with the exception of Carkl mRNA (**Figures 8I,J**), which showed a decrease. MPP+ treatment further increased LPS-IFN-γ-induced Glut1 mRNA expression (**Figure 8A**), while rotenone inhibited LPS-IFN-γ-induced Pfk1 (**Figure 8F**) and Hif1α (**Figure 8H**) mRNA expression. We also evaluated the expression of these mRNAs in the mixed glial cultures. MPP+ and rotenone alone increased the Glut1 mRNA (**Figures 9A,B**), MPP+ and Hif1α mRNA expression (**Figure 9G**). LPS/IFN-γ treatment inhibited the expression of the glycolytic genes Glut1 (**Figures 9A,B**), Hk1 (**Figures 9C,D**) and Pfk1 (**Figures 9E,F**), as well as Carkl mRNA expression (**Figures 9I,J**), and increased the expression of Hif1α (**Figures 9G,H**). Rotenone inhibited LPS/IFN-γ-induced Hif1α mRNA expression (**Figure 9H**).

DISCUSSION

In this study, we show that the response of glial cells to a pro-inflammatory stimulus is modified by the neurotoxic agents MPP+ and rotenone. MPP+ and rotenone treatment did not induce a significant pro-inflammatory phenotype in the primary mixed glial and microglial cultures *per se*. However, these neurotoxic agents, mainly rotenone, did impair the development of a pro-inflammatory phenotype in the LPS/IFN-γ-treated glial cultures. This effect was observed in the absence of significant cell death but in the presence of impaired metabolic activity.

The toxic effects of MPP+ and rotenone on neurons have repeatedly been demonstrated using primary neuronal cultures, with dopaminergic neurons showing the highest sensitivity to

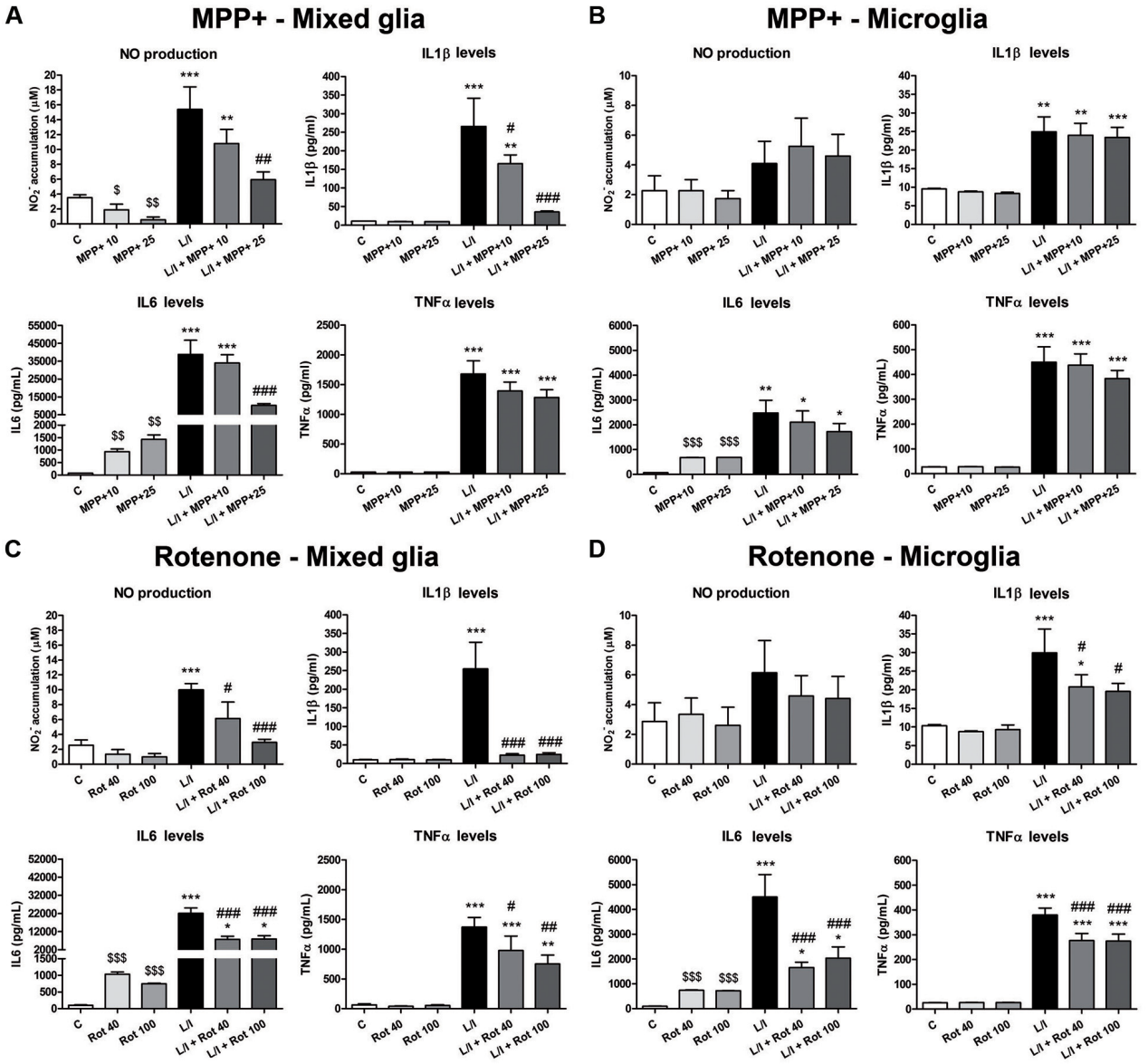

FIGURE 5 | Nitric oxide (NO) and pro-inflammatory cytokine production in the primary glial cell cultures treated with MPP+ and rotenone. NO production was estimated from nitrite accumulation and IL1β, IL6 and TNFα levels were determined by ELISA in the culture medium of the MPP+-treated mixed glial **(A)** and microglial **(B)** cultures, and the rotenone (Rot)-treated mixed glial **(C)** and microglial **(D)** cultures. The cell cultures were treated with 10 and 25 μM MPP+ or 40 and 100 nM Rot for 24 h, in the absence or in the presence of LPS/IFN-γ (L/I). Bars are means ± SEM of four independent experiments. $^{*}p < 0.5$, $^{**}p < 0.01$ and $^{***}p < 0.001$ vs. control (C); $^{\#}p < 0.05$, $^{\#\#}p < 0.01$ and $^{\#\#\#}p < 0.001$ vs. L/I; one-way ANOVA and Newman-Keuls post-test. $^{\$}p < 0.05$, $^{\$\$}p < 0.01$ and $^{\$\$\$}p < 0.001$ MPP+ and Rot alone vs. C, one-way ANOVA and Newman-Keuls post-test only considering the L/I-free groups. This latter analysis was performed to detect whether the high values observed in the L/I group may hinder the detection of a statistical significance of the effects of MPP+ and Rot alone.

the toxic effects of these compounds. In mouse primary cultures, dopaminergic neuron death is observed at concentrations from 0.1 μM MPP+ (1-week exposure; Kinugawa et al., 2013) or 3 μM MPP+ (48 h exposure; Henze et al., 2005), and 10 nM (1-week exposure; Gao et al., 2003) or 5 nM rotenone (48 h exposure; Radad et al., 2006). Exposure to higher concentrations of these neurotoxins is necessary to induce the death of non-dopaminergic neurons (Gao et al., 2003; Henze et al., 2005). The presence of microglial cells in neuronal cultures has been associated to the increased neurotoxicity of MPP+ and rotenone (Gao et al., 2002, 2003; Emmrich et al., 2013; Kinugawa et al., 2013). However, as MPP+- and rotenone-damaged neurons induce reactive microgliosis, which has a neurotoxic effect, it is difficult to establish the contribution of a direct effect of the toxins on glial cells in the neurotoxicity observed. In fact, although the neurotoxic effect of MPP+ and rotenone has been widely described using *in vivo* and *in vitro* experimental approaches, their direct effects on glial cells remain

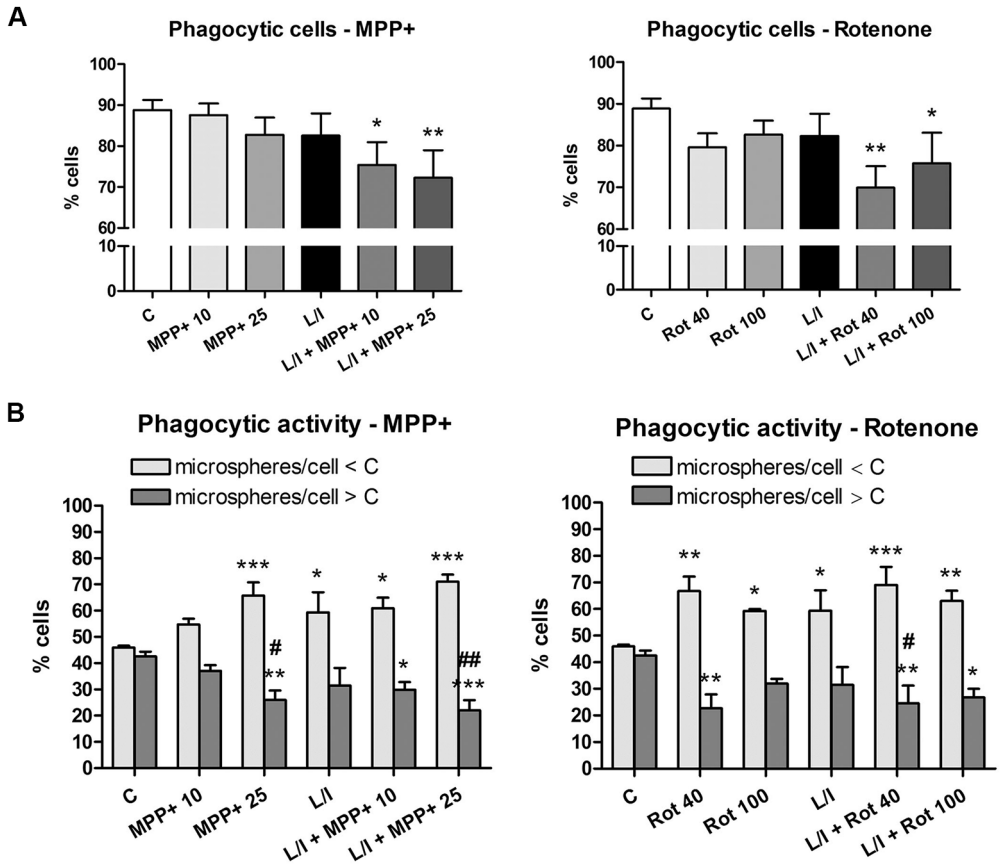

FIGURE 6 | Effect of MPP+ and rotenone treatment on the microglial cell phagocytosis in the primary microglial cell cultures. Phagocytic activity was evaluated through the ingestion of fluorescent microspheres after treating the cell cultures with 10 and 25 μM MPP+ or 40 and 100 nM rotenone (Rot) for 24 h, in both the absence and presence of LPS/IFN-γ (L/I). Internalization of microspheres was quantified after immunofluorescence labeling of the microglial cells using an anti-Iba1 antibody. **(A)** Percentage of cells with microspheres. Bars are means ± SEM of four independent experiments. $^{*}p < 0.05$ and $^{**}p < 0.01$ vs. control (C); one-way ANOVA and Newman-Keuls post-test. **(B)** Percentage of cells with low phagocytic activity (number of microspheres/cell < C) and cells with high phagocytic activity (number of microspheres/cells > C). Bars are means ± SEM of four independent experiments. $^{*}p < 0.05$, $^{**}p < 0.01$ and $^{***}p < 0.001$ vs. corresponding C; $^{\#}p < 0.05$ and $^{\#\#}p < 0.01$ vs. low-phagocytic cells; two-way ANOVA and Bonferroni post-test.

poorly characterized (Gao et al., 2003; Klintworth et al., 2009; Bournival et al., 2012; Du et al., 2014; Chen et al., 2015; Zhou et al., 2016). Most of the studies performed until now using glial cell cultures have tested whether these neurotoxins induce a pro-inflammatory phenotype in the microglial cells, and the results obtained are controversial. The range of concentrations used in these studies are higher than that used in neuronal cultures (0.1–500 μM MPP+ and 10 nM-1 μM rotenone; Gao et al., 2003; Henze et al., 2005; Klintworth et al., 2009; Bournival et al., 2012; Jin et al., 2012; Du et al., 2014). Some authors have reported no alterations (Klintworth et al., 2009; Ferger et al., 2010; Jin et al., 2012), but others have shown the induction of pro-inflammatory markers in the MPP+- and rotenone-treated microglial cultures (Du et al., 2014; Zhang et al., 2014; Liang et al., 2015; Zhou et al., 2016). Differences in the pattern of neurotoxin treatment (concentration and duration of the treatment) and the cell types used (primary cultures and cell lines from different species) may partially account for the differences observed. Most studies have considered microglial cell lines, while studies using primary microglial cultures are scarce. In this study, we show that concentrations of MPP+ and rotenone that did not affect cell viability in primary glial cultures at 24 h did not result in the induction of a significant pro-inflammatory phenotype (with the exception of IL6 production), but they interfered with the development of the pro-inflammatory phenotype induced by LPS/IFN-γ. Thus, MPP+ and rotenone inhibited pro-inflammatory cytokine production induced by LPS/IFN-γ in glial cells (IL1β in the case of MPP+, and also IL6 and TNFα in the case of rotenone). They also modified the expression of pro-inflammatory enzymes (iNOS, COX2 and/or gp91phox). In general, the alterations observed were more pronounced in the mixed glia than in the microglial cell cultures. In addition, the effect of rotenone was stronger than that of MPP+, although the concentrations of rotenone used were three orders of magnitude below those of MPP+. MPP+ and rotenone treatment also interfered in the phagocytic activity of the microglial cells, which was clearly inhibited after neurotoxin treatment, especially in the presence of LPS/IFN-γ. Altogether, these results suggest

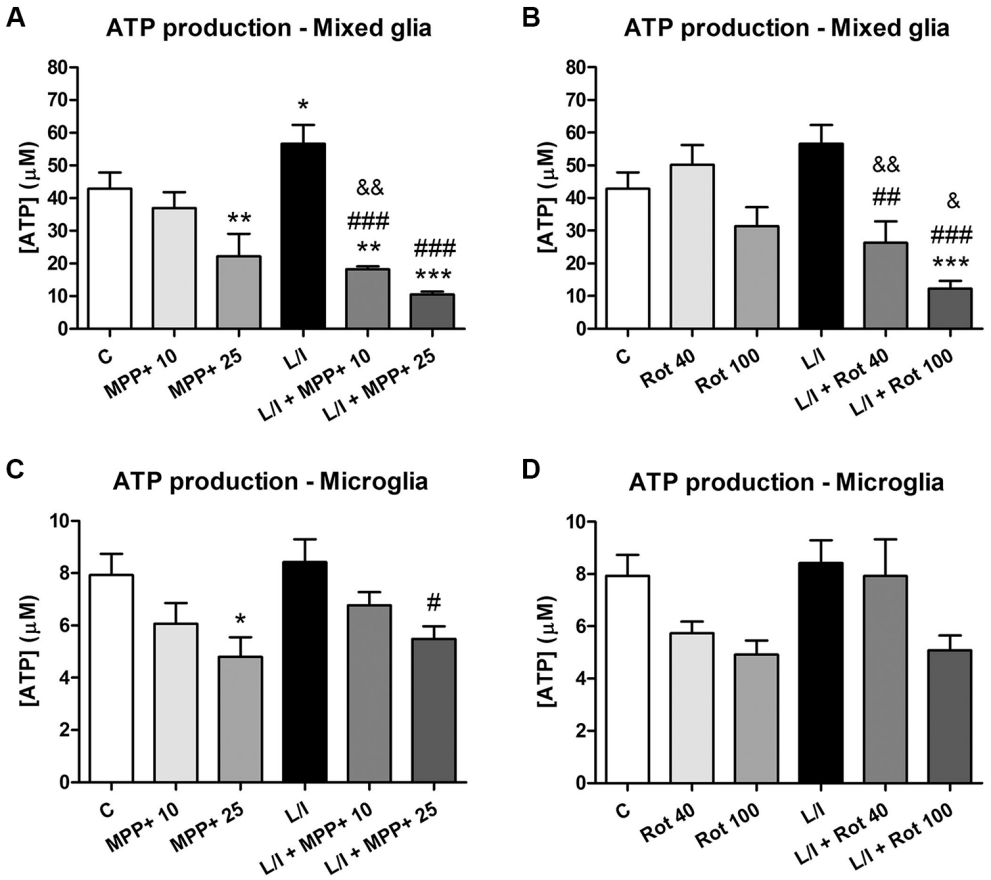

FIGURE 7 | Adenosine triphosphate (ATP) production in the primary glial cell cultures treated with MPP+ and rotenone. Intracellular ATP production was determined in the mixed glial cultures and microglial cultures treated with 10 and 25 μM MPP+ **(A,B)** or 40 and 100 nM rotenone (Rot; **C,D**) for 24 h, in the absence and in the presence of LPS/IFN-γ (L/I). Bars are means ± SEM of five independent experiments. $^{*}p < 0.5$, $^{**}p < 0.01$ and $^{***}p < 0.001$ vs. control **(C)**; $^{\#}p < 0.05$, $^{\#\#}p < 0.01$ and $^{\#\#\#}p < 0.001$ vs. L/I; $^{\&}p < 0.05$ and $^{\&\&}p < 0.01$ vs. MPP+ or Rot alone; one-way ANOVA and Newman-Keuls post-test.

that MPP+ and rotenone directly impair the ability of the glial cells to respond to a pro-inflammatory insult. In this sense, exposure to stimuli that affect the mitochondrial activity, such as hypoxia or respiratory chain inhibitors, has been suggested to alter the immune response of macrophages (Wiese et al., 2012).

At the cellular level, the main target of both MPP+ and rotenone is the mitochondrial electron transport chain, where they selectively inhibit complex I (Dauer and Przedborski, 2003). As a consequence, ATP production is compromised, O_2^- levels increase, and subsequent oxidative stress occurs. This is critical in neuronal cells, where energy production depends mainly on ATP synthesis through oxidative phosphorylation (reviewed in Bélanger et al., 2011). In contrast, astrocytes are mainly glycolytic (reviewed in Bélanger et al., 2011). In addition, astrocytes can generate lactate from glycogen *via* glycolysis under metabolic activation (Hertz et al., 2007). Macrophages/microglia have the capacity to generate ATP by both glycolytic and oxidative pathways (although in the case of microglial cells the field is still underexplored; Van den Bossche et al., 2017; Ghosh et al., 2018). Indeed, they are able to shift from oxidative phosphorylation to aerobic glycolysis (production of lactate in the presence of oxygen) to obtain ATP from different pathways according to the metabolic demands of their activation status (Haschemi et al., 2012; Galván-Peña and O'Neill, 2014; Orihuela et al., 2016). The classical activation or M1/pro-inflammatory phenotype is associated with inhibition of the respiratory chain and the potentiation of aerobic glycolysis, which results in more rapid ATP production to satisfy the metabolic demands associated with the quick pro-inflammatory response of the M1 phenotype. In this situation, the glycolytic and pentose phosphate pathways are potentiated, and oxidative phosphorylation is inhibited (Haschemi et al., 2012). A metabolic-epigenetic crosstalk is suggested to control macrophage activation (Baardman et al., 2015). In contrast, pro-inflammatory stimuli increase tricarboxylic acid activity in astrocytes (Gavillet et al., 2008). In mixed glial cultures, LPS/IFN-γ treatment increased ATP production, an effect that was clearly inhibited by MPP+ and rotenone. These results suggest that MPP+- and rotenone-treated cultures suffer metabolic stress that is aggravated when the cells increase their energetic demands after LPS/IFN-γ treatment. Consequently, activated glial cells may not fulfill their

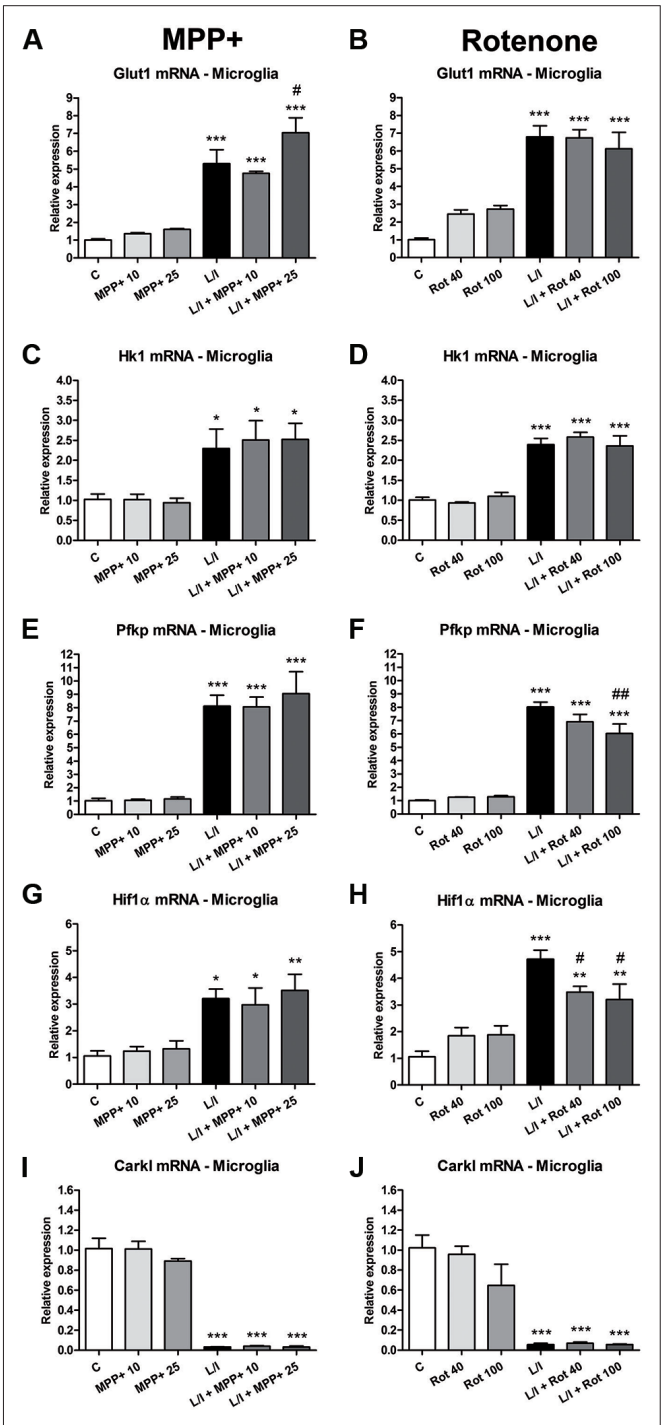

FIGURE 8 | Effect of MPP+ and rotenone treatment on the expression of genes involved in the control of the glycolysis in the microglial cell cultures. mRNA expression of the glucose transporter (Glut1; **A,B**) and the glycolytic enzymes hexokinase 1 (Hk1; **C,D**) and phosphofructokinase 1 (Pfk1; **E,F**), as well as Hif1α **(G,H)** and carbohydrate kinase-like protein 1 (Carkl; **I,J**). The primary microglial cultures were treated for 6 h with 10 and 25 μM MPP+ or 40 and 100 nM rotenone (Rot), both in the absence and the presence of LPS/IFN-γ (L/I). Rn18s and β-actin were used as housekeeping genes. Bars are means ± SEM of four independent experiments. $^{*}p < 0.05$, $^{**}p < 0.01$ and $^{***}p < 0.001$ vs. control (C); $^{\#}p < 0.05$ and $^{\#\#}p < 0.01$ vs. L/I; one-way ANOVA and Newman-Keuls post-test.

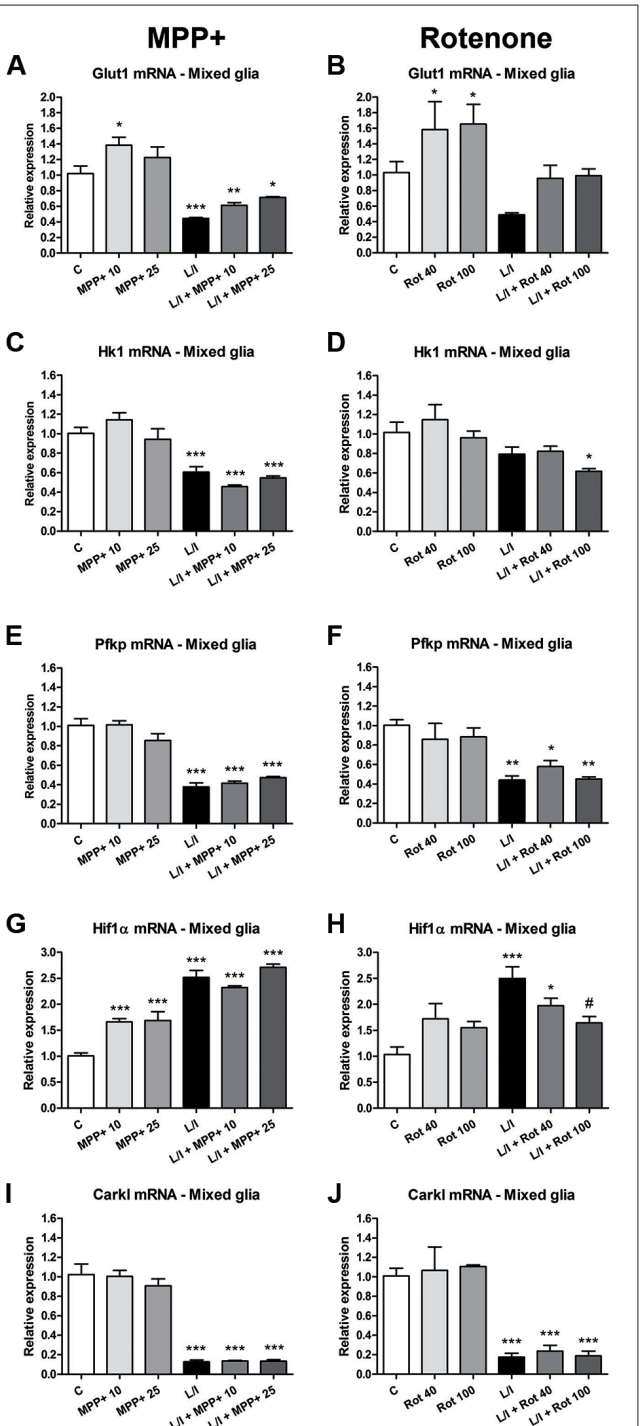

FIGURE 9 | Effect of MPP+ and rotenone treatment on the expression of genes involved in the control of glycolysis in the mixed glial cell cultures. mRNA expression of the glucose transporter Glut1 **(A,B)** and the glycolytic enzymes Hk1 **(C,D)** and Pfk1 **(E,F)**, as well as Hif1α **(G,H)** and Carkl **(I,J)**. The primary mixed glial cultures were treated for 6 h with 10 and 25 μM MPP+ or 40 and 100 nM rotenone (Rot), both in the absence and the presence of LPS/IFN-γ (L/I). Rn18s and β-actin were used as housekeeping genes. Bars are means ± SEM of four independent experiments. $^{*}p < 0.05$, $^{**}p < 0.01$ and $^{***}p < 0.001$ vs. control (C); $^{\#}p < 0.05$ vs. L/I; one-way ANOVA and Newman-Keuls post-test.

metabolic demands in the presence of MPP+ and rotenone, which would explain why mixed glial cultures exposed to these toxicants were not able to produce an appropriate pro-inflammatory response to LPS/IFN-γ. The effects of MPP+ and rotenone on ATP production were less drastic in the LPS-IFN-γ-treated microglial than the mixed glial cultures. ATP production was not significantly compromised in the LPS/IFN-γ-treated microglial cultures exposed to MPP+ and rotenone, with the exception of 25 μM MPP+ treatment. In addition, the response to LPS/IFN-γ was also impaired, to a lesser extent, in the microglial cultures than in the mixed glial cultures. Altogether, these results suggest that the microglial cells can better cope with the metabolic alterations induced by MPP+ and rotenone than astrocytes can, which accounts for 75% of the cells in the mixed glial cultures. A possible explanation is that while microglial cells developing a pro-inflammatory phenotype switch to glycolysis (Haschemi et al., 2012; Galván-Peña and O'Neill, 2014; Orihuela et al., 2016), astrocytes exposed to pro-inflammatory stimuli increase the activity of the tricarboxylic acid cycle (Gavillet et al., 2008), which in the presence of MPP+ and rotenone will encounter truncated oxidative phosphorylation. However, the involvement of a differential response of the activated microglial cells to the toxins in the presence of astrocytes (or impaired astrocytes) cannot be ruled out.

To assess whether the glycolytic switch mentioned above was behind the ATP production in activated glial cultures, we evaluated the expression of genes encoding critical proteins for the glycolytic pathway. In the microglial cultures, a switch to the glycolytic pathway in the LPS/IFN-γ-activated microglial cultures was suggested by the observed increase in the expression of Glut1, HK1, Pfk1 and Hif1α mRNA and the decreased expression of the Carkl mRNA. Increased expression of the glucose transporter Glut1 may result in more glucose uptake, while the increased expression of Hk1 and Pfk1, which regulate critical steps in glycolysis, may increase the glycolytic rate. It has been suggested that Hif activation contributes to macrophage polarization, and that Hifα-dependent glycolysis favors polarization to a M1 phenotype (Palazon et al., 2016; Taylor et al., 2016). In addition, metabolic intermediates such as succinate play a role in Hif1α stabilization and subsequent IL1β expression in LPS-treated macrophages (Tannahill et al., 2013). Inhibition of the Carkl expression potentiates the flux through the pentose phosphate pathway (Haschemi et al., 2012). Whereas MPP+ exposure resulted in a further increase in Glut1 expression in the LPS/IFN-γ-treated microglial cultures, rotenone exposure partially inhibited the LPS/IFN-γ-induced Pfk and Hifα mRNA expression. Consequently, in the case of microglial cultures, the attenuated pro-inflammatory response to LPS-IFN-γ mostly observed in the presence of rotenone may result from some alterations to the glycolytic switch. In addition, it cannot be ruled out that ATP production through oxidative phosphorylation may also partially contribute to the energy demand required to develop a pro-inflammatory response, even in situations where the switch to glycolysis occurs. In this sense, Wang et al. (2018) showed that 2-deoxyglucose, which blocks glycolysis and partially inhibits glycolytic-dependent oxidative phosphorylation, has a stronger inhibitory effect on the IFN-γ-induced inflammatory response in macrophages than inhibiting glycolysis when replacing glucose in the cell culture medium with galactose, which reduces glycolytic flux without interfering with oxidative phosphorylation. Interestingly, control of the pro-inflammatory macrophage response, through metabolic reprogramming, has been suggested as a potential therapeutic strategy to promote remission in chronic inflammatory diseases (Mills and O'Neill, 2016).

We observed contrasting effects in the LPS/IFN-γ-treated mixed glia and microglial cultures in terms of the mRNA expression of the glycolytic enzymes Glut1, Hk1, and Pfk1. Their expression was inhibited in the mixed glia, suggesting the contribution of astrocytes to the effects observed. Although astrocytes are mainly glycolytic (Bélanger et al., 2011), pro-inflammatory stimuli increase tricarboxylic acid activity in astrocytes (Gavillet et al., 2008). The decreased expression of the glycolytic enzymes we observed may reflect this switch. Consequently, the impaired response of the mixed glial cultures to LPS/IFN-γ in the presence of MPP+ and rotenone may be explained by the fact that oxidative phosphorylation, which would be responsible for the main ATP production from products of the tricarboxylic acid cycle, is inhibited by MPP+ and rotenone. However, the involvement of the microglial cells in the response of the mixed glial cultures to MPP+ and rotenone plus LPS/IFN-γ cannot be ruled out.

Finally, some studies show that MPP+ causes DNA damage (Zhang et al., 1995) and oxidative DNA damage in neuronal cells (Chen et al., 2005). In addition, rotenone-induced DNA damage (Goswami et al., 2016) and DNA methylation (Scola et al., 2014) in neurons have also been described. Although there are no reports on MPP+- and rotenone-induced DNA alterations on glial cells, we cannot discard that these alterations may be behind the decreased expression of inflammatory markers we detected in LPS/IFN-γ–treated glial cultures exposed to the neurotoxins.

CONCLUSION

In summary, the results of the present study show that the pro-inflammatory response induced by LPS/IFN-γ in mouse primary glial cell cultures, is impaired under MPP+ and rotenone exposure, mainly when both the astrocytes and microglia are present. This suggests that the immune response of the glial cells is compromised in the presence of neurotoxins that inhibit the mitochondrial electron transport chain. We are currently studying the possible effects of MPP+ and rotenone on the development of an anti-inflammatory phenotype by the glial cells. Although the involvement of the glial cells in the development of neurodegenerative diseases is widely accepted, the precise role they play in every neurodegenerative disorder remains to be established. As many genetic and environmental factors are probably involved in the etiopathogenesis of neurodegenerative diseases, many factors may also determine when and how the glial cells take part in the pathological process. In the case of pathologies where the exposure to certain neurotoxicants is a risk factor, such as PD, the direct effect of the toxic agents on glial cell function may be

an additional factor to take into account, as alterations in glial function will have an effect on neuronal function and CNS homeostasis. In this context, our results suggest that glial metabolic alterations induced by neurotoxin exposure compromises the brain's immune response. This impaired immune response may imply a more vulnerable brain, which can be a further aspect contributing to the development of PD.

DATA AVAILABILITY

All data generated or analyzed during this study are included in this published article.

AUTHOR CONTRIBUTIONS

NR-L and EX-E performed most of the experiments and analyzed the data. JSe participated in the processing of the samples and quantified the phagocytosis assay. JSa provided critical guidance and contributed to the final version of the manuscript. CS conceived and coordinated the experiments, provided guidance in the production of data and drafted the manuscript. All authors provided input and ideas throughout the process, and critically revised and approved the final manuscript.

FUNDING

NR-L was recipient of an FPU grant (FPU13/05491) from the Spanish *Ministerio de Educación, Cultura y Deporte*. This study was supported by grants PI14/00302 and PI15/00033 from the *Instituto de Salud Carlos III* (Spain) with joint financing by FEDER funds from the European Union.

ACKNOWLEDGMENTS

We thank Lucas Blasco and Andrés Jurado for their technical assistance. We acknowledge support for the publication fee, by the CSIC Open Access Publication Support Initiative through its Unit of Information Resources for Research (URICI).

REFERENCES

Baardman, J., Licht, I., de Winther, M. P. J., and Van den Bossche, J. (2015). Metabolic-epigenetic crosstalk in macrophage activation. *Epigenomics* 7, 1155–1164. doi: 10.2217/epi.15.71

Bélanger, M., Allaman, I., and Magistretti, P. J. (2011). Brain energy metabolism: focus on astrocyte-neuron metabolic cooperation. *Cell Metab.* 14, 724–738. doi: 10.1016/j.cmet.2011.08.016

Bournival, J., Plouffe, M., Renaud, J., Provencher, C., and Martolini, M. G. (2012). Quercetin and sesamin protect dopaminergic cells from MPP^+-induced neuroinflammation in a microglial (N9)-neuronal (PC12) coculture system. *Oxid. Med. Cell Longev.* 2012:921941. doi: 10.1155/2012/921941

Bové, J., and Perier, C. (2012). Neurotoxin-based models of Parkinson's disease. *Neuroscience* 211, 51–76. doi: 10.1016/j.neuroscience.2011.10.057

Chen, L. J., Gao, Y. Q., Li, X. J., Shen, D. H., and Sun, F. J. (2005). Melatonin protects against MPTP/MPP^+-induced mitochondrial DNA oxidative damage *in vivo* and *in vitro*. *J. Pineal Res.* 39, 34–42. doi: 10.1111/j.1600-079X.2005.00209.x

Chen, T., Hou, R., Xu, S., and Wu, C. (2015). Donepezil regulates 1-methyl-4-phenylpyridinium-induced microglial polarization in Parkinson's disease. *ACS Chem. Neurosci.* 6, 1708–1714. doi: 10.1021/acschemneuro.5b00026

Colonna, M., and Butovsky, O. (2017). Microglia function in the central nervous system during health and neurodegeneration. *Annu. Rev. Immunol.* 35, 441–468. doi: 10.1146/annurev-immunol-051116-052358

Dauer, W., and Przedborski, S. (2003). Parkinson's disease: mechanisms and models. *Neuron* 39, 889–909. doi: 10.1016/S0896-6273(03)00568-3

Dentesano, G., Serratosa, J., Tusell, J. M., Ramón, P., Valente, T., Saura, J., et al. (2014). CD200R1 and CD200 expression are regulated by PPAR-γ in activated glial cells. *Glia* 62, 982–998. doi: 10.1002/glia.22656

Du, C., Jin, M., Hong, Y., Li, Q., Wang, X. H., Xu, J. M., et al. (2014). Downregulation of cystathione β-synthase/hydrogen sulfide contributes to rotenone-induced microglia polarization toward M1 type. *Biochem. Biophys. Res. Commun.* 451, 239–245. doi: 10.1016/j.bbrc.2014.07.107

Emmrich, J. V., Hornik, T. C., Neher, J. J., and Brown, G. C. (2013). Rotenone induces neuronal death by microglial phagocytosis of neurons. *FEBS J.* 280, 5030–5038. doi: 10.1111/febs.12401

Ferger, A. I., Campanelli, L., Reimer, V., Muth, K. N., Merdian, I., Ludolph, A. C., et al. (2010). Effects of mitochondrial dysfunction on the immunological properties of microglia. *J Neuroinflammation* 7:45. doi: 10.1186/1742-2094-7-45

Galván-Peña, S., and O'Neill, L.A.J. (2014). Metabolic reprograming in macrophage polarization. *Front. Immunol.* 5:420. doi: 10.3389/fimmu.2014.00420

Gao, F., Chen, D., Hu, Q., and Wang, G. (2013). Rotenone directly induces BV2 cell activation via the p38 MAPK pathway. *PLos One* 8:e722046. doi: 10.1371/journal.pone.0072046

Gao, H.-M., Hong, J.-S., Zhang, W., and Liu, B. (2002). Distinct role for microglia in rotenone-induced degeneration of dopaminergic neurons. *J. Neurosci.* 22, 782–790. doi: 10.1523/JNEUROSCI.22-03-00782.2002

Gao, H.-M., Liu, B., Zhang, W., and Hong, J.-S. (2003). Critical role of microglial NADPH oxidase-derived free radicals in the *in vitro* MPTP model of Parkinson's disease. *FASEB J.* 17, 1954–1956. doi: 10.1096/fj.03-0109fje

Gavillet, M., Allaman, I., and Magistretti, P. J. (2008). Modulation of astrocytic metabolic phenotype by proinflammatory cytokines. *Glia* 56, 975–989. doi: 10.1002/glia.20671

Ghosh, S., Castillo, E., Frias, E. S., and Swanson, R. A. (2018). Bioenergetic regulation of microglia. *Glia* 66, 1200–1212. doi: 10.1002/glia.23271

Goldman, S. M. (2013). Environmental toxins and Parkinson's disease. *Annu. Rev. Pharmacol. Toxicol.* 54, 141–164. doi: 10.1146/annurev-pharmtox-011613-135937

Goswami, P., Gupta, S., Biswas, J., Joshi, N., Swarnkar, S., Nath, C., et al. (2016). Endoplasmic reticulum stress plays a key role in rotenone-induced apoptotic death of neurons. *Mol. Neurobiol.* 53, 285–298. doi: 10.1007/s12035-014-9001-5

Gresa-Arribas, N., Serratosa, J., Saura, J., and Solà, C. (2010). Inhibition of CCAAT/enhancer binding protein δ expression by chrysin in microglial cells results in anti-inflammatory and neuroprotective effects. *J. Neurochem.* 115, 526–536. doi: 10.1111/j.1471-4159.2010.06952.x

Haschemi, A., Kosma, P., Gille, L., Evans, C. R., Burant, C. F., Starkl, P., et al. (2012). The sedoheptulose kinase CARKL directs macrophage polarization through control of glucose metabolism. *Cell Metab.* 15, 813–826. doi: 10.1016/j.cmet.2012.04.023

Henze, C., Hartmann, A., Lescot, T., Hirsch, E. C., and Michel, P. P. (2005). Proliferation of microglial cells induced by 1-methyl-4-phenylpyridinium in mesencephalic cultures results from an astrocyte-dependent mechanism: role of granulocyte macrophage colony-stimulating factor. *J. Neurochem.* 95, 1069–1077. doi: 10.1111/j.1471-4159.2005.03416.x

Hertz, L., Peng, L., and Dienel, G. A. (2007). Energy metabolism in astrocytes: high rate of oxidative metabolism and spatiotemporal dependence on glycolysis/glycogenolysis. *J. Cereb. Blood Flow Metab.* 27, 219–249. doi: 10.1038/sj.jcbfm.9600343

Jin, M., Kim, B. W., Koppula, S., Kim, I. S., Park, J. H., Kumar, H., et al. (2012). Molecular effects of activated BV-2 microglia by mitochondrial toxin 1-methyl-4-phenylpyridinium. *Neurotoxicology* 33, 147–155. doi: 10.1016/j.neuro.2011.12.019

Kamel, F. (2013). Paths from pesticides to Parkinson's. *Science* 341, 722–723. doi: 10.1126/science.1243619

Kinugawa, K., Monnet, Y., Béchade, C., Alvarez-Fisher, D., Hirsch, E., Bessis, A., et al. (2013). DAP12 and CD11b contribute to the microglial-induced death of dopaminergic neurons *in vitro* but not *in vivo* in the MPTP mouse model of Parkinson's disease. *J. Neuroinflammation* 10:82. doi: 10.1186/1742-2094-10-82

Klintworth, H., Garden, G., and Xia, Z. (2009). Rotenone and paraquat do not directly activate microglia or induce inflammatory cytokine release. *Neurosci. Lett.* 462, 1–5. doi: 10.1002/jcp.27938

Langston, J. W., Ballard, P. A., Tetrud, J. W., and Irwin, I. (1983). Chronic parkinsonism in humans due to a product of meperidine-analog synthesis. *Science* 219, 979–980. doi: 10.1126/science.6823561

Liang, Y., Jing, X., Zeng, Z., Bi, W., Chen, Y., Wu, X., et al. (2015). Rifampicin attenuates rotenone-induced inflammation via suppressing NLRP3 inflammasome activation in microglia. *Brain Res.* 1622, 43–50. doi: 10.1016/j.brainres.2015.06.008

Livak, K. J., and Schmittgen, T. D. (2001). Analysis of relative gene expression data using real-time quantitative PCR and the $2^{-\Delta\Delta CT}$ method. *Methods* 25, 402–408. doi: 10.1006/meth.2001.1262

Mills, E. L., and O'Neill, L. A. (2016). Reprogramming mitochondrial metabolism in macrophages as an anti-inflammatory signal. *Eur. J. Immunol.* 46, 13–21. doi: 10.1002/eji.201445427

Mostafalou, S., and Abdollahi, M. (2013). Pesticides and human chronic diseases: evidences, mechanisms, and perspectives. *Toxicol. Appl. Pharmacol.* 268, 157–177. doi: 10.1016/j.taap.2013.01.025

Orihuela, R., McPherson, C. A., and Harry, G. J. (2016). Microglial M1/M2 polarization and metabolic states. *Br. J. Pharmacol.* 173, 649–665. doi: 10.1111/bph.13139

Palazon, A., Goldrath, A. W., Nizet, V., and Johnson, R. S. (2016). HIF transcription factors, inflammation, and immunity. *Immunity* 41, 518–528. doi: 10.1016/j.immuni.2014.09.008

Perry, V. H., Nicoll, J. A. R., and Clive, H. (2010). Microglia in neurodegenerative disease. *Nature Rev.* 6, 193–201. doi: 10.1038/nrneurol.2010.17

Radad, K., Rausch, W. D., and Gille, G. (2006). Rotenone induces cell death in primary dopaminergic culture by increasing ROS production and inhibiting mitochondrial respiration. *Neurochem. Int.* 49, 379–386. doi: 10.1016/j.neuint.2006.02.003

Salter, M. W., and Stevens, B. (2017). Microglia emerge as central players in brain disease. *Nat. Med.* 9, 1018–1027. doi: 10.1038/nm.4397

Saura, J., Tusell, J. M., and Serratosa, J. (2003). High-yield isolation of murine microglia by mild trypsinization. *Glia* 44, 183–189. doi: 10.1002/glia.10274

Scola, G., Kim, H. K., Young, L. T., Salvador, M., and Andreazza, A. C. (2014). Lithium reduces the effects of rotenone-induced complex I dysfunction on DNA methylation and hydroxymethylation in rat cortical primary neurons. *Psychopharmacology* 231, 4189–4198. doi: 10.1007/s00213-014-3565-7

Tannahill, G. M., Curtis, A. M., Adamik, J., Palsson-McDermott, E. M., McGettrick, A. F., Goel, G., et al. (2013). Succinate is an inflammatory signal that induces IL-1β through HIF-1α. *Nature* 496, 238–242. doi: 10.1038/nature11986

Tanner, C. M., Kamel, F., Ross, G. W., Hoppin, J. A., Goldman, S. M., Korell, M., et al. (2011). Rotenone, Paraquat, and Parkinson's disease. *Environm. Health Perspect.* 6, 866–872. doi: 10.1289/ehp.1002839

Taylor, C. T., Doherty, G., Fallon, P. G., and Cummins, E. P. (2016). Hypoxia-dependent regulation of inflammatory pathways in immune cells. *J. Clin. Invest.* 126, 3716–3724. doi: 10.1172/JCI84433

Van den Bossche, J., O'Neill, L. A., and Menon, D. (2017). Macrophage immunometabolism: where are we (going)? *Trends Immunol.* 38, 395–406. doi: 10.1016/j.it.2017.03.001

Wang, F., Zhang, S., Jeon, R., Vuckovic, I., Jiang, X., Lerman, A., et al. (2018). Interferon gamma induces reversible metabolic reprogramming of M1 macrophages to sustain cell viability and pro-inflammatory activity. *EBioMedicine* 30, 303–316. doi: 10.1016/j.ebiom.2018.02.009

Wiese, M., Gerlach, R. G., Popp, I., Matuszak, J., Mahapatro, M., Castiglione, K., et al. (2012). Hypoxia-mediated impairment of the mitochondrial respiratory chain inhibits the bactericidal activity of macrophages. *Infect. Immun.* 80, 1455–1466. doi: 10.1128/IAI.05972-11

Yuan, Y., Sun, J., Wu, M., Hu, J., Peng, S., and Chen, N. (2013). Rotenone could activate microglia through NFκB associated pathway. *Neurochem. Res.* 38, 1553–1560. doi: 10.1007/s11064-013-1055-7

Zhang, J., Pieper, A., and Snyder, S. H. (1995). Poly(ADP-ribose) synthetase activation: an early indicator of neurotoxic DNA damage. *J. Neurochem.* 65, 1411–1414. doi: 10.1046/j.1471-4159.1995.65031411.x

Zhang, X. Y., Chen, L., Yang, Y., Xu, D. M., Zhang, S. R., Li, C. T., et al. (2014). Regulation of rotenone-induced microglial activation by 5-lipoxygenase and cysteinyl leukotriene receptor 1. *Brain Res.* 1572, 59–71. doi: 10.1016/j.brainres.2014.05.026

Zhou, P., Weng, R., Chen, Z., Wang, R., Zou, J., Liu, X., et al. (2016). TLR4 signaling in MPP^+-induced activation of BV-2 cells. *Neural Plast.* 2016:5076740. doi: 10.1155/2016/5076740

Conflict of Interest Statement: The authors declare that the research was conducted in the absence of any commercial or financial relationships that could be construed as a potential conflict of interest.

frontiers in Aging Neuroscience

ORIGINAL RESEARCH
published: 04 February 2019
doi: 10.3389/fnagi.2019.00016

Iso-α-acids, Hop-Derived Bitter Components of Beer, Attenuate Age-Related Inflammation and Cognitive Decline

Yasuhisa Ano[1,2]*, *Rena Ohya*[1,2], *Keiji Kondo*[2] and *Hiroyuki Nakayama*[1]

[1]Graduate School of Agricultural and Life Sciences, The University of Tokyo, Tokyo, Japan, [2]Research Laboratories for Health Science & Food Technologies, Kirin Company Ltd, Yokohama, Japan

With the aging population rapidly increasing worldwide, preventive measures and treatments for age-related cognitive decline and dementia are of utmost importance. We have previously demonstrated that the consumption of iso-α-acids (IAA), which are hop-derived bitter compounds in beer, prevents the formation of disease pathology in a transgenic mouse model of Alzheimer's disease (AD). However, the effect of IAA consumption on age-related cognitive decline is unknown. In the present study, we examined the effect of long-term and short-term dietary consumption of IAA, on age-related memory impairments and inflammation in the hippocampus of aged mice. When compared with young mice, aged mice showed impairment in spatial working memory during the Y-maze spontaneous alternation test, impairment in object recognition memory during the novel object recognition test (NORT), a pro-inflammatory hippocampal microglial phenotype with increased CD86 expression and inflammatory cytokine production, increased levels of glutamate and amyloid β_{1-42}, and decreased levels of dopamine (DA). In aged mice fed IAA for 3 months, the age-related alterations in memory, microglial inflammation, and glutamate, amyloid β_{1-42}, and DA levels were all significantly attenuated. Additionally, the oral administration of IAA for 7 days in aged mice with memory impairment, also improved spatial and object recognition memory. These results suggest that IAA consumption prevents inflammation in the hippocampus and ameliorates age-related cognitive decline.

Keywords: aging, cognitive decline, hippocampus, inflammation, iso-α-acids, memory

OPEN ACCESS

Edited by:
Maria Jose Bellini, Consejo Nacional de Investigaciones Científicas y Técnicas (CONICET), Argentina

Reviewed by:
Fernando Correa, CONICET Centro de Estudios Farmacológicos y Botánicos (CEFYBO), Argentina
Florencia Labombarda, Instituto de Biología y Medicina Experimental (IBYME), Argentina

***Correspondence:**
Yasuhisa Ano
yasuhisa_ano@kirin.co.jp

Received: *15 November 2018*
Accepted: *17 January 2019*
Published: *04 February 2019*

Citation:
Ano Y, Ohya R, Kondo K and Nakayama H (2019) Iso-α-acids, Hop-Derived Bitter Components of Beer, Attenuate Age-Related Inflammation and Cognitive Decline. Front. Aging Neurosci. 11:16. doi: 10.3389/fnagi.2019.00016

INTRODUCTION

The increasing burden of dementia and cognitive impairment in rapidly expanding aging populations is shouldered not only by patients and their families but also by national healthcare systems. The lack of an effective disease-modifying therapy for dementia has garnered increasing attention on preventive approaches, such as diet, exercise, and learning. Etiological studies on lifestyle suggest that low to moderate consumption of alcohol, such as wine and beer, may reduce the risk of cognitive decline and the development of dementia. Individuals who consumed low to moderate levels of alcoholic beverages on a daily basis showed a significantly lower

Abbreviations: Aβ, amyloid β; DA, dopamine; DOPAC, 3,4-dihydroxyphenylacetic acid; ECD, electrochemical detection; DI, discrimination index; HVA, homovanillic acid; HPLC, high-performance liquid chromatography; IAA, iso-α-acids; NORT, novel object recognition test; PPAR-γ, peroxisome proliferator-activated receptor-γ.

risk of developing a neurodegenerative disease than those who either abstained from alcoholic beverages or drank heavily (Matsui et al., 2011; Neafsey and Collins, 2011; Horvat et al., 2015). These risk-reducing effects are thought to be because of the profile of compounds found in alcoholic beverages. Red wine is known to contain resveratrol, a polyphenolic compound with neuroprotective properties (Neafsey and Collins, 2011; Porquet et al., 2014; Witte et al., 2014). Conversely, beer has remained the most-consumed alcoholic beverage in the world for more than a thousand years; to date there are few reports on which constituents of beer could be beneficial for preventing cognitive decline.

Hops, the female inflorescences of the hop plant (*Humulus lupulus L.*), have been used in beer brewing since 822 AD and are used as both a preservative and a flavoring agent in the beer-brewing process. The bitter taste of beer originates from the α-acids found in hops. Owing to the fact that iso-α-acids (IAA) activate the peroxisome proliferator-activated receptor-γ (PPAR-γ; Yajima et al., 2004), the IAA found in beer have antioxidant and anti-metabolic syndrome properties and are also reported to prevent diet-induced obesity in rodents and to improve hyperglycemia, a result which has been confirmed in humans (Obara et al., 2009). We previously demonstrated that the long-term intake of IAA prevented Alzheimer's pathology in transgenic model mice (Ano et al., 2017). IAA suppressed microglial inflammation induced by the deposition of amyloid β (Aβ) in the brain and prevented cognitive decline. Additionally, IAA activated PPAR-γ and regulated microglial phagocytosis and inflammation. Our group has also demonstrated that IAA suppressed microglial inflammation in tauopathy mice and improved obesity-induced cognitive impairment by suppressing inflammation induced by a high-fat diet (Ano et al., 2018b; Ayabe et al., 2018). However, the effects of IAA on age-related cognitive decline and neuronal dysfunction have not yet been demonstrated. Most cases of cognitive decline are associated with aging; consequently, in this study, we examined the effects of IAA consumption on cognitive impairment and brain inflammatory processes in aged mice.

MATERIALS AND METHODS

Preparation of Iso-α-acids (IAA)

The α-acids predominantly comprised of the following three congeners: cohumulone, humulone, and adhumulone. During the brewing process, they were each isomerized into two epimeric isomers: cis-IAA and trans-IAA. We used isomerized hop extract (IHE; Hopsteiner, Mainburg, Germany) containing 30.5% (w/v) IAA and 65% H_2O as the IAA sample for our experiments. Based on the analysis in our previous report, IHE comprises six isomers: trans-isocohumulone (1.74% w/v), cis-isocohumulone (7.61% w/v), trans-isohumulone (3.05% w/v), cis-isohumulone (14.0% w/v), trans-isoadhumulone (0.737% w/v), and cis-isoadhumulone (3.37% w/v; Ano et al., 2017).

Animals

Male C57BL/6J mice (Charles River Japan, Tokyo, Japan) were maintained at the Kirin Company Ltd. The Animal Experiment Committee of Kirin Company Limited approved all experiments, which were conducted between 2016 and 2017 in strict accordance with their guidelines. We made every possible effort to minimize suffering. Mice were fed a standard purified rodent diet (AIN-93M, Oriental Yeast, Tokyo, Japan).

Our previous study showed that dietary intake of 0.05% (w/w) IAA reduced inflammation in the brain of Alzheimer's model mice (Ano et al., 2017). To study the effect of long-term IAA intake on age-related cognitive decline, aged mice (68 weeks of age) were fed AIN-93M with or without 0.05% (w/w) IAA for 3 months. Young control mice (7 weeks of age) were fed AIN-93M diet without IAA for 3 months. After a 3-month dietary intervention, the aged mice fed IAA (n = 10), control aged mice not fed IAA (n = 9), and control young mice (n = 12) underwent behavioral evaluation, after which brain samples were obtained for subsequent biochemical evaluation. The body weight of the aged mice with and without IAA did not differ between groups (**Supplementary Figure S1A**). To study the effect of short-term IAA intake, mice aged at 22 months were intragastrically administered IAA at either 0 mg/kg (distilled water as vehicle, n = 13) or 1 mg/kg (n = 14) for 9 days. Young mice aged at 7 months, that were administered with vehicle (n = 15), served as additional controls. At 7 days, mice were subjected to the spontaneous alternation test; at 8 and 9 days, mice were subjected to the novel object recognition test (NORT) at 1 h after the IAA administration.

Spontaneous Alternation Test

We evaluated spatial memory by performing a spontaneous alternation test using a Y-maze in accordance with our previous study (Ano et al., 2018a). The Y-maze is a 3-arm maze with equal angles between each black polyvinyl plastic arm (25 cm long × 5 cm wide × 20 cm high). Each mouse was initially placed in the start arm of the maze, and the number and sequence of subsequent arm entries was recorded over 8 min. We defined the alternation score (%) for each mouse as the ratio of the actual number of alternations to the total possible number of alternations (defined as the total number of arm entries minus 2) multiplied by 100 as follows: alternation score (%) = [(number of alternations)/(total arm entries − 2)] × 100.

NORT

We evaluated episodic memory by performing NORT in accordance with our previous study (Ano et al., 2018a). NORT was performed during the light period in a polyvinyl chloride box (25 cm × 40 cm × 20 cm) without a roof. For the acquisition trial, we used a pair of wooden triangle poles (4.5 cm × 4.5 cm × 4.5 cm) or wooden pyramids (4.5 cm × 4.5 cm × 4.5 cm); for the retention trial, we used one triangle pole or pyramid as the familiar object and a golf ball (4.5 cm diameter) as the novel object In all trials, we placed the objects 7.5 cm from the corner of the box. In the acquisition trial, each mouse was allowed 10-min exploration time in the box with the two identical objects at 1 h after intragastric administration of the test sample. At 24 h after the acquisition trial and 1 h after intragastric administration, mice were allowed to explore the box

with the novel and familiar objects for 5 min. The discrimination index (DI) was calculated by dividing the difference in time taken to explore the novel object and the familiar object, by the total time spent exploring both objects, that is, DI = (novel object exploration time − familiar object exploration time)/(total exploration time). Using this method, equal exploration of both objects was indicated by a DI of 0.

Measurements of Activity, Food Intake, and Water Intake in Home Cage

We monitored the amount of food intake, water intake, and ambulatory activity in the home cages using a three-point meter for 72 h (O'HARA & Co., Ltd., Tokyo, Japan). To monitor home cage activity, the interruption of infrared beams positioned on the X and Y axes around the cage detected the position of the mouse, automatically measuring their position and movement in their home cages. In this experiment, we measured the moving distance of each mouse over 5 min for a total of 72 h.

Aβ and Cytokine Measurement

To measure levels of cytokines, Aβ, and Tau, we homogenized the hippocampus of the left hemisphere in TBS buffer (Wako) with a multi-beads shocker (Yasui Kikai, Osaka, Japan). After centrifugation at 50,000× *g* for 20 min, we collected the supernatant. We measured the total protein concentration of each supernatant with a BCA protein assay kit (ThermoScientific, Yokohama, Japan). We assayed the supernatant to quantify soluble $A\beta_{1-42}$ (Wako), Tau (ThermoScientific), and phosphorylated Tau (pTau, pS199, ThermoScientific) by ELISA and cytokines by a Bio-Plex assay system (Bio-Rad, Hercules, CA, USA).

Microglial Analysis

We isolated microglial cells from the mouse brain by magnetic cell sorting after conjugation with anti-CD11b antibodies, as described previously (Ano et al., 2015). Isolated CD11b-positive cells (>90% pure, as evaluated by flow cytometry) were cultured in DMEM/F-12 (Gibco, Carlsbad, CA, USA) supplemented with 10% fetal calf serum (Gibco, Carlsbad, CA, USA) and 100 U/ml penicillin/streptomycin (Sigma-Aldrich, St. Louis, MO, USA). We treated the microglia with a leukocyte activation cocktail containing GolgiPlus (BD Biosciences, San Jose, CA, USA) for 12 h, fixed and permeabilized them with a Cytofix/Cytoperm Fixation/Permeabilization Kit (BD Biosciences, San Jose, CA, USA), and stained the microglia with FITC-conjugated anti-mouse TNF-α (MP6-XT22, eBioscience, San Diego, CA, USA), APC/Cy7-conjugated anti-mouse CD11b (M1/70, BD Pharmingen), and APC-conjugated anti-mouse CD86 (GL1, eBioscience, San Diego, CA, USA) antibodies. We analyzed populations of cytokine-producing cells and

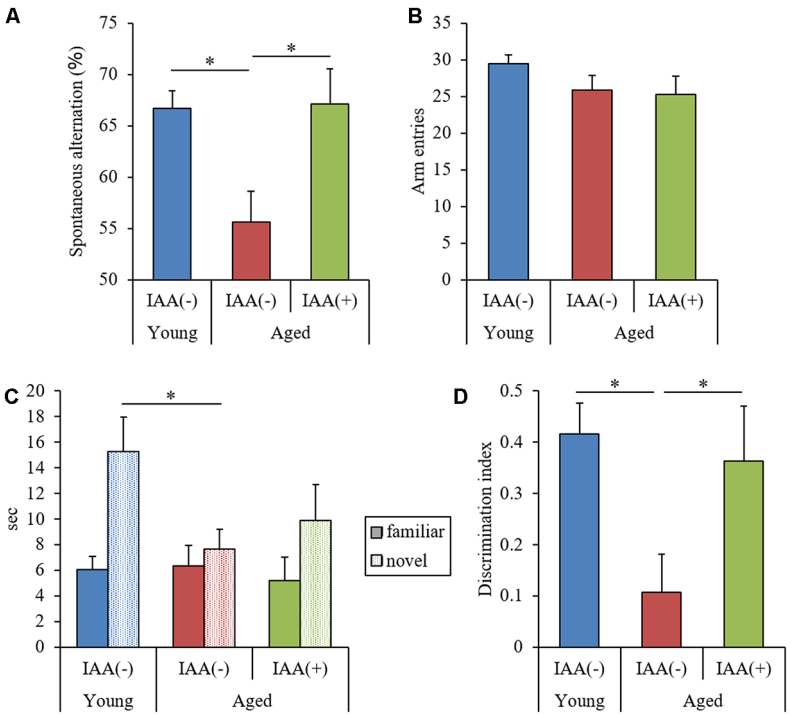

FIGURE 1 | Behavioral evaluation of cognitive functions. We fed C57BL/6J mice aged 7 weeks (young) and 68 weeks (aged) diets containing 0% or 0.05% (w/w) Iso-α-acids (IAA) for 3 months. We then performed behavioral evaluation in young mice (n = 12) and aged mice with (n = 10) or without (n = 9) dietary IAA. **(A,B)** We evaluated spatial memory using a Y-maze spontaneous alternation test to measure spontaneous alternation score **(A)** and total arm entries **(B)**. **(C,D)** We evaluated object recognition memory using a novel object recognition test (NORT). We measured the time taken to approach a novel or familiar object **(C)** and the discrimination index (DI) in NORT **(D)**. Data are presented as mean ± standard error of the mean (SE). We calculated p-values shown in the graph by one-way analysis of variance (ANOVA), followed by the Tukey-Kramer test. *$p < 0.05$.

the expression of cell markers with a flow cytometer (BD FACSCantoII, BD Biosciences, San Jose, CA, USA). We have expressed flow cytometry data as the mean median mode of the fluorescence intensity.

Monoamine Analysis

To evaluate the levels of the monoamine dopamine (DA) and its metabolites in the brain, we homogenized tissue in 0.2 M perchloric acid (Wako) containing 100 μM disodium EDTA (Sigma-Aldrich, St. Louis, MO, USA). After centrifugation, we analyzed the supernatant using high-performance liquid chromatography (HPLC) with an EICOMPAK SC-5ODS column and a PREPAK column (Eicom, Kyoto, Japan) with electrochemical detection (ECD). The mobile phase comprised of 83% 0.1 M acetic acid in citric acid buffer (pH 3.5), 17% methanol (Wako), 190 mg/ml sodium 1-octanesulfonate (Wako), and 5 mg/ml disodium EDTA. For ECD, we applied a voltage of 750 mV against an Ag/AgCl reference electrode.

Statistical Analyses

Data are presented as the mean with error bars representing the standard error of the mean (SE). We analyzed data by the one-way analysis of variance (ANOVA), followed by the Tukey-Kramer *post hoc* test. All statistical analyses were performed with Ekuseru-Toukei 2012 software (Social Survey Research Information, Tokyo, Japan). We considered a p-value of <0.05 to be statistically significant.

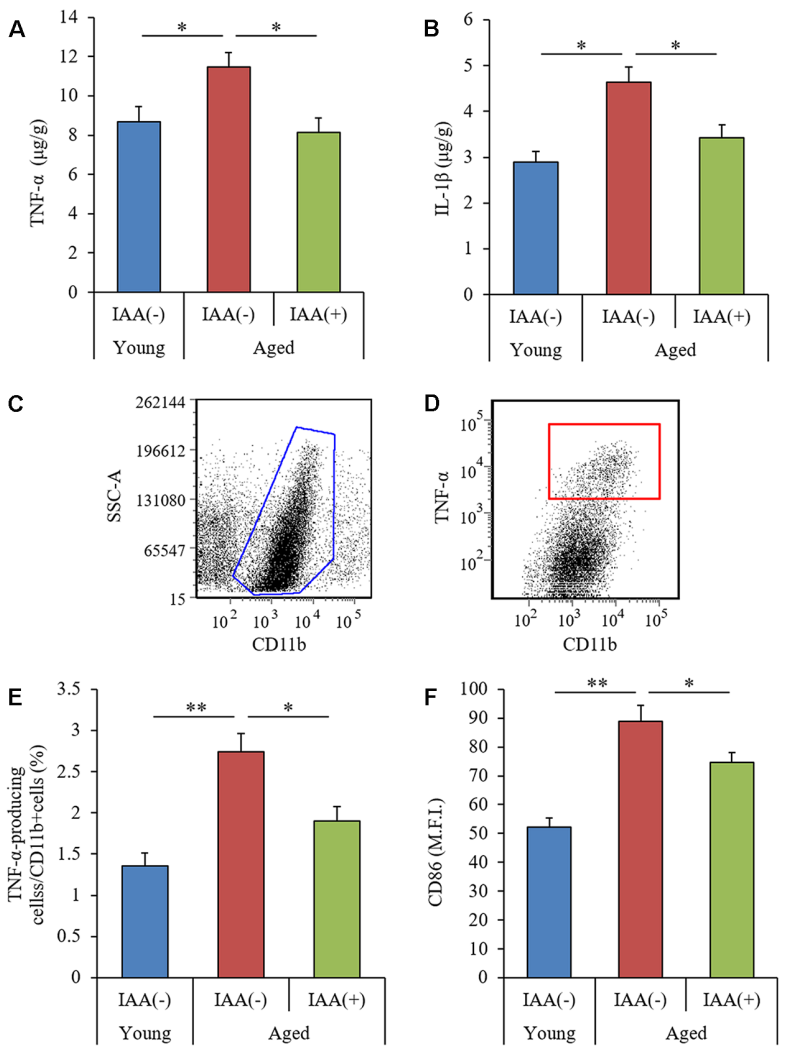

FIGURE 2 | Characteristics of microglial inflammation in aged mice. We fed C57BL/6J mice aged 7 weeks (young) and 68 weeks (aged) diets containing 0% or 0.05% (w/w) IAA for 3 months. We then obtained brain tissue for the analysis of microglial inflammation from young mice (n = 12) and aged mice with (n = 10) or without (n = 9) dietary IAA. **(A,B)** The levels of TNF-α **(A)** and IL-1β **(B)** in the hippocampus. **(C,D)** Flow cytometry characterization of TNF-α-production in CD11b-positive microglia isolated with magnetic cell sorting. **(E,F)** We collected CD11b-positive microglia using magnetic cell sorting and analyzed them using a flow cytometer, examining the ratio of TNF-α-producing cells to CD11b-positive cells **(E)** and the expression of CD86 on CD11b-positive cells **(F)**. Data are presented as mean ± SE. We calculated p-values shown in the graph by one-way ANOVA, followed by the Tukey-Kramer test. *$p < 0.05$ and **$p < 0.01$.

RESULTS

Preventive Effects of IAA on Age-Related Memory Impairment in Aged Mice

To evaluate the effects of IAA on memory impairment in aged mice, we fed mice a diet containing IAA for 3 months at 7 weeks old (young mice) and 68 weeks old (aged mice) and subjected them to behavioral memory evaluations using the spontaneous alternation test and NORT. In the Y-maze spontaneous alternation test, aged mice showed significantly lower alternation scores compared with young mice (**Figure 1A**), whereas the number of total arm entries was not different between the experimental groups (**Figure 1B**). In NORT, the time spent exploring the novel object (**Figure 1C**) and DI (**Figure 1D**) in aged mice were significantly decreased compared with those in young mice, whereas the total time taken to approach each object did not differ between groups. These results indicated that spatial working memory and object recognition memory declined with aging. However, IAA-fed aged mice showed significantly higher spontaneous alternations in the Y-maze (**Figure 1A**) and DI in NORT (**Figure 1D**) compared with the control aged mice, which indicated that dietary IAA intake for 3 months prevented age-related memory impairment. Food and water intake among the groups did not differ significantly (**Supplementary Figures S1B,C**, respectively).

Preventive Effects of IAA on Inflammation in Aged Mice

To evaluate the effects of IAA on age-related inflammation in the brain, we measured the level of cytokines in the hippocampus and analyzed the phenotype of brain microglia. Aged mice showed significant increases in TNF-α and IL-1β in the hippocampus compared with young mice (**Figures 2A,B**, respectively). The percentage of CD11b-positive microglia producing TNF-α (as gated in **Figures 2C,D**) and the microglial expression of CD86 were significantly increased in aged mice compared with young mice (**Figures 2E,F**, respectively). These results suggested that age-related microglial-mediated inflammation was present in the brain. Long-term dietary IAA in aged mice was able to attenuate the age-induced increase in hippocampal TNF-α and IL-1β levels and microglial inflammation, indicating that IAA downregulated aged-related inflammation in the brain. These results indicate that aging induces inflammation in the mouse hippocampus and that this inflammation can be reduced by IAA consumption.

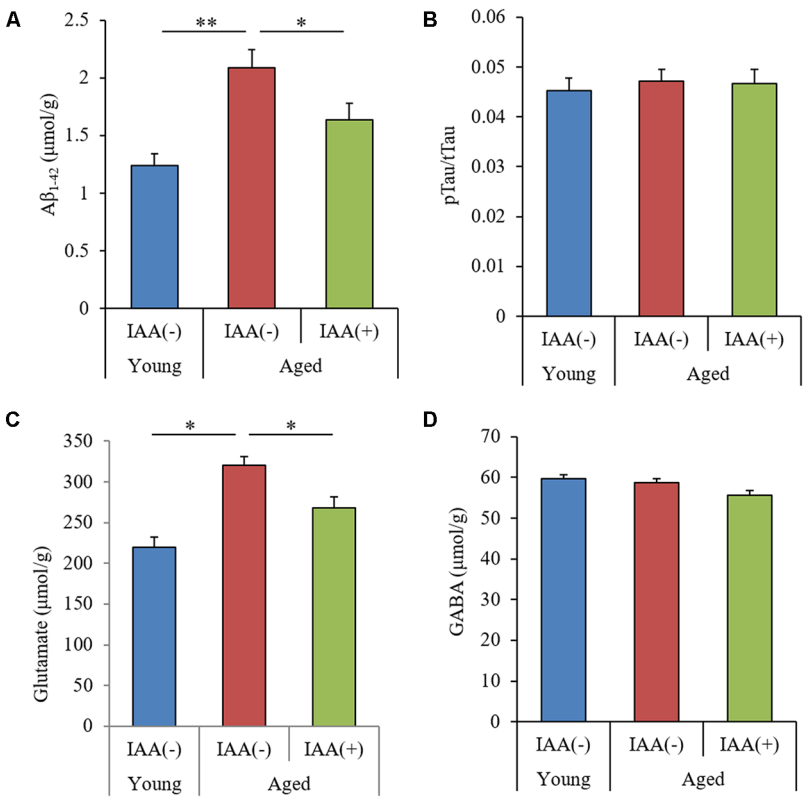

FIGURE 3 | Levels of amyloid β (Aβ), Tau, and glutamate in the hippocampus of aged mice. We fed C57BL/6J mice aged 7 weeks (young) and 68 weeks (aged) diets containing 0% or 0.05% (w/w) IAA for 3 months and then obtained brain tissue for analysis from young mice (n = 12) and aged mice with (n = 10) or without (n = 9) dietary IAA. **(A,B)** The levels of $A\beta_{1-42}$ **(A)** and phosphorylated Tau to total Tau (pTau/Tau; **B**) in TBS-soluble fractions of the hippocampus. **(C,D)** The amount of glutamate **(C)** and GABA **(D)** in the hippocampus. Data are presented as mean ± SE. We calculated the p-values shown in the graph by one-way ANOVA, followed by the Tukey-Kramer test. $^*p < 0.05$ and $^{**}p < 0.01$.

Effects of IAA on Molecules Inducing Inflammation in Aged Mice

We measured the level of $A\beta_{1-42}$, the ratio of pTau to total Tau (pTau/Tau), and the level of glutamate in aged mice to evaluate the effect of IAA on the production of inflammation-inducing molecules. Aβ is a major component of senile plaques (Hsiao et al., 1996), and the phosphorylation of Tau is known to cause neurofibrillary tangles (Wood et al., 1986). Glutamate can mediate neurotoxic effects and can induce inflammation in the brain (Novelli et al., 1988). We found that the hippocampus of aged mice had significantly higher levels of both TBS-soluble $A\beta_{1-42}$ and glutamate compared with the hippocampus of young mice (**Figures 3A,C**, respectively), but the ratio of pTau/Tau and the level of the inhibitory neurotransmitter GABA in the hippocampus did not differ between groups (**Figures 3B,D**, respectively). The age-related increases in Aβ and glutamate levels were significantly attenuated in aged mice provided with dietary IAA. These results indicated that $A\beta_{1-42}$ and glutamate, which have both been linked to inflammation and cognitive decline in the brain (Lambert et al., 1998; Brown and Bal-Price, 2003), increase in the hippocampus with aging and that dietary IAA was able to reduce the age-related increase in these molecules.

Effects of IAA on Monoamine Production in Aged Mice

DA is thought to be crucial for hippocampus-dependent memory (Li et al., 2003; Chan et al., 2017). To evaluate the effects of aging and IAA on monoamine production, we used an HPLC-ECD system to measure the levels of DA and DA metabolites, 3,4-dihydroxyphenylacetic acid (DOPAC), and homovanillic acid (HVA) in the hippocampus. The levels of DA and DOPAC were significantly decreased in aged mice compared with young mice (**Figures 4A,B**, respectively). However, the level of HVA and ratio of (DOPAC + HVA)/DA were not significantly altered by aging (**Figures 4C,D**, respectively). The level of norepinephrine did not differ between the experimental groups. These results indicated that the dopaminergic system function declined with aging but that the age-related decreases in DA and DOPAC could be significantly attenuated in aged mice that are administered dietary IAA.

Effects of Short-Term IAA Intake on Memory Impairments in Aged Mice

We demonstrated that the long-term intake of IAA suppressed cognitive decline and inflammation in the brain of aged mice. Next, to evaluate the effects of the short-term intake of IAA

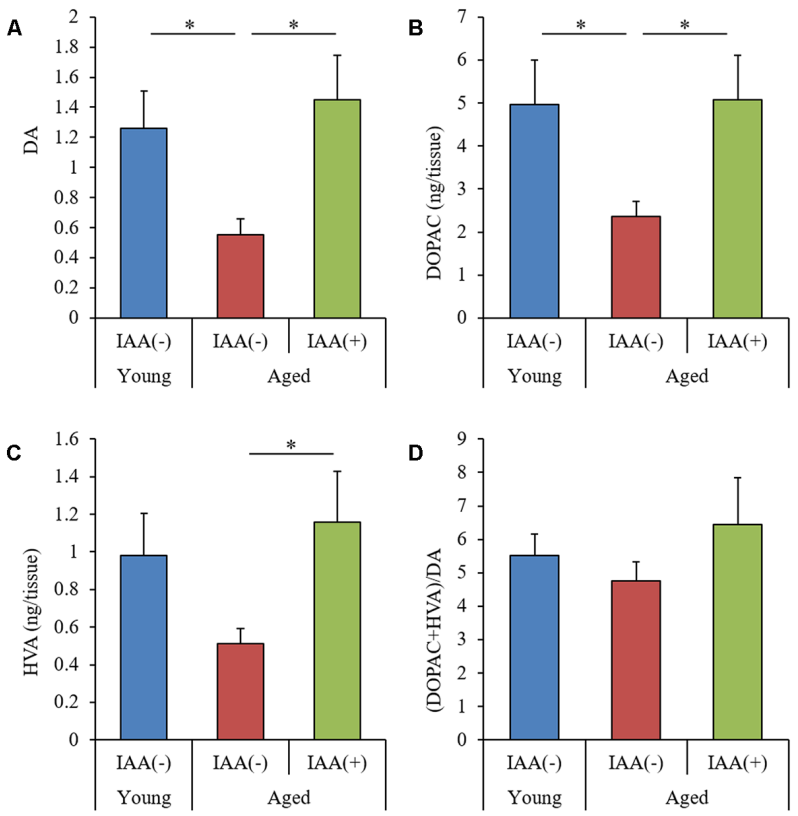

FIGURE 4 | Levels of dopamine (DA) and its metabolites in aged mice. We fed C57BL/6J mice aged 7 weeks (young) and 68 weeks (aged) diets containing 0% or 0.05% (w/w) IAA for 3 months and then obtained brain tissue for analysis of monoamine content in young mice (n = 12) and aged mice with (n = 10) or without (n = 9) dietary IAA. **(A–C)** The amount of DA **(A)**, 3, 4-dihydroxyphenylacetic acid (DOPAC; **B**), and homovanillic acid (HVA; **C**) in the hippocampus. **(D)** The ratio of (DOPAC + HVA)/DA. Data are presented as mean ± SE. We calculated the p-values shown in the graph by one-way ANOVA, followed by the Tukey-Kramer test. *$p < 0.05$.

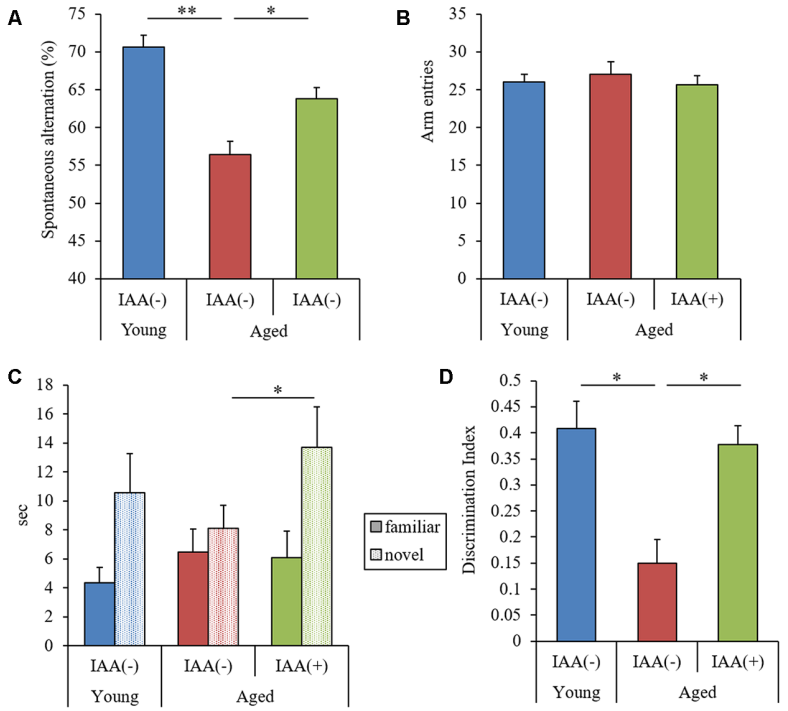

FIGURE 5 | Effects of the short-term administration of IAA in aged mice. C57BL/6J mice aged 7 months (young) and 22 months (aged) were orally administered 0 or 1 mg/kg IAA for 9 days. We performed behavioral characterization using the spontaneous alternation test at day 7 of administration and the NORT at days 8 and 9 at 1 h after the oral administration. For these behavioral tests, we used young mice (n = 15) and aged mice with (n = 14) and without (n = 13) dietary IAA. **(A,B)** We measured spontaneous alternation score **(A)** and arm entries **(B)** in the Y-maze spontaneous alternation test to evaluate spatial memory. **(C,D)** To evaluate object recognition memory, we measured the time taken to approach a novel or familiar object **(C)** and DI in NORT **(D)**. Data are presented as mean ± SE. We calculated the p-values shown in the graph by one-way ANOVA, followed by the Tukey-Kramer test. *$p < 0.05$ and **$p < 0.01$.

on memory function, we administered aged mice (22 months of age) IAA at 1 mg/kg for 9 days. In this experiment, both the spontaneous alternation score in the Y-maze and DI in NORT were significantly lower in aged mice than in young mice (7 months of age; **Figures 5A,D**, respectively). The total number of arm entries in the Y-maze did not differ between groups (**Figure 5B**). However, aged mice that received short-term oral administration of IAA showed significant improvements in the Y-maze spontaneous alternation score, the time taken to approach a novel object, and DI compared with control aged mice without orally administered IAA (**Figures 5A,C,D**, respectively). These results indicated that the short-term intake of IAA improved spatial and object recognition memory impairment that occurred in aging.

DISCUSSION

Given the worldwide increase in aging populations, it is imperative to discover novel preventive and treatment therapies for cognitive decline. Our study demonstrated that the consumption of IAA reduced inflammation in the brain and prevented the cognitive impairment associated with normal aging in mice. Aged mice displayed microglial inflammation in the hippocampus and impairments in spatial working memory and object recognition memory; but both the inflammation and the cognitive impairments were reduced by long-term dietary administration of IAA. In addition to these long-term preventive effects, short-term IAA administration also improved age-related cognitive impairment in aged mice.

In aged mice, the Aβ level in the hippocampus was increased and occurred in conjunction with a microglial inflammatory response and cognitive decline. Aβ, a well-known agent of Alzheimer's disease (AD; Kametani and Hasegawa, 2018), is gradually deposited in the brain over a long period, inducing chronic inflammation and accelerating disease pathology (Heppner et al., 2015). In aged mice, microglial inflammation is induced by Aβ and other antigens; activated microglia produce pro-inflammatory cytokines and reactive oxygen species, both of which lead to cognitive impairment (Sarlus and Heneka, 2017; Wendeln et al., 2018). Glutamate, a neurotransmitter that can confer neurotoxicity, is also produced by activated microglia (Barger et al., 2007; Takaki et al., 2012). Increased glutamate in the hippocampus of aged mice is thought to be involved in memory impairment (Tamminga et al., 2012). The short-term spatial memory tested in the Y-maze and long-term object recognition memory tested in NORT are hippocampus-dependent memory types (Cohen et al., 2013; Albani et al., 2014; Pioli et al., 2014). Inflammation in the hippocampus is reported to have impaired these types of memory, and the suppression of inflammation subsequently improved these

memory impairments (Miwa et al., 2011; Abareshi et al., 2016). Evidence from these reports together with the findings in our present study suggest that dietary IAA is capable of suppressing microglial inflammatory responses in aged mice, which might be associated with the prevention of the decline in hippocampal memory associated with aging. The behavioral evaluations in the present study cannot discriminate which specific step in memory (acquisition, retention, or recall) was improved by IAA consumption. Further evaluation of hippocampus-dependent memory acquisition and retention using the Morris water maze or radial arm maze will further elucidate the effects of IAA on memory impairments with aging.

We have previously demonstrated, as a mechanism underlying the suppression of inflammation by IAA in aged mice, that IAA activates PPAR-γ (Yajima et al., 2004), increases the expression of the "Aβ receptor" CD36, promotes phagocytosis of Aβ (Yu and Ye, 2015), and promotes microglial activation toward the M2 anti-inflammatory type (Ano et al., 2017). In AD model mice, Aβ deposition and inflammation in the hippocampus were reduced by IAA administration (Ano et al., 2017). In the present study, the increased expression of CD86 and production of TNF-α in aging are characteristic of the M1 inflammatory type of microglia (Zhou et al., 2017). The administration of IAA reduced these characteristics, suggesting that IAA suppressed the activity of M1 microglia. These results suggest that IAA consumption shifts microglial activation toward an anti-inflammatory phenotype in aged mice by activating PPAR-γ. Some studies report that the long- and short-term administration of PPAR-γ agonists, such as pioglitazone and rosiglitazone, suppressed cognitive decline in aged transgenic mice (Heneka et al., 2005; Escribano et al., 2010), but to date, the effects of PPAR-γ agonists on normally aged mice have not been demonstrated. In the present study, we demonstrated for the first time that IAA, a PPAR-γ agonist, prevent age-related cognitive decline in naturally aged mice.

Our study also demonstrated that the levels of DA and its metabolite DOPAC in the hippocampus of aged mice were reduced compared with those of young mice, and this reduction was ameliorated in aged mice by IAA. Levels of DA and DOPAC in the nucleus accumbens of aged mice were reported to be reduced when compared with those of young mice, whereas those in the striatum did not differ between groups, but to date, there has been no report on DA levels in the hippocampus of aged mice (Winner et al., 2017). In the hippocampus, DA is crucial for both spatial memory and object recognition memory. Inflammation in the brain is also reported to reduce the production of DA (Coffeen et al., 2010); accordingly, lipopolysaccharide endotoxin treatment reduced DA and DOPAC levels in rats (Noworyta-Sokolowska et al., 2013). We suggest that inflammation in the aging brain induces the reduction of DA level in the hippocampus, resulting in memory impairment.

In conclusion, our study demonstrated that consumption of IAA, the hop-derived component that imparts a bitter taste to beer, suppresses microglial activation and attenuates aged-related memory impairment in aged mice. This finding supports those of existing epidemiological studies and our previous research. Various brain disorders, including dementia, depression, and chronic fatigue, are associated with inflammation in the brain. The consumption of IAA might support the treatment or even reversal of various inflammation-related conditions such as cognitive decline.

DATA AVAILABILITY

The datasets generated for this study are available on request to the corresponding author.

AUTHOR CONTRIBUTIONS

YA conducted the experiment and wrote the manuscript. RO performed the experiment and the behavioral evaluations. KK and HN designed and conducted the research.

SUPPLEMENTARY MATERIAL

The Supplementary Material for this article can be found online at: https://www.frontiersin.org/articles/10.3389/fnagi.2019.00016/full#supplementary-material

FIGURE S1 | Weight and food/water consumption in aged mice. We fed C57BL/6J mice aged 7 weeks (young; $n = 12$) and 68 weeks (aged) diets containing 0% or 0.05% (w/w) IAA for 3 months (aged with dietary IAA, $n = 10$; aged without dietary IAA, $n = 9$). **(A)** Body weight was monitored every month. **(B,C)** Food **(B)** and water **(C)** consumption over 72 h. Data are presented as mean ± SE. We calculated the *p*-values shown in the graph by one-way analysis of variance (ANOVA), followed by the Tukey-Kramer test.

REFERENCES

Abareshi, A., Anaeigoudari, A., Norouzi, F., Shafei, M. N., Boskabady, M. H., Khazaei, M., et al. (2016). Lipopolysaccharide-induced spatial memory and synaptic plasticity impairment is preventable by captopril. *Adv. Med.* 2016:7676512. doi: 10.1155/2016/7676512

Albani, S. H., McHail, D. G., and Dumas, T. C. (2014). Developmental studies of the hippocampus and hippocampal-dependent behaviors: insights from interdisciplinary studies and tips for new investigators. *Neurosci. Biobehav. Rev.* 43, 183–190. doi: 10.1016/j.neubiorev.2014.04.009

Ano, Y., Ayabe, T., Kutsukake, T., Ohya, R., Takaichi, Y., Uchida, S., et al. (2018a). Novel lactopeptides in fermented dairy products improve memory function and cognitive decline. *Neurobiol. Aging* 72, 23–31. doi: 10.1016/j.neurobiolaging.2018.07.016

Ano, Y., Takaichi, Y., Uchida, K., Kondo, K., Nakayama, H., and Takashima, A. (2018b). Iso-α-acids, the bitter components of beer, suppress microglial inflammation in rTg4510 tauopathy. *Molecules* 23:3133. doi: 10.3390/molecules23123133

Ano, Y., Dohata, A., Taniguchi, Y., Hoshi, A., Uchida, K., Takashima, A., et al. (2017). Iso-α-acids, bitter components of beer, prevent inflammation and cognitive decline induced in a mouse model of Alzheimer's disease. *J. Biol. Chem.* 292, 3720–3728. doi: 10.1074/jbc.M116.763813

Ano, Y., Ozawa, M., Kutsukake, T., Sugiyama, S., Uchida, K., Yoshida, A., et al. (2015). Preventive effects of a fermented dairy product against Alzheimer's disease and identification of a novel oleamide with enhanced microglial phagocytosis and anti-inflammatory activity. *PLoS One* 10:e0118512. doi: 10.1371/journal.pone.0118512

Ayabe, T., Ohya, R., Kondo, K., and Ano, Y. (2018). Iso-α-acids, bitter components of beer, prevent obesity-induced cognitive decline. *Sci. Rep.* 8:4760. doi: 10.1038/s41598-018-23213-9

Barger, S. W., Goodwin, M. E., Porter, M. M., and Beggs, M. L. (2007). Glutamate release from activated microglia requires the oxidative burst and lipid peroxidation. *J. Neurochem.* 101, 1205–1213. doi: 10.1111/j.1471-4159.2007.04487.x

Brown, G. C., and Bal-Price, A. (2003). Inflammatory neurodegeneration mediated by nitric oxide, glutamate, and mitochondria. *Mol. Neurobiol.* 27, 325–355. doi: 10.1385/mn:27:3:325

Chan, J., Guan, X., Ni, Y., Luo, L., Yang, L., Zhang, P., et al. (2017). Dopamine D1-like receptor in lateral habenula nucleus affects contextual fear memory and long-term potentiation in hippocampal CA1 in rats. *Behav. Brain Res.* 321, 61–68. doi: 10.1016/j.bbr.2016.12.026

Coffeen, U., Ortega-Legaspi, J. M., de Gortari, P., Simón-Arceo, K., Jaimes, O., Amaya, M. I., et al. (2010). Inflammatory nociception diminishes dopamine release and increases dopamine D2 receptor mRNA in the rat's insular cortex. *Mol. Pain* 6:75. doi: 10.1186/1744-8069-6-75

Cohen, S. J., Munchow, A. H., Rios, L. M., Zhang, G., Asgeirsdottir, H. N., and Stackman, R. W. Jr. (2013). The rodent hippocampus is essential for nonspatial object memory. *Curr. Biol.* 23, 1685–1690. doi: 10.1016/j.cub.2013.07.002

Escribano, L., Simon, A. M., Gimeno, E., Cuadrado-Tejedor, M., López de Maturana, R., Garcia-Osta, A., et al. (2010). Rosiglitazone rescues memory impairment in Alzheimer's transgenic mice: mechanisms involving a reduced amyloid and tau pathology. *Neuropsychopharmacology* 35, 1593–1604. doi: 10.1038/npp.2010.32

Heneka, M. T., Sastre, M., Dumitrescu-Ozimek, L., Hanke, A., Dewachter, I., Kuiperi, C., et al. (2005). Acute treatment with the PPARγ agonist pioglitazone and ibuprofen reduces glial inflammation and Aβ1–42 levels in APPV717I transgenic mice. *Brain* 128, 1442–1453. doi: 10.1093/brain/awh452

Heppner, F. L., Ransohoff, R. M., and Becher, B. (2015). Immune attack: the role of inflammation in Alzheimer disease. *Nat. Rev. Neurosci.* 16, 358–372. doi: 10.1038/nrn3880

Horvat, P., Richards, M., Kubinova, R., Pajak, A., Malyutina, S., Shishkin, S., et al. (2015). Alcohol consumption, drinking patterns, and cognitive function in older Eastern European adults. *Neurology* 84, 287–295. doi: 10.1212/wnl.0000000000001164

Hsiao, K., Chapman, P., Nilsen, S., Eckman, C., Harigaya, Y., Younkin, S., et al. (1996). Correlative memory deficits, Aβ elevation, and amyloid plaques in transgenic mice. *Science* 274, 99–102. doi: 10.1126/science.274.5284.99

Kametani, F., and Hasegawa, M. (2018). Reconsideration of amyloid hypothesis and tau hypothesis in Alzheimer's disease. *Front. Neurosci.* 12:25. doi: 10.3389/fnins.2018.00025

Lambert, M. P., Barlow, A. K., Chromy, B. A., Edwards, C., Freed, R., Liosatos, M., et al. (1998). Diffusible, nonfibrillar ligands derived from Aβ1–42 are potent central nervous system neurotoxins. *Proc. Natl. Acad. Sci. U S A* 95, 6448–6453. doi: 10.1073/pnas.95.11.6448

Li, S., Cullen, W. K., Anwyl, R., and Rowan, M. J. (2003). Dopamine-dependent facilitation of LTP induction in hippocampal CA1 by exposure to spatial novelty. *Nat. Neurosci.* 6, 526–531. doi: 10.1038/nn1049

Matsui, T., Yoshimura, A., Toyama, T., Matsushita, S., and Higuchi, S. (2011). Preventive effect of moderation in drinking on dementia. *Nippon Rinsho* 69, 217–222.

Miwa, M., Tsuboi, M., Noguchi, Y., Enokishima, A., Nabeshima, T., and Hiramatsu, M. (2011). Effects of betaine on lipopolysaccharide-induced memory impairment in mice and the involvement of GABA transporter 2. *J. Neuroinflammation* 8:153. doi: 10.1186/1742-2094-8-153

Neafsey, E. J., and Collins, M. A. (2011). Moderate alcohol consumption and cognitive risk. *Neuropsychiatr. Dis. Treat.* 7, 465–484. doi: 10.2147/ndt.s23159

Novelli, A., Reilly, J. A., Lysko, P. G., and Henneberry, R. C. (1988). Glutamate becomes neurotoxic via the *N*-methyl-D-aspartate receptor when intracellular energy levels are reduced. *Brain Res.* 451, 205–212. doi: 10.1016/0006-8993(88)90765-2

Noworyta-Sokolowska, K., Górska, A., and Golembiowska, K. (2013). LPS-induced oxidative stress and inflammatory reaction in the rat striatum. *Pharmacol. Rep.* 65, 863–869. doi: 10.1016/s1734-1140(13)71067-3

Obara, K., Mizutani, M., Hitomi, Y., Yajima, H., and Kondo, K. (2009). Isohumulones, the bitter component of beer, improve hyperglycemia and decrease body fat in Japanese subjects with prediabetes. *Clin. Nutr.* 28, 278–284. doi: 10.1016/j.clnu.2009.03.012

Pioli, E. Y., Gaskill, B. N., Gilmour, G., Tricklebank, M. D., Dix, S. L., Bannerman, D., et al. (2014). An automated maze task for assessing hippocampus-sensitive memory in mice. *Behav. Brain Res.* 261, 249–257. doi: 10.1016/j.bbr.2013.12.009

Porquet, D., Griñán-Ferré, C., Ferrer, I., Camins, A., Sanfeliu, C., Del Valle, J., et al. (2014). Neuroprotective role of trans-resveratrol in a murine model of familial Alzheimer's disease. *J. Alzheimers Dis.* 42, 1209–1220. doi: 10.3233/jad-140444

Sarlus, H., and Heneka, M. T. (2017). Microglia in Alzheimer's disease. *J. Clin. Invest.* 127, 3240–3249. doi: 10.1172/JCI90606

Takaki, J., Fujimori, K., Miura, M., Suzuki, T., Sekino, Y., and Sato, K. (2012). L-glutamate released from activated microglia downregulates astrocytic L-glutamate transporter expression in neuroinflammation: the 'collusion' hypothesis for increased extracellular L-glutamate concentration in neuroinflammation. *J. Neuroinflammation* 9:275. doi: 10.1186/1742-2094-9-275

Tamminga, C. A., Southcott, S., Sacco, C., Wagner, A. D., and Ghose, S. (2012). Glutamate dysfunction in hippocampus: relevance of dentate gyrus and CA3 signaling. *Schizophr. Bull.* 38, 927–935. doi: 10.1093/schbul/sbs062

Wendeln, A. C., Degenhardt, K., Kaurani, L., Gertig, M., Ulas, T., Jain, G., et al. (2018). Innate immune memory in the brain shapes neurological disease hallmarks. *Nature* 556, 332–338. doi: 10.1038/s41586-018-0023-4

Winner, B. M., Zhang, H., Farthing, M. M., Karchalla, L. M., Lookingland, K. J., and Goudreau, J. L. (2017). Metabolism of dopamine in nucleus accumbens astrocytes is preserved in aged mice exposed to MPTP. *Front. Aging Neurosci.* 9:410. doi: 10.3389/fnagi.2017.00410

Witte, A. V., Kerti, L., Margulies, D. S., and Flöel, A. (2014). Effects of resveratrol on memory performance, hippocampal functional connectivity, and glucose metabolism in healthy older adults. *J. Neurosci.* 34, 7862–7870. doi: 10.1523/JNEUROSCI.0385-14.2014

Wood, J. G., Mirra, S. S., Pollock, N. J., and Binder, L. I. (1986). Neurofibrillary tangles of Alzheimer disease share antigenic determinants with the axonal microtubule-associated protein tau (tau). *Proc. Natl. Acad. Sci. U S A* 83, 4040–4043. doi: 10.1073/pnas.83.11.4040

Yajima, H., Ikeshima, E., Shiraki, M., Kanaya, T., Fujiwara, D., Odai, H., et al. (2004). Isohumulones, bitter acids derived from hops, activate both peroxisome proliferator-activated receptor α and γ and reduce insulin resistance. *J. Biol. Chem.* 279, 33456–33462. doi: 10.1074/jbc.M403456200

Yu, Y., and Ye, R. D. (2015). Microglial Aβ receptors in Alzheimer's disease. *Cell. Mol. Neurobiol.* 35, 71–83. doi: 10.1007/s10571-014-0101-6

Zhou, T., Huang, Z., Sun, X., Zhu, X., Zhou, L., Li, M., et al. (2017). Microglia polarization with M1/M2 phenotype changes in rd1 mouse model of retinal degeneration. *Front. Neuroanat.* 11:77. doi: 10.3389/fnana.2017.00077

Conflict of Interest Statement: YA, RO and KK are employed by Kirin Company Ltd.

The remaining author declares that the research was conducted in the absence of any commercial or financial relationships that could be construed as a potential conflict of interest.

frontiers in Aging Neuroscience

ORIGINAL RESEARCH
published: 28 February 2019
doi: 10.3389/fnagi.2019.00042

Emergence of Microglia Bearing Senescence Markers During Paralysis Progression in a Rat Model of Inherited ALS

Emiliano Trias[1†], Pamela R. Beilby[2,3†], Mariángeles Kovacs[1], Sofía Ibarburu[1], Valentina Varela[1], Romina Barreto-Núñez[1], Samuel C. Bradford[3], Joseph S. Beckman[2,3] and Luis Barbeito[1]**

[1] Institut Pasteur de Montevideo, Montevideo, Uruguay, [2] Department of Biochemistry and Biophysics, Oregon State University, Corvallis, OR, United States, [3] Linus Pauling Institute, Oregon State University, Corvallis, OR, United States

Age is a recognized risk factor for amyotrophic lateral sclerosis (ALS), a paralytic disease characterized by progressive loss of motor neurons and neuroinflammation. A hallmark of aging is the accumulation of senescent cells. Yet, the pathogenic role of cellular senescence in ALS remains poorly understood. In rats bearing the ALS-linked SOD1^{G93A} mutation, microgliosis contribute to motor neuron death, and its pharmacologic downregulation results in increased survival. Here, we have explored whether gliosis and motor neuron loss were associated with cellular senescence in the spinal cord during paralysis progression. In the lumbar spinal cord of symptomatic SOD1^{G93A} rats, numerous cells displayed nuclear p16^{INK4a} as well as loss of nuclear Lamin B1 expression, two recognized senescence-associated markers. The number of p16^{INK4a}-positive nuclei increased by four-fold while Lamin B1-negative nuclei increased by 1,2-fold, respect to non-transgenic or asymptomatic transgenic rats. p16^{INK4a}-positive nuclei and Lamin B1-negative nuclei were typically localized in a subset of hypertrophic Iba1-positive microglia, occasionally exhibiting nuclear giant multinucleated cell aggregates and abnormal nuclear morphology. Next, we analyzed senescence markers in cell cultures of microglia obtained from the spinal cord of symptomatic SOD1^{G93A} rats. Although microglia actively proliferated in cultures, a subset of them developed senescence markers after few days *in vitro* and subsequent passages. Senescent SOD1^{G93A} microglia in culture conditions were characterized by large and flat morphology, senescence-associated beta-Galactosidase (SA-β-Gal) activity as well as positive labeling for p16^{INK4a}, p53, matrix metalloproteinase-1 (MMP-1) and nitrotyrosine, suggesting a senescent-associated secretory phenotype (SASP). Remarkably, in the degenerating lumbar spinal cord other cell types, including ChAT-positive motor neurons and GFAP-expressing astrocytes, also displayed nuclear p16^{INK4a} staining. These results suggest that cellular senescence is closely associated with inflammation and motor neuron loss occurring after paralysis onset in SOD1^{G93A} rats. The emergence of senescent cells could mediate key pathogenic mechanisms in ALS.

Keywords: microglia, ALS, senescence, astrocytes, motor neurons, aging, SASP

OPEN ACCESS

Edited by:
Alberto Javier Ramos, Consejo Nacional de Investigaciones Científicas y Técnicas (CONICET), Argentina

Reviewed by:
Neil Cashman, University of British Columbia, Canada
Kaoru Tominaga, Jichi Medical University, Japan

****Correspondence:***
Joseph S. Beckman
joe.beckman@oregonstate.edu
Luis Barbeito
barbeito@pasteur.edu.uy;
barbeito2006@gmail.com

† These authors have contributed equally to this work

Received: *12 December 2018*
Accepted: *13 February 2019*
Published: *28 February 2019*

Citation:
Trias E, Beilby PR, Kovacs M, Ibarburu S, Varela V, Barreto-Núñez R, Bradford SC, Beckman JS and Barbeito L (2019) Emergence of Microglia Bearing Senescence Markers During Paralysis Progression in a Rat Model of Inherited ALS. Front. Aging Neurosci. 11:42. doi: 10.3389/fnagi.2019.00042

INTRODUCTION

Amyotrophic lateral sclerosis (ALS) is an adult-onset neurodegenerative disease characterized by progressive upper and lower motor neuron degeneration, leading to muscle weakness and paralysis (Tsai et al., 2017). Although the etiology of ALS remains unknown, age is considered the strongest independent risk factor, most patients being diagnosed between the ages of 50 and 85 (Kiernan et al., 2011). ALS is also characterized by the ineluctable progression of motor deficits, with a variable but short survival of about 20 months (Hardiman et al., 2017). Age of diagnosis is also considered a strong predictor of survival, with hazard ratios progressively increasing each decade for individuals older than 50 years (Crockford et al., 2018). Age-dependence of motor phenotypes has also been described in rodent and fly models (Iguchi et al., 2013; Sreedharan et al., 2015), further supporting ALS as an aging-related condition.

Various studies indicate that motor neuron degeneration in ALS is often associated with increased oxidative and nitrative damage, mitochondrial dysfunction, ER-stress, defective RNA processing, and protein homeostasis (Cassina et al., 2008; Morgan and Orrell, 2016). In parallel, glial cells also become activated, proliferate and display inflammatory features characteristic of gliosis (Philips and Rothstein, 2014; Trias et al., 2018a). These kinds of cellular stresses combined with DNA damage or strong mitogenic signaling in vulnerable cells have the potential to induce cellular senescence (Rodier et al., 2009), a basic and heterogenous mechanism by which damaged cells adapt to maintain survival and prevent potentially deleterious expansion or oncogenic transformation during aging (Munoz-Espin and Serrano, 2014). A fundamental feature of cellular senescence is the arrest of the cell cycle through $p16^{INK4A}$-mediated pathway, which is usually associated with p53 nuclear expression (Prieur et al., 2011). p53 becomes activated in response to a variety of cellular stressors including DNA damage and oxidative stress leading to an increased half-life of the p53 protein, phosphorylation and nuclear translocation. In turn, nuclear p53 can function as a transcription factor to regulate the cell cycle, apoptosis, genomic stability or senescence response (Rufini et al., 2013). Nuclear expression of $p16^{INK4A}$ is considered a robust molecular marker of cellular aging, as its expression increases in a variety of aged tissues (Baker et al., 2011). Another remarkable senescence-associated marker is the loss of nuclear Lamin B1 (Freund et al., 2012), which together with other lamins, is essential to maintain nucleus stability, size and shape (Dechat et al., 2008). The loss of nuclear Lamin B1 in particular is recognized as a senescence marker, functionally associated with the induction of $p16^{INK4A}$ and p53 (Freund et al., 2012).

In addition, senescent cells develop profound phenotypic and functional changes, including an increase in senescence-associated beta-galactosidase (SA-β-Gal) activity, reflecting an increased number of lysosomes (Dimri et al., 1995). In addition, senescent cells enlarge and flatten with a tendency to form multinucleated cell aggregates (Leikam et al., 2015), accumulate oxidative and nitrative damage (Lamoke et al., 2015) and typically display a senescent-associated secretory phenotype (SASP) (Tchkonia et al., 2013), releasing trophic factors, pro-inflammatory signaling molecules, extracellular matrix components and proteases (Rodier et al., 2009). Recent evidence indicate cells expressing senescence markers contribute to the chronic inflammatory environment and progressive degeneration in different tissues from aged animals (Childs et al., 2015), thus acquiring pathogenic significance.

Previous studies in neurodegenerative conditions show that the emergence of glial and neuronal senescent phenotypes displaying inflammatory features contribute to synaptic and neuronal loss (Arendt et al., 1996; Frost, 2016), with the senescence marker $p16^{INK4a}$ being frequently found in a subpopulation of astrocytes (Bhat et al., 2012). In accordance, a senescence phenotype in human astrocytes can be induced by toxic species of amyloid beta in cell cultures (Bhat et al., 2012). Also, brain astrocytes bearing senescence markers have been identified in normal aging and disease conditions (Salminen et al., 2011; Chinta et al., 2013). Both in ALS animal models and patients, aged astrocytes develop senescence markers such as $p16^{INK4A}$, p53, p21, and SA-β-gal, becoming toxic for motor neurons (Martin, 2000; Das and Svendsen, 2015; Turnquist et al., 2016), suggesting a causal pathogenic role in mediating motor neuron loss. To what extent activated microglia follow senescence-associated phenotypes during the course of paralysis progression in ALS remains to be analyzed.

Microgliosis is a recognized pathological feature in ALS patients (Brettschneider et al., 2012). Extensive microglia activation has also been described in transgenic rodent models of inherited ALS carrying SOD1 mutations (Lewis et al., 2014). In $SOD1^{G93A}$ rats, the rapid spread of paralysis is associated with marked microglial cell activation in the surroundings of motor neurons, leading to the emergence of aberrant phenotypes including astrocyte-like hypertrophic cells and giant multicellular clusters (Fendrick et al., 2007; Diaz-Amarilla et al., 2011; Trias et al., 2013). Activated microglia expressing mutant SOD1 in ALS have the potential to induce motor neuron death (Liao et al., 2012; Frakes et al., 2014). Removal of mutant SOD1 transgene from microglia and neurons significantly increases survival in of $SOD1^{G37R}$ mice (Boillee et al., 2006). The unique nature of microglia with the potential for self-renewal and telomere shortening led to the hypothesis that these cells can exhibit senescence (Eitan et al., 2014; Caldeira et al., 2017). Age-dependent and senescence-driven impairments of microglia functions and responses have been suggested to play essential roles during the onset and progression of neurodegenerative diseases (Luo et al., 2010; Spittau, 2017). However, it remains unknown whether deleterious gliosis and phenotypically aberrant glia in ALS are causally associated with the emergence of senescent cells in the degenerating spinal cord.

In this study, we analyzed the expression of senescence markers in the spinal cord and primary cultures of microglia from adult $SOD1^{G93A}$ rats. In an attempt to determine the relationship between the emergence of senescent glia phenotypes and progressive motor neuron loss, we analyzed senescence markers at disease onset and then at advanced paralysis, a time period of only 2 weeks while rapid paralysis develops in $SOD1^{G93A}$ rats.

MATERIALS AND METHODS

Animals and Study Approval

All procedures using laboratory animals were performed in accordance with the international guidelines for the use of live animals and were approved by either the Oregon State University Institutional Animal Care Use Committee or for experiments performed in Uruguay in strict accordance with the requirements of the Institut Pasteur de Montevideo Bioethics Committee under the ethical regulations of the Uruguayan Law N° 18.611 governing animal experimentation. Uruguayan law follows the Guide for the Care and Use of Laboratory Animals of the National Institutes of Health (United States). Male hemizygous NTac:SD-TgN(SOD1^{G93A})L26H rats (Taconic), originally developed by Howland et al. (2002), were bred locally by crossing with wild-type Sprague–Dawley female rats. Male SOD1^{G93A} progenies were used for further breeding to maintain the line. Rats were housed in a centralized animal facility with a 12-h light-dark cycle with *ad libitum* access to food and water. Symptomatic disease onset was determined by a periodic clinical examination for abnormal gait, typically expressed as subtle limping or dragging of one hind limb. Rats were killed well before they reached the end stage of the disease.

Experimental Conditions

At least three male rats were analyzed for each experiment. Four different conditions were studied as follow: (1) non-transgenic (NonTg) rats of 160–180 days; (2) transgenic SOD1^{G93A} rats of 125–135 days (asymptomatic); (3) transgenic SOD1^{G93A} rats of 170–180 days (onset); and (4) transgenic SOD1^{G93A} rats of 190–200 days (symptomatic 15d paralysis).

Determination of Disease Onset and End-Stage

As described previously (Trias et al., 2017), all rats were weighed and evaluated for motor activity daily. Disease onset was determined for each animal when pronounced muscle atrophy was accompanied by abnormal gait, typically expressed as subtle limping or dragging of one hind limb. When necessary, end-stage was defined by a lack of righting reflexes or the inability to reach food and water.

Immunohistochemical Staining of Rat Spinal Cords

Animals were deeply anesthetized and perfused transcardially with 0.9% saline and 4% paraformaldehyde in 0.1 M PBS (pH 7.2–7.4) at a constant flow of 1 mL/min. The fixed spinal cord was removed, post-fixed by immersion for 24 h, and then cut into transverse serial 25 μm sections with a cryostat. Serial sections were collected in PBS for immunohistochemistry. Free-floating sections were permeabilized for 30 min at room temperature with 0.3% Triton X-100 in PBS, passed through washing buffered solutions, blocked with 5% BSA:PBS for 1 h at room temperature, and incubated overnight at 4°C in a solution of 0.3% Triton X-100 and PBS containing the primary antibodies overnight at 4°C. After washing, sections were incubated in 1:1000-diluted secondary antibodies during 3 h at room temperature. Using a stereological approach, p16^{INK4a}-positive nuclei, Iba1-/p16^{INK4a}-positive cells, Lamin B1/DAPI and ChAT-/p16^{INK4a}-positive cells were counted in 25-μm spinal cord sections using confocal microphotograph with a magnification of 25×. At least 15 sections per spinal cord were analyzed (n = 3). ImageJ software was used for analysis. For p53 quantification in the spinal cord, p53 density was measured using ImageJ. At least five sections per animal were analyzed (n = 3) as previously described (Trias et al., 2018b).

Antibodies Used

Primary antibodies: 1:200 mouse monoclonal anti-CDKN2A/p16^{INK4a} (abcam, #ab54210), 1:300 rabbit polyclonal anti-p53 (abcam, #ab131442), 1:400 rabbit polyclonal anti-MMP-1 (Novus Biologicals, #NBP1-72209), 1:300 mouse monoclonal anti-Iba1 (Merck, #MABN92), 1:400 muse monoclonal anti-CD68 (abcam, #ab31630), 1:400 rabbit polyclonal anti-ChAT (Merck, #AB143), 1:500 rabbit polyclonal anti-GFAP (Sigma, #G9269), 1:300 mouse monoclonal anti-S100β (Sigma, #S2532), 1:250 rabbit polyclonal anti-Lamin B1 (abcam, #ab16048), 1:300 mouse monoclonal anti-misfolded SOD1 B8H19 (Medimabs, # MM-0070-P), and 1:250 rabbit polyclonal anti-Nitro tyrosine (abcam, #ab42789). Secondary antibodies: 1:500 goat anti-rabbit-AlexaFluor488 or AlexaFluor546 (Thermo Fisher Scientific, #A11035 or #A11034), 1:500 goat anti-mouse-AlexaFluor488, AlexaFluor546 or AlexaFluor633 (Thermo Fisher Scientific, #A11029, #A11030, or #A21052).

Microglia Cell Culture From Adult Symptomatic SOD1^{G93A} Rats

Microglia cells were isolated from adult symptomatic SOD1^{G93A} rats as previously described with slight modifications (Trias et al., 2013). Rats were terminally anesthetized and the spinal cords were dissected with the meninges carefully removed. The cords were mechanically chopped then enzymatically dissociated in 0.25% trypsin for 10 min at 37°C. Fetal Bovine Serum (FBS) 10% (vol/vol) in Dulbecco's Modified Eagle Medium (DMEM) was then added to halt trypsin digestion. Repetitive pipetting thoroughly disaggregated the tissue, which was then strained through an 80-μm mesh and spun down. The pellet was re-suspended in culture medium [DMEM + FBS 10% (vol/vol), HEPES buffer (3.6 g/mL), penicillin (100 IU/mL), and streptomycin (100 μg/mL)] and plated in glass-bottom p35 culture dishes for confocal microscopy or 25-cm^2 tissue culture flasks for flow cytometry analysis. Culture medium was replaced every 48 h.

Analysis of Aberrant Glial Cells After Phenotypic Transformation

As previously characterized (Trias et al., 2013), primary adult microglia isolated from symptomatic SOD1^{G93A} rats transitioned into aberrant glial cells after 12–15 days in culture. These aberrant glial cells can be maintained in culture for several passages (Diaz-Amarilla et al., 2011). In the present study, passages 2–4 of aberrant glial cells maintained *in vitro* (DMEM-10% FBS) in

glass-bottom p35 culture dishes for several days were analyzed for different senescent markers.

Senescence-Associated-β-Galactosidase (SA-β-Gal) Activity in Cell Cultures

Protocol for β-galactosidase staining was followed as described by manufacturer cell staining kit (Cell Signaling, #9860). Briefly, growth media was removed from the cells and washed with PBS. The 1X fixative solution was added for 15 min at room temperature. After two PBS washes, 1 mL of β-galactosidase staining solution was added overnight at 37°C in a dry incubator. After blue color was developed, β-galactosidase staining solution was removed and plates were mounted using 70% glycerol for long-term storage at 4°C. Both microglia and aberrant glial cells were analyzed at different time points during 12 days. 10×, 20×, and 100× images were acquired using an Olympus CX41 microscope connected to a Evolution^{TM}LC Color camera and using ImagePro Express software for acquisition. At least 10 fields per plate were acquired for quantitative analysis using ImageJ software.

Immunocytochemical Staining of Cultured Cells

Cultured cells were fixed with 4% PFA for 20 min at 4°C and then were washed three times with 10 mM PBS (pH 7.4). Cells were permeabilized using 0.3% Triton-X100 for 20 min. Nonspecific binding was blocked by incubating fixed cells with 5% BSA in PBS for 1 h at room temperature. Corresponding primary antibodies were diluted in blocking solution and incubated 3 h at room temperature. After washing, cells were incubated with secondary antibodies in blocking solution for 1 h at room temperature. For p16^{INK4a} and p53 staining, cells were permeabilized using 2M HCl solution during 15 min at room temperature before incubation with blocking solution. DAPI was used for nuclei staining. At least 10 fields per plate were acquired in a confocal microscope for quantitative analysis using ImageJ software.

Flow Cytometry of Senescence-Associated-β-Galactosidase (SA-β-gal) Activity

After 12 days *in vitro*, microglia were quantitatively analyzed for SA-β-Gal activity. Briefly, cells were treated with Bafilomycin A1 to inhibit lysosomal acidification, followed by incubation with C_{12}FDG (Molecular Probes/Life Technologies), a fluorogenic substrate for β-galactosidase for 2 h at 37°C with 5% CO_2. Microglia were then rinsed with PBS, harvested by trypsinization, centrifuged, and re-suspended in ice-cold PBS. Cells were immediately run on a Beckman-Coulter FC500 flow cytometer. Data were analyzed using Winlist (Verity Software).

Flow Cytometry of Cell Cycle Progression

Cells were trypsinized, washed, and centrifuged. The cell pellet was then resuspended in ice-cold 70% ethanol and incubated at −20°C for 30 min for fixation. Subsequently, cells were washed, centrifuged and re-suspended in 0.1% Triton X-100 in Dulbecco's Phosphate-Buffered Saline (DPBS). RNase A (10 μg/mL) and propidium iodide (20 μg/mL) were added and cells were incubated for 60 min at room temperature. They were then filtered through a 37-μm mesh and run on Beckman-Coulter FC500 flow cytometer and analyzed using Multi-Cycle (Phoenix Software).

Fluorescence Imaging

Fluorescence imaging was performed with a laser scanning Zeiss LSM 800 confocal microscope with either a 25× (1.2 numerical aperture) objective or 63× (1.3 numerical aperture) oil-immersion objective using Zeiss Zen Black software. Maximum intensity projections of optical sections were created with Zeiss Zen software.

Statistical Analysis

Quantitative data were expressed as mean ± SEM. Two-tailed Mann–Whitney test or Kruskal–Wallis followed by Dunn's multiple comparison tests were used for statistical analysis, with $p < 0.05$ considered significant. GraphPad Prism 7.03 software was used for statistical analyses.

RESULTS

Expression of Senescence Markers p16^{INK4a} and Lamin B1 in the Spinal Cord of SOD1^{G93A} Rats During Paralysis Progression

Based on a previous report showing an increase of p16^{INK4a} RNA levels in symptomatic SOD1^{G93A} rats (Das and Svendsen, 2015), we examined the number of p16^{INK4a}-positive nuclei and Lamin B1 expression in the ventral horn of the lumbar cord during paralysis progression. Immunohistochemistry analysis revealed a continuous increase in p16^{INK4a} nuclear expression in rats expressing mutant SOD1 as compared with non-transgenic rats (**Figure 1A**). The number of p16^{INK4a}-positive nuclei was significantly increased by 2.3-fold and 3.5-fold at paralysis onset and 15d of paralysis progression, respectively (graph in **Figure 1A**).

On the other hand, nuclear levels of Lamin B1 significantly declined during paralysis progression in SOD1 rats, 1 out of 4 nuclei exhibiting loss of Lamin B1 at 15d post-paralysis (arrows in **Figure 1D**), which is significantly different from non-transgenic and asymptomatic SOD1^{G93A} rats (**Figures 1B,D**). Moreover, the decline in Lamin B1 expression and nuclear Lamin B1 invaginations (asterisk in **Figure 1D**) were associated with aberrant nuclear shapes (arrowheads in **Figure 1D**).

Because cellular senescence is characterized by cell cycle arrest through p16^{INK4a}- and p53-mediated pathways (Prieur et al., 2011), we also assessed p53 expression in the lumbar ventral horn. As shown in **Supplementary Figure S1**, p53 immunoreactivity significantly increased in mutant SOD1 rats at paralysis onset and advanced paralysis with frequent colocalization of p16^{INK4a}

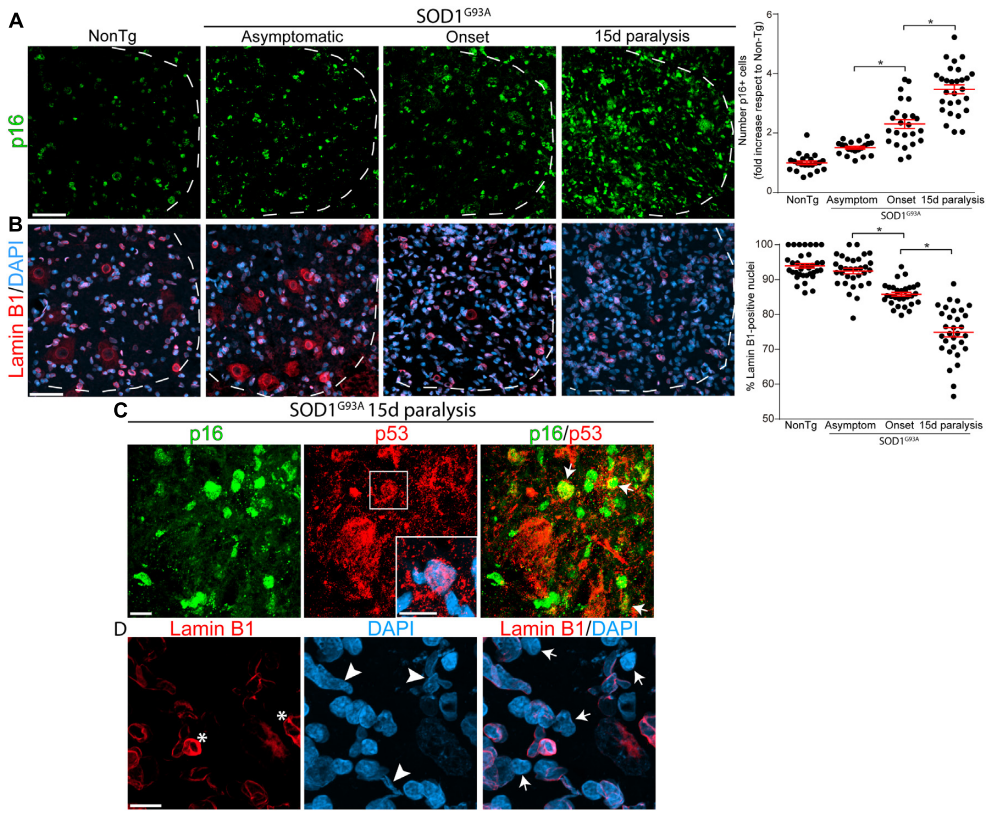

FIGURE 1 | Progressive change in senescence markers p16^{INK4a} and Lamin B1 during paralysis progression in SOD1^{G93A} rats ventral spinal cord. Representative confocal images showing the expression of p16^{INK4a} (green) and Lamin B1 (red) by immunohistochemistry in the degenerating spinal cord of SOD1^{G93A} animals and non-transgenic controls. **(A)** Progressive increase of the senescence marker p16^{INK4a} staining (green) in nuclei from the ventral horn of the spinal cord in symptomatic rat during paralysis progression (white dotted lines indicate the separation of white and gray matter). The graph to the right shows the quantitative analysis of the p16^{INK4a}-positive nuclei in the ventral spinal cord. Data are expressed as mean ± SEM; data were analyzed by Kruskal–Wallis followed by Dunn's multiple comparison tests, $p < 0.05$ was considered statistically significant. Scale bar: 50 μm. **(B)** Confocal microphotographs showing the staining for nuclear Lamin B1 (red) as a marker of non-senescent cells among analyzed groups. The graph to the right shows the quantitative analysis of Lamin B1-positive nuclei in the ventral horn of the spinal cord. Note the progressive loss of nuclear Lamin B1 expression with disease progression. Data are expressed as mean ± SEM; data were analyzed by Kruskal–Wallis followed by Dunn's multiple comparison tests, $p < 0.05$ was considered statistically significant. Scale bar: 50 μm. **(C)** The confocal images show co-expression of p16^{INK4a} (green) p53 (red) nuclear staining (white arrows) in the ventral horn of degenerating spinal cord at 15d post-paralysis. The inset shows the nuclear localization of p53 in a subset of cells. Scale bars: 10 μm. **(D)** High magnification confocal image showing the loss of nuclear Lamin B1 (red) expression (white arrows) and Lamin B1 invaginations (asterisks) associated to nuclear misshape. Scale bar: 10 μm.

(**Figure 1C**). p53 expression levels increased by 1.5- and 2-fold at onset and advanced paralysis, respectively, with respect to age-matched non-transgenic littermates (Graph in **Supplementary Figure S1**).

Nuclear p16^{INK4a} and Lamin B1 Expression in Spinal Cord Microglia During Paralysis Progression

Next, we analyzed whether p16^{INK4a} and Lamin B1 were expressed in Iba1-positive microglia, that typically proliferate and become hypertrophic near spinal motor neurons in symptomatic SOD1^{G93A} rats (Trias et al., 2013). As shown in **Figure 2A**, Iba1-positive microglia express high levels of nuclear p16^{INK4a} (white arrows) in rats developing paralysis. Compared with non-transgenic controls, p16^{INK4a} expression at onset and 15d of paralysis progression significantly increased by 2.6- and 4.8-fold, respectively (graph in **Figure 2A**). Remarkably, a high density of p16^{INK4a} nuclei was identified in multinucleated microglia clusters (**Figure 2B**) that are frequently found in the ventral horn of symptomatic SOD1^{G93A} rats (Fendrick et al., 2007), further indicating the correlation of senescence with microglia bearing aberrant phenotypes.

In addition, nuclear expression of Lamin B1 progressively declined in Iba1-positive cells during advance paralysis. **Figure 2C** shows subpopulation of Iba1-positive microglia that devoid of nuclear Lamin B1 (arrows) coexisting with microglia displaying normal pattern of Lamin B1 staining (arrowheads). Furthermore, nuclear Lamin B1 decline was observed in senescent multinucleated microglia clusters in the lumbar spinal cord (**Figure 2D**).

Next, we analyzed whether misfolded SOD1 was associated with senescent microglia in SOD1 rats. Misfolded SOD1 is a recognized hallmark of neuronal pathology in ALS linked to

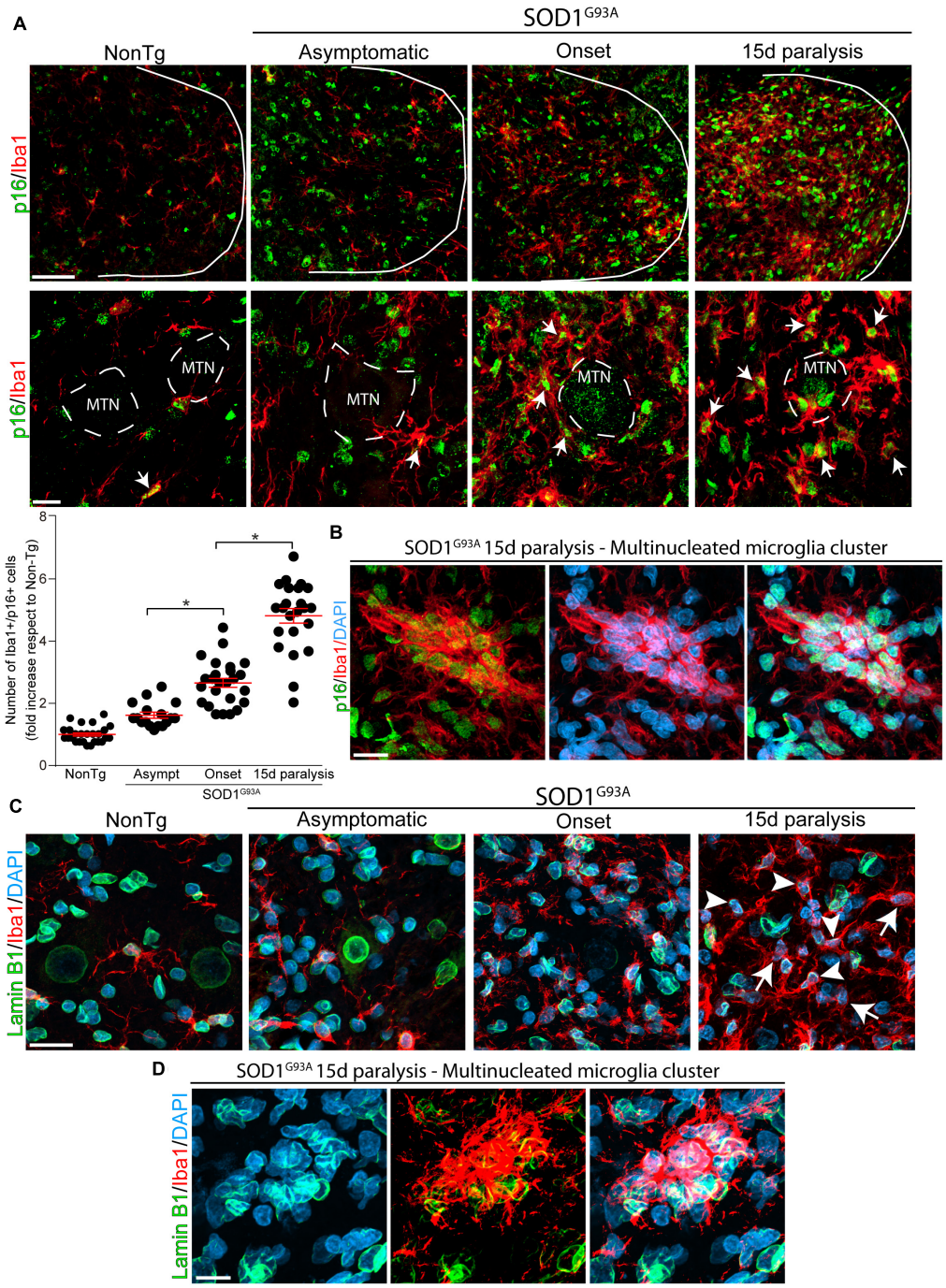

FIGURE 2 | Nuclear p16^{INK4a} and Lamin B1 expression in microglia during paralysis progression. **(A)** Confocal representative images showing the expression of the microglia marker Iba1 (red) and the senescence marker p16^{INK4a} (green) in the non-transgenic, asymptomatic, onset and 15d paralysis SOD1^{G93A} ventral spinal cord. The upper panels (low magnification) show the significant parallel increase of nuclear p16^{INK4a} in Iba1-positive cells during the symptomatic stage of the disease as compared with non-transgenic animals or SOD1^{G93A} asymptomatic stage. Lower panels show at high magnification images of p16^{INK4a}-positive swollen microglia (white arrows) surrounding motor neurons (MTN). The graph below shows the quantitative analysis of the expression of p16^{INK4a-} in Iba1-positive cells. Note the sharp increase of p16^{INK4a}–positive microglia at 15d post-paralysis. Data are expressed as mean ± SEM; data were analyzed by Kruskal–Wallis followed by Dunn's multiple comparison tests, $p < 0.05$ was considered statistically significant. Scale bars: 50 μm in low magnification panels and 10 μm in high magnification panels. **(B)** The confocal microphotograph shows a multinucleated microglia cluster expressing Iba1 (red) in a 15d paralysis rat. These Iba1-positive clusters express nuclear p16^{INK4a}. Scale bar: 20 μm. **(C)** Representative confocal microphotograph of the ventral spinal cord showing nuclear Lamin B1 expression in Iba1-positive cells (arrowheads). Note the loss of Lamin B1 expression in a subpopulation of cells (arrows) at 15d post-paralysis. Scale bar: 20 μm. **(D)** The confocal microphotograph shows a cluster of multinucleated microglia where Lamin B1 expression is absent in several nuclei (DAPI) at 15d post-paralysis. Scale bar: 20 μm.

SOD1 mutations (REF). As shown in **Supplementary Figure S2**, misfolded SOD1 was mainly detected in degenerating neuronal somas and dendrites in symptomatic SOD1^{G93A} rats and was not observed in non-transgenic or asymptomatic transgenic rats. However, the presence of misfolded SOD1 in microglia appeared to correspond to neuronal debris being engulfed by phagocytic microglia (arrows in **Supplementary Figure S2**).

Nuclear p16^{INK4a} Staining in a Subset of Spinal Motor Neurons and Astrocytes During Advanced Paralysis

Previous reports have shown astrocytes bearing senescent markers in the spinal cord of symptomatic SOD1^{G93A} rats (Das and Svendsen, 2015) as well as in post-mitotic neurons submitted to stress or aging (Jurk et al., 2012). Thus, we looked for p16^{INK4a}-expressing astrocytes and motor neurons in the lumbar spinal cord of SOD1^{G93A} rats during onset and 15d of paralysis progression. As shown in **Figure 3A**, a subset of ChAT-positive motor neurons expressed significant levels of nuclear p16^{NK4a} during the period of rapid motor neuron loss in advanced paralysis. In comparison, motor neurons bearing healthy morphology in asymptomatic SOD1^{G93A} rats were negative to p16^{NK4a}, suggesting senescence develops only in damaged motor neurons. Nuclear p16^{INK4a} was also observed in numerous GFAP-positive astrocytes that typically surround motor neurons in the ventral horn of symptomatic SOD1^{G93A} rats (**Figure 3B**).

Senescence-Associated β-Galactosidase Activity (SA-β-gal) in Primary Cultures of Microglia From Symptomatic SOD1^{G93A} Rats

We have previously shown that primary spinal cord cultures from symptomatic SOD1^{G93A} rats yield >98% of microglia (Trias et al., 2013). **Figure 4A** summarizes the behavior of these microglia cultures and its ability to actively proliferate and transform into flat enlarged cells after serial passages. In this context, we explored whether cultured microglia from symptomatic SOD1^{G93A} rats could develop senescence markers as observed in the degenerating spinal cord. Primary cultures of SOD1^{G93A} microglia maintained for 12 days *in vitro* progressively developed positive chromogenic SA-β-gal staining, with ∼8-fold increase between 1 DIV and 12 DIV (**Figure 4B**). Senescent microglia in cell cultures demonstrated an enlarged, flattened morphology (arrows in **Figure 4B**), morphological features previously described in other senescent cells (Carnero, 2013).

Flow cytometer analysis of microglia maintained in culture for 12 DIV showed 50% of the cells exhibiting SA-β-gal fluorescent staining (**Supplementary Figure S3**), with two distinct cell subpopulations, based on size as seen in the scatter diagram of the cells (**Supplementary Figure S3**). The subpopulation of smaller cells displays only 8% of SA-β-Gal activity and normal cell cycle behavior, corresponding to non-senescence cells (**Figures 4C,D**). In contrast, 92% of large size cells exhibited SA-β-gal activity and also significant S-phase arrest (**Figures 4E,F**), the latter being usually associated with inhibition of cell growth, proliferation and senescence in cell cultures (Blagosklonny, 2011).

Expression of Senescence Markers in Cell Cultures of SOD1^{G93A} Microglia

Next, we analyzed the phenotypic features of Iba1- and CD68-positive SOD1 microglia at 2- and 12-DIV to identify senescence cellular markers. As shown in **Figures 5A,B**, approximately 50% of microglia expressed p16^{INK4a} or p53 nuclear staining at 12DIV, as compared with approximately 15% at 2DIV (graphs in **Figures 5A,B**, and **Supplementary Figures S4A,B**). 12DIV microglial cells also displayed high levels of MMP-1 and NO_2Tyr in comparison with 2DIV isolated cells (**Supplementary Figure 4C**). In addition, p16^{INK4a}, p53, MMP-1, and NO_2Tyr were also found in multinucleated cell aggregates that are frequently found in culture conditions (**Figure 5C**), reproducing the aberrant features found in the degenerating spinal cord *in vivo*.

The emergence of senescent cells was also observed in serially passaged SOD1^{G93A} microglia cultures, which have undergone a phenotypic transformation (Trias et al., 2013). As shown in **Supplementary Figure 5A**, the number of SA-β-Gal-positive cells rapidly increased in the following 5 days after plating, ∼50% of these cells also displaying increased p16^{INK4a} and p53 nuclear staining (**Supplementary Figures 5B,C**).

DISCUSSION

Amyotrophic lateral sclerosis has been modeled as a multi-step process associating senescence-driven tissue dysfunction with underlying genetic defects and risk factors (Al-Chalabi et al., 2014). In this context, here we report that paralysis progression in a rat model of ALS is characterized by the emergence of numerous microglia, astrocytes and motor neurons displaying phenotypic markers of senescence. Senescent cells seem to be acutely induced after paralysis onset, suggesting a deleterious effect mediated by the ALS neurodegenerative cellular microenvironment and coincident to motor neuron loss. Senescence markers were also observed in cultures of microglia isolated from symptomatic SOD1^{G93A} rats, further indicating the inherent ability of these cells to develop a senescence program with secretory features. In agreement with previous reports showing senescence microglia in aged rodents (Rawji et al., 2016; Theriault and Rivest, 2016), the present data show evidence of a yet unknown mechanism associating microglia activation and cell senescence, with the emergence of secretory phenotypes in a rat model of ALS.

Activation of the p16^{INK4a}-pathway is essential for the induction of senescence in a variety of cell types (Prieur et al., 2011). The tumor suppressor p53 also contribute to the induction of cellular senescence in glial cells (Turnquist et al., 2016). We found that the basal levels in p16^{INK4a} and p53 expression were significantly increased in SOD1^{G93A} rats at asymptomatic and paralysis onset stages, respect to age-matched non-transgenic controls. Strikingly, p16^{INK4a} and p53 levels sharply increased after paralysis onset, coincident with extensive spinal cord microgliosis and motor neuron loss occurring in SOD1^{G93A} rats

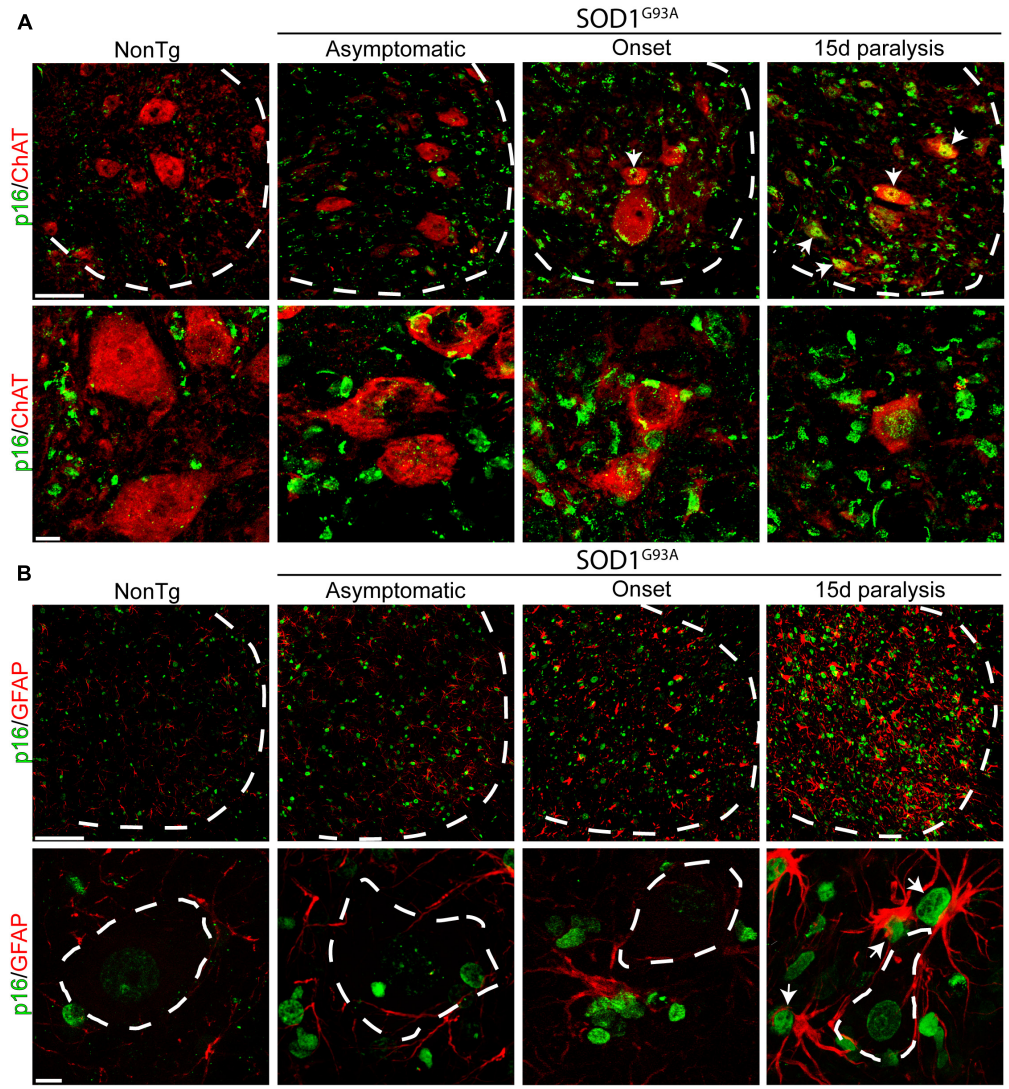

FIGURE 3 | Nuclear $p16^{INK4a}$ expression in a subpopulation of spinal motor neurons and astrocytes. **(A)** Representative confocal microphotograph of the ventral spinal cord of $SOD1^{G93A}$ rats showing ChAT-positive (red) motor neurons at low (upper row) and high (lower row) magnifications. During the symptomatic phase of the disease, a subpopulation of neurons expresses nuclear $p16^{INK4a}$ (white arrows). Dotted white line separate white from gray matter. Scale bars: 50 μm for low magnification panels and 10 μm for high magnification panel. **(B)** Photomicrographs showing $p16^{INK4a}$/GFAP stained lumbar spinal cord sections among groups. Low magnification panels (upper panels) show the notorious increase in the number of $p16^{INK4a}$-/GFAP-positive cells in the symptomatic rats, as compared to low markers co-expression in asymptomatic or non-transgenic rats. Note the expression of $p16^{INK4a}$ marker in a subpopulation of astrocytes that surround motor neurons. Scale bars: 50 μm for low magnification panels and 10 μm for high magnification panel.

(Howland et al., 2002). Increased levels of $p16^{INK4a}$ and p53 were shown to induce nuclear loss of Lamin B1 (REF). Such a decline in Lamin B1 level constitutes a recognized biomarker of cellular senescence (REF). This is the first report showing a significant increase in nuclear Lamin B1 loss in the degenerating spinal cord of $SOD1^{G93A}$ rats, which was associated with other pathological features of Lamin B1 and nuclear misshape. Senescent microglia showed Lamin B1 loss as well as abnormalities in nuclear Lamin B1 localization pattern. These findings agree with previous reports showing disruption of nuclear Lamin B1 in neural cells associated with Parkinson's disease and Tau pathologies (Frost et al., 2016; Chinta et al., 2018).

$p16^{INK4a}$ expression and nuclear Lamin B1 decline in microglia were typically observed in cells surrounding the damaged motor neurons. These cells also displayed large size, multinucleated formations as well as MMP-1 and nitrotyrosine staining in culture, suggesting phenotypic aberrations and secretory features. Thus, senescent microglia emerging in the degenerating spinal cord may explain the origin of aberrant glial phenotypes previously described during paralysis progression in $SOD1^{G93A}$ (Diaz-Amarilla et al., 2011; Trias et al., 2013). Taking together, these observations suggest that senescence microglia may result as a consequence of microglia activation, which involves the production of inflammatory mediators and oxidative

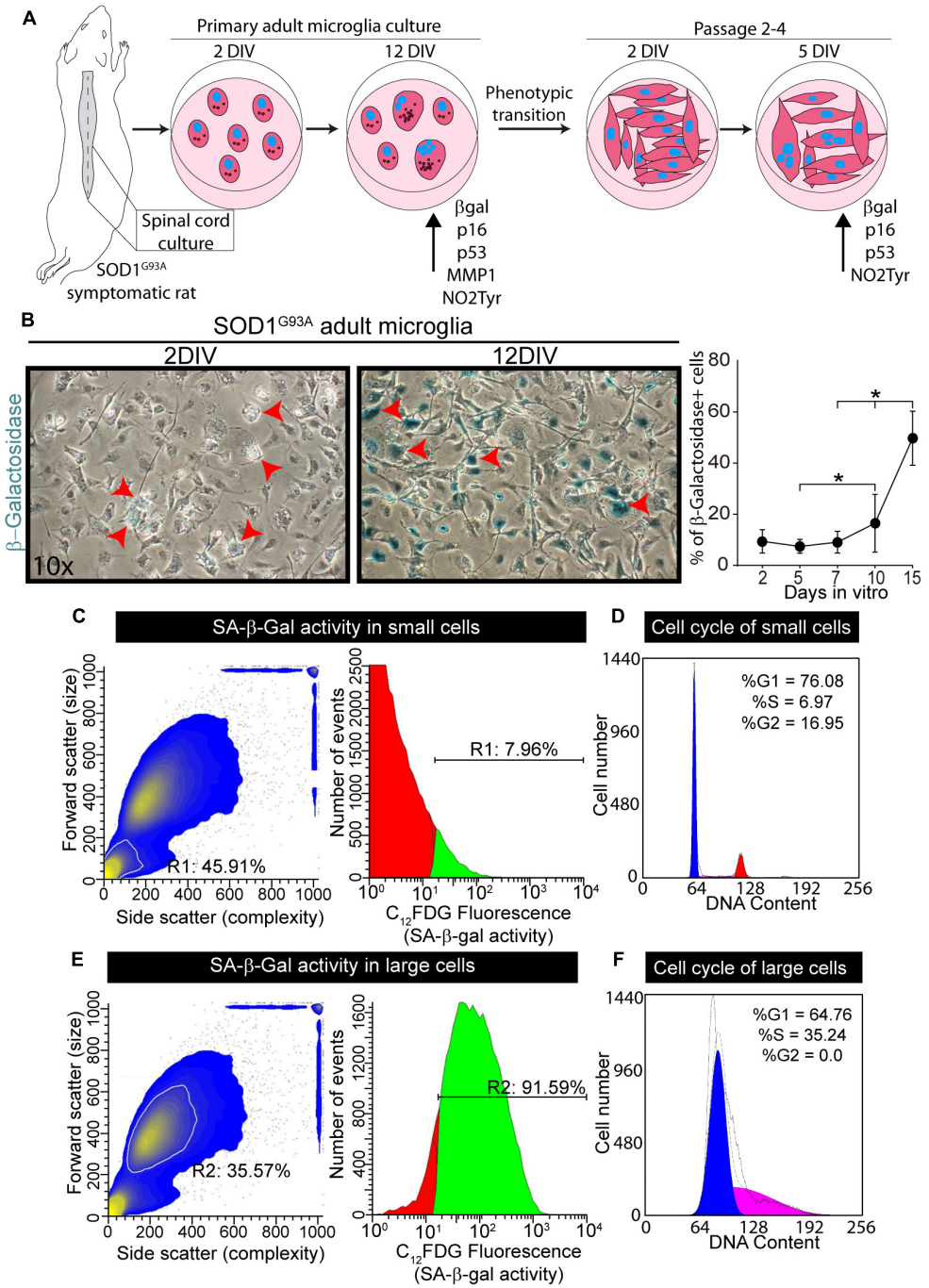

FIGURE 4 | Senescence-associated β-Galactosidase activity in primary cultures of microglia from symptomatic SOD1^{G93A} rats. **(A)** The scheme shows the procedure for adult microglia cell cultures from symptomatic SOD1^{G93A} rats. The spinal cord was plated on p35 culture dishes and SA-b-Gal was measured at different time points. Senescent markers increase their expression after several days in culture. After 2 weeks *in vitro*, microglia transitioned to aberrant glial cells. These transformed cells were also analyzed for SA-β-Gal and senescence markers at different time points in culture. **(B)** The phase contrast microphotographs show SA-β-Gal staining after 2 days *in vitro* (DIV) and 12 DIV. The graph to the right shows the quantitative analysis of SA-β-Gal activity in cultured adult microglia at different time points. Data are expressed as mean ± SEM; data were analyzed by Kruskal–Wallis followed by Dunn's multiple comparison tests, $p < 0.05$ was considered statistically significant. **(C)** SA-β-Gal activity analyzed by flow cytometry analysis. In the scatter diagram for the smaller population (inside white outline), R1 indicates the percentage of total population encompassed by this subset (45%). The gate for the smaller cell population indicates almost 8% of these cells are senescent. **(D)** The diagram shows the cell cycle analysis for the smaller cell population. **(E)** Scatter diagram for larger cell population (inside the white outline, R2). In the larger cell population, over 90% of the cells demonstrate SA-β-Gal activity. **(F)** The scatter diagram to the right shows the cell cycle analysis for the larger cell population.

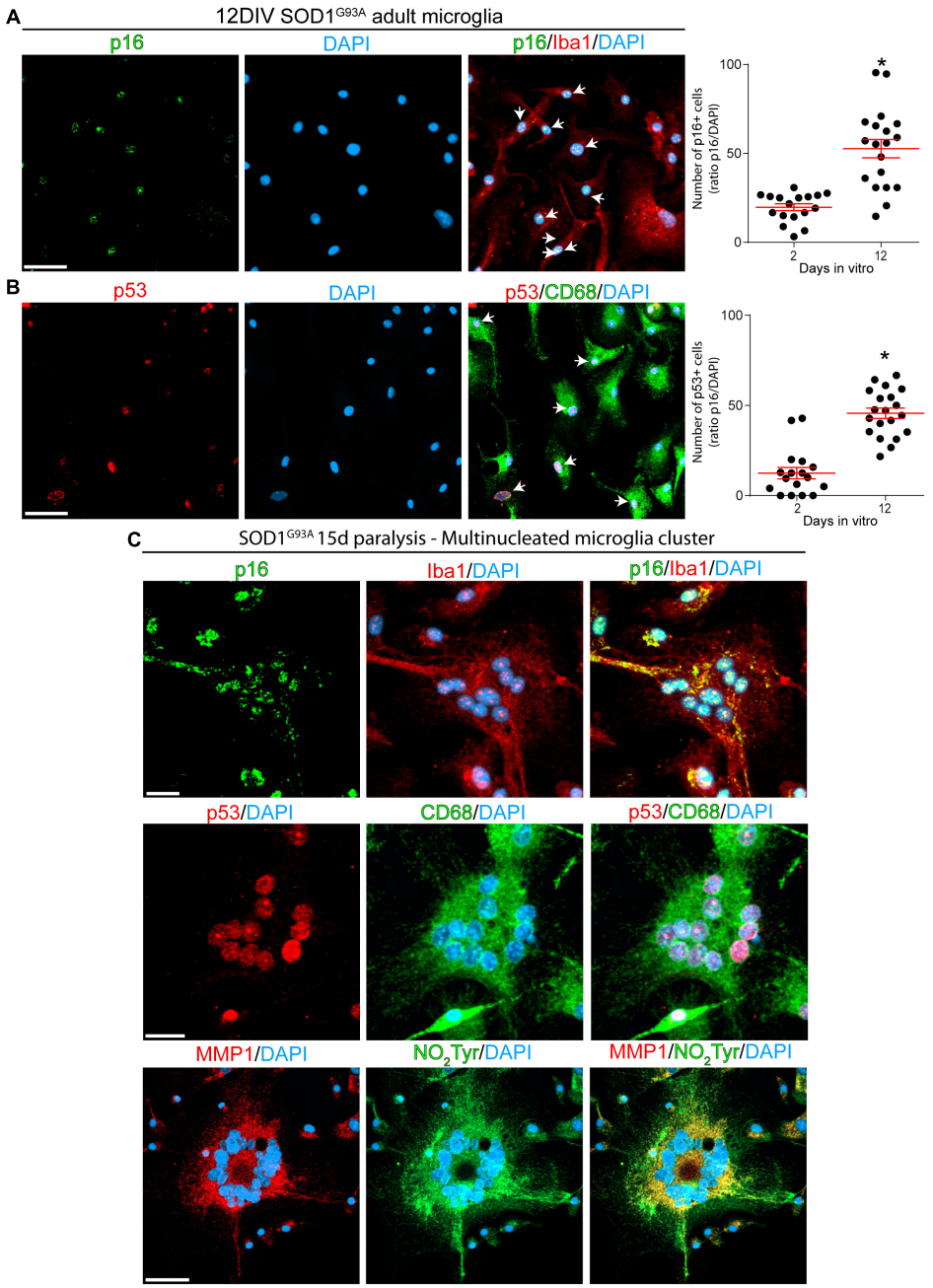

FIGURE 5 | Cultured adult microglia from SOD1^{G93A} symptomatic rats express senescence markers. Immunocytochemistry analysis of senescence markers on microglia isolated from SOD1^{G93A} symptomatic rats at 2 and 12DIV. **(A)** Isolated Iba1-positive microglia express nuclear p16^{INK4a}, which expression increase after several days in culture as shown in the graph to the right. Data are expressed as mean ± SEM: data were analyzed by Mann–Whitney test, 2-tailed, $p < 0.05$ was considered statistically significant. Scale bar: 50 μm. **(B)** CD68-positive microglia express increasing levels of nuclear p53 in culture. The graph to the right shows the comparative quantitative analysis of p53 expression. Data are expressed as mean ± SEM: data were analyzed by Mann-Whitney test, 2-tailed, $p < 0.05$ was considered statistically significant. Scale bar: 50 μm. **(C)** After 12 DIV, SOD1^{G93A} isolated microglia form Iba1-/CD68-positive multinucleated giant cells, which express several senescence markers such as p16^{INK4a}, p53, and MMP1. Also, these multinucleated cells express high levels of NO_2Tyr. Scale bars: 20 μm.

stress with potential genotoxic activity (Spittau, 2017). Thus, p53 induction in activated microglia from paralytic SOD1^{G93A} rats might not be only related to the senescence program but may also contribute to modulate the inflammatory phenotype as previously described (Aloi et al., 2015).

The finding that microglia isolated from symptomatic SOD1^{G93A} rats develop senescence features in culture conditions further support the inherent ability of these cells to undergo a senescence program. As cultures aged during several days, an increasing number of cells displayed senescence markers such

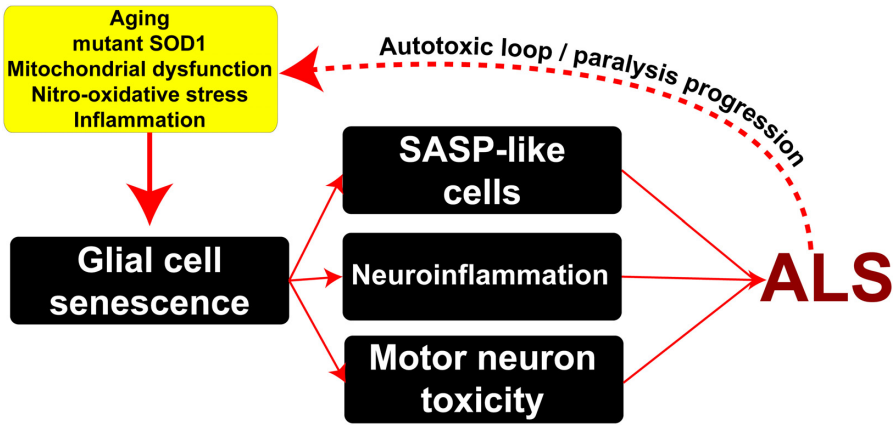

FIGURE 6 | Potential mechanisms underlying the emergence of senescent phenotypes in ALS and pathophysiological consequences. Risk factors such as aging, mitochondrial damage, nitro-oxidative stress, and inflammation may induce the appearance of senescent glial cells in the surroundings of motor neurons bearing SASP. In turn, these cells may exacerbate inflammation and induce motor neuron toxicity through the secretion of soluble toxic factors. This scenario might lead to a pathogenic autotoxic loop promoting the spread of motor neuron pathology and disease progression.

as SA-β-Gal activity, $p16^{INK4a}$, and MMP-1. SA-β-Gal activity, commonly used to distinguish senescent cells (Dimri et al., 1995), is perceptible due to the increased lysosomal content present in senescent cells (Kurz et al., 2000). Interestingly, senescent microglia *in vitro* expressed MMP-1, a marker of SASP (Strzyz, 2016), suggesting this phenotype could define a specific type of microglia polarization in ALS. Levels of matrix metalloproteinases increase with age in many tissues and organs and are associated with the SASP (Freund et al., 2010). MMP-1 levels in glial cells have been shown to be increased in Alzheimer's disease pathology (Bhat et al., 2012). Recent studies also suggest that metalloproteinases become increasingly dysregulated during disease progression in ALS (Soon et al., 2010), although this has not yet been considered in connection to cell senescence. In addition, senescent microglia isolated from symptomatic $SOD1^{G93A}$ rats showed a tendency to develop cell fusion and multinucleation. This cellular atypia has been previously described in the degenerating spinal cord of $SOD1^{G93A}$ rats (Fendrick et al., 2007). Our finding of microglia bearing SASP is in accordance with our previous reports in microglia in $SOD1^{G93A}$ rats displaying increased transcriptional expression of senescence-associated cytokines and inflammatory factors (Trias et al., 2016), as well as ultrastructural alterations in organelles occurring in cell senescence (Jimenez-Riani et al., 2017).

Cultures containing senescent microglia from symptomatic $SOD1^{G93A}$ rats were characterized by the fact that the emergence of senescent cells was coincident with a robust proliferation capacity of neighboring cells, which could be passaged many serial passages, as previously described (Diaz-Amarilla et al., 2011). Here, we have identified by flow cytometry that senescent microglia exhibited large size and cell cycle arrest, clearly differentiating from a subpopulation of smaller, SA-β-Gal-negative cells, with high proliferative capacity. Thus, SASP microglia in $SOD1^{G93A}$ rats could strongly promote the proliferation of neighboring non-senescent microglia by secretion of soluble factors. In accordance, we have shown that transplantation of $SOD1^{G93A}$ microglia into discrete sites of the lumbar spinal cord on non-transgenic rats, induced a massive microgliosis along the entire spinal cord (Ibarburu et al., 2017).

Because cultured $SOD1^{G93A}$ microglia from the rat paralytic spinal cord shows a high degree of activation, oxidative/nitrative stress and expression of inflammatory genes (Boillee and Cleveland, 2008; Thonhoff et al., 2012), we speculate that the triggering of the senescence program is a consequence of exacerbated cell damage or genotoxic stress, rather than aging *per se*. In accordance, we found that senescent microglia accumulate nitrotyrosine in proteins, indicating oxidative stress producing tyrosyl-radical formation and nitric oxide production (Zhao et al., 2004; Thonhoff et al., 2012). Increased levels of nitrotyrosine residues have been associated with endogenous production of peroxynitrite, a potent cellular oxidant and nitrating agent (Ischiropoulos et al., 1992; Pacher et al., 2007), which has not been previously associated with cellular senescence. In accordance, inflammatory stimulation of macrophages involving increase production of nitric oxide and superoxide also results in $p16^{INK4a}$ expression and SA-β-Gal activity (Hall et al., 2017).

Finally, we found evidence that motor neurons and astrocytes also express nuclear $p16^{INK4a}$ during the symptomatic stage, which might be related to the intriguing accumulation of misfolded SOD1 in motor neuron during advanced paralysis in $SOD1^{G93A}$ rats. This agrees with previous reports showing senescent neurons in aged mice and animal models of Alzheimer's disease (Jurk et al., 2012; Musi et al., 2018). Because neurons can develop a SASP, they can contribute to induce in inflammation in neighboring cells through the secretion of soluble factors (Appel et al., 2011; Komine and Yamanaka, 2015). Similarly, the finding of senescent astrocytes expressing nuclear $p16^{INK4a}$ in symptomatic $SOD1^{G93A}$ rat spinal cord suggest a role of defective astrocytes in ALS pathology. Astrocytes might exert their neurotoxic effect on motor neurons via the SASP, releasing several proinflammatory cytokines and trophic factors, such as

IL-6 (Haidet-Phillips et al., 2011; Das and Svendsen, 2015) and NGF species (Pehar et al., 2004). Astrocytes in ALS rodent models express different senescence markers which potentially turn them into a neurotoxic phenotype for motor neurons both *in vitro* and *in vivo* (Das and Svendsen, 2015; Turnquist et al., 2016). Thus, senescence-associated phenotypes in glial cells and neurons might be relevant pathogenic mechanisms in ALS. It remains unknown, however, whether prevention or eradication of senescence cells in ALS could result in delayed disease progression as has been reported in other neurological diseases (Bussian et al., 2018).

CONCLUSION

In conclusion, as summarized in **Figure 6**, here we show for the first time that senescent and secretory microglia emerge during paralysis progression in a rat model of inherited ALS. Risk factors such as aging together with mitochondrial dysfunction and nitro-oxidative damage linked to inflammation likely promote the emergence of senescent glial cells. Subsequently, senescent cells may promote profound changes in the cellular microenvironment through SASPs, exacerbating progressive neuroinflammation and motor neuron toxicity.

DATA AVAILABILITY

All datasets generated for this study are included in the manuscript and/or the **Supplementary Files**.

AUTHOR CONTRIBUTIONS

ET, PB, LB, and JB designed the research. ET, PB, MK, SI, VV, RB-N, and SB performed the research. ET, PB, SB, LB, and JB analyzed the data. ET, PB, LB, and JB wrote the paper.

FUNDING

This work was supported by Institut Pasteur de Montevideo – FOCEM Mercosur (COF 03/11), the Amyotrophic Lateral Sclerosis Association (00482), Department of Defense (AL140108), Agencia Nacional de Investigación e Innovación (ANII), and Programa de Desarrollo de las Ciencias Básicas (PEDECIBA).

ACKNOWLEDGMENTS

We want to thank the staff from the Transgenic and Experimental Animal Unit from Institut Pasteur de Montevideo. Finally, we wish to acknowledge the Confocal Microscopy Facility of the Center for Genome Research and Biocomputing at Oregon State University.

SUPPLEMENTARY MATERIAL

The Supplementary Material for this article can be found online at: https://www.frontiersin.org/articles/10.3389/fnagi.2019.00042/full#supplementary-material

FIGURE S1 | Progressive increase in spinal cord p53 expression during paralysis progression Confocal microphotographs show the staining for p53 (red) among analyzed groups. The graph to the right shows the quantitative analysis of p53 intensity. Note the increase in p53 expression with disease progression. Data are expressed as mean ± SEM; data were analyzed by Kruskal–Wallis followed by Dunn's multiple comparison tests, $p < 0.05$ was considered statistically significant. Scale bars: 50 μm.

FIGURE S2 | Interaction of microglia with degenerating motor neurons expressing misfolded SOD1. Confocal microphotograph showing Iba1-positive microglia clusters (red) surrounding damaged motor neurons accumulating high levels of misfolded SOD1 (green). Arrowheads indicate the microglia/motor neuron clustering. Note that misfolded SOD1 is mainly expressed in neuronal structures during paralysis, while its expression in microglia appears to be associated with the phagocytosis of misfolded SOD1 contained in degenerating neuronal structures (arrows). Scale bar: 20 μm.

FIGURE S3 | Senescence-associated β-Galactosidase activity in primary cultures of microglia from symptomatic $SOD1^{G93A}$ rats. The scatter diagram, a population density heat map, indicates the gate for the sample and includes the entire population of cells. The diagram to the right shows that approximately 50% of the cells demonstrate SA-β-activity.

FIGURE S4 | Expression of senescence markers $p16^{INK4a}$ and MMP1 in cultured adult microglia from $SOD1^{G93A}$ symptomatic rats. Immunocytochemistry analysis of senescence markers on microglia isolated from $SOD1^{G93A}$ symptomatic rats. **(A)** Isolated Iba1-positive microglia after 2 days in culture express nuclear $p16^{INK4a}$ **(A)** and p53 **(B)** in a small subpopulation of cells. Arrows indicate the respective nuclear localization of both markers. Scale bar: 20 μm. **(C)** Progressive increase of MMP1 and NO_2Tyr in adult cultured microglia. Note the increased expression of MMP1 and NO_2Tyr between 2 DIV (upper panel) and 12 DIV (lower panel). Scale bar: 20 μm.

FIGURE S5 | Serially passaged $SOD1^{G93A}$ microglia cultures express senescence markers. Senescence marker analysis in phenotypic transitioned $SOD1^{G93A}$ microglia in culture. **(A)** Transitioning microglia population display increasing SA-β-Gal activity (red arrows) at different time points (Passage 4). The graph to the right shows the quantitative analysis of SA-β-Gal activity in transformed microglia. Data are expressed as mean ± SEM; data were analyzed by Kruskal–Wallis followed by Dunn's multiple comparison tests, $p < 0.05$ was considered statistically significant. **(B)** After several days in culture, transformed microglia express increasing levels of $p16^{INK4a}$ and p53. Also, note the high expression of NO_2Tyr in those cells that express nuclear $p16^{INK4a}$. Graphs to the right show the quantitative comparative analysis of $p16^{INK4a}$ and p53 at different time points. Data are expressed as mean ± SEM; data were analyzed by Kruskal–Wallis followed by Dunn's multiple comparison tests, $p < 0.05$ was considered statistically significant. Scale bars: 20 μm.

REFERENCES

Al-Chalabi, A., Calvo, A., Chio, A., Colville, S., Ellis, C. M., Hardiman, O., et al. (2014). Analysis of amyotrophic lateral sclerosis as a multistep process: a population-based modelling study. *Lancet Neurol.* 13, 1108–1113. doi: 10.1016/S1474-4422(14)70219-4

Aloi, M. S., Su, W., and Garden, G. A. (2015). The p53 Transcriptional Network Influences Microglia Behavior and Neuroinflammation. *Crit. Rev. Immunol.* 35, 401–415.

Appel, S. H., Zhao, W., Beers, D. R., and Henkel, J. S. (2011). The microglial-motoneuron dialogue in ALS. *Acta Myol.* 30, 4–8.

Arendt, T., Rodel, L., Gartner, U., and Holzer, M. (1996). Expression of the cyclin-dependent kinase inhibitor p16 in Alzheimer's disease. *Neuroreport* 7, 3047–3049.

Baker, D. J., Wijshake, T., Tchkonia, T., LeBrasseur, N. K., Childs, B. G., van de Sluis, B., et al. (2011). Clearance of p16Ink4a-positive senescent cells delays ageing-associated disorders. *Nature* 479, 232–236. doi: 10.1038/nature10600

Bhat, R., Crowe, E. P., Bitto, A., Moh, M., Katsetos, C. D., Garcia, F. U., et al. (2012). Astrocyte senescence as a component of Alzheimer's disease. *PLoS One* 7:e45069. doi: 10.1371/journal.pone.0045069

Blagosklonny, M. V. (2011). Cell cycle arrest is not senescence. *Aging* 3, 94–101. doi: 10.18632/aging.100281

Boillee, S., and Cleveland, D. W. (2008). Revisiting oxidative damage in ALS: microglia, Nox, and mutant SOD1. *J. Clin. Invest.* 118, 474–478. doi: 10.1172/JCI34613

Boillee, S., Yamanaka, K., Lobsiger, C. S., Copeland, N. G., Jenkins, N. A., Kassiotis, G., et al. (2006). Onset and progression in inherited ALS determined by motor neurons and microglia. *Science* 312, 1389–1392. doi: 10.1126/science.1123511

Brettschneider, J., Toledo, J. B., Van Deerlin, V. M., Elman, L., McCluskey, L., Lee, V. M., et al. (2012). Microglial activation correlates with disease progression and upper motor neuron clinical symptoms in amyotrophic lateral sclerosis. *PLoS One* 7:e39216. doi: 10.1371/journal.pone.0039216

Bussian, T. J., Aziz, A., Meyer, C. F., Swenson, B. L., van Deursen, J. M., and Baker, D. J. (2018). Clearance of senescent glial cells prevents tau-dependent pathology and cognitive decline. *Nature* 562, 578–582. doi: 10.1038/s41586-018-0543-y

Caldeira, C., Cunha, C., Vaz, A. R., Falcao, A. S., Barateiro, A., Seixas, E., et al. (2017). Key aging-associated alterations in primary microglia response to beta-amyloid stimulation. *Front. Aging Neurosci.* 9:277. doi: 10.3389/fnagi.2017.00277

Carnero, A. (2013). Markers of cellular senescence. *Methods Mol. Biol.* 965, 63–81. doi: 10.1007/978-1-62703-239-1_4

Cassina, P., Cassina, A., Pehar, M., Castellanos, R., Gandelman, M., de Leon, A., et al. (2008). Mitochondrial dysfunction in SOD1G93A-bearing astrocytes promotes motor neuron degeneration: prevention by mitochondrial-targeted antioxidants. *J. Neurosci.* 28, 4115–4122. doi: 10.1523/JNEUROSCI.5308-07.2008

Childs, B. G., Durik, M., Baker, D. J., and van Deursen, J. M. (2015). Cellular senescence in aging and age-related disease: from mechanisms to therapy. *Nat. Med.* 21, 1424–1435. doi: 10.1038/nm.4000

Chinta, S. J., Lieu, C. A., Demaria, M., Laberge, R. M., Campisi, J., and Andersen, J. K. (2013). Environmental stress, ageing and glial cell senescence: a novel mechanistic link to Parkinson's disease? *J. Intern. Med.* 273, 429–436. doi: 10.1111/joim.12029

Chinta, S. J., Woods, G., Demaria, M., Rane, A., Zou, Y., McQuade, A., et al. (2018). Cellular senescence is induced by the environmental neurotoxin paraquat and contributes to neuropathology linked to Parkinson's Disease. *Cell Rep.* 22, 930–940. doi: 10.1016/j.celrep.2017.12.092

Crockford, C., Newton, J., Lonergan, K., Chiwera, T., Booth, T., Chandran, S., et al. (2018). ALS-specific cognitive and behavior changes associated with advancing disease stage in ALS. *Neurology* 91, e1370–e1380. doi: 10.1212/WNL.0000000000006317

Das, M. M., and Svendsen, C. N. (2015). Astrocytes show reduced support of motor neurons with aging that is accelerated in a rodent model of ALS. *Neurobiol. Aging* 36, 1130–1139. doi: 10.1016/j.neurobiolaging.2014.09.020

Dechat, T., Pfleghaar, K., Sengupta, K., Shimi, T., Shumaker, D. K., Solimando, L., et al. (2008). Nuclear lamins: major factors in the structural organization and function of the nucleus and chromatin. *Genes Dev.* 22, 832–853. doi: 10.1101/gad.1652708

Diaz-Amarilla, P., Olivera-Bravo, S., Trias, E., Cragnolini, A., Martinez-Palma, L., Cassina, P., et al. (2011). Phenotypically aberrant astrocytes that promote motoneuron damage in a model of inherited amyotrophic lateral sclerosis. *Proc. Natl. Acad. Sci. U.S.A.* 108, 18126–18131. doi: 10.1073/pnas.1110689108

Dimri, G. P., Lee, X., Basile, G., Acosta, M., Scott, G., Roskelley, C., et al. (1995). A biomarker that identifies senescent human cells in culture and in aging skin in vivo. *Proc. Natl. Acad. Sci. U.S.A.* 92, 9363–9367.

Eitan, E., Hutchison, E. R., and Mattson, M. P. (2014). Telomere shortening in neurological disorders: an abundance of unanswered questions. *Trends Neurosci.* 37, 256–263. doi: 10.1016/j.tins.2014.02.010

Fendrick, S. E., Xue, Q. S., and Streit, W. J. (2007). Formation of multinucleated giant cells and microglial degeneration in rats expressing a mutant Cu/Zn superoxide dismutase gene. *J. Neuroinflammation* 4:9. doi: 10.1186/1742-2094-4-9

Frakes, A. E., Ferraiuolo, L., Haidet-Phillips, A. M., Schmelzer, L., Braun, L., Miranda, C. J., et al. (2014). Microglia induce motor neuron death via the classical NF-kappaB pathway in amyotrophic lateral sclerosis. *Neuron* 81, 1009–1023. doi: 10.1016/j.neuron.2014.01.013

Freund, A., Laberge, R. M., Demaria, M., and Campisi, J. (2012). Lamin B1 loss is a senescence-associated biomarker. *Mol. Biol. Cell* 23, 2066–2075. doi: 10.1091/mbc.E11-10-0884

Freund, A., Orjalo, A. V., Desprez, P. Y., and Campisi, J. (2010). Inflammatory networks during cellular senescence: causes and consequences. *Trends Mol. Med.* 16, 238–246. doi: 10.1016/j.molmed.2010.03.003

Frost, B. (2016). Alzheimer's disease: an acquired neurodegenerative laminopathy. *Nucleus* 7, 275–283. doi: 10.1080/19491034.2016.1183859

Frost, B., Bardai, F. H., and Feany, M. B. (2016). Lamin dysfunction mediates neurodegeneration in tauopathies. *Curr. Biol.* 26, 129–136. doi: 10.1016/j.cub.2015.11.039

Haidet-Phillips, A. M., Hester, M. E., Miranda, C. J., Meyer, K., Braun, L., Frakes, A., et al. (2011). Astrocytes from familial and sporadic ALS patients are toxic to motor neurons. *Nat. Biotechnol.* 29, 824–828. doi: 10.1038/nbt.1957

Hall, B. M., Balan, V., Gleiberman, A. S., Strom, E., Krasnov, P., Virtuoso, L. P., et al. (2017). p16(Ink4a) and senescence-associated beta-galactosidase can be induced in macrophages as part of a reversible response to physiological stimuli. *Aging* 9, 1867–1884. doi: 10.18632/aging.101268

Hardiman, O., Al-Chalabi, A., Chio, A., Corr, E. M., Logroscino, G., Robberecht, W., et al. (2017). Amyotrophic lateral sclerosis. *Nat. Rev. Dis. Primers* 3:17071. doi: 10.1038/nrdp.2017.71

Howland, D. S., Liu, J., She, Y., Goad, B., Maragakis, N. J., Kim, B., et al. (2002). Focal loss of the glutamate transporter EAAT2 in a transgenic rat model of SOD1 mutant-mediated amyotrophic lateral sclerosis (ALS). *Proc. Natl. Acad. Sci. U.S.A.* 99, 1604–1609. doi: 10.1073/pnas.032539299

Ibarburu, S., Trias, E., Lago, N., Peluffo, H., Barreto-Nunez, R., Varela, V., et al. (2017). Focal transplantation of aberrant glial cells carrying the SOD1G93A mutation into rat spinal cord induces extensive gliosis. *Neuroimmunomodulation* 24, 143–153. doi: 10.1159/000480639

Iguchi, Y., Katsuno, M., Niwa, J., Takagi, S., Ishigaki, S., Ikenaka, K., et al. (2013). Loss of TDP-43 causes age-dependent progressive motor neuron degeneration. *Brain* 136(Pt 5), 1371–1382. doi: 10.1093/brain/awt029

Ischiropoulos, H., Zhu, L., Chen, J., Tsai, M., Martin, J. C., Smith, C. D., et al. (1992). Peroxynitrite-mediated tyrosine nitration catalyzed by superoxide dismutase. *Arch. Biochem. Biophys.* 298, 431–437.

Jimenez-Riani, M., Diaz-Amarilla, P., Isasi, E., Casanova, G., Barbeito, L., and Olivera-Bravo, S. (2017). Ultrastructural features of aberrant glial cells isolated from the spinal cord of paralytic rats expressing the amyotrophic lateral sclerosis-linked SOD1G93A mutation. *Cell Tissue Res.* 370, 391–401. doi: 10.1007/s00441-017-2681-1

Jurk, D., Wang, C., Miwa, S., Maddick, M., Korolchuk, V., Tsolou, A., et al. (2012). Postmitotic neurons develop a p21-dependent senescence-like phenotype driven by a DNA damage response. *Aging Cell* 11, 996–1004. doi: 10.1111/j.1474-9726.2012.00870.x

Kiernan, M. C., Vucic, S., Cheah, B. C., Turner, M. R., Eisen, A., Hardiman, O., et al. (2011). Amyotrophic lateral sclerosis. *Lancet* 377, 942–955. doi: 10.1016/S0140-6736(10)61156-7

Komine, O., and Yamanaka, K. (2015). Neuroinflammation in motor neuron disease. *Nagoya J. Med. Sci.* 77, 537–549.

Kurz, D. J., Decary, S., Hong, Y., and Erusalimsky, J. D. (2000). Senescence-associated β-galactosidase reflects an increase in lysosomal mass during replicative ageing of human endothelial cells. *J. Cell Sci.* 113(Pt 20), 3613–3622.

Lamoke, F., Shaw, S., Yuan, J., Ananth, S., Duncan, M., Martin, P., et al. (2015). Increased oxidative and nitrative stress accelerates aging of the retinal vasculature in the diabetic retina. *PLoS One* 10:e0139664. doi: 10.1371/journal.pone.0139664

Leikam, C., Hufnagel, A. L., Otto, C., Murphy, D. J., Muhling, B., Kneitz, S., et al. (2015). In vitro evidence for senescent multinucleated melanocytes as a source for tumor-initiating cells. *Cell Death Dis.* 6:e1711. doi: 10.1038/cddis.2015.71

Lewis, K. E., Rasmussen, A. L., Bennett, W., King, A., West, A. K., Chung, R. S., et al. (2014). Microglia and motor neurons during disease progression in the SOD1G93A mouse model of amyotrophic lateral sclerosis: changes in arginase1 and inducible nitric oxide synthase. *J. Neuroinflamm.* 11:55. doi: 10.1186/1742-2094-11-55

Liao, B., Zhao, W., Beers, D. R., Henkel, J. S., and Appel, S. H. (2012). Transformation from a neuroprotective to a neurotoxic microglial phenotype in a mouse model of ALS. *Exp. Neurol.* 237, 147–152. doi: 10.1016/j.expneurol.2012.06.011

Luo, X. G., Ding, J. Q., and Chen, S. D. (2010). Microglia in the aging brain: relevance to neurodegeneration. *Mol. Neurodegener.* 5:12. doi: 10.1186/1750-1326-5-12

Martin, L. J. (2000). p53 is abnormally elevated and active in the CNS of patients with amyotrophic lateral sclerosis. *Neurobiol. Dis.* 7(6 Pt B), 613–622. doi: 10.1006/nbdi.2000.0314

Morgan, S., and Orrell, R. W. (2016). Pathogenesis of amyotrophic lateral sclerosis. *Br. Med. Bull.* 119, 87–98. doi: 10.1093/bmb/ldw026

Munoz-Espin, D., and Serrano, M. (2014). Cellular senescence: from physiology to pathology. *Nat. Rev. Mol. Cell Biol.* 15, 482–496. doi: 10.1038/nrm3823

Musi, N., Valentine, J. M., Sickora, K. R., Baeuerle, E., Thompson, C. S., Shen, Q., et al. (2018). Tau protein aggregation is associated with cellular senescence in the brain. *Aging Cell* 17, e12840. doi: 10.1111/acel.12840

Pacher, P., Beckman, J. S., and Liaudet, L. (2007). Nitric oxide and peroxynitrite in health and disease. *Physiol. Rev.* 87, 315–424. doi: 10.1152/physrev.00029.2006

Pehar, M., Cassina, P., Vargas, M. R., Castellanos, R., Viera, L., Beckman, J. S., et al. (2004). Astrocytic production of nerve growth factor in motor neuron apoptosis: implications for amyotrophic lateral sclerosis. *J. Neurochem.* 89, 464–473. doi: 10.1111/j.1471-4159.2004.02357.x

Philips, T., and Rothstein, J. D. (2014). Glial cells in amyotrophic lateral sclerosis. *Exp. Neurol.* 262(Pt B), 111–120. doi: 10.1016/j.expneurol.2014.05.015

Prieur, A., Besnard, E., Babled, A., and Lemaitre, J. M. (2011). p53 and p16(INK4A) independent induction of senescence by chromatin-dependent alteration of S-phase progression. *Nat. Commun.* 2:473. doi: 10.1038/ncomms1473

Rawji, K. S., Mishra, M. K., Michaels, N. J., Rivest, S., Stys, P. K., and Yong, V. W. (2016). Immunosenescence of microglia and macrophages: impact on the ageing central nervous system. *Brain* 139(Pt 3), 653–661. doi: 10.1093/brain/awv395

Rodier, F., Coppe, J. P., Patil, C. K., Hoeijmakers, W. A., Munoz, D. P., Raza, S. R., et al. (2009). Persistent DNA damage signalling triggers senescence-associated inflammatory cytokine secretion. *Nat. Cell Biol.* 11, 973–979. doi: 10.1038/ncb1909

Rufini, A., Tucci, P., Celardo, I., and Melino, G. (2013). Senescence and aging: the critical roles of p53. *Oncogene* 32, 5129–5143. doi: 10.1038/onc.2012.640

Salminen, A., Ojala, J., Kaarniranta, K., Haapasalo, A., Hiltunen, M., and Soininen, H. (2011). Astrocytes in the aging brain express characteristics of senescence-associated secretory phenotype. *Eur. J. Neurosci.* 34, 3–11. doi: 10.1111/j.1460-9568.2011.07738.x

Soon, C. P., Crouch, P. J., Turner, B. J., McLean, C. A., Laughton, K. M., Atkin, J. D., et al. (2010). Serum matrix metalloproteinase-9 activity is dysregulated with disease progression in the mutant SOD1 transgenic mice. *Neuromuscul. Disord.* 20, 260–266. doi: 10.1016/j.nmd.2009.11.015

Spittau, B. (2017). Aging microglia-phenotypes, functions and implications for age-related neurodegenerative diseases. *Front. Aging Neurosci.* 9:194. doi: 10.3389/fnagi.2017.00194

Sreedharan, J., Neukomm, L. J., Brown, R. H. Jr., and Freeman, M. R. (2015). Age-dependent TDP-43-mediated motor neuron degeneration requires GSK3, hat-trick, and xmas-2. *Curr. Biol.* 25, 2130–2136. doi: 10.1016/j.cub.2015.06.045

Strzyz, P. (2016). Cell senescence: controlling the senescence-associated secretory phenotype. *Nat. Rev. Mol. Cell Biol.* 17:740. doi: 10.1038/nrm.2016.157

Tchkonia, T., Zhu, Y., van Deursen, J., Campisi, J., and Kirkland, J. L. (2013). Cellular senescence and the senescent secretory phenotype: therapeutic opportunities. *J. Clin. Invest.* 123, 966–972. doi: 10.1172/JCI64098

Theriault, P., and Rivest, S. (2016). Microglia: senescence impairs clearance of myelin debris. *Curr. Biol.* 26, R772–R775. doi: 10.1016/j.cub.2016.06.066

Thonhoff, J. R., Gao, J., Dunn, T. J., Ojeda, L., and Wu, P. (2012). Mutant SOD1 microglia-generated nitroxidative stress promotes toxicity to human fetal neural stem cell-derived motor neurons through direct damage and noxious interactions with astrocytes. *Am. J. Stem. Cells* 1, 2–21.

Trias, E., Barbeito, L., and Yamanaka, K. (2018a). Phenotypic heterogeneity of astrocytes in motor neuron disease. *Clin. Exp. Neuroimmunol.* 9, 225–234. doi: 10.1111/cen3.12476

Trias, E., King, P. H., Si, Y., Kwon, Y., Varela, V., Ibarburu, S., et al. (2018b). Mast cells and neutrophils mediate peripheral motor pathway degeneration in ALS. *JCI Insight* 3:123249. doi: 10.1172/jci.insight.123249

Trias, E., Diaz-Amarilla, P., Olivera-Bravo, S., Isasi, E., Drechsel, D. A., Lopez, N., et al. (2013). Phenotypic transition of microglia into astrocyte-like cells associated with disease onset in a model of inherited ALS. *Front. Cell. Neurosci.* 7:274. doi: 10.3389/fncel.2013.00274

Trias, E., Ibarburu, S., Barreto-Nunez, R., Babdor, J., Maciel, T. T., Guillo, M., et al. (2016). Post-paralysis tyrosine kinase inhibition with masitinib abrogates neuroinflammation and slows disease progression in inherited amyotrophic lateral sclerosis. *J. Neuroinflamm.* 13:177. doi: 10.1186/s12974-016-0620-9

Trias, E., Ibarburu, S., Barreto-Nunez, R., Varela, V., Moura, I. C., Dubreuil, P., et al. (2017). Evidence for mast cells contributing to neuromuscular pathology in an inherited model of ALS. *JCI Insight* 2:95934. doi: 10.1172/jci.insight.95934

Tsai, M. J., Hsu, C. Y., and Sheu, C. C. (2017). Amyotrophic lateral sclerosis. *N. Engl. J. Med.* 377:1602. doi: 10.1056/NEJMc1710379

Turnquist, C., Horikawa, I., Foran, E., Major, E. O., Vojtesek, B., Lane, D. P., et al. (2016). p53 isoforms regulate astrocyte-mediated neuroprotection and neurodegeneration. *Cell Death Differ.* 23, 1515–1528. doi: 10.1038/cdd.2016.37

Zhao, W., Xie, W., Le, W., Beers, D. R., He, Y., Henkel, J. S., et al. (2004). Activated microglia initiate motor neuron injury by a nitric oxide and glutamate-mediated mechanism. *J. Neuropathol. Exp. Neurol.* 63, 964–977.

Conflict of Interest Statement: The authors declare that the research was conducted in the absence of any commercial or financial relationships that could be construed as a potential conflict of interest.

frontiers in Aging Neuroscience

BRIEF RESEARCH REPORT
published: 05 March 2019
doi: 10.3389/fnagi.2019.00048

IGF1 Gene Therapy Modifies Microglia in the Striatum of Senile Rats

Eugenia Falomir-Lockhart[1], *Franco Juan Cruz Dolcetti*[1], *Luis Miguel García-Segura*[2,3], *Claudia Beatriz Hereñú*[4*†] and *Maria Jose Bellini*[1*†]

[1]Laboratorio de Bioquimica del Envejecimiento, Instituto de Investigaciones Bioquímicas de La Plata (INIBIOLP), Facultad de Ciencias Médicas, UNLP-CONICET, La Plata, Argentina, [2]Instituto Cajal, CSIC, Madrid, Spain, [3]Centro de Investigación, Biomédica en Red de Fragilidad y Envejecimiento Saludable (CIBERFES), Instituto de Salud Carlos III, Madrid, Spain, [4]Instituto de Farmacología Experimental de Córdoba-CONICET, Departamento de Farmacología, Facultad de Ciencias Químicas, UNC-CONICET, Córdoba, Argentina

Microglial cells become dystrophic with aging; this phenotypic alteration contributes to basal central nervous system (CNS) neuroinflammation being a risk factor for age related neurodegenerative diseases. In previous studies we have observed that insulin like growth factor 1 (IGF1) gene therapy is a feasible approach to target brain cells, and that is effective to modify inflammatory response *in vitro* and to ameliorate cognitive or motor deficits *in vivo*. Based on these findings, the main aim of the present study is to investigate the effect of IGF1 gene therapy on microglia distribution and morphology in the senile rat. We found that IGF1 therapy leads to a region-specific modification of aged microglia population.

Keywords: IGF1, microglia morphology, striatum, aging, gene therapy

OPEN ACCESS

Edited by:
George E. Barreto, Pontificia Universidad Javeriana, Colombia

Reviewed by:
Andrzej Bartke, Southern Illinois University School of Medicine, United States
Francisco G. Wandosell, Severo Ochoa Molecular Biology Center (CSIC-UAM), Spain

***Correspondence:**
Claudia Beatriz Hereñú
cherenu@fcq.unc.edu.ar
Maria Jose Bellini
mariajosebellini@yahoo.com; mariajosebellini@med.unlp.edu.ar

†These authors have contributed equally to this work

Received: *27 November 2018*
Accepted: *19 February 2019*
Published: *05 March 2019*

Citation:
Falomir-Lockhart E, Dolcetti FJC, García-Segura LM, Hereñú CB and Bellini MJ (2019) IGF1 Gene Therapy Modifies Microglia in the Striatum of Senile Rats. Front. Aging Neurosci. 11:48. doi: 10.3389/fnagi.2019.00048

INTRODUCTION

Microglia, the immune cells of the central nervous system (CNS), suffer a phenotypic alteration during aging that is characterized by decreased motility and inefficient surveillance (Streit et al., 2004; von Bernhardi et al., 2016; Koellhoffer et al., 2017). This dystrophic cellular phenotype of microglia is associated with the loss of their neuroprotective function, which contributes to increased basal CNS neuroinflammation with aging and may represent a risk factor for cognitive and motor impairment, depression or diverse age related neurodegenerative diseases (Streit and Xue, 2010; Cunningham, 2013; Patel et al., 2015; Pekny and Pekna, 2016; Ransohoff, 2016; Spittau, 2017).

A feasible approach to modulate microglia function in the aged brain is the use of neurotrophic factors that polarize these cells into a more neurotrophic/neuroprotective phenotype. Among these is insulin like growth factor 1 (IGF1; Arevalo et al., 2010; Suh et al., 2013; Acaz-Fonseca et al., 2014; Labandeira-Garcia et al., 2017), which exerts neuroprotective actions in the CNS (Piriz et al., 2011; Torres Aleman, 2012; Morel et al., 2016), including the aged brain (Piriz et al., 2011; Deak and Sonntag, 2012; Labandeira-Garcia et al., 2017). Previous studies have shown the viability of IGF1 gene therapy to target brain cells *in vivo* (Hereñú et al., 2009) and to

Abbreviations: IGF1, insulin like growth factor 1; RAd, recombinant adenovirus; DsRed, Discosoma Red fluorescent protein; CNS, central nervous system.

decrease behavioral functional impairments in aged rats (Nishida et al., 2011; Pardo et al., 2016). In the present study we report that IGF1 therapy lead to a region-specific modification in microglia number and morphology in the aged brain.

MATERIALS AND METHODS

Adenoviral Vectors

We employed recombinant adenoviral vectors (RAd) previously constructed in our laboratory (Hereñú et al., 2007) as carriers to deliver either the therapeutic cDNA of IGF1 gene (RAd-IGF1) or the red fluorescent protein from Discosoma sp DsRed (RAd-DsRed).

Animals and Experimental Procedures

Female senile Sprague-Dawley rats (28 months old) were used. These rats have a maximum life expectancy of 36 months (Mansilla et al., 2016). Animals were housed in a temperature-controlled room (22 ± 2°C) on a 12:12 h light/dark cycle and fed *ad libitum*, with a standard chow diet containing 12.08 kJ/g calories: 69.5% from carbohydrates, 5.6% from fat, and 24.9% from protein (Association de Cooperativas Argentinas-S.E.N.A.S.A. No. 04-288/A). All experiments with animals were performed according to the Animal Welfare Guidelines of NIH (INIBIOLP's Animal Welfare Assurance No A5647-01). The ethical acceptability of the animal protocols used here has been approved by our institutional IACUC (Protocol #T09-01-2013).

On day 0 (D0), rats were anesthetized with ketamine hydrochloride (40 mg/kg; i.p.) plus xylazine (8 mg/kg; i.m.) and placed in a stereotaxic apparatus. Rats were randomly divided into two groups (n = 10 per group): DsRed group, which received an injection of RAd-DsRed; and IGF1 group, which received an injection of RAd-IGF1. Bilateral injections in the lateral ventricles were performed placing the tip of a 26 G needle fitted to a 10 μL syringe at the following coordinates relative to the Bregma: −0.8 mm anteroposterior, −4.2 mm dorsoventral and ±1.5 mm mediolateral (Paxinos and Watson, 2007). Rats were injected bilaterally with 8 μL per side of a suspension containing 10^{10} plaque forming units (pfu) of the appropriate vector. Body weight was determined every 2 or 3 days from day −5 before surgery to experimental day 18. Animals were sacrificed at experimental day 18.

Immunohistochemistry

Animals were placed under deep anesthesia and perfused with phosphate buffered paraformaldehyde 4%, (pH 7.4) fixative. The brains were removed and stored in paraformaldehyde 4%, (pH 7.4) overnight at 4°C. Brains were kept in cryoprotective solution at −20°C until use. For immunohistochemical assessment, brains were cut coronally in 40 μm-thick sections with a Vibratome (Leica).

All immunohistochemical techniques were performed on free-floating sections under moderate shaking. Washes and incubations were done in 0.1 M phosphate buffer pH 7.4, containing 0.3% triton X-100 (washing buffer). The endogenous peroxidase activity was quenched for 15 min at room temperature in a solution of 3% hydrogen peroxide in 50% methanol. After several washes in buffer, sections were incubated overnight at 4°C with an Iba1 rabbit polyclonal antibody diluted 1:1,000 (WAKO CTG2683), marker of microglia/macrophages. Sections were then washed in buffer and incubated for 2 h at room temperature with an anti-rabbit biotinylated secondary antibody (1:1,000, BA-1000; Vector Labs). After several washes in buffer, sections were incubated for 90 min at room temperature with avidin-biotin-peroxidase complex (diluted 1:500, PK-6100; Vector ABC Elite Kit). The reaction product was revealed by incubating the sections with 3,3-diaminobenzidine (Sigma-Aldrich) and 0.01% hydrogen peroxide in 0.1 M phosphate buffer. Then, sections were dehydrated, mounted on gelatinized slides with mounting medium (Vectamount, Vector) and used for image analysis.

Morphometric Analysis

From each rat, 1 in every 12 brain serial sections was selected. For stereological analysis, we used an Olympus BX-51 microscope attached to an Olympus DP70 CCD video camera (Tokyo, Japan). All morphological parameters were assessed bilaterally. The density of microglia in the striatum (caudate-putamen), dorsal tier of substantia nigra pars compacta (SNCD), motor cortex, dorsolateral entorhinal cortex (DLEnt) and perirhinal cortex (PRh) was assessed. Areas of interest were defined in accordance with the rat brain atlas of Paxinos and Watson (2007). All Iba1-immunoreactive cells were manually quantified, according to the optical disector method, using a counting frame of 83 × 83 μm at 600× magnification. A total of 40–85 counting frames were analyzed. Cells in the uppermost focal plane and/or intersecting the exclusion boundaries of the counting frame were not counted. Cells counts are expressed as number/mm^3.

Iba1-immunoreactive cells were classified as: (1) non-reactive/ramified microglia; cells with small cell body and few large to no branches; and (2) reactive/ameboid microglia; cells with large or ameboid cell bodies, numerous retracted processes and intense Iba1 immunostaining (Acaz-Fonseca et al., 2015). The proportion of reactive vs. total microglia was determined for each brain region analyzed.

Statistical Analysis

Data shown in the figures are presented as the mean ± standard error of the mean (SEM). The size of the experimental groups is indicated in each figure legend. Gaussian distribution of data sets was assessed by Kolmogorov-Smirnov test. Statistical analysis was performed by using the software GraphPad Prism 6 (GraphPad Software). To determine significant differences in microglia densities and reactivity between groups, we used t-test analysis. P-values < 0.05 were considered to be significant.

RESULTS

Body Weight Gain

Animal weight was recorded every 2 or 3 days. At day two after administration of RAd-DsRed or RAd-IGF1, both groups experienced a transient loss of body weight due to the surgical procedure. Subsequently, both groups of rats recovered the initial

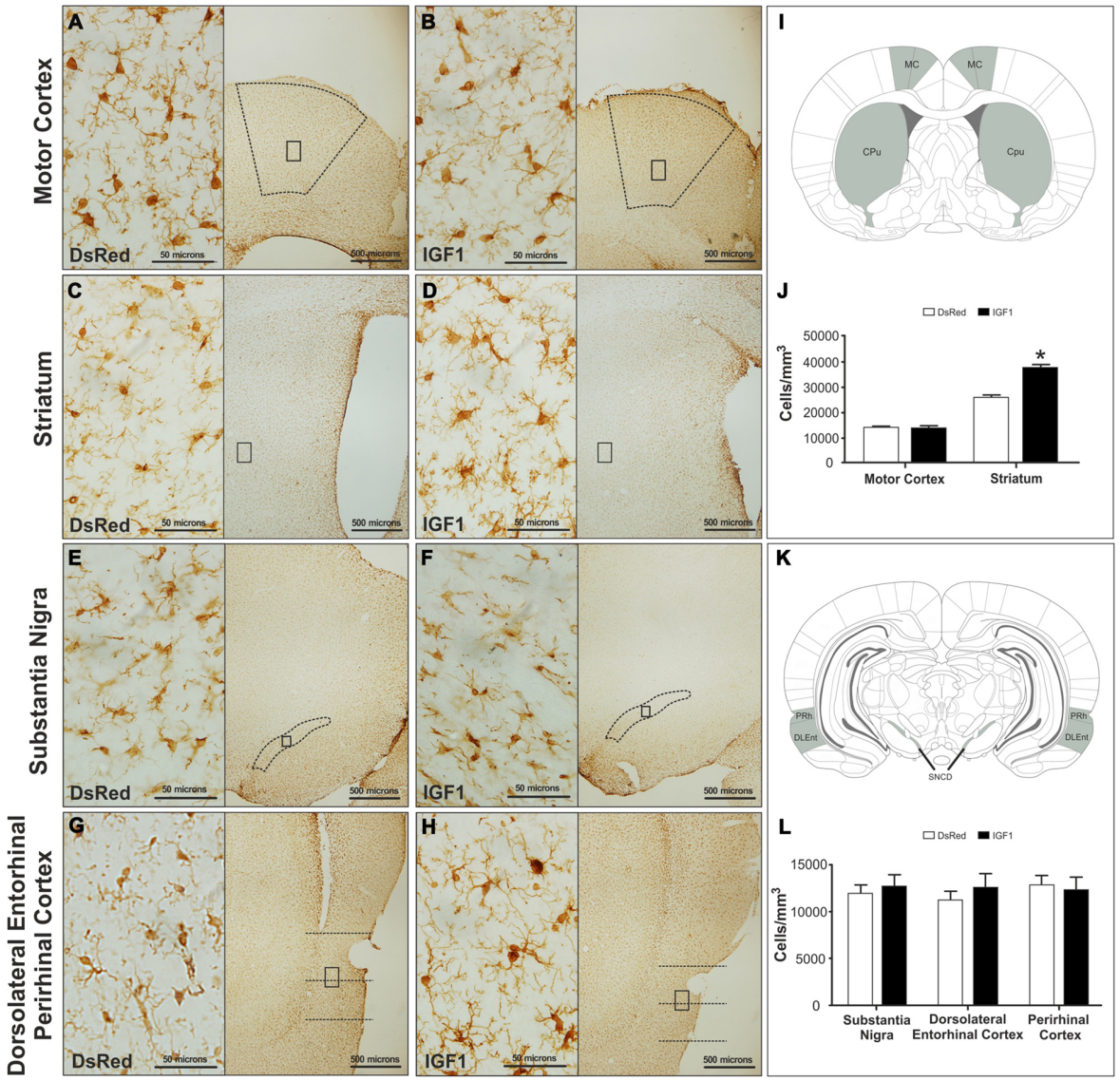

FIGURE 1 | Representative images of motor cortex **(A,B)**, striatum **(C,D)**, substantia nigra compact part dorsal **(E,F)** and dorsolateral entorhinal and perirhinal cortex **(G,H)** of the recombinant adenovirus (RAd)-discosoma Red fluorescent protein (DsRed; **A,C,E,G**) and RAd-Insulin like growth factor 1 (IGF1; **B,D,F,H**) groups at a magnification of 40X (scale bars: 500 microns), with insets at a magnification of 600X (scale bars: 50 microns). Panels (**I**; MC, motor cortex; Cpu, Striatum/caudate-putamen) and (**K**; PRh, perirhinal cortex; DLEnt, dorsolateral entorhinal cortex; and SNCD, substantia nigra compact part dorsal) show a representation of the coronal brain sections where the analyzed regions; are highlighted. Panels **(J,L)** show microglia densities in the different groups in the analyzed regions. Data are given as means ± SEM (N = 5/group). *Significant differences ($p < 0.05$).

weight and remained stable until the end of the experiment (**Supplementary Figure S1**).

Gene Therapy Affects the Number and Reactivity of Microglia

Iba-1 immunoreactive cells were analyzed in the motor cortex, striatum, substantia nigra, DLEnt and PRh. As shown in **Figure 1**, significant differences in the number of Iba-1 immunoreactive cells were detected in the striatum between the animals injected with RAd-DsRed and the animals injected with RAd-IGF1. Thus, there was a higher number of Iba-1 immunoreactive cells in the animals injected with RAd-IGF1 than in the animals injected with RAd-DsRed (**Figure 1**). No significant differences were detected in the number of Iba-1 immunoreactive cells in the motor cortex, substantia nigra and the PRh of the animals injected with RAd-IGF1 and the animals injected with RAd-DsRed (**Figure 1**).

In addition to the differences in total number, obvious qualitative differences were observed in the morphology of Iba-1 immunoreactive cells between the different experimental groups; with more cells with a reactive phenotype in the striatum of animals injected with Rad-IGF1 (**Figure 2**). Indeed,

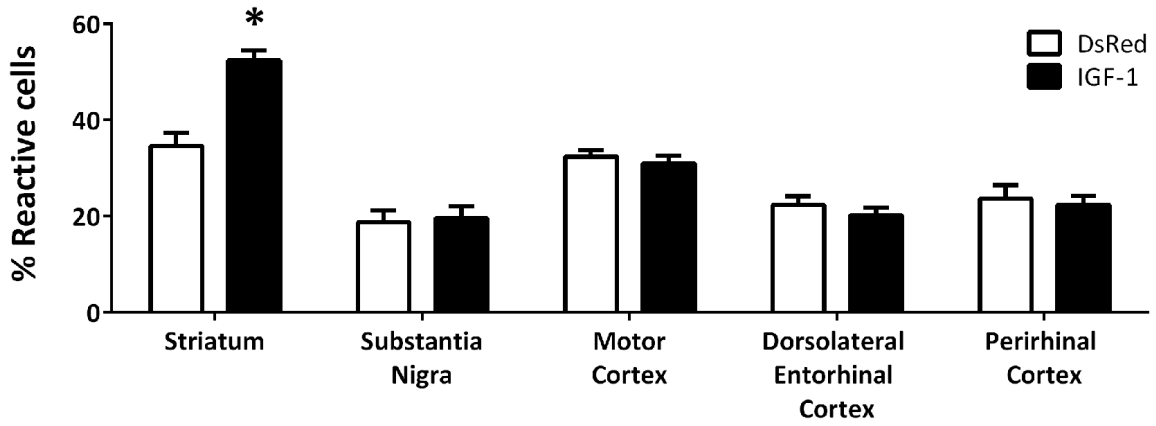

FIGURE 2 | Proportion of reactive microglia with ameboid morphology and enlarged cell body in RAd-DsRed and RAd-IGF1 groups in the different brain regions analyzed. Statistical results indicate significant differences between the experimental groups within the same brain region. Data are given as means ± SEM (N = 5/group). *Significant differences ($p < 0.05$).

the quantitative analysis of reactive/ameboid cells and non-reactive/ramified cells showed a significant increase in the proportion of reactive cells in the striatum of the animals injected with RAd-IGF1 in comparison with the striatum of RAd-DsRed injected rats. In contrast, no significant differences in the proportion of reactive and non-reactive phenotypes were detected in the other brain regions analyzed (**Figure 2**).

In summary, these findings indicate that the injection of RAd-IGF1 is able to increase the number of Iba-1 immunoreactive cells and the proportion of Iba-1 immunoreactive cells with a reactive phenotype in a specific brain region.

DISCUSSION

We previously demonstrated that ICV IGF1 gene therapy is effective to transduce brain ependymal cells with high efficiency, achieving effective release of transgenic IGF1 into the cerebrospinal fluid (CSF; Hereñú et al., 2009) and restoring motor performance in aged animals (Nishida et al., 2011). Thus, we decided to use the ependymal route to implement IGF1 gene therapy in aging rats with the goal to characterize microglia number and distribution in different brain regions related with cognition or motor performance.

ICV gene therapy caused a significant but transient decrease in weight gain in both DsRed and IGF1 groups. Body weigh may be affected by surgery and also by a temporary induction of endogenous neurotrophic factors, such as GDNF, which has been reported to cause body weight loss (Morel et al., 2010). This effect could be greater in the IGF1 group, since IGF1 may regulate the hypothalamic system controlling body weight and energy expenditure (Werner and LeRoith, 2014).

We expected that IGF1 gene therapy will decrease microglia reactivity, since this therapy has been shown to reduce the reactivity of astrocytes in response to proinflammatory stimuli *in vitro* (Bellini et al., 2011). And to exert neuroprotective and neuroreparative actions in experimental animal models of stroke (Zhu et al., 2008; Liu et al., 2017). However, other studies have reported detrimental actions of IGF1 receptor signaling in the brain of mouse models of Alzheimer's disease (Cohen et al., 2009; Freude et al., 2009; Gontier et al., 2015). In this study we found is that IGF1 gene therapy increased the number and the proportion of microglia with a reactive phenotype in a region dependent manner.

We have not a definitive explanation for the regional effect of RAd-IGF1 on striatal microglia. It is well established that microglia (Breese et al., 1996; Walter et al., 1999; Chesik et al., 2004; Suh et al., 2013; Rodriguez-Perez et al., 2016; Trueba-Saiz et al., 2017) and other cell types in the brain (Fernandez and Torres-Alemán, 2012) express IGF1 receptors. It is possible that regional differences in the expression of these receptors may cause a different sensitivity to IGF1 released and delivered to the ventricles by infected ependymal cells.

The functional consequences of these changes in microglia are unknown. However, it has been described that treatments that leads to the depletion of microglia in injury models increases neuronal death (Vinet et al., 2012). Reciprocally, repletion of microglia or introduction of exogenous microglia result in neuronal rescue, driven possibly by microglial production of trophic growth factors, or *via* the clearance of deleterious byproducts of metabolism and neurotransmission (Streit et al., 2004; Nissen, 2017). Therefore, it is possible that the increased number of microglia cells induced by IGF1 gene therapy may exert a protective function in the striatum of older rats. Indeed, previous studies have shown that the administration of RAd-IGF1 in the brain, following the protocol used in the present study, results in an improvement in motor function of senile rats (Nishida et al., 2011).

In summary, our findings indicate that ICV IGF1 gene therapy specifically modifies the number and phenotype of microglia in the striatum of senile rats, suggesting that such a therapy may be useful to alter the function of dystrophic microglia, at least in specific brain regions. Further studies should

determine whether the effect of IGF1 gene therapy on microglia is age-dependent and is also detected in male animals.

DATA AVAILABILITY

All datasets generated for this study are included in the manuscript and/or the supplementary files.

AUTHOR CONTRIBUTIONS

EF-L and MB designed the experiments. EF-L and FD performed the experiments. EF-L, FD, LG-S, CH and MB analyzed the data. EF-L, LG-S, CH and MB wrote the manuscript.

FUNDING

This study was supported in part by grants #PICT13-1119 from the Argentine Agency for the Promotion of Science and Technology and grant PIP0618 from the Argentine Research Council (CONICET) to MB, grant M184 from the Universidad Nacional de La Plata to CH and grant from Agencia Estatal de Investigación, Spain (BFU2017-82754-R), CIBERFES and Fondos Feder to LG-S.

ACKNOWLEDGMENTS

We thank Natalia Scelsio for technical assistance as well as to Oscar Vercellini, Araceli Bigres for animal care and to Mario Ramos for assistance with graphics design.

SUPPLEMENTARY MATERIAL

The Supplementary Material for this article can be found online at: https://www.frontiersin.org/articles/10.3389/fnagi.2019.00048/full#supplementary-material

FIGURE S1 | Time curve of body weight gains of RAd-DsRed and RAd-IGF1 rats. *Significant difference ($p < 0.05$). $N = 5$/group.

REFERENCES

Acaz-Fonseca, E., Duran, J. C., Carrero, P., Garcia-Segura, L. M., and Arevalo, M. A. (2015). Sex differences in glia reactivity after cortical brain injury. *Glia* 63, 1966–1981. doi: 10.1002/glia.22867

Acaz-Fonseca, E., Sanchez-Gonzalez, R., Azcoitia, I., Arevalo, M. A., and Garcia-Segura, L. M. (2014). Role of astrocytes in the neuroprotective actions of 17β-estradiol and selective estrogen receptor modulators. *Mol. Cell. Endocrinol.* 389, 48–57. doi: 10.1016/j.mce.2014.01.009

Arevalo, M.-A., Santos-Galindo, M., Bellini, M.-J., Azcoitia, I., and Garcia-Segura, L. M. (2010). Actions of estrogens on glial cells: implications for neuroprotection. *Biochim. Biophys. Acta* 1800, 1106–1112. doi: 10.1016/j.bbagen.2009.10.002

Bellini, M. J., Hereñú, C. B., Goya, R. G., and Garcia-Segura, L. M. (2011). Insulin-like growth factor-I gene delivery to astrocytes reduces their inflammatory response to lipopolysaccharide. *J. Neuroinflammation* 8:21. doi: 10.1186/1742-2094-8-21

Breese, C. R., Costa, A. D., Rollins, Y. D., Adams, C., Booze, R. M., Sonntag, W. E., et al. (1996). Expression of insulin-like growth factor-1 (IGF-1) and IGF-binding protein 2 (IGF-BP2) in the hippocampus following cytotoxic lesion of the dentate gyrus. *J. Comp. Neurol.* 404, 388–404. doi: 10.1002/(sici)1096-9861(19960603)369:3<388::aid-cne5>3.0.co;2-1

Chesik, D., De Keyser, J., and Wilczak, N. (2004). Involvement of insulin-like growth factor binding protein-2 in activated microglia as assessed in post mortem human brain. *Neurosci. Lett.* 362, 14–16. doi: 10.1016/s0304-3940(04)00098-9

Cohen, E., Paulsson, J. F., Blinder, P., Burstyn-Cohen, T., Du, D., Estepa, G., et al. (2009). Reduced IGF-1 signaling delays age-associated proteotoxicity in mice. *Cell* 139, 1157–1169. doi: 10.1016/j.cell.2009.11.014

Cunningham, C. (2013). Microglia and neurodegeneration: the role of systemic inflammation. *Glia* 61, 71–90. doi: 10.1002/glia.22350

Deak, F., and Sonntag, W. E. (2012). Aging, synaptic dysfunction, and insulin-like growth factor (IGF)-1. *J. Gerontol. A Biol. Sci. Med. Sci.* 67A, 611–625. doi: 10.1093/gerona/gls118

Fernandez, A. M., and Torres-Alemán, I. (2012). The many faces of insulin-like peptide signalling in the brain. *Nat. Rev. Neurosci.* 13, 225–239. doi: 10.1038/nrn3209

Freude, S., Hettich, M. M., Schumann, C., Stöhr, O., Koch, L., Köhler, C., et al. (2009). Neuronal IGF-1 resistance reduces Aβ accumulation and protects against premature death in a model of Alzheimer's disease. *FASEB J.* 23, 3315–3324. doi: 10.1096/fj.09-132043

Gontier, G., George, C., Chaker, Z., Holzenberger, M., and Aïd, S. (2015). Blocking IGF signaling in adult neurons alleviates Alzheimer's disease pathology through amyloid-β clearance. *J. Neurosci.* 35, 11500–11513. doi: 10.1523/JNEUROSCI.0343-15.2015

Hereñú, C. B., Cristina, C., Rimoldi, O. J., Becú-Villalobos, D., Cambiaggi, V., Portiansky, E. L., et al. (2007). Restorative effect of insulin-like growth factor-I gene therapy in the hypothalamus of senile rats with dopaminergic dysfunction. *Gene Ther.* 14, 237–245. doi: 10.1038/sj.gt.3302870

Hereñú, C. B., Sonntag, W. E., Morel, G. R., Portiansky, E. L., and Goya, R. G. (2009). The ependymal route for insulin-like growth factor-1 gene therapy in the brain. *Neuroscience* 163, 442–447. doi: 10.1016/j.neuroscience.2009.06.024

Koellhoffer, E. C., McCullough, L. D., and Ritzel, R. M. (2017). Old maids: aging and its impact on microglia function. *Int. J. Mol. Sci.* 18:E769. doi: 10.3390/ijms18040769

Labandeira-Garcia, J. L., Costa-Besada, M. A., Labandeira, C. M., Villar-Cheda, B., and Rodríguez-Perez, A. I. (2017). Insulin-like growth factor-1 and neuroinflammation. *Front. Aging Neurosci.* 9:365. doi: 10.3389/fnagi.2017.00365

Liu, Y., Wang, X., Li, W., Zhang, Q., Li, Y., Zhang, Z., et al. (2017). A sensitized IGF1 treatment restores corticospinal axon-dependent functions. *Neuron* 95, 817.e4–833.e4. doi: 10.1016/j.neuron.2017.07.037

Mansilla, E., Roque, G., Sosa, Y. E., Tarditti, A., and Goya, R. G. (2016). A rat treated with mesenchymal stem cells lives to 44 months of age. *Rejuvenation Res.* 19, 318–321. doi: 10.1089/rej.2015.1777

Morel, G. R., León, M. L., Uriarte, M., Reggiani, P. C., and Goya, R. G. (2016). Therapeutic potential of IGF-I on hippocampal neurogenesis and function during aging. *Neurogenesis* 4:e1259709. doi: 10.1080/23262133.2016.1259709

Morel, G. R., Sosa, Y. E., Bellini, M. J., Carri, N. G., Rodriguez, S. S., Bohn, M. C., et al. (2010). Glial cell line-derived neurotrophic factor gene therapy ameliorates chronic hyperprolactinemia in senile rats. *Neuroscience* 167, 946–953. doi: 10.1016/j.neuroscience.2010.02.053

Nishida, F., Morel, G. R., Hereñú, C. B., Schwerdt, J. I., Goya, R. G., and Portiansky, E. L. (2011). Restorative effect of intracerebroventricular insulin-like growth factor-I gene therapy on motor performance in aging rats. *Neuroscience* 177, 195–206. doi: 10.1016/j.neuroscience.2011.01.013

Nissen, J. C. (2017). Microglial function across the spectrum of age and gender. *Int. J. Mol. Sci.* 18:E561. doi: 10.3390/ijms18030561

Pardo, J., Uriarte, M., Cónsole, G. M., Reggiani, P. C., Outeiro, T. F., Morel, G. R., et al. (2016). Insulin-like growth factor-I gene therapy increases hippocampal neurogenesis, astrocyte branching and improves spatial memory in female aging rats. *Eur. J. Neurosci.* 44, 2120–2128. doi: 10.1111/ejn.13278

Patel, P., Lockey, R. F., and Kolliputi, N. (2015). Can inflammation regulate systemic aging? *Exp. Gerontol.* 67, 1–2. doi: 10.1016/j.exger.2015.04.011

Paxinos, G., and Watson, C. (2007). *The Rat Brain in Stereotaxic Coordinates.* 6th Edn. Amsterdam: Academic Press.

Pekny, M., and Pekna, M. (2016). Reactive gliosis in the pathogenesis of CNS diseases. *Biochim. Biophys. Acta* 1862, 483–491. doi: 10.1016/j.bbadis.2015.11.014

Piriz, J., Muller, A., Trejo, J. L., and Torres-Aleman, I. (2011). IGF-I and the aging mammalian brain. *Exp. Gerontol.* 46, 96–99. doi: 10.1016/j.exger.2010.08.022

Ransohoff, R. M. (2016). How neuroinflammation contributes to neurodegeneration. *Science* 353, 777–783. doi: 10.1126/science.aag2590

Rodriguez-Perez, A. I., Borrajo, A., Diaz-Ruiz, C., Garrido-Gil, P., and Labandeira-Garcia, J. L. (2016). Crosstalk between and angiotensin-II in dopaminergic neurons and glial cells: role in neuroinflammation and aging. *Oncotarget* 7, 30049–30067. doi: 10.18632/oncotarget.9174

Spittau, B. (2017). Aging microglia-phenotypes, functions and implications for age-related neurodegenerative diseases. *Front. Aging Neurosci.* 9:194. doi: 10.3389/fnagi.2017.00194

Streit, W. J., Sammons, N. W., Kuhns, A. J., and Sparks, D. L. (2004). Dystrophic microglia in the aging human brain. *Glia* 45, 208–212. doi: 10.1002/glia.10319

Streit, W. J., and Xue, Q. (2010). The brain's aging immune system. *Aging Dis.* 1, 254–261.

Suh, H.-S., Zhao, M.-L., Derico, L., Choi, N., and Lee, S. C. (2013). Insulin-like growth factor 1 and 2 (IGF1, IGF2) expression in human microglia: differential regulation by inflammatory mediators. *J. Neuroinflammation* 10:37. doi: 10.1186/1742-2094-10-37

Torres Aleman, I. (2012). Insulin-like growth factor-1 and central neurodegenerative diseases. *Endocrinol. Metab. Clin. North Am.* 41, 395–408, vii. doi: 10.1016/j.ecl.2012.04.016

Trueba-Saiz, A., Fernandez, A. M., Nishijima, T., Mecha, M., Santi, A., Munive, V., et al. (2017). Circulating insulin-like growth factor I regulates its receptor in the brain of male mice. *Endocrinology* 158, 349–355. doi: 10.1210/en.2016-1468

Vinet, J., Weering, H. R. J., Heinrich, A., Kälin, R. E., Wegner, A., Brouwer, N., et al. (2012). Neuroprotective function for ramified microglia in hippocampal excitotoxicity. *J. Neuroinflammation* 9:27. doi: 10.1186/1742-2094-9-27

von Bernhardi, R., Heredia, F., Salgado, N., and Muñoz, P. (2016). "Microglia function in the normal brain," in *Glial Cells in Health and Disease of the CNS. Advances in Experimental Medicine and Biology*, ed. R. von Bernhardi (Cham: Springer International Publishing), 67–92.

Walter, H. J., Berry, M., Hill, D., Cwyfan-Hughes, J. S., Holly, J. M. P., and Logan, A. (1999). Distinct sites of insulin-like growth factor (IGF)-II expression and localization in lesioned rat brain: possible roles of IGF binding proteins (IGFBPs) in the mediation of IGF-II activity. *Endocrinology* 140, 520–532. doi: 10.1210/en.140.1.520

Werner, H., and LeRoith, D. (2014). Insulin and insulin-like growth factor receptors in the brain: physiological and pathological aspects. *Eur. Neuropsychopharmacol.* 24, 1947–1953. doi: 10.1016/j.euroneuro.2014.01.020

Zhu, W., Fan, Y., Frenzel, T., Gasmi, M., Bartus, R. T., Young, W. L., et al. (2008). Insulin growth factor-1 gene transfer enhances neurovascular remodeling and improves long-term stroke outcome in mice. *Stroke* 39, 1254–1261. doi: 10.1161/strokeaha.107.500801

Conflict of Interest Statement: The authors declare that the research was conducted in the absence of any commercial or financial relationships that could be construed as a potential conflict of interest.

frontiers in Aging Neuroscience

REVIEW
published: 19 March 2019
doi: 10.3389/fnagi.2019.00059

Astrocyte Heterogeneity: Impact to Brain Aging and Disease

*Isadora Matias†, Juliana Morgado† and Flávia Carvalho Alcantara Gomes**

Laboratory of Cellular Neurobiology, Institute of Biomedical Sciences, Federal University of Rio de Janeiro, Rio de Janeiro, Brazil

Astrocytes, one of the largest glial cell population in the central nervous system (CNS), play a key function in several events of brain development and function, such as synapse formation and function, control of neurotransmitters release and uptake, production of trophic factors and control of neuronal survival. Initially described as a homogenous population, several evidences have pointed that astrocytes are highly heterogeneous, both morphologically and functionally, within the same region, and across different brain regions. Recent findings suggest that the heterogeneity in the expression profile of proteins involved in astrocyte function may predict the selective vulnerability of brain regions to specific diseases, as well as to the age-related cognitive decline. However, the molecular mechanisms underlying these changes, either in aging as well as in brain disease are scarce. Neuroinflammation, a hallmark of several neurodegenerative diseases and aging, is reported to have a dubious impact on glial activation, as these cells release pro- and anti-inflammatory cytokines and chemokines, anti-oxidants, free radicals, and neurotrophic factors. Despite the emerging evidences supporting that reactive astrocytes have a duality in their phenotype, neurotoxic or neuroprotective properties, depending on the age and stimuli, the underlying mechanisms of their activation, cellular interplays and the impact of regional astrocyte heterogeneity are still a matter of discussion. In this review article, we will summarize recent findings on astrocyte heterogeneity and phenotypes, as well as their likely impact for the brain function during aging and neural diseases. We will focus on the molecules and mechanisms triggered by

OPEN ACCESS

Edited by:
Maria Jose Bellini, Consejo Nacional de Investigaciones Científicas y Técnicas (CONICET), Argentina

Reviewed by:
Kyoungho Suk, Kyungpook National University, South Korea
Luca Steardo, Università degli Studi della Campania Luigi Vanvitelli Caserta, Italy

***Correspondence:**
Flávia Carvalho Alcantara Gomes
fgomes@icb.ufrj.br

†These authors have contributed equally to this work

Received: *08 January 2019*
Accepted: *01 March 2019*
Published: *19 March 2019*

Citation:
Matias I, Morgado J and Gomes FCA (2019) Astrocyte Heterogeneity: Impact to Brain Aging and Disease. Front. Aging Neurosci. 11:59. doi: 10.3389/fnagi.2019.00059

Abbreviations: AD, Alzheimer's disease; Aldh1L1, aldehyde dehydrogenase 1 family, member L1; ALS, amyotrophic lateral sclerosis; ATP, adenosine triphosphate; AQP4, aquaporin-4; APs, amyloid plaques; Aβ, amyloid-β; AβO, Aβ oligomers; BBB, blood-brain barrier; BDNF, brain-derived neurotrophic factor; BLBP, brain lipid binding protein; CaM-kinase, Ca^{2+}/calmodulin-dependent protein kinase; CNS, central nervous system; Cx30, connexin-30; Cx43, connexin-43; C1q, complement component 1q; C3, complement component 3; C4b, complement component 4b; EAAT1, excitatory amino acid transporter 1; EAAT2, excitatory amino acid transporter 2; ER, endoplasmic reticulum; GABA, gamma-aminobutyric acid; GFAP, glial fibrillary acidic protein; GLAST, astrocyte-specific glutamate-aspartate transporter; GLP1R, glucagon-like peptide-1 receptor; GLT-1, glutamate transporter-1; GDNF, glial-derived neurotrophic factor; GS, glutamine synthetase; HD, Huntington's disease; IFs, intermediate filaments; IFN-γ, interferon-γ; IL-6, interleukin-6; IL-8, interleukin-8; IL1R1, interleukin 1-receptor 1; IL-1α, interleukin-1α; IL-1ß, interleukin-1ß; JAK2, janus kinase 2; $K_{ir}4.1$, inwardly rectifying potassium channel 4.1; LPS, lipopolysaccharide; LTD, long-term depression; LTP, long-term potentiation; NGF, nerve growth factor; PD, Parkinson's disease; RG, radial glia cells; SNpc, substantia nigra pars compacta; SPARC, secreted protein-acidic and rich in cysteine; STAT3, signal transducer and activator of transcription 3; TGF-β, transforming growth factor-β; TGF-β1, transforming growth factor-β1; TLR4, toll-like receptor 4; TNF-α, tumor necrosis factor-α; TNT, tunneling nanotubes; TSP, thrombospondin; TSP-1, thrombospondin-1; WHO, World Health Organization.

astrocyte to control synapse formation in different brain regions. Finally, we will discuss new evidences on how the modulation of astrocyte phenotype and function could impact the synaptic deficits and glial dysfunction present in aging and pathological states.

Keywords: astrocyte, glial reactivity, aging, heterogeneity, neurodegenerative diseases

ASTROCYTES: AN OVERVIEW

The term "astrocytes" comprises a heterogeneous group of non-neuronal cells, involved in fundamental functions of the central nervous system (CNS). Even though astrocytes tile the entire brain, these cells have not always been considered active partners of neurons in the transfer of neural information as they are now, in the beginning of the XXI century.

In the XIX century, Virchow coined the term *nervenkitt* (neuroglia), to refer to the passive, connective elements in the brain, in which the other elements, the excitable ones, were embedded (Somjen, 1988). Further discoveries about the nature of neural cells came in the end of the XIX century, with new techniques of tissue staining developed by Italian physician and cytologist, Camillo Golgi and the Spanish neurohistologist, Ramón y Cajal. Golgi and Cajal were the first to highlight that neuroglia and nerve cells represented different populations and to further identify a variety of glial shapes and forms, as well as the glial network formed by these cells and other non-neuronal cells, such as the glial endfeet in close proximity to blood vessels (De Carlos and Borrell, 2007). At the end of the XIX century, the Hungarian anatomist and histologist, Lenhossék, introduced the term astrocyte to refer to a star-shaped glial cell; he raised the concept that even though astrocytes were electrically silent, they had functions as important as nerve cells (Somjen, 1988; Verkhratsky and Butt, 2013; Verkhratsky and Nedergaard, 2018).

In the last decades, an increasing amount of data has provided new insights on the plethora of functions performed by astrocytes. In the healthy tissue, these cells occupy unique spaces in which their extensive branching of fine processes occupy contiguous non-overlapping domains (Bushong et al., 2002). Their processes can contact synapses, other glial cells, blood vessels, and depending on the brain area, they have more specific roles. One of these key roles is in synaptic regulation, as astrocytes can act not only in the formation and maturation of synapses (Diniz et al., 2014a), but also in the maintenance, pruning and remodeling of synapses in the development, aging and diseases (Chung et al., 2013, 2015, 2016; Liddelow et al., 2017). Beyond the well-established concept of the tripartite synapse, in which perisynaptic astroglial processes are fundamental participants in the synapse, along with the pre- and post-synaptic components (Araque et al., 1999), it is now argued that the astroglial synaptic coverage could be far more extensive. It is theorized that the astroglial perisynaptic processes form a "synaptic cradle" around the synapse, embracing it, allowing the astrocyte to provide proper maintenance of the synapse, maintaining neurotransmitter, ion and volume homeostasis, releasing neuromodulators and keeping the specificity of the signaling, and providing synaptic isolation (Verkhratsky and Nedergaard, 2014, 2018). As astrocytes express a diversity of neurotransmitters' receptors and transporters, they can control the levels and activity of several neurotransmitters such as glutamate, gamma-aminobutyric acid (GABA), adenosine triphosphate (ATP) and D-serine (Rothstein et al., 1994, 1996). Some of these molecules, also known as gliotransmitters, can be secreted by astrocytes in the synaptic space and activate neuronal receptors, allowing astrocytes to act as modulators of neuronal activity (Volterra and Meldolesi, 2005).

Emerging evidence from the last decade have strongly challenged the concept that brain function is a result of solely neuronal networks' activity (Araque and Navarrete, 2010; Di Castro et al., 2011). Changes in synaptic function can cause the release of other gliotransmitters by astrocytes, such as thrombospondins (TSPs; Christopherson et al., 2005; Eroglu and Barres, 2010), hevin and secreted protein-acidic and rich in cysteine (SPARC; Kucukdereli et al., 2011), glypicans, and cytokines, including tumor necrosis factor-α (TNF-α; Stellwagen and Malenka, 2006) and transforming growth factor-β1 (TGF-β1; Diniz et al., 2012, 2014b). This could happen because neural activity cause excitability in the astrocyte's membrane, triggering the release of intracellular Ca^{2+}, which in turn, causes the release of some gliotransmitters (Perea and Araque, 2007; Araque et al., 2014); however, the mechanisms that govern astrocytes' influence on synaptic activity are not completely clear yet. Further, neuronal activity has also been implicated in the generation of spontaneous syncytial signaling through calcium waves in astrocytes (Shigetomi et al., 2010; Di Castro et al., 2011), even though this is not entirely dependent on neuronal activity (Nett et al., 2002). Physiological stimulation creates a flux of Ca^{2+} ions, changing the Ca^{2+} concentration throughout cell compartments, thus generating the waves. The waves can spread out (Kanemaru et al., 2014) and propagate the signal from one cell to the other through gap junction channels (De Bock et al., 2014). This could represent a specific kind of cell-cell communication, especially for long-range information transfer in astrocytic syncytia (Scemes and Giaume, 2006). However, the proper physiological role of calcium waves and the mechanism through which it happens remains to be explored.

Besides their roles in the synaptic function, astrocytes are responsible for ion homeostasis in the CNS, regulating the extracellular levels of potassium, chlorine and calcium ions, water homeostasis and maintenance of the cellular pH. They are also responsible for providing energetic metabolites required by neurons in neural networks, such as glucose (Rouach et al., 2008) and lactate (Qu et al., 2000; Figley, 2011; Sotelo-Hitschfeld et al., 2015), and trophic factors essential for neuronal survival and differentiation (Gomes et al., 1999, 2005;

Martinez and Gomes, 2002; Nones et al., 2012; Dezonne et al., 2013). Additionally, astrocytes maintain intimate contact along with endothelia and pericytes, thus contributing to the formation and function of the blood-brain barrier (BBB; Siqueira et al., 2018). More recently, a novel function has been attributed to astrocytes as part of the glymphatic system, in which astrocyte's endfeet contact the vasculature, surrounding it and forming a system of tunnels, through which compounds such as glucose and amino acids are distributed, and the excess of toxic waste products is removed, such as large proteins including β-amyloid and tau (Weller et al., 2009; Iliff et al., 2012; Jessen et al., 2015).

Given the large number of functions performed by astrocytes **(Figure 1)**, it is to be expected that deficits in these cells have a major impact on brain functioning. Such impact, however, due to the great diversity amongst these cells, vary among different brain areas and structures. This review article will focus on astrocyte diversity, highlighting the main findings on their morphological, functional and molecular differences amongst brain regions. We further discuss how such heterogeneity might contribute to shape the way astrocytes respond to different insults, such as those that rise from aging and in specific neurodegenerative diseases. Finally, we will argue that modulation of astrocyte phenotypes and functions, might shed light on new avenues to control aging and neural pathology.

MOLECULAR AND FUNCTIONAL HETEROGENEITY OF ASTROCYTES IN THE HEALTHY BRAIN

The neurocentric view of the brain has persisted for many years, and several studies have identified numerous neuronal

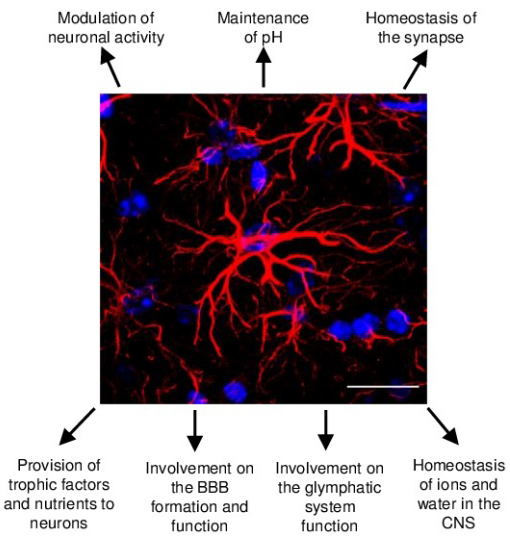

FIGURE 1 | Schematic representation of the main astrocyte functions in the central nervous system (CNS). Astrocytes in the healthy murine CNS are highly ramified cells responsible for a number of functions in the CNS development, homeostasis and function. Glial fibrillary acidic protein (GFAP; in red) and DAPI (in blue) staining of murine hippocampus tissue. Scale bars, 20 μm.

populations that differ molecularly and functionally (Kepecs and Fishell, 2014; Jiang et al., 2015; Mancinelli and Lodato, 2018). Even though astrocytes are in close contact to neurons, it was not clear whether astrocytes would be as diverse as neurons. Astrocyte heterogeneity was an underexplored topic for many years, and just recently, the plurality of functions that they can exert in different neuronal circuits has shed a light on the fact that perhaps these cells have more specialized roles locally than previously thought.

In the mammal CNS, it has long been recognized a variety of astrocyte subtypes that differ regarding their developmental origin, morphology, physiology and metabolism amongst regions (Zhang and Barres, 2010; Oberheim et al., 2012). The first evidences of morphological heterogeneity of astrocytes were introduced by Golgi and Cajal (for review, Garcia-Lopez et al., 2010), and by William Lloyd Andriezen, World Health Organization (WHO), in 1893, described two different types of glial cells present in white and gray matter, the fibrous and protoplasmic glia, respectively (Andriezen, 1893), even though he thought these cells had different developmental origins. Since then, numerous evidence have corroborated the concept that protoplasmic and fibrous astrocytes are different subsets of astrocytes based on morphologic and molecular criteria (Vaughn and Pease, 1967; Raff et al., 1984; Raff, 1989). The protoplasmic astrocytes represent the biggest population of astrocytes in the gray matter, mainly found in the hippocampus and cerebral cortex; their cell bodies are extremely ramified, which probably allows them to touch numerous synapses typical of these regions, thus performing a neuromodulatory role (Bushong et al., 2002; Oberheim et al., 2012). The fibrous astrocytes are organized along white matter tracts; they are smaller and have lesser branching points than the protoplasmic astrocytes and can contact the nodes of Ranvier, thus contributing to keep the homeostasis in the region (Lundgaard et al., 2014).

Besides these two main subtypes of astrocytes, other astrocyte-like cells are described: radial glia cells (RG), initially described as merely playing a role in neuronal migration during cerebral cortex development, today RG are known as the main neuronal/glial progenitor present during brain development (Sild and Ruthazer, 2011); Bergmann glia, astrocyte type specific for cerebellum that ensheaths and controls cerebellar synapses, and is involved in granular cell migration (Rakic, 1971; Gregory et al., 1988; Grosche et al., 2002); Müller glia, astrocyte type specific for retina, involved in cell migration, neuronal generation and control of synapses of the retina (Reichenbach, 1989; Reichenbach and Bringmann, 2010). These specific subtypes of astrocytes and their heterogeneity will not be the scope of this review, but they provide an insight on how diverse the astrocyte population can be, especially as these subsets can vary amongst themselves.

The astrocytes that populate the human CNS are unique. Not only the cortical protoplasmic astrocytes are nearly three-fold larger in diameter, they also extend ten times more primary processes than their rodent counterparts and contact nearly 100-fold more synapses located in their territorial domains

(Oberheim et al., 2009). The human brain also has exclusive subtypes of astrocytes, such as the *interlaminar astrocytes*, which cell body is located at the top cortical layer and sends long processes towards the deeper layers (Colombo et al., 1995) and the *varicose projection astrocytes*, which processes have many varicosities and extend 1–5 very long fibers towards all directions in the cerebral cortex (Oberheim et al., 2009, 2012). However, the whole extension of this diversity and its functional significance still remains to be investigated.

In rodents, by the end of gestation, RG-astrocyte differentiation is characterized, among several molecular mechanisms, by the replacement of RG markers, such as brain lipid binding protein (BLBP) and the intermediate filament (IF) protein, nestin, by astrocytic markers such as vimentin, the glial fibrillary acidic protein (GFAP), the glutamate transporter GLAST and the calcium binding protein S100β (Pixley and de Vellis, 1984) as discussed below. The correct timing of RG-astrocyte transformation is a crucial step to ensure correct number of neurons and cerebral cortex lamination. All things considered, the identification of astrocytic markers is crucial to the proper visualization of these cells, which may be the first step towards understanding how diverse they are. Although GFAP has become a classical marker for the identification of mature astrocytes, it has many limitations. One of the main ones is that it is not broadly expressed by all astrocytes across brain areas in the healthy CNS (Walz and Lang, 1998; Eng et al., 2000; Hol and Pekny, 2015).

GFAP has at least eight different isoforms generated by different splicing patterns, and they may be variably expressed in specific subsets of astrocytes (Middeldorp and Hol, 2011). Perhaps due to its importance in modulating astrocyte motility and shape by providing structural stability to astrocytic processes, GFAP expression is highly regulated including in injury and disease (Eng et al., 2000), and during aging in specific areas of the rodent brain, such as the corpus callosum, basal ganglia and hippocampus (Morgan et al., 1997, 1999) and in humans (Nichols et al., 1993). Another limitation is that GFAP has also been detected in peripheral glia, such as enteric glia (Kato et al., 1990), Schwann cells (Bianchini et al., 1992), and other non-neuronal cells, such as fibroblasts, and myoepithelial cells (Hainfellner et al., 2001). Other astrocytic markers include the glutamate transporters such as GLT-1 excitatory amino acid transporter 2 (EAAT2) and GLAST EAAT1, that stain a variety of astrocytes' subtypes, e.g., RG, Bergmann glia, Müller cells, etc. (Schmitt et al., 1997; Williams et al., 2005), glutamine synthetase (GS) which stains a wide array of astrocytes' subtypes in many regions where GFAP is not an effective marker (Anlauf and Derouiche, 2013); the glycoprotein S100β that is a more broadly expressed marker of astrocytes than GFAP in some regions (Ogata and Kosaka, 2002). However, these markers are less specific to astrocytes than GFAP, as S100β also stains oligodendrocytes and ependymal cells (Hachem et al., 2005; Steiner et al., 2007); GLT-1, GLAST and GS expression was also reported in neurons and oligodendrocytes (Cammer, 1990; D'Amelio et al., 1990; Schmitt et al., 2002). A few other markers have also been used to identify astrocytes such as aquaporin 4 (AQP4) and connexins 30 (Cx30) and Cx43, though these markers are mostly concentrated at astrocytes' endfeet, rather than throughout the cell soma (Nagy et al., 1999; Nagelhus and Ottersen, 2013).

The advent of genetics era in recent decades and identification of the transcriptional profile of astrocytes, represented a new tool to study the diversity of the astroglial lineage and provided useful insights in the physiological state of these cells. The genetic profiling of astrocytes has identified a wider array of new markers such as the aldehyde dehydrogenase 1 family, member L1 (Aldh1L1) gene. This metabolic enzyme is responsible for the folate metabolism, which is especially important during neurulation. Aldh1L1 is widely expressed throughout the whole cell, and it seems to be expressed by most astrocytes, but not by other cell types (Cahoy et al., 2008), which might make it a better tool to visualize astrocytes in the developing mouse brain.

All markers identified so far, have showed some kind of specificity depending on the area: while Aldh1L1 was reported mainly staining cortical astrocytes (Waller et al., 2016); GS labeled mainly astrocytes in the entorhinal cortex (EC) comparing to GFAP (Anlauf and Derouiche, 2013), whereas astrocytes in the hippocampus are widely stained for GFAP (Bushong et al., 2002; Chai et al., 2017).

Altogether, although these data suggest that there is some kind of selectivity of astrocytic protein expression among different areas, the lack of a universal astrocyte marker or specific astrocytic regional markers still represents a challenge for the identification of intrinsic differences between astrocytes from distinct brain regions.

Recently, Chai et al. (2017) demonstrated that astrocytes from the murine striatum and hippocampus differ morphologically, functionally and molecularly. They found that even though the cell density in both regions were equally high, astrocytes in the striatum have a larger territorial size and contact nearly twice as many neuronal somas than hippocampal astrocytes, but the latter display stronger and more numerous physical interactions with excitatory synapses. At the functional level, these cells displayed different Ca^{2+}-signaling dynamics and gap-junctional coupling. The transcriptomic and proteomic analysis of the astrocytes from these distinct regions showed that hippocampal and striatal astrocytes are molecularly distinct cell populations. Genes responsible for proteins with functional importance in astrocytes such as the ones encoding GLT-1, SPARC, the potassium channel inwardly rectifying potassium channel 4.1 ($K_{ir}4.1$) and a sodium-dependent GABA transporter were amongst the 40 most highly expressed genes common between the hippocampus and striatum, but the most highly expressed gene in the hippocampal astrocyte was the one encoding GFAP, and in the striatal astrocyte was that encoding the protein μ-crystallin, a protein related to the regulation of the thyroid-hormone T3 (Vié et al., 1997), whose proper function in the brain is still unknown. Although these data corroborated the already known limitations of GFAP as an astrocyte marker, it suggests that μ-crystallin might be a molecular

marker specific to striatal astrocytes (Francelle et al., 2015; Chai et al., 2017). Interestingly, they also found a gradient of expression of μ-crystallin within the striatum, suggesting that these cells may differ even depending on their subregion (Chai et al., 2017). Such differences have already been observed among astrocytes from the CA1 and CA3 subareas of the hippocampus demonstrating different physiological properties (D'Ambrosio et al., 1998), even though expressing a similar molecular marker profile (Sharif et al., 2004).

The functional implication of astrocyte heterogeneity in different neural circuits is still a matter of discussion. However, considering the key role of astrocytes in synapse formation, maturation and maintenance in different brain regions, it is likely that interactions between astrocytes and synapses vary accordingly to regional demands. Our group has recently compared the synaptogenic properties of astrocytes from four different brain regions: cerebral cortex, hippocampus, midbrain and cerebellum. We found that distinct populations of astrocytes have distinct synaptogenic profiles due to the differential expression of synaptogenic molecules such as TSP-1, glypicans 4 and 6, hevin, SPARC, TNF-α, brain-derived neurotrophic factor (BDNF) and TGF-β1 (Buosi et al., 2018). The synaptogenic properties of these astrocytes might reflect the differences in the requirement of astroglia's synaptic coverage amongst different brain regions: some regions, like the cerebellum, have nearly all their synapses covered by astrocytes endfeet, whilst less than 50% of cortical and hippocampal synapses are tripartite synapses (Lippman et al., 2008; Witcher et al., 2010). Further, the pool of synaptogenic and anti-synaptogenic molecules produced by astrocytes might contribute to shape distinct neural circuits. In the cerebral cortex, for example, astrocytes can control the balance between excitatory and inhibitory synapses by activating different downstream signaling pathways, as described by our group. Astrocytes secrete TGF-β1, which induces the formation of either excitatory synapses *via* activation of D-serine production (Diniz et al., 2012), or inhibitory synapses *via* the Ca^{2+}/Calmodulin-dependent protein kinase (CAM-kinase) pathway (Diniz et al., 2014b).

Together, data discussed here supports the idea that astrocytes display distinct inter- and intra-regional features, however, the functional significance of this is still a matter of discussion. The fact that astrocytic processes fill the local environment in non-overlapping domains suggest that a potential advantage of region-specified astrocytes might be their capacity to locally regulate neural circuit function (Emsley and Macklis, 2006; Oberheim et al., 2012). This raises a few unanswered questions: Can astrocyte heterogeneity primarily determine susceptibility of brain regions to different insults? Does astrocyte diversity impact the way brain regions age? Do astrocytes' dysfunctions contribute equally to neurodegenerative diseases throughout the nervous system? In the next sections, we will discuss some recent advances and alternative explanations for the distinct vulnerability of these cells to different insults, diseases and aging amidst brain areas and the roles that astrocytes may play in these processes.

HETEROGENEITY OF ASTROCYTE'S RESPONSE TO DIVERSE INSULTS: REACTIVE ASTROCYTES AND THEIR DIFFERENT PHENOTYPES

Astrocytes acquire different phenotypes in response to numerous pathological stimuli, such as stroke, neurodegenerative disorders, tumors, trauma, infection, ischemia and aging. These can trigger a response known as astrocyte reactivity, characterized by changes in the profile of astrocytes' gene expression, leading to both morphological and functional changes that may vary from cellular hypertrophy, or atrophy, to proliferation and scar formation. The extent of the astrocytic reaction is severely impacted by the size of the affected area, the nature of the insult and its severity, the intensity of BBB disruption and the inflammatory response.

The first concept of astrocyte reactivity emerged with Virchow, who characterized a necrotic spinal lesion surrounded by a thick, highly fibrillary scarring, probably composed by densely packed astrocyte processes (Virchow, 1856). Even though astrocytes themselves were not formally described at that moment, accumulating pieces of evidence since then resulted in the classical hallmarks of reactive astrocytes: overexpression of GFAP, which frequently is related to the degree of reactivity, hypertrophy of cell body and increase in the number of cellular processes (Bignami and Dahl, 1976; Eng et al., 2000; Anderson et al., 2016). More recently, additional reactive astrocyte markers have been described, such as lipocalin-2 (Lcn-2), an acute phase protein (Lee et al., 2009), overexpressed by reactive astrocytes induced not only by ischemic stroke and lipopolysaccharide (LPS) exposure (Zamanian et al., 2012), but also by inflammation and excitotoxicity (Chia et al., 2011); and Serpin3n, a serine protease inhibitor (Zamanian et al., 2012), that was already reported to have its levels increased after injury in the rat facial and hypoglossal nuclei (Gesase and Kiyama, 2007). Identification of specific astrocytic reactivity markers is a crucial step towards the understanding of the unique mechanisms underlying this cellular process in different diseases.

Recently, the idea of astrocyte reactivity has been revisited. Rather than an all-or-none phenomenon, the process of becoming activated is gradated, and may vary from subtle changes to a deep irreversible morphological alteration, regulated in a context-dependent manner (Wilhelmsson et al., 2006; Sofroniew, 2009; Anderson et al., 2014). Further, although it is recognized that astrocytes can present gain or loss of function at the site of the insult, it is not clear whether this is beneficial or damaging to their surroundings (Sofroniew, 2009; Pekny et al., 2014). The reason for this controversy is due to the fact that apart from the protective roles that can be enhanced by astrocyte's activation, such as production of anti-inflammatory factors, these cells can also acquire a toxic reactive phenotype, thus producing cytokines that exacerbate injuries in the spinal cord (Brambilla et al., 2009), increasing β-amyloid production (Nagele et al., 2003), or becoming atrophied and losing their neuroprotective functions in Alzheimer's disease (AD), as will be discussed soon (Diniz et al., 2017).

Astrocytic reactivity is coordinated by complex molecular mechanisms, mainly initiated through an inflammatory response to the insults, in which gene expression and cellular changes are regulated by a series of inter- and intracellular signaling. Zamanian et al. (2012), was one of the first to describe reactive astrogliosis from a molecular standpoint. By using two injury models, a middle cerebral artery occlusion to induce ischemia and a systemic LPS injection, they found that reactive astrogliosis consisted of a rapid change in gene expression, but the reactive astrocyte phenotype varied according to the type of insult. Both models induced inflammation and caused concomitantly microglia activation and reactive astrogliosis, although by different mechanisms. They found that over 1,000 genes related to many different biological processes had their levels at least twice as high, when compared to quiescent astrocytes, and 260 of these were induced at least four-fold more in expression, hinting at the highly complex change that the astrocytic activation represents. They also found high levels of IF proteins such as GFAP and vimentin, and of many cytokines and their receptors, such as interleukin-6 (IL-6) and IL-1 receptor 1 (IL-1R1), confirming a few already described hallmarks of reactive gliosis. They found that the insults had overlapping but distinct sets of induced genes: from 263 reactive glial genes identified, 150 were preferentially expressed by ischemic stroke-reactive astrocytes, and 57 by LPS reactive astrocytes, and while ischemia induced a reactive astrocyte phenotype that was more protective, the insult with LPS produced a reactive astrocyte that was neurotoxic (Zamanian et al., 2012).

Recently, two different types of reactive astrocytes have been described in response to different insults (Liddelow et al., 2017), A1 and A2. In an LPS-induced neuroinflammation scenario, activated microglia induced a neurotoxic reactive astrocyte phenotype by secreting IL-1α, TNFα and complement component 1q (C1q). The so-called A1 astrocyte showed loss of normal functions and gain of new, harmful, functions at the same time. They upregulate many of the markers mentioned previously on this review article, such as LCN-2, Serpina3, and the classical GFAP. Liddelow et al. (2017) have demonstrated that the A1 astrocyte loses normal functions, such as the ability to induce synapse formation and this could be due to the increased expression of many classical complement cascade genes that are toxic to synapses, even though the specific molecule toxic to neurons remains unknown.

On the other hand, other insults, such as ischemia, can induce a protective reactive astrocyte. In this case, reactive astrocytes may secrete neuroprotective molecules, such as TSPs that upregulate many neurotrophic factors, and promote CNS recovery and repair (Papadopoulos et al., 2004; Zador et al., 2009). This second phenotype is called A2 astrocytes, and they are known to secrete neuroprotective cytokines.

We previously demonstrated that, in a sepsis model, activated astrocytes were observed both in the hippocampus and cerebral cortex, whilst activated microglia was mainly observed in the hippocampus; moreover, both of these areas showed impairment of synapse function (Moraes et al., 2015). To further investigate the molecular effects of sepsis on these cell populations, we have used stimulation with LPS to mimic the inflammatory effect observed during sepsis. As result, LPS stimulation of glial cells generated distinct secretory profiles in astrocytes and microglia, which had direct, though contrasting, impacts on synapses. The conditioned medium of LPS-stimulated microglia induced synaptic elimination, whilst the medium of astrocytes treated with LPS increased synapse number. Both cell types showed increased production of TNFα and IL-6, and while astrocytes had increased production of TGF-β1, an anti-inflammatory and synaptogenic cytokine, microglia showed elevated secretion of IL-1β, a pro-inflammatory cytokine, especially in the hippocampus (Moraes et al., 2015). These data highlight different responses of glial cells under an insult; whereas LPS-activated microglia present a neurotoxic phenotype; LPS-activated astrocytes, presented a neuroprotective role, similar to those called A2 astrocytes.

The knowledge of how these cells act in the healthy brain just adds another layer of complexity to the immense possibilities of phenotypes that they can acquire after an insult or aging. It is theorized that there is a gradient between the A1, neurotoxic phenotype and the A2, neuroprotective phenotype, and, possibly, an interplay between different profiles (Liddelow and Barres, 2017). It is imperative to consider the diversity of astrocyte's roles and their heterogeneity in health in order to understand more deeply their roles in disease and aging, as we will discuss in the next sections.

AGING AND NEURODEGENERATIVE DISEASES: IMPACT ON ASTROCYTE REACTIVE PHENOTYPES

The concept of astrocyte heterogeneity has profoundly changed our view on astrocyte functions, astrocyte-neuron interactions as well as their impact in aging and neurodegenerative diseases. The first evidence on astrocyte heterogeneity referred to their inter and intra-regional diversity in morphology in the CNS (Oberheim et al., 2009). Moreover, besides morphology, astrocytes are highly diverse in terms of molecular expression pattern and functions, as discussed in the previous sections.

Emerging lines of evidences have shown that global features of astrocytic reactivity, such as changes in astrocyte morphology, transcriptional profile and function, are distinctly observed in specific brain regions during early stages of many neurodegenerative diseases, such as AD, Parkinson's disease (PD), Huntington's disease (HD), and amyotrophic lateral sclerosis (ALS; Phatnani and Maniatis, 2015). These observations raise two main questions: "Is astrocyte heterogeneity maintained throughout the aging and in neural diseases?" and "How might astrocyte heterogeneity affect the onset and progression of age-related cognitive decline and age-related diseases?" The next sections will shed light on the possible involvement of changes in astrocyte phenotype to brain aging and pathology.

Aging

Astrocyte reactivity is also a hallmark of physiological aging in rodents, non-human and human primates (Nichols et al., 1993;

Rodríguez et al., 2014; Robillard et al., 2016). It is interesting to note that similarly to some neurodegenerative diseases, during aging, astrocyte reactivity is mainly observed in specific brain regions primarily targets for synaptic loss and age-related cognitive decline, such as the hippocampus and frontal cortex (FC; Rodríguez et al., 2016). Nevertheless, the actual contribution of astrocytes to regional vulnerability of the nervous system to specific diseases remains to be investigated.

Interestingly, it has also been reported an intra-regional heterogeneity in astrocyte's response to brain aging. Astrocytes in the hippocampal dentate gyrus and CA1 presented an age-dependent hypertrophy, as observed by a reorganization of the cytoskeleton protein, GFAP, leading to an increased surface, volume and somata volume of astrocytes in aged mice; while the opposite effect was observed in the EC. On the other hand, S100β-immunostaining, which is a cytosolic protein and hence shows a more complete astrocyte arborization than GFAP, revealed an increased surface area and volume in aged astrocytes in the EC and dentate gyrus, but not in CA1. Therefore, these observations imply that morphological changes based only on GFAP-staining may not reflect the entire complexity of astrocytes, as observed in the EC, and hence it may cause misinterpretations. In conclusion, this study suggested that astrocytes undergo complex region-specific morphological and molecular changes upon aging (Rodríguez et al., 2014).

In agreement with these results, an age-dependent increase in hippocampal GFAP expression has also been shown by other groups in rodents (Hayakawa et al., 2007; Lynch et al., 2010; Cerbai et al., 2012) and most prominently in the human hippocampal formation (David et al., 1997), but also in the FC and temporal cortex (TC; Nichols et al., 1993). Nevertheless, functional implication of GFAP upregulation during aging is still a matter of discussion, as well as how and why particularly hippocampal astrocytes undergo these changes.

Within this context, several studies have been trying to elucidate the transcription profile of astrocytes from different brain regions during aging, taking advantage of new techniques for the isolation of purified cell populations from the mouse brain or post-mortem human brain tissues. These new approaches, combined with transcriptome analysis, have shed light on the molecular signature of aged astrocytes as well as their region-specific changes during the aging process.

The physiological aging is characterized by a chronic, low-grade and systemic inflammation, referred as "inflammaging", which is an important risk factor for morbidity and mortality in elderly people (Franceschi et al., 2000). It is also known that glial cells, specially microglia and astrocytes, play a preponderant role in controlling neuroinflammation. As previously discussed, glial cells undergo morphological, molecular and functional changes that will result in pro or anti-inflammatory phenotypes, depending on the pathological context and age (Colombo and Farina, 2016). However, only recently our knowledge on the role of astrocytes in inflammaging and their regional differences in response to the aging process have beginning to be better elucidated.

Orre et al. (2014) showed that astrocytes isolated from the aged mouse cerebral cortex present increased inflammatory phenotype, although decreased GFAP expression compared to young astrocytes. It is noteworthy that although an upregulation of GFAP is usually associated with astrocyte reactivity, this feature itself may not be entirely precise to characterize this process, either in aging or brain disease. This is due to several reasons, such as: the number of GFAP positive cells and the basal GFAP expression level notably vary between different brain regions (Kimelberg, 2004); alteration in GFAP expression is usually region-specific (Rodríguez et al., 2014) and it may depends on the type and stage of the disease, or even the time after injury (Kamphuis et al., 2014; Diniz et al., 2017; Cunha et al., 2018).

Supporting astrocyte heterogeneity in aging, evidence have shown that astrocytes from distinct brain regions present an unique molecular signature in both aged mouse and human brain tissue (Soreq et al., 2017; Boisvert et al., 2018; Clarke et al., 2018). Boisvert et al. (2018) performed RNA-seq on astrocytes isolated from four brain regions of adult and aged mice: motor and visual cortex, hypothalamus and cerebellum. Surprisingly, they found significantly more changes in these cells from the hypothalamus and cerebellum, than from the cortex. They found increased expression of genes for inflammatory response and astrocyte reactivity, including GFAP and Serpin3n, and synapse elimination pathways, mainly represented by proteins of the complement system, such as complement component 3 (C3) and complement component 4b (C4b), and decreased cholesterol synthesis enzymes (Boisvert et al., 2018).

Similarly, Clarke et al. (2018) compared the expression profile of astrocytes isolated from the hippocampus, cortex and striatum of young and aged mice. They observed that hippocampal and striatal astrocytes showed more pronounced changes compared to cortical astrocytes. Corroborating previous data, they observed the most prominent class of upregulated genes upon aging was related to astrocyte reactivity, immune response and synapse elimination (Clarke et al., 2018).

Therefore, these studies have suggested that murine astrocytes undergo age-dependent changes in gene expression that may contribute to age-related synapse loss and neuroinflammation. Further, they reinforce the region-specificity of astrocyte responses to the aging process. Nevertheless, there is still a lack of evidence concerning the functional implications of these changes in gene expression to astrocyte function and cellular interplays in aging. Moreover, whether human astrocytes behave similarly to their murine counterparts is still a matter of discussion.

Within this context, Soreq and collaborators reported the first evidence of glial region-specific gene expression in the human brain aging, by analyzing ten different brain regions from the post-mortem human tissue of individuals aged from 16 to 102 years. They demonstrated that while a general upregulation of microglial and endothelial genes was observed upon aging in all brain regions analyzed; astrocyte- and oligodendrocyte-specific genes showed a more complex shift in their expression pattern, prominently observed in the hippocampus and substantia nigra (SN). On the other hand, these changes were not evident for the neuron-specific genes

(Soreq et al., 2017). Altogether, these data might suggest another view on the concept of "selective vulnerability" in aging and age-related diseases; a concept that primarily refers to an increased vulnerability of specific brain regions or groups of cells to a pathological state or injury. The vulnerability of neuronal populations has been mainly studied and characterized in neurodegenerative diseases, as reviewed by other works (Saxena and Caroni, 2011; Fu et al., 2018). However, recently new evidence has pointed that major changes in the transcriptional profile and function of glial cells might also contribute to predict the human brain aging and to understand the selective region-specific vulnerability in these age-related neurodegenerative diseases.

Neurodegenerative Diseases

During the last decades, a growing number of evidence has suggested that astrocytes and microglia play a key role in synaptic dysfunction, neuronal loss and cognitive impairments associated with several neurodegenerative diseases, such as AD; ALS, HD and PD. Interestingly, changes in astrocytes arise early in the course of these conditions and most prominently in specific brain regions known to be primarily vulnerable to a particular pathology. However, the cellular and molecular basis that define the selective vulnerability of specific regions in neurodegenerative diseases remain poorly understood. Understanding astrocyte heterogeneity in this context certainly represents an important step to unveil the mechanisms underlying the onset and progression of neurodegenerative diseases.

In this section, we will discuss recent studies on how astrocytes' changes and heterogeneity might impact in the onset of two neurodegenerative diseases, AD and PD.

Alzheimer's Disease

AD is the most common cause of dementia and one of the main public health concerns nowadays (Scheltens et al., 2016). According to the WHO a considerable increase in incidence of dementia and age-related diseases, especially AD, is expected for the next few years. Within this context, many efforts have been done to better elucidate the mechanisms involved in AD pathology and unveil possible cellular and molecular targets for diagnosis, prevention and/or therapy.

Clinically, AD is characterized by cognitive deficits, mainly represented by learning impairments and memory loss. Histopathologically, the two major hallmarks of AD are extracellular amyloid plaques (APs) depositions, composed of amyloid β (Aβ) peptides, and intracellular neurofibrillary tangles, constituted by hyperphosphorylated Tau protein (Ballard et al., 2011). Initially, it was thought that Aβ deposition would be the primary event in AD pathology, triggering neurofibrillary tangle formation and neuronal death, which led to the "amyloid cascade hypothesis" (Hardy and Higgins, 1992). However, it has been demonstrated that the most neurotoxic forms of Aβ are their soluble ligands, Aβ oligomers (AβOs), shedding light on the "Aβ oligomer hypothesis" (Lambert et al., 1998).

AβOs accumulate at early stages in AD pathology, before plaque formation, and clinical symptoms, in humans and animal models (Gong et al., 2003; Noguchi et al., 2009; Pham et al., 2010; Lesné et al., 2013). Currently, it is well known that AβOs induce memory impairment, disruption of long-term potentiation (LTP) and long-term depression (LTD; Townsend et al., 2006; Shankar et al., 2008), synapse dysfunction and loss (Brito-Moreira et al., 2017; Diniz et al., 2017), oxidative stress (Sponne et al., 2003; De Felice et al., 2007), endoplasmic reticulum (ER) stress (Umeda et al., 2011; Lourenco et al., 2013) and neuroinflammation (Forny-Germano et al., 2014).

AD pathology initiates in a region-specific manner, meaning that specific brain regions or group of cells are more vulnerable to AD than others. The selective vulnerability of neuronal populations has been better elucidated and reported in the EC, subiculum and the hippocampal CA1 region (Reilly et al., 2003; Stranahan and Mattson, 2010), but also in the basal forebrain (Whitehouse et al., 1982) and locus coeruleus (Bondareff et al., 1987). For a more complete view on neuronal selective vulnerability we recommend additional review (Fu et al., 2018). Besides neuronal contribution, several evidences have shown that glial changes are also present early, before neuronal death and clinical symptoms, during the pathogenesis of AD.

The likely involvement of astrocytes in AD pathology has been already reported by Alzheimer (1910), through the observation of association between glial cells and senile plaques in demented brains (Alzheimer, 1910; Verkhratsky et al., 2010). Subsequent studies have shown that astrocytes undergo complex morphological, transcriptional and functional alterations in AD. Morphologically, astrocytes may become either atrophic or hypertrophic depending on the stage of the disease and proximity to APs depositions (Rodríguez-Arellano et al., 2016; **Figure 2**).

Astrocyte atrophy has been observed during early stages of AD pathology as well as in non-plaque associated astrocytes along disease progression in the EC, medial prefrontal cortex, dentate gyrus and CA1 hippocampal region in 3xTg-AD mouse model (Olabarria et al., 2010; Kulijewicz-Nawrot et al., 2012; Yeh, 2013), PDAPP-J20 transgenic mice (Beauquis et al., 2013), and in CA1 of adult mice intracerebroventricularly injected with AβOs (Diniz et al., 2017). The functional meaning of this observation is still a matter of discussion. A possibility is that a reduction in astrocyte territorial domains might result in diminished synaptic coverage and impaired neuro-vascular unit; two important features that might be involved in synaptic dysfunction and loss of metabolic support at early stages of AD. Nevertheless, the underlying mechanisms of astrocyte atrophy as well as the functional impact of that to the onset of AD pathology have not been completely elucidated so far.

Within this context, recent data from our group have reinforced that astrocytes are targets for AβOs and that these neurotoxins induce molecular and functional changes in these cells, leading to astrocyte activation and impairments in their synaptogenic and synaptical-protective capacity (Diniz et al., 2017). We showed that AβOs rapidly interacted with astrocytes and triggered astrocyte activation *in vitro*. Further, the intracerebroventricular injection of AβOs in adult mice acutely induced astrocyte atrophy in the CA1 hippocampal region, as observed by reduced number of primary processes, area and

intensity of GFAP per cell. Following these changes, we verified that AβOs reduced the levels of TGF-β1 in astrocytes, an event that was related to an impairment in the synaptogenic and neuroprotective potential of astrocytes (Diniz et al., 2017). These data together with the fact that TGF-β1 is an important cytokine that promotes inhibitory and excitatory synapse formation in the CNS (Diniz et al., 2012, 2014b; Araujo et al., 2016), shed light on a new possible mechanism involved in synapse dysfunction and loss at early stages of AD pathology, mediated by astrocytes.

In contrast, many evidences have shown that during later stages of AD, astrocytes nearby plaques become highly hypertrophic and produce increased levels of GFAP (Olabarria et al., 2010; Heneka et al., 2015). Such features have also been observed in post-mortem human brain tissue, which seems to accompany the Braak stage progression (Simpson et al., 2010; Kamphuis et al., 2014). In addition, a transcriptomic analysis of astrocytes isolated from aged APPswe/PS1dE9 transgenic AD mice revealed that these cells acquired a pro-inflammatory phenotype, as well as a less supportive capacity to neuronal communication, represented by reduced expression of genes involved in that process (Orre et al., 2014). Altogether, these evidences suggest that the reactive phenotype of astrocytes in AD might contribute to neuroinflammation, synaptic deficits and neuronal dysfunctions during disease progression. Interestingly, a recent study has corroborated that hypothesis through the genetic inhibition of astrocyte reactivity in an AD mouse model. Ceyzériat et al. (2018) have shown that the inhibition of the astrocytic janus kinase 2 (JAK2)/signal transducer and activator of transcription 3 (STAT3) pathway efficiently controlled the reactivity of these cells in the hippocampus of AD mice, which was followed by a reduction in amyloid deposition, synaptic deficits and spatial learning improvements.

Therefore, altogether, these data strongly point to the key involvement of reactive astrocytes in the progression of AD pathology, revealing their detrimental actions on neuronal communication and cognitive performance. Nevertheless, apart from being the two major hallmarks of astrocyte reactivity, it remains elusive the functional meaning of astrocyte hypertrophy and upregulation of GFAP levels at later stages of AD.

Furthermore, since these alterations are mostly reported in vulnerable brain regions to AD pathology, in which neuronal degeneration is mainly observed, it is possible that astrocyte heterogeneity plays a role in this selective vulnerability. It has been suggested that the pre-clinical stage of AD begins decades before clinical symptoms, which is called the cellular phase of AD pathology (De Strooper and Karran, 2016). During this phase, extensive changes occur in glial cells and vasculature, which may orchestrate subsequent neuronal deficits. In fact, Soreq et al. (2017) have found that age-related changes in gene expression profile of astrocytes take place particularly in the hippocampus and SN in human tissue, two regions primarily affected during the pathogenesis of AD and PD. Therefore, these observations strengthen the likely involvement of astrocyte heterogeneity to the regional selective vulnerability in AD onset and progression. However, a direct link between astrocytes morphological/molecular changes to functional alterations still remains to be determined.

Parkinson's Disease

PD is the second most common type of neurodegenerative disease, affecting 2%–3% of the elderly population. Similarly to AD, the majority of PD cases is sporadic, while less than 10% are associated to genetic causes (Poewe et al., 2017). Clinically, PD is primarily characterized by motor abnormalities, mainly represented by tremor at rest, rigidity, bradykinesia and postural

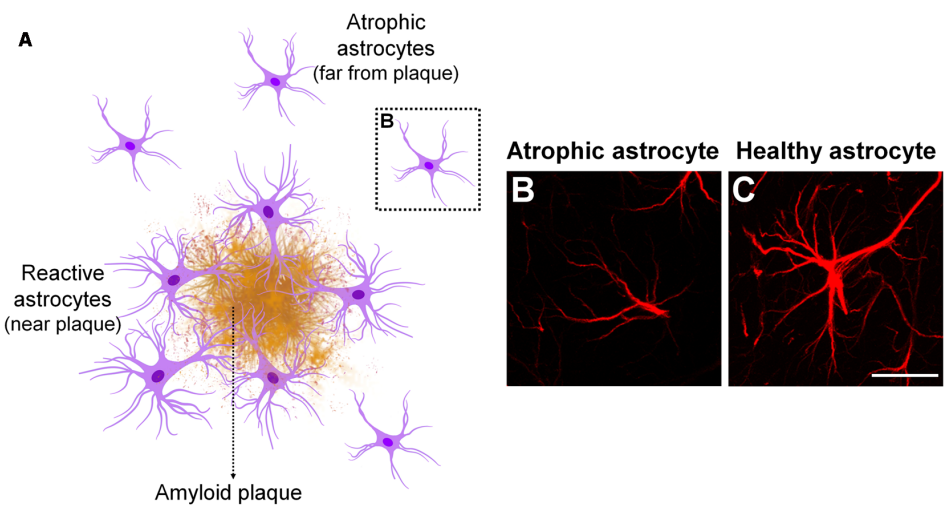

FIGURE 2 | Astrocyte phenotype in Alzheimer's disease (AD). In AD pathology, morphological changes in astrocytes depend on the stage of disease and proximity to amyloid plaques (APs; **A**). Astrocyte atrophy occurs at early stages of AD, before plaque formation, as well as in non-plaque associated astrocytes at later stages of disease **(B)**. Atrophic astrocytes present reduced number and thinner cellular processes, which is accompanied by diminished volume and somata volume, compared to healthy or resting astrocytes **(C)**. Astrocyte hypertrophy is mainly observed in astrocytes surrounding APs at later stages of AD. They show opposite features in comparison to atrophic astrocytes.

instability (Jankovic, 2008), symptoms that have been linked to a progressive and selective degeneration of dopaminergic neurons in SN pars compacta (SNpc) during early stages of the disease (Dauer and Przedborski, 2003). However, several other CNS and peripheral nervous system (PNS) structures are also affected early or during the disease progression, a fact that is responsible for the non-motor symptoms of PD, which include, for example, autonomic dysfunction, olfactory deficits and cognitive decline (Schapira et al., 2017).

Histopathologically, aggregates of the synaptic protein α-synuclein are usually found in the cell bodies and neurites, called respectively Lewy bodies and Lewy neurites, in specific classes of neurons in several brain regions in all PD patients (Poewe et al., 2017). Although it is still debated, Braak et al. (2003) have proposed that Lewy bodies' pathology spread from one region to another following a specific and predictive progression during the course of PD. Interestingly, more recently it has been suggested a prion-like propagation of α-synuclein aggregates. In this hypothesis, α-synuclein might be transmitted from neuron to neuron, along axons, secreted into the extracellular space and internalized by neighboring cells, including neurons and glial cells. Once internalized, it may induce the aggregation of the native proteins in the host, contributing and exacerbating the aggregate spreading (Brundin et al., 2010). Although this hypothesis has been proven in both *in vitro* and *in vivo* models (Desplats et al., 2009; Hansen et al., 2011), it remains to be determined whether this mechanism explains the spreading of Lewy's body pathology in humans.

Several lines of evidence have shown that impairments in α-synuclein proteostasis strongly contribute to PD pathogenesis, as well as may impact other cellular pathways and functions also implicated in PD, such as mitochondria dysfunction, oxidative stress and neuroinflammation (Poewe et al., 2017). Moreover, astrocytes and microglia seem to play an important role in all of these pathological mechanisms, contributing to PD onset and progression (Halliday and Stevens, 2011).

Astrocytes accumulate α-synuclein aggregates in the SN and extra nigral regions in patients with PD, which is correlated with the severity of neuronal loss (Wakabayashi et al., 2000). Interestingly, it has also been reported that particularly protoplasmic astrocytes presented inclusions of protein aggregates in PD, which was not observed in fibrous astrocytes (Song et al., 2009). Braak et al. (2007) have shown that α-synuclein immunoreactive astrocytes are present in several brain regions of PD patients, which appears to accompany the formation of Lewy bodies and neurites. Moreover, these immunoreactive astrocytes were also found in the striatum and dorsal thalamus, regions where Lewy's bodies do not develop, suggesting that astrocytes might internalize α-synuclein released by dysfunctional axon terminals in these regions. This is supported by observations that astrocytes can take up α-synuclein released by neurons, which, in turns, induce gene expression changes in astrocytes, mainly represented by an up-regulation of pro-inflammatory genes (Lee et al., 2010). Conversely, an *in vitro* study has proposed that human astrocytes are similarly able to transfer aggregated α-synuclein to neighboring astrocytes, *via* direct contact and tunneling nanotubes (TNTs; Rostami et al., 2017). Moreover, accumulation of α-synuclein in astrocytes may impair their lysosomal-autophagosomal machinery as well as lead to ER swelling and mitochondria damage (Rostami et al., 2017). Nevertheless, it remains to be investigated whether these events also occur *in vivo* and their overall impact to the aggregate spreading in PD pathology.

The direct functional impact of non-cell autonomous mechanisms on neurodegeneration in PD has been reported in mouse models in which solely astrocytes expressed PD-related A53T α-synuclein mutation. In this case, α-synuclein aggregation in astrocytes resulted in severe astrogliosis, disruption in the BBB and down-regulation of glutamate transporters. Moreover, microglial activation was also pronounced especially in the brainstem and SN, in which neuronal loss occurred (Gu et al., 2010). Additional studies have unraveled the molecular mechanisms underlying astrocyte and microglia activation in PD. The treatment of astroglial and microglial cell cultures with recombinant α-synuclein induced cell activation, as observed by a strong inflammatory response and production of reactive oxygen species (ROS), effects dependent on Toll-like receptor 4 (TLR4) activation in both cell types. Further, the ablation of TLR4 in α-synuclein-treated microglia and astrocytes suppressed their pro-inflammatory response, although the uptake of α-synuclein by astrocytes was independent of TLR4 (Fellner et al., 2013; Rannikko et al., 2015). These studies have shed light on new signaling pathways involved in α-synuclein-induced neuroinflammation in PD, as well as the key role of glial cells in disease progression.

Although the underlying mechanisms involved in PD pathology have been extensively investigated, there is still a lack of evidence concerning the cellular and molecular determinants of regional selective vulnerability in PD. Curiously, as discussed above, astrocytes changes are largely present in regions primarily affected during the onset of PD in humans (Wakabayashi et al., 2000; Braak et al., 2007); further, the non-cell autonomous mechanisms of dopaminergic neuronal loss have also been proved in PD animal models (Gu et al., 2010; Booth et al., 2017). However, although these evidences point to the likely involvement of astrocytes in PD, they still do not explain why degeneration begins at specific brain regions. Within this context, new studies on the inter-regional molecular heterogeneity of astrocytes have shed light on the role of these cells in predicting the human brain aging, with implications to age-related diseases, such as PD.

Notably, it has been shown that the main age-related shifts in gene expression profile of astrocytes occur in the hippocampus and SN from post-mortem human tissue (Soreq et al., 2017). Since the aging process is a risk factor for PD, it is possible that the glial alterations in SN along aging may play a role in determining the selective vulnerability of this region to PD.

Recently, an outstanding study has strengthened the role of astrocyte-microglia interplay in PD pathology. It is well known that the state of microglia activation may have a direct impact on the astrocyte phenotype in different pathologies (Liddelow and Barres, 2017; Shinozaki et al., 2017). Recently,

this hypothesis was strongly demonstrated for PD. By using the agonist of the glucagon-like peptide-1 receptor (GLP1R), NLY01, the authors control the pro-inflammatory profile of microglia treated with α-synuclein preformed fibrils (α-syn PFF) *in vitro*. NLY01 pre-treatment indirectly controls astrocyte reactivity by reducing microglial secretion of molecules involved in astrogliosis, such as IL-1β, TNF-α and C1q. Similarly, astrocyte reactivity in the ventral midbrain was inhibited in PD mice pre-treated with NLY01. These effects were accompanied by a prevention of dopaminergic neuronal loss, reduced dopamine levels and motor deficits in PD mice (Yun et al., 2018).

Several evidences have highlighted the key involvement of glial cells in neurodegenerative diseases. However, many unanswered questions remain concerning the contribution of glial cells to the selective vulnerability of the nervous system to these diseases. Altogether, elucidating the molecular and functional heterogeneity of astrocytes arise as a fundamental step to understand the underlying mechanisms of age-related cognitive decline and associated neurodegenerative diseases. Further, it might reveal new therapeutic targets to modulate astrocyte phenotype in order to prevent and/or delay these processes.

FUTURE DIRECTIONS: GLIAL CELLS AS NOVEL TARGETS FOR THERAPEUTIC STRATEGIES

Astrocyte reactivity is a common feature in aging and age-related diseases. As discussed in this review article, although its functional implications are not completely understood yet, new evidence have suggested that reactive astrocytes comprise a heterogeneous group constituted by subpopulations of astrocytes that may differ from each other in terms of molecular signature, function and response to several physiological and pathological stimuli. These cells can undergo atrophy and hypertrophy amongst other changes according to the insult (**Figure 3**), therefore altering their functions in the region.

Differently from previously thought, astrocyte reactivity is not just a hallmark of aging and brain diseases, but a key mechanism involved in the pathogenesis and progression of these conditions. It is worth noting that, as there is a crosstalk between microglia and astrocytes, these cells can greatly influence each other's phenotype (for review see Jha et al., 2018), therefore, by modulating microglia phenotypes, it would be possible to change the way astrocytes respond to injury and disease as well. As described before, microglia can respond to inflammatory insults by becoming activated and influence astrocyte's response by secreting cytokines and complement cascade molecules such as TNF-α and C1q (Liddelow et al., 2017), and during aging, extensive neuroinflammation is also observed (Franceschi et al., 2000). Therefore, as it can determine the fate of astrocytes, it is important to consider microglia when designing new drugs that could modulate astrocyte's phenotypes, especially as the modulation of microglia towards an anti-inflammatory phenotype may provide neuroprotective effects, contributing to the recovery of the diseased brain (Cherry et al., 2014; Song and Suk, 2017). Suk (2017), suggested that more importantly than blocking glial cells reactivity, the focus should be on new strategies that could modulate glial cells activated phenotype.

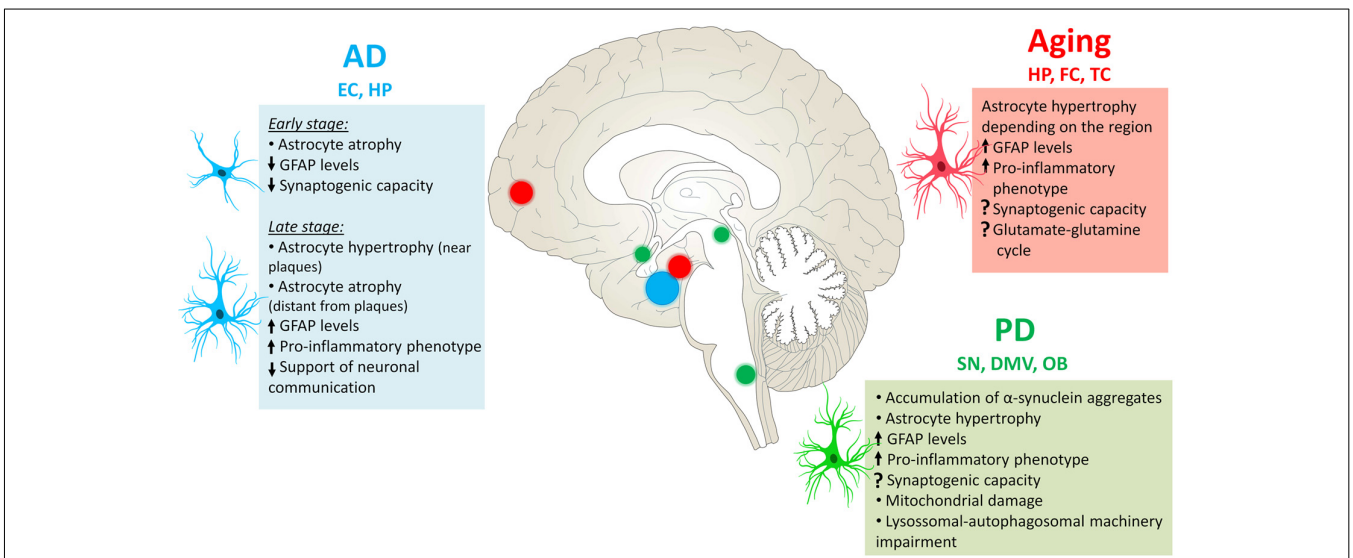

FIGURE 3 | Astrocytes' changes in aging and neurodegenerative diseases. During the physiological aging, astrocytes in the hippocampus (HP), frontal cortex (FC) and temporal cortex (TC) become reactive, with increased levels of GFAP and pro-inflammatory phenotype. In AD, astrocyte reactivity is mainly observed in the entorhinal cortex (EC) and HP, where these cells can be either atrophic or hypertrophic depending on the stage of the disease and their proximity to AP. In Parkinson's disease (PD), astrocytes accumulate α-synuclein aggregates in several CNS regions, particularly in the substantia nigra (SN) and extra-nigral regions affected in PD pathology, such as the dorsal motor nucleus of the vagus (DMV) and olfactory bulb (OB). The functional changes exposed here are not necessarily observed in all mentioned regions, more information can be found in the text.

Thus, modulation of astrocyte reactivity state emerged as an important venue for the development of new preventive and therapeutic strategies (Yun et al., 2018). Within this context, molecules and compounds, including natural or synthetics, able to control astrocyte reactivity and function have been viewed as potential drugs to neurodegenerative diseases.

Within the natural compounds, the biggest class of polyphenols in nature and also in the human diet comprises the flavonoids. These molecules are ubiquitously found in vegetables, cereals, fruits, tea, chocolate and wine (Tsao, 2010). Epidemiological studies have shown that the long-term consumption of polyphenols is associated to a reduced risk in developing cardiovascular diseases, diabetes, cancer, and neurodegenerative diseases (Arts and Hollman, 2005; Graf et al., 2005).

The consumption of polyphenol-rich diets has been linked to an enhanced cognitive performance and delay in age-related cognitive decline in humans (Devore et al., 2012; Brickman et al., 2014). In agreement, the administration of flavonoids or polyphenol-rich extracts may promote learning and memory improvements in aged animals (Zeng et al., 2012; Bensalem et al., 2018), as well as in several mouse models for neurodegenerative diseases, including AD (Zhang et al., 2014), ALS (Koh et al., 2006) and PD (Rojas et al., 2012), for review see (Solanki et al., 2015). However, the cellular and molecular mechanisms underlying the flavonoids actions are still not fully understood. Besides their remarkable antioxidant effect, flavonoids can also directly interact with cellular receptors as well as modulate signaling pathways in neurons and glial cells (Williams and Spencer, 2012).

Due to the prominent involvement of astrocyte reactivity/inflammation in aging and neurodegenerative diseases, a growing number of studies has pointed that these cells may be important targets for the natural compounds in the CNS (Matias et al., 2016). Strikingly, flavonoids have been also reported to modulate astrocyte reactivity and hence attenuating neuroinflammation. It has been shown that the flavonoids luteolin and quercetin were able to inhibit IL-1β-induced astrocyte activation, which was characterized by a reduced secretion of pro-inflammatory cytokines and chemokines, such as IL-6, IL-8, IP-10, MCP-1, an up-regulation of antioxidant enzymes, SOD1 and thioredoxin (TRX1), as well as an down-regulation of the GFAP levels in astrocytes (Sharma et al., 2007). In agreement, Bahia et al. (2008) demonstrated that the flavonoid (−) epicatechin specifically induced the activation of the antioxidant response element (ARE) pathway in astrocytes, which was followed by an increase in the glutathione (GSH) levels, an important antioxidant enzyme.

Furthermore, the pre-treatment of glial cell cultures (astrocytes and microglia) with the flavonoids naringenin, hesperidin, (+)-catechin or (−)-epicatechin significantly attenuated the production of TNF-α by these cells when exposed to LPS/interferon-γ (IFN-γ). Most prominently, naringenin not only reduced glial cell activation, but also promoted neuronal survival in a co-culture system with neurons and glia (Vafeiadou et al., 2009). Altogether, these studies have pointed that the modulation of astrocyte reactivity may have an indirect beneficial effect on neuronal physiology.

Further effects of flavonoids in controlling astrocyte reactivity have also been suggested by other groups in animal models of aging and neurodegenerative diseases. Aged rats treated with the polyphenol resveratrol showed increased neurogenesis and microvasculature and reduced astrocyte hypertrophy, as well as more ramified microglia (non-activated) within different hippocampal regions. These effects were accompanied by improvement in memory performance (Kodali et al., 2015).

In APPswe/PS1dE9 double transgenic AD mouse model, the long-term oral administration of fisetin significantly reduced astrocyte reactivity, mainly observed by a reversal of astrocyte hypertrophy and a down-regulation of the GFAP levels in AD mice (Currais et al., 2014). Similar results have also been observed in p25Tg AD mouse model treated with the phenolic compound Curcumin (Sundaram et al., 2017).

Data from our group have recently suggested beneficial effects of flavonoids also in the healthy brain. We have shown that hesperidin and casticin increased the neuroprotective potential of astrocytes *in vitro*, by modulating the secretion of protective factors (de Sampaio e Spohr et al., 2010; Nones et al., 2012). Although the identity of those factors is not fully characterized, further studies have suggested a number of neurotrophic factors that might be target for the flavonoids' actions. A screening of thirty-three different flavonoids revealed that calycosin, isorhamnetin, luteolin, and genistein were more promising in inducing the synthesis and secretion of the nerve growth factor (NGF), glial-derived neurotrophic factor (GDNF), and BDNF by astrocytes in culture (Xu et al., 2013).

More recently, our group raised evidences of the beneficial effects of the flavonoids in the healthy brain *in vivo*. The treatment of adult mice with the flavanone hesperidin induced improvements in memory performance, which were accompanied by increased synaptic density in the hippocampal CA1 region, as well as activation of the TGF-β pathway in the same region. We also showed that hesperidin was able to enhance the synaptogenic potential of astrocytes, by modulating the TGF-β1 pathway and levels (Matias et al., 2017), a pathway previously involved in the regulation of synapse formation in the CNS (Diniz et al., 2014a). Deficits in this pathway is implicated in neurodegenerative diseases, including AD (Diniz et al., 2017, 2018). Whether the effect of hesperidin/TGF-β1 in astrocytes and thus in cognitive decline is related to their anti-inflammatory activities or not, remains to be elucidated. Nevertheless, modulation of the astrocytic TGF-β1 pathway might arise as a valuable strategy in promoting cognitive improvements in both physiological and pathological contexts. Based on that, targeting of specific signaling pathways that modulates astrocyte phenotypes emerged as a promise therapeutic strategy.

Recently, modulation of the JAK/STAT3 pathway has been shown as a useful strategy to control astrocyte reactivity *in vivo*. By specifically inhibiting the astrocytic JAK/STAT3 activation in an AD mouse model, Ceyzériat et al. (2018) reduced astrocytes reactivity and amyloid deposition, thus leading to improvements in their cognitive performance. Similarly, as previously discussed, block of A1 astrocyte conversion by microglia by the agonist

(NLY01) of the GLP1R has proven to be neuroprotective in models of PD. The treatment of PD mouse models with NLY01 significantly prevented the dopaminergic neuronal loss in the ventral midbrain, restored dopamine levels as well as ameliorated the motor deficits observed in PD mice (Yun et al., 2018). Despite all the new advances, there are still many unanswered questions in this field, such as "Is it possible to convert a neurotoxic reactive astrocyte in a neuroprotective one?"; "Are the human astrocytes more diverse in terms of reactive phenotypes?"; "Are the mechanisms involved in the induction of A1 and A2 astrocytes similar in different species, such as rodents and humans?".

In addition, due to the large genetic variability in human population and the fact that human astrocytes are unique in terms of morphological and functional complexity (Colombo et al., 1995; Oberheim et al., 2009), new studies are needed to investigate whether our knowledge on murine astrocytes can be applied to their human counterparts. Interestingly, a new study has shown that changes in astrocyte gene signature may have functional implications to the age-related cognitive decline as well as may predict the human aging with greater precision than the neuron gene signature. Curiously, these changes were more evident in the hippocampus and substantia nigra, regions where AD and PD pathology seem to begin. Therefore, they have highlighted the likely involvement of human astrocyte heterogeneity in predicting the regional selective vulnerability in aging and age-related diseases, such as AD and PD.

Altogether, the fact that astrocyte reactivity and dysfunction play a key role in AD and PD pathology make these cells interesting targets for the actions of synthetic and natural compounds in ameliorating cognitive performance or even restoring brain function in disease contexts, based on astrocyte biology.

AUTHOR CONTRIBUTIONS

All authors wrote sections of the manuscript and contributed to manuscript revision. All authors approved the submitted version of the manuscript.

FUNDING

This work was supported by grants from Conselho Nacional de Desenvolvimento Científico e Tecnológico (CNPq), Coordenação de Aperfeiçoamento de Pessoal de Nível Superior (CAPES), Departamento de Ciência e Tecnologia do Ministério da Saúde (Decit), and Fundação Carlos Chagas Filho de Amparo à Pesquisa do Estado do Rio de Janeiro (FAPERJ).

REFERENCES

Alzheimer, A. (1910). "Beiträge zur kenntnis der pathologischen neuroglia und ihrer beziehungen zu den Abbauvorgängen im nervengewebe," in *Histologische und Histopathologische Arbeiten über die Grosshirnrinde mit Besonderer Berücksichtigung der Pathologischen Anatomie der Geisteskrankheiten*, eds F. Nissl and A. Alzheimer (Jena: Gustav Fischer), 401–562.

Anderson, M. A., Ao, Y., and Sofroniew, M. V. (2014). Heterogeneity of reactive astrocytes. *Neurosci. Lett.* 565, 23–29. doi: 10.1016/j.neulet.2013.12.030

Anderson, M. A., Burda, J. E., Ren, Y., Ao, Y., O'Shea, T. M., Kawaguchi, R., et al. (2016). Astrocyte scar formation AIDS central nervous system axon regeneration. *Nature* 532, 195–200. doi: 10.1038/nature17623

Andriezen, W. L. (1893). The neuroglia elements in the human brain. *Br. Med. J.* 2, 227–230. doi: 10.1136/bmj.2.1700.227

Anlauf, E., and Derouiche, A. (2013). Glutamine synthetase as an astrocytic marker: its cell type and vesicle localization. *Front. Endocrinol.* 4:144. doi: 10.3389/fendo.2013.00144

Araque, A., and Navarrete, M. (2010). Glial cells in neuronal network function. *Philos. Trans. R. Soc. Lond. B Biol. Sci.* 365, 2375–2381. doi: 10.1098/rstb.2009.0313

Araque, A., Carmignoto, G., Haydon, P. G., Oliet, S. H. R., Robitaille, R., and Volterra, A. (2014). Gliotransmitters travel in time and space. *Neuron* 81, 728–739. doi: 10.1016/j.neuron.2014.02.007

Araque, A., Parpura, V., Sanzgiri, R. P., and Haydon, P. G. (1999). Tripartite synapses: glia, the unacknowledged partner. *Trends Neurosci.* 22, 208–215. doi: 10.1016/s0166-2236(98)01349-6

Araujo, A. P., Diniz, L. P., Eller, C. M., de Matos, B. G., Martinez, R., and Gomes, F. C. (2016). Effects of transforming growth factor β 1 in cerebellar development: role in synapse formation. *Front. Cell. Neurosci.* 10:104. doi: 10.3389/fncel.2016.00104

Arts, I. C., and Hollman, P. C. (2005). Polyphenols and disease risk in epidemiologic studies. *Am. J. Clin. Nutr.* 81, 317S–325S. doi: 10.1093/ajcn/81.1.317s

Bahia, P. K., Rattray, M., and Williams, R. J. (2008). Dietary flavonoid (−)epicatechin stimulates phosphatidylinositol 3-kinase-dependent anti-oxidant response element activity and up-regulates glutathione in cortical astrocytes. *J. Neurochem.* 106, 2194–2204. doi: 10.1111/j.1471-4159.2008.05542.x

Ballard, C., Gauthier, S., Corbett, A., Brayne, C., Aarsland, D., and Jones, E. (2011). Alzheimer's disease. *Lancet* 377, 1019–1031. doi: 10.1016/S0140-6736(10)61349-9

Beauquis, J., Pavia, P., Pomilio, C., Vinuesa, A., Podlutskaya, N., Galvan, V., et al. (2013). Environmental enrichment prevents astroglial pathological changes in the hippocampus of APP transgenic mice, model of Alzheimer's disease. *Exp. Neurol.* 239, 28–37. doi: 10.1016/j.expneurol.2012.09.009

Bensalem, J., Dudonne, S., Gaudout, D., Servant, L., Calon, F., Desjardins, Y., et al. (2018). Polyphenol-rich extract from grape and blueberry attenuates cognitive decline and improves neuronal function in aged mice. *J. Nutr. Sci.* 7:e19. doi: 10.1017/jns.2018.10

Bianchini, D., De Martini, I., Cadoni, A., Zicca, A., Tabaton, M., Schenone, A., et al. (1992). GFAP expression of human Schwann cells in tissue culture. *Brain Res.* 570, 209–217. doi: 10.1016/0006-8993(92)90583-u

Bignami, A., and Dahl, D. (1976). The astroglial response to stabbing. Immunofluorescence studies with antibodies to astrocyte-specific protein (GFA) in mammalian and submammalian vertebrates. *Neuropathol. Appl. Neurobiol.* 2, 99–110. doi: 10.1111/j.1365-2990.1976.tb00488.x

Boisvert, M. M., Erikson, G. A., Shokhirev, M. N., and Allen, N. J. (2018). The aging astrocyte transcriptome from multiple regions of the mouse brain. *Cell Rep.* 22, 269–285. doi: 10.1016/j.celrep.2017.12.039

Bondareff, W., Mountjoy, C. Q., Roth, M., Rossor, M. N., Iversen, L. L., Reynolds, G. P., et al. (1987). Neuronal degeneration in locus ceruleus and cortical correlates of Alzheimer disease. *Alzheimer Dis. Assoc. Disord.* 1, 256–262. doi: 10.1097/00002093-198701040-00005

Booth, H. D. E., Hirst, W. D., and Wade-Martins, R. (2017). The role of astrocyte dysfunction in Parkinson's disease pathogenesis. *Trends Neurosci.* 40, 358–370. doi: 10.1016/j.tins.2017.04.001

Braak, H., Del Tredici, K., Rub, U., de Vos, R. A., Jansen Steur, E. N., and Braak, E. (2003). Staging of brain pathology related to sporadic Parkinson's disease. *Neurobiol. Aging* 24, 197–211. doi: 10.1016/s0197-4580(02)00065-9

Braak, H., Sastre, M., and Del Tredici, K. (2007). Development of α-synuclein immunoreactive astrocytes in the forebrain parallels stages of intraneuronal pathology in sporadic Parkinson's disease. *Acta Neuropathol.* 114, 231–241. doi: 10.1007/s00401-007-0244-3

Brambilla, R., Hurtado, A., Persaud, T., Esham, K., Pearse, D. D., Oudega, M., et al. (2009). Transgenic inhibition of astroglial NF-κB leads to increased axonal sparing and sprouting following spinal cord injury. *J. Neurochem.* 110, 765–778. doi: 10.1111/j.1471-4159.2009.06190.x

Brickman, A. M., Khan, U. A., Provenzano, F. A., Yeung, L. K., Suzuki, W., Schroeter, H., et al. (2014). Enhancing dentate gyrus function with dietary flavanols improves cognition in older adults. *Nat. Neurosci.* 17, 1798–1803. doi: 10.1038/nn.3850

Brito-Moreira, J., Lourenco, M. V., Oliveira, M. M., Ribeiro, F. C., Ledo, J. H., Diniz, L. P., et al. (2017). Interaction of amyloid-β (Aβ) oligomers with neurexin 2α and neuroligin 1 mediates synapse damage and memory loss in mice. *J. Biol. Chem.* 292, 7327–7337. doi: 10.1074/jbc.m116.761189

Brundin, P., Melki, R., and Kopito, R. (2010). Prion-like transmission of protein aggregates in neurodegenerative diseases. *Nat. Rev. Mol. Cell Biol.* 11, 301–307. doi: 10.1038/nrm2873

Buosi, A. S., Matias, I., Araujo, A. P. B., Batista, C., and Gomes, F. C. A. (2018). Heterogeneity in synaptogenic profile of astrocytes from different brain regions. *Mol. Neurobiol.* 55, 751–762. doi: 10.1007/s12035-016-0343-z

Bushong, E. A., Martone, M. E., Jones, Y. Z., and Ellisman, M. H. (2002). Protoplasmic astrocytes in CA1 stratum radiatum occupy separate anatomical domains. *J. Neurosci.* 22, 183–192. doi: 10.1523/jneurosci.22-01-00183.2002

Cahoy, J. D., Emery, B., Kaushal, A., Foo, L. C., Zamanian, J. L., Christopherson, K. S., et al. (2008). A transcriptome database for astrocytes, neurons, and oligodendrocytes: a new resource for understanding brain development and function. *J. Neurosci.* 28, 264–278. doi: 10.1523/JNEUROSCI.4178-07.2008

Cammer, W. (1990). Glutamine synthetase in the central nervous system is not confined to astrocytes. *J. Neuroimmunol.* 26, 173–178. doi: 10.1016/0165-5728(90)90088-5

Cerbai, F., Lana, D., Nosi, D., Petkova-Kirova, P., Zecchi, S., Brothers, H. M., et al. (2012). The neuron-astrocyte-microglia triad in normal brain ageing and in a model of neuroinflammation in the rat hippocampus. *PLoS One* 7:e45250. doi: 10.1371/journal.pone.0045250

Ceyzériat, K., Haim, L. B., Denizot, A., Pommier, D., Matos, M., Guillemaud, O., et al. (2018). Modulation of astrocyte reactivity improves functional deficits in mouse models of Alzheimer's disease. *Acta Neuropathol. Commun.* 6:104. doi: 10.1186/s40478-018-0606-1

Chai, H., Diaz-Castro, B., Shigetomi, E., Monte, E., Octeau, J. C., Yu, X., et al. (2017). Neural circuit-specialized astrocytes: transcriptomic, proteomic, morphological, and functional evidence. *Neuron* 95, 531.e9–549.e9. doi: 10.1016/j.neuron.2017.06.029

Cherry, J. D., Olschowka, J. A., and O'Banion, M. K. (2014). Neuroinflammation and M2 microglia: the good, the bad, and the inflamed. *J. Neuroinflammation* 11:98. doi: 10.1186/1742-2094-11-98

Chia, W.-J., Dawe, G. S., and Ong, W.-Y. (2011). Expression and localization of the iron-siderophore binding protein lipocalin 2 in the normal rat brain and after kainate-induced excitotoxicity. *Neurochem. Int.* 59, 591–599. doi: 10.1016/j.neuint.2011.04.007

Christopherson, K. S., Ullian, E. M., Stokes, C. C. A., Mullowney, C. E., Hell, J. W., Agah, A., et al. (2005). Thrombospondins are astrocyte-secreted proteins that promote CNS synaptogenesis. *Cell* 120, 421–433. doi: 10.1016/j.cell.2004.12.020

Chung, W. S., Allen, N. J., and Eroglu, C. (2015). Astrocytes control synapse formation, function, and elimination. *Cold Spring Harb. Perspect. Biol.* 7:a020370. doi: 10.1101/cshperspect.a020370

Chung, W. S., Clarke, L. E., Wang, G. X., Stafford, B. K., Sher, A., Chakraborty, C., et al. (2013). Astrocytes mediate synapse elimination through MEGF10 and MERTK pathways. *Nature* 504, 394–400. doi: 10.1038/nature12776

Chung, W.-S., Verghese, P. B., Chakraborty, C., Joung, J., Hyman, B. T., Ulrich, J. D., et al. (2016). Novel allele-dependent role for APOE in controlling the rate of synapse pruning by astrocytes. *Proc. Natl. Acad. Sci. U S A* 113, 10186–10191. doi: 10.1073/pnas.1609896113

Clarke, L. E., Liddelow, S. A., Chakraborty, C., Münch, A. E., Heiman, M., and Barres, B. A. (2018). Normal aging induces A1-like astrocyte reactivity. *Proc. Natl. Acad. Sci. U S A* 115, E1896–E1905. doi: 10.1073/pnas.1800165115

Colombo, E., and Farina, C. (2016). Astrocytes: key regulators of neuroinflammation. *Trends Immunol.* 37, 608–620. doi: 10.1016/j.it.2016.06.006

Colombo, J. A., Yáñez, A., Puissant, V., and Lipina, S. (1995). Long, interlaminar astroglial cell processes in the cortex of adult monkeys. *J. Neurosci. Res.* 40, 551–556. doi: 10.1002/jnr.490400414

Cunha, C., Santos, C., Gomes, C., Fernandes, A., Correia, A. M., Sebastião, A. M., et al. (2018). Downregulated glia interplay and increased miRNA-155 as promising markers to track ALS at an early stage. *Mol. Neurobiol.* 55, 4207–4224. doi: 10.1007/s12035-017-0631-2

Currais, A., Prior, M., Dargusch, R., Armando, A., Ehren, J., Schubert, D., et al. (2014). Modulation of p25 and inflammatory pathways by fisetin maintains cognitive function in Alzheimer's disease transgenic mice. *Aging Cell* 13, 379–390. doi: 10.1111/acel.12185

D'Ambrosio, R., Wenzel, J., Schwartzkroin, P. A., McKhann, G. M., and Janigro, D. (1998). Functional specialization and topographic segregation of hippocampal astrocytes. *J. Neurosci.* 18, 4425–4438. doi: 10.1523/jneurosci.18-12-04425.1998

D'Amelio, F., Eng, L. F., and Gibbs, M. A. (1990). Glutamine synthetase immunoreactivity is present in oligodendroglia of various regions of the central nervous system. *Glia* 3, 335–341. doi: 10.1002/glia.440030504

Dauer, W., and Przedborski, S. (2003). Parkinson's disease: mechanisms and models. *Neuron* 39, 889–909. doi: 10.1016/S0896-6273(03)00568-3

David, J. P., Ghozali, F., Fallet-Bianco, C., Wattez, A., Delaine, S., Boniface, B., et al. (1997). Glial reaction in the hippocampal formation is highly correlated with aging in human brain. *Neurosci. Lett.* 235, 53–56. doi: 10.1016/s0304-3940(97)00708-8

De Bock, M., Decrock, E., Wang, N., Bol, M., Vinken, M., Bultynck, G., et al. (2014). The dual face of connexin-based astroglial Ca^{2+} communication: a key player in brain physiology and a prime target in pathology. *Biochim. Biophys. Acta* 1843, 2211–2232. doi: 10.1016/j.bbamcr.2014.04.016

De Carlos, J. A., and Borrell, J. (2007). A historical reflection of the contributions of Cajal and Golgi to the foundations of neuroscience. *Brain Res. Rev.* 55, 8–16. doi: 10.1016/j.brainresrev.2007.03.010

De Felice, F. G., Velasco, P. T., Lambert, M. P., Viola, K., Fernandez, S. J., Ferreira, S. T., et al. (2007). Aβ oligomers induce neuronal oxidative stress through an N-methyl-D-aspartate receptor-dependent mechanism that is blocked by the Alzheimer drug memantine. *J. Biol. Chem.* 282, 11590–11601. doi: 10.1074/jbc.m607483200

de Sampaio e Spohr, T. C. L., Stipursky, J., Sasaki, A. C., Barbosa, P. R., Martins, V., Benjamim, C. F., et al. (2010). Effects of the flavonoid casticin from Brazilian Croton betulaster in cerebral cortical progenitors *in vitro*: direct and indirect action through astrocytes. *J. Neurosci. Res.* 88, 530–541. doi: 10.1002/jnr.22218

De Strooper, B., and Karran, E. (2016). The cellular phase of Alzheimer's disease. *Cell* 164, 603–615. doi: 10.1016/j.cell.2015.12.056

Desplats, P., Lee, H. J., Bae, E. J., Patrick, C., Rockenstein, E., Crews, L., et al. (2009). Inclusion formation and neuronal cell death through neuron-to-neuron transmission of α-synuclein. *Proc. Natl. Acad. Sci. U S A* 106, 13010–13015. doi: 10.1073/pnas.0903691106

Devore, E. E., Kang, J. H., Breteler, M. M., and Grodstein, F. (2012). Dietary intakes of berries and flavonoids in relation to cognitive decline. *Ann. Neurol.* 72, 135–143. doi: 10.1002/ana.23594

Dezonne, R. S., Stipursky, J., Araujo, A. P. B., Nones, J., Pavão, M. S. G., Porcionatto, M., et al. (2013). Thyroid hormone treated astrocytes induce maturation of cerebral cortical neurons through modulation of proteoglycan levels. *Front. Cell. Neurosci.* 7:125. doi: 10.3389/fncel.2013.00125

Di Castro, M. A., Chuquet, J., Liaudet, N., Bhaukaurally, K., Santello, M., Bouvier, D., et al. (2011). Local Ca^{2+} detection and modulation of synaptic release by astrocytes. *Nat. Neurosci.* 14, 1276–1284. doi: 10.1038/nn.2929

Diniz, L. P., Almeida, J. C., Tortelli, V., Lopes, C. V., Setti-Perdigão, P., Stipursky, J., et al. (2012). Astrocyte-induced synaptogenesis is mediated by transforming growth factor β signaling through modulation of D-serine levels in cerebral cortex neurons. *J. Biol. Chem.* 287, 41432–41445. doi: 10.1074/jbc.M112.380824

Diniz, L. P., Matias, I. C. P., Garcia, M. N., and Gomes, F. C. A. (2014a). Astrocytic control of neural circuit formation: highlights on TGF-β signaling. *Neurochem. Int.* 78, 18–27. doi: 10.1016/j.neuint.2014.07.008

Diniz, L. P., Tortelli, V., Garcia, M. N., Araujo, A. P., Melo, H. M., Silva, G. S., et al. (2014b). Astrocyte transforming growth factor β 1 promotes inhibitory synapse formation via CaM kinase II signaling. *Glia* 62, 1917–1931. doi: 10.1002/glia.22713

Diniz, L. P., Matias, I., Siqueira, M., Stipursky, J., and Gomes, F. C. A. (2018). Astrocytes and the TGF-β1 pathway in the healthy and diseased brain: a double-edged sword. *Mol. Neurobiol.* doi: 10.1007/s12035-018-1396-y [Epub ahead of print].

Diniz, L., Tortelli, V., Matias, I., Morgado, J., Bérgamo Araujo, A. P., Melo, H. M., et al. (2017). Astrocyte TGF-β1 protects synapses against Aβ oligomers in Alzheimer's disease model. *J. Neurosci.* 37, 6797–6809. doi: 10.1523/JNEUROSCI.3351-16.2017

Emsley, J. G., and Macklis, J. D. (2006). Astroglial heterogeneity closely reflects the neuronal-defined anatomy of the adult murine CNS. *Neuron Glia Biol.* 2, 175–186. doi: 10.1017/s1740925x06000202

Eng, L. F., Ghirnikar, R. S., and Lee, Y. L. (2000). Glial fibrillary acidic protein: GFAP-thirty-one years(1969–2000). *Neurochem. Res.* 25, 1439–1451. doi: 10.1023/A:1007677003387

Eroglu, C., and Barres, B. A. (2010). Regulation of synaptic connectivity by glia. *Nature* 468, 223–231. doi: 10.1038/nature09612

Fellner, L., Irschick, R., Schanda, K., Reindl, M., Klimaschewski, L., Poewe, W., et al. (2013). Toll-like receptor 4 is required for α-synuclein dependent activation of microglia and astroglia. *Glia* 61, 349–360. doi: 10.1002/glia.22437

Figley, C. R. (2011). Lactate transport and metabolism in the human brain: implications for the astrocyte-neuron lactate shuttle hypothesis. *J. Neurosci.* 31, 4768–4770. doi: 10.1523/jneurosci.6612-10.2011

Forny-Germano, L., Lyra e Silva, N. M., Batista, A. F., Brito-Moreira, J., Gralle, M., Boehnke, S. E., et al. (2014). Alzheimer's disease-like pathology induced by amyloid-β oligomers in nonhuman primates. *J. Neurosci.* 34, 13629–13643. doi: 10.1523/JNEUROSCI.1353-14.2014

Francelle, L., Galvan, L., Gaillard, M.-C., Guillermier, M., Houitte, D., Bonvento, G., et al. (2015). Loss of the thyroid hormone-binding protein Crym renders striatal neurons more vulnerable to mutant huntingtin in Huntington's disease. *Hum. Mol. Genet.* 24, 1563–1573. doi: 10.1093/hmg/ddu571

Franceschi, C., Bonafè, M., Valensin, S., Olivieri, F., De Luca, M., Ottaviani, E., et al. (2000). Inflamm-aging. An evolutionary perspective on immunosenescence. *Ann. N Y Acad. Sci.* 908, 244–254. doi: 10.1111/j.1749-6632.2000.tb06651.x

Fu, H., Hardy, J., and Duff, K. E. (2018). Selective vulnerability in neurodegenerative diseases. *Nat. Neurosci.* 21, 1350–1358. doi: 10.1038/s41593-018-0221-2

Garcia-Lopez, P., Garcia-Marin, V., and Freire, M. (2010). The histological slides and drawings of cajal. *Front. Neuroanat.* 4:9. doi: 10.3389/neuro.05.009.2010

Gesase, A. P., and Kiyama, H. (2007). Peripheral nerve injury induced expression of mRNA for serine protease inhibitor 3 in the rat facial and hypoglossal nuclei but not in the spinal cord. *Ital. J. Anat. Embryol.* 112, 157–168.

Gomes, F. C. A., Maia, C. G., de Menezes, J. R. L., and Neto, V. M. (1999). Cerebellar astrocytes treated by thyroid hormone modulate neuronal proliferation. *Glia* 25, 247–255. doi: 10.1002/(sici)1098-1136(19990201)25:3<247::aid-glia5>3.0.co;2-2

Gomes, F., Sousa Vde, O., and Romão, L. (2005). Emerging roles for TGF-β1 in nervous system development. *Int. J. Dev. Neurosci.* 23, 413–424. doi: 10.1016/j.ijdevneu.2005.04.001

Gong, Y., Chang, L., Viola, K. L., Lacor, P. N., Lambert, M. P., Finch, C. E., et al. (2003). Alzheimer's disease-affected brain: presence of oligomeric A β ligands (ADDLs) suggests a molecular basis for reversible memory loss. *Proc. Natl. Acad. Sci. U S A* 100, 10417–10422. doi: 10.1073/pnas.1834302100

Graf, B. A., Milbury, P. E., and Blumberg, J. B. (2005). Flavonols, flavones, flavanones, and human health: epidemiological evidence. *J. Med. Food* 8, 281–290. doi: 10.1089/jmf.2005.8.281

Gregory, W. A., Edmondson, J. C., Hatten, M. E., and Mason, C. A. (1988). Cytology and neuron-glial apposition of migrating cerebellar granule cells *in vitro*. *J. Neurosci.* 8, 1728–1738. doi: 10.1523/JNEUROSCI.08-05-01728.1988

Grosche, J., Kettenmann, H., and Reichenbach, A. (2002). Bergmann glial cells form distinct morphological structures to interact with cerebellar neurons. *J. Neurosci. Res.* 68, 138–149. doi: 10.1002/jnr.10197

Gu, X.-L., Long, C.-X., Sun, L., Xie, C., Lin, X., and Cai, H. (2010). Astrocytic expression of Parkinson's disease-related A53T α-synuclein causes neurodegeneration in mice. *Mol. Brain* 3:12. doi: 10.1186/1756-6606-3-12

Hachem, S., Aguirre, A., Vives, V., Marks, A., Gallo, V., and Legraverend, C. (2005). Spatial and temporal expression of S100B in cells of oligodendrocyte lineage. *Glia* 51, 81–97. doi: 10.1002/glia.20184

Hainfellner, J. A., Voigtländer, T., Ströbel, T., Mazal, P. R., Maddalena, A. S., Aguzzi, A., et al. (2001). Fibroblasts can express glial fibrillary acidic protein (GFAP) *in vivo*. *J. Neuropathol. Exp. Neurol.* 60, 449–461. doi: 10.1093/jnen/60.5.449

Halliday, G. M., and Stevens, C. H. (2011). Glia: initiators and progressors of pathology in Parkinson's disease. *Mov. Disord.* 26, 6–17. doi: 10.1002/mds.23455

Hansen, C., Angot, E., Bergström, A.-L., Steiner, J. A., Pieri, L., Paul, G., et al. (2011). α-synuclein propagates from mouse brain to grafted dopaminergic neurons and seeds aggregation in cultured human cells. *J. Clin. Invest.* 121, 715–725. doi: 10.1172/JCI43366

Hardy, J. A., and Higgins, G. A. (1992). Alzheimer's disease: the amyloid cascade hypothesis. *Science* 256, 184–185. doi: 10.1126/science.1566067

Hayakawa, N., Kato, H., and Araki, T. (2007). Age-related changes of astorocytes, oligodendrocytes and microglia in the mouse hippocampal CA1 sector. *Mech. Ageing Dev.* 128, 311–316. doi: 10.1016/j.mad.2007.01.005

Heneka, M. T., Carson, M. J., Khoury, J. E., Landreth, G. E., Brosseron, F., Feinstein, D. L., et al. (2015). Neuroinflammation in Alzheimer's disease. *Lancet Neurol.* 14, 388–405. doi: 10.1016/S1474-4422(15)70016-5

Hol, E. M., and Pekny, M. (2015). Glial fibrillary acidic protein (GFAP) and the astrocyte intermediate filament system in diseases of the central nervous system. *Curr. Opin. Cell Biol.* 32, 121–130. doi: 10.1016/j.ceb.2015.02.004

Iliff, J. J., Wang, M., Liao, Y., Plogg, B. A., Peng, W., Gundersen, G. A., et al. (2012). A paravascular pathway facilitates CSF flow through the brain parenchyma and the clearance of interstitial solutes, including amyloid β. *Sci. Transl. Med.* 4:147ra111. doi: 10.1126/scitranslmed.3003748

Jankovic, J. (2008). Parkinson's disease: clinical features and diagnosis. *J. Neurol. Neurosurg. Psychiatry* 79, 368–376. doi: 10.1136/jnnp.2007.131045

Jessen, N. A., Munk, A. S. F., Lundgaard, I., and Nedergaard, M. (2015). The glymphatic system: a beginner's guide. *Neurochem. Res.* 40, 2583–2599. doi: 10.1007/s11064-015-1581-6

Jha, M. K., Kim, J. H., Song, G. J., Lee, W. H., Lee, I. K., Lee, H. W., et al. (2018). Functional dissection of astrocyte-secreted proteins: Implications in brain health and diseases. *Prog. Neurobiol.* 162, 37–69. doi: 10.1016/j.pneurobio.2017.12.003

Jiang, X., Shen, S., Cadwell, C. R., Berens, P., Sinz, F., Ecker, A. S., et al. (2015). Principles of connectivity among morphologically defined cell types in adult neocortex. *Science* 350:aac9462. doi: 10.1126/science.aac9462

Kamphuis, W., Middeldorp, J., Kooijman, L., Sluijs, J. A., Kooi, E.-J., Moeton, M., et al. (2014). Glial fibrillary acidic protein isoform expression in plaque related astrogliosis in Alzheimer's disease. *Neurobiol. Aging* 35, 492–510. doi: 10.1016/j.neurobiolaging.2013.09.035

Kanemaru, K., Sekiya, H., Xu, M., Satoh, K., Kitajima, N., Yoshida, K., et al. (2014). *In vivo* visualization of subtle, transient, and local activity of astrocytes using an ultrasensitive Ca^{2+} indicator. *Cell Rep.* 8, 311–318. doi: 10.1016/j.celrep.2014.05.056

Kato, H., Yamamoto, T., Yamamoto, H., Ohi, R., So, N., and Iwasaki, Y. (1990). Immunocytochemical characterization of supporting cells in the enteric nervous system in Hirschsprung's disease. *J. Pediatr. Surg.* 25, 514–519. doi: 10.1016/0022-3468(90)90563-o

Kepecs, A., and Fishell, G. (2014). Interneuron cell types are fit to function. *Nature* 505, 318–326. doi: 10.1038/nature12983

Kimelberg, H. K. (2004). The problem of astrocyte identity. *Neurochem. Int.* 45, 191–202. doi: 10.1016/s0197-0186(03)00286-9

Kodali, M., Parihar, V. K., Hattiangady, B., Mishra, V., Shuai, B., and Shetty, A. K. (2015). Resveratrol prevents age-related memory and mood dysfunction with increased hippocampal neurogenesis and microvasculature and reduced glial activation. *Sci. Rep.* 5:8075. doi: 10.1038/srep08075

Koh, S.-H., Lee, S. M., Kim, H. Y., Lee, K.-Y., Lee, Y. J., Kim, H.-T., et al. (2006). The effect of epigallocatechin gallate on suppressing disease progression of ALS model mice. *Neurosci. Lett.* 395, 103–107. doi: 10.1016/j.neulet.2005.10.056

Kucukdereli, H., Allen, N. J., Lee, A. T., Feng, A., Ozlu, M. I., Conatser, L. M., et al. (2011). Control of excitatory CNS synaptogenesis by astrocyte-secreted proteins Hevin and SPARC. *Proc. Natl. Acad. Sci. U S A* 108, E440–E449. doi: 10.1073/pnas.1104977108

Kulijewicz-Nawrot, M., Verkhratsky, A., Chvátal, A., Syková, E., and Rodríguez, J. J. (2012). Astrocytic cytoskeletal atrophy in the medial prefrontal

cortex of a triple transgenic mouse model of Alzheimer's disease. *J. Anat.* 221, 252–262. doi: 10.1111/j.1469-7580.2012.01536.x

Lambert, M. P., Barlow, A. K., Chromy, B. A., Edwards, C., Freed, R., Liosatos, M., et al. (1998). Diffusible, nonfibrillar ligands derived from A 1–42 are potent central nervous system neurotoxins. *Proc. Natl. Acad. Sci. U S A* 95, 6448–6453. doi: 10.1073/pnas.95.11.6448

Lee, S., Park, J.-Y., Lee, W.-H., Kim, H., Park, H.-C., Mori, K., et al. (2009). Lipocalin-2 is an autocrine mediator of reactive astrocytosis. *J. Neurosci.* 29, 234–249. doi: 10.1523/JNEUROSCI.5273-08.2009

Lee, H.-J., Suk, J.-E., Patrick, C., Bae, E.-J., Cho, J.-H., Rho, S., et al. (2010). Direct transfer of α-synuclein from neuron to astroglia causes inflammatory responses in synucleinopathies. *J. Biol. Chem.* 285, 9262–9272. doi: 10.1074/jbc.m109.081125

Lesné, S. E., Sherman, M. A., Grant, M., Kuskowski, M., Schneider, J. A., Bennett, D. A., et al. (2013). Brain amyloid-β oligomers in ageing and Alzheimer's disease. *Brain J. Neurol.* 136, 1383–1398. doi: 10.1093/brain/awt062

Liddelow, S. A., and Barres, B. A. (2017). Reactive astrocytes: production, function, and therapeutic potential. *Immunity* 46, 957–967. doi: 10.1016/j.immuni.2017.06.006

Liddelow, S. A., Guttenplan, K. A., Clarke, L. E., Bennett, F. C., Bohlen, C. J., Schirmer, L., et al. (2017). Neurotoxic reactive astrocytes are induced by activated microglia. *Nature* 541, 481–487. doi: 10.1038/nature21029

Lippman, J. J., Lordkipanidze, T., Buell, M. E., Yoon, S. O., and Dunaevsky, A. (2008). Morphogenesis and regulation of Bergmann glial processes during Purkinje cell dendritic spine ensheathment and synaptogenesis. *Glia* 56, 1463–1477. doi: 10.1002/glia.20712

Lourenco, M. V., Clarke, J. R., Frozza, R. L., Bomfim, T. R., Forny-Germano, L., Batista, A. F., et al. (2013). TNF-α mediates PKR-dependent memory impairment and brain IRS-1 inhibition induced by Alzheimer's β-amyloid oligomers in mice and monkeys. *Cell Metab.* 18, 831–843. doi: 10.1016/j.cmet.2013.11.002

Lundgaard, I., Osório, M. J., Kress, B. T., Sanggaard, S., and Nedergaard, M. (2014). White matter astrocytes in health and disease. *Neuroscience* 276, 161–173. doi: 10.1016/j.neuroscience.2013.10.050

Lynch, A. M., Murphy, K. J., Deighan, B. F., O'Reilly, J.-A., Gun'ko, Y. K., Cowley, T. R., et al. (2010). The impact of glial activation in the aging brain. *Aging Dis.* 1, 262–278.

Mancinelli, S., and Lodato, S. (2018). Decoding neuronal diversity in the developing cerebral cortex: from single cells to functional networks. *Curr. Opin. Neurobiol.* 53, 146–155. doi: 10.1016/j.conb.2018.08.001

Martinez, R., and Gomes, F. C. A. (2002). Neuritogenesis induced by thyroid hormone-treated astrocytes is mediated by epidermal growth factor/mitogen-activated protein kinase-phosphatidylinositol 3-kinase pathways and involves modulation of extracellular matrix proteins. *J. Biol. Chem.* 277, 49311–49318. doi: 10.1074/jbc.m209284200

Matias, I., Buosi, A. S., and Gomes, F. C. A. (2016). Functions of flavonoids in the central nervous system: astrocytes as targets for natural compounds. *Neurochem. Int.* 95, 85–91. doi: 10.1016/j.neuint.2016.01.009

Matias, I., Diniz, L. P., Buosi, A., Neves, G., Stipursky, J., and Gomes, F. C. A. (2017). Flavonoid hesperidin induces synapse formation and improves memory performance through the astrocytic TGF-β1. *Front. Aging Neurosci.* 9:184. doi: 10.3389/fnagi.2017.00184

Middeldorp, J., and Hol, E. M. (2011). GFAP in health and disease. *Prog. Neurobiol.* 93, 421–443. doi: 10.1016/j.pneurobio.2011.01.005

Moraes, C. A., Santos, G., de SaMpaio e Spohr, T. C., D'Avila, J. C., Lima, F. R. S., Benjamim, C. F., et al. (2015). Activated microglia-induced deficits in excitatory synapses through IL-1β: implications for cognitive impairment in sepsis. *Mol. Neurobiol.* 52, 653–663. doi: 10.1007/s12035-014-8868-5

Morgan, T. E., Rozovsky, I., Goldsmith, S. K., Stone, D. J., Yoshida, T., and Finch, C. E. (1997). Increased transcription of the astrocyte gene GFAP during middle-age is attenuated by food restriction: implications for the role of oxidative stress. *Free Radic. Biol. Med.* 23, 524–528. doi: 10.1016/s0891-5849(97)00120-2

Morgan, T. E., Xie, Z., Goldsmith, S., Yoshida, T., Lanzrein, A. S., Stone, D., et al. (1999). The mosaic of brain glial hyperactivity during normal ageing and its attenuation by food restriction. *Neuroscience* 89, 687–699. doi: 10.1016/s0306-4522(98)00334-0

Nagele, R. G., D'Andrea, M. R., Lee, H., Venkataraman, V., and Wang, H.-Y. (2003). Astrocytes accumulate Aβ42 and give rise to astrocytic amyloid plaques in Alzheimer disease brains. *Brain Res.* 971, 197–209. doi: 10.1016/s0006-8993(03)02361-8

Nagelhus, E. A., and Ottersen, O. P. (2013). Physiological roles of aquaporin-4 in brain. *Physiol. Rev.* 93, 1543–1562. doi: 10.1152/physrev.00011.2013

Nagy, J. I., Patel, D., Ochalski, P. A. Y., and Stelmack, G. L. (1999). Connexin30 in rodent, cat and human brain: selective expression in gray matter astrocytes, co-localization with connexin43 at gap junctions and late developmental appearance. *Neuroscience* 88, 447–468. doi: 10.1016/s0306-4522(98)00191-2

Nett, W. J., Oloff, S. H., and McCarthy, K. D. (2002). Hippocampal astrocytes *in situ* exhibit calcium oscillations that occur independent of neuronal activity. *J. Neurophysiol.* 87, 528–537. doi: 10.1152/jn.00268.2001

Nichols, N. R., Day, J. R., Laping, N. J., Johnson, S. A., and Finch, C. E. (1993). GFAP mRNA increases with age in rat and human brain. *Neurobiol. Aging* 14, 421–429. doi: 10.1016/0197-4580(93)90100-p

Noguchi, A., Matsumura, S., Dezawa, M., Tada, M., Yanazawa, M., Ito, A., et al. (2009). Isolation and characterization of patient-derived, toxic, high mass amyloid β-protein (Aβ) assembly from Alzheimer disease brains. *J. Biol. Chem.* 284, 32895–32905. doi: 10.1074/jbc.M109.000208

Nones, J., Spohr, T. C., and Gomes, F. C. A. (2012). Effects of the flavonoid hesperidin in cerebral cortical progenitors *in vitro*: indirect action through astrocytes. *Int. J. Dev. Neurosci.* 30, 303–313. doi: 10.1016/j.ijdevneu.2012.01.008

Oberheim, N. A., Goldman, S. A., and Nedergaard, M. (2012). Heterogeneity of astrocytic form and function. *Methods Mol. Biol.* 814, 23–45. doi: 10.1007/978-1-61779-452-0_3

Oberheim, N. A., Takano, T., Han, X., He, W., Lin, J. H. C., Wang, F., et al. (2009). Uniquely hominid features of adult human astrocytes. *J. Neurosci.* 29, 3276–3287. doi: 10.1523/JNEUROSCI.4707-08.2009

Ogata, K., and Kosaka, T. (2002). Structural and quantitative analysis of astrocytes in the mouse hippocampus. *Neuroscience* 113, 221–233. doi: 10.1016/s0306-4522(02)00041-6

Olabarria, M., Noristani, H. N., Verkhratsky, A., and Rodriguez, J. J. (2010). Concomitant astroglial atrophy and astrogliosis in a triple transgenic animal model of Alzheimer's disease. *Glia* 58, 831–838. doi: 10.1002/glia.20967

Orre, M., Kamphuis, W., Osborn, L. M., Jansen, A. H. P., Kooijman, L., Bossers, K., et al. (2014). Isolation of glia from Alzheimer's mice reveals inflammation and dysfunction. *Neurobiol. Aging* 35, 2746–2760. doi: 10.1016/j.neurobiolaging.2014.06.004

Papadopoulos, M. C., Manley, G. T., Krishna, S., and Verkman, A. S. (2004). Aquaporin-4 facilitates reabsorption of excess fluid in vasogenic brain edema. *FASEB J.* 18, 1291–1293. doi: 10.1096/fj.04-1723fje

Pekny, M., Wilhelmsson, U., and Pekna, M. (2014). The dual role of astrocyte activation and reactive gliosis. *Neurosci. Lett.* 565, 30–38. doi: 10.1016/j.neulet.2013.12.071

Perea, G., and Araque, A. (2007). Astrocytes potentiate transmitter release at single hippocampal synapses. *Science* 317, 1083–1086. doi: 10.1126/science.1144640

Pham, E., Crews, L., Ubhi, K., Hansen, L., Adame, A., Cartier, A., et al. (2010). Progressive accumulation of amyloid-β oligomers in Alzheimer's disease and in amyloid precursor protein transgenic mice is accompanied by selective alterations in synaptic scaffold proteins. *FEBS J.* 277, 3051–3067. doi: 10.1111/j.1742-4658.2010.07719.x

Phatnani, H., and Maniatis, T. (2015). Astrocytes in neurodegenerative disease. *Cold Spring Harb. Perspect. Biol.* 7:a020628. doi: 10.1101/cshperspect.a020628

Pixley, S. K., and de Vellis, J. (1984). Transition between immature radial glia and mature astrocytes studied with a monoclonal antibody to vimentin. *Brain Res.* 317, 201–209. doi: 10.1016/0165-3806(84)90097-x

Poewe, W., Seppi, K., Tanner, C. M., Halliday, G. M., Brundin, P., Volkmann, J., et al. (2017). Parkinson disease. *Nat. Rev. Dis. Primer* 3:17013. doi: 10.1038/nrdp.2017.13

Qu, H., Håberg, A., Haraldseth, O., Unsgård, G., and Sonnewald, U. (2000). ^{13}C MR spectroscopy study of lactate as substrate for rat brain. *Dev. Neurosci.* 22, 429–436. doi: 10.1159/000017472

Raff, M. C. (1989). Glial cell diversification in the rat optic nerve. *Science* 243, 1450–1455. doi: 10.1126/science.2648568

Raff, M. C., Abney, E. R., and Miller, R. H. (1984). Two glial cell lineages diverge prenatally in rat optic nerve. *Dev. Biol.* 106, 53–60. doi: 10.1016/0012-1606(84)90060-5

Rakic, P. (1971). Guidance of neurons migrating to the fetal monkey neocortex. *Brain Res.* 33, 471–476. doi: 10.1016/0006-8993(71)90119-3

Rannikko, E. H., Weber, S. S., and Kahle, P. J. (2015). Exogenous α-synuclein induces toll-like receptor 4 dependent inflammatory responses in astrocytes. *BMC Neurosci.* 16:57. doi: 10.1186/s12868-015-0192-0

Reichenbach, A. (1989). Attempt to classify glial cells by means of their process specialization using the rabbit retinal Müller cell as an example of cytotopographic specialization of glial cells. *Glia* 2, 250–259. doi: 10.1002/glia.440020406

Reichenbach, A., and Bringmann, A. (2010). "Müller Cells in the Healthy Retina," in *Müller Cells in the Healthy and Diseased Retina*, eds A. D. Fryer, A. Reichenbach and A. Bringmann (New York, NY: Springer New York), 35–214.

Reilly, J. F., Games, D., Rydel, R. E., Freedman, S., Schenk, D., Young, W. G., et al. (2003). Amyloid deposition in the hippocampus and entorhinal cortex: quantitative analysis of a transgenic mouse model. *Proc. Natl. Acad. Sci. U S A* 100, 4837–4842. doi: 10.1073/pnas.0330745100

Robillard, K. N., Lee, K. M., Chiu, K. B., and MacLean, A. G. (2016). Glial cell morphological and density changes through the lifespan of rhesus macaques. *Brain Behav. Immun.* 55, 60–69. doi: 10.1016/j.bbi.2016.01.006

Rodríguez, J. J., Butt, A. M., Gardenal, E., Parpura, V., and Verkhratsky, A. (2016). Complex and differential glial responses in Alzheimer's disease and ageing. *Curr. Alzheimer Res.* 13, 343–358. doi: 10.2174/1567205013666160229112911

Rodríguez, J. J., Yeh, C. Y., Terzieva, S., Olabarria, M., Kulijewicz-Nawrot, M., and Verkhratsky, A. (2014). Complex and region-specific changes in astroglial markers in the aging brain. *Neurobiol. Aging* 35, 15–23. doi: 10.1016/j.neurobiolaging.2013.07.002

Rodríguez-Arellano, J. J., Parpura, V., Zorec, R., and Verkhratsky, A. (2016). Astrocytes in physiological aging and Alzheimer's disease. *Neuroscience* 323, 170–182. doi: 10.1016/j.neuroscience.2015.01.007

Rojas, P., Montes, P., Rojas, C., Serrano-Garcia, N., and Rojas-Castaneda, J. C. (2012). Effect of a phytopharmaceutical medicine, Ginko biloba extract 761, in an animal model of Parkinson's disease: therapeutic perspectives. *Nutrition* 28, 1081–1088. doi: 10.1016/j.nut.2012.03.007

Rostami, J., Holmqvist, S., Lindstrom, V., Sigvardson, J., Westermark, G. T., Ingelsson, M., et al. (2017). Human astrocytes transfer aggregated α-synuclein via tunneling nanotubes. *J. Neurosci.* 37, 11835–11853. doi: 10.1523/JNEUROSCI.0983-17.2017

Rothstein, J. D., Dykes-Hoberg, M., Pardo, C. A., Bristol, L. A., Jin, L., Kuncl, R. W., et al. (1996). Knockout of glutamate transporters reveals a major role for astroglial transport in excitotoxicity and clearance of glutamate. *Neuron* 16, 675–686. doi: 10.1016/s0896-6273(00)80086-0

Rothstein, J. D., Martin, L., Levey, A. I., Dykes-Hoberg, M., Jin, L., Wu, D., et al. (1994). Localization of neuronal and glial glutamate transporters. *Neuron* 13, 713–725. doi: 10.1016/0896-6273(94)90038-8

Rouach, N., Koulakoff, A., Abudara, V., Willecke, K., and Giaume, C. (2008). Astroglial metabolic networks sustain hippocampal synaptic transmission. *Science* 322, 1551–1555. doi: 10.1126/science.1164022

Saxena, S., and Caroni, P. (2011). Selective neuronal vulnerability in neurodegenerative diseases: from stressor thresholds to degeneration. *Neuron* 71, 35–48. doi: 10.1016/j.neuron.2011.06.031

Scemes, E., and Giaume, C. (2006). Astrocyte calcium waves: what they are and what they do. *Glia* 54, 716–725. doi: 10.1002/glia.20374

Schapira, A. H. V., Chaudhuri, K. R., and Jenner, P. (2017). Non-motor features of Parkinson disease. *Nat. Rev. Neurosci.* 18, 435–450. doi: 10.1038/nrn.2017.62

Scheltens, P., Blennow, K., Breteler, M. M., de Strooper, B., Frisoni, G. B., Salloway, S., et al. (2016). Alzheimer's disease. *Lancet* 388, 505–517. doi: 10.1016/S0140-6736(15)01124-1

Schmitt, A., Asan, E., Lesch, K.-P., and Kugler, P. (2002). A splice variant of glutamate transporter GLT1/EAAT2 expressed in neurons: cloning and localization in rat nervous system. *Neuroscience* 109, 45–61. doi: 10.1016/s0306-4522(01)00451-1

Schmitt, A., Asan, E., Püschel, B., and Kugler, P. (1997). Cellular and regional distribution of the glutamate transporter GLAST in the CNS of rats: nonradioactive *in situ* hybridization and comparative immunocytochemistry. *J. Neurosci.* 17, 1–10. doi: 10.1523/jneurosci.17-01-00001.1997

Shankar, G. M., Li, S., Mehta, T. H., Garcia-Munoz, A., Shepardson, N. E., Smith, I., et al. (2008). Amyloid-β protein dimers isolated directly from Alzheimer's brains impair synaptic plasticity and memory. *Nat. Med.* 14, 837–842. doi: 10.1038/nm1782

Sharif, A., Renault, F., Beuvon, F., Castellanos, R., Canton, B., Barbeito, L., et al. (2004). The expression of PEA-15 (phosphoprotein enriched in astrocytes of 15 kDa) defines subpopulations of astrocytes and neurons throughout the adult mouse brain. *Neuroscience* 126, 263–275. doi: 10.1016/j.neuroscience.2004.02.039

Sharma, V., Mishra, M., Ghosh, S., Tewari, R., Basu, A., Seth, P., et al. (2007). Modulation of interleukin-1β mediated inflammatory response in human astrocytes by flavonoids: implications in neuroprotection. *Brain Res. Bull.* 73, 55–63. doi: 10.1016/j.brainresbull.2007.01.016

Shigetomi, E., Kracun, S., Sofroniew, M. V., and Khakh, B. S. (2010). A genetically targeted optical sensor to monitor calcium signals in astrocyte processes. *Nat. Neurosci.* 13, 759–766. doi: 10.1038/nn.2557

Shinozaki, Y., Shibata, K., Yoshida, K., Shigetomi, E., Gachet, C., Ikenaka, K., et al. (2017). Transformation of astrocytes to a neuroprotective phenotype by microglia via P2Y1 receptor downregulation. *Cell Rep.* 19, 1151–1164. doi: 10.1016/j.celrep.2017.04.047

Sild, M., and Ruthazer, E. S. (2011). Radial glia: progenitor, pathway and partner. *Neuroscientist* 17, 288–302. doi: 10.1177/1073858410385870

Simpson, J. E., Ince, P. G., Lace, G., Forster, G., Shaw, P. J., Matthews, F., et al. (2010). Astrocyte phenotype in relation to Alzheimer-type pathology in the ageing brain. *Neurobiol. Aging* 31, 578–590. doi: 10.1016/j.neurobiolaging.2008.05.015

Siqueira, M., Francis, D., Gisbert, D., Gomes, F. C. A., and Stipursky, J. (2018). Radial Glia cells control angiogenesis in the developing cerebral cortex through TGF-β1 signaling. *Mol. Neurobiol.* 55, 3660–3675. doi: 10.1007/s12035-017-0557-8

Sofroniew, M. V. (2009). Molecular dissection of reactive astrogliosis and glial scar formation. *Trends Neurosci.* 32, 638–647. doi: 10.1016/j.tins.2009.08.002

Solanki, I., Parihar, P., Mansuri, M. L., and Parihar, M. S. (2015). Flavonoid-based therapies in the early management of neurodegenerative diseases. *Adv. Nutr.* 6, 64–72. doi: 10.3945/an.114.007500

Somjen, G. G. (1988). Nervenkitt: notes on the history of the concept of neuroglia. *Glia* 1, 2–9. doi: 10.1002/glia.440010103

Song, G. J., and Suk, K. (2017). Pharmacological Modulation of Functional Phenotypes of Microglia in Neurodegenerative Diseases. *Front. Aging Neurosci.* 9:139. doi: 10.3389/fnagi.2017.00139

Song, Y. J., Halliday, G. M., Holton, J. L., Lashley, T., O'Sullivan, S. S., McCann, H., et al. (2009). Degeneration in different parkinsonian syndromes relates to astrocyte type and astrocyte protein expression. *J. Neuropathol. Exp. Neurol.* 68, 1073–1083. doi: 10.1097/nen.0b013e3181b66f1b

Soreq, L., Rose, J., Soreq, E., Hardy, J., Trabzuni, D., Cookson, M. R., et al. (2017). Major shifts in glial regional identity are a transcriptional hallmark of human brain aging. *Cell Rep.* 18, 557–570. doi: 10.1016/j.celrep.2016.12.011

Sotelo-Hitschfeld, T., Niemeyer, M. I., Mächler, P., Ruminot, I., Lerchundi, R., Wyss, M. T., et al. (2015). Channel-mediated lactate release by K^+-stimulated astrocytes. *J. Neurosci.* 35, 4168–4178. doi: 10.1523/JNEUROSCI.5036-14.2015

Sponne, I., Fifre, A., Drouet, B., Klein, C., Koziel, V., Pincon-Raymond, M., et al. (2003). Apoptotic neuronal cell death induced by the non-fibrillar amyloid-β peptide proceeds through an early reactive oxygen species-dependent cytoskeleton perturbation. *J. Biol. Chem.* 278, 3437–3445. doi: 10.1074/jbc.m206745200

Steiner, J., Bernstein, H.-G., Bielau, H., Berndt, A., Brisch, R., Mawrin, C., et al. (2007). Evidence for a wide extra-astrocytic distribution of S100B in human brain. *BMC Neurosci.* 8:2. doi: 10.1186/1471-2202-8-2

Stellwagen, D., and Malenka, R. C. (2006). Synaptic scaling mediated by glial TNF-α. *Nature* 440, 1054–1059. doi: 10.1038/nature04671

Stranahan, A. M., and Mattson, M. P. (2010). Selective vulnerability of neurons in layer II of the entorhinal cortex during aging and Alzheimer's disease. *Neural Plast.* 2010:108190. doi: 10.1155/2010/108190

Suk, K. (2017). Glial phenotype modulators. *Oncotarget* 8, 22309–22310. doi: 10.18632/oncotarget.16245

Sundaram, J. R., Poore, C. P., Sulaimee, N. H. B., Pareek, T., Cheong, W. F., Wenk, M. R., et al. (2017). Curcumin ameliorates neuroinflammation, neurodegeneration and memory deficits in p25 transgenic mouse model that bears hallmarks of Alzheimer's disease. *J. Alzheimers Dis.* 60, 1429–1442. doi: 10.3233/jad-170093

Townsend, M., Shankar, G. M., Mehta, T., Walsh, D. M., and Selkoe, D. J. (2006). Effects of secreted oligomers of amyloid β-protein on hippocampal synaptic plasticity: a potent role for trimers. *J. Physiol.* 572, 477–492. doi: 10.1113/jphysiol.2005.103754

Tsao, R. (2010). Chemistry and biochemistry of dietary polyphenols. *Nutrients* 2, 1231–1246. doi: 10.3390/nu2121231

Umeda, T., Tomiyama, T., Sakama, N., Tanaka, S., Lambert, M. P., Klein, W. L., et al. (2011). Intraneuronal amyloid β oligomers cause cell death via endoplasmic reticulum stress, endosomal/lysosomal leakage and mitochondrial dysfunction *in vivo*. *J. Neurosci. Res.* 89, 1031–1042. doi: 10.1002/jnr.22640

Vafeiadou, K., Vauzour, D., Lee, H. Y., Rodriguez-Mateos, A., Williams, R. J., and Spencer, J. P. (2009). The citrus flavanone naringenin inhibits inflammatory signalling in glial cells and protects against neuroinflammatory injury. *Arch. Biochem. Biophys.* 484, 100–109. doi: 10.1016/j.abb.2009.01.016

Vaughn, J. E., and Pease, D. C. (1967). Electron microscopy of classically stained astrocytes. *J. Comp. Neurol.* 131, 143–154. doi: 10.1002/cne.901310206

Verkhratsky, A., and Butt, A. (2013). *Glial Physiology and Pathophysiology*. New York, NY: John Wiley and Sons.

Verkhratsky, A., and Nedergaard, M. (2014). Astroglial cradle in the life of the synapse. *Philos. Trans. R. Soc. Lond. B Biol. Sci.* 369:20130595. doi: 10.1098/rstb.2013.0595

Verkhratsky, A., and Nedergaard, M. (2018). Physiology of astroglia. *Physiol. Rev.* 98, 239–389. doi: 10.1152/physrev.00042.2016

Verkhratsky, A., Olabarria, M., Noristani, H. N., Yeh, C. Y., and Rodriguez, J. J. (2010). Astrocytes in Alzheimer's disease. *Neurotherapeutics* 7, 399–412. doi: 10.1016/j.nurt.2010.05.017

Vié, M. P., Evrard, C., Osty, J., Breton-Gilet, A., Blanchet, P., Pomérance, M., et al. (1997). Purification, molecular cloning and functional expression of the human nicodinamide-adenine dinucleotide phosphate-regulated thyroid hormone-binding protein. *Mol. Endocrinol. Baltim. Md* 11, 1728–1736. doi: 10.1210/mend.11.11.9915

Virchow, R. (1856). *Gesammelte Abhandlungen zyr wissenschaftlischen Medizin*. Frankfurt: Verlag von Meidinger Sohn & Comp.

Volterra, A., and Meldolesi, J. (2005). Astrocytes, from brain glue to communication elements: the revolution continues. *Nat. Rev. Neurosci.* 6, 626–640. doi: 10.1038/nrn1722

Wakabayashi, K., Hayashi, S., Yoshimoto, M., Kudo, H., and Takahashi, H. (2000). NACP/α-synuclein-positive filamentous inclusions in astrocytes and oligodendrocytes of Parkinson's disease brains. *Acta Neuropathol.* 99, 14–20. doi: 10.1007/pl00007400

Waller, R., Woodroofe, M. N., Wharton, S. B., Ince, P. G., Francese, S., Heath, P. R., et al. (2016). Gene expression profiling of the astrocyte transcriptome in multiple sclerosis normal appearing white matter reveals a neuroprotective role. *J. Neuroimmunol.* 299, 139–146. doi: 10.1016/j.jneuroim.2016.09.010

Walz, W., and Lang, M. K. (1998). Immunocytochemical evidence for a distinct GFAP-negative subpopulation of astrocytes in the adult rat hippocampus. *Neurosci. Lett.* 257, 127–130. doi: 10.1016/s0304-3940(98)00813-1

Weller, R. O., Djuanda, E., Yow, H.-Y., and Carare, R. O. (2009). Lymphatic drainage of the brain and the pathophysiology of neurological disease. *Acta Neuropathol.* 117, 1–14. doi: 10.1007/s00401-008-0457-0

Whitehouse, P. J., Price, D. L., Struble, R. G., Clark, A. W., Coyle, J. T., and Delon, M. R. (1982). Alzheimer's disease and senile dementia: loss of neurons in the basal forebrain. *Science* 215, 1237–1239. doi: 10.1126/science.7058341

Wilhelmsson, U., Bushong, E. A., Price, D. L., Smarr, B. L., Phung, V., Terada, M., et al. (2006). Redefining the concept of reactive astrocytes as cells that remain within their unique domains upon reaction to injury. *Proc. Natl. Acad. Sci. U S A* 103, 17513–17518. doi: 10.1073/pnas.0602841103

Williams, R. J., and Spencer, J. P. (2012). Flavonoids, cognition and dementia: actions, mechanisms and potential therapeutic utility for Alzheimer disease. *Free Radic. Biol. Med.* 52, 35–45. doi: 10.1016/j.freeradbiomed.2011.09.010

Williams, S. M., Sullivan, R. K. P., Scott, H. L., Finkelstein, D. I., Colditz, P. B., Lingwood, B. E., et al. (2005). Glial glutamate transporter expression patterns in brains from multiple mammalian species. *Glia* 49, 520–541. doi: 10.1002/glia.20139

Witcher, M. R., Park, Y. D., Lee, M. R., Sharma, S., Harris, K. M., and Kirov, S. A. (2010). Three-dimensional relationships between perisynaptic astroglia and human hippocampal synapses. *Glia* 58, 572–587. doi: 10.1002/glia.20946

Xu, S. L., Bi, C. W., Choi, R. C., Zhu, K. Y., Miernisha, A., Dong, T. T., et al. (2013). Flavonoids induce the synthesis and secretion of neurotrophic factors in cultured rat astrocytes: a signaling response mediated by estrogen receptor. *Evid. Based Complement. Alternat. Med.* 2013:127075. doi: 10.1155/2013/127075

Yeh, C.-Y. (2013). *Cortical Astroglial Atrophy in Ageing and Alzheimer's Disease*. Manchester: University of Manchester.

Yun, S. P., Kam, T. I., Panicker, N., Kim, S., Oh, Y., Park, J. S., et al. (2018). Block of A1 astrocyte conversion by microglia is neuroprotective in models of Parkinson's disease. *Nat. Med.* 24, 931–938. doi: 10.1038/s41591-018-0051-5

Zador, Z., Stiver, S., Wang, V., and Manley, G. T. (2009). Role of aquaporin-4 in cerebral edema and stroke. *Handb. Exp. Pharmacol.* 190, 159–170. doi: 10.1007/978-3-540-79885-9_7

Zamanian, J. L., Xu, L., Foo, L. C., Nouri, N., Zhou, L., Giffard, R. G., et al. (2012). Genomic analysis of reactive astrogliosis. *J. Neurosci.* 32, 6391–6410. doi: 10.1523/JNEUROSCI.6221-11.2012

Zeng, Y., Lv, F., Li, L., Yu, H., Dong, M., and Fu, Q. (2012). 7,8-dihydroxyflavone rescues spatial memory and synaptic plasticity in cognitively impaired aged rats. *J. Neurochem.* 122, 800–811. doi: 10.1111/j.1471-4159.2012.07830.x

Zhang, Y., and Barres, B. A. (2010). Astrocyte heterogeneity: an underappreciated topic in neurobiology. *Curr. Opin. Neurobiol.* 20, 588–594. doi: 10.1016/j.conb.2010.06.005

Zhang, Z., Liu, X., Schroeder, J. P., Chan, C.-B., Song, M., Yu, S. P., et al. (2014). 7,8-Dihydroxyflavone prevents synaptic loss and memory deficits in a mouse model of Alzheimer's disease. *Neuropsychopharmacology* 39, 638–650. doi: 10.1038/npp.2013.243

Conflict of Interest Statement: The authors declare that the research was conducted in the absence of any commercial or financial relationships that could be construed as a potential conflict of interest.

frontiers in Molecular Neuroscience

ORIGINAL RESEARCH
published: 21 May 2019
doi: 10.3389/fnmol.2019.00120

Phosphorylation of Glutamine Synthetase on Threonine 301 Contributes to Its Inactivation During Epilepsy

Deborah Huyghe[1†], Andrew R. Denninger[2†], Caroline M. Voss[3], Pernille Frank[3], Ning Gao[2], Nicholas Brandon[4,5], Helle S. Waagepetersen[3], Andrew D. Ferguson[6], Menelas Pangalos[7], Peter Doig[2] and Stephen J. Moss[1,8]**

[1]Department of Neuroscience, Tufts University School of Medicine, Boston, MA, United States, [2]Mechanistic Biology & Profiling, Discovery Sciences, IMED Biotech Unit, AstraZeneca, Boston, MA, United States, [3]Department of Drug Design and Pharmacology, Faculty of Health and Medical Sciences, University of Copenhagen, Copenhagen, Denmark, [4]Neuroscience, IMED Biotech Unit, AstraZeneca, Boston, MA, United States, [5]AstraZeneca Tufts Laboratory for Basic and Translational Neuroscience, Boston, MA, United States, [6]Structure & Biophysics, Discovery Sciences, IMED Biotech Unit, AstraZeneca, Boston, MA, United States, [7]IMED Biotech Unit, AstraZeneca, Cambridge, United Kingdom, [8]Department of Neuroscience, Physiology and Pharmacology, University College, London, United Kingdom

OPEN ACCESS

Edited by:
Maria Jose Bellini, National Council for Scientific and Technical Research (CONICET), Argentina

Reviewed by:
Yijuang Chern, National Research Program for Biopharmaceuticals, Taiwan
Arthur Joseph Cooper, New York Medical College, United States

***Correspondence:**
Peter Doig
peter.doig@astrazeneca.com
Stephen J. Moss
stephen.moss@tufts.edu

[†]*Joint-first authors*

Received: *06 December 2018*
Accepted: *25 April 2019*
Published: *21 May 2019*

Citation:
Huyghe D, Denninger AR, Voss CM, Frank P, Gao N, Brandon N, Waagepetersen HS, Ferguson AD, Pangalos M, Doig P and Moss SJ (2019) Phosphorylation of Glutamine Synthetase on Threonine 301 Contributes to Its Inactivation During Epilepsy. Front. Mol. Neurosci. 12:120. doi: 10.3389/fnmol.2019.00120

The astrocyte-specific enzyme glutamine synthetase (GS), which catalyzes the amidation of glutamate to glutamine, plays an essential role in supporting neurotransmission and in limiting NH_4^+ toxicity. Accordingly, deficits in GS activity contribute to epilepsy and neurodegeneration. Despite its central role in brain physiology, the mechanisms that regulate GS activity are poorly defined. Here, we demonstrate that GS is directly phosphorylated on threonine residue 301 (T301) within the enzyme's active site by cAMP-dependent protein kinase (PKA). Phosphorylation of T301 leads to a dramatic decrease in glutamine synthesis. Enhanced T301 phosphorylation was evident in a mouse model of epilepsy, which may contribute to the decreased GS activity seen during this trauma. Thus, our results highlight a novel molecular mechanism that determines GS activity under both normal and pathological conditions.

Keywords: glutamine synthetase, phosphorylation, epilepsy, astrocyte, cAMP-dependent protein kinase

INTRODUCTION

The glutamate/GABA-glutamine cycle plays a fundamental role in the central nervous system (CNS) by detoxifying the brain of excess neurotransmitters and ammonia as well as supplying neurons with glutamine, which is a precursor of both GABA and glutamate. Glutamine synthetase (GS) catalyzes an essential step in this pathway, the ATP-dependent condensation of glutamate and ammonia into glutamine (Schousboe et al., 2013).

GS is expressed in several organs; however, its expression in the CNS is mainly restricted to astrocytes (Suárez et al., 2002). Previous studies have shown that GS is essential to survival, both in rodents and in humans (Häberle et al., 2005; He et al., 2010). Moreover, inhibition of GS activity *in vivo* induces seizures in animal models (Rowe and Meister, 1970; Eid et al., 2008; Boissonnet et al., 2012). Consistent with its central role in neurotransmitter recycling and neurotransmission, GS expression and/or activity are dramatically decreased in several neurological disorders, including mesial temporal lobe epilepsy

(MTLE; Eid et al., 2004; van der Hel et al., 2005). Moreover, a recent study has demonstrated that conditional ablation of GS expression selectively in the mouse cortex of mice induces spontaneous seizures (Zhou et al., 2018).

MTLE is a recurrent, complex pathology characterized by neuronal loss and astrogliosis in the hippocampus and is the most common type of drug-resistant epilepsy (Asadi-Pooya et al., 2017). Several studies have shown that the cycling of glutamate to glutamine is slower and glutamate levels are increased in MTLE patients (Petroff et al., 2002; Cavus et al., 2005, 2008). Consistent with these findings, GS activity is significantly reduced in the sclerotic hippocampus (Eid et al., 2004; van der Hel et al., 2005), leading to the hypothesis that the loss of the enzyme's function might contribute to the pathological state of this disorder. However, the molecular mechanisms regulating the activity of GS within astrocytes remain to be explored.

Here, we report that cAMP-dependent protein kinase (PKA) phosphorylates GS on both threonine 301 (T301) and serine 343 (S343). Additionally, we show that the main site of phosphorylation, T301, plays a fundamental role in regulating the enzyme's activity and is significantly increased in a mouse model of epilepsy. Taken together, these results suggest that PKA-dependent phosphorylation of T301 regulates the activity of GS. Moreover, enhanced phosphorylation of this residue may contribute to the deficits in GS activity arising during epilepsy.

MATERIALS AND METHODS

Animals

Eight to 12-week-old C57BL/6 male mice were used for phospho-specific antibody characterization and kainate injections. All mice were housed in a 12-h light/dark cycle. All mice were bred in-house at the Tufts University School of Medicine and handled according to protocols approved by the Institutional Animal Care and Use Committee (IACUC).

Antibodies and Expression Constructs

The following antibodies were used for Western-blotting: GS mouse antibodies (Millipore, cat number MAB302 and Santa Cruz, cat number sc-398034), tubulin mouse antibody, pT301 and pS343 antibodies (created by PhosphoSolutions). GS rabbit antibody (Sigma, cat number G2781) was used for immunoprecipitation. GS was cloned into prK5 from mouse genome (ATTG) and a MYC tag was inserted between amino acids 372–373. A mutagenesis kit was used to substitute T301 and S343 into alanine (T>A: 5′AACGCCCGGCGTCTGGCTGGATTCCACGAAACC, S>A: 5′ GAAGACCGTCGGCCTGCTGCCAATTGTGACCCC).

Cell Culture and Transfection

COS-7 cells were maintained in Dulbecco's modified Eagle's medium/F12 (1:1) nutrient mix with 10% fetal bovine serum and 1% of PenStrep (Thermo Fisher, cat number 11330–057). The cells were transfected by electroporation (3 μg of DNA/condition) and used 24 h after transfection. Astrocytes were prepared from forebrain of 1–4 day-old mouse pups of either sex as previously described (Schildge et al., 2013). Cells were grown in Advanced modified Eagle's medium supplemented with 10% FBS and 1% P/S (Thermo Fisher, cat number 11995073). Confluent cultures were shaken to obtain an enriched astrocytes culture. The cells were trypsinized once a week and used 3 weeks after shaking.

Western-Blotting

Cells or brain tissues were sonicated in lysis buffer consisting of Tris, pH 8 20 mM, NaCl 150 mM, Triton 1%, EDTA 5 mM, NaF 10 mM, Na_3VO_4 2 mM, and Na pyrophosphate 10 mM. In order to detect GS, pT301 and pS343 signal, 15, 30 and 45 μg were loaded respectively from cell in culture lysates and 15, 45 and 60 μg were loaded respectively from brain lysates. Proteins separated by SDS-PAGE (10% gel) were then transferred to nitrocellulose membranes and blocked in 6% milk in PBST for 6 h. Membranes were further incubated with the appropriate primary antibody (6% milk in PBST overnight), and after extensive washes, they were probed with HRP-conjugated secondary antibodies for 1 h. Western blots were developed using an enhanced chemiluminescence system as per the manufacturer's instructions (Amresco). Membranes were imaged (ChemiDoc MP, Bio-Rad, Hercules, CA, USA) and analyzed using ImageJ (National Institutes of Health, Bethesda, MD, USA). For quantification, the ratio between GS, pT301 and pS343 and the reporter protein (tubulin) was first analyzed. We then normalized this value to the total GS to compare the variation of T301 and S343 phosphorylation change between each condition. In order to purify the signal of pT301 antibody, it was premixed with non-phospho peptide overnight before each use.

Immunoprecipitation and *in vitro* PKA Assay

Cells were lysed in lysis buffer consisting of 20 mM Tris, pH 8, 150 mM NaCl, 1% Triton X-100, 5 mM EDTA, 10 mM NaF, 2 mM Na_3VO_4, and 10 mM Na pyrophosphate for 1 h at 4°C on a circular rotor. Lysates were precleared with rabbit IgG attached to protein G beads for 4 h at 4°C. Lysates were then incubated overnight with 50 μL of protein G sepharose and 3 μg of GS antibody. Precipitated immunocomplexes were twice washed in lysis buffer. Half of the sample was then incubated in 50 μl of 40 mM Tris-HCl, pH 7.5, 5 mM magnesium acetate with 200 μm ATP, and 0.1 μg of the catalytic subunit of PKA for 30 min at 30°C, and the other half was incubated in the same reaction buffer without ATP as negative control.

Cloning, Expression and Purification of Mouse GS

The gene sequence encoding mouse GS (2–373, Uniprot assession #P15105) was synthesized with an N-terminal 6×His-AVI-TEV tag (MHHHHHHGLNDIFEAQKIEWHEENLYFQG) and cloned into pET-24a(+) to yield pNG189 (Blue Sky Bioservices, Worcester, MA, USA). GS mutants T301A and S343A were synthesized and cloned similarly (numbering refers to the native mouse sequence). All sequences were codon optimized for expression in *Escherichia coli*. GS mutants T301E and T301V were generated with the QuikChange II Site-Directed

Mutagenesis Kit (Agilent, Santa Clara, CA, USA) using pNG189 as a template according to the manufacturer's protocol.

For expression of GS, pNG189 was transformed into BL21 (DE3) cells (New England Biolabs, Ipswich, MA, USA). Cultures were grown in LB medium with 25 μg/mL kanamycin at 37°C with shaking until they reached an OD of 0.6, at which point they were induced by addition of isopropyl β-D-1-thiogalactopyranoside to a final concentration of 500 μM. After induction, cultures were incubated at 16°C overnight with shaking. Cells were harvested by centrifugation and stored at −20°C until further use. For protein purification, all steps were performed at 4°C. Two liters worth of cells were thawed and resuspended in lysis buffer containing 50 mM sodium phosphate pH 7.5, 500 mM NaCl, 10% glycerol, 500 μM TCEP, 10 mM imidazole, and 1× Halt Protease Inhibitor Cocktail, EDTA-Free (Thermo Scientific, Waltham, MA, USA). Cells were lysed by passage through a French press. Lysates were cleared by high-speed centrifugation and loaded onto a HisTrap HP column (GE Healthcare, Chicago, IL, USA) pre-equilibrated with 50 mM sodium phosphate pH 7.5, 500 mM NaCl, 10% glycerol, 500 μM TCEP, and 10 mM imidazole. The column was washed with the same buffer before eluting with a gradient of 1 M imidazole. Fractions containing GS were identified by SDS-PAGE, pooled, and concentrated to ∼2 mL. Crude GS was then loaded onto a HiLoad 16/600 Superdex 200 pg column (GE Healthcare, Chicago, IL, USA) pre-equilibrated with 50 mM sodium phosphate pH 7.5, 500 mM NaCl, 10% glycerol, and 500 μM TCEP. GS was eluted with the same buffer at a flow rate of 1 mL/min. Fractions containing GS were identified by SDS-PAGE, pooled, supplemented with 1 mM $MgCl_2$ and ATP, and concentrated. Protein concentration was determined by the Bradford method (Bio-Rad; #500–006) using bovine serum albumin as a standard (Thermo Scientific, Waltham, MA, USA; #23209). GS was stored at −80°C. GS mutants were expressed and purified similarly.

Thermal Shift Assays

Twenty-five-microliter reactions containing 5 μM wild-type (WT) or mutant GS, 5× SyproOrange (Life Technologies, Carlsbad, CA, USA; #S6651) and varying concentrations of $MgCl_2$ and ATP in 20 mM HEPES pH 7.5, 300 mM NaCl, 10% glycerol, and 500 μM TCEP were prepared in white 96-well PCR plates (ThermoFisher, Waltham, MA, USA; #AB0700/W). Plates were incubated in a Bio-Rad CFX96 thermocylcer at 25°C for 2 min then heated to 95°C at a rate of 0.2°C/5 s. Plates were read at every 0.2°C interval. Melting temperatures (T_m) were determined by the maximum point of the dF/dT curve of the HEX channel.

In vitro Phosphorylation Assays

Fifty-microliter reactions containing 5 μM WT or mutant GS and 2.5 μM Protein Kinase A (PKA; Sigma; #P2645) in 50 mM imidazole pH 7.5, 10 mM $MgCl_2$, 100 μM EDTA, 2 mM DTT, and 1 mM ATP were prepared and incubated overnight at room temperature with or without 5 μM PKI 6-22 (Calbiochem; #539684). Kinase reactions lacking PKI were stopped by the addition of PKI. Intact mass spectrometry analysis was performed on a TripleTOF 5,600+ (AB Sciex) equipped with a Duo Spray Ion Source and a Shimadzu LC 20-AD HPLC system (Shimadzu Scientific Instruments). Samples were diluted to 1 μM in 0.1% formic acid and separated on a Poroshell 300SB-C8 75 × 2.1 mm, 5 μm column (Agilent) at 30°C with a gradient of acetonitrile (5%–95%) in 0.1% formic acid. The mass spectrometer was operated in positive ion and intact protein mode. LC-MS data were acquired in TOF MS mode for m/z+ between 600 and 2,000. Peak areas for protein species were determined following spectrum deconvolution using PeakView (version 2.2) software.

GS Activity Assays

GS activity was measured using the γ-glutamyl hydroxamate assay (Pamiljans et al., 1962). For recombinant GS, reactions were prepared in 384-well plates (Greiner; #781101) in a final volume of 10 μL by mixing 5 μL of a concentrated substrate mix containing 0–700 mM glutamate, 40 mM ATP, and 40 mM hydroxylamine in assay buffer (40 mM imidazole pH 7.4, 20 mM $MgCl_2$, 1 mM DTT, and 0.01% Triton X-100) with 5 μL of concentrated enzyme mix containing either 150 nM WT GS, 700 nM GS T301A, 700 nM GS T301E, or 200 nM GS T301V in assay buffer. Negative controls lacking glutamate were prepared in parallel. Reactions were allowed to proceed at room temperature for 1 h. Reactions were terminated by the addition of 50 μL of a stop/developer solution containing 163 mM $FeCl_3$, 98 mM trichloroacetic acid, and 202 mM HCl. Stopped reactions were mixed thoroughly, and their absorbances were read at 540 nm. Background absorbance from negative controls lacking glutamate was subtracted from all measurements. These data were compared to standard curves containing genuine γ-glutamyl hydroxamate (Sigma; #G2253), which were prepared in assay buffer and developed as above; kinetic parameters were extracted from non-linear fits of these data.

Assays in tissue lysates were performed as above with slight modifications. Samples were lysed by sonication in assay buffer supplemented with 1% Triton X-100, 150 mM NaCl, 25 mM β-glycerophosphate, 2.5 mM sodium orthovanadate, and 1× Protease Inhibitor Cocktail (Sigma; #P1860) and centrifuged to remove insoluble material. Several common protease and phosphatase inhibitors, including sodium fluoride, sodium pyrophosphate, phenylmethylsulfonyl fluoride, and 4-(2-aminoethyl) benzenesulfonyl fluoride were found to inhibit GS (not shown) and should be avoided. Reactions were prepared in 200 μL PCR tubes in a final volume of 20 μL by mixing 10 μL of cleared lysate and 10 μL of a concentrated substrate mix containing 700 mM glutamate, 40 mM ATP, and 40 mM hydroxylamine in assay buffer. Negative controls lacking glutamate were prepared in parallel. Reactions were allowed to proceed at room temperature for 30, 40, 50, or 60 min to ensure linearity. Reactions were terminated by adding 100 μL of stop/developer solution, after which they were centrifuged to remove insoluble material. One-hundred microliters of each supernatant was transferred to the well of a 384-well plate, and their absorbances were read at 540 nm. Background absorbance from negative controls lacking glutamate was subtracted from

all measurements. Activity in lysates was compared to standard curves containing genuine γ-glutamyl hydroxamate as above and normalized by protein concentration using the Bradford method.

PKA Inhibition Assay

The effect of methionine sulfoximine (MSO; Sigma; #M5379) on PKA (EMD Millipore; #539481) activity was measured using the PKA Colorimetric Activity Kit (Invitrogen; #EIAPKA) according to the manufacturer's protocol.

Data Analysis

Data were analyzed using GraphPad PRISM, and statistical significance was determined at $p < 0.05$ using one-way ANOVA followed by Dunnett's multiple comparison *post hoc* test or Student's *t*-test for two groups.

RESULTS

GS Is Phosphorylated by PKA *in vitro*

In mammals, GS is a homomeric decamer comprising two stacked pentameric rings that catalyzes the ATP-dependent condensation of ammonia and glutamate to glutamine (Krajewski et al., 2008). Protein sequence comparison between rodents and human shows a high percentage of similarity (98%, **Figure 1A**). Interestingly, both species exhibit two consensus sites for PKA-dependent phosphorylation near the active site of the protein localized on threonine 301 and serine 343 (T301 and S343, **Figure 1A**). However, neither of these predicted sites of phosphorylation are found in prokaryotic forms of GS (**Figure 1B**), suggesting that phosphorylation may play a species-specific role in controlling enzyme activity.

In order to assess the possible role that phosphorylation plays in determining GS activity, we initially expressed WT and mutant versions of mouse GS modified with an N-terminal 6× His-Avi-TEV tag in *E. coli*. WT GS and mutants in which T301 and S343 were mutated to alanine (T301A and S343A) were affinity purified and exposed to the catalytic subunit of PKA in the presence or absence of a peptide inhibitor of PKA (PKI). Intact mass spectrometry analyses revealed that WT GS and GS S343A were substrates for PKA-dependent phosphorylation (**Figure 1C**), as indicated by an increase in mass consistent with the addition of a single phosphoryl group in the absence of PKI. Mutating T301 to alanine completely abolished GS phosphorylation, thus indicating that T301 is the primary phosphorylation site of PKA-mediated phosphorylation of GS *in vitro*.

PKA Phosphorylation Decreases GS Activity

T301 is located within the "glutamate flap," a flexible active site loop that enhances the binding of both glutamate and ammonia and is thought to shield the active site from water, thereby preventing premature hydrolysis of reactive intermediates (**Figure 2A**, **Supplementary Figure S1**; Liaw and Eisenberg, 1994; Alibhai and Villafranca, 1994; Gill and Eisenberg, 2001; Gill et al., 2002; Krajewski et al., 2008). Previous mutational studies of GS from *Bacillus subtilis* have demonstrated that mutations in the flap can dramatically affect the enzymatic activity of GS (Fisher et al., 2002; Wray and Fisher, 2010). In order to understand how phosphorylation of T301 affects GS activity, we treated GS with PKA in the presence or absence of PKI and measured the initial velocities of γ-glutamyl hydroxamate formation at various concentrations of glutamate (Pamiljans et al., 1962). We found that unphosphorylated GS (+PKI) was highly active and displayed a low affinity for glutamate ($K_{m\ app}$ = 21 ± 1 mM; n = 3; **Figure 2B**), which is consistent with previous studies on GS from other rodents (Richterich-Van Baerle et al., 1957; Wu, 1963; Lund, 1970). Importantly, treatment of GS with PKA in the absence of PKI decreased the specific activity of GS by approximately 40% at the highest glutamate concentration tested but did not significantly alter glutamate affinity. The decrease in activity correlated with a 74 ± 7% (n = 3) degree of phosphorylation of GS as measured by intact mass spectrometry (**Figure 1B**).

PKA Mediates Its Effects on GS Activity *via* T301

To determine if the effects of PKA on GS activity are mediated *via* direct phosphorylation we used site-directed mutagenesis. First, we mutated T301 to glutamate (T301E), whose negative charge mimics that of a phosphoryl group. We then tested the activity of GS T301E and found, as expected, that it had very low activity (about 25% of that of WT at maximum glutamate concentration; **Figure 2B**) and was insensitive to PKA-treatment.

To further explore structure-function relationships at position 301, we tested the activity of GS T301A, which we expected to exhibit WT-like activity but lack the capacity for regulation by phosphorylation. GS T301A was insensitive to PKA-treatment; however, its activity was similar to GS T301E (approximately 20% of that of WT, **Figure 2B**). In light of the low activity observed for GS T301A, we questioned whether WT-like activity would be maintained by the introduction of a bulkier valine residue, which is found at this position in several bacterial species (Krajewski et al., 2008; Wray and Fisher, 2010). Therefore, we generated a T301V mutant and tested its activity. GS T301V exhibited a similar specific activity to WT GS but displayed a significantly lower affinity for glutamate ($K_{m\ app}$ = 145 ± 12 mM, **Figure 2B**). As expected, PKA-treatment did not affect T301V activity.

In addition to alterations in glutamate-binding and activity, mutations within the glutamate flap have been shown to reduce the sensitivity of GS to the inhibitor MSO (Wray and Fisher, 2010). MSO binds to the glutamate binding site of GS in an initially reversible manner but is rapidly phosphorylated by GS in the presence of ATP; in WT GS, the glutamate flap forms strong hydrogen bonds with MSO phosphate, resulting in non-covalent but nearly irreversible inhibition (Eisenberg et al., 2000; Gill and Eisenberg, 2001; Jeitner and Cooper, 2014). We found that the IC_{50} of MSO for WT GS was 182 ± 14 μM (**Figure 2C**). The IC_{50} of MSO for GS T301V was 40-fold higher (7.6 ± 0.5 mM) and >100 mM for GS T301E and GS T301A.

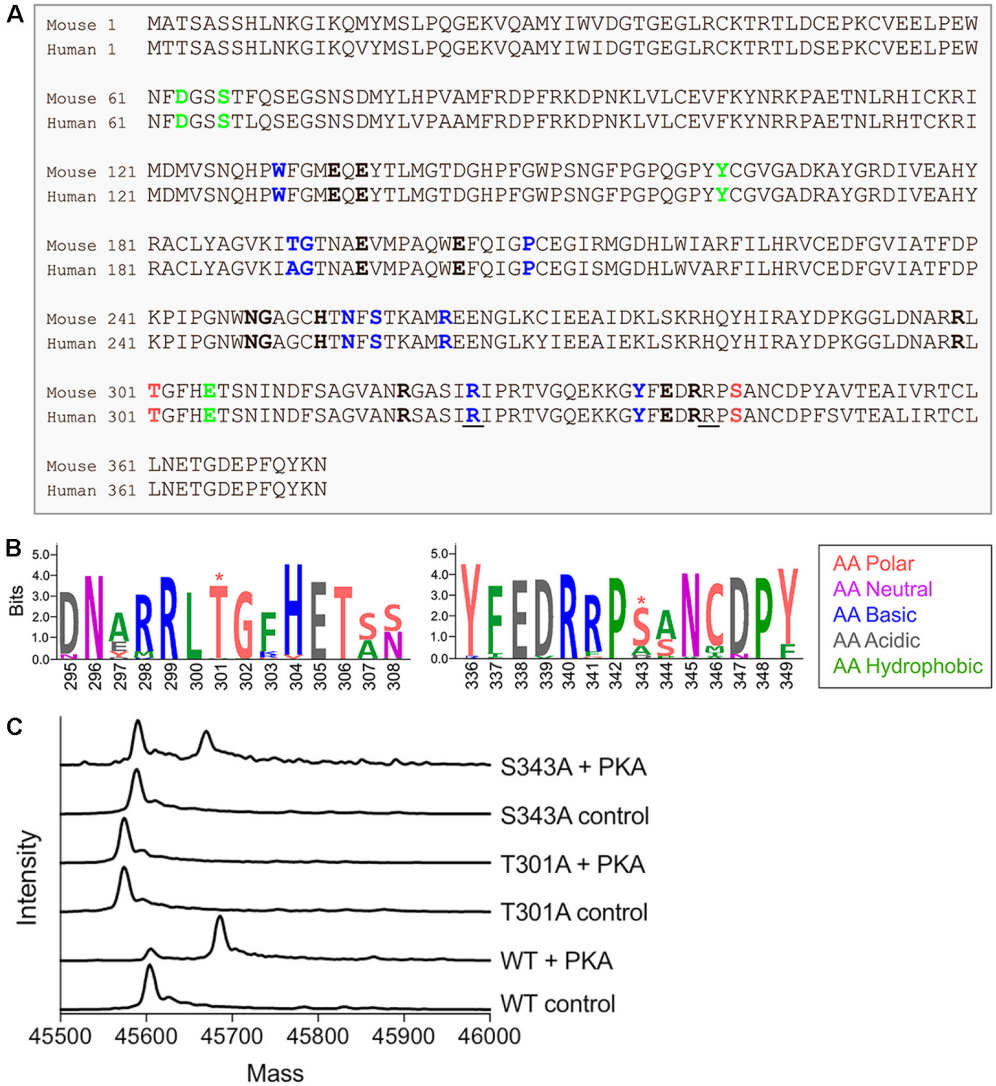

FIGURE 1 | Glutamine synthetase (GS) is phosphorylated by protein kinase A (PKA) *in vitro*. **(A)** Sequence alignment between mouse and human GS protein sequences. The amino acids that bind ammonia, ATP and glutamate are respectively labeled in bold green, blue and black. The underlined amino acids highlight the reported lethal mutations in human and the red amino acids indicate the two consensus sites for PKA-dependent phosphorylation. **(B)** The weblogo motif for an alignment between bacteria (*Escherichia coli*), yeast (*Saccharomyces cerevisiae*), plant (*Arabidopsis thaliana*), worm (*Caenorhabditis elegans*), chicken (*Gallus gallus*), dog (*Canis lupus*), mouse (*Mus musculus*) and human (http://weblogo.berkeley.edu/, *highlights the putative PKA-dependent phosphorylation sites). **(C)** Representative spectra from intact mass spectrometry analysis of purified WT and mutant GS treated with PKA in the presence (control) or absence (+ PKA) of PKI. A single phosphorylation event is indicated by an 80-Da increase in mass in "+ PKA" samples relative to controls.

In order to rule out the possibility that the observed differences in GS activity resulted from changes in GS stability or Mg- or ATP-binding, we performed thermal shift assays on GS in the presence of varying concentrations of MgATP, which has been shown to stabilize GS (Krajewski et al., 2008). We found that the melting temperatures of all GS constructs used in this study were similar (approximately 55°C) and that incubation with MgATP increased their melting temperatures to similar extents, indicating that the respective mutations do not impact on enzyme stability or ability to bind MgATP (**Figure 2D**). Collectively, these results indicate that residue T301 is essential for efficient catalysis and that alterations at this site, either by phosphorylation or mutation, can be a strong negative regulator of GS activity. Additionally, these findings are consistent with the idea that T301 phosphorylation exerts its effects on GS activity by perturbing the position or dynamics of the glutamate flap.

Analyses of GS Phosphorylation in Cell Lines and the Brain Using Mass Spectrometry

In order to assess the significance of our measurements using purified GS, we expressed GS in COS-7 cells (Huyghe et al., 2014). GS was immunoprecipitated from transfected COS-7 cells

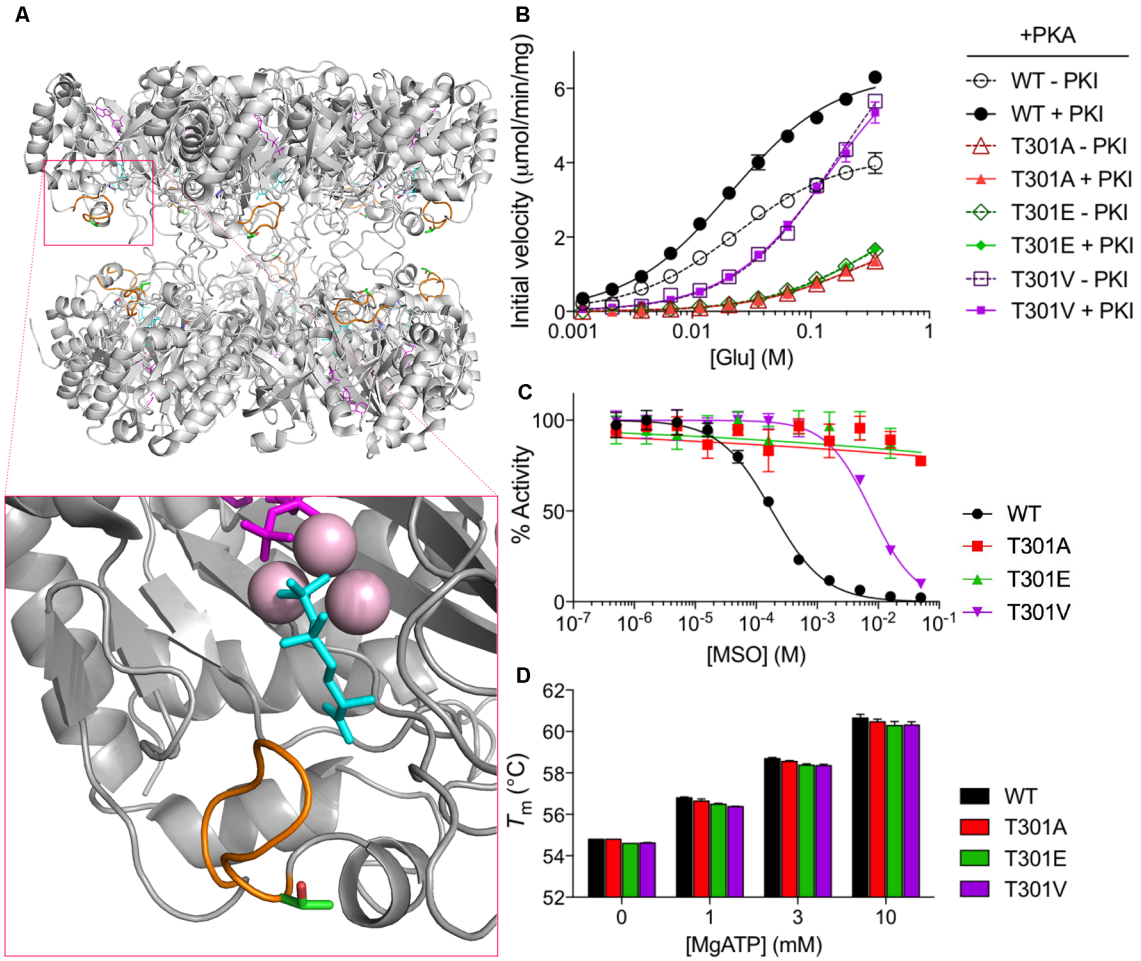

FIGURE 2 | PKA phosphorylation decreases GS activity. **(A)** Overall structure of a mammalian GS decamer, with an expanded view of the active site of GS (inset) showing the locations of the glutamate flap (T301–N308; orange), T301 (carbon in green; oxygen in red), methionine sulfoximine (MSO; cyan) in the glutamate binding site, manganese ions (pink), and ADP (magenta). Based on PDB ID 2QC8. **(B)** Initial velocity vs. glutamate concentration of purified WT and mutant GS treated with PKA in the presence or absence of PKI as measured by the γ-glutamyl hydroxamate assay. Graph shows the mean ± standard error of the mean (SEM; $n = 3$). **(C)** Activity of purified WT and mutant GS pretreated with MSO for 1 h at the indicated concentrations (with 20 mM ATP in assay buffer) as measured by the γ-glutamyl hydroxamate assay. Results are normalized to the maximum activity for each protein. Graph shows the mean ± SEM ($n = 3$–5). **(D)** Melting temperatures of purified WT and mutant GS in the presence of various concentrations of MgATP as measured by differential scanning fluorimetry. Graph shows the mean ± SEM ($n = 3$).

and incubated with active PKA in the presence or absence of ATP. The samples were then subjected to SDS-PAGE and stained with Coomassie blue. The major band at 45 kDa was then digested with trypsin and phosphorylation was examined using liquid chromatography coupled with mass spectroscopy (LC-MS/MS). Possible sites of phosphorylation were then ranked according to their ambiguity score (Ascore; Beausoleil et al., 2006). Both T301 and S343 exhibited Ascores >19 compared to control (-ATP), suggesting both residues are substrates for PKA-dependent phosphorylation (**Figure 3A**). Encouraged by our experiments using "back-phosphorylation," we assessed phosphorylation of GS in the brain. To do so, GS was immunoprecipitated from mice hippocampal lysates. Following SDS-PAGE and Coomassie blue staining, the principal band at 45 kDa was subjected to LC-MS/MS as detailed above. Ascores >19 were seen for both T301 and S343 (**Figures 3B,C**). Thus, our experiments in COS-7 cells and brain reveal that in common with our experiments *in vitro*, T301 is phosphorylated by PKA. In addition, these findings suggest that GS is also phosphorylated on residue S343 in cell lines and in the brain.

Characterization of Phospho-specific Antibodies Against GS

The results obtained using *in vitro* measurements of GS phosphorylation and our LC-MS/MS studies prompted us to create phospho-specific antibodies against T301 and S343 (pT301 and pS343, respectively). Accordingly, rabbits were immunized with a highly purified (>95%) synthetic peptide centered and chemically phosphorylated on the residue corresponding to T301 (bold) in GS: KGGLDNARRL**T**GFHETSNIND. Antibodies were raised

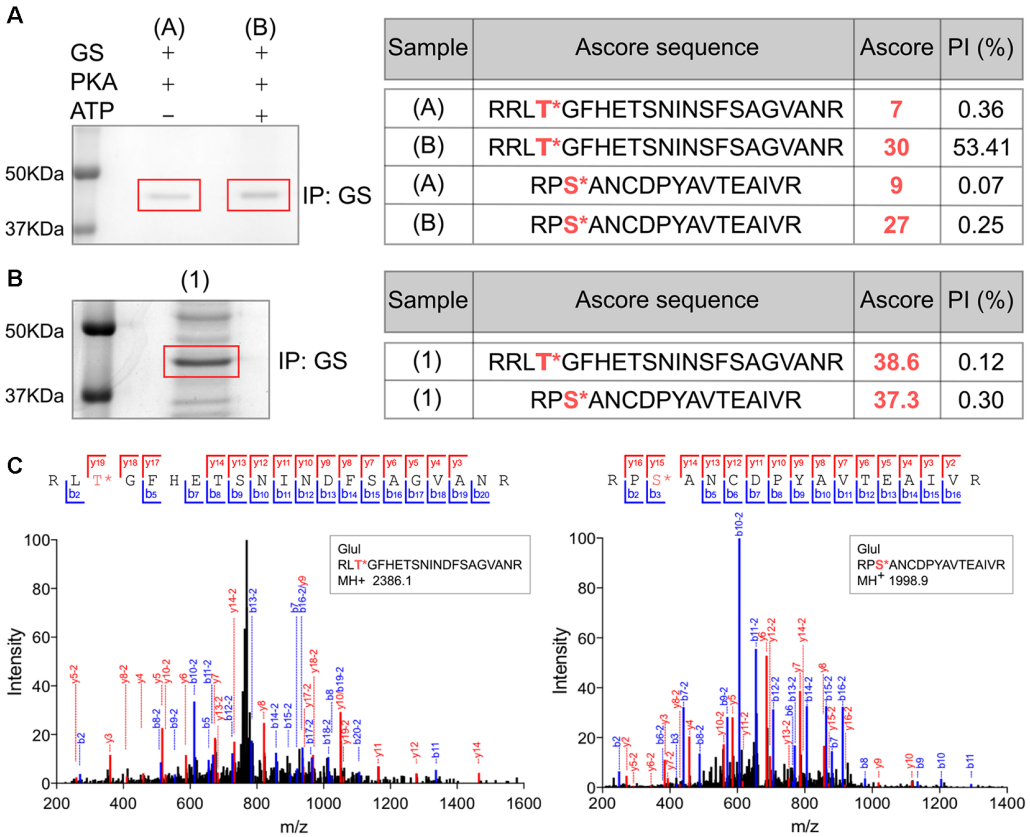

Sample	Ascore sequence	Ascore	PI (%)
(A)	RRLT*GFHETSNINSFSAGVANR	7	0.36
(B)	RRLT*GFHETSNINSFSAGVANR	30	53.41
(A)	RPS*ANCDPYAVTEAIVR	9	0.07
(B)	RPS*ANCDPYAVTEAIVR	27	0.25

Sample	Ascore sequence	Ascore	PI (%)
(1)	RRLT*GFHETSNINSFSAGVANR	38.6	0.12
(1)	RPS*ANCDPYAVTEAIVR	37.3	0.30

FIGURE 3 | Analyses of GS phosphorylation in cell lines and the brain using mass spectrometry. **(A)** Lysates from COS-7 cells transiently transfected with WT GS were used to immunoprecipitate GS followed by an *in vitro* PKA assay. The sample (A) is the negative control (no ATP) and (B) is the experimental condition in the presence of purified PKA and 200 μM ATP (n = 1). The samples were analyzed by LC/MS/MS and the associated table shows the ambiguity score for each peptide (Ascore) the ratio between the peak intensity between phospho and non-phospho peptide (PI). The potential phosphorylation sites are labeled in red. **(B)** Lysates from WT mice brain (1) were used to immnoprecipitate GS (n = 1). The samples were analyzed by LC/MS/MS and the associated table shows the results. **(C)** Representative LC/MS/MS spectra associated for two phosphopeptides identified from GS immunoprecipitated from brain samples.

against S343 by injecting mice with synthetic peptide centered and chemically phosphorylated on the residue corresponding to S343 (bold): KKGYFEDRRP**S**ANCDPYAVTE. High titer antisera were then subject to tandem affinity purification on the phospho- and dephospho-antigens (Jovanovic et al., 2004; Saliba et al., 2012).

To test the specificity of these antibodies we expressed WT GS, T301A and S343A in COS-7 cells (**Figures 4A,D** respectively). Our laboratory previously determined that COS-7 cells do not express GS endogenously; therefore, those cells are a great system to study the specificity of GS phospho antibodies (Huyghe et al., 2014). Extracts of cells expressing the respective constructs were then immunoblotted with pT301, pS343 and GS antibodies. The pT301 antibody recognized a major band of 45 kDa in cells expressing WT GS, as well as a lighter band at the same molecular weight with GS T301A (**Figure 4A**, n = 4). We then performed a peptide competition assay by pre-mixing the antibody with the phospho or non-phospho peptide (**Supplementary Figure S2**). We observed that the pT301 signal disappears when pre-mixed with the phospho peptide but not with the non-phospho peptide, demonstrating that the pT301 antibody specifically recognizes the T301 phosphorylation site; however, the lighter band observed with the T301A point mutant also suggests that pT301 antibody recognizes a second epitope on the phospho peptide. Therefore, we tested whether we could increase the specificity of this antibody by adding an extra purification step consisting of pre-mixing pT301 with the non-phospho peptide. Detection of this band was prevented by incubation with the de-phospho-antigen (**Supplementary Figure S2**); therefore, we added this extra step of antibody purification for the rest of the study.

The same method was used to assess the specificity of the pS343 antibody. In contrast to T301, no basal phosphorylation of S343 was seen in COS-7 cells. In order to determine whether S343 phosphorylation could be detected by increasing PKA activity, the cells were treated with forskolin for 15 min (FSK; 20 μM), which resulted in the detection of a 45-kDa band in cells expressing WT GS but not GS S343A (**Figure 4D**). Significantly, the detection of this band was blocked by absorption with the phospho- but not the dephospho-antigen and by pretreatment with λ-phosphatase (**Supplementary Figure S2**).

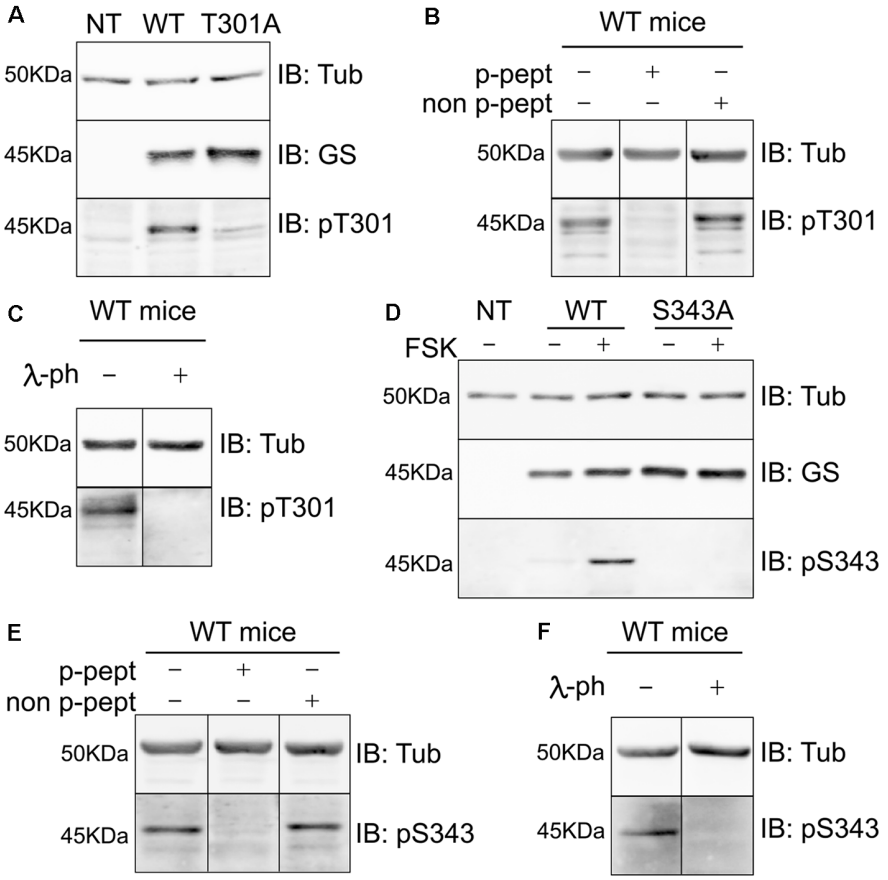

FIGURE 4 | Characterization of phospho-specific antibodies against GS. **(A)** Characterization of pT301 antibody using lysates from COS-7 cells transiently transfected with GS WT or T301A point mutant. Total lysates were immnunoblotted with tubulin, GS or pT301 antibodies. Lysate from non-transfected COS-7 cells was used as an additional negative control (NT, $n = 4$). **(B)** Lysates from WT mice forebrain were used for peptide competition assays to test pT301 specificity in brain. Total lysates were immunoblotted with tubulin and pT301 antibodies ($n = 3$). **(C)** Lysates from WT mice forebrains were used for lambda-phosphatase assays and immunoblotted with tubulin and pT301 antibodies ($n = 3$). **(D)** Characterization of pS343 antibody using lysates from COS-7 cells transiently transfected with GS WT or S343A point mutant and immunoblotted with tubulin, GS or pS343 antibodies. PKA activator forskolin (FSK, 20 μM for 15 min) was used to increase S343 phosphorylation signal. Total lysate from non-transfected COS-7 cells was used as an additional negative control (NT, $n = 3$). **(E)** Lysates from WT mice forebrain were used for peptide competition assays to test pS343 specificity in brain. Total lysates were immunoblotted with tubulin and pS343 antibodies ($n = 3$). **(F)** Lysates from WT mice forebrains were used for lambda-phosphatase assays and immunoblotted with tubulin and pS343 antibodies ($n = 3$).

In agreement with our studies conducted in COS-7 cells (**Figures 4A,D**, **Supplementary Figure S2**), pT301 and pS343 antibodies recognized bands of 45 kDa in brain extracts, the detection of which was prevented by peptide competition (**Figures 4B,E**) and λ-phosphatase treatment (**Figures 4C,F**). Collectively, these findings show that the antibodies directed against pT301 and pS343 recognize specifically the phosphorylated sites of GS. Moreover, these results suggest that the enzyme is phosphorylated on residues T301 and S343 in cell lines and the brain.

GS Is Preferentially Phosphorylated on T301 in COS-7 Cells and Astrocytes

To further assess GS phosphorylation, we expressed GS in COS-7 cells and compared the effects of FSK treatment on the phosphorylation of both residues T301 and S343 over a time course of 60 min. Consistent with our initial studies, only T301 exhibited basal phosphorylation, and FSK significantly increased phosphorylation of T301 and S343 over time. Significantly, PKA-dependent phosphorylation of T301 occurs faster (**Figure 5A**, 15 min = 1.77 ± 0.21, $p = 0.011$, $n = 4$) than on S343 (**Figure 5A**, 30 min = 0.13 ± 0.009, $p = 0.046$, $n = 4$). Next, we examined the levels of basal phosphorylation for each site in cultured astrocytes. While robust phosphorylation of T301 was seen in these primary cells, S343 phosphorylation was not detected (**Figure 5B**, $n = 3$). Collectively, these results in cultured cells suggest that GS is preferentially phosphorylated on T301.

MSO Binding Decreases T301 Phosphorylation

MSO is a well-characterized GS inhibitor that binds irreversibly to the glutamate binding site within this enzyme (Eisenberg et al., 2000; Cloix et al., 2010). Given the strategic

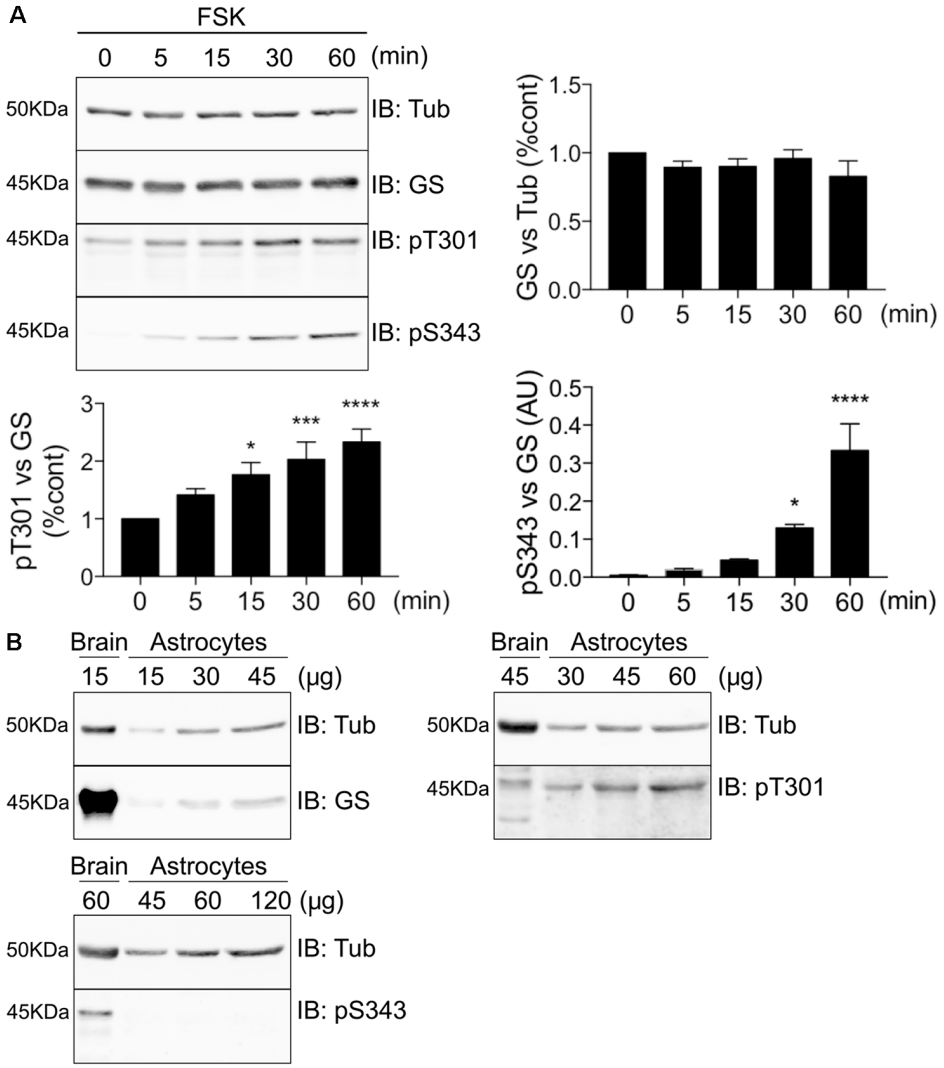

FIGURE 5 | GS is preferentially phosphorylated on T301 in COS-7 cells and astrocytes. **(A)** Lysates from COS-7 cells transfected with GS WT and treated with forskolin (FSK, 20 μM) for different time-point were analyzed by immunoblotting with tubulin, GS, pT301 and pS343 antibodies. Graphs show the mean ± SEM (*$p < 0.05$, ***$p < 0.001$, ****$p < 0.0001$, ANOVA Dunnett's multiple comparison, $n = 4$). **(B)** Basal phosphorylation of pT301 and pS343 in cultured astrocytes was determined by running an increasing range of protein concentration followed by immunoblotting with tubulin, GS, pT301 and pS343 antibodies. Total forebrain lysate was used as an additional control ($n = 3$).

localization of T301 within the active site, we further sought to assess whether MSO affects the ability of PKA to phosphorylate GS. To do so, COS-7 cells transfected with WT GS were exposed to 1 mM MSO for 60 min followed by 20 μM FSK for 30 min. Pre-treatment with MSO partially blocked the FSK-induced potentiation of T301 phosphorylation compared to control (**Figure 6A**, FSK = 3.41 ± 1.15, MSO+FSK = 2.19 ± 0.88, $n = 4$). Likewise, we observed that MSO tended to partially reduce FSK-induced potentiation of S343 phosphorylation; however, a significant increase was still observed compared to control condition (**Figure 6A**, FSK = 0.46 ± 0.11, MSO+FSK = 0.35 ± 0.12, $n = 4$, $p = 0.03$).

To assess the significance of the results obtained in COS-7 cells for events in the brain, mice were injected with either saline or a pro-convulsive dose of MSO (75 mg/kg, Bernard-Helary et al., 2000; Cloix et al., 2010). All MSO-injected mice started seizing between 4 and 6 h after injection. After 8 h, the mice were sacrificed and total GS levels and phosphorylation of T301 and S343 were analyzed from hippocampal lysates. MSO treatment significantly decreased T301 phosphorylation relative to vehicle-treated controls (**Figure 6C**, MSO = 0.70 ± 0.06, $p = 0.0185$, $n = 5$). We did not observe any significant change in S343 phosphorylation in MSO-injected mice compared to controls (**Figure 6C**, MSO = 1.11 ± 0.07, $n = 5$). These results suggest that MSO treatment specifically reduces phosphorylation of residue T301 in the hippocampus of WT mice. However, a previous study has shown that MSO binding impairs the antibody-antigen recognition that might lead to misinterpreting

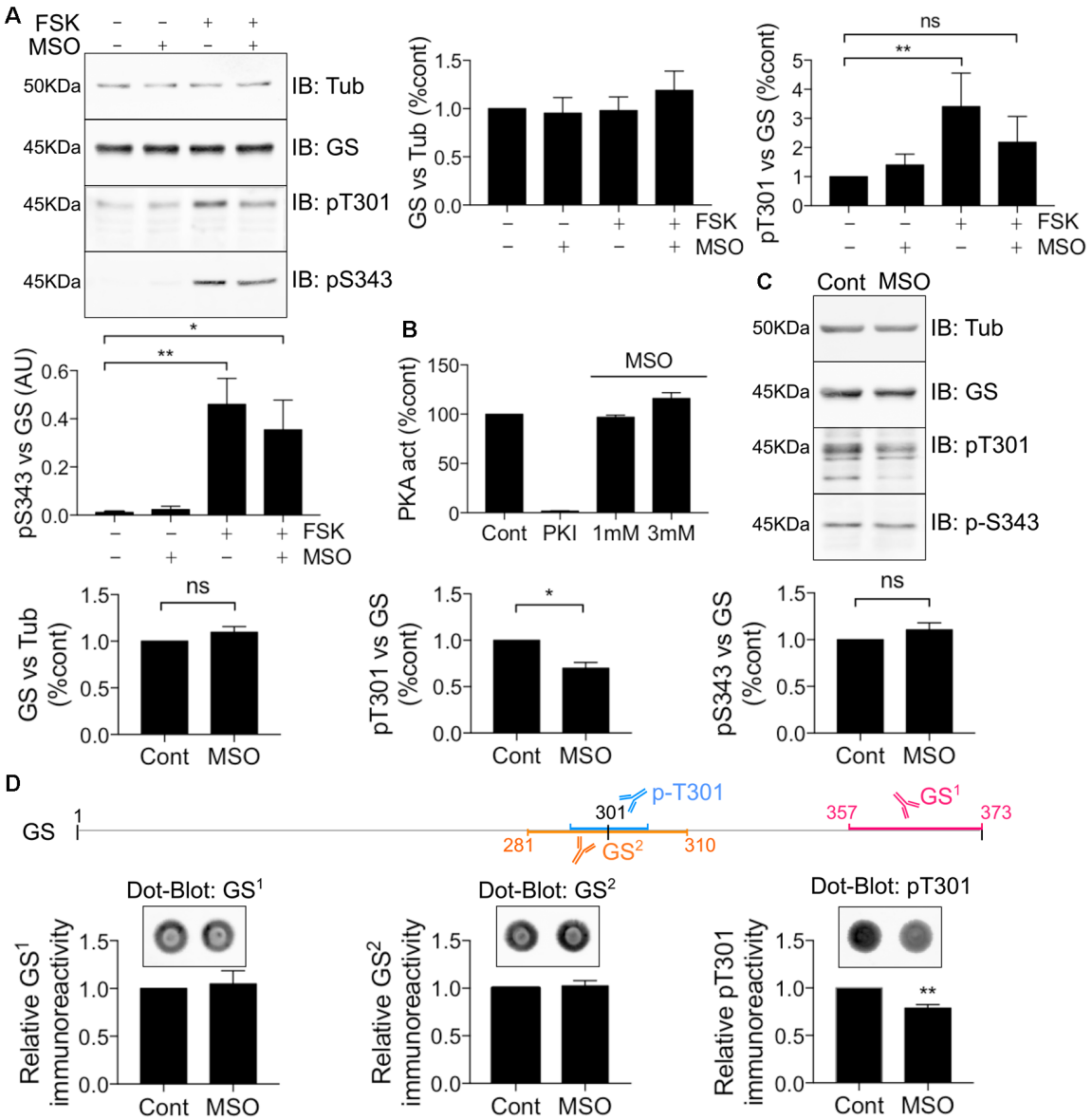

FIGURE 6 | MSO binding decreases T301 phosphorylation. **(A)** COS-7 cells transiently transfected with GS WT were treated with either MSO (1 mM for 60 min) or corresponding control followed by forskolin treatment (FSK, 20 μM for 30 min). Lysates were analyzed by immunoblotting with tubulin, GS, pT301 and pS343 antibodies. Graphs show the mean ± SEM (*$p < 0.05$, **$p < 0.01$, ns, not significant, ANOVA Dunnett's multiple comparison test, $n = 4$). **(B)** Relative activity of purified mouse PKA treated with either PKI (1 mM) or MSO as measured by an ELISA-based assay using an immobilized peptide substrate. Graph shows the mean ± SEM ($n = 3$). **(C)** WT male mice (8–12 weeks) were injected intraperitoneally by saline or MSO (75 mg/kg). Dissections of the hippocampi were performed 8 h after injection and the tissues lysates were analyzed by immunoblotting with tubulin, GS, pT301 and pS343 antibodies. Graphs show the mean ± SEM (*$p < 0.05$, ns, not significant, unpaired t-test, $n = 5$). **(D)** The schema represents the antigen region recognized by different GS antibodies. Hippocampal lysates used in **(C)** were analyzed by Dot-blot for pT301 and two different GS antibodies (GS^1 and GS^2). Graphs show the mean ± SEM (**$p < 0$ 0.01, unpaired t-test, $n = 5$).

the reduction of the signal for a decrease in protein levels (Bidmon et al., 2008). To circumvent this technical issue, the hippocampal samples from the saline or MSO-injected mice were used to perform dot-blot analyses to compare their respective immunoreactivity after an additional denaturation step (10 min at boiling temperature). As an additional control, a GS antibody targeting the region surrounding the T301 residue was also used (GS^2). We did not detect any change in GS signal using the regular GS antibody (GS^1) or GS^2, however, a reduction in the T301 signal was still evident (**Figure 6D**). Therefore, MSO binding leads to a decrease of T301 phosphorylation *in vivo*. Finally, to investigate any possible direct inhibitory effects of MSO on PKA activity, we directly tested how MSO affected the enzyme activity of PKA *in vitro*. Under these conditions, MSO did not directly modify PKA activity (**Figure 6B**). Accordingly, these results provide further evidence that T301 phosphorylation

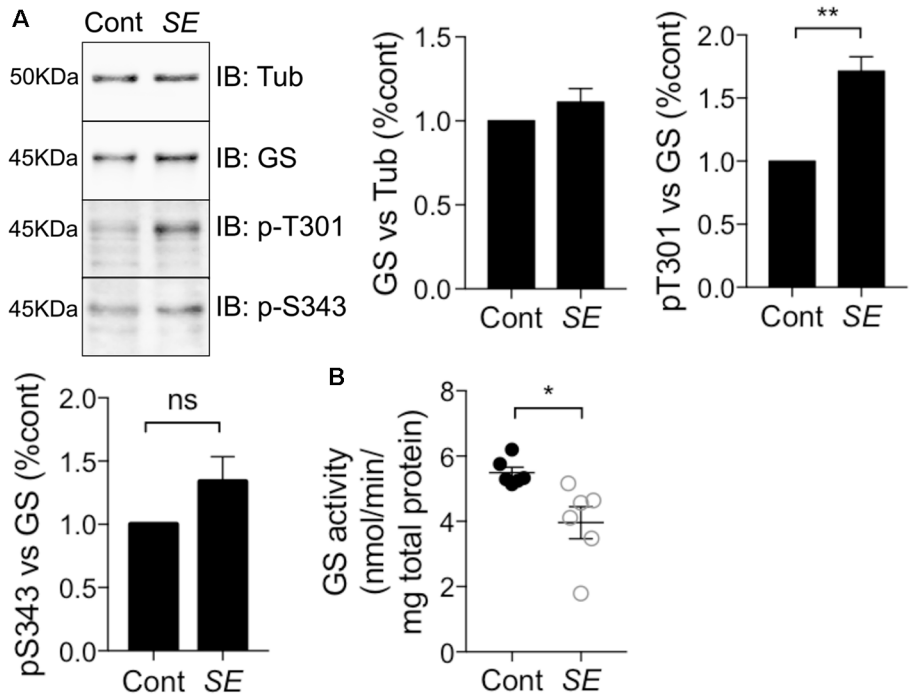

FIGURE 7 | T301 phosphorylation is increased and GS activity is decreased in chemico-induced *Status Epilepticus (SE)*. **(A)** WT male mice (8–12 weeks) were injected intraperitoneally by saline or kainate (KA, 20 mg/kg). Dissections of the hippocampi were performed 1 h after SE and the tissues lysates were analyzed by immunoblotting with tubulin, GS, pT301 and pS343 antibodies. Graphs show the mean ± SEM (*$p < 0.01$, ns: not significant, unpaired *t*-test, $n = 6$). **(B)** GS activity in hippocampal lysates from kainate- (*SE*) or saline-injected (Cont) mice as measured by the γ-glutamyl hydroxamate assay. Graph shows the mean ± SEM (*$p < 0.05$, unpaired *t*-test with unequal variances, $n = 6$).

is intimately linked to the catalytic mechanism of GS in the hippocampus of WT mice.

T301 Phosphorylation Is Increased and GS Activity Is Decreased in Chemico-induced *Status Epilepticus*

Epilepsy leads to deficits in GS activity (Eid et al., 2004; van der Hel et al., 2005); however, the underlying molecular mechanisms are ill-defined. Thus, we assessed if alterations in GS phosphorylation may be of significance in a mouse model of epilepsy. To do so, we injected mice with the chemico-convulsant kainic acid (KA; 20 mg/kg, Silayeva et al., 2015). Subsequent to KA injection, the development of *Status Epilepticus (SE)* was measured by the development of stage V seizures as defined on the Racine Scale (Racine et al., 1972). Sixty minutes after entrance into *SE*, mice were sacrificed and hippocampal lysates were subjected to immunoblotting with GS, pT301 and pS343 antibodies. This revealed that T301 phosphorylation was significantly increased in *SE* relative to control (**Figure 7A**, $SE = 1.71 \pm 0.12$, $n = 5$, $p = 0.0017$). In contrast, pS343 signal ($SE = 1.41 \pm 0.14$, $n = 5$, $p = 0.27$) and total GS ($SE = 1.11 \pm 0.04$, $n = 5$, $p = 0.85$) were not affected in KA-treated mice. Finally, we assessed if in addition to modifying GS phosphorylation, *SE* impacts on its activity using the γ-glutamyl hydroxamate assay. The results revealed that GS activity was reduced by about 25% in KA-injected mice relative to saline-injected controls (**Figure 7B**, control $= 5.5 \pm 0.17$, $SE = 3.4 \pm 0.49$, $n = 6$, $p = 0.02$). Thus, increased phosphorylation of T301 may contribute to the reduced activity of GS activity observed in epilepsy.

DISCUSSION

In the brain, GS expression is restricted to astrocytes where it plays a critical role in regulating glutamate levels and ammonia by catalyzing their conversation to glutamine. Thus, GS is accepted to play a central role in regulating amino acid-mediated neurotransmission. Studies in peripheral tissues and the CNS suggest that GS activity is modulated by posttranslational mechanisms that include acetylation, tyrosine nitration, oxidation, and ubiquitination (Bidmon et al., 2008; Castegna et al., 2011; Nguyen et al., 2016).

GS shows remarkable phylogenic conservation, but it is notable that all mammalian isoforms contain consensus sites for phosphorylation by some protein kinases, including PKA, that are not found in prokaryotes. To assess the importance of phosphorylation—the most common protein covalent modification—in regulating GS activity, we expressed and purified the murine enzyme from *E. coli*. *In vitro*, GS is phosphorylated by PKA to a final stoichiometry of 70% solely on T301. T301 is within the glutamate flap region of GS, which plays

a critical role in substrate binding and is essential for efficient catalysis (Alibhai and Villafranca, 1994; Liaw and Eisenberg, 1994; Gill and Eisenberg, 2001; Gill et al., 2002). Phosphorylation of GS significantly reduced its ability to synthesize glutamine, an effect that was critically dependent on T301, as demonstrated by mutation.

Mutation of T301 to either a glutamate residue, which mimics the negative charge of a phosphoryl group or a conservative alanine residue dramatically decreases enzyme activity and increases the apparent K_m for glutamate. In prokaryotes, a hydrophobic valine residue is found at this position, and conversion of T301 to valine in murine GS results in a relatively mild reduction in glutamate affinity. In addition to these effects on the catalytic properties of GS, mutating T301 greatly reduced the affinity of GS for its inhibitor MSO. Importantly, mutations of T301 did not modify GS stability or its ability to bind ATP and magnesium, providing further evidence that these mutations selectively impact glutamate binding. Collectively these results suggest a vital role for the phosphorylation of T301 in modulating the activity of GS, consistent with its role in substrate binding (Krajewski et al., 2008; Wray and Fisher, 2010).

To better understand the significance of our *in vitro* measurements, we examined the phosphorylation of GS when expressed in COS-7 cells and the brain. Confirming our experiments with purified PKA, LC-MS/MS revealed that T301 was phosphorylated in both systems. In addition, a second site of phosphorylation, S343, was detected. In contrast to T301, S343 is buried near the monomer-monomer interface (**Supplementary Figure S1**), and its role remains unknown. In agreement with our LC-MS/MS measurements, several high-throughput mass spectrometry studies have detected both T301 and S343 phosphorylation in the murine brain (Goswami et al., 2012; Trinidad et al., 2012). To further study GS phosphorylation, we produced phospho-specific antibodies against T301 and S343. These tools confirmed that both residues were phosphorylated in COS-7 cells and brain lysates. Significantly, in COS-7 cells, phosphorylation of T301 was faster than S343 upon activation of PKA. In cultured astrocytes, phosphorylation of S343 was not detected under basal conditions, but robust phosphorylation of T301 was seen. Collectively, these results suggest that T301 is preferentially phosphorylated upon the activation of PKA. They further suggest that S343 phosphorylation may be regulated in a cell type- and/or context-specific manner.

To further assess the relationship between phosphorylation of T301 and GS structure, mice were injected with MSO, which irreversibly binds to the enzyme's active site. Eight hours after MSO injection, decreased T301 phosphorylation was evident in the brain, while S343 and total GS levels were unaffected. Thus, these results suggest that phosphorylation of T301 is intimately linked with the catalytic mechanism of GS in the brain. Finally, we assessed the effects of *SE* on GS phosphorylation and activity. Deficits in GS activity and increased T301 phosphorylation were evident in mice exhibiting *SE*, while total GS levels and S343 phosphorylation were unaltered. Therefore, enhanced T301 phosphorylation may contribute to the deficits in GS activity that have been reported in human patients and animal models of epilepsy (Eid et al., 2004; van der Hel et al., 2005; Eid et al., 2012).

Collectively, our studies have revealed that GS is subject to PKA-mediated phosphorylation, which leads to its inhibition after *SE*. Thus, preventing its phospho-dependent inactivation may be a potent mechanism to upregulate GS activity, which may be of therapeutic value in epilepsy. Consistent with this notion, PKA activity has been shown to be elevated in animal models of *SE* and in human epileptic foci (Rakhade et al., 2005; Lee et al., 2007; Bracey et al., 2009). It is important to note that T301 in addition to S343 may also be subject to phosphorylation by other protein kinases such as protein kinase C. Thus, the phosphorylation of GS may be subject to modulation by multiple cell signaling pathways under control conditions and during seizures. Finally, as decreased GS activity has been implicated in schizophrenia (Steffek et al., 2008) and Alzheimer's disease (Smith et al., 1991), alterations in its phosphorylation may also be relevant to these pathologies.

ETHICS STATEMENT

All mice were bred in-house at the Tufts University School of Medicine and handled according to protocols approved by the Institutional Animal Care and Use Committee (IACUC).

AUTHOR CONTRIBUTIONS

DH performed cell culture, dissections, mutagenesis, antibody characterization, *in vivo* injection and Western blotting, and data analysis. AD performed enzyme purifications, *in vitro* phosphorylation, enzyme assays, thermal shift assays and data analysis. CV and PF performed antibody characterization, cell culture, Western-blotting. NG performed intact mass spectrometry. Experiments were designed by DH, AD, PD and SM. The manuscript was written by DH, AD and SM with input from PD, CV, NB, PF, HW, NG, AF, MP. DH and SM conceived the project.

FUNDING

This work was supported by NIH-NINDS grants NS101888, NS081735, NS087662, NIMH grants MH097446, MH106954 and NIH-DA grant DA037170.

ACKNOWLEDGMENTS

AD is a fellow of the AstraZeneca postdoc programme. We thank Emily Schwenger for technical assistance.

SUPPLEMENTARY MATERIAL

The Supplementary Material for this article can be found online at: https://www.frontiersin.org/articles/10.3389/fnmol.2019.00120/full#supplementary-material

REFERENCES

Alibhai, M., and Villafranca, J. J. (1994). Kinetic and mutagenic studies of the role of the active site residues Asp-50 and Glu-327 of *Escherichia coli* glutamine synthetase. *Biochemistry* 33, 682–686. doi: 10.1021/bi00169a008

Asadi-Pooya, A. A., Stewart, G. R., Abrams, D. J., and Sharan, A. (2017). Prevalence and incidence of drug-resistant mesial temporal lobe epilepsy in the United States. *World Neurosurg.* 99, 662–666. doi: 10.1016/j.wneu.2016.12.074

Beausoleil, S. A., Villén, J., Gerber, S. A., Rush, J., and Gygi, S. P. (2006). A probability-based approach for high-throughput protein phosphorylation analysis and site localization. *Nat. Biotechnol.* 24, 1285–1292. doi: 10.1038/nbt1240

Bernard-Helary, K., Lapouble, E., Ardourel, M., Hévor, T., and Cloix, J. F. (2000). Correlation between brain glycogen and convulsive state in mice submitted to methionine sulfoximine. *Life Sci.* 67, 1773–1781. doi: 10.1016/s0024-3205(00)00756-6

Bidmon, H. J., Görg, B., Palomero-Gallagher, N., Schleicher, A., Haussinger, D., Speckmann, E. J., et al. (2008). Glutamine synthetase becomes nitrated and its activity is reduced during repetitive seizure activity in the pentylentetrazole model of epilepsy. *Epilepsia* 49, 1733–1748. doi: 10.1111/j.1528-1167.2008.01642.x

Boissonnet, A., Hévor, T., and Cloix, J. F. (2012). Phenotypic differences between fast and slow methionine sulfoximine-inbred mice: seizures, anxiety and glutamine synthetase. *Epilepsy Res.* 98, 25–34. doi: 10.1016/j.eplepsyres.2011.08.012

Bracey, J. M., Kurz, J. E., Low, B., and Churn, S. B. (2009). Prolonged seizure activity leads to increased protein kinase A activation in the rat pilocarpine model of status epilepticus. *Brain Res.* 1283, 167–176. doi: 10.1016/j.brainres.2009.05.066

Castegna, A., Palmieri, L., Spera, I., Porcelli, V., Palmieri, F., Fabis-Pedrini, M. J., et al. (2011). Oxidative stress and reduced glutamine synthetase activity in the absence of inflammation in the cortex of mice with experimental allergic encephalomyelitis. *Neuroscience* 185, 97–105. doi: 10.1016/j.neuroscience.2011.04.041

Cavus, I., Kasoff, W. S., Cassaday, M. P., Jacob, R., Gueorguieva, R., Sherwin, R. S., et al. (2005). Extracellular metabolites in the cortex and hippocampus of epileptic patients. *Ann. Neurol.* 57, 226–235. doi: 10.1002/ana.20380

Cavus, I., Pan, J. W., Hetherington, H. P., Abi-Saab, W., Zaveri, H. P., Vives, K. P., et al. (2008). Decreased hippocampal volume on MRI is associated with increased extracellular glutamate in epilepsy patients. *Epilepsia* 49, 1358–1366. doi: 10.1111/j.1528-1167.2008.01603.x

Cloix, J. F., Tahi, Z., Martin, B., and Hevor, T. (2010). Selection of two lines of mice based on latency to onset of methionine sulfoximine seizures. *Epilepsia* 51, 118–128. doi: 10.1111/j.1528-1167.2009.02200.x

Eid, T., Behar, K., Dhaher, R., Bumanglag, A. V., and Lee, T. S. (2012). Roles of glutamine synthetase inhibition in epilepsy. *Neurochem. Res.* 37, 2339–2350. doi: 10.1007/s11064-012-0766-5

Eid, T., Ghosh, A., Wang, Y., Beckstrom, H., Zaveri, H. P., Lee, T. S., et al. (2008). Recurrent seizures and brain pathology after inhibition of glutamine synthetase in the hippocampus in rats. *Brain* 131, 2061–2070. doi: 10.1093/brain/awn133

Eid, T., Thomas, M. J., Spencer, D. D., Runden-Pran, E., Lai, J. C., Malthankar, G. V., et al. (2004). Loss of glutamine synthetase in the human epileptogenic hippocampus: possible mechanism for raised extracellular glutamate in mesial temporal lobe epilepsy. *Lancet* 363, 28–37. doi: 10.1016/s0140-6736(03)15166-5

Eisenberg, D., Gill, H. S., Pfluegl, G. M., and Rotstein, S. H. (2000). Structure-function relationships of glutamine synthetases. *Biochim. Biophys. Acta* 1477, 122–145. doi: 10.1016/s0167-4838(99)00270-8

Fisher, S. H., Brandenburg, J. L., Wray, L. V. Jr. (2002). Mutations in bacillus subtilis glutamine synthetase that block its interaction with transcription factor TnrA. *Mol. Microbiol.* 45, 627–635. doi: 10.1046/j.1365-2958.2002.03054.x

Gill, H. S., and Eisenberg, D. (2001). The crystal structure of phosphinothricin in the active site of glutamine synthetase illuminates the mechanism of enzymatic inhibition. *Biochemistry* 40, 1903–1912. doi: 10.1021/bi002438h

Gill, H. S., Pfluegl, G. M., and Eisenberg, D. (2002). Multicopy crystallographic refinement of a relaxed glutamine synthetase from mycobacterium tuberculosis highlights flexible loops in the enzymatic mechanism and its regulation. *Biochemistry* 41, 9863–9872. doi: 10.1021/bi020254s

Goswami, T., Li, X., Smith, A. M., Luderowski, E. M., Vincent, J. J., Rush, J., et al. (2012). Comparative phosphoproteomic analysis of neonatal and adult murine brain. *Proteomics* 12, 2185–2189. doi: 10.1002/pmic.201200003

Häberle, J., Görg, B., Rutsch, F., Schmidt, E., Toutain, A., Benoist, J. F., et al. (2005). Congenital glutamine deficiency with glutamine synthetase mutations. *N. Engl. J. Med.* 353, 1926–1933. doi: 10.1056/NEJMoa050456

He, Y., Hakvoort, T. B., Vermeulen, J. L., Labruyere, W. T., De Waart, D. R., Van Der Hel, W. S., et al. (2010). Glutamine synthetase deficiency in murine astrocytes results in neonatal death. *Glia* 58, 741–754. doi: 10.1002/glia.20960

Huyghe, D., Nakamura, Y., Terunuma, M., Faideau, M., Haydon, P., Pangalos, M. N., et al. (2014). Glutamine synthetase stability and subcellular distribution in astrocytes are regulated by gamma-aminobutyric type B receptors. *J. Biol. Chem.* 289, 28808–28815. doi: 10.1074/jbc.M114.583534

Jeitner, T. M., and Cooper, A. J. (2014). Inhibition of human glutamine synthetase by L-methionine-S,R-sulfoximine-relevance to the treatment of neurological diseases. *Metab. Brain Dis.* 29, 983–989. doi: 10.1007/s11011-013-9439-6

Jovanovic, J. N., Thomas, P., Kittler, J. T., Smart, T. G., and Moss, S. J. (2004). Brain-derived neurotrophic factor modulates fast synaptic inhibition by regulating $GABA_A$ receptor phosphorylation, activity and cell-surface stability. *J. Neurosci.* 24, 522–530. doi: 10.1523/JNEUROSCI.3606-03.2004

Krajewski, W. W., Collins, R., Holmberg-Schiavone, L., Jones, T. A., Karlberg, T., and Mowbray, S. L. (2008). Crystal structures of mammalian glutamine synthetases illustrate substrate-induced conformational changes and provide opportunities for drug and herbicide design. *J. Mol. Biol.* 375, 217–228. doi: 10.1016/j.jmb.2007.10.029

Lee, T. S., Mane, S., Eid, T., Zhao, H., Lin, A., Guan, Z., et al. (2007). Gene expression in temporal lobe epilepsy is consistent with increased release of glutamate by astrocytes. *Mol. Med.* 13, 1–13. doi: 10.2119/2006-00079.Lee

Liaw, S. H., and Eisenberg, D. (1994). Structural model for the reaction mechanism of glutamine synthetase, based on five crystal structures of enzyme-substrate complexes. *Biochemistry* 33, 675–681. doi: 10.1021/bi00169a007

Lund, P. (1970). A radiochemical assay for glutamine synthetase and activity of the enzyme in rat tissues. *Biochem. J.* 118, 35–39. doi: 10.1042/bj1180035

Nguyen, T. V., Lee, J. E., Sweredoski, M. J., Yang, S. J., Jeon, S. J., Harrison, J. S., et al. (2016). Glutamine triggers acetylation-dependent degradation of glutamine synthetase via the thalidomide receptor cereblon. *Mol. Cell* 61, 809–820. doi: 10.1016/j.molcel.2016.02.032

Pamiljans, V., Krishnaswamy, P. R., Dumville, G., and Meister, A. (1962). Studies on the mechanism of glutamine synthesis; isolation and properties of the enzyme from sheep brain. *Biochemistry* 1, 153–158. doi: 10.1021/bi00907a023

Petroff, O. A., Errante, L. D., Rothman, D. L., Kim, J. H., and Spencer, D. D. (2002). Glutamate-glutamine cycling in the epileptic human hippocampus. *Epilepsia* 43, 703–710. doi: 10.1046/j.1528-1157.2002.38901.x

Racine, R. J., Gartner, J. G., and Burnham, W. M. (1972). Epileptiform activity and neural plasticity in limbic structures. *Brain Res.* 47, 262–268. doi: 10.1016/0006-8993(72)90268-5

Rakhade, S. N., Yao, B., Ahmed, S., Asano, E., Beaumont, T. L., Shah, A. K., et al. (2005). A common pattern of persistent gene activation in human neocortical epileptic foci. *Ann. Neurol.* 58, 736–747. doi: 10.1002/ana.20633

Richterich-Van Baerle, R., Goldstein, L., and Dearborn, E. H. (1957). Kidney glutaminases. III. Glutamine synthesis in the guinea pig kidney. *Enzymologia* 18, 327–336.

Rowe, W. B., and Meister, A. (1970). Identification of L-methionine-S-sulfoximine as the convulsant isomer of methionine sulfoximine. *Proc. Natl. Acad. Sci. U S A* 66, 500–506. doi: 10.1073/pnas.66.2.500

Saliba, R. S., Kretschmannova, K., and Moss, S. J. (2012). Activity-dependent phosphorylation of $GABA_A$ receptors regulates receptor insertion and tonic current. *EMBO J.* 31, 2937–2951. doi: 10.1038/emboj.2012.109

Schildge, S., Bohrer, C., Beck, K., and Schachtrup, C. (2013). Isolation and culture of mouse cortical astrocytes. *J. Vis. Exp.* 71:50079. doi: 10.3791/50079

Schousboe, A., Bak, L. K., and Waagepetersen, H. S. (2013). Astrocytic control of biosynthesis and turnover of the neurotransmitters glutamate and GABA. *Front. Endocrinol.* 4:102. doi: 10.3389/fendo.2013.00102

Silayeva, L., Deeb, T. Z., Hines, R. M., Kelley, M. R., Munoz, M. B., Lee, H. H., et al. (2015). KCC2 activity is critical in limiting the onset and severity of status epilepticus. *Proc. Natl. Acad. Sci. U S A* 112, 3523–3528. doi: 10.1073/pnas.1415126112

Smith, C. D., Carney, J. M., Starke-Reed, P. E., Oliver, C. N., Stadtman, E. R., Floyd, R. A., et al. (1991). Excess brain protein oxidation and enzyme dysfunction in normal aging and in Alzheimer disease. *Proc. Natl. Acad. Sci. U S A* 88, 10540–10543. doi: 10.1073/pnas.88.23.10540

Steffek, A. E., McCullumsmith, R. E., Haroutunian, V., and Meador-Woodruff, J. H. (2008). Cortical expression of glial fibrillary acidic protein and glutamine synthetase is decreased in schizophrenia. *Schizophr. Res.* 103, 71–82. doi: 10.1016/j.schres.2008.04.032

Suárez, I., Bodega, G., and Fernández, B. (2002). Glutamine synthetase in brain: effect of ammonia. *Neurochem. Int.* 41, 123–142. doi: 10.1016/s0197-0186(02)00033-5

Trinidad, J. C., Barkan, D. T., Gulledge, B. F., Thalhammer, A., Sali, A., Schoepfer, R., et al. (2012). Global identification and characterization of both O-GlcNAcylation and phosphorylation at the murine synapse. *Mol. Cell. Proteomics* 11, 215–229. doi: 10.1074/mcp.o112.018366

van der Hel, W. S., Notenboom, R. G., Bos, I. W., van Rijen, P. C., van Veelen, C. W., and de Graan, P. N. (2005). Reduced glutamine synthetase in hippocampal areas with neuron loss in temporal lobe epilepsy. *Neurology* 64, 326–333. doi: 10.1212/01.WNL.0000149636.44660.99

Wray, L. V. Jr., and Fisher, S. H. (2010). Functional roles of the conserved Glu304 loop of bacillus subtilis glutamine synthetase. *J. Bacteriol.* 192, 5018–5025. doi: 10.1128/JB.00509-10

Wu, C. (1963). Glutamine synthetase. I. A comparative study of its distribution in animals and its inhibition by Dl-allo-σ-hydroxylysine. *Comp. Biochem. Physiol.* 9, 335–351. doi: 10.1016/0010-406x(63)90169-5

Zhou, Y., Dhaher, R., Parent, M., Hu, Q. X., Hassel, B., Yee, S. P., et al. (2018). Selective deletion of glutamine synthetase in the mouse cerebral cortex induces glial dysfunction and vascular impairment that precede epilepsy and neurodegeneration. *Neurochem. Int.* 123, 22–33. doi: 10.1016/j.neuint.2018.07.009

Conflict of Interest Statement: AD, NG, NB, PD and MP are current employees of AstraZeneca. SM acts as a consultant for AstraZeneca and SAGE Therapeutics, relationships that are governed by Tufts University.

The remaining authors declare that the research was conducted in the absence of any commercial or financial relationships that could be construed as a potential.

frontiers in Aging Neuroscience

ORIGINAL RESEARCH
published: 31 May 2019
doi: 10.3389/fnagi.2019.00123

Humanin, a Mitochondrial-Derived Peptide Released by Astrocytes, Prevents Synapse Loss in Hippocampal Neurons

Sandra Cristina Zárate[1,2]*, *Marianela Evelyn Traetta*[3,4], *Martín Gabriel Codagnone*[3,4‡], *Adriana Seilicovich*[1,2†] *and Analía Gabriela Reinés*[3,4†]

[1]*Instituto de Investigaciones Biomédicas (INBIOMED, UBA-CONICET), Facultad de Medicina, Universidad de Buenos Aires, Buenos Aires, Argentina,* [2]*Departamento de Histología, Embriología, Biología Celular y Genética, Facultad de Medicina, Universidad de Buenos Aires, Buenos Aires, Argentina,* [3]*Instituto de Biología Celular y Neurociencias "Prof. E. De Robertis" (IBCN, UBA-CONICET), Facultad de Medicina, Universidad de Buenos Aires, Buenos Aires, Argentina,* [4]*Departamento de Farmacología, Facultad de Farmacia y Bioquímica, Universidad de Buenos Aires, Buenos Aires, Argentina*

OPEN ACCESS

Edited by:
Maria Jose Bellini, National Council for Scientific and Technical Research (CONICET), Argentina

Reviewed by:
Alexei Verkhratsky, University of Manchester, United Kingdom
Estefanía Acaz-Fonseca, Spanish National Research Council (CSIC), Spain

***Correspondence:**
Sandra Cristina Zárate
szarate@fmed.uba.ar

†These authors have contributed equally to this work

‡Present address:
Martín Gabriel Codagnone, APC Microbiome Ireland, University College Cork, Cork, Ireland; Department of Anatomy and Neuroscience, University College Cork, Cork, Ireland

Received: *16 January 2019*
Accepted: *09 May 2019*
Published: *31 May 2019*

Citation:
Zárate SC, Traetta ME, Codagnone MG, Seilicovich A and Reinés AG (2019) Humanin, a Mitochondrial-Derived Peptide Released by Astrocytes, Prevents Synapse Loss in Hippocampal Neurons. Front. Aging Neurosci. 11:123. doi: 10.3389/fnagi.2019.00123

Astroglial cells are crucial for central nervous system (CNS) homeostasis. They undergo complex morpho-functional changes during aging and in response to hormonal milieu. Ovarian hormones positively affect different astroglia parameters, including regulation of cell morphology and release of neurotrophic and neuroprotective factors. Thus, ovarian hormone loss during menopause has profound impact in astroglial pathophysilogy and has been widely associated to the process of brain aging. Humanin (HN) is a secreted mitochondrial-encoded peptide with neuroprotective effects. It is localized in several tissues with high metabolic rate and its expression decreases with age. In the brain, humanin has been found in glial cells in physiological conditions. We previously reported that surgical menopause induces hippocampal mitochondrial dysfunction that mimics an aging phenotype. However, the effect of ovarian hormone deprivation on humanin expression in this area has not been studied. Also, whether astrocytes express and release humanin and the regulation of such processes by ovarian hormones remain elusive. Although humanin has also proven to be beneficial in ameliorating cognitive impairment induced by different insults, its putative actions on structural synaptic plasticity have not been fully addressed. In a model of surgical menopause in rats, we studied hippocampal humanin expression and localization by real-time quantitative polymerase chain reaction (RT-qPCR) and double immunohistochemistry, respectively. Humanin production and release and ovarian hormone regulation of such processes were studied in cultured astrocytes by flow cytometry and ELISA, respectively. Humanin effects on glutamate-induced structural synaptic alterations were determined in primary cultures of hippocampal neurons by immunocytochemistry.

Abbreviations: CNS, Central nervous system; GFAP, glial fibrillary acidic protein; HN, humanin; HNr, rattin; AD, Alzheimer's disease; ORF, open reading frame; rRNA, ribosomal RNA; NMDA, *N*-methyl-D-aspartate; CNTFR-α, ciliary neurotrophic factor α; DMEM, Dulbecco's Modified Eagle Medium; FCS, fetal calf serum; OVX, ovariectomized; HPRT, hypoxanthine-guanine phosphoribosyltransferase; FITC, fluorescein isothiocyanate; DAPI, 4′,6 diamidino-2-phenilindoledihydrocloride; E, 17β-estradiol; P, progesterone; MTT, 3-(4, 5-dimethylthiazol-2-yl)-2, 5-diphenyltetrazolium bromide; DIV, day *in vitro*; GH, growth hormone; IGF-1, insulin-like growth factor-1; TFAM, mitochondrial transcription factor A; mtDNA, mitochondrial DNA; DG, dentate gyrus; GABA, γ-aminobutyric acid.

Humanin expression was lower in the hippocampus of ovariectomized rats and its immunoreactivity colocalized with astroglial markers. Chronic ovariectomy also promoted the presence of less complex astrocytes in this area. Ovarian hormones increased humanin intracellular content and release by cultured astrocytes. Humanin prevented glutamate-induced dendritic atrophy and reduction in puncta number and total puncta area for pre-synaptic marker synaptophysin in cultured hippocampal neurons. In conclusion, astroglial functional and morphological alterations induced by chronic ovariectomy resemble an aging phenotype and could affect astroglial support to neuronal function by altering synaptic connectivity and functionality. Reduced astroglial-derived humanin may represent an underlying mechanism for synaptic dysfunction and cognitive decline after menopause.

Keywords: astrocytes, ovarian hormones, mitochondria, humanin, synapse, hippocampus

INTRODUCTION

Proper functioning of the central nervous system (CNS) requires the tight intercommunication between two main cell types: neurons and glial cells. It is now well accepted that glia functions go much beyond mere structural and metabolic support to neurons, indeed they are now recognized as key players in diverse physiological processes such as synaptic communication and plasticity, homeostasis and network-level activity in the adult brain (Allen and Lyons, 2018). Neuron-glia interplay is highly dynamic and prone to changes as a result of the natural process of aging as well as alterations associated to different pathologies (Verkhratsky et al., 2014). During aging, both structural and physiological changes that occur in the brain have been attributed to changes in glial cells, which reduce their number and modify gene expression (Palmer and Ousman, 2018). In fact, glial rather than neuronal-specific genes have been proposed to be better predictors of age (Soreq et al., 2017). Among glial cells, astrocytes are crucial for maintaining synaptic connectivity throughout life by means of creating a perisynaptic sheath that accumulates molecules responsible for synaptic support (Verkhratsky et al., 2015). Aged astrocytes undergo profound morpho-functional alterations, which involve retraction of their cytoplasmic processes and a decline in the production of metabolic and trophic factors. These alterations have a direct impact in CNS health, as aged astrocytes reduce their neuroprotective and homeostatic capacity, altering, in turn, neuronal synaptic connectivity and functionality (Verkhratsky et al., 2010, 2014; Palmer and Ousman, 2018).

Ovarian hormones estradiol and progesterone have trophic effects involved in the maintenance of both reproductive and non-reproductive functions in different tissues (Nilsen and Brinton, 2002; Morrison et al., 2006). In the brain, they exert potent antioxidant and neuroprotective actions that promote cognitive health. In fact, their loss during aging and natural or induced menopause has been linked to several pathological conditions, such as neuroinflammation, mitochondrial dysfunction, synaptic decline, cognitive impairment and increased risk of neurodegenerative disorders (Zárate et al., 2017b). It has been reported that the density of dendritic spines as well as synapse number in the CA1 area of the hippocampus decrease with natural or surgical loss of ovarian hormones (Gould et al., 1990; Woolley and McEwen, 1992, 1993; Adams et al., 2001). Many of the beneficial effects of these hormones are mediated through their direct actions on neurons. However, astrocytes are also cellular targets of ovarian hormones and thus are highly involved in the protective and reparative actions of estradiol and progesterone (Acaz-Fonseca et al., 2014). Through binding to sex hormone receptors in astrocytes, ovarian hormones regulate several cellular, molecular and functional parameters in these cells, including the growth of astroglial cytoplasmic processes, the expression of glial fibrillary acidic protein (GFAP), glutamate transport and the release of neurotrophic and neuroprotective factors (Acaz-Fonseca et al., 2014, 2016; Palmer and Ousman, 2018). Considering the active role of astrocytes in regulating synaptic maintenance and plasticity and the dependence on ovarian hormone signaling for several of their neuroprotective functions, it is expected that decline in sex hormones after menopause results in impaired astroglial synaptic function.

Humanin (HN) is a cytoprotective 24 amino acid peptide which was originally isolated from a cDNA library constructed from nervous tissue of a patient with familial Alzheimer's disease (AD). Since then, it has been identified in different species such as mice, nematodes and rats (Niikura et al., 2004). The rat humanin homolog rattin (HNr) is a 38 amino acid peptide encoded and translated from an open reading frame (ORF) within the mitochondrial 16S ribosomal RNA (rRNA) gene (Caricasole et al., 2002; Paharkova et al., 2015). Several studies have demonstrated that HN is a potent pro-survival factor for neurons exposed to multiple cell stressors, such as Aβ oligomers and over-expression of familial AD-related genes (Hashimoto et al., 2001; Caricasole et al., 2002), serum deprivation (Kariya et al., 2002), stroke (Xu et al., 2006; Gao et al., 2017) and *N*-methyl-D-aspartate (NMDA)-induced excitotoxicity (Cui et al., 2014). HN and its derivatives have also proven to be beneficial in ameliorating cognitive impairment induced by Aβ, muscarinic receptor antagonists and aging in rodents (Mamiya and Ukai, 2001; Krejcova et al., 2004; Tajima et al., 2005; Niikura et al., 2011; Zhang et al., 2012; Yen et al., 2018).

Moreover, HN and HNr were reported to prevent Aβ-induced spatial learning and memory impairments in rats by a mechanism involving changes in long-term potentiation (Chai et al., 2014; Wang et al., 2014), synaptic protein expression, dendritic branch number and spine density in the hippocampus (Chai et al., 2014).

It has been reported that HN exerts its neuroprotective action from the extracellular space through binding to a trimeric IL-6-receptor-related receptor(s) on the cell surface involving the receptor for ciliary neurotrophic factor α (CNTFR-α), WSX-1 and glycoprotein 130 kDa (gp130) subunits (Matsuoka and Hashimoto, 2010) and further modulation of tyrosin kinase, ERK1/2, AkT, STAT3 and JNK signaling cascades (Hashimoto et al., 2005; Matsuoka and Hashimoto, 2010; Takeshita et al., 2013; Kim et al., 2016). HN has been ubiquitously detected in different adult tissues with high metabolic rate, including skeletal and cardiac muscle, cerebral cortex, hippocampus and liver both in humans and in rodents (Caricasole et al., 2002; Kariya et al., 2005; Muzumdar et al., 2009). The mechanisms regulating HN expression are not fully elucidated. It has been shown that HN levels decrease with age in human and mice plasma as well as in the rat hypothalamus (Muzumdar et al., 2009; Bachar et al., 2010). Also, there is a sexual dimorphism in the expression of HN in rat anterior pituitary cells, suggesting that sex hormones are involved in the regulation of HN biosynthesis in this gland (Gottardo et al., 2014). In the brain, HN has been widely localized both in neurons and glial cells, albeit the former only in pathological conditions (Tajima et al., 2002). Thus, glial cells have been suggested to be the main production sites of this peptide in the brain in physiological conditions (Niikura et al., 2004). However, astroglial HN expression and release and the regulation of such processes by ovarian hormones have not been studied so far.

All things considered, the aim of this work was to evaluate the expression of HNr in the hippocampus of a rat model of surgical-induced menopause. We also aimed at determining whether astroglia is able to produce and release HNr *in vitro* and ovarian hormone dependence on these processes. HN putative actions on structural synaptic plasticity in a model of glutamate-induced dendritic atrophy were also studied.

MATERIALS AND METHODS

Drugs

All drugs and reagents were obtained from Sigma Chemical Co., St. Louis, MO, USA except for Dulbecco's Modified Eagle Medium (DMEM) and supplements (Gibco, Invitrogen Carlsbad, CA, USA) fetal calf serum (FCS; Natocor, Córdoba, Argentina) and the materials indicated below.

Animals

Adult female Wistar rats were housed in groups of four in controlled conditions of light (12 h light-dark cycles) and temperature (20–22°C). Rats were fed standard lab chow and water *ad libitum* and kept in accordance with the National Institutes of Health Guide for the Care and Use of Laboratory Animals. Animal protocols were previously approved by the Ethics Committee of the School of Medicine, University of Buenos Aires (Res. No. 2249).

For *in vivo* experiments, rats were ovariectomized (OVX) or sham-operated (SHAM) at 3 months of age under ketamine (100 mg/kg, i.p.) and xylazine (10 mg/kg, i.p.) anesthesia and ketoprofen (5 mg/kg) for analgesia. Beginning on week 10 post-surgery, rat hormonal status was monitored daily by vaginal smears. SHAM animals had 4–5 days estrous cycles while OVX animals presented continuous diestrus status. Eleven weeks after the surgery, rats were subjected to behavioral tests as described below. Twelve weeks after the surgery, rats were either deeply anesthetized (100 mg/kg ketamine and 6 mg/kg xylazine, i.p.), transcardially perfused with heparinized saline solution and fixed with 4% paraformaldehyde in 0.1 M phosphate buffer (for free-floating immunostaining of brain sections) or euthanized in a CO_2 chamber followed by decapitation (for real-time quantitative polymerase chain reaction (RT-qPCR) assays).

Behavioral Tests

Open Field Test

The open field test was performed to evaluate animal general locomotor activity and exploratory behavior (Gould et al., 2009). The arena consisted of a squared open field (60 × 60 cm) limited by a 40 cm-height wall with a grided floor divided into squares (15 × 15 cm) by lines. Animals were individually placed in the center of the open field arena and were allowed to freely explore for 10 min. The frequency with which the animal crossed grid lines with all four paws (crossings) was recorded as a measure of locomotor activity. After each animal was tested, the open field was cleaned with a 10% ethanol-damp cloth. Testing was performed between 10:00 and 14:00 h in a quiet room illuminated with a 75 W electric bulb, hung 75 cm above the open field apparatus.

Y-Maze Spontaneous Alternation Test

Spontaneous alternation behavior in a Y-maze was recorded to evaluate animal spatial working memory (Miedel et al., 2017). The apparatus consisted of three identical black arms (50 × 10 × 40 cm, length × width × height). Animals were habituated to the testing room for at least 30 min prior to the test. At the beginning of the session, animals were placed individually at the end of one same arm of the Y-maze and allowed to freely explore for 6 min. The whole session was recorded using a SONY CCD-TRV75 video camera recorder connected to a personal computer with AVerTV A833 video capture. The number of total arm entries and the number of triads (referred as entries to a different arm of the maze in each of three consecutive arm entries) were recorded and the percentage of alternation was calculated as [number of alternations/(total arm entries-2)] × 100 (Miedel et al., 2017).

Elevated Plus Maze

The elevated plus maze test was carried out to evaluate animal anxiety-like behavior (Walf and Frye, 2007). The apparatus consisted of a plus-shaped maze containing two open arms (50 × 10 cm, length × width) and two enclosed arms by 40 cm high walls arranged such that the two open arms were opposite

to each other. The apparatus was placed on four legs so that it was elevated 50 cm off the floor. Testing was performed between 10:00 and 16:00 h in a quiet room illuminated with a dim light hung 75 cm above the center of the maze. At the beginning of the session, each animal was placed in the center of the maze facing a close arm and allowed to freely explore for 5 min. The whole session was recorded and behavior was assessed offline. The number of times the animal entered an arm with all four paws was recorded. The percentage of open arm entries was calculated as [number of open arm entries/total arm entries] × 100.

Forced Swimming Test

The forced swimming test was performed to evaluate animal depressive-like behaviors by quantifying their mobility and immobility and associated behaviors (Overstreet, 2012). Each rat was individually placed in a plastic cylinder (diameter, 40 cm; height, 35 cm) containing water (23−25°C) up to 25 cm from the bottom for 5 min. At 5 s intervals throughout the test session, the predominant behavior was assigned to one of the followings categories: (1) immobility: lack of movement, except for the ones needed to keep the head above water; (2) swimming: swimming movement throughout the cylinder or (3) climbing: vigorous movements of the forepaws in and out of the water, usually directed against the walls. After each animal was tested, the water was changed and the cylinder rinsed with clean water. Following the session, each animal was dried and placed to its housing cage in a temperature-controlled room. All swimming sessions were carried out between 10:00 and 16:00 h.

RNA Isolation and Reverse-Transcription Real-Time Quantitative Polymerase Chain Reaction (RT-qPCR)

Immediately after decapitation, hippocampi from SHAM and OVX rats were dissected on ice, snap-frozen and kept at −80°C until use. Total RNA was extracted from frozen tissue using QuickZol reagent (Kalium Technologies, Buenos Aires, Argentina) according to the manufacturer's protocol. One μg of total RNA was treated with 2 U DNAse (Promega Corp., Madison, WI, USA) and then reverse transcribed using SuperScript II Reverse Transcriptase (Invitrogen, Thermo Fisher Scientific) following the manufacturer's instructions. Amplification of the products from RT reactions was performed in duplicate using specific primers (HNr forward 5′-GAG GGT TCA ACT GTC TCT TAC TTT CA-3′, reverse 5′-GTG AAG AGG CTG GAA TCT CCC-3′; HPRT forward 5′-CTC ATG GAC TGA TTA TGG ACA GGA C-3′, reverse 5′-GCA GGT CAG CAA AGA ACT TAT AGC C-3; Invitrogen, Thermo Fisher Scientific) and SYBR Green Select Master Mix (Invitrogen, Thermo Fisher Scientific) on a StepOne™ Real-Time PCR System (Applied Biosystems, Thermo Fisher Scientific). PCR product specificity was verified by a melting curve analysis. Negative RT controls were performed by omitting the addition of the reverse transcriptase enzyme in the RT reaction, while negative template controls were performed by addition of nuclease-free water instead of cDNA. Both primer sets were pre-validated to check similar efficiency ∼2 and for the use of $2^{-\Delta\Delta Ct}$ method as the quantification method (Livak and Schmittgen, 2001). Lack of statistically significant variation of endogenous reference gene HPRT expression between SHAM and OVX animals was determined (**Supplementary Figure S1**). Gene expression was normalized to HPRT using Step-One Software (Applied Biosystems, Thermo Fisher Scientific), and expressed as fold-changes relative to the control group.

Free-Floating Immunostaining of Tissue Sections

After animal intracardiac perfusion, brains were dissected, postfixed with 4% paraformaldehyde in 0.1 M phosphate buffer and equilibrated in 25% (w/v) sucrose in the same buffer. The hippocampus was serially sectioned in a freezing microtome and the free-floating coronal 30-μm-thick tissue sections were stored at −20°C in 25% (w/v) sucrose in phosphate buffer until use. The sections were blocked with 10% (v/v) normal goat serum and incubated for 48 h with primary antibodies against HNr (1:1,500), anti-GFAP (1:500, Millipore), NF-200 (1:1,000), OLIG2 (1:50,000, Millipore) or S100B (1:1,000) followed by an hour incubation with Alexa 594- or FITC-labeled secondary antibodies (Jackson ImmunoResearch). 4′,6 diamidino-2-phenilindoledihydrocloride (DAPI) was used for DNA staining. Negative controls were incubated in the absence of primary antibodies (**Supplementary Figure S2**).

Astroglial Cell Culture

Astroglial cell cultures were prepared from neonatal rat pups of 3–4 days old. Hippocampi and cortices from four to six pups were isolated, cut into small fragments using scissors and then cells were mechanically dispersed by extrusion through a Pasteur pipette in Hank's Balanced Salt Solution. After decanting tissue, supernatant was transferred to a new tube and pelleted. The procedure was repeated twice and finally the cells were plated in poly-D-lysine coated bottles with high glucose DMEM supplemented with 10% FCS, 100 μg/ml penicillin-streptomicin (DMEM-S) and 1 μg/ml fungizone. After the first 24 h and every 3–4 days, media was replaced with fresh DMEM-S. When the cells reached confluence (10–12 days), they were subjected to shaking at 180 rpm for two consecutive 24 h-periods at 37°C to detach microglia and oligodendrocytes. The cells were then incubated with 0.625% 5-fluorouracil for further 24 h, washed and incubated in fresh DMEM supplemented with 10% FCS previously treated with 0.025% dextran-0.25% charcoal (FCS-DCC) to remove steroids for additional 48 h. Then the cells were tripsinized and re-seeded onto 12 well plates in DMEM FCS-DCC for 24–48 h. Cultures obtained with this procedure showed 93 ± 0.04% GFAP-positive astrocytes ($n = 3$ independent cultures), as reported in the literature (Villarreal et al., 2014). Then, the cells were cultured for 4 h in DMEM FCS-DCC containing 1 nM 17β-estradiol (E) and 1 μM progesterone (P) or vehicle (ethanol, 20 μl/l), washed and cultured for further 20 h in fresh DMEM FCS-DCC.

Expression of HNr in Astroglial Cells by Flow Cytometry

Cultured astroglial cells were harvested with 0.025% trypsin-EDTA, washed in cold PBS, fixed with 4% paraformaldehyde

and permeabilized with 0.1% saponin in PBS (MP Biomedicals Inc., OH, USA) for 10 min. Then, the cells were incubated with rabbit anti-HNr antibody (1 μg/μl) in PBS-0.05% saponin for 1 h at 37°C followed by 40-min incubation with a FITC-conjugated anti-rabbit secondary antibody (1:100) in the same buffer. To determine the cut-off for HNr fluorescence, cells were incubated with secondary antibody only. Cells were washed, resuspended in PBS and analyzed by flow cytometry using a FACScan (Becton Dickinson). Data were analyzed with WinMDI 98 software.

ELISA

HNr levels in supernatants from astroglial cultures were measured by ELISA using a commercial kit HN(N) (Rat)-EIA Kit (Phoenix Pharmaceuticals) following the manufacturer's instructions and normalized to 50 μg of total protein in cell lysates from corresponding wells. Attached astrocytes were harvested as described above. Cells were lysed in lysis buffer containing 150 mM NaCl, 1% Igepal, 0.02% sodium azide, 0.1% sodium dodecyl sulfate (SDS), in 50 mM Tris-HCl pH 7.4 and a protease inhibitor cocktail (1:50). Cell lysate was collected and clarified by centrifugation at 16,000× *g* for 30 min and total protein content was determined by the Bradford protein assay (BioRad Laboratories, CA, USA) using bovine serum albumin as standard.

Metabolic Activity of Viable Cells

The metabolic activity of viable cells was determined by the 3-(4,5-dimethylthiazol-2-yl)-2,5-diphenyltetrazolium bromide (MTT) assay (Promega, Madison, WI, USA). Cells were washed twice and incubated for 4 h in 100 μl Krebs buffer plus 50 μg MTT reagent in PBS at 37°C. The developed crystals were dissolved in 100 μl 0.04 N HCl in isopropanol and the OD was read in a microplate spectrophotometer at a wavelength of 600 nm. The quantity of formazan product is directly proportional to the number of living cells in culture.

Primary Neuronal Cultures and Glutamate Treatment

Hippocampal neuronal cultures were prepared from dissected embryonic day 18 hippocampi as previously reported (Reinés et al., 2012; Podestá et al., 2014). Briefly, hippocampal tissue was trypsinized and mechanically dissociated. Then, dispersed cells were seeded on poly-D-lysine-coated glass coverslips at a density of 2×10^4 cells/cm^2 in Neurobasal medium supplemented with 2% (v/v) B27 and 0.5 mM glutamine. On day 13 *in vitro* (DIV), neurons were treated with 5 μM glutamate or vehicle for 3 min at 37°C, media was immediately removed and cells were washed with Hank's balanced salt solution. Immediately after, neurons were incubated with Humanin peptide (HN, 0.01–1 μM; Genemed Synthesis, Inc., San Antonio, TX, USA) in supplemented culture media for 24 h and then fixed for immunostaining as described below.

Immunostaining of Fixed Cells

Neurons in culture (14 DIV) were fixed in 4% (w/v) paraformaldehyde/4% (w/v) sucrose in PBS solution, pH 7.2 for 20 min at room temperature (RT) and permeabilized with 0.2% (v/v) Triton X-100 for 10 min at RT followed by a blockade with 5% (v/v) normal goat serum for 1 h at RT. The cells were then incubated overnight at 4°C with MAP-2 (1:500) or SYN (1:2,000; Chemicon, Millopre) primary antibodies in PBS. The next day, cells were washed and incubated for 1 h at RT with the appropriate secondary antibodies followed by DAPI for DNA staining. Negative controls were incubated in the absence of primary antibodies (**Supplementary Figure S3**). Finally, cells were mounted using Mowiol.

Image Acquisition and Quantification

A Zeiss Axiophot microscope (Carl Zeiss, Oberkochen, Germany) equipped with an Olympus Q-Color 5 camera or a Olympus IX81 microscope equipped with a CCD model DP71 digital camera were employed in immunohistochemistry or immunocytochemistry assays, respectively. Confocal images were acquired using Fluoview version 3.3 software using an Olympus FV300 confocal microscope. Immuno-positive structures were quantified as relative immunoreactive area (immunoreactive area/total area) as described elsewhere using the ImageJ (NIH) software (Reinés et al., 2008; Aviles-Reyes et al., 2010; Codagnone et al., 2015). In immunohistochemistry assays, the total area corresponded to the hilus, granular and molecular layers in the superior and inferior blades of the dentate gyrus (DG) and to pyramidal and stratum lucidum and radiatum in CA1. Briefly, microscopic images were captured with a digital camera, transformed to an 8-bit gray scale and an interactive threshold was determined. Then, the area fraction covered by immunostained structures obtained using this threshold, which remained fixed for the entire experiment, was quantified with the particle counting tool of the software. In immunocytochemistry assays, dendritic tree area per neuron was calculated by subtracting the area corresponding to the immunolabeled soma from the total MAP-2 immunostaining. The number of synaptic puncta, total puncta area and individual puncta area for SYN was calculated as previously described (Podestá et al., 2014). Figures were prepared using Adobe Photoshop 7.0 software (Adobe Systems Inc.). Brightness and contrast were kept constant between the experimental groups. Each immunohistochemistry assay consisted of 5–6 hippocampal serial sections of each animal per group. The average data obtained from the quantification of sections from the same animal was considered $n = 1$. Results of immunohistochemistry assays are expressed as mean values (±SEM) of $n = 3$–5 animals per group. Each experiment was repeated 2–4 times. Each immunocytochemistry assay consisted of 1–3 coverslips per experimental condition. Results of immunocytochemistry assays are expressed as mean values (±SEM) of 20–40 neurons per experimental condition from two to three independent cultures. The experiments were repeated at least twice.

Statistical Analysis

Results are expressed as mean ± SEM and evaluated by unpaired Student's *t*-test or nonparametric Mann-Whitney *U* test. HNr content in conditioned media determined by ELISA was evaluated by one-way ANOVA followed by Tukey's

test. Dendritic tree area, total SYN puncta area, number and individual SYN puncta area were evaluated by two-way ANOVA followed by Tukey's test. Differences were considered significant if $p < 0.05$.

RESULTS

Behavioral Characterization of OVX-Induced Model of Menopause

It is now accepted that ovariectomized (OVX) adult rodents share common features with aged animals regarding brain function, including changes in mitochondrial function, synaptic plasticity, behavior and cognition (Zárate et al., 2017b). To characterize our animal model of surgical menopause in adult Wistar rats at the behavioral level, we assessed parameters of spatial working memory, anxiety and depression, which are known to be modulated by ovarian hormones (Diz-Chaves et al., 2012; Kiss et al., 2012; Cao et al., 2013; Rodríguez-Landa et al., 2017; Hampson, 2018; da Silva Moreira et al., 2016). Twelve-week ovarian hormone-deprived rats showed lower spontaneous alternation behavior in the Y-maze, indicating impaired spatial working memory (**Figure 1A**). They also spent less time in the open arms and more time immobile when subjected to the elevated plus maze and the forced swimming test, respectively. These results show that long-term ovarian hormone deprivation increases anxiety-like and depressive-like behaviors (**Figures 1B,C**). There were no differences in spontaneous locomotion and exploratory behavior between OVX and control groups, as assessed in the open field test (**Figure 1D**), indicating that the observed behaviors in OVX rats cannot be attributed to altered locomotion.

HNr Expression in the Hippocampus

Circulating levels of mitochondrial-encoded HN are known to decline with age in mice and humans and in the rat hypothalamus (Muzumdar et al., 2009; Bachar et al., 2010). Indeed, this peptide has been suggested to participate in the endocrine regulation of the aging process (Lee et al., 2014). We have previously reported that long-term ovarian hormone deprivation induces functional and structural alterations in hippocampal mitochondria, which resembles a mitochondrial aging phenotype (Zárate et al., 2017a). We thus evaluated HNr expression in the hippocampus of OVX rats by RT-qPCR. Hippocampal expression of HNr was lower in OVX rats compared to control rats (**Figure 2**). In order to identify cell types expressing this peptide, we performed immunohistochemistry for both HNr and different brain cell markers. HNr immunostaining

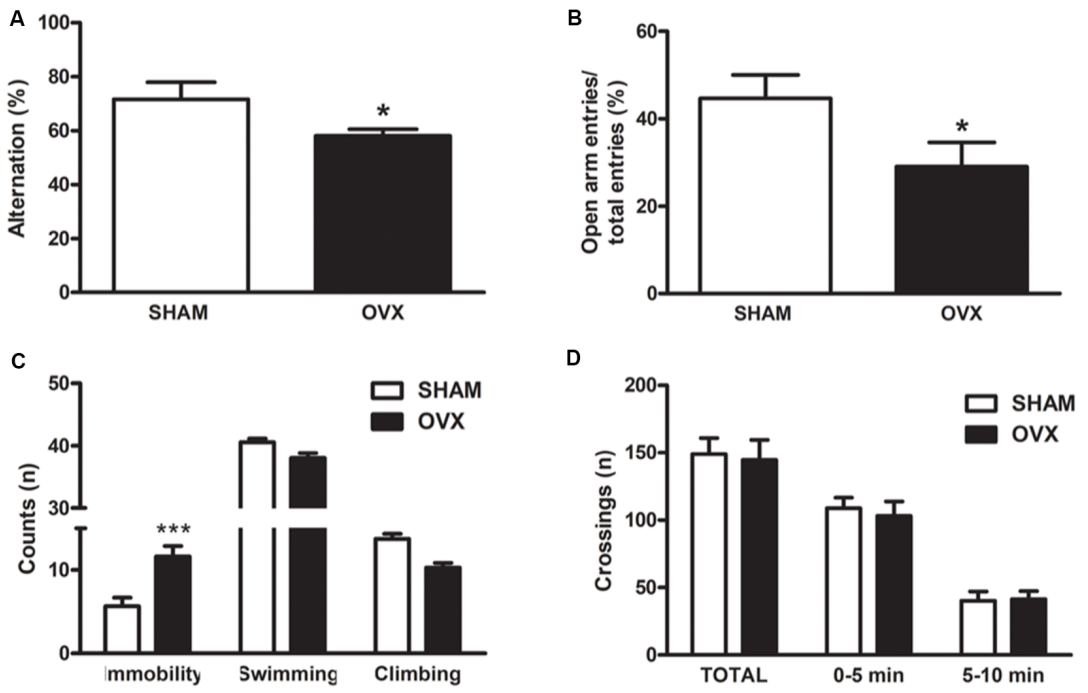

FIGURE 1 | Behavioral characterization of an animal model of surgical menopause in adult rats. Adult Wistar female rats were ovariectomized (OVX) or sham-operated (SHAM). Twelve weeks after surgery, the animals were subjected to behavioral tests as described in "Materials and Methods" section. **(A)** Y-maze spontaneous alternation test: for each animal, the number of total arm entries and the number of triads in 6 min was recorded. **(B)** Elevated plus maze test: each animal was allowed to freely explore for 5 min and the number of times the animal entered an arm with all four paws was recorded. **(C)** Forced swimming test: every 5 s, a time-sampling technique was used to score the presence of immobility, swimming or climbing behavior. **(D)** SHAM or OVX rats were placed individually in the center of a field marked with a grid of 16 equal squares for 10 min. The number of times the animal crossed each line was registered. Each column represents the mean ± SEM of **(A)** the percentage of alternation, **(B)** the percentage of open arm entries, **(C)** the number of counts or **(D)** the number of crossings per session (n = 4–12 animals/group); $^{*}p < 0.05$, $^{***}p < 0.001$, Student's t-test.

colocalized with astroglial marker S100B and GFAP, but not with neuronal or oligodendroglial markers NF-200 and OLIG-2, respectively (**Figures 3**, **4A**). Noteworthy, some HNr staining could be observed in the extracellular space, suggesting the presence of secreted HNr. Further evaluation of HNr and GFAP expression levels in different hippocampal subregions showed that HNr relative immunoreactive area was lower in the CA1 region of the hippocampus of OVX rats while there was no difference between HNr relative immunoreactive area from OVX and control rats in the DG (**Figure 4B**). OVX rats also showed lower relative immunoreactive area for GFAP in all hippocampal subregions studied (**Figure 4B**). Remarkably, there was a positive correlation for HNr and GFAP levels in both OVX and control groups (**Figure 4C**).

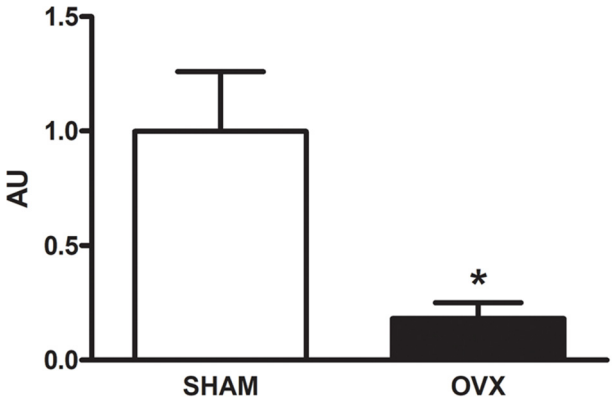

FIGURE 2 | Expression of HNr in the hippocampus. The expression of HNr RNA was evaluated in hippocampi from SHAM and OVX rats by real-time quantitative polymerase chain reaction (RT-qPCR). Each column represents the mean ± SEM of the concentration of HNr RNA relative to its internal control HPRT expressed as fold-changes relative to SHAM group (AU; $n = 3$ animals/group); $^*p < 0.05$, Student's t-test.

HNr Production and Release by Astroglia

Glial cells have been proposed as the main site of HNr production in the brain in physiological conditions (Tajima et al., 2002). Indeed, our results show that HNr immunoreactivity colocalizes with astroglial markers and that OVX rats display lower expression of HNr in the hippocampus. However, the production and release of this peptide by astroglial cells as well as the regulation of these processes by ovarian hormones remain to be determined. To address this issue, cultured astrocytes were incubated with ovarian hormones 17β-estradiol (E) and progesterone (P) alone or in combination and released

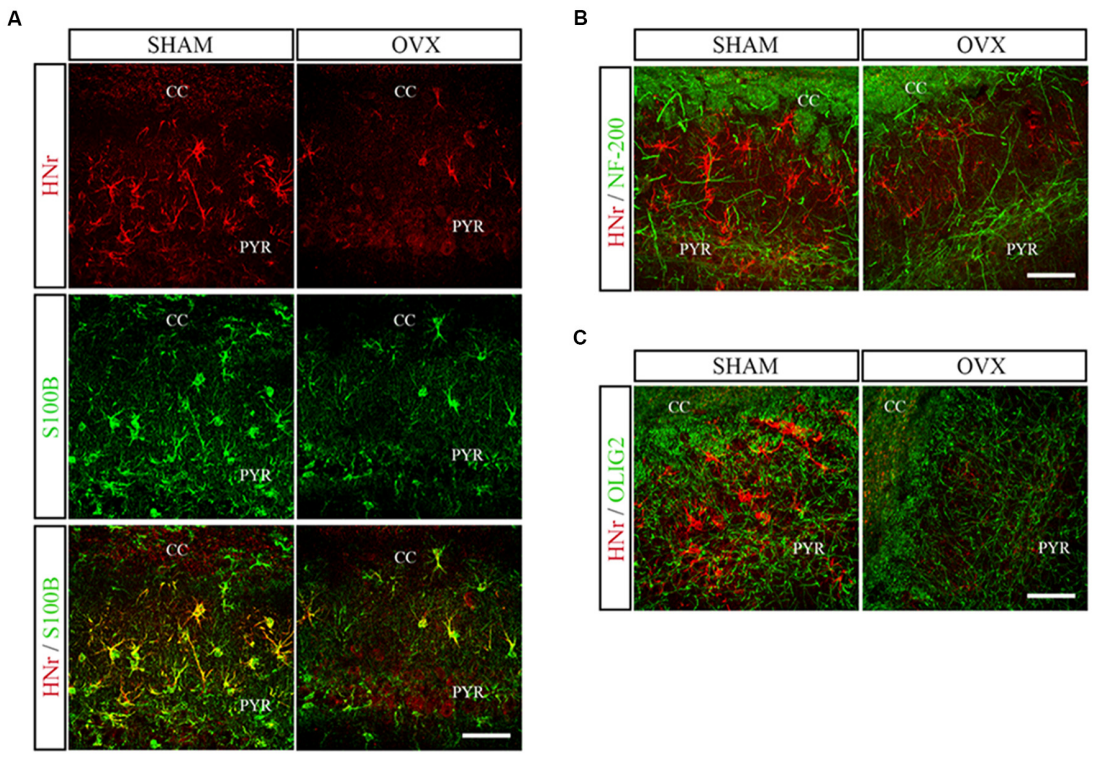

FIGURE 3 | Double immunostaining for HNr and astroglial, neuronal or oligodendroglial markers. Coronal sections from the hippocampus of SHAM and OVX animals were processed for double immunohistochemistry for HNr and **(A)** astroglial (S100B), **(B)** neuronal (NF-200) or **(C)** oligodendroglial (OLIG-2) markers. Representative confocal microphotographs from CA1 stratum oriens (600×) show the expression of HNr (red), S100B, NF-200 or OLIG2 (green) and the merged image (yellow). PYR, pyramidal layer; CC, corpus callosum. Scale bar = 50 μm.

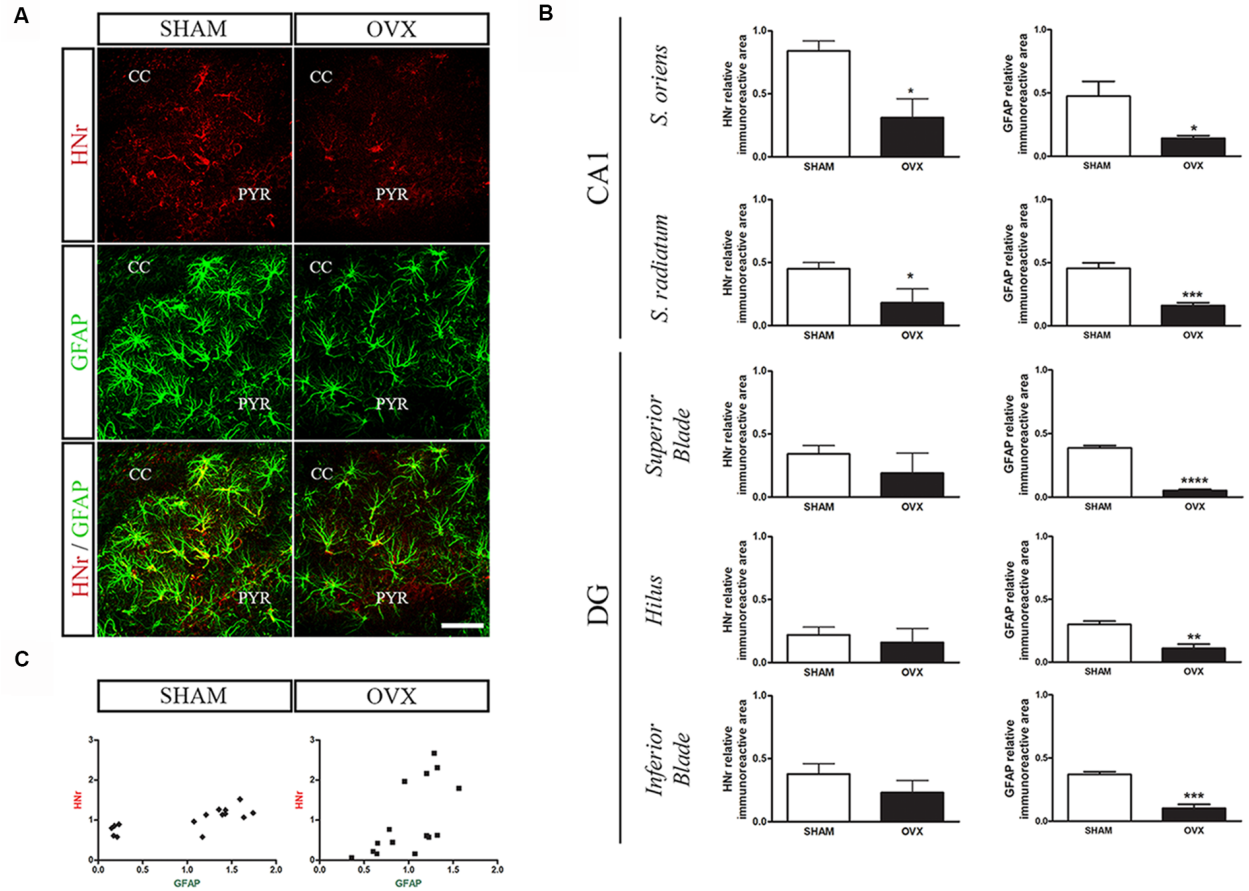

FIGURE 4 | Effects of long-term ovarian hormone deprivation on HNr and glial fibrillary acidic protein (GFAP) immunoreactivity in the hippocampus. Coronal sections from the hippocampus of SHAM and OVX animals were processed for double immunohistochemistry for HNr and GFAP. **(A)** Representative confocal microphotographs from CA1 stratum oriens (600×) show the expression of HNr (red), GFAP (green) and the merged image (yellow). **(B)** Quantification of relative immunoreactive area (immunoreactive area/total area) for HNr and GFAP using ImageJ software. Each column represents the mean ± SEM of relative immunoreactive area (n = 3 animals/group). *$p < 0.05$, **$p < 0.01$, ***$p < 0.001$, Student's t-test. **(C)** HNr and GFAP expression levels expressed as relative immunopositive area for each protein were normalized with respect to each corresponding hippocampal subregion (SHAM $r = 0.74$, $p < 0.01$; OVX $r = 0.63$, $p < 0.05$, Pearson correlation test). PYR, pyramidal layer; CC, corpus callosum; DG, dentate gyrus. Scale bar = 50 μm.

HNr content was determined in the conditioned media of cultured astrocytes by ELISA. There was a two-fold increase in HNr levels in the conditioned media of astrocytes incubated with E + P (**Figure 5A**). Then, intracellular astroglial HNr levels were determined by immunocytochemistry and flow cytometry. Ovarian hormones increased the intracellular content of HNr per cell without changing the number of astrocytes expressing this peptide (**Figures 5B,C**), indicating that ovarian hormones increase both the expression and the release of HNr by these cells.

HN Effect on Structural Synaptic Plasticity in the Hippocampus

It has been extensively reported that ovariectomy decreases the number of synapses and induces dendritic alterations in hippocampal neurons (Gould et al., 1990; Woolley and McEwen, 1992, 1993; Adams et al., 2001). However, HN effects on these synaptic parameters have not been explored yet. To this aim, cultured hippocampal neurons were subjected to a brief exposure to a low glutamate concentration, a condition that has previously been reported to induce dendritic atrophy in the absence of neuronal death (Podestá et al., 2014). Immediately after glutamate exposure, neurons were incubated with HN in two different concentrations and cell viability and synaptic parameters were studied 24 h later. Neither glutamate nor HN affected cell viability, as assessed by MTT assay (**Figure 6**). As expected, immunostaining for the specific dendritic marker MAP-2 was reduced 24 h after glutamate insult, rendering into a decreased neuronal dendritic area. Remarkably, HN prevented glutamate-induced dendritic atrophy in both concentrations studied (**Figure 7**). Pre-synaptic marker SYN immunostaining was also altered in glutamate-treated neurons, as previously reported (Podestá et al., 2014). Remarkably, while glutamate decreased SYN puncta number and total puncta area, both concentrations of HN prevented glutamate actions over SYN synaptic profile. Neither

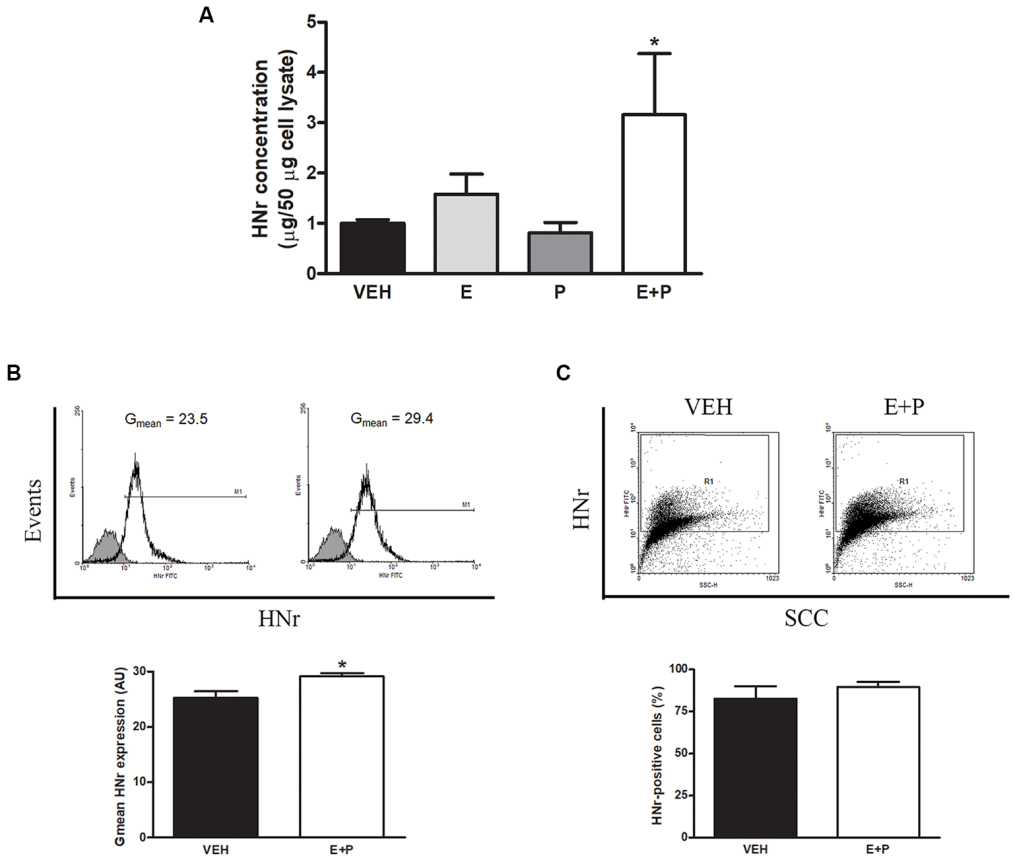

FIGURE 5 | HNr production and release by astrocytes *in vitro*. Cultured astrocytes were incubated with estradiol (E) and progesterone (P). HNr secreted levels were determined in conditioned media by ELISA. Harvested cells from additional cultures were immunostained for HNr and analyzed by flow cytometry. Each column represents the mean ± SEM of **(A)** the concentration of HNr in conditioned media normalized to 50 μg of total protein in corresponding cell lysate, **(B)** the fluorescence intensity of HNr staining (Gmean) or **(C)** the percentage of HNr-positive cells. The upper panels in **(B,C)** show representative histograms and dot plots of HNr expression in astrocytes incubated with VEH or E + P (n = 3–4 wells per group from three independent experiments). **(A)** $^*p < 0.05$ vs. respective control without E; ANOVA followed by Tukey's test, **(B,C)** $^*p < 0.05$; Student's t-test.

glutamate nor HN induced changes in SYN individual puncta area (**Figure 8**).

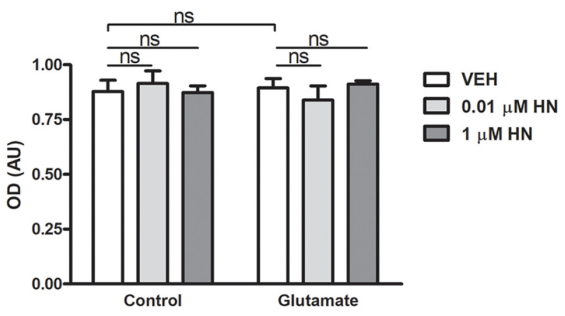

FIGURE 6 | Effects of glutamate and HN on hippocampal neuronal cell viability *in vitro*. Cultured embryonic neurons (DIV13) were subjected to a 3-min incubation with glutamate (5 μM) immediately followed by a 24-h incubation with HN (0.01–1 μM). Cell viability was assessed by MTT assay. Each column represents the mean ± SEM of five wells from one experiment representative of three independent experiments. ns, non-significant; ANOVA.

DISCUSSION

Mitochondrial DNA has been classically described as a maternally-inherited, small DNA encoding only 13 mitochondrial proteins involved in oxidative phosphorylation and 24 structural RNAs required for their translation. However, recent research has challenged this view (Capt et al., 2016; Luo et al., 2018). In fact, several mitochondrial-derived peptides encoded as genes-within-genes in short ORFs dispersed throughout the mitochondrial genome have been recently described (Capt et al., 2016; Kim et al., 2017). Among them, humanin (HN) has received much attention due to its neuroprotective effect against different types of stress and disease models (Lee et al., 2013). Encoded within the 16S rRNA, HN has been detected in several tissues and in circulation in rodents and humans (Caricasole et al., 2002; Kariya et al., 2005; Muzumdar et al., 2009) and its expression is age-dependent (Muzumdar et al., 2009; Bachar et al., 2010). HN circulating levels both in mice and humans are regulated by the growth hormone and insulin-like growth factor-1 (GH/IGF-1) axis, a well conserved

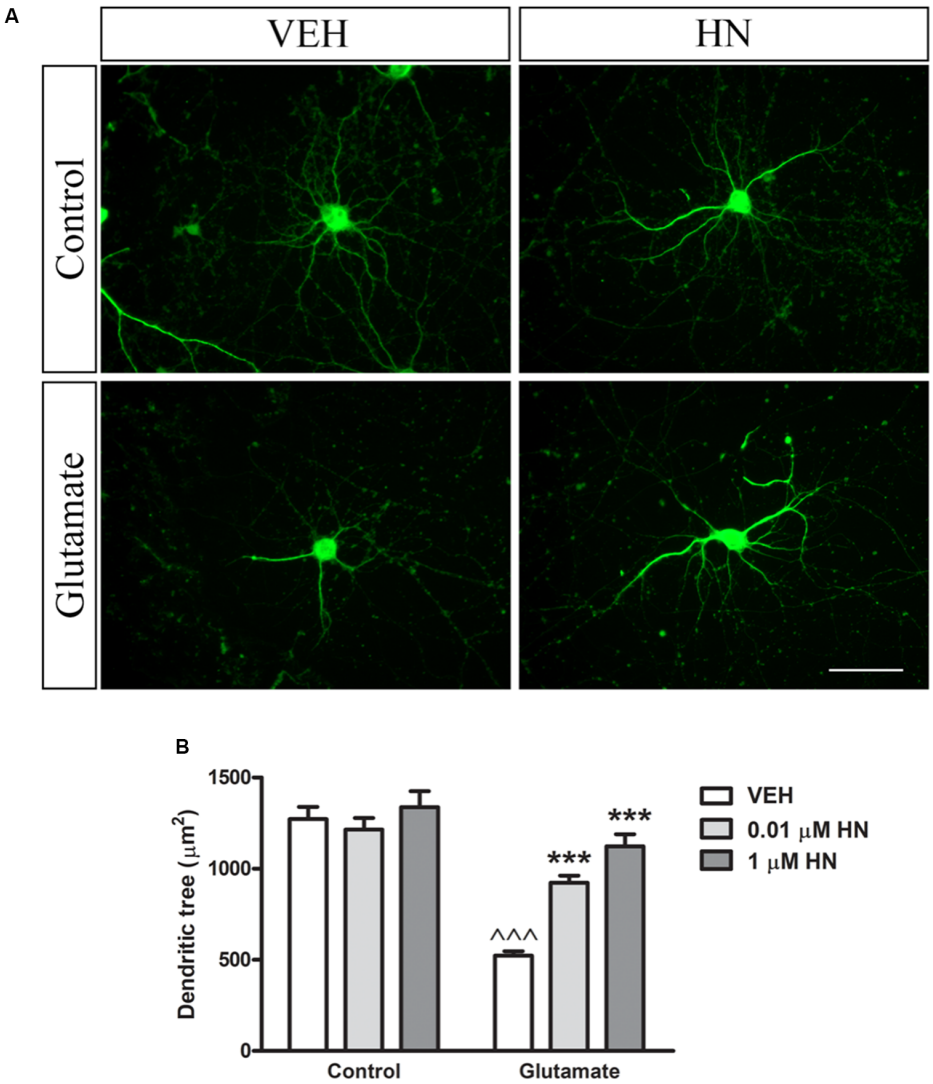

FIGURE 7 | Effect of HN on neuronal dendritic tree area in hippocampal neurons *in vitro*. Hippocampal neurons in culture (DIV 13) were briefly exposed to glutamate (5 μM), immediately incubated with HN (0.01–1 μM) and evaluated 24 h later. **(A)** Representative microphotographs of hippocampal neurons in culture immunostained for MAP-2. Microphotographs corresponding to 0.01 μM HN are shown, **(B)** Quantification of MAP-2 immunostaining using ImageJ software. Each column represents the mean ± SEM of 20–40 neurons per experimental condition. ^^^$p < 0.01$ vs. respective control without glutamate, ***$p < 0.001$ vs. respective control without HN; two-way ANOVA followed by Tukey's test. Scale bar = 50 μm.

endocrine system that controls the process of aging. In fact, HN has been suggested to be a mitochondrial signaling peptide that is secreted and acts as a hormone involved in the endocrine regulation of the aging process (Lee et al., 2014). We previously reported that 12-week ovarian hormone deprivation, a model of surgical menopause, induces mitochondrial dysfunction in the rat hippocampus (Zárate et al., 2017a). These alterations comprise slower active respiration and ATP production rates as well as decreased membrane potential together with changes in the lipid composition of mitochondrial membranes. Remarkably, these functional and structural features are found in mitochondria from aged animals (Pamplona, 2008; Gómez and Hagen, 2012), further supporting the idea that ovarian hormone loss promotes an accelerated aging phenotype, as previously suggested (Yao et al., 2009). Ovarian hormones, especially estrogens, are well-known regulators of mitochondrial function, which is crucial in organs and tissues with high energy demand like the CNS (Zárate et al., 2017b). Estrogen regulation of mitochondrial metabolism, biogenesis and morphology has been reported to occur in neuronal tissue (Garcia-Segura et al., 1998; Nilsen and Brinton, 2003; Arnold et al., 2008; Brinton, 2008; Hara et al., 2014; Kemper et al., 2014; Klinge, 2017). Since ovarian hormone loss has been associated to the process of aging and estrogens are well-known regulators of mitochondrial gene expression (Virbasius and Scarpulla, 1994; Kang et al., 2007), we hypothesized that the levels of a mitochondrial-encoded

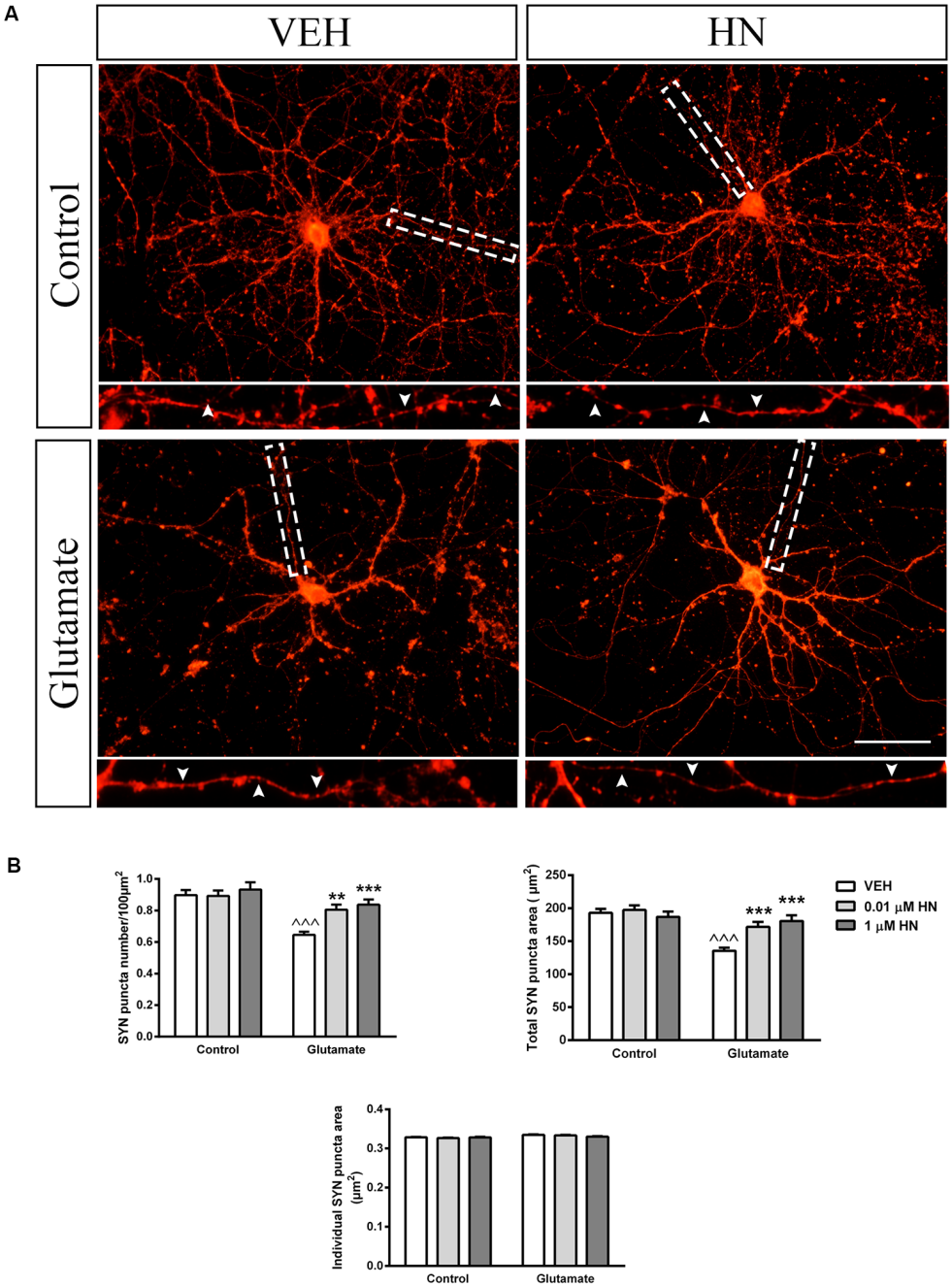

FIGURE 8 | Effect of HN on SYN synaptic profile in hippocampal neurons *in vitro*. Hippocampal neurons in culture (DIV 13) were briefly exposed to glutamate (5 μM), immediately incubated with HN (0.01–1 μM) and evaluated 24 h later. **(A)** Representative microphotographs of hippocampal neurons in culture immunostained for SYN. Microphotographs corresponding to 0.01 μM HN are shown. Insets (3× magnification) detail SYN immunostaining pattern. **(B)** Quantification of total SYN puncta area, SYN puncta number and individual SYN puncta area using ImageJ software. Each column represents the mean ± SEM of 20–40 neurons per experimental condition. ^^^$p < 0.01$ vs. respective control without glutamate, **$p < 0.01$, ***$p < 0.001$ vs. respective control without HN; two-way ANOVA followed by Tukey's test. Scale bar = 50 μm.

gene like HN would be decreased in hormone-deprived animals. Indeed, herein we found that long-term ovariectomy reduced the expression of HNr in the hippocampus. It is to note that, although initially transcribed as long polycistronic precursor transcripts (Ojala et al., 1981), the levels of individual mitochondrial RNAs varies in different tissues and cell types due to post-transcriptional processing mechanisms (Mercer et al., 2011; Sanchez et al., 2015). Such mechanisms have been shown to respond to the tissue hormonal milieu (Sanchez et al., 2015). In fact, estrogen treatment has been shown to increase the

amount of mitochondrial-encoded RNAs (Stirone et al., 2005; Klinge, 2008). Moreover, 16S rRNA levels have been reported to decrease with aging due to reduced rate of mitochondrial RNA transcription (Calleja et al., 1993). Remarkably, female rats express more 16S rRNA than males of the same chronological age (Borras et al., 2003), suggesting a putative role of sex hormones in the regulation of its expression. Considering that HNr is encoded within the mitochondrial 16S rRNA molecule, it can be speculated that similar post-transcriptional processing mechanisms induced by hormonal environment can affect HNr expression. Also, HN peptide seems to be associated with lipids in different tissues (Tajima et al., 2002), suggesting that alterations in tissue lipid composition induced by age or disease may affect HN effective levels. Interestingly, hippocampal mitochondria membranes from OVX rats display an altered lipid profile consisting of increased membrane peroxidability index together with decreased cardiolipin levels (Zárate et al., 2017a), which could also affect HN levels and/or distribution within this tissue.

Different cells comprise the highly specialized and complex nervous tissue. Although an early report showed the presence of HN immunoreactivity in both normal and AD human brains (Tajima et al., 2002), the specific cell types expressing this peptide remained elusive. Tajima et al. (2002) showed HN immunoreactivity to be located in round cells resembling glia widely distributed in the brain, mainly in the hippocampus. However, the identity of such glial cells was not investigated then. HN immunoreactivity was also detected in some neurons of the occipital lobe in the AD brain but not in an age-matched normal brain (Tajima et al., 2002). By means of double immunohistochemistry using neuronal, astroglial and olidodendroglial markers in the hippocampus, we detected HNr immunoreactivity to be located only in astrocytes, both in OVX and control animals. However, co-immunostaining with microglial markers was not studied and HNr localization in microglial cells cannot be ruled out. Considering that microglia are highly regulated by both estrogen and progesterone, further studies are warranted to elucidate whether microglial cells also express HNr *in vivo*.

The role of astroglial cells as supportive cells in the CNS is well established. They are not only the major contributors to cell homeostasis in the CNS but also play a central role in the control of synaptic transmission through different mechanisms. Perisynaptic astroglial membranous sheaths are known to cover a high number of all synaptic contacts in the hippocampus, thus finely regulating synaptic transmission by means of establishing physical contact with synapses and also by secreting a plethora of bioactive agents (Verkhratsky and Nedergaard, 2018). These astroglial processes have been reported to be devoid of organelles but may contain mitochondria, which, in light of our results, could be the source of mitochondria-derived peptides with a local role in the neighboring synapse. Considering the effect of HN in the prevention of glutamate-induced structural synaptic alterations shown herein, this peptide could be considered as another bioactive molecule locally secreted by astroglia to regulate synaptic plasticity in pathophysiological conditions. In this way, our results add new evidence for astroglial role as a major contributor to proper signal transmission in the CNS and therefore to higher cognitive function.

In vitro assays using cultured astrocytes further confirmed that this cell type is able to produce and release HNr and that ovarian hormones positively regulate these processes. It is well known that estradiol and progesterone exert their actions on astrocytes through classical and non-classical receptor signaling initiated at the nucleus, membrane or cytoplasm levels (Acaz-Fonseca et al., 2016). By inducing the transcription of nuclear-encoded mitochondrial transcription factor A (TFAM), estrogens are able to promote transcription of mitochondrial DNA (mtDNA) through a classical mechanism (Virbasius and Scarpulla, 1994; Kang et al., 2007). Also, estrogen and progesterone receptors have been localized within mitochondria, suggesting that they might regulate mitochondrial transcription through direct binding to hormone-response element-like sequences in mtDNA (Demonacos et al., 1996; Chen et al., 2004). Further studies are warranted to determine ovarian hormone mechanism involved in HNr expression and release by astroglial cells.

Estradiol and progesterone are well-known regulators of astroglial cell morphology and GFAP expression. Evidence supporting this includes changes in the surface density of GFAP-immunoreactive cells in the DG of the hippocampus along the estrous cycle (Luquin et al., 1993). Moreover, GFAP-immunoreactive cell density in this brain area decreases after ovariectomy and is increased by treatment with estradiol alone or in combination with progesterone in a dose-dependent manner (Luquin et al., 1993). It has been suggested that ovarian hormones promote the increase in the size and/or branching of cell processes without affecting astrocyte cell number (Tranque et al., 1987). We evidenced the presence of qualitatively smaller, less complex astrocytes with thinner cytoplasmic processes, which resulted in lower GFAP relative immunoreactive area in all subregions of the hippocampus from OVX animals. Similar alterations in astrocyte phenotype have been described in aged rodents, primates and humans (Castiglioni et al., 1991; Amenta et al., 1998; Kanaan et al., 2010; Cerbai et al., 2012; Jyothi et al., 2015; Robillard et al., 2016). For example, Cerbai et al reported the presence of fewer, smaller and less complex GFAP-positive astrocytes in the CA1 region of the hippocampus from 22-month old rats (Cerbai et al., 2012). These morphological changes are accompanied with loss of homeostatic function, which represents an underlying mechanism for impaired neuroprotection and disrupted neuronal connectivity (Verkhratsky et al., 2014). Indeed, several recent reports have shown that the atrophic astrocyte is the main astroglial phenotype not only in natural aging but also in the early stages of neurodegenerative diseases (Verkhratsky et al., 2014). This phenotype is characterized not only by smaller and less complex astrocytes but also by a decrease in glutamate uptake and glutamate synthase activity, which may contribute to the observed general imbalance in both excitatory and inhibitory neurotransmission as well as alterations at the synapse level (Verkhratsky et al., 2014). It is of note that astrocyte cytoplasmic processes form close structural contacts with synapses to regulate all aspects of synaptic function *via* the secretion of several factors (Pfrieger, 2010). Thus, it can be

speculated that OVX may negatively impact astroglial support to neuronal function by means of reduced synapse maintenance.

Accumulating evidence indicates that the CA1 region of the hippocampus highly responds to natural or surgical ovarian hormone loss by decreasing synapse number and spine density in rats (Gould et al., 1990; Woolley and McEwen, 1992, 1993; Adams et al., 2001), which has been directly associated to cognitive impairment. Interestingly, quantification of HN immunoreactivity in the hippocampus of OVX rats evidenced lower HN protein levels in the CA1 region without changes in the DG between experimental groups, which was temporally correlated with impaired spatial working memory. A HN derivative has been reported to improve cognitive impairments in different genetic mouse models of AD (Niikura et al., 2011; Zhang et al., 2012) as well as blunt learning and memory decline induced by Aβ peptides (Tajima et al., 2005). Also, HN ameliorates spatial working memory deficits induced by cholinergic antagonism- and GABA agonist-induced amnesia in mice (Mamiya and Ukai, 2001; Krejcova et al., 2004; Tajima et al., 2005). It has been recently reported that HN treatment improves cognition in aged mice. Also, there is a positive correlation between decreased HN circulating levels and accelerated cognitive aging in humans (Yen et al., 2018). Moreover, intrahippocampal injection of HN into the CA1 region is able to prevent Aβ-induced memory deficits (Chai et al., 2014). Thus, it can be hypothesized that decreased HN expression in the CA1 region of the hippocampus could be the underlying mechanism for cognitive impairment induced by OVX.

It is well recognized that structural synaptic plasticity, which involves changes in synaptic architecture and number, is an important biological basis of learning and memory (Lamprecht and LeDoux, 2004). *In vivo* treatment with HN has been shown to prevent Aβ-induced dendritic atrophy in the CA1 region of the hippocampus by promoting dendritic branching and spine density. These HN-induced effects occur concomitantly with an increase in pre- and post-synaptic proteins in this hippocampal subregion (Chai et al., 2014). To our knowledge, ours is the first *in vitro* study showing that HN has a direct effect at the synaptic level preventing glutamate-induced structural synaptic alterations in hippocampal neurons.

HN has been shown to protect cultured rat cortical neurons from NMDA-induced neurotoxicity, an effect that seems to be time- and concentration-dependent (Cui et al., 2014, 2017; Yang et al., 2018). In this study, we aimed at studying HN effects on structural synaptic plasticity in glutamate-induced dendritic atrophy and synapse alterations (Podestá et al., 2014). This approach, which consists on subjecting cultured hippocampal neurons to a brief exposure to a low glutamate concentration, proved to be mediated by NMDA receptor (Podestá et al., 2014). Our results show that HN is able to prevent glutamate-induced dendritic atrophy even at the lowest concentration studied. Interestingly, we also detected a reduction in synapse number, evidenced by decreased SYN puncta number and total SYN puncta area, which occurs simultaneously with dendritic retraction. Remarkably, HN prevented these structural synaptic alterations at concentrations that are comparable to HNr levels detected in astrocyte conditioned media by ELISA, suggesting that HN could be exerting its actions in pathophysiological conditions.

In summary, our results indicate that long-term ovarian hormone deprivation promotes structural changes in hippocampal astrocytes, which is positively correlated with reduced HN expression in this brain area. Our results *in vitro* show that ovarian hormones positively regulate astroglial HN expression and release and that this peptide prevents glutamate-induced structural synaptic alterations of cultured hippocampal neurons. Thus, OVX-induced functional and morphological alterations in astrocytes discussed above could impair astroglial support to neuronal function and may represent an underlying mechanism for synaptic dysfunction after menopause. Our study could help find new therapeutic targets for interventions that may promote a healthier lifespan for post-menopausal women.

ETHICS STATEMENT

Animals were kept in accordance with the National Institutes of Health Guide for the Care and Use of Laboratory Animals. Animal protocols were previously approved by the Ethics Committee of the School of Medicine, University of Buenos Aires (Res. N° 2249).

AUTHOR CONTRIBUTIONS

SZ and AR contributed to the conception and design of the study. SZ and MT performed the experiments. MC contributed to the design and performance of behavioral tests. SZ wrote the first draft of the manuscript. SZ, AR and AS discussed results. AR and AS revised the first draft of the manuscript. All authors contributed to the revision of the final version of the manuscript, read and approved the submitted version.

FUNDING

This study was supported by Agencia Nacional de Promoción Científica y Tecnológica (ANPCYT; PICT 2014-1769 and PICT 2014-0334), Consejo Nacional de Investigaciones Científicas y Técnicas (CONICET; PIP 11220130100212CO) and Universidad de Buenos Aires (UBA; UBACyT 20020150200250BA, 20020130100020BA and 20020170100478BA). The funders had no role in study design, data collection and analysis, decision to publish, or preparation of the manuscript.

SUPPLEMENTARY MATERIAL

The Supplementary Material for this article can be found online at: https://www.frontiersin.org/articles/10.3389/fnagi.2019.00123/full#supplementary-material

FIGURE S1 | Validation of the $2^{-\Delta\Delta Ct}$ method for quantitative polymerase chain reaction (qPCR) data quantification. The efficiency of amplification of **(A)** the target gene (HNr) and **(B)** housekeeping control (HPRT) was examined using real-time PCR and SYBR Green detection. Using reverse transcriptase, cDNA was synthesized from 1 μg total RNA isolated from sham-operated (SHAM) and

ovariectomized (OVX) rat hippocampi. Serial dilutions of cDNA were amplified by real-time PCR using gene-specific primers. The most concentrated sample contained 200 ng of cDNA. **(C)** The ΔCT (Ct_{HNr}-Ct_{HPRT}) was calculated for each cDNA dilution. The data were fit using least-squares linear regression analysis (n = 2–3). **(D)** Validation of HPRT as housekeeping gene. The expression of HPRT RNA was evaluated in hippocampi from SHAM and OVX rats by RT-qPCR. Each column represents the mean ± SEM of the concentration of HPRT RNA expressed as fold-changes relative to SHAM group (AU; n = 3 animals/group); p = 0.0802, Student's t-test.

FIGURE S2 | Negative controls for immunohistochemistry assays. Coronal sections from the hippocampus of SHAM or OVX animals were processed for double immunohistochemistry for HNr and GFAP. **(A)** Representative microphotographs from CA1 stratum oriens show the lack of signal in the 488 (green) and 594 (red) channels in sections incubated only with secondary antibodies (double negative control). **(B)** Representative microphotographs from CA1 stratum oriens show the expression of GFAP (green) or HNr (red) together with the lack of signal in the 594 (red) or 488 (green) channels respectively in sections incubated in the presence of each primary antibody as indicated in the figure and both secondary antibodies (single negative control). Nuclear staining is shown in blue (DAPI). Scale bar = 50 μm.

FIGURE S3 | Negative controls for immunocytochemistry assays. Hippocampal neurons in culture (DIV 13) were immunostained for double immunohistochemistry for MAP-2 and SYN. **(A)** Representative microphotographs show the lack of signal in the 488 (green) and 590 (red) channels in neurons incubated only with secondary antibodies (double negative control). **(B)** Representative microphotographs show the expression of SYN (red) or MAP-2 (green) together with the lack of signal in the 488 (green) or 590 (red) channels respectively in neurons incubated in the presence of each primary antibody as indicated in the figure and both secondary antibodies (single negative control). Nuclear staining is shown in blue (DAPI). Scale bar = 50 μm.

REFERENCES

Acaz-Fonseca, E., Avila-Rodriguez, M., Garcia-Segura, L. M., and Barreto, G. E. (2016). Regulation of astroglia by gonadal steroid hormones under physiological and pathological conditions. *Prog. Neurobiol.* 144, 5–26. doi: 10.1016/j.pneurobio.2016.06.002

Acaz-Fonseca, E., Sanchez-Gonzalez, R., Azcoitia, I., Arevalo, M. A., and Garcia-Segura, L. M. (2014). Role of astrocytes in the neuroprotective actions of 17β-estradiol and selective estrogen receptor modulators. *Mol. Cell. Endocrinol.* 389, 48–57. doi: 10.1016/j.mce.2014.01.009

Adams, M. M., Shah, R. A., Janssen, W. G., and Morrison, J. H. (2001). Different modes of hippocampal plasticity in response to estrogen in young and aged female rats. *Proc. Natl. Acad. Sci. U S A* 98, 8071–8076. doi: 10.1073/pnas.141215898

Allen, N. J., and Lyons, D. A. (2018). Glia as architects of central nervous system formation and function. *Science* 362, 181–185. doi: 10.1126/science.aat0473

Amenta, F., Bronzetti, E., Sabbatini, M., and Vega, J. A. (1998). Astrocyte changes in aging cerebral cortex and hippocampus: a quantitative immunohistochemical study. *Microsc. Res. Tech.* 43, 29–33. doi: 10.1002/(sici)1097-0029(19981001)43:1<29::aid-jemt5>3.0.co;2-h

Arnold, S., de Araújo, G. W., and Beyer, C. (2008). Gender-specific regulation of mitochondrial fusion and fission gene transcription and viability of cortical astrocytes by steroid hormones. *J. Mol. Endocrinol.* 41, 289–300. doi: 10.1677/jme-08-0085

Aviles-Reyes, R. X., Angelo, M. F., Villarreal, A., Rios, H., Lazarowski, A., and Ramos, A. J. (2010). Intermittent hypoxia during sleep induces reactive gliosis and limited neuronal death in rats: implications for sleep apnea. *J. Neurochem.* 112, 854–869. doi: 10.1111/j.1471-4159.2009.06535.x

Bachar, A. R., Scheffer, L., Schroeder, A. S., Nakamura, H. K., Cobb, L. J., Oh, Y. K., et al. (2010). Humanin is expressed in human vascular walls and has a cytoprotective effect against oxidized LDL-induced oxidative stress. *Cardiovasc. Res.* 88, 360–366. doi: 10.1093/cvr/cvq191

Borras, C., Sastre, J., Garcia-Sala, D., Lloret, A., Pallardó, F. V., and Viña, J. (2003). Mitochondria from females exhibit higher antioxidant gene expression and lower oxidative damage than males. *Free Radic Biol. Med.* 34, 546–552. doi: 10.1016/s0891-5849(02)01356-4

Brinton, R. D. (2008). The healthy cell bias of estrogen action: mitochondrial bioenergetics and neurological implications. *Trends Neurosci.* 31, 529–537. doi: 10.1016/j.tins.2008.07.003

Calleja, M., Peña, P., Ugalde, C., Ferreiro, C., Marco, R., and Garesse, R. (1993). Mitochondrial DNA remains intact during *Drosophila* aging, but the levels of mitochondrial transcripts are significantly reduced. *J. Biol. Chem.* 268, 18891–18897.

Cao, F., Zhang, H., Meng, X., Feng, J., Li, T., Wei, S., et al. (2013). Ovariectomy-mediated impairment of spatial working memory, but not reference memory, is attenuated by the knockout of the dopamine D_3 receptor in female mice. *Behav. Brain Res.* 247, 27–33. doi: 10.1016/j.bbr.2013.03.014

Capt, C., Passamonti, M., and Breton, S. (2016). The human mitochondrial genome may code for more than 13 proteins. *Mitochondrial DNA A DNA Mapp. Seq. Anal.* 27, 3098–3101. doi: 10.3109/19401736.2014.1003924

Caricasole, A., Bruno, V., Cappuccio, I., Melchiorri, D., Copani, A., and Nicoletti, F. (2002). A novel rat gene encoding a Humanin-like peptide endowed with broad neuroprotective activity. *FASEB J.* 16, 1331–1333. doi: 10.1096/fj.02-0018fje

Castiglioni, A. J., Legare, M. E., Busbee, D. L., and Tiffany-Castiglioni, E. (1991). Morphological changes in astrocytes of aging mice fed normal or caloric restricted diets. *Age* 14, 102–106. doi: 10.1007/bf02435015

Cerbai, F., Lana, D., Nosi, D., Petkova-Kirova, P., Zecchi, S., Brothers, H. M., et al. (2012). The neuron-astrocyte-microglia triad in normal brain ageing and in a model of neuroinflammation in the rat hippocampus. *PLoS One* 7:e45250. doi: 10.1371/journal.pone.0045250

Chai, G.-S., Duan, D.-X., Ma, R.-H., Shen, J.-Y., Li, H.-L., Ma, Z.-W., et al. (2014). Humanin attenuates Alzheimer-like cognitive deficits and pathological changes induced by amyloid β-peptide in rats. *Neurosci. Bull.* 30, 923–935. doi: 10.1007/s12264-014-1479-3

Chen, J. Q., Eshete, M., Alworth, W. L., and Yager, J. D. (2004). Binding of MCF-7 cell mitochondrial proteins and recombinant human estrogen receptors a and b to human mitochondrial DNA estrogen response elements. *J. Cell. Biochem.* 93, 358–373. doi: 10.1002/jcb.20178

Codagnone, M. G., Podestá, M. F., Uccelli, N. A., and Reinés, A. (2015). Differential local connectivity and neuroinflammation profiles in the medial prefrontal cortex and hippocampus in the valproic acid rat model of autism. *Dev. Neurosci.* 37, 215–231. doi: 10.1159/000375489

Cui, A.-L., Li, J. Z., Feng, Z.-B., Ma, G.-L., Gong, L., Li, C.-L., et al. (2014). Humanin rescues cultured rat cortical neurons from NMDA-induced toxicity not by NMDA receptor. *ScientificWorldJournal* 2014:341529. doi: 10.1155/2014/341529

Cui, A.-L., Zhang, Y.-H., Li, J.-Z., Song, T., Liu, X.-M., Wang, H., et al. (2017). Humanin rescues cultured rat cortical neurons from NMDA-induced toxicity through the alleviation of mitochondrial dysfunction. *Drug Des. Devel. Ther.* 11, 1243–1253. doi: 10.2147/dddt.s133042

da Silva Moreira, S. F., Nunes, E. A., Kuo, J., de Macedo, I. C., Muchale, A., de Oliveira, C., et al. (2016). Hypoestrogenism alters mood: ketamine reverses depressive-like behavior induced by ovariectomy in rats. *Pharmacol. Rep.* 68, 109–115. doi: 10.1016/j.pharep.2015.06.009

Demonacos, C. V., Karayanni, N., Hatzoglou, E., Tsiriyiotis, C., Spandidos, D. A., and Sekeris, C. E. (1996). Mitochondrial genes as sites of primary action of steroid hormones. *Steroids* 61, 226–232. doi: 10.1016/0039-128x(96)00019-0

Diz-Chaves, Y., Kwiatkowska-Naqvi, A., Von Hülst, H., Pernía, O., Carrero, P., and Garcia-Segura, L. M. (2012). Behavioral effects of estradiol therapy in ovariectomized rats depend on the age when the treatment is initiated. *Exp. Gerontol.* 47, 93–99. doi: 10.1016/j.exger.2011.10.008

Gao, G., Fan, H., Zhang, X., Zhang, F., Wu, H., Qi, F., et al. (2017). Neuroprotective effect of G^{14}-humanin on global cerebral ischemia/reperfusion by activation of SOCS3—STAT3—MCL-1 signal transduction pathway in rats. *Neurol. Res.* 39, 895–903. doi: 10.1080/01616412.2017.1352187

Garcia-Segura, L. M., Cardona-Gomez, P., Naftolin, F., and Chowen, J. A. (1998). Estradiol upregulates Bcl-2 expression in adult brain neurons. *Neuroreport* 9, 593–597. doi: 10.1097/00001756-199803090-00006

Gómez, L. A., and Hagen, T. M. (2012). Age-related decline in mitochondrial bioenergetics: does supercomplex destabilization determine lower oxidative capacity and higher superoxide production? *Semin. Cell Dev. Biol.* 23, 758–767. doi: 10.1016/j.semcdb.2012.04.002

Gottardo, M. F., Jaita, G., Magri, M. L., Zárate, S., Moreno Ayala, M., Ferraris, J., et al. (2014). Antiapoptotic factor humanin is expressed in normal and tumoral pituitary cells and protects them from TNF-α-induced apoptosis. *PLoS One* 9:e111548. doi: 10.1371/journal.pone.0111548

Gould, T. D., Dao, D. T., and Kovacsics, C. E. (2009). "The open field test. Mood and anxiety related phenotypes in mice", in *Neuromethods*, ed. T. Gould (Totowa, NJ: Humana Press), 1–20. doi: 10.1007/978-1-60761-303-9_1

Gould, E., Woolley, C. S., Frankfurt, M., and McEwen, B. S. (1990). Gonadal steroids regulate dendritic spine density in hippocampal pyramidal cells in adulthood. *J. Neurosci.* 10, 1286–1291. doi: 10.1523/JNEUROSCI.10-04-01286.1990

Hampson, E. (2018). Estrogens, aging, and working memory. *Curr. Psychiatry Rep.* 20:109. doi: 10.1007/s11920-018-0972-1

Hara, Y., Yuk, F., Puri, R., Janssen, W. G., Rapp, P. R., and Morrison, J. H. (2014). Presynaptic mitochondrial morphology in monkey prefrontal cortex correlates with working memory and is improved with estrogen treatment. *Proc. Natl. Acad. Sci. U S A* 111, 486–491. doi: 10.1073/pnas.1311310110

Hashimoto, Y., Niikura, T., Tajima, H., Yasukawa, T., Sudo, H., Ito, Y., et al. (2001). A rescue factor abolishing neuronal cell death by a wide spectrum of familial Alzheimer's disease genes and Aβ. *Proc. Natl. Acad. Sci. U S A* 98, 6336–6341. doi: 10.1073/pnas.101133498

Hashimoto, Y., Suzuki, H., Aiso, S., Niikura, T., Nishimoto, I., and Matsuoka, M. (2005). Involvement of tyrosine kinases and STAT3 in Humanin-mediated neuroprotection. *Life Sci.* 77, 3092–3104. doi: 10.1016/j.lfs.2005.03.031

Jyothi, H. J., Vidyadhara, D. J., Mahadevan, A., Philip, M., Parmar, S. K., Manohari, S. G., et al. (2015). Aging causes morphological alterations in astrocytes and microglia in human substantia nigra pars compacta. *Neurobiol. Aging* 36, 3321–3333. doi: 10.1016/j.neurobiolaging.2015.08.024

Kanaan, N. M., Kordower, J. H., and Collier, T. J. (2010). Age-related changes in glial cells of dopamine midbrain subregions in rhesus monkeys. *Neurobiol. Aging* 31, 937–952. doi: 10.1016/j.neurobiolaging.2008.07.006

Kang, D., Kim, S. H., and Hamasaki, N. (2007). Mitochondrial transcription factor A (TFAM): roles in maintenance of mtDNA and cellular functions. *Mitochondrion* 7, 39–44. doi: 10.1016/j.mito.2006.11.017

Kariya, S., Hirano, M., Furiya, Y., Sugie, K., and Ueno, S. (2005). Humanin detected in skeletal muscles of MELAS patients: a possible new therapeutic agent. *Acta Neuropathol.* 109, 367–372. doi: 10.1007/s00401-004-0965-5

Kariya, S., Takahashi, N., Ooba, N., Kawahara, M., Nakayama, H., and Ueno, S. (2002). Humanin inhibits cell death of serum-deprived PC12h cells. *Neuroreport* 13, 903–907. doi: 10.1097/00001756-200205070-00034

Kemper, M. F., Stirone, C., Krause, D. N., Duckles, S. P., and Procaccio, V. (2014). Genomic and non-genomic regulation of PGC1 isoforms by estrogen to increase cerebral vascular mitochondrial biogenesis and reactive oxygen species protection. *Eur. J. Pharmacol.* 723, 322–329. doi: 10.1016/j.ejphar.2013.11.009

Kim, S. J., Guerrero, N., Wassef, G., Xiao, J., Mehta, H. H., Cohen, P., et al. (2016). The mitochondrial-derived peptide humanin activates the ERK1/2, AKT, and STAT3 signaling pathways and has age-dependent signaling differences in the hippocampus. *Oncotarget* 7, 46899–46912. doi: 10.18632/oncotarget.10380

Kim, S. J., Xiao, J., Wan, J., Cohen, P., and Yen, K. (2017). Mitochondrially derived peptides as novel regulators of metabolism. *J. Physiol.* 595, 6613–6621. doi: 10.1113/jp274472

Kiss, A., Delattre, A. M., Pereira, S. I., Carolino, R. G., Szawka, R. E., Anselmo-Franci, J. A., et al. (2012). 17β-estradiol. Replacement in young, adult and middle-aged female ovariectomized rats promotes improvement of spatial reference memory and an antidepressant effect and alters monoamines and BDNF levels in memory- and depression-related brain areas. *Behav. Brain Res.* 227, 100–108. doi: 10.1016/j.bbr.2011.10.047

Klinge, C. M. (2008). Estrogenic control of mitochondrial function and biogenesis. *J. Cell. Biochem.* 105, 1342–1351. doi: 10.1002/jcb.21936

Klinge, C. M. (2017). Estrogens regulate life and death in mitochondria. *J. Bioenerg. Biomembr.* 49, 307–324. doi: 10.1007/s10863-017-9704-1

Krejcova, G., Patocka, J., and Slaninova, J. (2004). Effect of humanin analogues on experimentally induced impairment of spatial memory in rats. *J. Pept. Sci.* 10, 636–639. doi: 10.1002/psc.569

Lamprecht, R., and LeDoux, J. (2004). Structural plasticity and memory. *Nat. Rev. Neurosci.* 5, 45–54. doi: 10.1038/nrn1301

Lee, C., Wan, J., Miyazaki, B., Fang, Y., Guevara-Aguirre, J., Yen, K., et al. (2014). IGF-I regulates the age-dependent signaling peptide humanin. *Aging Cell* 13, 958–961. doi: 10.1111/acel.12243

Lee, C., Yen, K., and Cohen, P. (2013). Humanin: a harbinger of mitochondrial-derived peptides? *Trends Endocrinol. Metab.* 24, 222–228. doi: 10.1016/j.tem.2013.01.005

Livak, K. J., and Schmittgen, T. D. (2001). Analysis of relative gene expression data using real-time quantitative PCR and the $2^{-\Delta\Delta CT}$ method. *Methods* 25, 402–408. doi: 10.1006/meth.2001.1262

Luo, S., Valencia, C. A., Zhang, J., Lee, N. C., Slone, J., Gui, B., et al. (2018). Biparental inheritance of mitochondrial DNA in humans. *Proc. Natl. Acad. Sci. U S A* 115, 13039–13044. doi: 10.1073/pnas.1810946115

Luquin, S., Naftolin, F., and Garcia-Segura, L. M. (1993). Natural fluctuation and gonadal hormone regulation of astrocyte immunoreactivity in dentate gyrus. *J. Neurobiol.* 24, 913–924. doi: 10.1002/neu.480240705

Mamiya, T., and Ukai, M. (2001). [Gly^{14}]-humanin improved the learning and memory impairment induced by scopolamine *in vivo*. *Br. J. Pharmacol.* 134, 1597–1599. doi: 10.1038/sj.bjp.0704429

Matsuoka, M., and Hashimoto, Y. (2010). Humanin and the receptors for humanin. *Mol. Neurobiol.* 41, 22–28. doi: 10.1007/s12035-009-8090-z

Mercer, T. R., Neph, S., Dinger, M. E., Crawford, J., Smith, M. A., Shearwood, A. M., et al. (2011). The human mitochondrial transcriptome. *Cell* 146, 645–658. doi: 10.1016/j.cell.2011.06.051

Miedel, C. J., Patton, J. M., Miedel, A. N., Miedel, E. S., and Levenson, J. M. (2017). Assessment of spontaneous alternation, novel object recognition and limb clasping in transgenic mouse models of amyloid-β and tau neuropathology. *J. Vis. Exp.* 123:55523. doi: 10.3791/55523

Morrison, J. H., Brinton, R. D., Schmidt, P. J., and Gore, A. C. (2006). Estrogen, menopause and the aging brain: how basic neuroscience can inform hormone therapy in women. *J. Neurosci.* 26, 10332–10348. doi: 10.1523/JNEUROSCI.3369-06.2006

Muzumdar, R. H., Huffman, D. M., Atzmon, G., Buettner, C., Cobb, L. J., Fishman, S., et al. (2009). Humanin: a novel central regulator of peripheral insulin action. *PLoS One* 4:e6334. doi: 10.1371/journal.pone.0006334

Niikura, T., Chiba, T., Aiso, S., Matsuoka, M., and Nishimoto, I. (2004). Humanin: after the discovery. *Mol. Neurobiol.* 30, 327–340. doi: 10.1385/mn:30:3:327

Niikura, T., Sidahmed, E., Hirata-Fukae, C., Aisen, P. S., and Matsuoka, Y. (2011). A humanin derivative reduces amyloid β accumulation and ameliorates memory deficit in triple transgenic mice. *PLoS One* 6:e16259. doi: 10.1371/journal.pone.0016259

Nilsen, J., and Brinton, R. D. (2002). Impact of progestins on estrogen-induced neuroprotection: synergy by progesterone and 19-norprogesterone and antagonism by medroxyprogesterone acetate. *Endocrinology* 143, 205–212. doi: 10.1210/endo.143.1.8582

Nilsen, J., and Brinton, R. D. (2003). Mechanism of estrogen-mediated neuroprotection: regulation of mitochondrial calcium and Bcl-2 expression. *Proc. Natl. Acad. Sci. U S A* 100, 2842–2847. doi: 10.1073/pnas.0438041100

Ojala, D., Montoya, J., and Attardi, G. (1981). tRNA punctuation model of RNA processing in human mitochondria. *Nature* 290, 470–474. doi: 10.1038/290470a0

Overstreet, D. H. (2012). Modeling depression in animal models. *Methods Mol. Biol.* 829, 125–144. doi: 10.1007/978-1-61779-458-2_7

Paharkova, V., Alvarez, G., Nakamura, H., Cohen, P., and Lee, K. W. (2015). Rat Humanin is encoded and translated in mitochondria and is localized to the mitochondrial compartment where it regulates ROS production. *Mol. Cell. Endocrinol.* 413, 96–100. doi: 10.1016/j.mce.2015.06.015

Palmer, A. L., and Ousman, S. S. (2018). Astrocytes and aging. *Front. Aging Neurosci.* 10:337. doi: 10.3389/fnagi.2018.00337

Pamplona, R. (2008). Membrane phospholipids, lipoxidative damage and molecular integrity: a causal role in aging and longevity. *Biochim. Biophys. Acta* 1777, 1249–1262. doi: 10.1016/j.bbabio.2008.07.003

Pfrieger, F. W. (2010). Role of glial cells in the formation and maintenance of synapses. *Brain Res. Rev.* 63, 39–46. doi: 10.1016/j.brainresrev.2009.11.002

Podestá, M. F., Yam, P., Codagnone, M. G., Uccelli, N. A., Colman, D., and Reinés, A. (2014). Distinctive PSA-NCAM and NCAM hallmarks in glutamate-induced dendritic atrophy and synaptic disassembly. *PLoS One* 9:e108921. doi: 10.1371/journal.pone.0108921

Reinés, A., Bernier, L. P., McAdam, R., Belkaid, W., Shan, W., Koch, A. W., et al. (2012). N-cadherin prodomain processing regulates synaptogenesis. *J. Neurosci.* 32, 6323–6334. doi: 10.1523/JNEUROSCI.0916-12.2012

Reinés, A., Cereseto, M., Ferrero, A., Sifonios, L., Podestá, M. F., and Wikinski, S. (2008). Maintenance treatment with fluoxetine is necessary to sustain normal levels of synaptic markers in an experimental model of depression: correlation with behavioral response. *Neuropsychopharmacology* 33, 1896–1908. doi: 10.1038/sj.npp.1301596

Robillard, K. N., Lee, K. M., Chiu, K. B., and MacLean, A. G. (2016). Glial cell morphological and density changes through the lifespan of rhesus macaques. *Brain Behav. Immun.* 55, 60–69. doi: 10.1016/j.bbi.2016.01.006

Rodríguez-Landa, J. F., Cueto-Escobedo, J., Puga-Olguín, A., Rivadeneyra-Domínguez, E., Bernal-Morales, B., Herrera-Huerta, E. V., et al. (2017). The phytoestrogen genistein produces similar effects as 17β-estradiol on anxiety-like behavior in rats at 12 weeks after ovariectomy. *Biomed. Res. Int.* 2017:9073816. doi: 10.1155/2017/9073816

Sanchez, M. I., Shearwood, A. M., Chia, T., Davies, S. M., Rackham, O., and Filipovska, A. (2015). Estrogen-mediated regulation of mitochondrial gene expression. *Mol. Endocrinol.* 29, 14–27. doi: 10.1210/me.2014-1077

Soreq, L., UK Brain Expression Consortium, North American Brain Expression Consortium, Rose, J., Soreq, E., Hardy, J., et al. (2017). Major shifts in glial regional identity are a transcriptional hallmark of human brain aging. *Cell Rep.* 18, 557–570. doi: 10.1016/j.celrep.2016.12.011

Stirone, C., Duckles, S. P., Krause, D. N., and Procaccio, V. (2005). Estrogen increases mitochondrial efficiency and reduces oxidative stress in cerebral blood vessels. *Mol. Pharmacol.* 68, 959–965. doi: 10.1124/mol.105.014662

Tajima, H., Kawasumi, M., Chiba, T., Yamada, M., Yamashita, K., Nawa, M., et al. (2005). A humanin derivative, S14G-HN, prevents amyloid-β-induced memory impairment in mice. *J. Neurosci. Res.* 79, 714–723. doi: 10.1002/jnr.20391

Tajima, H., Niikura, T., Hashimoto, Y., Ito, Y., Kita, Y., Terashita, K., et al. (2002). Evidence for *in vivo* production of Humanin peptide, a neuroprotective factor against Alzheimer's disease-related insults. *Neurosci. Lett.* 324, 227–231. doi: 10.1016/s0304-3940(02)00199-4

Takeshita, Y., Hashimoto, Y., Nawa, M., Uchino, H., and Matsuoka, M. (2013). SH3-binding protein 5 mediates the neuroprotective effect of the secreted bioactive peptide humanin by inhibiting c-Jun NH2-terminal kinase. *J. Biol. Chem.* 288, 24691–24704. doi: 10.1074/jbc.m113.469692

Tranque, P. A., Suarez, I., Olmos, G., Fernandez, B., and Garcia-Segura, L. M. (1987). Estradiol—induced redistribution of glial fibrillary acidic protein immunoreactivity in the rat brain. *Brain Res.* 406, 348–351. doi: 10.1016/0006-8993(87)90805-5

Verkhratsky, A., and Nedergaard, M. (2018). Physiology of astroglia. *Physiol. Rev.* 98, 239–389. doi: 10.1152/physrev.00042.2016

Verkhratsky, A., Nedergaard, M., and Hertz, L. (2015). Why are astrocytes important? *Neurochem. Res.* 40, 389–401. doi: 10.1007/s11064-014-1403-2

Verkhratsky, A., Olabarria, M., Noristani, H. N., Yeh, C. Y., and Rodriguez, J. J. (2010). Astrocytes in Alzheimer's disease. *Neurotherapeutics* 7, 399–412. doi: 10.1016/j.nurt.2010.05.017

Verkhratsky, A., Rodríguez, J. J., and Parpura, V. (2014). Neuroglia in ageing and disease. *Cell Tissue Res.* 357, 493–503. doi: 10.1007/s00441-014-1814-z

Villarreal, A., Seoane, R., González Torres, A., Rosciszewski, G., Angelo, M. F., Rossi, A., et al. (2014). S100B protein activates a RAGE-dependent autocrine loop in astrocytes: implications for its role in the propagation of reactive gliosis. *J. Neurochem.* 131, 190–205. doi: 10.1111/jnc.12790

Virbasius, J. V., and Scarpulla, R. C. (1994). Activation of the human mitochondrial transcription factor A gene by nuclear respiratory factors: a potential regulatory link between nuclear and mitochondrial gene expression in organelle biogenesis. *Proc. Natl. Acad. Sci. U S A* 91, 1309–1313. doi: 10.1073/pnas.91.4.1309

Walf, A. A., and Frye, C. A. (2007). The use of the elevated plus maze as an assay of anxiety-related behavior in rodents. *Nat. Protoc.* 2, 322–328. doi: 10.1038/nprot.2007.44

Wang, Z. J., Han, W. N., Yang, G. Z., Yuan, L., Liu, X. J., Li, Q. S., et al. (2014). The neuroprotection of Rattin against amyloid β peptide in spatial memory and synaptic plasticity of rats. *Hippocampus* 24, 44–53. doi: 10.1002/hipo.22202

Woolley, C. S., and McEwen, B. S. (1992). Estradiol mediates fluctuation in hippocampal synapse density during the estrous cycle in the adult rat. *J. Neurosci.* 12, 2549–2554. doi: 10.1523/JNEUROSCI.12-07-02549.1992

Woolley, C. S., and McEwen, B. S. (1993). Roles of estradiol and progesterone in regulation of hippocampal dendritic spine density during the estrous cycle in the rat. *J. Comp. Neurol.* 336, 293–306. doi: 10.1002/cne.903360210

Xu, X., Chua, C. C., Gao, J., Hamdy, R. C., and Chua, B. H. (2006). Humanin is a novel neuroprotective agent against stroke. *Stroke* 37, 2613–2619. doi: 10.1161/01.str.0000242772.94277.1f

Yang, X., Zhang, H., Wu, J., Yin, L., Yan, L. J., and Zhang, C. (2018). Humanin attenuates NMDA-induced excitotoxicity by inhibiting ROS-dependent JNK/p38 MAPK pathway. *Int. J. Mol. Sci.* 19:E2982. doi: 10.3390/ijms19102982

Yao, J., Irwin, R. W., Zhao, L., Nilsen, J., Hamilton, R. T., and Brinton, R. D. (2009). Mitochondrial bioenergetic deficit precedes Alzheimer's pathology in female mouse model of Alzheimer's disease. *Proc. Natl. Acad. Sci. U S A* 106, 14670–14675. doi: 10.1073/pnas.0903563106

Yen, K., Wan, J., Mehta, H. H., Miller, B., Christensen, A., Levine, M. E., et al. (2018). Humanin prevents age-related cognitive decline in mice and is associated with improved cognitive age in humans. *Sci. Rep.* 8:14212. doi: 10.1038/s41598-018-32616-7

Zárate, S., Astiz, M., Magnani, N., Imsen, M., Merino, F., Álvarez, S., et al. (2017a). Hormone deprivation alters mitochondrial function and lipid profile in the hippocampus. *J. Endocrinol.* 233, 1–14. doi: 10.1530/joe-16-0451

Zárate, S., Stevnsner, T., and Gredilla, R. (2017b). Role of estrogen and other sex hormones in brain aging. neuroprotection and DNA repair. *Front. Aging Neurosci.* 9:430. doi: 10.3389/fnagi.2017.00430

Zhang, W., Zhang, W., Li, Z., Hao, J., Zhang, Z., Liu, L., et al. (2012). S14G-humanin improves cognitive deficits and reduces amyloid pathology in the middle-aged APPswe/PS1dE9 mice. *Pharmacol. Biochem. Behav.* 100, 361–369. doi: 10.1016/j.pbb.2011.09.012

Conflict of Interest Statement: The authors declare that the research was conducted in the absence of any commercial or financial relationships that could be construed as a potential conflict of interest.

The handling Editor declared a shared affiliation, though no other collaboration, with the authors.

frontiers in Neuroscience

ORIGINAL RESEARCH
published: 20 December 2019
doi: 10.3389/fnins.2019.01340

Microglial Ultrastructure in the Hippocampus of a Lipopolysaccharide-Induced Sickness Mouse Model

*Julie C. Savage[1,2], Marie-Kim St-Pierre[2], Chin Wai Hui[1,2,3] and Marie-Eve Tremblay[1,2]**

[1] Axe Neurosciences, Centre de Recherche du CHU de Québec-Université Laval, Quebec, QC, Canada, [2] Département de Médecine Moléculaire, Faculté de Médecine, Université Laval, Quebec, QC, Canada, [3] Division of Life Science, The Hong Kong University of Science and Technology, Kowloon, Hong Kong

Sickness behavior is a set of behavioral changes induced by infections and mediated by pro-inflammatory cytokines. It is characterized by fatigue, decreased appetite and weight loss, changes in sleep patterns, cognitive functions, and lost interest in social activity. It can expedite recovery by conserving energy to mount an immune response involving innate immunity. To provide insights into microglial implication in sickness behavior with special focus on cognitive and social impairment, we investigated changes in their ultrastructure and interactions with synapses using a toxemia mouse model. Adult mice were injected with 1 mg/kg lipopolysaccharide (LPS) or saline, and assayed for signs of sickness behavior. LPS treated mice displayed reduced activity in open-field tests 24 h post-injection, while social avoidance and weight gain/loss were not significantly different between treatment groups. Microglia were investigated using electron microscopy to describe changes in their structure and function at nanoscale resolution. Microglial cell bodies and processes were investigated in the hippocampus CA1, a region responsible for learning and memory that is often impacted after peripheral LPS administration. Microglia in LPS treated animals displayed larger cell bodies as well as less complex processes at the time point examined. Strikingly, microglial processes in LPS injected animals were also more likely to contact excitatory synapses and contained more phagocytic material compared with saline injected controls. We have identified at the ultrastructural level significant changes in microglia-synapse interactions shortly after LPS administration, which draws attention to studying the roles of microglia in synaptic rewiring after inflammatory stimuli.

Keywords: sickness behavior, lipopolysaccharide, neuroinflammation, microglia, phagocytosis, hippocampus, mouse, electron microscopy

OPEN ACCESS

Edited by:
Yolanda Diz-Chaves, University of Vigo, Spain

Reviewed by:
Robert Dantzer, University of Texas MD Anderson Cancer Center, United States
Harris A. Gelbard, University of Rochester Medical Center, United States

***Correspondence:**
Marie-Eve Tremblay
tremblay0202@gmail.com

Specialty section:
This article was submitted to Neurodegeneration, a section of the journal Frontiers in Neuroscience

Received: *27 June 2019*
Accepted: *27 November 2019*
Published: *20 December 2019*

Citation:
Savage JC, St-Pierre M-K, Hui CW and Tremblay M-E (2019) Microglial Ultrastructure in the Hippocampus of a Lipopolysaccharide-Induced Sickness Mouse Model. Front. Neurosci. 13:1340. doi: 10.3389/fnins.2019.01340

INTRODUCTION

Sickness behavior is a well-defined set of cognitive and behavioral adaptations recruited in response to bacterial or viral infection or peripheral increases in proinflammatory cytokines. It is characterized by fatigue, joint and muscle pain, coldness, and reduced appetite (Dantzer, 2009) accompanied by psychological, emotional, and behavioral disturbance (Dantzer et al., 2008). Sepsis

is a life-threatening condition caused by the body's immune response to infection. Massive increases in blood and serum levels of cytokines and chemokines can cause organ failure and breakdown of the blood-brain barrier (BBB). Septic-associated encephalopathy is a serious complication, with symptoms including cognitive impairment and seizures.

Peripheral macrophages are able to recognize viruses, bacteria, fungi, and other invading pathogens using cell-surface receptors which recognize pathogen and danger associated molecular patterns (PAMPs and DAMPs). Upon recognition of dangerous materials, these cell surface receptors initiate signaling cascades, and culminate into a robust inflammatory response to kill and phagocytose the microorganism. PAMPs often cause the initial cascade of proinflammatory signaling in the early stages of illness, and this inflammation can damage nearby cells, thus releasing DAMPs into circulation and initiating a snowball proinflammatory signaling cascade (Hanisch and Kettenmann, 2007). Macrophages recognize gram-negative bacterial endotoxin lipopolysaccharide (LPS) using a receptor complex including toll-like receptor 4 (TLR4), CD14, and complement proteins, and secrete reactive oxygen and reactive nitrogen species to destroy the pathogen and proinflammatory cytokines in order to call nearby microglia to aid in the response (Lund et al., 2006). While this response is beneficial in most cases of infection, high levels of PAMPs and DAMPs also cause immune cells to release dangerously high levels of cytokines. As such, PAMPs, DAMPs, and cytokines have been targeted in recent therapeutics designed to treat sepsis (Gruda et al., 2018).

Microglia, the brain's resident macrophages, survey the brain and respond to any disturbances in their environment, resulting in morphological and functional changes during peripheral inflammation and infection (Butovsky and Weiner, 2018). As the main immune effector cell within the brain, they play intimate roles in the mechanisms behind sickness behaviors. During peripheral inflammation driven by increased circulating levels of proinflammatory cytokines, microglia express high levels of inducible nitric oxide producing enzymes, which remain elevated for several days. High levels of nitric oxide can result in destruction of bacteria, but also cause apoptosis of nearby neurons (Heneka et al., 1998). Elevated nitric oxide levels have been linked to synaptic loss in a protein kinase-G dependent manner (Sunico et al., 2010). Additionally, complement-mediated synaptic pruning has been implicated in normal brain development, cognitive aging, and neurodegenerative disease (Presumey et al., 2017). Systemic LPS injection has also been shown to have both disruptive and non-disruptive effects on the BBB during and after inflammation (Varatharaj and Galea, 2017).

Various mouse models of endotoxemia have revealed reduction of synapses in the CA1 region of the hippocampus (Moraes et al., 2015; Zhang et al., 2017). Reduced levels of NMDA protein were reported in the CA1 region of two different mouse sickness models (Zhang et al., 2017), while other studies have found reductions in excitatory synapse number in the hippocampus using cecal ligation and puncture (CLP) models (Moraes et al., 2015). Behavioral deficits, including spatial memory tasks, have been found to be microglia-dependent as pre-emptive minocycline treatment reduced neuroinflammation, oxidative stress, and neuronal dysfunction following CLP (Michels et al., 2015, 2017). Additionally, hippocampal-dependent context discrimination memory is impaired in rats following a single peripheral injection of LPS (Czerniawski and Guzowski, 2014). Recent human studies have similarly found long-term cognitive dysfunction in sepsis survivors. Sickness behavior in humans also includes memory impairment (Capuron et al., 1999; Reichenberg et al., 2001) and even very low doses of endotoxins can cause anxiety and depressive symptoms in humans (Reichenberg et al., 2001; Krabbe et al., 2005). Cognitive dysfunction and sickness behavior was exacerbated in aged mice in response to intracerebroventricular LPS administration (Huang et al., 2008). Synaptic loss is considered the best known correlate of cognitive dysfunction, but the direct role of microglia in synaptic loss in sepsis or sickness behavior has not yet been investigated.

To provide insights into this possible involvement, the present study aimed to investigate changes in microglial ultrastructure and interactions with synaptic elements in the *strata radiatum* and *lacunosum-moleculare* of the hippocampal CA1 region, 24 h after peripheral LPS administration in mice. We chose a 24 h timepoint as previous studies have found changes in ultrastructural interactions between microglia and cortical neurons, and disruptions in inhibitory synapses 24 h after peripheral LPS injection (Chen et al., 2014). We focused on the CA1 as it is the main region implicated in spatial memory tasks, where deficits were seen in prior studies in both human cases and mouse models of illness (Michels et al., 2015; Calsavara et al., 2018; Barichello et al., 2019). Our quantitative analysis determined that microglial cell body and process ultrastructure, as well as interactions with the neuropil, including synaptic clefts, were significantly modified following peripheral LPS administration.

MATERIALS AND METHODS

Animal Model

All experimental procedures were performed in agreement with the guidelines of the Institutional Animal Ethics committees, in conformity with the Canadian Council on Animal Care and the Animal Care Committee of *Université Laval*. Animals were group housed three to five animals per cage under a 12-h light-dark cycle at 22–25 °C with free access to food and water. Four month old CX3CR1-GFP heterozygous mice on C57BL/6J background (The Jackson Laboratory) were injected intraperitoneally (i.p.) with saline or 1 mg/kg of LPS derived from *Escherichia coli* serotype O55:B5 (Sigma Aldrich). CX3CR1-GFP mice were used considering that a subset of mice from the same protocol were imaged using two-photon *in vivo* microscopy (Abiega et al., 2016; Paris et al., 2018). The dose and timing of LPS was defined by the minimal dose required to induce sickness behavior while preventing mortality in our and other studies, and coinciding with changes in microglia-neuron interactions in previous studies in mouse cortex (Chen et al., 2014; Hoogland et al., 2015). A small cohort (four saline and five LPS injected animals) were treated to verify this dose and afterward utilized for two-photon *in vivo*

microscopy (Abiega et al., 2016; Paris et al., 2018). Following LPS injection, murine sickness score (MSS) was assessed every 2 h as previously described (Shrum et al., 2014) by an observer blinded to the experimental conditions. Coat appearance, level of consciousness, activity, response to stimulus, eye appearance, and respiration rate and quality were assessed every 2 h until 10 h post-injection. Male and female mice were split evenly between groups. Seven saline and seven LPS injected animals were used for open-field behavior studies, keeping only those with an optimal ultrastructural preservation (five saline and six LPS injected animals) for electron microscopy studies.

Open-Field Test

Twenty four hours after injection, mice were subjected to open-field testing (Hui et al., 2018). Carefully, one mouse was placed at the center of the apparatus (i.e., 50 × 50 cm white laminated cardboard box) and allowed to move freely for ten minutes. The movement was recorded with the ANY-maze system (version 4.8, Stoelting, Wood Dale, IL, United States). The total distance traveled, lines crossed, distance traveled at the center, entrances into the center, body rotations, freezes and immobile episodes were determined. The apparatus was cleaned between each mouse with 70% ethanol.

Animal Sacrifice and Tissue Processing

Immediately after open-field testing, mice were anesthetized with a cocktail of 80 mg/kg ketamine and 10 mg/kg xylazine. The animals were then transcardially perfused with ice-cold phosphate-buffered saline (PBS; 50 mM at pH 7.4) followed by 3.5 % acrolein and 4% paraformaldehyde (PFA) both diluted in phosphate buffer (PB; 100 mM at pH 7.4). Brains were harvested and post-fixed 2 h in ice-cold 4% PFA. Following post-fixation, brains were washed with PBS to remove excess PFA. Fifty-micrometer thick coronal brain sections were generated in PBS using a vibratome (Leica VT1000s). Brain sections were stored in a solution of cryoprotectant and stored at −20°C (Bisht et al., 2016a).

Tissue Preparation Staining for Electron Microscopy

Immunohistochemistry was performed against ionized calcium-binding adaptor protein 1 (IBA1) which provides an excellent visualization of microglial fine processes by immunocytochemical electron microscopy, as described previously (Savage et al., 2018). Briefly, brain sections between −2.0 mm and −2.3 mm Bregma levels were selected and washed in PBS to remove cryoprotectant, then incubated in 0.3% hydrogen peroxide followed by 0.1 % sodium borohydride. Sections were incubated 1 h in blocking buffer (10% fetal bovine serum, 3% bovine serum albumin, 0.03% Triton X-100) then overnight at 4°C in primary rabbit anti-IBA1 antibody in blocking buffer (Wako). Sections were next incubated for 90 min in goat-anti-rabbit IgGs conjugated to biotin (1/300, diluted in TBS, Jackson ImmunoResearch) followed by ABC reagent (Vector Laboratories) and developed with a solution containing 0.05% 3,3′-diaminobenzidine and 0.015% hydrogen peroxide. A 30-min incubation of sections with 1% osmium tetroxide to fix lipids was performed followed by an ethanol dehydration of increasing concentration, washing in propylene oxide and overnight infiltration in Durcupan resin. The next day, the sections were embedded with Durcupan resin between ACLAR embedding films (Electron Microscopy Sciences) for 72 h at 55°C.

The CA1 of the dorsal hippocampus was excised, affixed to a resin block and cut into 70–75 nanometer-thick sections using an ultramicrotome (Leica Ultracut UC7). The ultrathin sections were collected on copper mesh grids. In each animal, 10 microglial cell bodies and 150–250 microglial processes were randomly selected and imaged at a magnification of 6800× using a transmission electron microscope (FEI Tecnai Spirit G2) equipped with an ORCA-HR digital camera (Hamamatsu; 10 MP). Microglial cell bodies were identified based on their positive staining for IBA1 and their unique ultrastructure. Microglia generally have smaller cell bodies and nuclei than neighboring astrocytes or neurons, characteristic heterochromatin patterns in their nuclei, as well as long and narrow stretches of endoplasmic reticulum (ER) (Savage et al., 2018). Microglial processes were identified based on their positive staining for IBA1 and their lack of nucleus, ER or Golgi apparatus. Intracellular organelles were identified as previously described (El Hajj et al., 2019).

Ultrastructural Analysis of Microglia

Images of the microglial cell bodies and processes were blinded to the experimental conditions prior to analysis to prevent bias. The area, perimeter, circularity, solidity, number of phagosomes, percentage of cells with phagosomes and presence of ER dilation was determined for each cell body using FIJI. Additionally, the maximum distance from nuclear membrane to cellular membrane was measured, as well as the number of cells displaying proximal processes. A proximal process was defined as a region which narrows to below 0.3 microns and does not contain ER or Golgi apparatus. Excitatory synapses (asymmetric synapses) were defined by the presence of a presynaptic axon terminal containing 40-nanometer vesicles in close apposition to a postsynaptic dendritic spine displaying an asymmetric postsynaptic density thickening (Colonnier, 1968). The perimeter, area, percentage touching synapses, percentage with phagosomes and percentage associated with extended extracellular space pockets was determined for each process (El Hajj et al., 2019). Phagosomes were identified by their ovoid shape with a clear cytoplasm. ER was characterized as dilated if the distance between the two membranes enclosing the lumen was greater than 60 nanometers. Extracellular space pockets were identified by clear space surrounding the microglia, without delineating membranes and lacking acute angles seen in astrocytic processes (Tremblay et al., 2010).

Statistics

Data was analyzed using GraphPad Prism 7. LPS versus saline injected mice were compared using a non-parametric Mann–Whitney test. The sample size (n) refers to individual

microglial cell bodies or processes, as previously reported in our ultrastructural analyses (El Hajj et al., 2019). All data is reported as mean ± standard error of the mean (SEM).

RESULTS

To determine the ultrastructural changes of microglia and their interactions with synaptic structures during sickness behavior, we injected 4 month old CX3CR1-GFP heterozygous mice i.p. with 1 mg/kg LPS or saline (see **Figure 1A** for experimental paradigm). An observer blinded to animal treatment monitored the injected mice for sickness behavior during 10 h following injection (**Figure 1B**), and was able to correctly identify LPS from control mice, as control mice displayed a score of 0 on the MSS at every timepoint investigated. Mice injected with LPS displayed time-dependent increases in MSS (**Figure 1B**). Twenty-four hours after injection, mice were subjected to open-field behavior testing to verify sickness behavior. Mice displayed sickness behavior including decreased distance traveled both in total and in the center of the open-field, and decreases in the number of line crossings (**Figures 1C–G**), consistent with other rodent sickness behavior models (Shrum et al., 2014; Furube et al., 2018; Mansour et al., 2018).

Following verification of LPS injection causing sickness behavior, we analyzed microglia at nanoscale resolution to determine changes in ultrastructure and interactions with synapses. We focused on the *strata radiatum* and *lacunosum-moleculare* of the dorsal CA1, which has been implicated in microglial-mediated behavioral deficits in mouse models of sickness behavior (Michels et al., 2015; Zhang et al., 2017). Microglial cell bodies and processes were identified by their immunoreactivity against IBA1, with cell bodies displaying characteristic bean-shaped nuclei, long stretches of ER and numerous mitochondria (**Figures 2A–D**).

Microglial cell bodies were more likely to contain phagosomes in LPS injected *versus* saline injected animals (84.62 percent versus 43.75 percent, **Table 1**). LPS injected animals also displayed increased numbers of phagosomes per microglial cell body (**Figure 2E**). Most of these phagosomes were lucent and contained fully digested contents. However, many phagosomes contained partially degraded membranes and in one case contained what may appear to be two partially digested postsynaptic densities. Cell bodies were also more likely to display attached proximal processes, defined by a narrowing to less than 300 nanometers in width at some point also devoid of ER and Golgi (**Figure 2E**). Attached proximal processes are very rarely seen in ultrathin sections when investigating healthy brain tissue, but were significantly increased after LPS injection (14.58 percent in saline injected controls *versus* 44.23 percent in LPS injected animals, **Table 1**). The cytosol of microglial cell bodies from LPS injected animals was also thicker and more expansive compared with saline injected controls, as determined by the longest distance measured between cellular and nuclear membranes (**Figure 2E**).

While microglial cell bodies in LPS injected animals contained a larger area of cytosolic space (10.75 μm^2 versus 6.72 μm^2, **Table 1**), they were not significantly different in total area or perimeter. Roughly 60 percent of cell bodies contacted pockets of extracellular space in both conditions (56.25 percent in saline injected *versus* 59.62 percent in LPS injected mice). Previous studies from our group have defined dark microglia, recognized by their electron dense cytoplasm and nucleoplasm, as cells displaying signs of metabolic stress including dilated ER (Bisht et al., 2016b). These cells are rare in healthy young adult mice, but they increase in number among the hippocampus CA1 *strata radiatum* and *lacunosum-moleculare* of maternal immune activation, chronic stress, aging or Alzheimer model mice (Bisht et al., 2016b; Hui et al., 2018). We found no dark microglia in either experimental group, indicating that acute sickness induced by a single LPS injection is an insufficient stressor to induce microglial cytoplasmic/nucleoplasmic condensation, the hallmark identifying ultrastructural feature of dark microglia, at least in this brain region and at the time point examined.

TABLE 1 | Quantification of ultrastructural changes induced by LPS in 4 month old mice.

	Saline	LPS	*p*-value
Cell bodies			
Area (μm^2)	20.41 ± 1.11	23.65 ± 1.727	0.116
Perimeter (μm)	22.41 ± 0.88	25.58 ± 1.32	0.0477
Circularity	0.525 ± 0.02	0.482 ± 0.02	0.136
Roundness	0.5591 ± 0.023	0.5733 ± 0.023	0.658
Solidity	0.844 ± 0.014	0.814 ± 0.014	0.126
Phagocytic cells (%)	43.75 ± 7.24	84.62 ± 5.05	<0.0001
Phagosomes per cell (n)	1.083 ± 0.22	3 ± 0.231	<0.0001
Lipid bodies (%)	20.83 ± 5.9	21.15 ± 5.7	0.969
Lipid bodies per cell (n)	0.4583 ± 0.1657	0.4615 ± 0.1516	0.988
Extracellular space pockets (%)	56.25 ± 7.2	59.62 ± 6.87	0.7365
ER dilation (%)	12.5 ± 4.8	30.77 ± 6.46	0.0276
Attached proximal processes (%)	14.58 ± 5.15	44.23 ± 6.96	0.001
Cell body cytoplasmic size (μm^2)	6.724 ± 0.516	10.75 ± 1.11	0.0018
Distance nucleus to membrane (μm)	1.679 ± 0.180	2.956 ± 0.314	0.0002
Processes			
Area (μm^2)	0.278 ± 0.016	0.334 ± 0.017	0.86
Perimeter (μm)	2.49 ± 0.092	2.51 ± 0.073	0.43
Circularity	0.559 ± 0.008	0.589 ± 0.006	0.007
Roundness	0.523 ± 0.008	0.527 ± 0.006	0.725
Solidity	0.826 ± 0.005	0.842 ± 0.004	0.016
Touching synapse (%)	9.646 ± 1.19	15.53 ± 1.08	0.0005
Number of synaptic clefts per process (n)	0.111 ± 0.015	0.173 ± 0.013	0.002
Axon terminals per process (n)	0.129 ± 0.018	0.221 ± 0.017	0.0005
Spines per process (n)	0.133 ± 0.018	0.201 ± 0.016	0.005
Phagocytic (%)	20.9 ± 1.6	22.7 ± 1.25	0.337
Number of phagosomes per process (n)	0.338 ± 0.035	0.430 ± 0.028	0.365
Extracellular space pockets (%)	40.68 ± 1.97	37.89 ± 1.45	0.253

While no dark microglia were identified, occasional stressed or degenerating dendritic spines were observed based on their darkened cytoplasm and altered organelles, often in contact with microglial processes (**Figure 2B**).

In addition to investigating microglial cell bodies, we utilized anti-IBA1 staining to identify at the ultrastructural level microglial processes discontinuous to their cell body in ultrathin section. Because IBA1 is distributed throughout the cytosol, we were able to investigate processes and their interactions with the surrounding neuropil. Although microglial processes did not change size following LPS injection, they were rounder and increased in solidity compared with the saline injected controls (**Figures 2B,D**). This is in line with light-level analyses of microglia conducted in other sickness behavior models (Hoogland et al., 2015). Microglial processes in LPS injected animals were also significantly more likely to interact with excitatory synapses. In particular, processes from LPS injected animals were much more likely to directly touch synaptic clefts (15.53 percent versus 9.6 percent, **Table 1**) and interact with both presynaptic axon terminals and postsynaptic dendritic spines (**Figure 2F**) than those of saline injected controls.

DISCUSSION

Microglia have been implicated in the initiation of neuronal death and damage across a myriad of neurodegenerative conditions including models of sickness behavior and sepsis survivors (Block et al., 2007; Sankowski et al., 2015; Zhao et al., 2019). We are reporting the first quantitative ultrastructural characterization of microglia within the hippocampus CA1 (*strata radiatum* and *lacunosum-moleculare*) of an LPS induced mouse sickness model. Our results uncovered increases in phagosomes 24 h after peripheral exposure. As we performed all of our TEM analysis on individual ultrathin sections and not serial sections, we cannot rule out the possibility that these phagosomes could

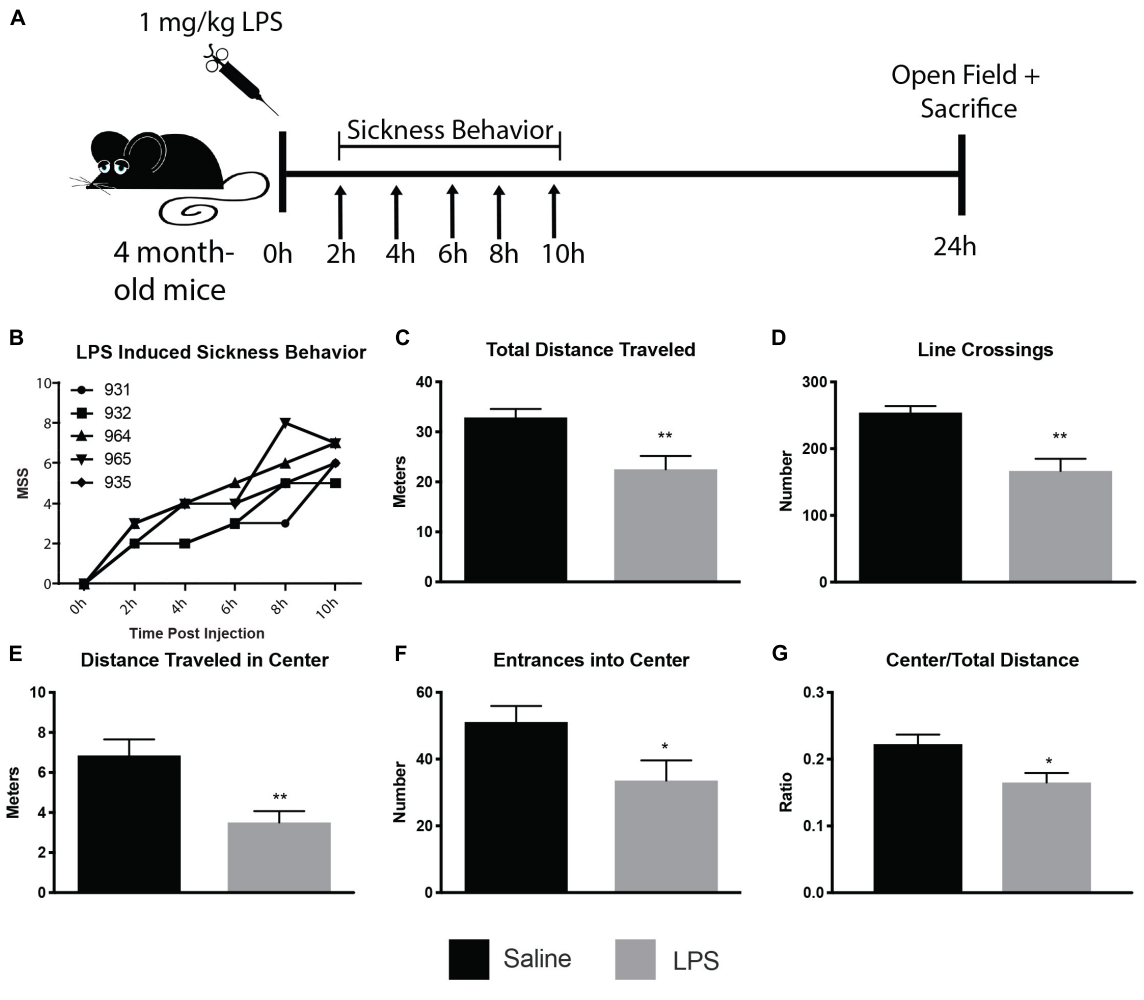

FIGURE 1 | LPS induced sickness behavior in 4 month old mice. Mice were injected with 1 mg/kg LPS or saline and assayed for sickness behavior, using the murine sickness score (MSS) tallied every 2 h for 10 h post-injection and open field behavior assay 24 h post-injection **(A)**. LPS-injected mice displayed increases in MSS **(B)** and decreases in total distance traveled **(C)**, line crossings **(D)**, distance traveled in the center **(E)**, entrances into center **(F)**, and center/total distance traveled **(G)**. $*p < 0.05$, $**p < 0.01$.

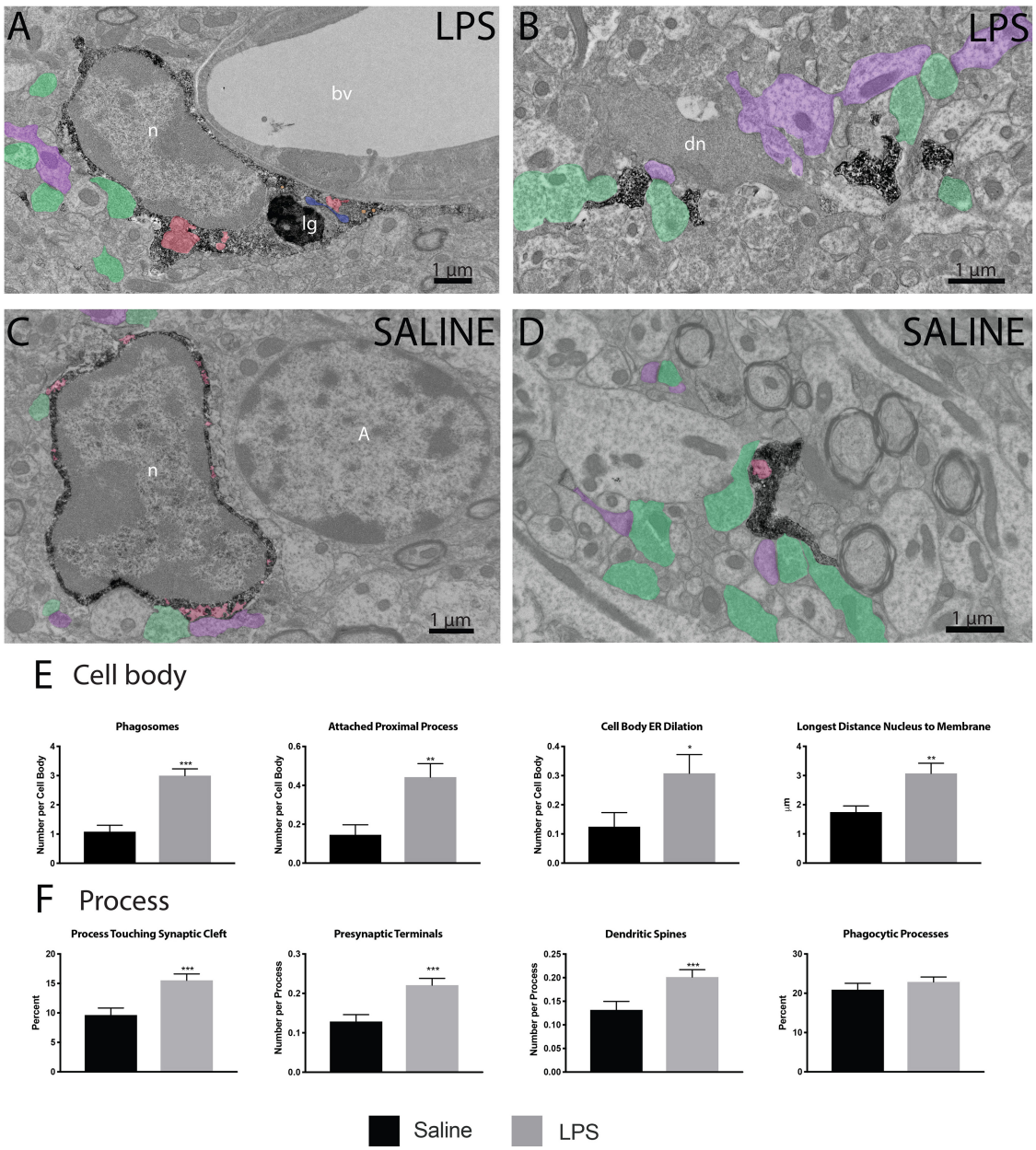

FIGURE 2 | LPS induced variations in microglial ultrastructure. Microglial cell bodies **(A,B)** and processes **(C,D)** within the *strata radiatum* and *lacunosum-moleculare* region of CA1 hippocampus were stained with anti-IBA1 antibody and investigated using transmission electron microscopy. Microglial cell bodies in LPS treated animals often contained long processes connected to their cell bodies, numerous lipidic (lg) and phagocytic inclusions (red) as well as dilated endoplasmic reticulum (ER; blue). Microglial processes often contacted asymmetric synapses including presynaptic terminals (green) and postsynaptic dendritic spines and shafts (purple). In panel **(B)**, a dark dendrite is also seen extending a dark spine that receives a synaptic contact from a healthy-looking axon terminal. The interaction of microglial cell bodies **(E)** was quantified, including number of phagosomes, attached proximal processes, and number of dilated ER stretches per cell body, as well as the longest distance between the cell body and nucleus. The interaction of microglial processes **(F)** with the neuropil was also quantified, including interactions with synaptic structures comprising synaptic clefts, presynaptic terminals and postsynaptic dendritic spines. $^{*}p < 0.05$, $^{**}p < 0.01$, $^{***}p < 0.001$. bv – blood vessel, n – nucleus, lg – lipid granule, dn – dark neuron, A - astrocyte.

be incidences of extracellular digestion or "exophagy" (Haka et al., 2016) viewed in 70–75 nanometer-thick profile. However, the incidence of microglia-associated extracellular space pockets was not significantly different between LPS and saline injected controls. In addition to increases in putative phagosomes, we also detected increased microglial interactions with synaptic structures when observed 24 h after peripheral LPS injection.

Dark microglia have been described in the hippocampus CA1 region of various mouse models in conjunction with disruptions in their inflammatory signaling, including animals

subjected to chronic unpredictable stress, repeated social defeat, maternal immune activation, aging, Alzheimer pathology and CX3CR1 deficiency (Bisht et al., 2016b; Hui et al., 2018; El Hajj et al., 2019). While a single dose of LPS was sufficient to induce proinflammatory signaling and significant changes in microglial cell body and process ultrastructure, we found no evidence of dark microglia in the CA1 (*strata radiatum* and *lacunosum-moleculare*) of LPS injected animals. It appears that the acute reaction to a single dose of LPS is insufficient to induce the dark microglia phenotype in 4 month old animals. This could imply that such a shift in microglial phenotype requires chronic increases in inflammatory signaling. Further studies are required to investigate the long-term consequences of LPS induced sickness and recovery on microglial ultrastructure.

While we did not observe dark microglia in the CA1 of LPS injected animals, we identified dark neuronal spines and cell bodies, for the first time in a sickness behavior model. These dark neurons, which could represent a subset of susceptible neurons, were previously described in aged mice and in mice experiencing stressful challenges, including sensory loss (Peters et al., 1991; Tremblay et al., 2012), as well as neurodegenerative disease pathology (Turmaine et al., 2000). Our data is in line with previous studies showing that mice subjected to i.p. LPS display reductions in neuronal projections (microtubule associated protein 2 staining) accompanied by neuronal cell body loss in the hippocampus (Zhao et al., 2019). Additionally, mouse models of sepsis have lower levels of glutamatergic NMDA receptors, as well as reduced numbers of doublecortin-positive newborn neurons and parvalbumin interneurons in the hippocampus (Valero et al., 2014; Ji et al., 2015; Zhang et al., 2017). These alterations were shown to be triggered by inflammatory pathways, most likely through increased microglial secretion of proinflammatory cytokines and reactive oxygen species.

Microglia in LPS injected animals contained increased amounts of phagocytic material. It is well established in the literature that peripheral administration of LPS can cause a shift in microglial morphology toward a more amoeboid shape (Buttini et al., 1996; Hoogland et al., 2015). It is possible that exposing microglia to proinflammatory cytokines shifts their activity to a more pro-phagocytic state. In our study, microglial cell bodies in animals injected with LPS contained nearly three times the phagocytic cargo observed in those injected with saline. These data imply that proinflammatory cytokines, at least in the short term of 24 h, significantly increase microglial phagocytic activity. However, further studies focused on the expression of proinflammatory cytokines, chemokines, and phagocytic cell surface receptors by these cells is required to directly link LPS administration with increases in microglial phagocytosis.

While several models of microglial morphology have implied that more amoeboid cells are associated with cell body migration and phagocytosis at the expense of surveillance (Walker et al., 2014), microglia in LPS injected animals were significantly more likely to interact with excitatory synapses (both elements and clefts). This is not immediately intuitive as microglia were previously defined with phenotypes somewhere on a spectrum between surveillant (interacting with synapses) and reactive (increasing cytokine/chemokine response to invading pathogens followed by phagocytic clearance) (Kreutzberg, 1996; Butovsky and Weiner, 2018). However, microglia involved in the phagocytosis of newborn neurons generated through adult neurogenesis or synapses during normal brain development were previously shown to display a ramified morphology with 'ball and chain' structures of phagocytic pouches on ramified processes (Sierra et al., 2010; Tremblay et al., 2010; Schafer et al., 2012). In the context of chronic stress, microglia which are involved in neuronal circuit rewiring (Milior et al., 2016; Wohleb et al., 2018) were either shown to display reduced or hyper-ramified processes depending on the model and time course (Hinwood et al., 2013; Hellwig et al., 2016; Milior et al., 2016). The synaptic contacts we observed did not appear to be sites of active proteolytic degradation, as there was no change in the amount of microglia-associated extracellular debris, marked by partially degraded membranes located in the large pockets of extracellular space between microglial membranes and surrounding neuropil, between either group of microglia. However, several microglial cell bodies displayed putative phagosomes containing seeming intact neuropil, while partially digested membranes and possible postsynaptic densities were also found in LPS injected mice.

Microglia have previously been implicated in synaptic pruning in a cellular mechanism known as "trogocytosis" (Weinhard et al., 2018). Weinhard and colleagues demonstrated that microglial processes in postnatal day 15 animals removed small parts of axon terminals averaging between 0.1 and 0.5 μm^3, much smaller than traditionally phagocytosed elements, without extracellular space between the neuronal and microglial membrane. It is possible that these excess synaptic contacts in LPS injected animals were undergoing trogocytosis, although further studies using 3-dimensional electron microscopy would be necessary to verify complete engulfment. It is also possible that these processes are engaged in synaptic stripping, by which a microglia remove synapses by interjecting a process into the synaptic cleft, physically separating the presynaptic terminal from the dendritic spine or shaft (Blinzinger and Kreutzberg, 1968). Synaptic stripping has been described in cortical samples from mice sacrificed 24 h after peripheral LPS injection (Chen et al., 2014).

Our study focused on the microglial response 24 h after a single injection of LPS, which has allowed us an ultrastructural snapshot of what occurs inside the brain during recovery from acute sickness. Numerous studies have studied acute (2–6 h post LPS injection) sickness behavior in rodents but have found increases in depressive-like behavior 24 h after injection (Dantzer et al., 2008). Human studies have also uncovered both acute and long-term implications of peripheral inflammation on the emergence of depression and other psychiatric disorders (Savitz and Harrison, 2018). Other studies in rodents have noted various long-term changes to microglial morphology after single or multiple exposures to LPS, being present in some cases as much as a year after injection (Hoogland et al., 2015). As this is the first ultrastructural characterization of microglia in the hippocampus in response to systemic LPS administration we focused on a single timepoint during initial sickness behavior. While we investigated both male and female mice there were no overt differences between the microglial ultrastructure between the two sexes in response to LPS, although the response to

LPS administration was rather robust and our sample size was insufficient to detect possibly small changes due to sex differences. In addition to sex differences, there are numerous questions to be addressed in follow-up studies, including exploration of acute *versus* chronic ultrastructural changes of microglia in response to a single dose or multiple doses of LPS, as well as investigation into other brain regions and along the aging trajectory. In complement, it would also be important to use additional techniques than electron microscopy, beyond the scope of this short communication study, to provide cellular and molecular insights into the microglial activities, such as neuronal circuit rewiring, mediated during sickness behavior.

DATA AVAILABILITY STATEMENT

The datasets generated for this study are available on request to the corresponding author.

ETHICS STATEMENT

The animal study was reviewed and approved by the Université Laval.

AUTHOR CONTRIBUTIONS

M-ET obtained funding for the study. JS designed and performed the experiments with CH. JS and M-KS-P prepared and analyzed the electron microscopy pictures and behavioral data. JS wrote the first draft of the manuscript. M-ET edited the subsequent versions to which all authors contributed. All authors read and approved the final version of the manuscript.

FUNDING

This study was supported by the ERA-NET TracInflam grant. JS and CH were supported by the Fonds de Recherche du Québec–Santé (FRQS) fellowships, M-KS-P holds a Canadian Institute of Health Research scholarship, while M-ET holds a Tier II Canada Research Chair of *Neuroimmune plasticity in health and therapy*.

ACKNOWLEDGMENTS

We would like to thank Nathalie Vernoux for technical assistance and experimental guidance, as well as Julie-Christine Lévesque at the Bio-Imaging platform of the Infectious Disease Research Centre, funded by an equipment and infrastructure grant from the Canadian Foundation Innovation (CFI).

REFERENCES

Abiega, O., Beccari, S., Diaz-Aparicio, I., Nadjar, A., Layé, S., Leyrolle, Q., et al. (2016). Neuronal hyperactivity disturbs ATP microgradients, impairs microglial motility, and reduces phagocytic receptor expression triggering apoptosis/microglial phagocytosis uncoupling. *PLoS Biol.* 14:e1002466. doi: 10.1371/journal.pbio.1002466

Barichello, T., Sayana, P., Giridharan, V. V., Arumanayagam, A. S., Narendran, B., Della Giustina, A., et al. (2019). Long-term cognitive outcomes after sepsis: a translational systematic review. *Mol. Neurobiol.* 56, 186–251. doi: 10.1007/s12035-018-10482

Bisht, K., El Hajj, H., Savage, J. C., Sánchez, M. G., and Tremblay, M.-È (2016a). Correlative light and electron microscopy to study microglial interactions with β-amyloid plaques. *J. Vis. Exp.* 2016:54060. doi: 10.3791/54060

Bisht, K., Sharma, K. P., Lecours, C., Gabriela Sánchez, M., El Hajj, H., Milior, G., et al. (2016b). Dark microglia: a new phenotype predominantly associated with pathological states. *Glia* 64, 826–839. doi: 10.1002/glia.22966

Blinzinger, K., and Kreutzberg, G. (1968). Displacement of synaptic terminals from regenerating motoneurons by microglial cells. *Z. Für Zellforsch. Mikrosk. Anat.* 85, 145–157. doi: 10.1007/BF00325030

Block, M. L., Zecca, L., and Hong, J.-S. (2007). Microglia-mediated neurotoxicity: uncovering the molecular mechanisms. *Nat. Rev. Neurosci.* 8, 57–69. doi: 10.1038/nrn2038

Butovsky, O., and Weiner, H. L. (2018). Microglial signatures and their role in health and disease. *Nat. Rev. Neurosci.* 19, 622–635. doi: 10.1038/s41583-018-0057-5

Buttini, M., Limonta, S., and Boddeke, H. W. (1996). Peripheral administration of lipopolysaccharide induces activation of microglial cells in rat brain. *Neurochem. Int.* 29, 25–35. doi: 10.1016/0197-0186(95)00141-7

Calsavara, A. J. C., Costa, P. A., Nobre, V., and Teixeira, A. L. (2018). Factors associated with short and long term cognitive changes in patients with sepsis. *Sci. Rep.* 8:4509. doi: 10.1038/s41598-018-22754-3

Capuron, L., Lamarque, D., Dantzer, R., and Goodall, G. (1999). Attentional and mnemonic deficits associated with infectious disease in humans. *Psychol. Med.* 29, 291–297. doi: 10.1017/s0033291798007740

Chen, Z., Jalabi, W., Hu, W., Park, H.-J., Gale, J. T., Kidd, G. J., et al. (2014). Microglial displacement of inhibitory synapses provides neuroprotection in the adult brain. *Nat. Commun.* 5:4486. doi: 10.1038/ncomms5486

Colonnier, M. (1968). Synaptic patterns on different cell types in the different laminae of the cat visual cortex. an electron microscope study. *Brain Res.* 9, 268–287. doi: 10.1016/0006-8993(68)90234-5

Czerniawski, J., and Guzowski, J. F. (2014). Acute neuroinflammation impairs context discrimination memory and disrupts pattern separation processes in hippocampus. *J. Neurosci. Off. J. Soc. Neurosci.* 34, 12470–12480. doi: 10.1523/JNEUROSCI.0542-14.2014

Dantzer, R. (2009). Cytokine, sickness behavior, and depression. *Immunol. Allergy Clin. North Am.* 29, 247–264. doi: 10.1016/j.iac.2009.02.002

Dantzer, R., O'Connor, J. C., Freund, G. G., Johnson, R. W., and Kelley, K. W. (2008). From inflammation to sickness and depression: when the immune system subjugates the brain. *Nat. Rev. Neurosci.* 9, 46–56. doi: 10.1038/nrn2297

El Hajj, H., Savage, J. C., Bisht, K., Parent, M., Vallières, L., Rivest, S., et al. (2019). Ultrastructural evidence of microglial heterogeneity in Alzheimer's disease amyloid pathology. *J. Neuroinflammation* 16:87. doi: 10.1186/s12974-019-1473-9

Furube, E., Kawai, S., Inagaki, H., Takagi, S., and Miyata, S. (2018). Brain region-dependent heterogeneity and dose-dependent difference in transient microglia population increase during lipopolysaccharide-induced inflammation. *Sci. Rep.* 8:2203. doi: 10.1038/s41598-018-206433

Gruda, M. C., Ruggeberg, K.-G., O'Sullivan, P., Guliashvili, T., Scheirer, A. R., Golobish, T. D., et al. (2018). Broad adsorption of sepsis-related PAMP and DAMP molecules, mycotoxins, and cytokines from whole blood using CytoSorb® sorbent porous polymer beads. *PloS One* 13:e0191676. doi: 10.1371/journal.pone.0191676

Haka, A. S., Barbosa-Lorenzi, V. C., Lee, H. J., Falcone, D. J., Hudis, C. A., Dannenberg, A. J., et al. (2016). Exocytosis of macrophage lysosomes leads to digestion of apoptotic adipocytes and foam cell formation. *J. Lipid Res.* 57, 980–992. doi: 10.1194/jlr.M064089

Hanisch, U.-K., and Kettenmann, H. (2007). Microglia: active sensor and versatile effector cells in the normal and pathologic brain. *Nat. Neurosci.* 10, 1387–1394. doi: 10.1038/nn1997

Hellwig, S., Brioschi, S., Dieni, S., Frings, L., Masuch, A., Blank, T., et al. (2016). Altered microglia morphology and higher resilience to stress-induced depression-like behavior in CX3CR1-deficient

mice. *Brain. Behav. Immun.* 55, 126–137. doi: 10.1016/j.bbi.2015.11.008

Heneka, M. T., Löschmann, P. A., Gleichmann, M., Weller, M., Schulz, J. B., Wüllner, U., et al. (1998). Induction of nitric oxide synthase and nitric oxide-mediated apoptosis in neuronal PC12 cells after stimulation with tumor necrosis factor-alpha/lipopolysaccharide. *J. Neurochem.* 71, 88–94. doi: 10.1046/j.1471-4159.1998.71010088.x

Hinwood, M., Tynan, R. J., Charnley, J. L., Beynon, S. B., Day, T. A., and Walker, F. R. (2013). Chronic stress induced remodeling of the prefrontal cortex: structural re-organization of microglia and the inhibitory effect of minocycline. *Cereb. Cortex N. Y. N* 1991, 1784–1797. doi: 10.1093/cercor/bhs151

Hoogland, I. C. M., Houbolt, C., van Westerloo, D. J., van Gool, W. A., and van de Beek, D. (2015). Systemic inflammation and microglial activation: systematic review of animal experiments. *J. Neuroinflammation* 12:114. doi: 10.1186/s12974-015-0332-6

Huang, Y., Henry, C. J., Dantzer, R., Johnson, R. W., and Godbout, J. P. (2008). Exaggerated sickness behavior and brain proinflammatory cytokine expression in aged mice in response to intracerebroventricular lipopolysaccharide. *Neurobiol. Aging* 29, 1744–1753. doi: 10.1016/j.neurobiolaging.2007.04.012

Hui, C. W., St-Pierre, A., El Hajj, H., Remy, Y., Hébert, S. S., Luheshi, G. N., et al. (2018). Prenatal immune challenge in mice leads to partly sex-dependent behavioral, microglial, and molecular abnormalities associated with schizophrenia. *Front. Mol. Neurosci.* 11:13. doi: 10.3389/fnmol.2018.00013

Ji, M.-H., Qiu, L.-L., Tang, H., Ju, L.-S., Sun, X.-R., Zhang, H., et al. (2015). Sepsis-induced selective parvalbumin interneuron phenotype loss and cognitive impairments may be mediated by NADPH oxidase 2 activation in mice. *J. Neuroinflammation* 12:182. doi: 10.1186/s12974-015-0401-x

Krabbe, K. S., Reichenberg, A., Yirmiya, R., Smed, A., Pedersen, B. K., and Bruunsgaard, H. (2005). Low-dose endotoxemia and human neuropsychological functions. *Brain. Behav. Immun.* 19, 453–460. doi: 10.1016/j.bbi.2005.04.010

Kreutzberg, G. W. (1996). Microglia: a sensor for pathological events in the CNS. *Trends Neurosci.* 19, 312–318. doi: 10.1016/0166-2236(96)10049-7

Lund, S., Christensen, K. V., Hedtjärn, M., Mortensen, A. L., Hagberg, H., Falsig, J., et al. (2006). The dynamics of the LPS triggered inflammatory response of murine microglia under different culture and in vivo conditions. *J. Neuroimmunol.* 180, 71–87. doi: 10.1016/j.jneuroim.2006.07.007

Mansour, H. A., Hassan, W. A., and Georgy, G. S. (2018). Neuroinflammatory reactions in sickness behavior induced by bacterial infection: protective effect of minocycline. *J. Biochem. Mol. Toxicol.* 32:e22020 doi: 10.1002/jbt.22020

Michels, M., Sonai, B., and Dal-Pizzol, F. (2017). Polarization of microglia and its role in bacterial sepsis. *J. Neuroimmunol.* 303, 90–98. doi: 10.1016/j.jneuroim.2016.12.015

Michels, M., Vieira, A. S., Vuolo, F., Zapelini, H. G., Mendonça, B., Mina, F., et al. (2015). The role of microglia activation in the development of sepsis-induced long-term cognitive impairment. *Brain. Behav. Immun.* 43, 54–59. doi: 10.1016/j.bbi.2014.07.002

Milior, G., Lecours, C., Samson, L., Bisht, K., Poggini, S., Pagani, F., et al. (2016). Fractalkine receptor deficiency impairs microglial and neuronal responsiveness to chronic stress. *Brain. Behav. Immun.* 55, 114–125. doi: 10.1016/j.bbi.2015.07.024

Moraes, C. A., Santos, G., de Sampaio e Spohr, T. C., D'Avila, J. C., Lima, F. R. S., Benjamim, C. F., et al. (2015). Activated microglia-induced deficits in excitatory synapses through IL-1β: implications for cognitive impairment in sepsis. *Mol. Neurobiol.* 52, 653–663. doi: 10.1007/s12035-014-8868-5

Paris, I., Savage, J. C., Escobar, L., Abiega, O., Gagnon, S., Hui, C.-W., et al. (2018). ProMoIJ: a new tool for automatic three-dimensional analysis of microglial process motility. *Glia* 66, 828–845. doi: 10.1002/glia.23287

Peters, A., Palay, S. L., and Webster, H. D. (1991). *Fine Structures of the Nervous System: Neurons and their Supporting Cells*, 3rd Edn. Oxford: Oxford University Press.

Presumey, J., Bialas, A. R., and Carroll, M. C. (2017). Complement system in neural synapse elimination in development and disease. *Adv. Immunol.* 135, 53–79. doi: 10.1016/bs.ai.2017.06.004

Reichenberg, A., Yirmiya, R., Schuld, A., Kraus, T., Haack, M., Morag, A., et al. (2001). Cytokine-associated emotional and cognitive disturbances in humans. *Arch. Gen. Psychiatry* 58, 445–452. doi: 10.1001/archpsyc.58.5.445

Sankowski, R., Mader, S., and Valdés-Ferrer, S. I. (2015). Systemic inflammation and the brain: novel roles of genetic, molecular, and environmental cues as drivers of neurodegeneration. *Front. Cell. Neurosci.* 9:28. doi: 10.3389/fncel.2015.00028

Savage, J. C., Picard, K., González-Ibáñez, F., and Tremblay, M. -È (2018). A brief history of microglial ultrastructure: distinctive features, phenotypes, and functions discovered over the past 60 years by electron microscopy. *Front. Immunol.* 9:803. doi: 10.3389/fimmu.2018.00803

Savitz, J., and Harrison, N. A. (2018). Interoception and Inflammation in psychiatric disorders. *Biol. Psychiatry Cogn. Neurosci. Neuroimaging* 3, 514–524. doi: 10.1016/j.bpsc.2017.12.011

Schafer, D. P., Lehrman, E. K., Kautzman, A. G., Koyama, R., Mardinly, A. R., Yamasaki, R., et al. (2012). Microglia sculpt postnatal neural circuits in an activity and complement-dependent manner. *Neuron* 74, 691–705. doi: 10.1016/j.neuron.2012.03.026

Shrum, B., Anantha, R. V., Xu, S. X., Donnelly, M., Haeryfar, S. M. M., McCormick, J. K., et al. (2014). A robust scoring system to evaluate sepsis severity in an animal model. *BMC Res. Notes* 7:233. doi: 10.1186/1756-0500-7-233

Sierra, A., Encinas, J. M., Deudero, J. J. P., Chancey, J. H., Enikolopov, G., Overstreet-Wadiche, L. S., et al. (2010). Microglia shape adult hippocampal neurogenesis through apoptosis-coupled phagocytosis. *Cell Stem Cell* 7, 483–495. doi: 10.1016/j.stem.2010.08.014

Sunico, C. R., González-Forero, D., Domínguez, G., García-Verdugo, J. M., and Moreno-López, B. (2010). Nitric oxide induces pathological synapse loss by a protein kinase G-, Rho kinase-dependent mechanism preceded by myosin light chain phosphorylation. *J. Neurosci. Off. J. Soc. Neurosci.* 30, 973–984. doi: 10.1523/JNEUROSCI.3911-09.2010

Tremblay, M. -È, Lowery, R. L., and Majewska, A. K. (2010). Microglial interactions with synapses are modulated by visual experience. *PLoS Biol.* 8:e1000527. doi: 10.1371/journal.pbio.1000527

Tremblay, M. -È, Zettel, M. L., Ison, J. R., Allen, P. D., and Majewska, A. K. (2012). Effects of aging and sensory loss on glial cells in mouse visual and auditory cortices. *Glia* 60, 541–558. doi: 10.1002/glia.22287

Turmaine, M., Raza, A., Mahal, A., Mangiarini, L., Bates, G. P., and Davies, S. W. (2000). Nonapoptotic neurodegeneration in a transgenic mouse model of Huntington's disease. *Proc. Natl. Acad. Sci. U.S.A.* 97, 8093–8097. doi: 10.1073/pnas.110078997

Valero, J., Mastrella, G., Neiva, I., Sánchez, S., and Malva, J. O. (2014). Long-term effects of an acute and systemic administration of LPS on adult neurogenesis and spatial memory. *Front. Neurosci.* 8:83. doi: 10.3389/fnins.2014.00083

Varatharaj, A., and Galea, I. (2017). The blood-brain barrier in systemic inflammation. *Brain. Behav. Immun.* 60, 1–12. doi: 10.1016/j.bbi.2016.03.010

Walker, F. R., Beynon, S. B., Jones, K. A., Zhao, Z., Kongsui, R., Cairns, M., et al. (2014). Dynamic structural remodelling of microglia in health and disease: a review of the models, the signals and the mechanisms. *Brain. Behav. Immun.* 37, 1–14. doi: 10.1016/j.bbi.2013.12.010

Weinhard, L., di Bartolomei, G., Bolasco, G., Machado, P., Schieber, N. L., Neniskyte, U., et al. (2018). Microglia remodel synapses by presynaptic trogocytosis and spine head filopodia induction. *Nat. Commun.* 9:1228. doi: 10.1038/s41467-018-03566-5

Wohleb, E. S., Terwilliger, R., Duman, C. H., and Duman, R. S. (2018). Stress-induced neuronal CSF1 provokes microglia-mediated neuronal remodeling and depressive-like behavior. *Biol. Psychiatry* 83, 38–49. doi: 10.1016/j.biopsych.2017.05.026

Zhang, S., Wang, X., Ai, S., Ouyang, W., Le, Y., and Tong, J. (2017). Sepsis-induced selective loss of NMDA receptors modulates hippocampal neuropathology in surviving septic mice. *PloS One* 12:e0188273. doi: 10.1371/journal.pone.0188273

Zhao, J., Bi, W., Xiao, S., Lan, X., Cheng, X., Zhang, J., et al. (2019). Neuroinflammation induced by lipopolysaccharide causes cognitive impairment in mice. *Sci. Rep.* 9:5790. doi: 10.1038/s41598-019-42286-8

Conflict of Interest: The authors declare that the research was conducted in the absence of any commercial or financial relationships that could be construed as a potential conflict of interest.

frontiers in Aging Neuroscience

ORIGINAL RESEARCH
published: 12 March 2020
doi: 10.3389/fnagi.2020.00024

Boosting Antioxidant Self-defenses by Grafting Astrocytes Rejuvenates the Aged Microenvironment and Mitigates Nigrostriatal Toxicity in Parkinsonian Brain *via* an *Nrf2-Driven Wnt/β-Catenin* Prosurvival Axis

Maria Francesca Serapide[1], *Francesca L'Episcopo*[2], *Cataldo Tirolo*[2], *Nunzio Testa*[2], *Salvatore Caniglia*[2], *Carmela Giachino*[2] *and Bianca Marchetti*[1,2]*

[1]*Pharmacology Section, Department of Biomedical and Biotechnological Sciences, Medical School, University of Catania, Catania, Italy,* [2]*Section of Neuropharmacology, OASI Research Institute-IRCCS, Troina, Italy*

OPEN ACCESS

Edited by:
Alberto Javier Ramos, National Council for Scientific and Technical Research (CONICET), Argentina

Reviewed by:
Zhigang Liu, Northwest A&F University, China
Juan Ferrario, National Council for Scientific and Technical Research (CONICET), Argentina

***Correspondence:**
Bianca Marchetti
biancamarchetti@libero.it

Received: *04 October 2019*
Accepted: *22 January 2020*
Published: *12 March 2020*

Citation:
Serapide MF, L'Episcopo F, Tirolo C, Testa N, Caniglia S, Giachino C and Marchetti B (2020) Boosting Antioxidant Self-defenses by Grafting Astrocytes Rejuvenates the Aged Microenvironment and Mitigates Nigrostriatal Toxicity in Parkinsonian Brain via an Nrf2-Driven Wnt/β-Catenin Prosurvival Axis. Front. Aging Neurosci. 12:24. doi: 10.3389/fnagi.2020.00024

Astrocyte (As) bidirectional dialog with neurons plays a fundamental role in major homeostatic brain functions, particularly providing metabolic support and antioxidant self-defense against reactive oxygen (ROS) and nitrogen species (RNS) *via* the activation of *NF-E2-related factor 2* (*Nrf2*), a master regulator of oxidative stress. Disruption of As–neuron crosstalk is chiefly involved in neuronal degeneration observed in Parkinson's disease (PD), the most common movement disorder characterized by the selective degeneration of dopaminergic (DAergic) cell bodies of the substantia nigra (SN) pars compacta (SNpc). Ventral midbrain (VM)-As are recognized to exert an important role in DAergic neuroprotection *via* the expression of a variety of factors, including wingless-related MMTV integration site 1 (*Wnt1*), a principal player in DAergic neurogenesis. However, whether As, by themselves, might fulfill the role of chief players in DAergic neurorestoration of aged PD mice is presently unresolved. Here, we used primary postnatal mouse VM-As as a graft source for unilateral transplantation above the SN of aged 1-methyl-4-phenyl-1,2,3,6-tetrahydropyridine (MPTP) mice after the onset of motor symptoms. Spatio-temporal analyses documented that the engrafted cells promoted: (i) a time-dependent nigrostriatal rescue along with increased high-affinity synaptosomal DA uptake and counteraction of motor deficit, as compared to mock-grafted counterparts; and (ii) a restoration of the impaired microenvironment *via* upregulation of As antioxidant self-defense through the activation of *Nrf2/Wnt/β-catenin* signaling, suggesting that grafting As has the potential to switch the SN neurorescue-unfriendly environment to a beneficial antioxidant/anti-inflammatory prosurvival milieu. These findings highlight As-derived factors/mechanisms as the crucial key for successful therapeutic outcomes in PD.

Keywords: Parkinson's disease, aging, astrocyte–neuron crosstalk, neuroinflammation, dopaminergic neurons, neuroprotection

INTRODUCTION

Astrocyte (As) bidirectional dialog with neurons plays a fundamental role in major homeostatic brain functions. Besides their physical and metabolic support to neurons, As regulate central nervous system (CNS) synaptogenesis, promote neuronal development and plasticity, guide axon pathfinding, modulate the blood–brain barrier, and contribute to neuroprotection *via* the production of different growth and neurotrophic factors, antioxidant and anti-inflammatory molecules, through a concerted crosstalk with neurons (Marchetti and Abbracchio, 2005; Bélanger and Magistretti, 2009; Sofroniew and Vinters, 2010; Molofsky et al., 2012; Sun and Jakobs, 2012). Notably, As display region-specific properties, as the nature of As-derived factors can vary as a function of the CNS region, the age and sex of the host, and the type of brain lesion/injury (Gallo et al., 1995; Marchetti, 1997; Barkho et al., 2006; Jiao and Chen, 2008; Oberheim et al., 2012). Specifically, As of the ventral midbrain (VM-As) represent a primary source of survival, neurotrophic and neuroprotective molecules for dopaminergic (DAergic) neurons (Engele and Bohn, 1991; Takeshima et al., 1994; Morale et al., 2006; Sandhu et al., 2009; L'Episcopo et al., 2010a), the neuronal cell population that progressively degenerates in Parkinson's disease (PD).

Here, the selective death of DAergic neurons of the substantia nigra pars compacta (SNpc) and their terminals in the striatum (Str) are responsible for the gradual impairment of motor function leading to the classical motor features of PD (i.e., bradykinesia, rest tremor, rigidity, and postural instability; Schapira et al., 2014; Jankovic, 2019). While the causes and mechanisms are not completely understood, current evidence indicates that a complex interplay between several genes and many environmental factors affecting the regulation of crucial pathways involved in inflammatory glial activation, mitochondrial function, protein misfolding/aggregation, and autophagy contribute to DAergic neuron demise in PD (Marchetti and Abbracchio, 2005; Frank-Cannon et al., 2008; Gao et al., 2011; Lastres-Becker et al., 2012; Cannon and Greenamyre, 2013; Hirsch et al., 2013; Dzamko et al., 2015, 2017; Langston, 2017; Blauwendraat et al., 2019).

Especially, in this context, dopamine (DA) oxidative metabolism represents a vulnerability factor linking both mitochondrial and lysosomal dysfunctions to PD pathogenesis (Hirsch and Hunot, 2009; Johri and Beal, 2012), whereby As play a critical antioxidant self-protective role. Hence, oxidative stress upregulates the expression of *Nuclear factor erythroid 2* like 2 (*NFE2L2/Nrf2*), which translocates to the nucleus and binds to antioxidant responsive elements (AREs; Tebay et al., 2015; Zhang et al., 2017). Besides other activated genes, the antioxidant, anti-inflammatory, and cytoprotective *Heme oxygenase 1* (*HO1*) and superoxide dismutase 1 (SOD1; Chen et al., 2009; Sandhu et al., 2009; Surh et al., 2009; Zhang et al., 2017) likely play an important role in DAergic neuroprotection against oxidative damage (Burbulla et al., 2017; Giguère et al., 2018; Surmeier, 2018; Nguyen et al., 2019).

Notably, aging represents a chief risk factor for PD development, as with advancing age, nigrostriatal DAergic neurons progressively deteriorate (Rodriguez et al., 2015; Wyss-Coray, 2016; Poewe et al., 2017). With age, the "adaptive" or "compensatory" capacity of midbrain DAergic neurons gradually fails, which may contribute to the slow nigrostriatal degeneration of PD (Hornykiewicz, 1993; Bezard and Gross, 1998; Blesa et al., 2017). In fact, aging is associated to a gradual decline in the ability of DAergic neurons to recover upon an insult (Bezard and Gross, 1998; Ho and Blum, 1998; Boger et al., 2010). Aging exacerbates inflammation and oxidative stress, which are crucial hallmarks of PD and 1-methyl-4-phenyl-1,2,3,6-tetrahydropyridine (MPTP)–induced PD (Di Monte and Langston, 1995; Langston, 2017).

In fact, microglial cells show age-dependent and region-specific changes in morphology such as structural deterioration or dystrophy, decreased expression of growth/neurotrophic factors, and an impaired phagocytic activity in the face of increased marker expression and upregulation of pro-inflammatory molecules (see Niraula et al., 2017, and references herein), all of which are associated to a gradual loss of As and microglia neuroprotective capacity. Reportedly, microglia switch to a so-called "primed" status, endowed with a strong neurotoxic, pro-inflammatory M1 phenotype with harmful consequences for As–neuron interactions (Miller and Streit, 2007; Liddelow et al., 2017; Rosciszewski et al., 2018, 2019) and DAergic neuron survival upon injury (L'Episcopo et al., 2011a,b,c, 2018a,b).

Notably, genetics, environmental toxicity, and particularly "inflammaging" differentially affect the nature, quality, and outcome of As–neuron crosstalk, directing to either neurodegeneration/repair (L'Episcopo et al., 2018a,b). Hence, the neuroprotective functions of VM-As are impaired, including their ability to mount a self-protective neurorepair strategy thanks to the expression of several pro-neurogenic, neurotrophic, and antioxidant molecules (Marchetti et al., 2013).

Besides others, we uncovered the *Wnt/β-catenin* signaling pathway, a chief player in neurodevelopmental processes (Salinas, 2012; Arenas, 2014; Joksimovic and Awatramani, 2014; Wurst and Prakash, 2014; Brodski et al., 2019; Marchetti et al., 2020), as a crucial signaling system involved in the physiopathology of nigrostriatal DAergic neurons (see Marchetti, 2018, for extensive review). The hallmark of the Wnt/β-catenin pathway after binding the Wnt's receptors, Frizleds (Fzds), is the cytoplasmic accumulation of β-catenin and its nuclear translocation, finally activating the transcription of Wnt target genes involved in DAergic neurogenesis and neuroprotection (Marchetti, 2018). Notably, VM-As express region-specific transcription factors including Wnt glycoproteins (Marchetti et al., 2013). Especially, wingless-related MMTV integration site 1 (*Wnt1*) is critically involved in DAergic neuroprotection against several neurotoxic and inflammatory insults (Marchetti and Pluchino, 2013).

Of specific mention, with age, Wnt signaling becomes dysfunctional, with potential consequences for neuron–glia crosstalk, DAergic neuron plasticity, and repair (Marchetti, 2018). Notably, deregulation of Wnt signaling has been reported in major neurodegenerative diseases including PD (Berwick and Harvey, 2012; Galli et al., 2014; Harvey and Marchetti, 2014;

Marchetti, 2018; Tapia-Rojas and Inestrosa, 2018; Palomer et al., 2019). Additionally, an increasing number of reports corroborate a Wnt connection for neuron survival and regeneration (Singh et al., 2016; Wang et al., 2017; Marchetti et al., 2020).

To date, there are no effective treatments that can stop or reverse the neurodegeneration process in PD, and current treatments rely on DAergic drugs, including levodopa (L-DOPA) and DAergic agonists, which only temporarily alleviate motor symptoms (Olanow and Schapira, 2013; Obeso et al., 2017; Olanow, 2019). Thus, different lines of research are being pursued to develop novel therapeutic regimens for PD, including cell therapies, aimed at protecting or enhancing the intrinsic regenerative potential of DAergic neurons.

Hence, an increasing number of studies focus on the ability of neural stem progenitor cells (NSCs) harvested from the adult brain to engraft in the injured brain of experimental neurodegenerative diseases and exert positive effects (Yasuhara et al., 2006; Redmond et al., 2007) promoting local trophic support and immune modulation, thus synergizing with the restorative responses of the endogenous NSC population (Madhavan et al., 2009; Zuo et al., 2015; Bacigaluppi et al., 2016). Recently, we performed a carefully constructed time-course analysis of the degenerative changes occurring at the nigrostriatal level of aged male mice upon exposure to MPTP and studied the effects of the unilateral transplantation of syngeneic somatic NSCs within the SNpc. In this aged mouse model, the compensatory DAergic mechanisms are lost, and MPTP induces a long-lasting nigrostriatal degeneration with no repair (Collier et al., 2007).

Interestingly, we found that grafted adult NSCs mostly differentiated into reactive As activating intrinsic cues instructing endogenous As to incite DAergic neuroprotection/neurorestoration, thus efficiently counteracting neurotoxin-induced long-lasting DA degeneration (L'Episcopo et al., 2018b).

Based on this background, VM-As appear uniquely positioned to drive neuroprotective and regenerative programs in PD, and recent preclinical studies used co-transplantation of As to promote the regenerative effects of co-transplanted stem cells in rodent PD models (Yang et al., 2014; Song et al., 2018). However, how the aged brain responds to pharmacological or cellular therapeutical interventions is not well documented. In particular, whether transplantation of VM-As by themselves might fulfill the role of chief players in DAergic neurorestoration of aged PD mice is presently unresolved.

Here, we combined different recognized environmental risk factors for human PD, i.e., aging, male gender, inflammation, and exposure to MPTP (Langston, 2017), to explore the capacity of As grafting to mitigate the harmful SN microenvironment and DAergic toxicity. To this end, we used primary mouse postnatal [postnatal days 2–3 (P2–3)] VM-As as a graft source for unilateral transplantation above the SN of middle-aged mice treated with MPTP, after the onset of motor symptoms. We herein report that the engrafted VM-As survived, expressed As markers, and promoted a remarkable reduction of DAergic neuron loss within the MPTP-lesioned SN associated to striatal DAergic reinnervation and functionality. Gene expression analyses coupled to immunofluorescence and functional data *in vivo, ex vivo*, and *in vitro*, suggest the ability of AS grafts to increase Nrf2-antioxidant self-defense, to mitigate MPTP-induced oxidative stress and inflammation, thus switching the harmful As–neuron crosstalk, *via* activation of an *Nrf2/Wnt/β-catenin* prosurvival axis.

MATERIALS AND METHODS

Mice and Treatments

Middle-aged (9- to 11-month-old) male C57BL/J (Charles River, Calco, Italy) mice were maintained under standard laboratory conditions. All surgeries were performed under anesthesia. The mice received $n = 4$ intraperitoneal (i.p.) injections of vehicle (saline) or MPTP-HCl (Sigma-Adrich, St. Louis, MO, USA) dissolved in saline, 3 h apart during 1 day, at a dose of 12 mg/kg^{-1} free base, according to titration studies that produced long-lasting depletion of DA end points with no recovery in both Str and SNpc of aged mice without causing toxicity (L'Episcopo et al., 2013). MPTP was handled in accordance with the reported guidelines (Jackson-Lewis and Przedborski, 2007). Based on our time-course analysis of the degenerative changes occurring in aging male mice upon exposure to MPTP (L'Episcopo et al., 2013, 2018b), a window of 7 days post-MPTP was selected for transplantation of VM-As (**Supplementary Figure S1**).

Experimental Design

Middle-aged male mice exhibiting a long-lasting nigrostriatal DAergic toxicity with no recovery upon MPTP treatment (L'Episcopo et al., 2018b) were used to study the neuroprotective/neurorescue effects of unilateral transplantation of As derived from the ventral midbrain (tVM-As), above the SN (**Supplementary Figure S1**). We designed in *vivo*, *ex vivo*, and *in vitro* experiments. The studies included the SN and the Str and were performed both in basal condition and at different time points (tps) after MPTP ± VM-As/mock transplants, covering 1–5 weeks post-MPTP. The quantification of the different parameters studied included immunohistochemical, neurochemical, gene expression, and behavioral analyses (see **Supplementary Figure S1**). Based on our gene profiling analysis of the MPTP response in young and aged mice (L'Episcopo et al., 2011b, 2013, 2018b), this study focused on inflammation and oxidative stress, and Wnt signaling genes that are specifically altered in aging mice (see Marchetti, 2018). The microglial response was studied using quantitative immunohistochemistry, and at both gene and protein levels. For the As response, both *ex vivo* and *in vitro* experiments were carried out to address molecular and functional changes according to: (i) the different experimental groups; (ii) the different pharmacological challenges; and (iii) the different As–neuron coculture paradigms established with primary mesencephalic neurons, according to our previous studies (L'Episcopo et al., 2011b, 2014a, 2018a,b).

Ventral Midbrain As Cultures

Primary astroglial cell cultures were obtained from mouse VM at P2–3 according to Booher and Sensenbrenner (1972), with slight modifications, as described in full detail (Gallo

et al., 2000a; Gennuso et al., 2004). The cultures were allowed to grow and differentiate until they reached confluency, at which time (15–20 days *in vitro*, DIV) the loosely adherent microglial cells were separated by shaking for 2 h at 37°C and 190 rpm. The attached cells were then washed with sterile phosphate buffered saline (PBS) and incubated for 1–2 h at 37°C, at 5% CO^2, before overnight shaking at 37°C and 210 rpm. The supernatant media containing oligodendrocyte precursors and other cell types were discarded. The glial [more than 95% of the cells were glial fibrillary acidic protein (GFAP)–immunoreactive (IR) As] monolayers were then rinsed with sterile PBS and pulsed with the nucleotide analog bromodeoxyuridine (BrdU, 5 μM) 24 h before transplantation. Part of the cultures were replated at a final density of 0.4–0.6 × 10^5 cells/cm^2 in poly-D-lysine (10 μg/ml)–coated 6-, 12- or 24-well plates, or in insert membranes (0.4 μm polyethylene terephthalate) for direct or indirect coculture (BD Biosciences) with primary mesencephalic neurons, and processed as described for RT-PCR or immunocytochemistry (**Figures 1**, **2**).

Transplantation of VM-As

Upon verification of the purity, proliferation, and neuroprotective potential, VM-As, tagged *in vitro* with BrdU, were then transplanted at different concentrations in pilot experiments conducted for optimization of cell number (50–200 × 10^3 VM-As; n = 6 mice/experimental group) and timing of transplantation after MPTP (1, 7, or 21 days post-MPTP, n = 6 mice/tp). The dose of 150 × 10^3 VM-As and 7-day post-MPTP interval were selected, as a higher number of VM-As and TH^+ neurons were recovered by 1 week post-implant (wpt). On the day of transplantation (i.e., day 7 post-MPTP), MPTP-injected mice exhibiting a significant motor deficit were randomly (**Supplementary Figure S1**) assigned to MPTP + PBS, MPTP + VM-As grafts, or MPTP + mock [VM dead cells (VMCs), Madhavan et al., 2009]. Mice were anesthetized with chloral hydrate (600 mg/kg) and positioned in a stereotaxic apparatus. The following stereotaxic coordinates were used: 3.2 posterior to the Bregma, 1.5 mm lateral to the midline, and 3.6 mm ventral to the surface of the dura mater. VM-As or mock (150 × 10^3) was injected unilaterally above the left SN (over a period of 2 min). The needle was kept in place for 5 min after each infusion before retraction. Saline-injected controls received the same volume of PBS.

Motor Behavior Analysis With the Rotarod

An accelerating rotarod (five-lane accelerating rotarod; Ugo Basile, Comerio, Italy) was used to measure motor coordination in mice. Mice had to keep their balance on a horizontal rotating rod (diameter, 3 cm) and rotation speed was increased every 30 s by 4 rpm. Five mice were tested at the same time, separated by large disks. A trial started when the mouse was placed on the rotating rod, and it stopped when the mouse fell down or when 5 min were completed. Falling down activated a switch that automatically stopped a timer. On the testing day, each mouse was submitted to five trials with an intertrial interval of 30 min. Mice housed five per cage were acclimated to a 12 h shift in light/dark cycle so that the exercise occurred during the animals' normal wake period. Saline- and MPTP-treated mice (10/experimental group) were assessed for their rotarod performance on days −7, 1, 7, 14, 21, and 28 after MPTP injection.

Immunohistochemistry

On the day of sacrifice, mice were anesthetized and transcardially perfused with 0.9% saline, followed by 4% paraformaldehyde in phosphate buffer (pH 7.2 at 4°C); the brains were carefully removed and processed as described in full detail (Morale et al., 2004). Tissues were frozen and stored at −80° C until further analyses. Serial coronal sections (14 μm thick), encompassing the Str (Bregma 1.54 to Bregma −0.46) and the SNpc (Bregma −2.92 to Bregma −3.8 mm) according to Franklin and Paxinos (2007), were collected, mounted on poly-L-lysine–coated slides, and processed as previously described in full detail (L'Episcopo et al., 2011b). The following pre-absorbed primary antibodies were used: rabbit anti-tyrosine hydroxylase (TH, Chemicon International, Temecula, CA, USA), the rate limiting enzyme in DA synthesis; rabbit anti-TH (Peel Freez Biochemicals, Rogers, AR, USA); mouse anti-TH (Boehringer Mannheim Bioc., Philadelphia, PA, USA), rat anti-dopamine transporter (DAT, Chemicon, Int. USA); mouse anti-neuron specific nuclear protein (NeuN, US Biologicals, Swampscott, MA, USA); rabbit anti-GFAP (GFAP, Dako, Cytomation, Denmark), mouse anti-GFAP (Sigma-Adrich, St. Louis, MO, USA) as an As-specific cell marker; goat anti-ionized calcium-binding adapter molecule 1 (IBA1, Novus Biologicals, Littleton, CO, USA) a microglia-specific marker; goat anti-heme oxygenase 1 (anti-Hmox, 1:150, Santa Cruz Biotechnology, Santa Cruz, CA, USA); rabbit polyclonal, anti-inducible nitric oxide synthase (iNOS;1:200; Santa Cruz Biotechnology, Santa Cruz, CA, USA); and rabbit anti-3-nitrotyrosine (3-NT; 1:200; Millipore, Kankakee, IL, USA; see also complete list of Abs in **Supplementary Table S1**). Nuclei were counterstained with 4′,6-diamidino-2-phenylindole (DAPI) in mounting medium (Vector Laboratories, Burlingame, CA, USA). Visualization of incorporated BrdU requires DNA denaturation performed by incubating the sections in HCl for 30 min at 65°C. After overnight incubation, sections were washed extensively and incubated with fluorochrome (FITC, CY3, CY5)–conjugated species-specific secondary antibodies for immunofluorescent detection. TH immunoreactivity was also detected using biotinylated secondary antibodies (Vector Laboratories, Burlingame, CA, USA) and diaminobenzidine (DAB, Vector Laboratories, Burlingame, CA, USA) as the developing agent as described (L'Episcopo et al., 2011b). Cresyl violet (CV) was used to visualize the Nissl substance.

In all of these protocols, blanks were processed as for experimental samples except that the primary antibodies were replaced with PBS.

DAergic End Points

Quantitative analysis of DAergic neurons in the SNpc was carried out by serial section analysis of the total number of TH-positive (TH^+) and NeuN-positive ($NeuN^+$) neurons throughout the entire rostro-caudal axis of the SNpc (Franklin

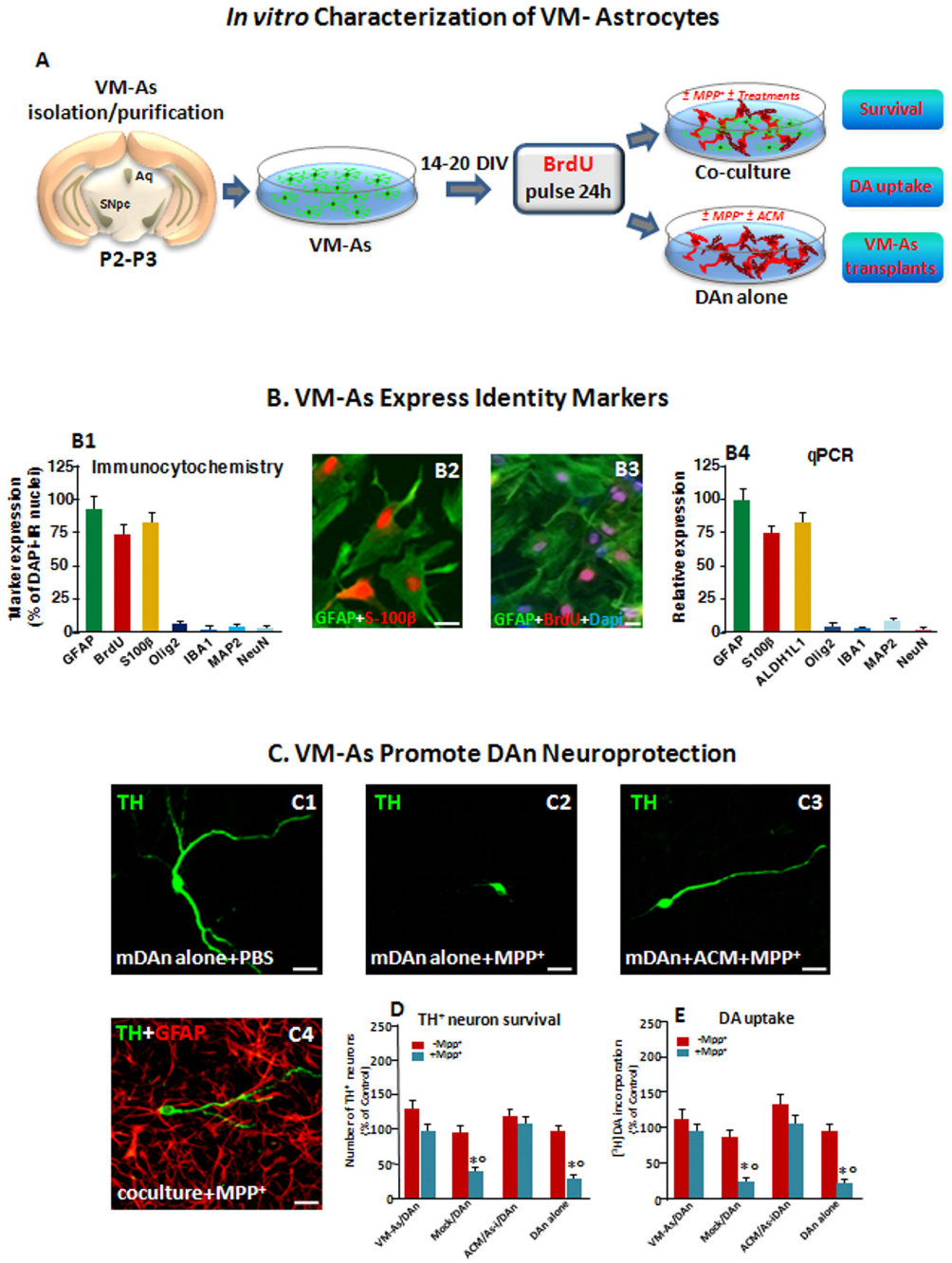

FIGURE 1 | Identity markers and neuroprotective properties of primary ventral midbrain astrocytes (VM-As). **(A)** Scheme of VM-As isolation and purification and direct (coculture) or indirect (As-conditioned medium, ACM) culture paradigms with purified primary mesencephalic dopaminergic neurons (DAn). VM-As pulsed with bromodeoxyuridine (BrdU) were used as a graft source for transplantation. **(B)** Expression of As markers estimated by immunocytochemical (**B1–B3**; $n = 3$ independent experiments) and quantitative real-time (qPCR, **B4**) analyses ($n = 3$ replicates). Quantification of proliferation, glial or neural differentiation markers (mean ± SEM) expressed as percentage of immunoreactive (IR) cells over total glial fibrillary acidic protein–positive ($GFAP^+$)/$Dapi^+$ cells **(B1–B3)**, and qPCR analysis **(B4)** supported the astrocytic identity of the cultures, revealed by co-expression with S100β (**B1,B2**, in red) and ALDH1L1 **(B4)** and the poor expression of IBA1, Olig2, and MAP2 or NeuN, at both gene and protein levels **(B1,B4)**. Bars: 25 μm. When pulsed with the nucleotide analog, BrdU, a large proportion of $GFAP^+$ cells were co-stained after 24 h (B3). **(C–E)** VM-As promote DAn neuroprotection against MPP^+. **(C1–C4)** Confocal images of tyrosine hydroxylase–positive (TH^+; green) neurons cultured alone in the absence **(C1)** or presence of MPP^+ without **(C2)** or in the presence of ACM, or in coculture with VM-As **(C4)**. *Bars*: 25 μm. **(D)** Quantification of TH^+ neuron survival at 10 days *in vitro* (DIV) in the different culture paradigms (direct or indirect coculture between VM-As or mock with purified DAn vs. DAn alone) and DA uptake levels measured by [^{3}H]DA incorporation (**E**; $n = 3$ independent experiments). Comparable results were obtained in the indirect coculture paradigms (DAn exposure to ACM or to VM-As inserts, As-), and values were pooled together. $^*p \leq 0.01$ vs. -MPP^+ within the same experimental group; $^\circ p \leq 0.01$ vs. VM-As groups (direct and indirect coculture) by ANOVA followed by Newman–Keuls test.

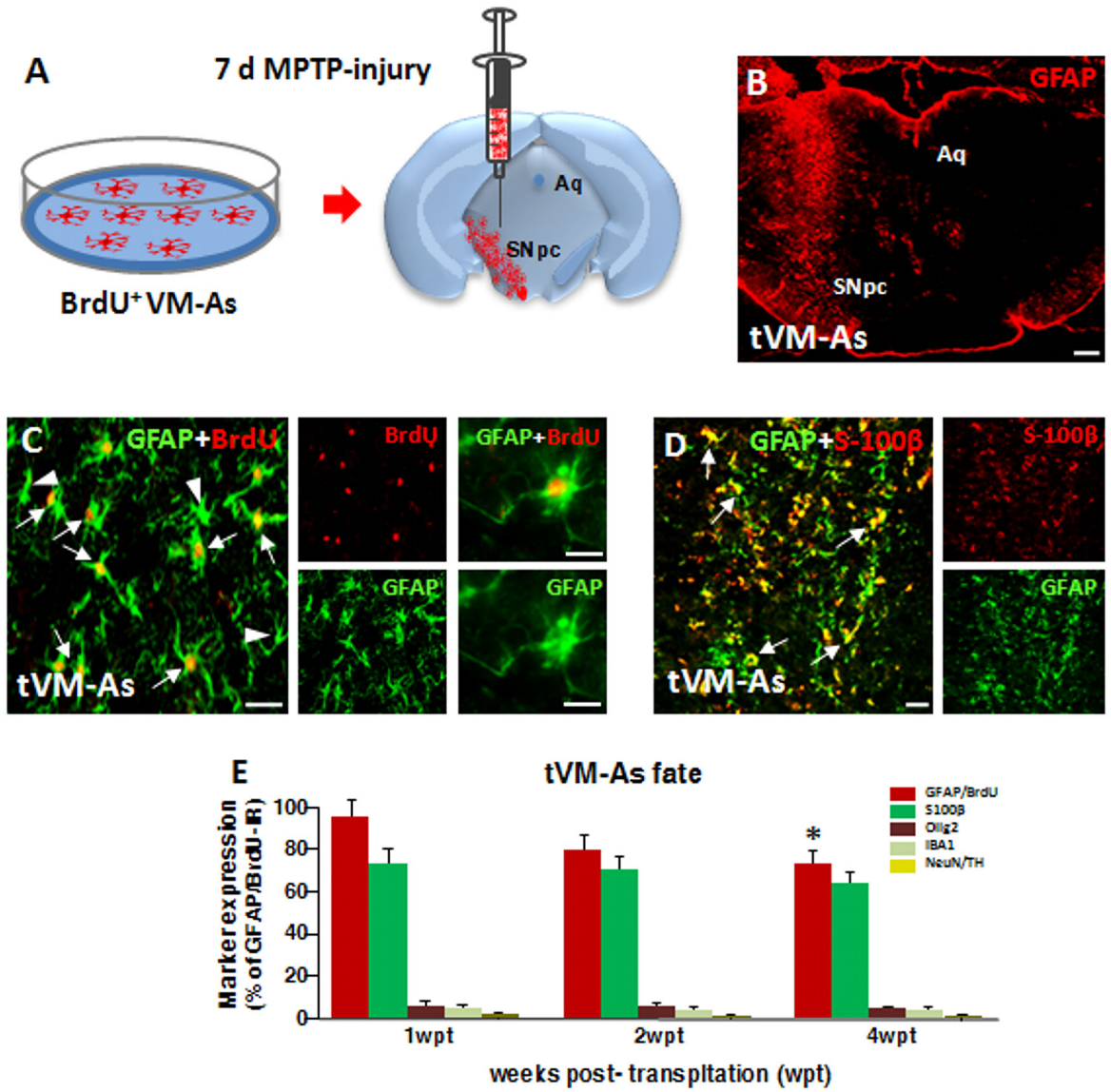

FIGURE 2 | Grafted VM-As survive, express identity markers, and integrate into the aged 1-methyl-4-phenyl-1,2,3,6-tetrahydropyridine (MPTP)-lesioned host substantia nigra pars compacta (SNpc). **(A)** Purified VM-As pulsed with BrdU were unilaterally transplanted above the SNpc, and analyses were carried out 1–4 weeks post-implant (wpt). **(B)** Confocal microscopic image of a coronal midbrain section at the level of the SNpc showing GFAP$^+$ As injection. Scale bar: 600 μm. **(C,D)** Grafted GFAP$^+$ astrocytes expressing BrdU (**C**, arrows) and BrdU$^-$ (**C**, arrowhead) cells and S100β **(D)** are shown. *Scale bars*: **(C)**, 50 μm; **(C)** magnification, 20 μm; **(D)**, 50 μm. **(E)** Relative quantification of transplanted BrdU$^+$GFAP$^+$ astrocytes at the SN level. Data (mean± SEM, n = 6 brains/time point, tp) are percentage of BrdU$^+$GFAP$^+$ cells over 1 wpt (100%) and expression of glial or neural differentiation markers by grafted VM-As at 1–3 wpt. Time-course analyses indicated that more than 60–70% of the engrafted BrdU$^+$GFAP$^+$ cells expressed S100β, whereas only 2–3% of tVM-astros were IR for the oligodendroglial cell marker Olig2$^+$ and the microglial marker IBA1, and only occasionally did BrdU$^+$/GFAP$^+$ cells colocalize with neuronal (NeuN) or DAergic (TH) markers. By 4 wpt, an almost 25–30% decline of BrdU$^+$/GFAP$^+$/S100β$^+$ astrocytes was observed within the lesioned SNpc. Data (mean ± SEM) expressed as percentage of IR cells over total BrdU$^+$GFAP$^+$ cells. *$p \leq 0.05$ vs. 1 wpt by ANOVA followed by Newman–Keuls test.

and Paxinos, 2007) as previously described (L'Episcopo et al., 2011b). Total numbers of TH- and CV-stained neurons in adjacent tissue sections were estimated in parallel to validate TH$^+$ neuron survival, using Abercrombie correction (Abercrombie, 1946).

Striatal TH- and DAT-immunoreactive (IR) fiber staining was assessed in n = 3 coronal sections at three levels (Bregma coordinates: +0.5, +0.86, and 1.1 mm, respectively) of the caudate putamen (CPu), in n = 6 mice/group/time (Burke et al., 1990). Fluorescence intensity (FI) of TH- and

DAT-staining above a fixed threshold used the corpus callosum for background subtraction.

For synaptosomal, high-affinity DA uptake, at the indicated time intervals, mice were sacrificed by cervical dislocation, and the brains rapidly removed and immediately placed on ice-cold saline. The right and left striata were then dissected on an ice-cold plastic dish and processed as described in full detail (L'Episcopo et al., 2011a,b). Synaptosomal, high-affinity DA uptake was assessed in the presence of 10 μM mazindol, according to Morale et al. (2004).

Glial Cell Counts

Cell counts were obtained for $GFAP^+$ As and ameboid $IBA1^+$ microglial cells (Kreutzberg, 1996). For SN cell counts, at least three sections were obtained from each animal representing each of the five representative planes from −2.92 mm to −3.8 mm relative to Bregma according to the stereotaxic coordinates of Franklin and Paxinos (2007). $GFAP^+$ As and $IBA1^+$ microglial cell number per unit of surface area was determined in 8–10 randomly selected fields per section on both sides, the counts averaged for each animal, and the mean number of cells per mm^2 was estimated. Classification of microglia activation was carried out according to Kreutzberg (1996); as described in **Supplementary Table S3**, the glial counts were confirmed by two different observers.

Confocal Laser Scanning Microscopy, Image Analysis, and Quantification of Immunostaining

All the quantifications were performed by investigators blind to treatment conditions. Immunostaining was examined using a Leica LCS-SPE confocal microscope. For FI assessments and colocalizations, midbrain sections were labeled by immunofluorescence, and images were acquired by sequential scanning of 12–16 serial optical sections (Gennuso et al., 2004; L'Episcopo et al., 2011a,b,c, 2013). Three dimensional reconstructions from z-series were used to verify colocalization in the x–y, y–z, and x–z planes. Serial fluorescent images were captured in randomly selected areas, the number of labeled cells per field (n = 6–8 fields/section) was manually counted in 4–6 midbrain sections per brain (n = 6/treatment group) using Olympus cellSense Dimension software, and cell counts obtained were averaged (mean ± SEM); the percentages of $HO1^+/GFAP^+$ cells out of the total $GFAP^+$ cells were estimated in each condition, in ≥100 cells, read from at least four VM sections per brain, in six mice per experimental group, and results expressed as mean ±SEM (Gennuso et al., 2004).

RNA Extraction, Reverse Transcription, and Real-Time PCR

RNA was extracted from tissues/cell samples, as previously detailed (L'Episcopo et al., 2011a,b). Briefly, after purification using a QIAquick PCR Purification kit (Qiagen), 250 ng of cDNA was used for real-time PCR using pre-developed TaqMan assay reagents (Applied Biosystems). Real-time quantitative PCR was performed using the Step One Detection System (Applied Biosystems) according to the manufacturer's protocol, using the TaqMan Universal PCR master mix (#4304437). The assay IDs are reported in **Supplementary Table S2**. For each sample, we designed a duplicate assay. β-actin (Applied Biosystems #4352341E) was selected as the housekeeping gene, according to our previous (L'Episcopo et al., 2011b, 2018b) and present pilot studies indicating that it does not modify its expression between conditions. Quantification of the abundance of target gene expression was determined relative to β-actin with regard to the control group by using the delta C_t ($2^{-\Delta\Delta Ct}$) comparative method, with the results expressed as arbitrary units (AU). Relative fold changes over saline/PBS or MPTP/PBS are indicated.

Enriched Neuronal Cultures and Primary Midbrain Astroglial–Neuron Cultures

For *in vitro* establishment of primary mesencephalic neuronal cultures, timed pregnant Sprague–Dawley rats (Charles River Breeding Laboratories, Milan, Italy) were killed in accordance with the Society for Neuroscience guidelines and Italian law. Primary mesencephalic neurons were prepared from the brain on embryonic day 13–14, as detailed (L'Episcopo et al., 2011b). Briefly, mesencephalic tissues were isolated and dissociated with gentle mechanical trituration. Cells were diluted to 1.5×10^6/ml in maintenance medium (MEM supplemented with 10% heat-inactivated FBS, 10% heat-inactivated horse serum, 1 g/L glucose, 2 mM glutamine, 1 mM sodium pyruvate, 100 μM nonessential amino acids, 50 U/ml penicillin, and 50 μg/ml streptomycin) and seeded into 24-well culture plates precoated with poly-D-lysine (20 μg/ml). Plates were maintained at 37°C in a humidified atmosphere of 5% CO_2 and 95% air. To obtain neuron-enriched cultures, cytosine β-D-arabinofuranoside (Ara-c) was added to a final concentration of 6 μM 36 h after seeding the cells, to suppress glia proliferation (L'Episcopo et al., 2011b). Cultures were changed back to maintenance medium 2 days later and were used for treatment 7 DIV after initial seeding. Neuronal enrichment was verified by immunocytochemistry using GFAP-, TH-, and NeuN-Abs as described. Ara-c treatment reduced glial expression by 95%.

Both purified neuronal cultures and astroglial–neuron cultures at 7 DIV received MPP^+ (10 μM). The specificity of the As neuroprotective effect was further verified in purified neuronal cultures exposed to astroglial conditioned media (ACM) or to As inserts (As-i, indirect As–neuron coculture). In this experimental paradigm, the inserts containing the As monolayer were added on the top of the purified neurons. These inserts allowed diffusion of factors from the glia monolayer to the mesencephalic neurons and vice versa, without direct contact between cells (Gallo et al., 1995, 2000a,b). DAergic neuron survival was estimated after 24 h, by counting the number of TH^+ neurons over the DAPI-positive nuclei and TH^+ neurons expressed as percent (%) of control (-MPTP), and by determination of [^{3}H]DA incorporation, which reflects DAergic cell count and functionality. Uptake of [^{3}H]DA was performed essentially as previously described, by incubating the cell cultures for 20 min at 37° with 1 μM [^{3}H]DA in Krebs-Ringer buffer

[16 mM sodium phosphate, 119 mM NaCl, 4.7 mM KCl, 1.8 mM $CaCl_2$, 1.2 mM $MgSO_4$, 1.3 mM EDTA, and 5.6 mM glucose (pH 7.4)]. Non-specific DA uptake was blocked by mazindol (10 μM). Cells were then collected in 1 N NaOH after washing in ice-cold Krebs-Ringer buffer. Radioactivity was determined by liquid scintillation and specific [^{3}H]DA uptake calculated by subtracting the mazindol counts from the wells without the uptake inhibitor (Morale et al., 2004; L'Episcopo et al., 2011a,b,c).

Ex vivo Isolation of As

Ex vivo isolation and culture of glial cells from the adult brain were previously detailed (Schwartz and Wilson, 1992; L'Episcopo et al., 2012, 2013). Isolated As from middle-aged mice of the studied groups (m-astro, >95%, GFAP$^+$ cells) were counted and plated at a final density of 0.4–0.6 × 10^5 cells/cm^2 in poly-D-lysine (10 μg/ml)–coated 6-, 12-, or 24-well plates, and their conditioned media were collected and stored at −70°. Some of the glial cells were exposed to different treatments and processed for qPCR or functional analyses or were used for direct coculture with primary mesencephalic neurons, as detailed in the previous section.

Mitochondrial Activity With the 3-(4,5-dimethylthiazol-2-yl)-2,5-diphenyltetrazolium Bromide Assay

The colorimetric 3-(4,5-dimethylthiazol-2-yl)-2,5-diphenyltetrazolium bromide (MTT) assay was used to measure mitochondrial functionality in glial cells (Gennuso et al., 2004). Briefly, cells were incubated with 0.25 mg/ml MTT for 3 h at 37°C, and mitochondrial enzyme activity was measured in culture supernatants in a spectrophotometer (Molecular Devices) at 570 nm, with a reference wavelength of 630 nm. Results are expressed as percentage changes of control.

ROS and RNS

For reactive oxygen species (ROS) measurement, the redox membrane-permeant probe 2′,7′-dichlorofluorescein diacetate (DCFH-DA, 50 μM) was added for 1 h at 37°C, and cells were viewed under the confocal microscope (Gennuso et al., 2004). Measurement of iNOS-derived NO was carried out in cell free supernatant using Griess reagent (Marchetti et al., 2002; L'Episcopo et al., 2011c). To study the effect of inhibition of oxidative and nitrosative stress mediators, the freshly prepared GFAP$^+$ cells were cultured in the absence or the presence of the ROS antagonist, apocynin (Apo, 0.5 mM), and the specific iNOS inhibitor, L-Nil [L-N6-(1-iminoethyl)-lysine, 50 μM, Sigma] (Marchetti et al., 2002; Morale et al., 2004), applied after plating and determinations carried out 24–48 h after treatment (**Figure 6**).

Enzyme-Linked Immunosorbent Assay

Levels of cytokines were determined in tissue homogenates/cells using enzyme-linked immunosorbent assay (ELISA) kits (DuoSet ELISA Development System; R&D Systems, McKinley Place, MN, USA) following the manufacturer's protocol (Marchetti et al., 2002; L'Episcopo et al., 2011c).

Data Analysis

Statistical significance between means ± SEM was analyzed by a two-way analysis of variance (ANOVA). Experimental series performed on different days were compared by the Student–Newman–Keuls *t*-test. A value of $p < 0.05$ was considered to be statistically significant.

RESULTS

In vitro Characterization of VM-As Displaying Neuroprotective Properties

As a first step of our transplantation protocol, primary VM-As cultures established from P2–3 and cultured as described for 14–20 DIV were processed for qPCR and immunocytochemical analyses to identify astrocytic (GFAP, S100B, ALDHL1) markers and verify the purity of the preparation by testing several non-astrocytic (i.e., microglial IBA1, oligodendrocyte, Olig2, and neuronal MAP2, NeuN) identity markers (**Figures 1A,B**). As observed, the astrocytic identity was confirmed by As co-expression with S100b, and ALDH1L1, two As-associated genes, whereas IBA1, Olig2, and MAP2 or NeuN were only poorly expressed, at both gene and protein levels (**Figure 1B**), thus confirming the full differentiation and purity of the VM-astro cultures. Additionally, when pulsed with the nucleotide analog, BrdU, a large proportion of GFAP$^+$ cells were co-stained after 24 h.

Our previous studies on neuron-As interactions first reported the region and growth factor specificity of As-derived molecules for neuronal development and growth, for acquisition of the mature neuronal phenotype, as well as for neuroprotection (Gallo et al., 1995; Morale et al., 2006; L'Episcopo et al., 2011a,b). Especially, P2–3 VM-As were shown to promote the differentiation of adult midbrain- but not subventricular zone (SVZ) NSCs into functionally active DAergic neurons, *in vitro* (L'Episcopo et al., 2011b, 2014a). Here the neuroprotective ability of VM-As was further verified in the coculture paradigm, where purified mesencephalic neurons (DAn) were layered on the top of VM-As in both the presence and the absence of the toxic MPTP metabolite, Mpp$^+$ (10 μM; **Figures 1C–E**). In accord with our previous findings (L'Episcopo et al., 2011a,b), in enriched primary mesencephalic neuronal cultures at 7 DIV, MPP$^+$ promoted the well-known neuron toxicity as demonstrated by the loss of TH$^+$ neurons, DAn atrophy, and inhibition of [^{3}DA] incorporation (**Figures 1C, 2,D,E**). On the other hand, in VM-As–neuron cocultures, MPP$^+$ failed to induce DAergic cell death, as reflected by the greater TH$^+$ neuronal number and DA uptake levels measured (**Figures 1D,E**), with the TH$^+$ neurons cocultured with VM-As showing longer ramified neurites compared with those without As coculture (**Figure 1C2** vs. **Figure 1C4**). Accordingly, exposure of enriched DAn to either VM-As–conditioned medium (ACM) or VM-As insert paradigms similarly exerted a significant degree of TH$^+$ neuron protection against MPP$^+$ (**Figures 1C3,D,E**).

Together, these findings supported the differentiation, proliferative, and neuroprotective properties of our VM-As cultures, *in vitro* (**Figures 1A–C**).

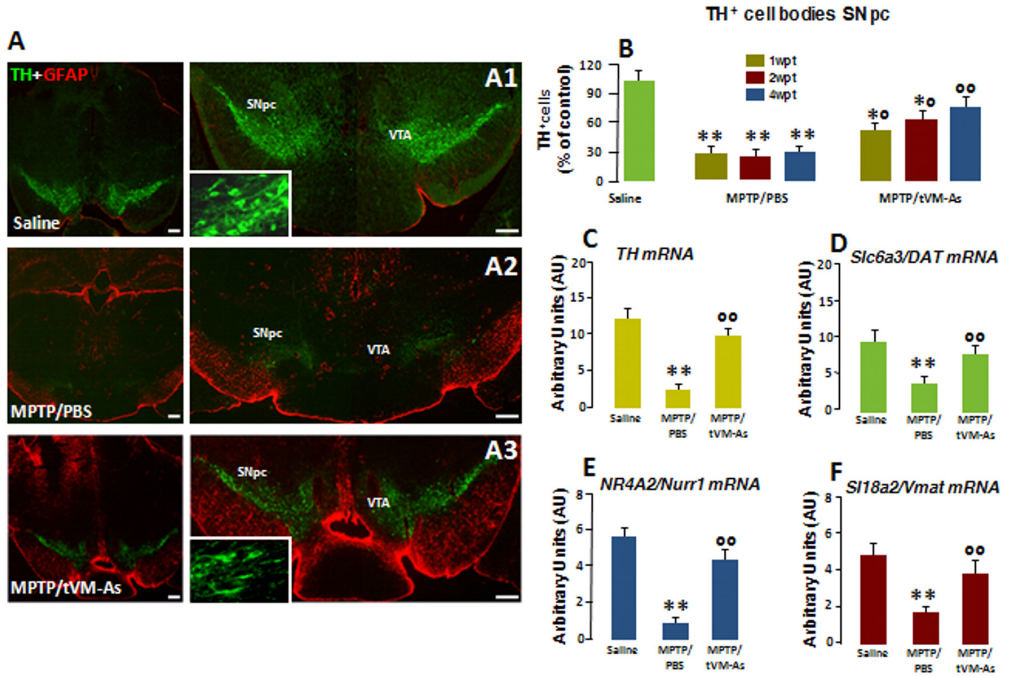

FIGURE 3 | tVM-As promote the rescue of endogenous TH$^+$ neurons in the SNpc. **(A1–A3)** Confocal images of the SNpc in middle-aged (9- to 11-month-old) saline-**(A1)**, MPTP/PBS-**(A2)** and aged-matched VM-As–grafted mice **(A3)** at 4 wpt. Scale bars: 600 μm. Magnifications in the *boxed areas*. **(B)** Total number of TH$^+$ neurons in the right and left SNpc (mean ± SEM) at 1, 2, and 4 wpt showing that tVM-As grafts increase TH$^+$ neuron survival in MPTP mice in a time-dependent fashion. **(C–F)** qRT-PCR in SNpc showing 2- to 3-fold upregulation of typical DAergic transcripts, *TH* **(C)**, *Slc6a3* (*DAT*, **D**), *Nr4A2* (*Nurr1*, **E**), and *Slc18a2* (*Vmat*, **F**) mRNAs of MPTP/tVM-As over 1-methyl-4-phenyl-1,2,3,6-tetrahydropyridine (MPTP)/phosphate buffered saline (PBS). Values (arbitrary units, AU, mean % ± SEM of $n = 5$ samples/experimental group) are expressed as fold changes over control. $^{**}p \leq 0.01$. vs. saline/PBS; $^{*\circ}p \leq 0.05$. $^{\circ\circ}p \leq 0.01$ vs. MPTP/PBS, at each time interval respectively, by ANOVA followed by *post hoc* Newman–Keuls test.

Grafted VM-As Survive, Express Identity Markers, and Integrate Into the Aged MPTP-Lesioned Host SNpc

As a second step of our transplantation protocol, we verified the engraftment, proliferation, and distribution of VM-As tagged by incorporation of BrdU, which were unilaterally transplanted 7 days post-MPTP in the SNpc of middle-aged 9- to 11-month-old mice (**Figures 2A,B**). Spatio-temporal immunohistochemical, neurochemical, molecular, and motor behavioral analyses were carried out 1–3 wpt (**Supplementary Figure S1**).

By 1 week post-transplant (wpt), tVM-astros showed robust ipsilateral engraftment at all the SN rostro-caudal levels analyzed. Quantitative colocalization analyses in midbrain sections at 1 wpt (1 wpt = 100%) indicated that more than 70% of the engrafted BrdU$^+$GFAP$^+$ cells expressed S100β, whereas only 3–5% of tVM-astros were IR for the oligodendroglial cell marker Olig2$^+$ and the microglial marker IBA1, and we did not observe colocalization of tVM-As with neuronal (NeuN) or DAergic (TH) markers (**Figure 2C**). Additionally, time-course analyses indicated that by 3 wpt, an almost 25–30% decline of GFAP$^+$/BrdU$^+$ cells was observed within the lesioned SNpc (**Figure 2D**).

Together, tVM-As displaying *in vitro* well-recognized neuroprotective features, when transplanted unilaterally in the SNpc of middle-aged mice engrafted within the lesioned SNpc, expressed typical astrocytic, but not neuronal, nor microglial or oligodendroglial, markers and survived up to 4 wpt.

tVM-As Promote the Rescue of Endogenous TH$^+$ Neurons in the SNpc

To investigate the effect of the transplantation of tVM-astros on MPTP-induced neuronal loss in middle-aged mice, the number of DAergic cell bodies in the SNpc was assessed by TH immunoreactivity (**Figures 3A1–A3** and **Figure 3B**). Stereological quantification of TH$^+$ and Nissl$^+$ neurons in SNpc was performed to validate TH$^+$ neuron survival. tVM-astros grafted into MPTP-lesioned mice (MPTP/tVM-As) showed a significant ($p \leq 0.05$) increase in endogenous TH$^+$ immunoreactivity and TH$^+$ neuron survival at both early (1 wpt) and later (4 wpt) tps (**Figures 3A1–A3** and **Figure 3B**) vs. control MPTP mice receiving an intranigral injection of PBS (MPTP/PBS; **Figures 3A1–A3** and **Figure 3B**). The observed increase in the number of TH$^+$ neurons appears specific for VM-As, since transplantation of a mock cell preparation (VMCs) failed to increase TH$^+$ neuron survival (not shown). By 4 wpt, the number of TH$^+$ neurons in MPTP/tVM-astro mice became almost comparable with unlesioned (saline/PBS) mice (**Figure 3B**).

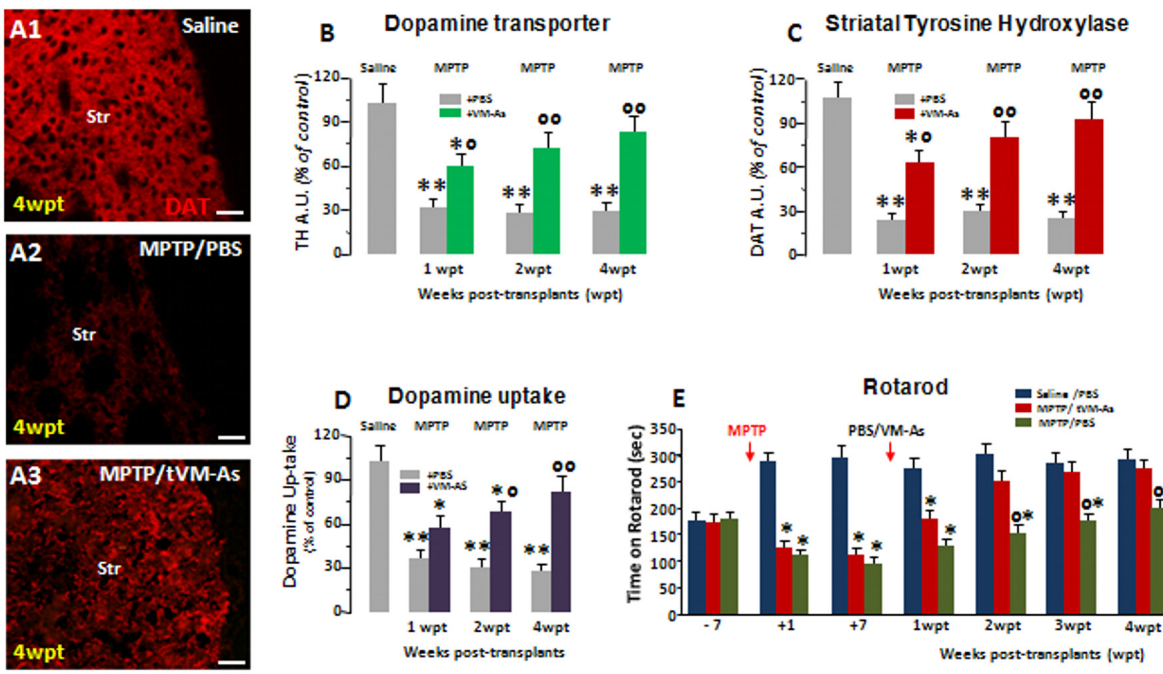

FIGURE 4 | tVM-As grafts counteract MPTP-induced loss of DAergic innervation and synaptosomal dopamine (DA) uptake in the striatum, and revert Parkinson's disease (PD) motor deficits. **(A1–A3)** tVM-As increase dopamine transporter (DAT)–fluorescence intensity (FI, **A3**) as compared to MPTP/PBS **(A2)**, showing the recognized loss of striatal DAT as opposed to Saline-treated controls **(A1)**. **(B–C)** DAT- **(B)** and TH-**(C)** immunofluorescent staining measured by image analysis. Scale bars: 50 μm. **(D)** VM-As grafts increase high-affinity striatal (*Str*) DA uptake assessed by [^{3}H]DA incorporation (mean % ± SEM). **(E)** Motor performances on rotarod showing recovery from motor impairment in MPTP/tVM-As but not MPTP/PBS mice. *$p \leq 0.05$, **$p \leq 0.01$ vs. saline/PBS; °$p \leq 0.05$, °°$p \leq 0.01$ vs. MPTP/PBS, at each time interval respectively, by ANOVA followed by *post hoc* Newman–Keuls test.

Next, we studied the expression levels of several DAergic mRNA species by applying quantitative real-time polymerase chain reaction (qRT-PCR) in MPTP-injured SNpc tissues. Here, we found that in MPTP/tVM-astro mouse *Th*, the high-affinity DA transporter *Slc6a3* (DAT), the vesicular monoamine transporter *Slc18a2* (VMAT), and the DA-specific transcription factor *Nr4a2* (Nurr1) required for the mature DA phenotype and survival (Kadkhodaei et al., 2009) showed an upregulation (by 2- to 3-fold), vs. MPTP/PBS control mice (**Figures 3C–F**).

Together, the tVM-As graft had a significant time-dependent rescue effect on endogenous TH neurons, which occurs at tissue, gene, and protein levels. Moreover, this effect was tVM-astro–specific and was not attributable to a direct differentiation of transplanted tVM-astros into TH$^+$ neurons but, rather, to a rescue effect on endogenous cells.

tVM-As Grafts Counteract MPTP-Induced Loss of DAergic Innervation and Synaptosomal DA Uptake in the Str and Revert PD Motor Deficits

We next investigated the ability of tVM-astro grafts to increase the functionality of new TH$^+$ neurons, using quantitative confocal laser microscopy on striatal sections, the high-affinity synaptosomal DA uptake levels, and the analysis of motor behavior.

Hence, tVM-As grafts efficiently counteracted the MPTP-induced loss of striatal TH and DAT innervation (**Figures 4A1–A3** and **Figures 4B–C**). By contrast, corresponding levels in control MPTP/PBS mice were found to be significantly lower, compared with both MPTP/tVM-As ($p \leq 0.05$) and saline/PBS controls ($p \leq 0.01$) at each tp tested. Measuring the striatal uptake of radiolabeled DA([^{3}H]-DA) in presynaptic terminals of middle-aged MPTP mice, we found that MPTP/tVM-As mice showed a significant ($p \leq 0.05$) recovery of high-affinity striatal synaptosomal DA uptake (vs. MPTP/PBS) by 2 wpt (**Figure 4D**). This effect in MPTP/tVM-As mice increased over time, reaching values similar to those of saline/PBS controls by 4 wpt. On the contrary, MPTP/PBS mice showed a constant significant ($p \leq 0.01$) reduction of synaptosomal DA uptake over time, vs. saline/PBS controls.

Behavior analyses confirmed that these structural and functional striatal changes were coupled with a full recovery of motor coordination deficits in MPTP/tVM-As mice, vs. MPTP/PBS controls, which started to be significant ($p \leq 0.05$) at 2 wpt (**Figure 4E**).

Together, besides the effects of tVM-As on SNpc-DA neuronal cell bodies, tVM-As would promote a progressive

recovery of the host striatal DA terminal region function, which further supports their role in enhancing endogenous recovery mechanisms in the aged brain.

tVM-As Rejuvenate the SN Microenvironment: Downmodulation of Microglial Pro-inflammatory Status

With age, both As and microglial cells become dysfunctional. As lose their neuroprotective, antioxidant, and pro-neurogenic potential, and microglia acquire a "primed" status (Streit, 2010; Njie et al., 2012; Niraula et al., 2017), capable of producing upregulated levels of pro-inflammatory cytokines when challenged with inflammatory/neurotoxic stimuli (L'Episcopo et al., 2010a,b, 2011c, 2018a,b). We thus questioned whether tVM-As might affect this "harmful" setting, thus ameliorating the injured microenvironment of middle-aged MPTP mice. To this end we first examined the effect of tVM-As on microglial response to MPTP. Notably, glial inflammatory mechanisms have long been recognized to contribute to both nigrostriatal degeneration and self-repair (see Marchetti and Abbracchio, 2005; Marchetti et al., 2005a,b,c; McGeer and McGeer, 2008; Marchetti et al., 2011; Przedborski, 2010; Gao et al., 2011; L'Episcopo et al., 2018a,b). We thus examined the microglial cell number and phenotype *in vivo* (**Figures 5A–D**) and found that tVM-As induced a significant ($p \leq 0.01$) counteraction of MPTP-induced increased IBA1$^+$ microglial cells (**Figure 5B**) displaying the morphology of activated macrophage-like microglia (**Figures 5A1,A2**). Hence, in MPTP/PBS middle-aged mice, we observed a greater number of stage 3 IBA1$^+$, ameboid microglia, showing a round-shaped body with short, thick, and stout processes, or stage 4 phagocytic glial cells (**Supplementary Table S3**), with round-shaped cells and no processes, indicative of an M1-activated phenotype (Kreutzberg, 1996). In stark contrast, MPTP/tVM-As mice displayed a ramified, more quiescent phenotype, with elongated-shaped cell bodies and long and thicker processes, comparable to stages 1–2 (**Figures 5A3,A4**, **Supplementary Table S3**), which suggested a switch towards the M2 less-reactive phenotype. Accordingly, using qPCR, we found that the expression levels of the pro-inflammatory M1-cytokines *IL1*-β, *IL-6*, and *TNF*-α were significantly ($p \leq 0.01$) upregulated by about 5- to 6-fold in MPTP/PBS, as compared to saline-injected controls, in the face of no changes of the low levels of expression of the anti-inflammatory M2-cytokine, *IL-10* (**Figure 5C**). By contrast, tVM-As significantly ($p \leq 0.01$) reduced *IL1*-β, *IL-6*, and *TNF*-α to values almost comparable to saline/PBS mice, while *IL-10* gene expression increased significantly ($p \leq 0.05$) at both 2 and 4 wpt (**Figure 5D**). Supporting these results, when the cytokine protein levels were determined in VM tissues of the different groups at 4 wpt, by ELISA, we found significantly ($p \leq 0.01$) greater levels of *IL1*-β, *IL-6*, and *TNF*-α in MPTP/PBS as compared to MPTP/tVM-As treated mice, exhibiting cytokine values comparable to those determined in saline/PBS-injected mice (**Figure 5E**). Additionally, MPTP/tVM-As mice, but not MPTP/PBS mice, had increased IL-10 protein levels (**Figure 5E**).

Thus, tVM-As efficiently override the microglial pro-inflammatory status and reduce the number of activated IBA1$^+$ cells within the middle-aged MPTP-lesioned SNpc during the studied experimental period. This effect was associated with a significant downregulation of the pro-inflammatory cytokines, TNF-α, IL-6, and IL-1β, associated to an increase of the anti-inflammatory cytokine, IL-10, at both gene and protein levels.

tVM-As Upregulate As Antioxidant Self-defense *in vivo and ex vivo*: Contribution of Wnt/β-Catenin Signaling

Given the central role of As in antioxidant self-defense brain functions, we then looked at critical As-oxidative/nitrosative stress markers in SN tissues isolated from MPTP/PBS and MPTP/tVM-As, *in vivo* (**Figure 6A**). To differentiate the As-specific mRNAs vs. the SN-expressed mRNAs, we used *ex vivo* As cultures acutely isolated from MPTP/tVM-As and MPTP/PBS-As at 1 wpt (**Figure 6B**). Nrf2 is a conserved basic leucine zipper transcription factor which affords cytoprotection against xenobiotics and ROS through induction of antioxidant (ARE) and electrophile (EpRE) response elements (see Tebay et al., 2015; Zhang et al., 2017). HO1 is a principal mediator of cellular adaptive (i.e., antioxidant and anti-inflammatory) responses (Chen et al., 2009; Surh et al., 2009). SOD1 is critical for enhancing antioxidant self-defense during aging and neurodegenerative conditions, whereas its deficiency results in an accelerating aging phenotype (see Zhang et al., 2017).

Hence, we found that in response to MPTP, *Nrf2* and the antioxidant gene, *HO1*, but not *HO2*, were sharply upregulated ($p \leq 0.01$), together with *SOD1*, in aging MPTP/tVM-As–grafted vs. MPTP/PBS mice, which instead failed to activate an antioxidant self-defense response to the MPTP challenge (**Figures 6A,B**). Notably, tVM-astros greatly ($p \leq 0.01$) increased Nrf2-antioxidant genes as compared to saline/PBS mice exhibiting very low transcript levels (**Figures 6A,B**). Within the nicotinamide adenine dinucleotide phosphate (NADPH) oxidases, Nox2 is the predominant oxidase family member expressed in As, at both the mRNA and protein level (Belarbi et al., 2017). Here, we detected decreased activation/expression of *Nox2* in SN tissues from MPTP/tVM-As when compared to MPTP/PBS counterparts (**Figures 6A,B**) exhibiting an almost 3-fold increase over saline/PBS-injected mice. Additionally, tVM-As significantly counteracted the exacerbated expression of the harmful pro-inflammatory mediator, *iNOS*, vs. MPTP/PBS, showing instead a 3-fold upregulation ($p \leq 0.01$, vs. saline-injected mice; **Figures 6A,B**). Remarkably, dual immunofluorescent stainings evidenced the neuroprotective effect of tVM-As and close interactions with both TH neurons and microglial cells, as suggested by the long GFAP$^+$ processes close to the rescued TH$^+$ neuronal cell body (**Figures 6D1,D2**), and in close contact with the long, ramified IBA1$^+$ processes (**Figures 6D4,D5**). On the

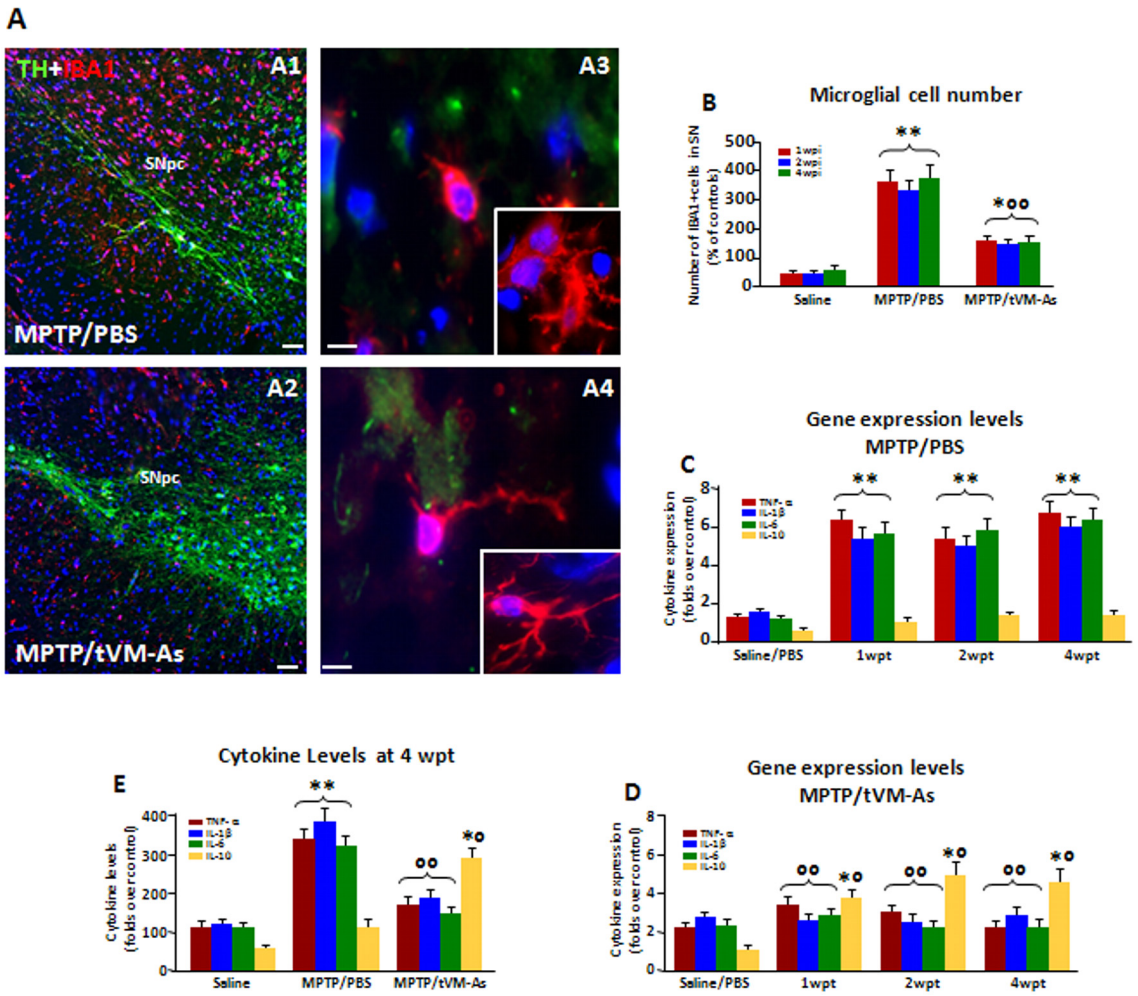

FIGURE 5 | tVM-As downregulate microglial pro-inflammatory phenotype in SNpc. **(A,B)** tVM-As reverse MPTP-induced reactive microglial cells displaying the morphology of activated macrophage-like microglia **(A1,A3)** and the increased IBA1$^+$/Dapi$^+$ microglial cell numbers in midbrain sections at the level of the SNpc **(B)**. Note the ramified microglia in SNpc of tVM-As mice **(A2,A4)**. *Scale bars*: **(A1,A2)**, 100 μm; **(A3,A4)**, 25 μm. **(C,D)** SNpc tissues were processed for gene expression analyses of mRNA species using qRT-PCR. Values (AU, mean % ± SEM of $n = 5$ samples/experimental group) are expressed as fold changes. In MPTP/PBS, inflammatory (*Tnfa*, *Il1*, *IL-6*) mRNAs are upregulated by about 5- to 6-fold ($p \leq 0.01$) over saline-injected controls **(C)**, whereas the anti-inflammatory cytokine *IL-10* is not affected. Transplantation of VM-As in MPTP mice induced a significant ($p \leq 0.01$) downregulation of pro-inflammatory markers at all tps but increased *IL-10* expression vs. MPTP/PBS **(D)**. **(E)** Evaluation of IL-1β, TNF-α, IL-6, and IL-10 at a protein level, as determined by enzyme-linked immunosorbent assay (ELISA) in homogenate tissue samples (mean % ± SEM of $n = 5$ samples/experimental group), documents the ability of tVM-As to suppress the pro-inflammatory cytokines in the face of a significant increase in the anti-inflammatory cytokine, IL-10, when levels are compared to MPTP/PBS mice. $^*p \leq 0.05$, $^{**}p \leq 0.01$ vs. saline/PBS; $^{\circ\circ}p \leq 0.01$ vs. MPTP/PBS; $^{*\circ}p \leq 0.01$ vs. saline/PBS and MPTP/PBS, at each time interval respectively, by ANOVA with *post hoc* Newman–Keuls.

other hand, a severe neuronal loss, poor GFAP$^+$–TH$^+$ neuron interactions (**Figures 6C1,C2**) were observed in MPTP/PBS, where only round-shaped IBA1$^+$ cells were seen close to the reactive GFAP$^+$ As (**Figure 6C6**), thus supporting the failure of middle-aged MPTP-injured As to mount a neuroprotective response against MPTP.

Consistently, dual staining with GFAP and HO1 followed by confocal laser microscopic analyses uncovered an abundant co-expression of HO1 in tVM-As ($p \leq 0.01$, vs. saline- and MPTP-injected mice) as determined by the sharp increase in the percentage of GFAP$^+$/HO1$^+$ out of the total GFAP$^+$ cells (77 ± 11%) in MPTP/tVM-As, when compared to MPTP/PBS (20 ± 4%) and saline/PBS mice (12 ± 4%; **Figure 6C3**). These results coupled to the abundant expression of iNOS in GFAP$^+$ As of MPTP/PBS (**Figure 6C5**) as opposed to MPTP/tVM-As mice suggested failure of aged As to activate the antioxidant and anti-inflammatory response upon MPTP challenge. Given that when iNOS and NADPH oxidase are present together, a potent toxin, peroxynitrite (ONOO-), may be generated which promotes the nitration of proteins (Gao et al., 2011), we then looked at the colocalization of 3-NT and found an

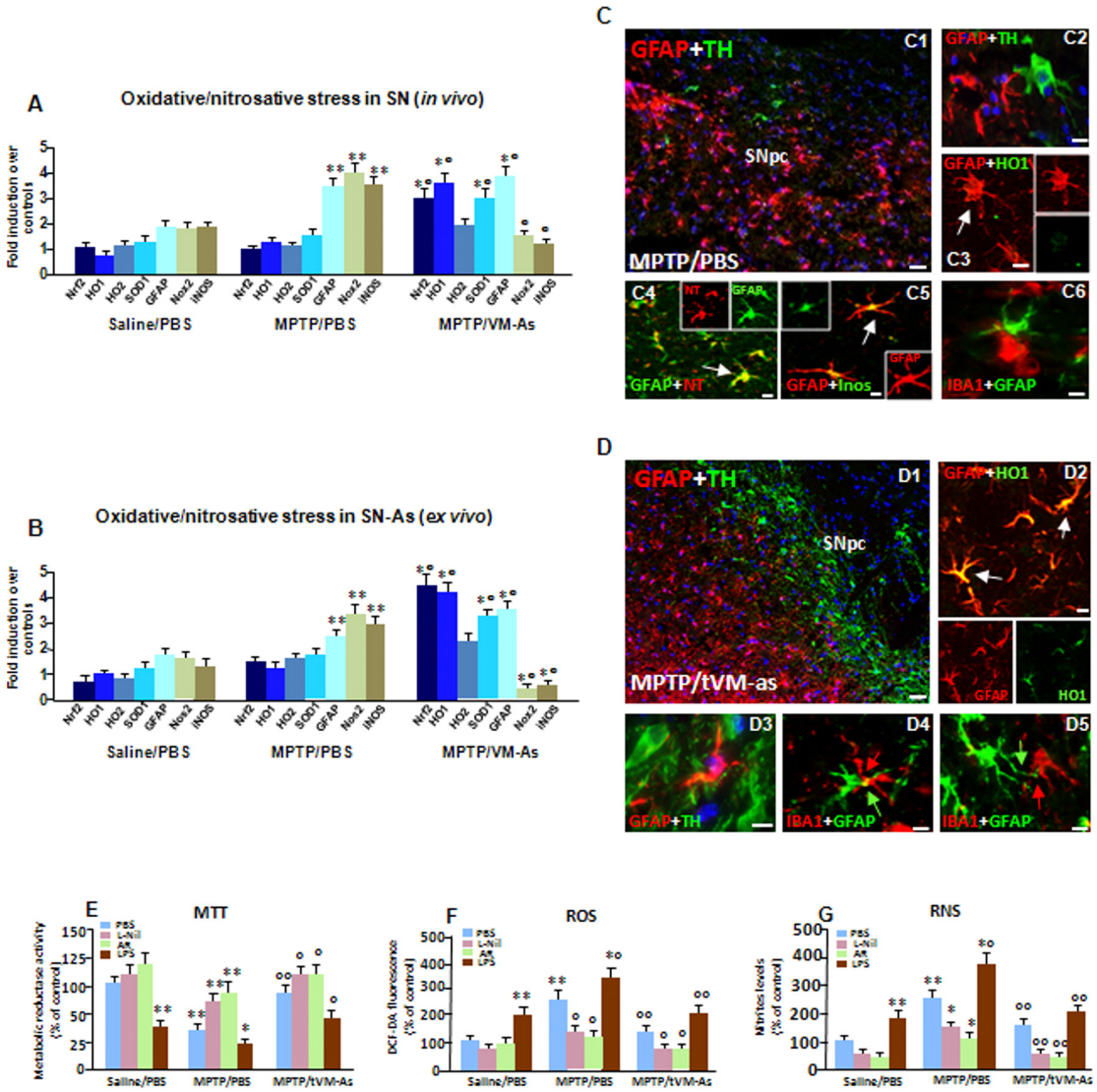

FIGURE 6 | tVM-As upregulate antioxidant self-defense *in vivo and ex vivo*. **(A,B)** Oxidative and nitrosative stress markers were analyzed by quantitative real-time PCR (qPCR) in SNpc tissues derived from MPTP/PBS and MPTP/tVM-As mice, *in vivo* **(A)**, and acutely isolated As, *ex vivo*, from both d groups **(B)**. Values (AU, mean % ± SEM of $n = 5$ samples/experimental group) are expressed as fold changes over control. VM-As grafts upregulated *Nrf2, HO1, and* superoxide dismutase 1 (SOD1), whereas *Nox2 and* inducible nitric oxide synthase (iNOS) are downregulated vs. MPTP/PBS both in SN tissues **(A)** and As-derived cultures **(B)**. $^{**}p \leq 0.01$ vs. saline/PBS; $^{\circ\circ}p \leq 0.01$ vs. MPTP/PBS, within each treatment group, respectively, by ANOVA followed by *post hoc* Newman–Keuls test. **(C,D)** Dual staining with TH (green) and GFAP (red) in midbrain sections from MPTP/PBS **(C1,C2)** and MPTP/tVM-As **(D1–D3)** showing the ability of VM-As grafts to revert MPTP-induced TH neuronal loss. In tVM-As, GFAP$^+$ cells extend the long process in close contact, almost embracing TH$^+$ neurons (D2, D3, *arrows*), and co-express HO1 **(D4)**. Scale bars: **(C1)**, 100 μm; **(C2–C5)**, 25 μm. By contrast, in MPTP/PBS, GFAP$^+$ As (red) do not colocalize with HO (green, **C3**), but express iNOS (green) at high levels **(C5)**. Likewise, the reactive oxygen (ROS) and nitrogen species (RNS) footprint, 3-nitrotyrosine (red), is abundantly expressed in GFAP$^+$ (green) cells **(C3)**. Note that in tVM-As–grafted mice, dual staining of GFAP and ionized calcium-binding adapter molecule 1 (IBA1), showing a GFAP$^+$ cell in close contact with a ramified IBA1$^+$cell phenotype **(D5)**, as opposed to MPTP/PBS, IBA1$^+$ cells with a rounded morphology, is seen close to reactive GFAP$^+$ As **(C6)**. Scale bars: **(D1)**, 100 μm; **(D2–D4)**, 25 μm. **(E–G)** Accordingly, in astrocyte cultures acutely isolated from MPTP/PBS, the production of ROS measured with the redox membrane-permeant probe 2′,7′-dichlorofluorescein diacetate (DCFH-DA, F) and the generation of iNOS-derived RNS **(G)**, in cell free supernatant, are sharply increased, resulting in a significant inhibition of mitochondrial reductase activity (MTT, **E**). These effects were efficiently counteracted in tVM-As cultures, with the application of the specific iNOS inhibitor, L-N6-(1-iminoethyl)-lysine (L-Nil) **(E–G)**. Activation of Wnt/β-catenin signaling counteracts ROS and RNS production and reverts mitochondrial dysfunction of MPTP/PBS-As **(E–G)**. By contrast, lipopolysaccharide (LPS) application further exacerbated oxidative/nitrosative stress in MPTP/PBS- vs. MPTP/tVM-As (E–G). $^{*}p \leq 0.05$, $^{**}p \leq 0.01$ vs. saline/PBS; $^{*\circ}p \leq 0.01$ vs. saline/PBS and MPTP/PBS; $^{\circ\circ}p \leq 0.01$ vs. MPTP/PBS.

abundant expression of 3-NT in GFAP$^+$ As of MPTP/PBS (**Figure 6C4**) but not of MPTP/tVM-As (not shown). These findings suggested the potential of tVM-As to ameliorate the exacerbated endogenous oxidative/nitrosative glial status of the aged injured SN milieu *via* an upregulation of antioxidant functions.

As a proof of concept, we next studied some functional properties of tVM-As derived from MPTP/PBS and MPTP/tVM-As mice, looking at the mitochondrial activity with the MTT assay, the production of ROS with the redox membrane-permeant probe DCFH-DA, and the generation of iNOS-derived NO, in cell free supernatant using the Griess reagent (**Figures 6E–G**). To study the effect of inhibition of oxidative and nitrosative stress mediators, the freshly prepared $GFAP^+$ cells were cultured in the absence or the presence the specific iNOS inhibitor, L-Nil (Marchetti et al., 2002; Morale et al., 2004), whereas to study the effect of an exogenous inflammatory trigger, lipopolysaccharide (LPS) was applied at a dose of 100 ng/ml. Finally, the effect of Wnt/β-catenin activation was studied using AR, a drug that antagonizes GSK-3β (i.e., the kinase that phosphorylates β-catenin, leading to its degradation).

First we found that mitochondrial activity was increased in tVM-As when compared to MPTP/PBS-As metabolic activity, showing significantly ($p \leq 0.01$) reduced activity vs. saline/PBS-As (**Figure 6G**). This effect is in line with the reduced amounts of both ROS and reactive nitrogen species (RNS) produced by MPTP/tVM-As vs. MPTP/PBS (**Figures 6E,F**), exhibiting significantly ($p \leq 0.01$) greater levels vs. saline/PBS-As. These results thus support increased antioxidant properties of tVM-As. Accordingly, the specific iNOS-NO inhibitor, L-Nil, efficiently counteracted the sharp increase in oxidative and nitrosative stress of MPTP/PBS-As vs. MPTP/tVM-As counterparts (**Figures 6F,G**), with a beneficial effect on mitochondrial reductase activity (**Figure 6E**). Conversely, application of LPS counteracted the low ROS and RNS levels of MPTP/tVM-As, reducing mitochondrial activity, and further increased the already elevated ROS and RNS of MPTP/PBS-As (**Figures 6E–G**).

Given the decline of As-derived Wnts with age, we asked whether Wnt/β-catenin signaling activation might affect the exacerbated redox status of MPTP/PBS-As. Remarkably, we found a significant counteraction of both ROS and RNS upregulation of MPTP/PBS-As in AR-treated vs. untreated As cultures, to levels almost comparable to those measured in tVM-As (**Figures 6F,G**), which resulted in increased metabolic activity (**Figure 6E**).

Together, tVM-As grafts downregulate the exacerbated oxidative/nitrosative status of the aged MPTP-injured SNpc and As cultures *via* an increase of Nrf2-antioxidant genes, thereby shifting the pro-inflammatory and oxidative SN microenvironment. Additionally, the ability of Wnt/β-catenin activation to revert ROS- and RNS-exacerbated production of MPTP/PBS-As further suggested the contribution of Wnt/β-catenin signaling in redox properties of VM-As.

tVM-As Promote Upregulation of Wnt/β-Catenin Genes and Protect DAergic Neurons Against MPTP/MPP^+: Crosstalk With Oxidative Stress Pathways

Previous findings clearly indicated that the aging process is associated with a sharp decline of As Wnts in the face of an increase of endogenous Wnt antagonists (L'Episcopo et al., 2011a,b, 2013, 2014b; Okamoto et al., 2011; Seib et al., 2013; Orellana et al., 2015; reviewed in Marchetti, 2018). We thus hypothesized that an As-driven disbalance of the *Nrf2-ARE* axis in middle-aged mice might contribute to aging-induced loss of Wnt signaling, and looked at the ability of tVM-As to override this hostile Wnt setting. Hence, both SNpc tissues from tVM-As (**Figure 7A**) and tVM-As–derived cultures (**Figure 7B**) enriched the expression of Wnt signature genes ($p \leq 0.01$), including *Wnt1* and β-*catenin*, together with *Fzd-1* receptor, vs. MPTP/PBS SNpc tissues and MPTP/PBS-As cultures (**Figures 7A,B**). By contrast, a number of endogenous Wnt signaling inhibitors, including the *Dkk1, sFrp1*, and *GSK-3*β, were markedly ($p \leq 0.01$) downregulated by 1 wpt in tVM-As, compared to MPTP/PBS exhibiting significantly ($p \leq 0.01$) increased levels compared to saline-injected controls (**Figures 7A,B**), suggesting that tVM-As promoted a switch of the redox- and inflammation-sensitive Wnt/β-catenin signaling response. Hence, by reverting the age-dependent decline of endogenous Wnt tone, this, in turn, might enhance the ensuing DAergic neuronal survival. To test this hypothesis, primary (E18) mesencephalic TH^+ neurons were grown on the top of MPTP/PBS-As (**Figure 7E1**) or tVM-As (**Figure 7E2**), for 5–7 DIV, and the survival and growth of TH^+ neurons as well as their functionality were studied using immunocytochemistry and DA uptake assay (**Figures 7C,D**). Hence, we found increased TH^+ neuron numbers and increased neurite extension and DA uptake levels when cocultured with tVM-As (**Figures 7C,D,E3,E4**). By contrast, TH^+ neurons grown on the top of MPTP/PBS-As exhibited a marked inhibition of neuronal survival, growth and functionality (**Figures 7C,D,E3,E4**). Accordingly, activating Wnt/β-catenin signaling with AR by lowering ROS and RNS and ameliorating MPTP/PBS-As metabolic activity (see **Figures 6E–G**) in turn increased both TH^+ neuron survival and DA uptake in MPTP/PBS-As cocultures (**Figures 7C,D,E5**), and further increased both parameters in the tVM-As–neuronal cocultures (**Figures 7C,D,E6**). By contrast, antagonizing Wnt/β-catenin signaling by the exogenous application of Dkk1 to tVM-As coculture reduced both neuronal numbers and function, thereby supporting increased As-Wnt tone as a crucial event involved in DAn growth. On the other hand, in MPTP/PBS-As overexpressing Dkk1, exogenous Dkk1 only slightly affected the already inhibited neuronal numbers found in MPTP/PBS-As–neuron cultures (**Figures 7C,D**). Finally, lowering ROS and RNS by the application of the antioxidant Apo, or L-Nil, in MPTP/PBS-As increased the number of TH^+ neurons and DA uptake levels vs. the untreated cocultures ($p \leq 0.05$), but these effects were significantly ($p \leq 0.05$) lower when compared to their tVM/As counterparts, where L-Nil and Apo induced a further increase in neuronal growth and DA uptake vs. the untreated tVM-As–neuronal cocultures (**Figures 7C,D**).

Together, these data suggest the potential of grafted VM-As to reverse the As decline of canonical Wnt's signaling components, downregulate major Wnt antagonists, and trigger the activation of an *Nrf2/Hmox/Wnt/*β-*catenin* axis favoring the "rejuvenation" of the aged, injured microenvironment, likely contributing to the DAergic neuroprotection and neurorescue herein observed.

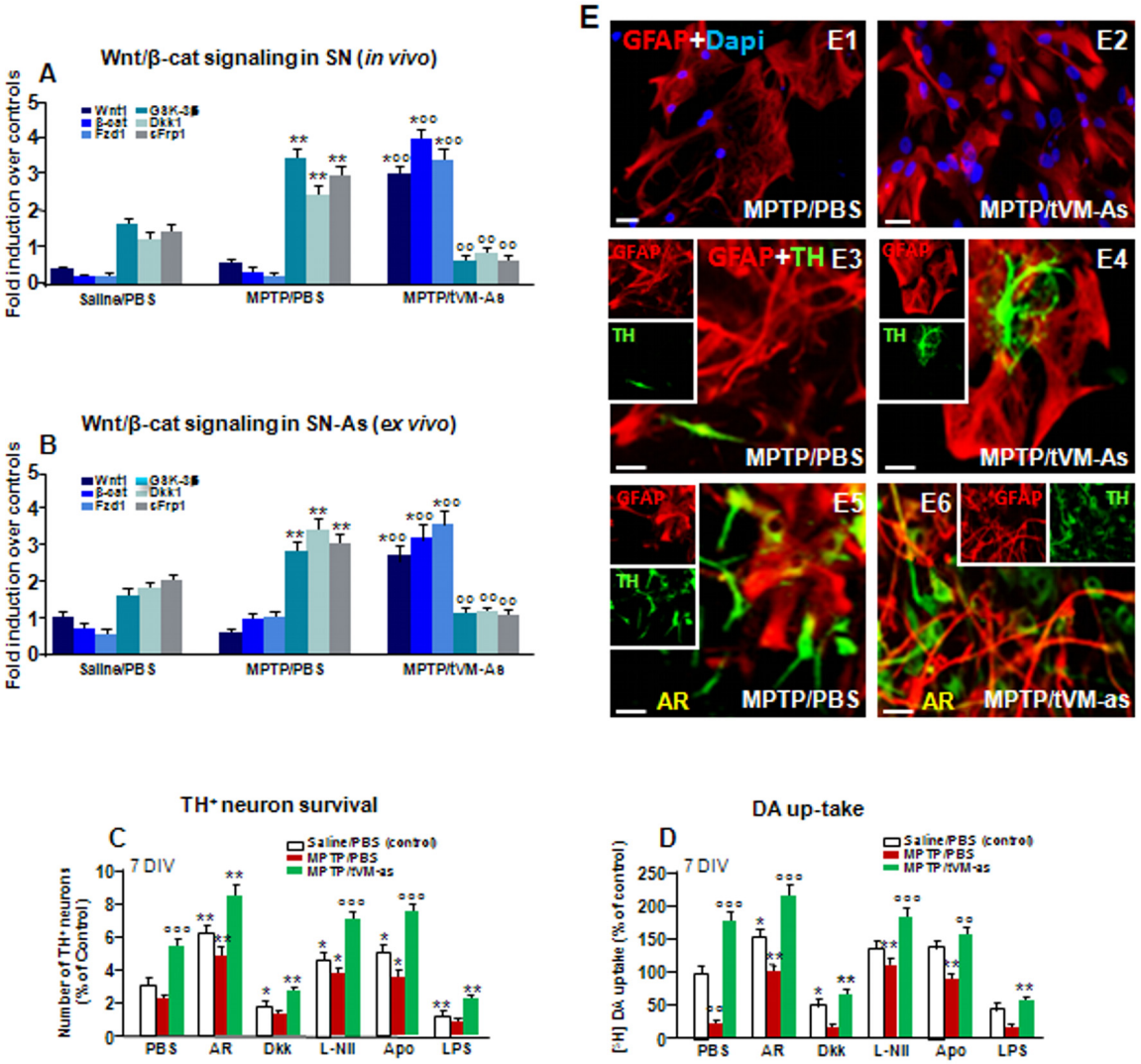

FIGURE 7 | tVM-As grafts promote activation of Wnt/β-catenin signaling in SN tissue and As and reverse the impaired DAn growth *in vitro*. **(A,B)** Wnt/β-catenin signaling transcripts were analyzed by quantitative real-time PCR (qPCR) in SNpc tissues derived from MPTP/PBS- and MPTP/tVM-As mice, *in vivo* **(A)**, and acutely isolated As, *ex vivo*, from both groups **(B)**. Values (AU, mean % ± SEM of $n = 5$ samples/experimental group) are expressed as fold changes over control. VM-As grafts upregulated *Wnt1*, β-*catenin*, and *Fzd1 receptor*, whereas the endogenous Wnt antagonists, *Dkk1, sFrp, and GSK-3*β are downregulated vs. MPTP/PBS in both SN tissues **(A)** and As-derived cultures **(B)** at 1 wpi. $^{**}p \leq 0.01$ vs. saline/PBS; $^{\circ\circ}p \leq 0.01$ vs. MPTP/PBS; $^{*\circ\circ}p \leq 0.01$ vs. saline/PBS and MPTP/PBS, within each treatment group, respectively, by ANOVA followed by *post hoc* Newman–Keuls test. **(C,D)** Quantification of TH^+ neuron number at 7 DIV **(C)** and DA uptake levels measured by [^{3}H]DA incorporation **(D)** in a direct coculture paradigm between MPTP/PBS- and MPTP/tVM-As acutely isolated, *ex vivo*, and primary mesencephalic DAn grown on the top of As, in the absence or the presence of the GSK-3β inhibitor AR, the Wnt antagonist Dkk1, the antioxidant apocynin (Apo), or the specific iNOS inhibitor L-Nil. Wnt signaling activation with AR increased TH neuron number and DA uptake levels in MPTP/PBS-As–DAn coculture **(C–D,E5)** and significantly magnified TH neuron number and functionality of MPTP/tVM-As–DAn coculture **(C–D,E6)**. Lowering oxidative and nitrosative stress with Apo and L-Nil also increased TH neuron number and DA uptake in MPTP/PBS-As–DAn coculture, albeit to a lower extent vs. their tVM-As–DAn treated counterparts **(C,D)**. Mean ± SEM values ($n = 3$ different culture preparations) are reported. $^{*}p \leq 0.05$, $^{**}p \leq 0.01$ vs. saline/PBS control; $^{\circ\circ}p \leq 0.01$ vs. PBS; $^{\circ\circ\circ}p \leq 0.01$ vs. all treatments, within each group, respectively, by ANOVA followed by *post hoc* Newman–Keuls test. **(E1–E6)** Confocal images of $GFAP^+$ (*red*) in As cultures from MPTP/PBS **(E1)** and MPTP/tVM-As **(E2)**, and TH neurons (green) and GFAP (red) in the coculture from MPTP/PBS- **(E3)** and MPTP/tVM-As **(E4)**, showing TH+ neuron growth at 5–7 DIV neurons in the presence of tVM-As **(E4)**, compared to the impaired TH neuron development in MPTP/PBS-As coculture **(E3)**. Activation of Wnt/β-catenin signaling improved TH neuron growth in MPTP/PBS-As **(E5)**, an effect that was magnified in MPTP/tVM-As–DAn coculture **(E6)**. *Bars*: **(E1,E2)**, 23 μm; **(E3–E6)**, 20 μm.

DISCUSSION

Given that aging is the leading risk factor for PD development, and that by middle age, several parameters of astroglial and DAergic neuronal functionality start to be impaired, we focused on the middle-aged (9–11 months) male midbrain microenvironment to address the ability of primary fully differentiated tVM-As to activate intrinsic mechanisms that

might rejuvenate As–neuronal dialog and promote DAergic neurorepair in MPTP-induced DAergic neurotoxicity. We herein report for the first time that grafting VM-As derived from postnatal (P2–3) midbrain within the middle-aged MPTP-injured SN can trigger a significant time-dependent endogenous nigrostriatal DAergic neurorescue. Clearly, various interactions between exogenous tVM-As and the pathological host milieu may underlie the improvement herein observed, and further time-course studies and in-depth molecular analyses both at a tissue and at a single-cell level are clearly needed to unravel how tVM-As grafts may drive a DAergic neurorescue program. However, from the presented results and based on our previous (see L'Episcopo et al., 2012, 2013, 2014b, 2018a,b; and as reviewed by Marchetti, 2018) and the recent literature findings (Tebay et al., 2015; Zhang et al., 2015, 2017; Zheng et al., 2017; Rizor et al., 2019), it seems tempting to speculate that the observed changes might result from a beneficial tVM-As–to–host SN crosstalk, promoting the rejuvenation of the host microenvironment, through the activation of an astrocytic *Nrf2/ARE/Wnt/*β*-catenin* prosurvival axis.

Notably, complex mechanisms are responsible for SNpc-DAergic cell death in PD, where the demise of this mesencephalic neuronal population is a process that is very long and is still not yet clarified (Del Tredici and Braak, 2012), as opposed to MPTP-induced DAergic degeneration (Langston, 2017), and extrapolations must be very careful. In the present study, our approach was aimed at combining: (i) the effect of age with; (ii) neurotoxin exposure; (iii) the consequent exacerbated inflammation; and (iv) male gender (representing four strong risk factors for PD), to address the ability of As grafting to mitigate the SN microenvironment and DAergic cell death.

Here, we found that, within the aged microenvironment, the proliferating tVM-As expressed S100β, but not microglia or neuronal markers, and survived for at least 4 wpt. At the SN level, tVM-As counteracted aging and MPTP-induced DAergic cell body loss, and at the striatal level, tVM-As promoted the recovery of DAT- and TH-IR, which was corroborated by the increased striatal synaptosomal DA uptake capacity and the reversal of motor impairment of aged MPTP mice, indicating the ability of tVM-As to restore nigrostriatal DAergic neurons and reinstate DAergic functionality at least for the studied time window of 4 wpt; further studies are needed to confirm, at a protein level, the capacity of tVM-As to revert the downregulation of the studied DA-signaling genes, as observed by qPCR analyses.

By analyzing microglial cells, we found that tVM-As efficiently counteracted aging and MPTP-induced increase of microglial cell number within the injured midbrain and shifted microglial morphological appearance from the M1 macrophage–like to the M2 more quiescent glial phenotype. Especially, in MPTP/PBS mice, glial cells showed round-shaped bodies with either short and thick processes or no processes, as observed in activated microglial cells (Kreutzberg, 1996), whereas in tVM-As mice, microglial cells exhibited more elongated cell bodies and longer, ramified processes, similar to the M2 glial phenotype. Accordingly, tVM-astros reversed the upregulated levels of the pro-inflammatory M1 cytokines, TNF-α, IL-6, and IL1-β, at both gene and protein expression levels in SN tissues, as compared to MPTP/PBS mice, but significantly increased the anti-inflammatory cytokine, IL-10, therefore supporting tVM-As ability to downregulate microglial exacerbation of aged MPTP/PBS mice. While further studies are clearly needed to address tVM-As–microglial interactions, their close contacts coupled to the observed change in glial phenotype may favor the possibility of a "beneficial" As–microglia crosstalk in tVM-As–grafted vs. MPTP/PBS mice, likely contributing to the downregulation of inflammation and DAergic neurorescue. In stark contrast, when the microglia is chronically activated, as observed in MPTP/PBS aging mice, As can lose both immunomodulatory and neuroprotective properties with harmful consequences for the dysfunctional DAergic neurons, as herein observed.

We then focused on the astrocytic compartment and found that tVM-As grafts sharply increased the expression of *Nrf2*, a chief astrocytic regulator of oxidative stress and inflammation, and upregulated the antioxidant and anti-inflammatory HO1 and *SOD1* transcripts, in the face of a marked suppression of *iNOS*. Clearly, from our gene expression analysis, it is not possible to differentiate the exogenous tVM-As vs. the endogenous As-expressed mRNAs, albeit using *ex vivo* As cultures from MPTP/tVM-As and MPTP/PBS-As at 1 wpt, we delineated a clear upregulation of antioxidant and Wnt signaling genes in MPTP/tVM-As vs. their MPTP/PBS-As counterparts. Especially, we found VM-As of middle-aged MPTP-lesioned mice as a critical source of Wnt antagonists likely responsible for their failure to exert neuroprotection. Hence, at a functional level, tVM-As generated significantly lower amounts of ROS and RNS compared to the exacerbated reactive mediators of MPTP/PBS-As, resulting in As mitochondrial impairment, whereas Wnt signaling activation in MPTP/PBS-As efficiently reversed the upregulated ROS and RNS to levels measured in L-Nil–treated As levels, suggesting crosstalk between Wnt signaling and oxidative stress pathways. Remarkably, tVM-astros promoted Wnt/β-catenin activation within the middle-aged, MPTP-injured SN *in vivo* and in *ex vivo* direct As–neuron coculture paradigms, where MPTP/tVM-As promoted the growth and functionality of developing primary mesencephalic DAn, as compared to their counterparts derived from MPTP/PBS mice, which failed to exhibit the critical supportive properties and instead inhibited TH^+ neuron survival and functionality.

Thus, switching the SN neurorescue-unfriendly environment, grafted As promoted a beneficial antioxidant/anti-inflammatory "*Wnt-on*" prosurvival milieu, highlighting *As*-derived factors/mechanisms as the crucial keys for successful therapeutic outcomes in PD.

As Grafting Switched the Harmful SN Milieu of Aging MPTP Mice Driving the Master Regulator of the Oxidative Stress and Inflammatory Response

With advancing age, the decline of the nigrostriatal DAergic system coupled with the progressive loss of DAergic neuron adaptive potential is believed to contribute to the slow nigrostriatal degeneration of PD (Hornykiewicz, 1993; Bezard

et al., 2000; Collier et al., 2007; de la Fuente-Fernández et al., 2011; Blesa et al., 2017). In fact, the activation of endogenous compensatory mechanisms is thought to mask the appearance of PD before the appearance of the first clinical symptoms (Zigmond et al., 2009; Blesa et al., 2017), which raises the possibility that some individuals with PD suffer from a reduction of these neuroprotective mechanisms and that treatments that boost these mechanisms may provide therapeutic benefit (see Zigmond et al., 2009). Interestingly, while young adult rodents experience a time-dependent recovery/repair from neurotoxic or immunological challenges, aging mice fail to recover for their entire life span (L'Episcopo et al., 2011a,b,c). With aging, the glial adaptive mechanisms are reduced, resulting in increased DAergic neuron vulnerability to various risk factors, including genetic, inflammatory, and environmental toxic exposures, such as MPTP (L'Episcopo et al., 2018a).

In fact, declined Nrf2-antioxidant signaling during aging leads to accumulation of ROS/RNS and oxidative stress, which is either causally linked or associated with numerous health problems including neurodegenerative conditions; thus, targeting Nrf2 has been suggested as a promising therapeutical avenue in neurodegeneration (Abdalkader et al., 2018). Remarkably, previous studies of Chen et al. (2009) indicated that *Nrf2* expression restricted to As is sufficient to protect against MPTP toxicity, suggesting that As modulation of the Nrf2-ARE pathway is a promising target for therapeutics aimed at reducing or preventing neuronal death in PD (Chen et al., 2009). Significantly, Lastres-Becker et al. (2012) reported that α-synuclein expression and Nrf2 deficiency cooperate to aggravate protein aggregation, neuronal death, and inflammation in early-stage PD, and very recent findings further define As oxidative/nitrosative stress as a key etiopathogenetic factor in PD (Rizor et al., 2019). Additionally, we pinpointed that by middle age, a significant decrease of *Nrf2/HO1* response to MPTP in striatal and SVZ-As played a prominent role and synergized with the heightened inflammatory SVZ milieu to downregulate SVZ neurogenesis (L'Episcopo et al., 2013). Here, we further uncovered that VM-As grafts promoted a switch of inflammatory M1 microglia phenotype and turned the aged As into a supportive and neuroprotective A2 phenotype.

In fact, amongst glial cytotoxic molecules, iNOS-derived NO, a superoxide from the plasma membrane NADPH oxidase, associated with a number of potent inflammatory cytokines, including TNF-α, IL-1β, IL-6, and IFN-γ, is known to exert detrimental effects in DAergic neurons (see Gao and Hong, 2008; Hirsch and Hunot, 2009). Indeed, when iNOS and NADPH oxidase are present together, a potent toxin, ONOO-, may be generated, which promotes the nitration of proteins (Gao and Hong, 2008), with harmful consequences for DAergic neurons. Conversely, As-secreted antioxidant factors represent a critical self-protective system against MPTP and 6-OHDA cytotoxicity (Chen et al., 2009). In fact, the prolonged dysfunction of As and activation of microglia accelerate degeneration of DAergic neurons in the rat SN and block compensation of early motor dysfunction induced by 6-OHDA (Kuter et al., 2018).

Here, we uncovered the ability of VM-As grafts to override the strong oxidant and pro-inflammatory status of the SN milieu of middle-aged MPTP-injured As overexpressing iNOS and the harmful RNS footprint, 3NT, by decreasing the number activated macrophage-like microglia and the expression of major inflammatory transcripts and proteins, *in vivo*, resulting in suppression of the exacerbated ROS and RNS production of MPTP-injured As, *ex vivo*.

Coupled to the critical role of As mitigating mitochondrial dysfunctions in human DAergic neurons derived from iPSC (Du et al., 2018), these present findings support the ability of VM-As grafts to boost antioxidant self-defenses, as a potential mechanistic link in the herein observed DAergic neurorescue effects.

As Grafting Triggering Wnt/Nrf2/HO1 Crosstalk Mitigates Inflammation Promoting DAn Neurorescue

The Wnt/β-catenin signaling pathway is of utmost importance owing to its ability to promote tissue repair and regeneration of stem cell activity in diverse organs, and in light of its crucial role in age-related pathogenesis and therapy of disease (Nusse and Clevers, 2017; García-Velázquez and Arias, 2017; Marchetti et al., 2020). In the last decade, we characterized As-derived *Wnt1* as crucial actor in As–DAn crosstalk involved in neuroprotection against several neurotoxic and inflammatory insults (Marchetti and Pluchino, 2013; Marchetti et al., 2013; Marchetti, 2018) and the regulation of neurogenesis and SVZ plasticity *via* crosstalk with inflammatory and oxidative stress signaling pathways during aging and MPTP-induced parkinsonism (Marchetti et al., 2020).

Indeed, a major finding of aging is the decline of Wnt signaling and that this "*Wnt-off*" state very likely drives the decline of neurogenesis and the exacerbation of inflammation, thus increasing DAn vulnerability to a number of cytotoxic and inflammatory insults (Marchetti and Pluchino, 2013; L'Episcopo et al., 2018a,b; Marchetti, 2018). Here, we further unveiled that VM-As grafts promoted an enriched expression of canonical *Wnt* signature genes in the middle-aged MPTP-injured VM, which included *Wnt1*, β-*catenin*, and *Fzd1* receptor, thus triggering a *Wnt-on* state, likely contributing to DAergic neurorescue. Accordingly, a number of endogenous Wnt signaling antagonists, such as *GSK-3β, Dkk1, and sFrp1*, were downregulated by 1 wpt in tVM-As SN tissues and As cultures, when compared to their MPTP/PBS-As counterparts exhibiting a significant upregulation of endogenous Wnt antagonists, supporting the *Wnt-off* state of the aged MPTP-injured midbrain, as observed in our previous studies (Marchetti, 2018). Here, As overexpression of Wnt antagonists and upregulated ROS and RNS levels of MPTP/PBS mice impaired As–neuron interactions *in vivo* and *ex vivo*, thus resulting in a marked inhibition of DAn survival and growth, whereas activating Wnt/β-catenin signaling, as observed in VM-As–grafted mice and VM-As–derived cultures, or MPTP/PBS-As–derived cultures treated with the GSK-3β antagonist, powerfully reverted oxidative/nitrosative stress markers promoting DAn survival and growth.

Thus, in light of the role of Wnt signaling in the inflammatory and oxidative stress response and the crosstalk between inflammatory and Wnt signaling components (Chong et al., 2007, 2010; Halleskog et al., 2011; Kilander et al., 2011; L'Episcopo et al., 2011b; Schaale et al., 2011; Halleskog and Schulte, 2013; Marchetti and Pluchino, 2013; Ma and Hottiger, 2016; Zheng et al., 2017; L'Episcopo et al., 2018a,b; Marchetti, 2018), it seems tempting to suggest that the *Wnt-off* state of MPTP/PBS mice likely exacerbates the pro-inflammatory microglial phenotype of MPTP/PBS mice, in turn responsible for the hostile SN milieu that synergizes with the downregulation of MPTP/PBS-As antioxidant self-defenses.

In stark contrast, Wnt/β-catenin activation of tVM-As–grafted mice might well promote a beneficial effect, switching the microglial M1 phenotype to a likely more quiescent anti-inflammatory state (see L'Episcopo et al., 2018a,b). Especially, a lack of As-derived Wnt-microglial dialog might well contribute to the loss of major Nrf2-antioxidant genes responsible for As failure to protect and rescue/repair the injured DAn of middle-aged MPTP mice.

Together, these findings argue in favor of reciprocal As/microglial/neuron interactions and suggest the *Nrf2/HO1/Wnt/β-catenin* axis as a critical mediator in promoting neuroprotection.

CONCLUSIONS

We have shown that grafting tVM-astros can override the aged hostile SN milieu and drive DAergic neurorescue in MPTP-induced nigrostriatal toxicity triggering the activation of a "beneficial" astrocytic *Nrf2/Hmox1/Wnt/β-catenin* axis that rejuvenates the SN microenvironment and favors DAergic neurorescue/neurorepair.

In light of the emerging implications of dysfunctional As in major human NDs (Endo et al., 2015; Anderson et al., 2016; L'Episcopo et al., 2016, 2018a,b; Booth et al., 2017; Patel et al., 2019), together with the critical role of As and As-derived factors in both pharmacological and cell therapeutical interventions (Kondo et al., 2014; Yang et al., 2014; Nicaise et al., 2015; Hall et al., 2017; Rivetti di Val Cervo et al., 2017; Barker et al., 2018; Du et al., 2018; Kuter et al., 2018; Song et al., 2018; Bali et al., 2019; Klapper et al., 2019; Rizor et al., 2019), our findings highlight As-focused therapies as the crucial key for beneficial outcomes in PD.

DATA AVAILABILITY STATEMENT

All datasets generated for this study are included in the article/**Supplementary Material**.

ETHICS STATEMENT

This study has been approved by the local Ethics Committee "Comitato Etico IRCCS Sicilia-Oasi Maria SS" of the Associazione Oasi Maria SS., based in Troina (Italy), Via Conte Ruggero, 73.

AUTHOR CONTRIBUTIONS

Authors contributing to the presented experimental findings and manuscript editing. BM: conception and design, data analysis and interpretation, manuscript writing. MS: astrocyte transplantation, histopathology, data analyses and interpretation, manuscript writing and final approval of manuscript. CT, NT, FL'E, SC, and CG: performed experiments, data analyses and interpretation, final approval of manuscript.

FUNDING

This research program has received support from different funding agencies, in particular, the Italian Ministry of Health (Ricerca Corrente-2016-2019), the Italian Ministry of Education, University and Research (MIUR), CHANCE Grant 2016–2019, the OASI Research Institute–IRCCS, Troina, Italy, and BIOMETEC at the University of Catania, Medical School, Catania, Italy.

SUPPLEMENTARY MATERIAL

The Supplementary Material for this article can be found online at: https://www.frontiersin.org/articles/10.3389/fnagi.2020.00024/full#supplementary-material.

REFERENCES

Abdalkader, M., Lampinen, R., Kanninen, K. M., Malm, T. M., and Liddell, J. R. (2018). Targeting Nrf2 to suppress ferroptosis and mitochondrial dysfunction in neurodegeneration. *Front. Neurosci.* 10:466. doi: 10.3389/fnins.2018.00466

Abercrombie, M. (1946). Estimation of nuclear population from microtome sections. *Anat. Rec.* 94, 239–247. doi: 10.1002/ar.1090940210

Anderson, M. A., Burda, J. E., Ren, Y., Ao, Y., O'Shea, T. M., Kawaguchi, R., et al. (2016). Astrocyte scar formation aids central nervous system axon regeneration. *Nature* 532, 195–200. doi: 10.1038/nature17623

Arenas, E. (2014). Wnt signaling in midbrain dopaminergic neuron development and regenerative medicine for Parkinson's disease. *J. Mol. Cell Biol.* 6, 42–53. doi: 10.1093/jmcb/mju001

Bacigaluppi, M., Russo, G. L., Peruzzotti-Jametti, L., Rossi, S., Sandrone, S., Butti, E., et al. (2016). Neural stem cell transplantation induces stroke recovery by upregulating glutamate transporter GLT-1 in astrocytes. *J. Neurosci.* 36, 10529–10544. doi: 10.1523/JNEUROSCI.1643-16.2016

Bali, P., Banik, A., Nehru, B., and Anand, A. (2019). Neurotrophic factors mediated activation of astrocytes ameliorate memory loss by amyloid clearance after transplantation of lineage negative stem cells. *Mol. Neurobiol.* 56, 8420–8434. doi: 10.1007/s12035-019-01680-z

Barker, R. A., Götz, M., and Parmar, M. (2018). New approaches for brain repair—from rescue to reprogramming. *Nature* 557, 329–334. doi: 10.1038/s41586-018-0087-1

Barkho, B. Z., Song, H., Aimone, J. B., Smrt, R. D., Kuwabara, T., Nakashima, K., et al. (2006). Identification of astrocyte-expressed factors that modulate neural stem/progenitor cell differentiation. *Stem Cells Dev.* 15, 407–421.

Bélanger, M., and Magistretti, P. J. (2009). The role of astroglia in neuroprotection. *Dialogue Clin. Neurosci.* 11, 281–295.

Belarbi, K., Cuvelier, E., Destée, A., Gressier, B., and Chartier-Harlin, M. C. (2017). NADPH oxidases in Parkinson's disease: a

systematic review. *Mol. Neurodegener.* 12:84. doi: 10.1186/s13024-017-0225-5

Berwick, D. C., and Harvey, K. (2012). The importance of Wnt signalling for neurodegeneration in Parkinson's disease. *Biochem. Soc. Trans.* 40, 1123–1128. doi: 10.1042/bst20120122

Bezard, E., and Gross, C. E. (1998). Compensatory mechanisms in experimental and human parkinsonism: towards a dynamic approach. *Prog. Neurobiol.* 55, 93–116. doi: 10.1016/s0301-0082(98)00006-9

Bezard, E., Jaber, M., Gonon, F., Boireau, A., Bloch, B., and Gross, C. E. (2000). Adaptive changes in the nigrostriatal pathway in response to increased 1-methyl-4-phenyl-1,2,3,6-tetrahydropyridine-induced neurodegeneration in the mouse. *Europ. J. Neurosci.* 12, 2892–2900. doi: 10.1046/j.1460-9568.2000.00180.x

Blauwendraat, C., Heilbron, K., Vallerga, C. L., Bandres-Ciga, S., von Coelln, R., Pihlstrøm, L., et al. (2019). Parkinson's disease age at onset genome-wide association study: defining heritability, genetic loci and α-synuclein mechanisms. *Mov. Disord.* 34, 866–875. doi: 10.1002/mds.27659

Blesa, J., Trigo-Damas, I., Dileone, M., Del Rey, N. L., Hernandez, L. F., and Obeso, J. A. (2017). Compensatory mechanisms in Parkinson's disease: circuits adaptations and role in disease modification. *Exp. Neurol.* 298, 148–161. doi: 10.1016/j.expneurol.2017.10.002

Boger, H. A., Granholm, A. C., McGinty, J. F., and Middaugh, L. D. (2010). A dual-hit animal model for age-related parkinsonism. *Prog. Neurobiol.* 90, 217–229. doi: 10.1016/j.pneurobio.2009.10.013

Booher, J., and Sensenbrenner, M. (1972). Growth and cultivation of dissociated neurons and glial cells from embryonic chick, rat and human brain in flask cultures. *Neurobiology* 2, 97–105.

Booth, H. D. E., Hirst, W. D., and Wade-Martins, R. (2017). The role of astrocyte dysfunction in Parkinson's disease pathogenesis. *Trend Neurosci.* 40, 358–370. doi: 10.1016/j.tins.2017.04.001

Brodski, C., Blaess, S., Partanen, J., and Prakash, N. (2019). Crosstalk of intercellular signaling pathways in the generation of midbrain dopaminergic neurons *in vivo* and from stem cells. *J. Dev. Biol.* 7:E3. doi: 10.3390/jdb7010003

Burbulla, L. F., Song, P., Mazzulli, J. R., Zampese, E., Wong, Y. C., Jeon, S., et al. (2017). Dopamine oxidation mediates mitochondrial and lysosomal dysfunction in Parkinson's disease. *Science* 357, 1255–1261. doi: 10.1126/science.aam9080

Burke, R. E., Cadet, J. L., Kent, J. D., Karanas, A. L., and Jackson-Lewis, V. (1990). An assessment of the validity of densitometric measures of striatal tyrosine hydroxylase-positive fibers: relationship to apomorphine-induced rotation in 6-hydroxydopamine lesioned rats. *J. Neurosci. Methods* 35, 63–73. doi: 10.1016/0165-0270(90)90095-w

Cannon, J. R., and Greenamyre, J. T. (2013). Gene-environment interactions in Parkinson's disease: specific evidence in humans and mammalian models. *Neurobiol. Dis.* 57, 38–46. doi: 10.1016/j.nbd.2012.06.025

Chen, P. C., Vargas, M. R., Pani, A. K., Smeyne, R. J., Johnson, D. A., Kan, Y. W., et al. (2009). Nrf2-mediated neuroprotection in the MPTP mouse model of Parkinson's disease: critical role for the astrocyte. *Proc. Natl. Acad. Sci. U S A* 106, 2933–2938. doi: 10.1073/pnas.0813361106

Chong, Z. Z., Li, F., and Maiese, K. (2007). Cellular demise and inflammatory microglial activation during β-amyloid toxicity are governed by Wnt1 and canonical signalling pathways. *Cell. Signal.* 19, 1150–1162. doi: 10.1016/j.cellsig.2006.12.009

Chong, Z. Z., Shang, Y. C., Hou, J., and Maiese, K. (2010). Wnt1 neuroprotection translates into improved neurological function during oxidant stress and cerebral ischemia through AKT1 and mitochondrial apoptotic pathways. *Oxid. Med. Cell. Longev.* 3, 153–165. doi: 10.4161/oxim.3.2.11758

Collier, T. J., Lipton, J., Daley, B. F., Palfi, S., Chu, Y., Sortwell, C., et al. (2007). Aging-related changes in the nigrostriatal dopamine system and the response to MPTP in nonhuman primates: diminished compensatory mechanisms as a prelude to parkinsonism. *Neurobiol. Dis.* 26, 56–65. doi: 10.1016/j.nbd.2006.11.013

de la Fuente-Fernández, R., Schulzer, M., Kuramoto, L., Cragg, J., Ramachandiran, N., Au, W. L., et al. (2011). Age-specific progression of nigrostriatal dysfunction in Parkinson's disease. *Ann. Neurol.* 69, 803–810. doi: 10.1002/ana.22284

Del Tredici, K., and Braak, H. (2012). Lewy pathology and neurodegeneration in premotor Parkinson's disease. *Mov. Disord.* 27, 597–607. doi: 10.1002/mds.24921

Di Monte, D. A., and Langston, J. W. (1995). "Idiopathic and 1-methyl-4phenyl-1,2,3,6-tetrahydropyridine (MPTP)-induced Parkinsonism," in *Neuroglia Chapter 65*, eds H. Kettenmann and B. R. Ransom (Oxford University Press), 989–997.

Du, F., Yu, Q., Chen, A., Chen, D., and Yan, S. S. (2018). Astrocytes attenuate mitochondrial dysfunctions in human dopaminergic neurons derived from iPSC. *Stem Cell Reports* 10, 366–374. doi: 10.1016/j.stemcr.2017.12.021

Dzamko, N., Geczy, C. L., and Halliday, G. M. (2015). Inflammation is genetically implicated in Parkinson's disease. *Neuroscience* 302, 89–102. doi: 10.1016/j.neuroscience.2014.10.028

Dzamko, N., Gysbers, A., Perera, G., Bahar, A., Shankar, A., Gao, J., et al. (2017). Toll-like receptor 2 is increased in neurons in Parkinson's disease brain and may contribute to α-synuclein pathology. *Acta Neuropathol.* 133, 303–319. doi: 10.1007/s00401-016-1648-8

Endo, F., Komine, O., Fujimori-Tonou, N., Katsuno, M., Jin, S., Watanabe, S., et al. (2015). Astrocyte-derived TGF-β1 accelerates disease progression in ALS mice by interfering with the neuroprotective functions of microglia and T cells. *Cell Rep.* 11, 592–604. doi: 10.1016/j.celrep.2015.03.053

Engele, J., and Bohn, M. C. (1991). The neurotrophic effects of fibroblast growth factors on dopaminergic neurons *in vitro* are mediated by mesencephalic glia. *J. Neurosci.* 11, 3070–3078. doi: 10.1523/JNEUROSCI.11-10-03070.1991

Frank-Cannon, T. C., Tran, T., Ruhn, K. A., Martinez, T. N., Hong, J., Marvin, M., et al. (2008). Parkin deficiency increases vulnerability to inflammation-related nigral degeneration. *J. Neurosci.* 28, 10825–10834. doi: 10.1523/JNEUROSCI.3001-08.2008

Franklin, K. B. J., and Paxinos, G. (2007). *The Mouse Brain in Stereotaxic Coordinates*, 3rd Edn. San Diego, CA: Academic Press.

Galli, S., Lopes, D. M., Ammari, R., Kopra, J., Millar, S. E., Gibb, A., et al. (2014). Deficient Wnt signalling triggers striatal synaptic degeneration and impaired motor behaviour in adult mice. *Nat. Commun.* 5:4992. doi: 10.1038/ncomms5992

Gallo, F., Morale, M. C., Avola, R., and Marchetti, B. (1995). Cross-talk between luteinizing hormone-releasing hormone (LHRH) neurons and astroglial cells: developing glia release factors that accelerate neuronal differentiation and stimulate LHRH release from GT(1–1) neuronal cell line and LHRH neurons induce astroglia proliferation. *Endocrine* 3, 863–874. doi: 10.1007/bf02738891

Gallo, F., Morale, M. C., Spina-Purrello, V., Tirolo, C., Testa, N., Farinella, Z., et al. (2000a). Basic fibroblast growth factor (bFGF) acts on both neurons and glia to mediate the neurotrophic effects of astrocytes on LHRH neurons in culture. *Synapse* 36, 233–253. doi: 10.1002/(SICI)1098-2396(20000615)36:4<233::AID-SYN1>3.0.CO;2-I

Gallo, F., Morale, M. C., Tirolo, C., Testa, N., Farinella, Z., Avola, R., et al. (2000b). Basic fibroblast growth factor priming increases the responsiveness of immortalized hypothalamic luteinizing hormone releasing hormone neurones to neurotrophic factors. *J. Neuroendocrinol.* 12, 941–959. doi: 10.1046/j.1365-2826.2000.00554.x

García-Velázquez, L., and Arias, C. (2017). The emerging role of Wnt signaling dysregulation in the understanding and modification of age-associated diseases. *Ageing Res. Rev.* 37, 135–145. doi: 10.1016/j.arr.2017.06.001

Gao, H. M., and Hong, J. S. (2008). Why neurodegenerative diseases are progressive: uncontrolled inflammation drives disease progression. *Trends Immunol.* 29, 357–365. doi: 10.1016/j.it.2008.05.002

Gao, H. M., Zhang, F., Zhou, H., Kam, W., Wilson, B., and Hong, J. S. (2011). Neuroinflammation and α-synuclein dysfunction potentiate each other, driving chronic progression of neurodegeneration in a mouse model of Parkinson's disease. *Environ. Health Perspect.* 119, 807–814. doi: 10.1289/ehp.1003013

Gennuso, F., Fernetti, C., Tirolo, C., Testa, N., L'Episcopo, F., Caniglia, S., et al. (2004). Bilirubin protects astrocytes from its own toxicity inducing up-regulation and translocation of multigrug resistance-associated protein 1 (Mrp 1). *Proc. Natl. Acad. Sci. U S A* 101, 2470–2475. doi: 10.1073/pnas.0308452100

Giguère, N., Burke Nanni, S., and Trudeau, L. E. (2018). On cell loss and selective vulnerability of neuronal populations in Parkinson's disease. *Front. Neurol.* 19:455. doi: 10.3389/fneur.2018.00455

Hall, C. E., Yao, Z., Choi, M., Tyzack, G. E., Serio, A., Luisier, R., et al. (2017). Progressive motor neuron pathology and the role of astrocytes in a human stem cell model of VCP-related ALS. *Cell Rep.* 19, 1739–1749. doi: 10.1016/j.celrep.2017.05.024

Halleskog, C., Mulder, J., Dahlström, J., Mackie, K., Hortobágyi, T., Tanila, H., et al. (2011). WNT signaling in activated microglia is proinflammatory. *Glia* 59, 119–131. doi: 10.1002/glia.21081

Halleskog, C., and Schulte, G. (2013). WNT-3A and WNT-5A counteract lipopolysaccharide-induced pro-inflammatory changes in mouse primary microglia. *J. Neurochem.* 125, 803–808. doi: 10.1111/jnc.12250

Harvey, K., and Marchetti, B. (2014). Regulating Wnt signaling: a strategy to prevent neurodegeneration and induce regeneration. *J. Mol. Cell Biol.* 6, 1–2. doi: 10.1093/jmcb/mju002

Hirsch, E. C., and Hunot, S. (2009). Neuroinflammation in Parkinson's disease: a target for neuroprotection? *Lancet Neurol.* 8, 382–397. doi: 10.1016/S1474-4422(09)70062-6

Hirsch, E. C., Jenner, P., and Przedborski, S. (2013). Pathogenesis of Parkinson's disease. *Mov. Disord.* 28, 24–30. doi: 10.1002/mds.25032

Ho, A., and Blum, M. (1998). Induction of interleukin-1 associated with compensatory dopaminergic sprouting in the denervated striatum of young mice: model of aging and neurodegenerative disease. *J. Neurosci.* 18, 5614–5629. doi: 10.1523/JNEUROSCI.18-15-05614.1998

Hornykiewicz, O. (1993). Parkinson's disease and the adaptive capacity of the nigrostriatal dopamine system: possible neurochemical mechanisms. *Adv. Neurol.* 60, 140–147.

Jackson-Lewis, V., and Przedborski, S. (2007). Protocol for the MPTP model of Parkinson's disease. *Nat. Protoc.* 2, 141–151. doi: 10.1038/nprot.2006.342

Jankovic, J. (2019). Pathogenesis-targeted therapeutic strategies in Parkinson's disease. *Mov. Disord.* 34, 41–44. doi: 10.1002/mds.27534

Jiao, J., and Chen, D. F. (2008). Induction of neurogenesis in nonconventional neurogenic regions of the adult central nervous system by niche astrocyte-produced signals. *Stem Cells* 26, 1221–1230. doi: 10.1634/stemcells.2007-0513

Johri, A., and Beal, M. F. (2012). Mitochondrial dysfunction in neurodegenerative diseases. *J. Pharmacol. Exp. Ther.* 342, 619–630. doi: 10.1124/jpet.112.192138

Joksimovic, M., and Awatramani, R. (2014). Wnt/β-catenin signaling in midbrain dopaminergic neuron specification and neurogenesis. *J. Mol. Cell Biol.* 6, 27–33. doi: 10.1093/jmcb/mjt043

Kadkhodaei, B., Ito, T., Joodmardi, E., Mattsson, B., Rouillard, C., and Carta, M. (2009). Nurr1 is required for maintenance of maturing and adult midbrain dopamine neurons. *J. Neurosci.* 29, 15923–15932. doi: 10.1523/JNEUROSCI.3910-09.2009

Kilander, M. B., Halleskog, C., and Schulte, G. (2011). Recombinant WNTs differentially activate β-catenin-dependent and -independent signalling in mouse microglia-like cells. *Acta Physiol.* 203, 363–372. doi: 10.1111/j.1748-1716.2011.02324.x

Klapper, S. D., Garg, P., Dagar, S., Lenk, K., Gottmann, K., and Nieweg, K. (2019). Astrocyte lineage cells are essential for functional neuronal differentiation and synapse maturation in human iPSC-derived neural networks. *Glia* 67, 1893–1909. doi: 10.1002/glia.23666

Kondo, T., Funayama, M., Tsukita, K., Hotta, A., Yasuda, A., Nori, S., et al. (2014). Focal transplantation of human iPSC-derived glial-rich neural progenitors improves lifespan of ALS mice. *Stem Cell Reports* 3, 242–249. doi: 10.1016/j.stemcr.2014.05.017

Kreutzberg, G. W. (1996). Microglia: a sensor for pathological events in the CNS. *Trends Neurosci.* 19, 312–318. doi: 10.1016/0166-2236(96)10049-7

Kuter, K., Olech, L., and Glowacka, U. (2018). Prolonged dysfunction of astrocytes and activation of microglia accelerate degeneration of dopaminergic neurons in the rat substantia nigra and block compensation of early motor dysfunction induced by 6-OHDA. *Mol. Neurobiol.* 55, 3049–3066. doi: 10.1007/s12035-017-0529-z

Langston, J. W. (2017). The MPTP story. *J. Parkinsons Dis.* 7, S11–S19. doi: 10.3233/jpd-179006

Lastres-Becker, I., Ulusoy, A., Innamorato, N. G., Sahin, G., Rábano, A., Kirik, D., et al. (2012). α-Synuclein expression and Nrf2-deficiency cooperate to aggravate protein aggregation, neuronal death and inflammation in early-stage Parkinson's disease. *Hum. Mol. Genet.* 21, 3173–3192. doi: 10.1093/hmg/dds143

L'Episcopo, F., Drouin-Ouellet, J., Tirolo, C., Pulvirenti, A., Giugno, R., Testa, N., et al. (2016). GSK-3β-induced Tau pathology drives hippocampal neuronal cell death in Huntington's disease: involvement of astrocyte-neuron interactions. *Cell Death Dis.* 7:e2206. doi: 10.1038/cddis.2016.104

L'Episcopo, F., Serapide, M. F., Tirolo, C., Testa, N., Caniglia, S., Morale, M. C., et al. (2011a). A Wnt1 regulated Frizzled-1/β-catenin signaling pathway as a candidate regulatory circuit controlling mesencephalic dopaminergic neuron-astrocyte crosstalk: therapeutical relevance for neuron survival and neuroprotection. *Mol. Neurodeg.* 6:49. doi: 10.1186/1750-1326-6-49

L'Episcopo, F., Tirolo, C., Testa, N., Caniglia, S., Morale, M. C., Cossetti, C., et al. (2011b). Reactive astrocytes and Wnt/β-catenin signaling link nigrostriatal injury to repair in 1-methyl-4-phenyl-1,2,3,6-tetrahydropyridine model of Parkinson's disease. *Neurobiol. Dis.* 41, 508–527. doi: 10.1016/j.nbd.2010.10.023

L'Episcopo, F., Tirolo, C., Testa, N., Caniglia, S., Morale, M. C., Impagnatiello, F., et al. (2011c). Switching the microglial harmful phenotype promotes lifelong restoration of subtantia nigra dopaminergic neurons from inflammatory neurodegeneration in aged mice. *Rejuvenation Res.* 14, 411–424. doi: 10.1089/rej.2010.1134

L'Episcopo, F., Tirolo, C., Caniglia, S., Testa, N., Serra, P. A., Impagnatiello, F., et al. (2010a). Combining nitric oxide release with anti-inflammatory activity preserves nigrostriatal dopaminergic innervation and prevents motor impairment in a 1-methyl-4-phenyl-1,2,3,6-tetrahydropyridine model of Parkinson's disease. *J. Neuroinflam.* 7:83. doi: 10.1186/1742-2094-7-83

L'Episcopo, F., Tirolo, C., Testa, N., Caniglia, S., Morale, M. C., and Marchetti, B. (2010b). Glia as a turning point in the therapeutic strategy of Parkinson's disease. *CNS Neurol. Disord. Drug Targets* 9, 349–372. doi: 10.2174/187152710791292639

L'Episcopo, F., Tirolo, C., Caniglia, S., Testa, N., Morale, M. C., Serapide, M. F., et al. (2014a). Targeting Wnt signaling at the neuroimmune interface for dopaminergic neuroprotection/repair in Parkinson's disease. *J. Mol. Cell Biol.* 6, 13–26. doi: 10.1093/jmcb/mjt053

L'Episcopo, F., Tirolo, C., Testa, N., Caniglia, S., Morales, C., Serapide, M. F., et al. (2014b). Wnt/β-catenin signaling is required to rescue midbrain dopaminergic progenitors and promote neurorepair in ageing mouse model of Parkinson's disease. *Stem Cells* 32, 2147–2163. doi: 10.1002/stem.1708

L'Episcopo, F., Tirolo, C., Peruzzotti-Jametti, L., Serapide, M. F., Testa, N., Caniglia, S., et al. (2018a). Neural stem cell grafts promote astroglia-driven neurorestoration in the aged Parkinsonian brain *via* Wnt/β-catenin signaling. *Stem Cells* 36, 1179–1197. doi: 10.1002/stem.2827

L'Episcopo, F., Tirolo, C., Serapide, M. F., Caniglia, S., Testa, N., Leggio, L., et al. (2018b). Microglia polarization, gene-environment interactions and Wnt/β-catenin signaling: emerging roles of glia-neuron and glia-stem/neuroprogenitor crosstalk for dopaminergic neurorestoration in aged parkinsonian brain. *Front. Neurosci.* 10:12. doi: 10.3389/fnagi.2018.00012

L'Episcopo, F., Tirolo, C., Testa, N., Caniglia, S., Morale, M. C., Impagnatiello, F., et al. (2013). Aging-induced Nrf2-ARE pathway disruption in the subventricular zone (SVZ) drives neurogenic impairment in parkinsonian mice *via* PI3K-Wnt/β-catenin dysregulation. *J. Neurosci.* 33, 1462–1485. doi: 10.1523/JNEUROSCI.3206-12.2013

L'Episcopo, F., Tirolo, C., Testa, N., Caniglia, S., Morale, M. C., Serapide, M. F., et al. (2012). Plasticity of subventricular zone neuroprogenitors in MPTP (1-methyl-4-phenyl-1,2,3,6-tetrahydropyridine) mouse model of Parkinson's disease involves crosstalk between inflammatory and Wnt/β-catenin signaling pathways: functional consequences for neuroprotection and repair. *J. Neurosci.* 32, 2062–2085. doi: 10.1523/JNEUROSCI.5259-11.2012

Liddelow, S. A., Guttenplan, K. A., Clarke, L. E., Bennett, F. C., Bohlen, C. J., Schirmer, L., et al. (2017). Neurotoxic reactive astrocytes are induced by activated microglia. *Nature* 541, 481–487. doi: 10.1038/nature21029

Ma, B., and Hottiger, M. O. (2016). Crosstalk between Wnt/β-catenin and NF-κB signaling pathway during inflammation. *Front. Immunol.* 7:378. doi: 10.3389/fimmu.2016.00378

Madhavan, L., Daley, B. F., Paumier, K. L., and Collier, T. J. (2009). Transplantation of subventricular zone neural precursors induces an

endogenous precursor cell response in a rat model of Parkinson's disease. *J. Comp. Neurol.* 515, 102–115. doi: 10.1002/cne.22033

Marchetti, B. (1997). Cross-talk signals in the CNS: role of neurotrophic and hormonal factors, adhesion molecules and intercellular signaling agents in luteinizing hormone-releasing hormone (LHRH) neuron-astroglia interactive network. *Trends Biosci.* 2:d88-125. doi: 10.2741/a177

Marchetti, B. (2018). Wnt/β-catenin signaling pathway governs a full program for dopaminergic neuron survival, neurorescue and regeneration in the mptp mouse model of Parkinson's disease. *Int. J. Mol. Sci.* 19:E3743. doi: 10.3390/ijms19123743

Marchetti, B., and Abbracchio, M. P. (2005). To be or not to be (inflammed)—is that the question in anti-inflammatory drug therapy of neurodegenerative diseases? *Trends Pharmacol. Sci.* 26, 517–525. doi: 10.1016/j.tips.2005.08.007

Marchetti, B., Kettenmann, H., and Streit, W. J. (2005a). Glia-neuron crosstalk in neuroinflammation, neurodegeneration and neuroprotection. *Brain Res. Rev.* 482, 129–489. doi: 10.1016/j.brainresrev.2004.12.002

Marchetti, B., L'Episcopo, F., Tirolo, C., Testa, N., Caniglia, S., and Morale, M. C. (2011). "Vulnerability to Parkinson's disease: towards an unifying theory of disease etiology," in *Encyclopedia of Environmental Health*, ed. J. O. Nriagu, 690–704.

Marchetti, B., Morale, M. C., Brouwer, J., Tirolo, C., Testa, N., Caniglia, S., et al. (2002). Exposure to a dysfunctional glucocorticoid receptor from early embryonic life programs the resistance to experimental autoimmune encephalomyelitis via nitric oxide-induced immunosuppression. *J. Immunol.* 168, 5848–5859. doi: 10.4049/jimmunol.168.11.5848

Marchetti, B., Serra, P. A., L'Episcopo, F., Tirolo, C., Caniglia, S., Testa, N., et al. (2005b). Hormones are key actors in gene x environment interactions programming the vulnerability to Parkinson's disease: glia as a common final pathway. *Ann. N Y Acad. Sci.* 1057, 296–318. doi: 10.1196/annals.1356.023

Marchetti, B., Serra, P. A., Tirolo, C., L'Episcopo, F., Caniglia, S., Gennuso, F., et al. (2005c). Glucocorticoid receptor-nitric oxide crosstalk and vulnerability to experimental Parkinsonism: pivotal role for glia-neuron interactions. *Brain Res. Rev.* 48, 302–321. doi: 10.1016/j.brainresrev.2004.12.030

Marchetti, B., L'Episcopo, F., Morale, M. C., Tirolo, C., Testa, N., Caniglia, S., et al. (2013). Uncovering novel actors in astrocyte-neuron crosstalk in Parkinson's disease: the Wnt/β-catenin signaling cascade as the common final pathway for neuroprotection and self-repair. *Eur. J. Neurosci.* 37, 1550–1563. doi: 10.1111/ejn.12166

Marchetti, B., and Pluchino, S. (2013). Wnt your brain be inflamed? Yes, it Wnt! *Trends Mol. Med.* 19, 144–156. doi: 10.1016/j.molmed.2012.12.001

Marchetti, B., Tirolo, C., L'Episcopo, F., Caniglia, S., Testa, N., Smith, J., et al. (2020). Parkinson's disease, aging and adult neurogenesis: Wnt/β-catenin signalling as the key to unlock the mystery of endogenous brain repair. *Aging Cell* 12:e13101. doi: 10.1111/acel.13101

McGeer, P. L., and McGeer, E. G. (2008). Glial reactions in Parkinson's disease. *Mov. Disord.* 23, 474–483. doi: 10.1002/mds.21751

Miller, K. R., and Streit, W. J. (2007). The effect of aging, injury and disease on microglial function: a case for cellular senescence. *Neuron Glia Biol.* 3, 245–253. doi: 10.1017/s1740925x08000136

Molofsky, A. V., Krencik, R., Ullian, E. M., Tsai, H. H., Deneen, B., Richardson, W. D., et al. (2012). Astrocytes and disease: a neurodevelopmental perspective. *Genes Dev.* 26, 891–907. doi: 10.1101/gad.188326.112

Morale, M. C., Serra, P., Delogu, M. R., Migheli, R., Rocchitta, G., Tirolo, C., et al. (2004). Glucocorticoid receptor deficiency increases vulnerability of the nigrostriatal dopaminergic system: critical role of glial nitric oxide. *FASEB J.* 18, 164–166. doi: 10.1096/fj.03-0501fje

Morale, M. C., Serra, P. A., L'Episcopo, F., Tirolo, C., Caniglia, S., Testa, N., et al. (2006). Estrogen, neuroinflammation and neuroprotection in Parkinson's disease: glia dictates resistance versus vulnerability to neurodegeneration. *Neuroscience* 138, 869–878. doi: 10.1016/j.neuroscience.2005.07.060

Nguyen, M., Wong, Y. C., Ysselstein, D., Severino, A., and Krainc, D. (2019). Synaptic, mitochondrial, and lysosomal dysfunction in Parkinson's disease. *Trends Neurosci.* 42, 140–149. doi: 10.1016/j.tins.2018.11.001

Nicaise, C., Mitrecic, D., Falnikar, A., and Lepore, A. C. (2015). Transplantation of stem cell-derived astrocytes for the treatment of amyotrophic lateral sclerosis and spinal cord injury. *World J. Stem Cells* 7, 380–398. doi: 10.4252/wjsc.v7.i2.380

Niraula, A., Sheridan, J. F., and Godbout, J. P. (2017). Microglia priming with aging and stress. *Neuropsychopharmacology* 42, 318–333. doi: 10.1038/npp.2016.185

Njie, E. G., Boelen, E., Stassen, F. R., Stassen, F. R., Steinbusch, H. W., Borchelt, D. R., et al. (2012). Ex vivo cultures of microglia from young and agent rodent brain reveal age-related changes in microglial function. *Neurobiol. Aging* 33, 195.e1–195.e12. doi: 10.1016/j.neurobiolaging.2010.05.008

Nusse, R., and Clevers, H. (2017). Wnt/β-catenin signaling, disease, and emerging therapeutic modalities. *Cell* 169, 985–999. doi: 10.1016/j.cell.2017.05.016

Oberheim, N. A., Goldman, S. A., and Nedergaard, M. (2012). Heterogeneity of astrocytic form and function. *Methods Mol. Biol.* 814, 23–45. doi: 10.1007/978-1-61779-452-0_3

Obeso, J. A., Stamelou, M., Goetz, C. G., Poewe, W., Lang, A. E., Weintraub, D., et al. (2017). Past, present, and future of Parkinson's disease: a special essay on the 200th Anniversary of the Shaking Palsy. *Mov. Disord.* 32, 1264–1310. doi: 10.1002/mds.27115

Okamoto, M., Inoue, K., Iwamura, H., Terashima, K., Soya, H., Asashima, M., et al. (2011). Reduction in paracrine Wnt3 factors during aging causes impaired adult neurogenesis. *FASEB J.* 25, 3570–3582. doi: 10.1096/fj.11-184697

Olanow, C. W. (2019). Levodopa is the best symptomatic therapy for PD: nothing more, nothing less. *Mov. Disord.* 34, 812–815. doi: 10.1002/mds.27690

Olanow, C. W., and Schapira, A. (2013). Therapeutic prospects for parkinson's disease. *Ann. Neurol.* 74, 337–347. doi: 10.1002/ana.24011

Orellana, A. M., Vasconcelos, A. R., Leite, J. A., de Sá Lima, L., Andreotti, D. Z., Munhoz, C. D., et al. (2015). Age-related neuroinflammation and changes in AKT-GSK-3β and WNT/β-CATENIN signaling in rat hippocampus. *Aging* 7, 1094–1108. doi: 10.18632/aging.100853

Palomer, E., Buechler, J., and Salinas, P. C. (2019). Wnt signaling deregulation in the aging and Alzheimer's brain. *Front. Cell. Neurosci.* 13:227. doi: 10.3389/fncel.2019.00227

Patel, D. C., Tewari, B. P., Chaunsali, L., and Sontheimer, H. (2019). Neuron-glia interactions in the pathophysiology of epilepsy. *Nat. Rev. Neurosci.* 20, 282–297. doi: 10.1038/s41583-019-0126-4

Poewe, W., Seppi, K., Tanner, C. M., Halliday, G. M., Brundin, P., Volkmann, J., et al. (2017). Parkinson disease. *Nat. Rev. Dis. Primers* 3:17013. doi: 10.1038/nrdp.2017.13

Przedborski, S. (2010). Inflammation and Parkinson's disease pathogenesis. *Mov. Disord.* 25, S55–S57. doi: 10.1002/mds.22638

Redmond, D. E. Jr., Bjugstad, K. B., Teng, Y. D., Ourednik, V., Ourednik, J., Wakeman, D. R., et al. (2007). Behavioral improvement in a primate Parkinson's model is associated with multiple homeostatic effects of human neural stem cells. *Proc. Natl. Acad. Sci. U S A* 104, 12175–12180. doi: 10.1073/pnas.0704091104

Rivetti di Val Cervo, P., Romanov, R. A., Spigolon, G., Masini, D., Martín-Montañez, E., Toledo, E. M., et al. (2017). Induction of functional dopamine neurons from human astrocytes *in vitro* and mouse astrocytesin a Parkinson's disease model. *Nat. Biotechnol.* 35, 444–452. doi: 10.1038/nbt.3835

Rizor, A., Pajarillo, E., Johnson, J., Aschner, M., and Lee, E. (2019). Astrocytic oxidative/nitrosative stress contributes to Parkinson's disease pathogenesis: the dual role of reactive astrocytes. *Antioxidants* 8:E265. doi: 10.3390/antiox8080265

Rodriguez, M., Rodriguez-Sabate, C., Morales, I., Sanchez, A., and Sabate, M. (2015). Parkinson's disease as a result of aging. *Aging Cell* 14, 293–308. doi: 10.1111/acel.12312

Rosciszewski, G., Cadena, V., Auzmendi, J., Cieri, M. B., Lukin, J., Rossi, A. R., et al. (2019). Detrimental effects of HMGB-1 require microglial-astroglial interaction: implications for the status epilepticus -induced neuroinflammation. *Front. Cell. Neurosci.* 13:380. doi: 10.3389/fncel.2019.00380

Rosciszewski, G., Cadena, V., Murta, V., Lukin, J., Villarreal, A., Roger, T., et al. (2018). Toll-like receptor 4 (TLR4) and triggering receptor expressed on myeloid Cells-2 (TREM-2) activation balance astrocyte polarization into a proinflammatory phenotype. *Mol. Neurobiol.* 55, 3875–3888. doi: 10.1007/s12035-017-0618-z

Salinas, P. C. (2012). Wnt signaling in the vertebrate central nervous system: from axon guidance to synaptic function. *Cold Spring Harb. Perspect. Biol.* 4:a008003. doi: 10.1101/cshperspect.a008003

Sandhu, J. K., Gardaneh, M., Iwasiow, R., Lanthier, P., Gangaraju, S., Ribecco-Lutkiewicz, M., et al. (2009). Astrocyte-secreted GDNF and glutathione antioxidant system protect neurons against 6OHDA cytotoxicity. *Neurobiol. Dis.* 33, 405–414. doi: 10.1016/j.nbd.2008.11.016

Schaale, K., Neumann, J., Schneider, D., Ehlers, S., and Reiling, N. (2011). Wnt signaling in macrophages: augmenting and inhibiting mycobacteria-induced inflammatory responses. *Eur. J. Cell Biol.* 90, 553–559. doi: 10.1016/j.ejcb.2010.11.004

Schapira, A. H., Olanow, C. W., Greenamyre, J. T., and Bezard, E. (2014). Slowing of neurodegeneration in Parkinson's disease and Huntington's disease: future therapeutic perspectives. *Lancet* 384, 545–555. doi: 10.1016/s0140-6736(14)61010-2

Schwartz, J. P., and Wilson, D. J. (1992). Preparation and characterization of type 2 astrocytes cultured from adult rat cortex, cerebellum, and striatum. *Glia* 5, 75–80. doi: 10.1002/glia.440050111

Seib, D. R. M., Corsini, N. S., Ellwanger, K., Plaas, C., Mateos, A., Pitzer, C., et al. (2013). Loss of Dickkopf-1 restores neurogenesis in old age and counteracts cognitive decline. *Cell Stem Cell* 12, 204–214. doi: 10.1016/j.stem.2012.11.010

Singh, S., Mishra, A., and Shukla, S. (2016). ALCAR exerts neuroprotective and pro-neurogenic effects by inhibition of glial activation and oxidative stress *via* activation of the Wnt/β-catenin signaling in Parkinsonian rats. *Mol. Neurobiol.* 53, 4286–4301. doi: 10.1007/s12035-015-9361-5

Sofroniew, M., and Vinters, H. B. (2010). Astrocytes: biology and pathology. *Acta Neuropathol.* 119, 7–35. doi: 10.1007/s00401-009-0619-8

Song, J. J., Oh, S. M., Kwon, O. C., Wulansari, N., Lee, H. S., Chang, M. Y., et al. (2018). Cografting astrocytes improves cell therapeutic outcomes in a Parkinson's disease. *J. Clin. Invest.* 128, 463–482. doi: 10.1172/JCI93924

Streit, W. J. (2010). Microglial activation and neuroinflammation in Alzheimer's disease: a critical examination of recent history. *Front. Aging Neurosci.* 2:22. doi: 10.3389/fnagi.2010.00022

Sun, D., and Jakobs, T. C. (2012). Structural remodeling of astrocytes in the injured CNS. *Neuroscientist* 18, 567–588. doi: 10.1177/1073858411423441

Surh, Y. J., Kundu, J. K., Li, M. H., Na, H. K., and Cha, Y. N. (2009). Role of Nrf2-mediated heme oxygenase-1 upregulation in adaptive survival response to nitrosative stress. *Arch. Pharm. Res.* 32, 1163–1176. doi: 10.1007/s12272-009-1807-8

Surmeier, D. J. (2018). Determinants of dopaminergic neuron loss in Parkinson's disease. *FEBS J.* 285, 3657–3668. doi: 10.1111/febs.14607

Takeshima, T., Johnston, J. M., and Commissiong, J. W. (1994). Mesencephalic type 1 astrocytes rescue dopaminergic neurons from death induced by serum deprivation. *J. Neurosci.* 14, 4769–4779. doi: 10.1523/JNEUROSCI.14-08-04769.1994

Tapia-Rojas, C., and Inestrosa, N. C. (2018). Loss of canonical Wnt signaling is involved in the pathogenesis of Alzheimer's disease. *Neural Regen. Res.* 13, 1705–1710. doi: 10.4103/1673-5374.238606

Tebay, L. E., Robertson, H., Durant, S. T., Vitale, S. R., Penning, T. M., Dinkova-Kostova, A. T., et al. (2015). Mechanisms of activation of the transcription factor Nrf2 by redox stressors, nutrient cues, and energy status and the pathways through which it attenuates degenerative disease. *Free Radic. Biol. Med.* 88, 108–146. doi: 10.1016/j.freeradbiomed.2015.06.021

Wang, L. L., Li, J., Gu, X., Wei, L., and Yu, S. P. (2017). Delayed treatment of 6-bromoindirubin-3′oxime stimulates neurogenesis and functional recovery after focal ischemic stroke in mice. *Int. J. Dev. Neurosci.* 57, 77–84. doi: 10.1016/j.ijdevneu.2017.01.002

Wurst, W., and Prakash, N. (2014). Wnt-1 regulated genetic networks in midbrain dopaminergic neuron development. *J. Mol. Cell Biol.* 6, 34–41. doi: 10.1093/jmcb/mjt046

Wyss-Coray, T. (2016). Ageing, neurodegeneration and brain rejuvenation. *Nature* 539, 180–186. doi: 10.1038/nature20411

Yang, F., Liu, Y., Tu, J., Wan, J., Zhang, J., Wu, B., et al. (2014). Activated astrocytes enhance the dopaminergic differentiation of stem cells and promote brain repair through bFGF. *Nat. Commun.* 5:5627. doi: 10.1038/ncomms6627

Yasuhara, T., Matsukawa, N., Hara, K., Yu, G., Xu, L., Maki, M., et al. (2006). Transplantation of human neural stem cells exerts neuroprotection in a rat model of Parkinson's disease. *J. Neurosci.* 26, 12497–12511. doi: 10.1523/JNEUROSCI.3719-06.2006

Zhang, J., Götz, S., Vogt Weisenhorn, D. M., Simeone, A., Wurst, W., and Prakash, N. (2015). A WNT1-regulated developmental gene cascade prevents dopaminergic neurodegeneration in adult $En1^{+/-}$ mice. *Neurobiol. Dis.* 82, 32–45. doi: 10.1016/j.nbd.2015.05.015

Zhang, Y., Unnikrishnan, A., Deepa, S. S., Liu, Y., Li, Y., Ikeno, Y., et al. (2017). A new role for oxidative stress in aging: the accelerated aging phenotype in $Sod1^{-/-}$ mice is correlated to increased cellular senescence. *Redox Biol.* 11, 30–37. doi: 10.1016/j.redox.2016.10.014

Zheng, H., Jia, L., Liu, C. C., Rong, Z., Zhong, L., Yang, L., et al. (2017). TREM2 promotes microglial survival by activating Wnt/β-catenin pathway. *J. Neurosci.* 37, 1772–1784. doi: 10.1523/JNEUROSCI.2459-16.2017

Zigmond, M. J., Cameron, J. L., Leak, R. K., Mirnics, K., Russell, V. A., Smeyne, R. J., et al. (2009). Triggering endogenous neuroprotective processes through exercise in models of dopamine deficiency. *Parkinsonism Relat. Disord.* 15, S42–S45. doi: 10.1016/S1353-8020(09)70778-3

Zuo, F., Bao, X. J., Sun, X. C., Wu, J., Bai, Q. R., Chen, G., et al. (2015). Transplantation of human neural stem cells in a Parkinsonian model exerts neuroprotection *via* regulation of the host microenvironment. *Int. J. Mol. Sci.* 16, 26473–26492. doi: 10.3390/ijms161125966

Conflict of Interest: The authors declare that the research was conducted in the absence of any commercial or financial relationships that could be construed as a potential conflict of interest.

Advantages of publishing in Frontiers

OPEN ACCESS
Articles are free to read for greatest visibility and readership

FAST PUBLICATION
Around 90 days from submission to decision

HIGH QUALITY PEER-REVIEW
Rigorous, collaborative, and constructive peer-review

TRANSPARENT PEER-REVIEW
Editors and reviewers acknowledged by name on published articles

Frontiers
Avenue du Tribunal-Fédéral 34
1005 Lausanne | Switzerland

Visit us: www.frontiersin.org
Contact us: info@frontiersin.org | +41 21 510 17 00

REPRODUCIBILITY OF RESEARCH
Support open data and methods to enhance research reproducibility

DIGITAL PUBLISHING
Articles designed for optimal readership across devices

FOLLOW US
@frontiersin

IMPACT METRICS
Advanced article metrics track visibility across digital media

EXTENSIVE PROMOTION
Marketing and promotion of impactful research

LOOP RESEARCH NETWORK
Our network increases your article's readership